THESIS

DETAIL DESIGN OF PROTOTYPE PORTABLE CORDLESS REINFORCING STEEL COMBINATION CUTTER AND BENDER

Submitted by

Kinnon Kenneth Pang

School of Engineering, Computer and Mathematical Sciences

Faculty of Design and Creative Technologies

In fulfillment of the requirements for the degree of

Master of Engineering

Auckland University of Technology

Auckland, New Zealand

September 2018

Supervisors

Dr. Michael Gschwendtner

Dr. David White

Statement of Originality

I, Kinnon Kenneth Pang hereby declare that this submission is my own work. That, to the best of my knowledge and belief it contains no material previously published or written by another person nor material which, to a substantial extent, has been accepted for the qualification of any other degree or diploma of this university or other institution of higher learning, except where due acknowledgment is made.

Kinnon Kenneth Pang BE

21st of September 2018

Executive Summary

This project was commissioned by Bill Ross, owner of Bay of Plenty Gear Cutters, to design a prototype portable handheld reinforced steel-rod combination bender and cutter for use on construction sites; where access to a power source is limited. This thesis covers the research of current cutters and benders on the market, concept generation, development, materials selection, and detailed design involving the analysis of the components in the device in both first principles and a finite element analysis (FEA) performed on mainly SolidWorks. The proposed new tool will require further development, refinement and optimisation before it can be released for sale.

Acknowledgements

I would like to thank Dr. Michael Gschwendtner, Dr. David White, and Mr. Bill Ross for their knowledge, guidance and, support; I also wish to thank Callaghan Innovation for the Research and Development Fellowship Grant that made this project possible. I would like to make a few special mentions here to acknowledge Mr. Tony Mackenzie for his invaluable knowledge of FEA simulations, Miss Danielle Yang and Mr. Jeffery Chen for their proof reading, humour, and continuous support throughout this degree. Last but not least, acknowledgement must be made to my parents, Chi Chuen Pang and Oi Yin Pang née Lo, for their unwavering unconditional support throughout past 26 years.

Table of Contents

Table of Figures

List of Tables

Nomenclature

Symbol	Definition	Units
$\mathfrak{A}$	Area bound by the centre line of cross-section	m^2
α_P	Pressure angle	°, rad
β	Cam angle	°, rad
ε	Strain	-
ε_{cen}	Eccentricity	m
θ, $\angle$	Angle	°, rad
ρ	Radius of Curvature	m
ω	Angular velocity	$rads^{-1}$
σ	Stress	Pa, MPa
τ	Shear Stress	Pa, MPa
υ	Poisson's Ratio	-
A	Area	m^2
a_{con}	x axis half dimension of ellipse	m
A_{con}	Principle Relative Curvature	m^{-1}
B_{con}	Principle Relative Curvature	m^{-1}
b	Contact half width	m
b_{con}	y axis half dimension of ellipse	m
C_a	Non-dimensional Coefficient	-
C_b	Non-dimensional Coefficient	-
C_f	Maximum Direct Stress Coefficient	-
c	Maximum Value of y (radius of rebar)	m
D	Diameter	m, mm
E	Young's Modulus of Elasticity	GPa, MPa
F	Force	N

F_S	Factor of safety	-
h	Maximum rise of follower	m
I	Moment of Inertia, Second Moment of Area	m^4
~~I~~	Current	A
J	Polar Moment of Inertia	m^4
K	Stress Concentration Factor	-
$k_{1, 2\ldots}$	Material Constant	m^2N^{-1}
k	Spring Constant	Nm^{-1}
L	Length	m, mm
M	Bending Moment	Nm
m	Module	-
P	Power	W
Q	First Moment of Area (shaded area)/Shape Factor	m^3
R	Modulus of Rigidity	-
R_P	Base Circle Radius	m
r	Radius	m, mm
R	Radius of Gyration	m
$R_{11, 12, 21, 22}$	Principal Radius of Curvature of Body	m
R_e	Resistance	Ω
R_p	Prime radius	m
T	Torque	Nm
t	Time	s
~~V~~	Voltage	V
V	Linear velocity	ms^{-1}
W	Width	m

w	Calculation Parameter	-
y	Values of y along y axis of rebar	m
y_y	Half Height of Elastic Core	m
$\bar{y}$	Distance from Equal Area Axis/Neutral Axis to centroid	m
$\dot{y}$	Follower Velocity	ms^{-1}
$y(\theta)$	Cam profile displacement	m
$y'(\theta)$	Cam profile velocity	m
$y''(\theta)$	Cam profile acceleration	m
z	Width of Cross-section	m

Subscripts

1	Follower
2	Cam
All	Allowable
arm	Bending arm
B	Bending
b	Bearing
c	Compression
cam	Cam
con	contact
d	Depth
e	Equivalent
f	Follower
max	Maximum
p	Plastic Deformation
s	Shear

t	Tension
UTS	Ultimate Tensile Stress
x	x direction, direction normal to cross-sectional area
Y	Yield

1 Introduction

The purpose of this project is to develop a hand tool that can cut and bend reinforced steel rod, hereinafter referred to as “rebar,” of varying diameters, which will be used in the heavy construction industry for reinforced concrete. All currently available tools that have this combination of cutting and bending capacity require power to be delivered from a mains power point. Although there are current power tools on the market that have a bending and cutting combination feature, none of these tools have an independent power source be it electrical or otherwise. This restriction can be a nuisance or danger on a construction site, as this tool is usually used before electricity is connected to the building and large generators are clumsy to manoeuvre, especially on unsealed surfaces found at construction sites. Having a portable tool that possesses its own power source would allow the construction workers to use this tool with greater ease.

As previously mentioned, construction sites have limited access to power sources. Reinforced steel is used in the initial stages of construction, and if the reinforced steel is bent incorrectly or cut to the wrong length, the builders would have to send the steel back to the manufacturer for correction. This, of course, would delay construction and would have financial ramifications; this tool seeks to eliminate this risk by making the job of bending and shearing rebar easier.

1.1 Client specifications

The client of this project has requested that:

- The power tool can bend and cut rebar to a maximum diameter of 20 mm.
- The power tool must also be electrically powered; the most likely source of power will be a standard drill battery.
- The rebar bender mechanism should be able to bend 20 mm diameter rebar 180° within 15 seconds.
- Shear 20 mm rebar within 10 seconds.
- The power tool should not be heavier than 15 kg if possible.
- Safety features will include a “dead man switch” (the switch, if released at any time would switch off the tool).
- Power tool will be internally torque-balanced so that the user will not have to wrestle with the tool when in use.

2 Research

This chapter will focus on researching the rebar bender and cutters that are currently available, methods in which metal is cut, sheared and bent. The material properties and applications of rebar used in New Zealand will also be discussed as well as the possible transmission methods that could be utilised to achieve the cutting and bending of rebar. The opinions of the end user will also be part of this research.

2.1 Similar Products

Currently on the market, there are several cordless cutters and benders of reinforced steel. However, these products do not have a cutter/bender combination feature. There are however corded power tools that have this feature of a cutter and bender combination, but the main drawback is that they require a 230 V 50 Hz power supply.

Figure 2.1: Diamond DBC-16H Portable Combination Rebar Cutter/Bender ('Rebar and Mesh Conversion Supplies (Pty) Ltd , n.d.)

The combination rebar cutter/bender by Diamond, shown in *Figure 2.1*, has the rebar bender located on the side of the tool while the rebar cutter is located at the front of the tool. According to the manufacturer's specifications for this device, it can bend a steel bar to a maximum diameter of 16 mm in 5.5 seconds with a maximum bend angle of 180°. It is also able to cut through a steel bar in 2.5 seconds.

Hitachi has developed a similar product to that of Diamond; both power tools employ the same method of cutting, but Hitachi provides more accurate bending, as bend angles are pre-set. It also allows the user to manually control the angle of bend if the desired angle is not provided on the pre-sets.

Figure 2.2: Hitachi rebar cutter and bender ('Hitachi VB16Y 8 Amp Rebar Bender and Cutter', 2018)

The yellow guard covers the cutter while it is not in use. Both the Hitachi and the Diamond rebar cutter and benders share the same problem of their reliance on a mains power supply.

Figure 2.3: Rebar cutting on Hitachi (Hitachi VB16Y 8.0-Amp Portable Variable-Speed Rebar Cutter / Bender, 2018)

There are several battery-powered hand-held products offered by numerous other brands. However, these products only either offer cutting or bending, but not both. *Figure 2.4* shows one such cordless rebar bender; the Ogura HBB-19180DF can bend 16 mm diameter rebar 180° in 16 seconds; it uses an 18 V lithium-ion battery. The electric motor does not directly drive the bending mechanism but rather the motor drives a hydraulic pump to generate 60,000 kPa output to bend the rebar.

Figure 2.4: Ogura HBB-19180DF cordless bender ('HBB-19180DF cordless rebar benders from Stainelec Hydraulic Equipment', 2011)

Figure 2.5: Cordless Makita XCS01Z rebar cutter ('Makita Power Tools - XCS01Z', 2018)

Makita has developed a rebar cutter capable of cutting a 16 mm diameter rebar in 6.5 seconds; it uses the standard Makita 18 V lithium-ion battery which is compatible with the rest of the Makita range of power tools. The blades have been rated for 4000 cuts before replacement is required.

There are numerous brands offering similar cordless and corded solutions for cutting and bending rebar. However, there are no cordless combination 20 mm rebar cutter and bender currently on the market.

2.2 Alternative Methods of Cutting

There are alternative methods of cutting steel to the metal shear method used on most rebar cutters. One such method is to use a circular saw. Circular saw blades are highly accessible but would significantly increase the size of the device. It would also require a great deal of guarding to protect the user from its high rotational velocity. Another downfall of this method is sparks generated from cutting steel; this would present a fire hazard and restrict the device's use in certain environments. The time required to cut through a 16 mm diameter rebar using a circular saw is comparable to that of conventional methods used by rebar cutting products currently on the market. The same goes for cutting discs, although cutting discs would be more compact.

Figure 2.6: Circular saw blade (Roofing Tools, 2011)

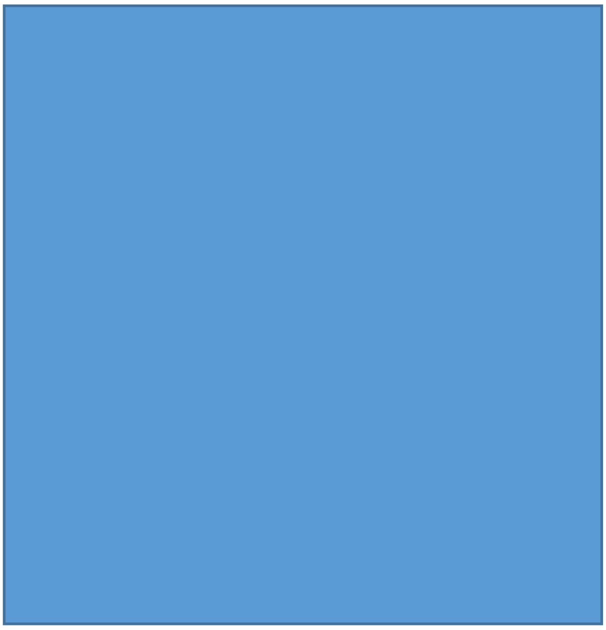

Figure 2.7: Cutting disc for angle grinders ('Bosch', n.d.)

There are other methods of cutting steel such as laser cutting, water jet, and the use of oxyacetylene which are used in industry, but for this application, these options may prove impractical. However, all options must be considered and will be briefly discussed below.

Laser cutting (CO_2 laser cutting) is one of the most accurate and the quickest methods of cutting steel, but laser cutting produces a significant amount of smoke and heat. It also has a risk of warping the material due to the heat produced by the laser. However, the major drawback of laser cutting is that there is currently no battery powered laser powerful enough to cut through steel; a laser cutting through steel requires approximately 6000 W.

Water jet cutting is one of the most straightforward methods of cutting through steel and many other materials. Waterjet cutting uses high-pressure water, “in excess of 50,000 psi (344738 kPa)” (WARDJet, n.d.), which is then concentrated into a jet stream diameter between 0.25 ~ 0.36 mm. The smaller the jet stream diameter, the slower the cutting speed. The larger the diameter, the faster the cutting speed but lower precision of cut. Water jet cutting has several drawbacks including requiring a continuous supply of water and abrasive particles.

Oxyacetylene gas cutting works by applying oxygen to the heated metal; the oxygen reacts to the metal forming an oxide which is below the melting point of the metal being cut. The torch then burns through the oxide and cuts through the metal. Using an oxyacetylene gas-cutting torch does require some skill and training; it also presents a fire hazard and may prevent its use on some construction sites.

2.3 Methods of Bending

There are two most common methods of bending found on electric rebar benders. The first pushes the rebar inwards against two stationary pins which then forms a bend, as shown in *Figure 2.8.* The flaw of this method is that it cannot make 180° bends; as the power tool, will obstruct the rebar's path. However, there is a variation of this tool that bends the rebar in the opposite direction which eliminates this problem, see *Figure 2.9.*

Figure 2.8: Linear rebar bender (Stainlec Hydraulic Equipment, 2014)

Figure 2.9: Variation of linear rebar bender ('Stainelec EDILGRAPPA REBAR BENDERS', 2014)

The second method most commonly found on benders uses a radial system. The rebar is placed between a stationary pin and a roller that moves in a rotational motion (*Figure 2.10)*, which gives more variety in bend angles compared to the linear rebar bender. The cordless version also incorporates a hydraulic pump.

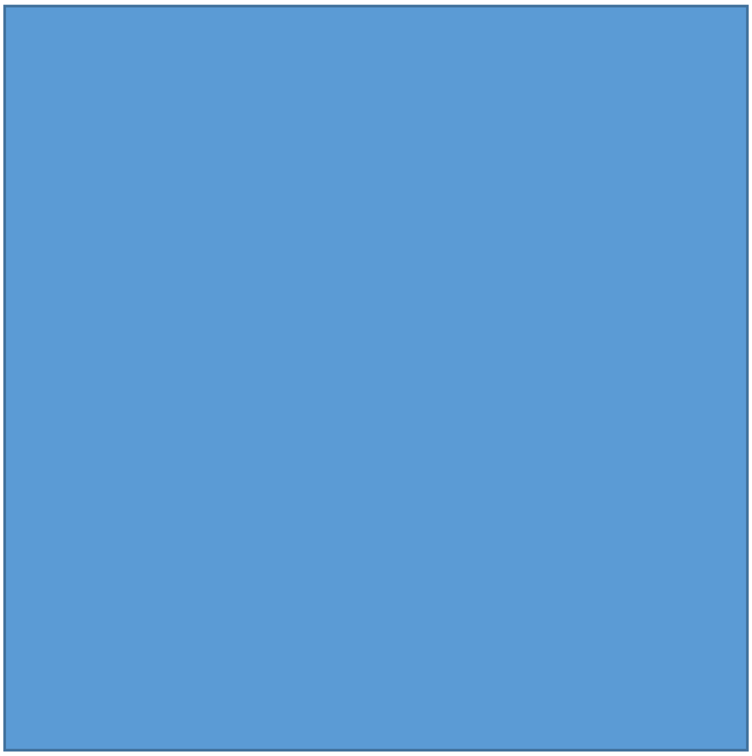

Figure 2.10: Radial rebar bender (RMCS, n.d.)

Both methods have their advantages and disadvantages; the radial rebar bender is more compact compared to the linear rebar bender and would be easier to store when not in use. However, the radial rebar bender would not be well suited for hand-held use as it will be top-heavy, while the linear rebar bender would have better balance for hand-held use.

There are also alternative methods for shaping steel. The following methods may or may not be practical to this project, but all avenues must be explored and will be briefly discussed. There are several conventional methods of bending; these are: induction bending, roll bending, and synchronized incremental bending. There is also a method of forming steel utilising explosives.

Induction bending involves heating the piece with a heating coil, and the workpiece is moved at a constant speed so that a specific temperature could be achieved. As it moves through the heating coil, the piece is bent to its desired shape. Once the desired shape is obtained, the piece is then cooled. One of the drawbacks of this method is that the mechanical properties of the rebar will change due to heating, which may put the structural integrity of the building at risk.

Roll bending involves running a workpiece of metal through three rollers arranged in a triangle, *(Figure 2.11)*, with the three rollers rotating independently. The radius of the bend is achieved by changing the distances between the rollers. However, it will take several passes to achieve the desired radius.

Figure 2.11: Roll bending/pyramid rolling (Shell Rolling Procedure, 2013)

The synchronised incremental bending method (*Figure 2.12*) is similar to point bending, which is the method used by linear rebar benders. Synchronised incremental bending has several bending points (unlike point bending with only one bending point) which are applied to either section of the metal piece or the entire length of the piece depending on the desired shape or bend radius. This method produces bends with little distortion.

Figure 2.12: Synchronised incremental bending (Albina, 2018)

Explosive hydroforming uses explosive charges placed on the sheet-metal surface (see *Figure 2.13*), it is then submerged underwater over a die, to which the charge is detonated. This is known as the Contact Method. The second method of hydroforming is called the Standoff Method in which a layer of material, usually water, oil, or air, is placed in-between the explosive and the sheet metal. The sheet metal is also placed over a die and submerged in water. This method is similar to hydroforming; the difference is instead of using an explosive to generate pressure, hydraulic fluid is pumped into a mould with the sheet metal in place. The punch will then push down against the sheet metal and give the desired shape (*Figure 2.14)*; a similar method is used with tubes to obtain the desired shape, where the hydraulic fluid is pumped into the tube (*Figure 2.15)* which expands the tube wall up against the die and punch.

Figure 2.13: Explosive hydroforming sheet metal ('Explosive Forming & Hydro Forming Services Provided at Pacaero', 2018)

Figure 2.14: Hydroforming sheet metal ('Hydroforming of tubes, extrusions, and sheet', 2018)

Figure 2.15: Hydroforming tubes ('Hydroforming of tubes, extrusions, and sheet', n.d.)

2.4 Types of Rebar

There are two types of rebar; plain and deformed (*Figure 2.16)*. Plain rebars are used in applications where the concrete and the bar are required to slide against one another. An example of this application is pavements. Throughout the day, concrete pavements will expand and contract. Here, adhesion between concrete and rebar would result in cracking. The most common rebars in use are the deformed rebars; which have ridges, a repeating pattern, or a custom pattern as required by a customer. The ridges allow better contact with the concrete; it is mainly used for beams, columns, and other pre-cast concrete applications. There are also epoxy-coated and galvanised rebar; these are usually used in environments where corrosion is a significant issue, and they are usually more expensive.

Figure 2.16: Plain and deformed rebars (Betons, 2017)

2.4.1 Rebar Bending

Rebar must be bent to the specification as outlined in NZS 3109: 1997 Concrete construction, and depending on the type and diameter, minimum bend diameters must be adhered to *Table 1*.

Table 1: Minimum rebar bend diameter (Molloy, June)

With most grades of rebar, initial cold-bending is permitted. Re-bending or straightening is to be avoided for 300E, but for 500-grade rebar, re-bending or straightening is strictly forbidden. Rebar bending is also performed cold, although hot bending is allowed. It must be completed in strict control, as high temperatures would degrade the mechanical properties of the rebar. This results in welding specific grades of rebar being forbidden, (*Table 2*).

Table 2: Rebar conditions (Molloy, June)

2.4.2 Rebar Applications

Concrete is best suited to applications where compression is experienced; however, concrete may experience some external forces that will cause tension to occur. Without reinforcement, excessive tensile forces within the concrete would cause it to crack or fail. In order to combat tension, steel rods (rebar) are utilised in the concrete to direct the tension away from the concrete. Rebar will most often be seen in concrete beams, columns, walls, and foundations (*Figure 2.17)*.

Figure 2.17: Applications of rebar (Integrated Publishing Construction, n.d.)

Rebar is also used for ties and stirrups. The former for preventing shear in concrete beams, and the latter to prevent the main vertical-rebar in columns from separating due to compressive loads.

2.4.3 Rebar Metal Composition and Mechanical Properties

Rebar used in New Zealand construction is sourced from both overseas (China, India, etc.) and locally. The quality control of steel used in rebar overseas is unknown. However, it is known that the primary local supplier of rebar in New Zealand is Pacific Steel. Steel manufactured by New Zealand Steel (supplied to Pacific Steel) adheres to the Australian and New Zealand standard AS/NZS 4671:2001. This standard describes the chemical, geometrical, and mechanical properties that all rebar produced in New Zealand and

Australia must comply. According to Pacific Steel, for the two most commonly used rebar grades, the mechanical and chemical properties for grades 500E and 300E are as follows in *Table 3*.

Table 3: Seismic 500E and 300E Grade Rebar Mechanical and Chemical Properties ('SEISMIC® Pacific Steel', 2018)

<table>
<tr><td rowspan="4">Grade 300E</td><td>Elements</td><td>C</td><td>S</td><td>P</td><td>Ce</td></tr>
<tr><td>Max [%]</td><td>0.22</td><td>0.05</td><td>0.05</td><td>0.43</td></tr>
<tr><td colspan="2">Yield Stress [MPa]</td><td colspan="2">Tensile Ratios [MPa]</td><td>Uniform Elongation at max load [%]</td></tr>
<tr><td colspan="2">300-380</td><td colspan="2">1.15-1.5</td><td>Min. 15 %</td></tr>
<tr><td rowspan="4">Grade 500E</td><td>Elements</td><td>C</td><td>S</td><td>P</td><td>Ce</td></tr>
<tr><td>Max [%]</td><td>0.22</td><td>0.05</td><td>0.05</td><td>0.49</td></tr>
<tr><td colspan="2">Yield Stress [MPa]</td><td colspan="2">Tensile Ratios [MPa]</td><td>Uniform Elongation at max load [%]</td></tr>
<tr><td colspan="2">500-600</td><td colspan="2">1.15-1.4</td><td>Min. 10 %</td></tr>
</table>

The variations in the mechanical properties in *Table 3* could be due to New Zealand Steel mixing recycled steel into their new steel. According to New Zealand Steel (2018), the average recycled content of steel produced by New Zealand Steel is approximately 12% from pre-consumer scrap. It should be noted that New Zealand Steel tests its scrap steel composition before mixing it into the batch. *Figure 2.18* shows the stress-strain curve of 500E grade rebar steel; this grade of rebar steel will be used for all analysis pertaining to the design of the rebar cutter and bender. From *Figure 2.18*, the yield stress is between 500 – 600 MPa; for the analysis in bending, 600 MPa will be used and for shear, the Ultimate Tensile Stress (UTS) of 726 MPa, will be used. The red lines on *Figure 2.18* show the offset stresses at yield and ultimate tensile stress.

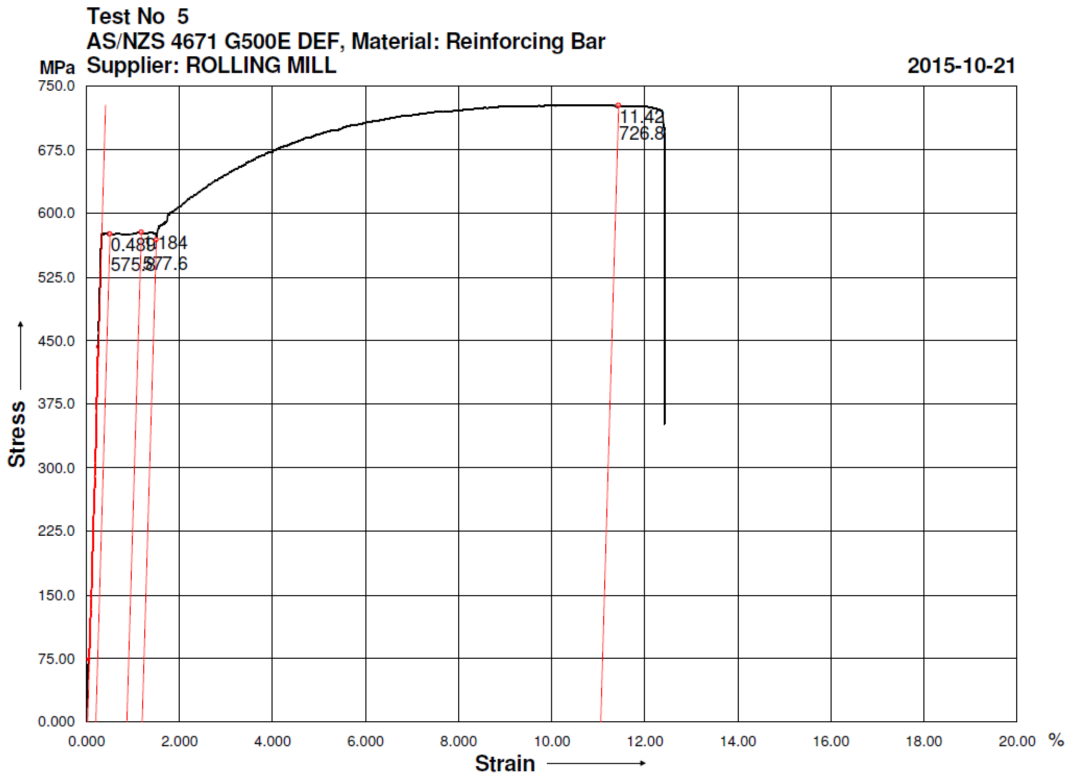

Test No	BNo	d mm	ReL (abs.) kN	Fm kN	Agt %	At %	Rm/ReL	ReL MPa	Rp0.2 MPa	Rm MPa	ReH MPa	Rm/Rp0.2	m g	Lt mm	Ag %	Comment	t	E GPa	RH	RW1	RW2	LS	K	Bend	SPA
5		25.00	279.2	357.2	11.44	12.41	1.279	568.8	575.8	727.7	577.8	1.264	2372	618.0	11.05		0.000	186.7	1.420	3.780	3.740	12.73	1.000	PAS	0

Figure 2.18: Stress Strain Curve of 500E grade rebar steel (Palmer, M. personal communication, October 26, 2017)

2.4.4 Rebar Shearing

As the tool both shears and bends, the one with the higher power requirement will be used to select a suitable electric motor. Before the calculations can be carried out, the various stages of shearing metal must be considered, as shown in *Figure 2.19*.

Figure 2.19: Stages of shearing ('Sheet Metal Cutting (Shearing)', 2009)

From *Figure 2.19*, the stages of shearing can be seen. The reflective surface is the roll-over and burnish depth; these two features combined is the shear depth. The surface with the duller finish is where the fracture has occurred. The values from *Table 4* were obtained from a reinforcing plant. The rebar was sheared on the MEP Syntax Line 25 rebar cutter and bender.

Table 4: 20mm 500E Fracture Samples

Samples	Fracture Height [mm]	Shear Depth [mm]	Change in Diameter [mm]
Sample 1	13	4	2
Sample 2	14	4	2
Sample 3	14	4	2
Sample 4	14	4	2
Sample 5	13	4	2

From *Table 4* and *Figure 2.20*, it can be deduced that the first event that occurs when the blade is lowered onto the rebar is that it deforms. The rebar is “crushed” before it begins to shear, and the blade travels 6 mm before the rebar fractures.

Figure 2.20: 20 mm 500E Rebar fracture surface

2.5 Gearbox types

It can be assumed that shearing and bending rebar will require a high torque from the electric motor. However, finding a battery powered motor that produces a torque that can bend or shear rebar without the need for a gearbox would be unlikely. A battery-powered electric motor can only produce a limited amount of torque at high speed, thus, a gearbox would be required to increase the torque output and to produce a more reasonable operating output speed.

After selecting the motor, a gearbox was required to reduce the output speed and to magnify the torque output of the motor. The most common gearboxes that were found were worm and planetary gearboxes, with numerous manufacturers offering a variety of sizes, gear ratios, and torque capacities.

Worm gearboxes are quite simple; the gearbox consists of a worm gear and worm, (*Figure 2.21)*. It provides low-noise operation, it can accommodate a large reduction ratio, and it is relatively easy to maintain.

Figure 2.21: Cut away diagram of worm gearbox unit ('Worm Gearbox', 2014)

However, the worm gearboxes are not without their limitations. As the reduction ratio increases, so does the volume of the gearbox, making the gearbox unmanageable to hold, and the efficiency of the gearbox is comparatively low at higher reductions (300:1 efficiency roughly at 79%, and 5:1 efficiency is approximately 90%). The low efficiency is partly due to the increase in helix angle. As the helix angle increases, the contact area also increases between the worm, and the worm gear, which creates a higher amount of friction.

Planetary gearboxes are another commonly used gearbox. These gearboxes can accommodate large reduction ratios, they are smaller compared to worm gearboxes (at high reduction ratios), and have minimal noise during use. However, planetary gearboxes are significantly complex, *(Figure 2.22)*.

Figure 2.22: Single stage planetary gearbox cut-away (Rohloff, n.d.)

The efficiency of planetary gearboxes is higher than that of the worm gearbox, depending on the number of stages that gearbox has (97% efficiency at single stage 88% efficiency at third stage). According to Pinho Silva Dias da Costa (2015), efficiency depends on the number of mesh points between the sun and the ring gears, the friction in the bearings, the lubrication used, and the operating speed of the gearbox.

With higher reduction ratios, planetary gearboxes require implementation of additional stages (consisting of planet and sun gears as shown in *Figure 2.22*) to the existing stage. The standard number of stages found in commercially available planetary gearboxes are three. With extra stages added, the gearbox can become large, especially with high-torque output requirements.

Cycloidal gearboxes (also known as cycloidal drives) give high reductions with similar efficiencies of a planetary gearbox. According to Darali (2012), a cycloidal drive gearbox with a single stage is 93% efficient, and a two-stage 86% efficient). The cycloidal gearbox has the advantage of having more than two teeth engage with the ring gear at any given time (*Figure 2.24*), meaning that the gearbox has higher load capabilities. The cycloidal gearbox also allows for much higher reduction ratios than planetary and worm gearboxes without increasing its volume drastically; according to Sumitomo (2018), its reduction ratio ranges between "3:1 to 119:1 (single stage), 121:1 to 7569:1 (second stage) and 8041:1 to 658503:1 (third stage)". However cycloidal gearboxes have their disadvantages, for instance, they cannot be back-driven, and at high rotational velocities, vibration could become an issue due to the eccentric cycloidal discs.

Figure 2.23: Exploded diagram of cycloidal gearbox (Gorla, et al., 2008)

Figure 2.24: Anatomy of cycloidal gearbox ("Opinions on Cycloid gear", 2011)

With the advantages of high reduction ratios, high efficiency, compactness, and high load capacity; the cycloidal gearbox is the most suitable gearbox for this application. A further improvement has been made to the two-stage cycloidal gearbox, minimising the number moving of parts, and thus, reducing the overall weight of the gearbox. In a traditional two-stage cycloidal gearbox, four cycloidal discs would be required as shown in *Figure 2.25*, but in the new design, only two cycloidal discs are required (*Figure 2.26*). The main difference is that in a traditional cycloidal gearbox the output shaft is driven by the cycloidal discs, while in the new design, the roles have been changed. The second stage cycloidal disc now drives the second stage ring gear which is also the output shaft (*Figure 2.27* and *2.28*). The new two-stage cycloidal gearbox has “significantly fewer rollers than the one stage cycloidal speed reducer. Having fewer rollers could have substantial advantages in lowering the required stress (due an increase of the rollers’ diameter)” (Blagojevic, Marjanovic, Djordjevic, Stojanovic, and Disic, 2011).

Figure 2.25: The old design of a 2-stage cycloidal gearbox. (1) Input shaft, (2) First stage cycloidal disc, (3) First stage ring gear, (4) First stage output, (5) Input shaft of second stage, (6) Second stage cycloidal disc, (7) Second stage ring gear, (8) Second stage output (Blagojevic, Marjanovic, Djordjevic, Stojanovic, and Disic, 2011).

Figure 2.26: Anatomy of new two stage cycloidal drive. (1) Input shaft, (2) first stage cycloidal disc, (3) first stage ring gear, (4) central disc, (5) second stage cycloidal disc, (6) second stage ring gear (Blagojevic, Marjanovic, Djordjevic, Stojanovic, and Disic, 2011)

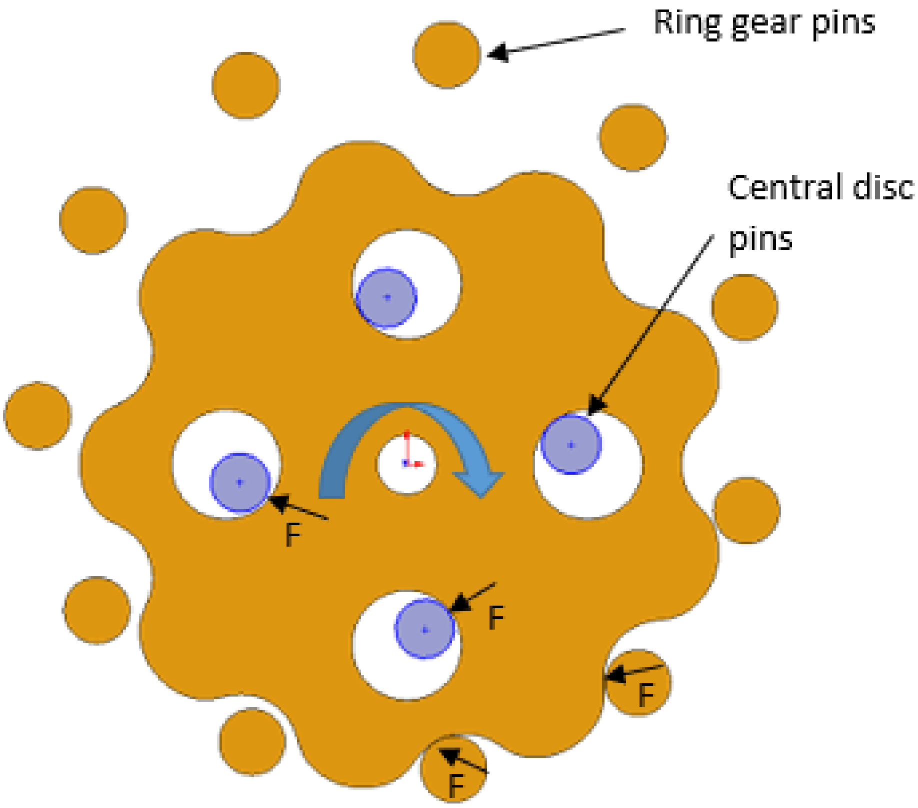

Figure 2.27: Force exerted on cycloidal disc tooth by ring gear. Which then exerts force onto the central disc pins. The cycloidal disc is rotating clockwise as indicated by the blue arrow

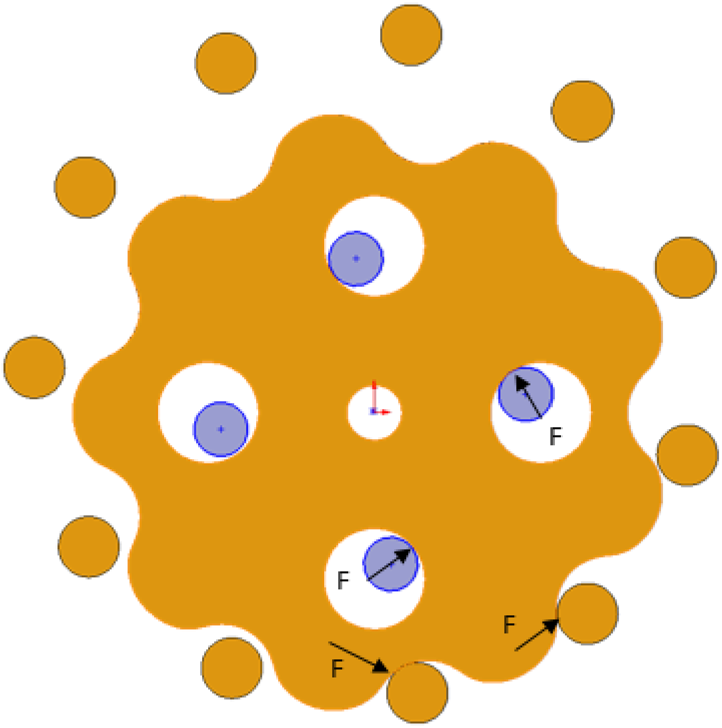

Figure 2.28: The central disc pins now drive the second stage cycloidal disc, which in turn drives the second stage ring gear

2.6 Electric Motors

The client has specified that the tool is to be powered by a cordless drill battery, restricting the design to a choice between a brush and brushless electric motors. As with any portable power tool, the aim is to try and minimise the tools' bulk and mass. From this reasoning, it was decided that a brushed "pancake" motor will be used. A pancake motor is considerably thinner than a conventional motor; however, the trade-off is that the diameter of the motor is quite large. A brushed electric motor does not require a motor controller (unlike a brushless motor) which simplifies the circuitry of the power tool.

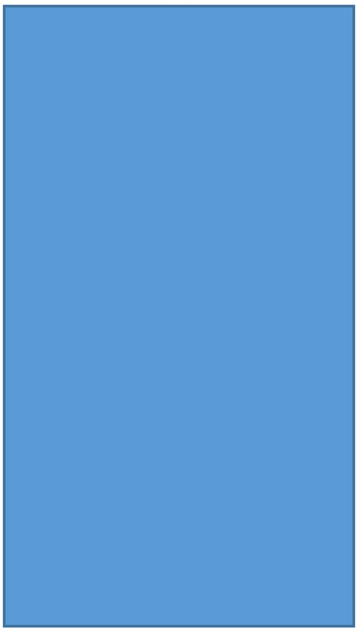

Figure 2.29: Brushed DC pancake motor ("Brushed Pancake Motors" ,2018)

2.7 Hydraulic Transmission

An alternative option to an electric motor and gearbox is a hydraulic transmission. A hydraulic transmission consists of an electric motor, reservoir, pump and actuator (*Figure 2.30*).

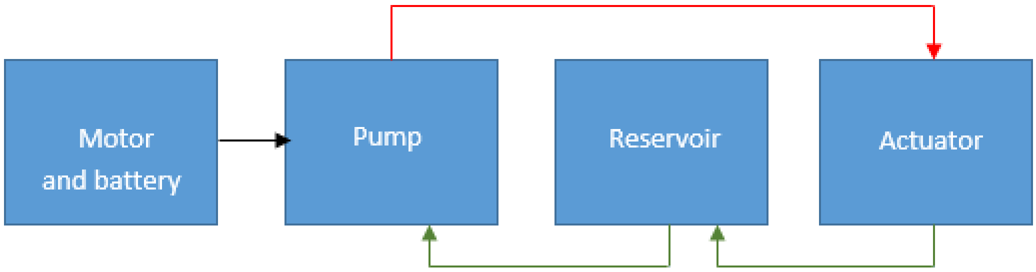

Figure 2.30: Hydraulic transmission schematic

The fundamental working principle is the electric motor pumping the fluid from the reservoir tank to the actuator. Linear and rotary hydraulic actuators are commonly available and come in a variety of different designs for different applications; in order to explain, a simplified schematic of both rotary and linear actuators will be used (*Figure 2.31* and *2.32*).

Figure 2.31: Single acting hydraulic actuator (Gonzalez, 2015)

The linear actuator comes in two forms, either it has a spring retraction or it has a fluid retraction. A linear actuator with two power strokes means that the hydraulic fluid is both used to extend and retract the piston rod. While the single-acting actuator only has hydraulic fluid pumped in on one side of the piston, it then relies on a return spring to retract the piston rod. The double-acting linear actuator would be useful only if there is loading on both the extension and retraction phase of the actuator. The rotary actuator works on a similar principle to the fluid return linear actuator (*Figure 2.32*).

Figure 2.32: Hydraulic rotary actuator (Hydraulic Actuators, 2005)

The hydraulic fluid is pumped into the actuator's chamber (indicated in red), the fluid then pushes the arm around its shaft. By pushing the arm around it also forces the unpressurised hydraulic fluid (indicated in blue) back into the reservoir tank. In order to reverse the motion of the actuator, the hydraulic fluid will need to be pumped into the fluid-out port.

2.8 End User Input

As part of the design process, input from the end users to assist in the design of this tool is most important. In order to obtain their opinions and experience, a questionnaire was sent out to construction companies across New Zealand. Before the questionnaires could be distributed an ethics approval was required, (AUT Ethics Committee Approval, AUTEC 17/259). This is to assure that the questionnaire would be fair and without bias as well as to make sure that the questionnaire would respect the culture and backgrounds of the people who were to answer them (*Appendices E* and *F*). From the feedback gathered, it was found that the weight/bulk of the tool is one of the main issues as the tool will be carried everywhere on site. The most common grade of rebar used is 500, and the diameters range between 10 mm – 40 mm, the most used angles are 45°, and 90° and the rebar are not cut or bent when embedded in concrete. Over 100 rebars will be bent a day, which, however, is entirely dependent on the size of the construction site. It can be assumed that this tool will be exposed to the harshest conditions of dust, mud, water, low maintenance, and heavy-duty wear and tear.

Observing construction workers bending rebar using the linear bending method, showed that it had a major drawback. As the rebar was being bent, the construction worker would bend down with the rebar (*Figure 2.33*); this will be a problem if space is limited and the bend angle is 90° or greater. It also poses an ergonomic issue as the user would have to kneel at an unfavourable angle to remove the bender once the desired angle is achieved. Gripping the tool while in use is also inconvenient, although the user would not have to bear the weight of the tool. They too would have to move with the tool as it bends in-order to operate it. However, according to W. Rowlands (personal communication, 29 January 2017), from the Ministry of Business, Innovation, and Employment, bending rebar partially embedded in concrete is generally not allowed unless an engineer approves. The rebar being bent in this case should be far enough away from the concrete to minimise the risk of damaging the concrete during the process.

It has been observed that each piece of rebar is first cut and bent to shape before being placed in its appropriate location in the foundations. Rebar is usually bent and cut on the ground, but it must be noted that the people observed were using manual rebar benders and circular saws.

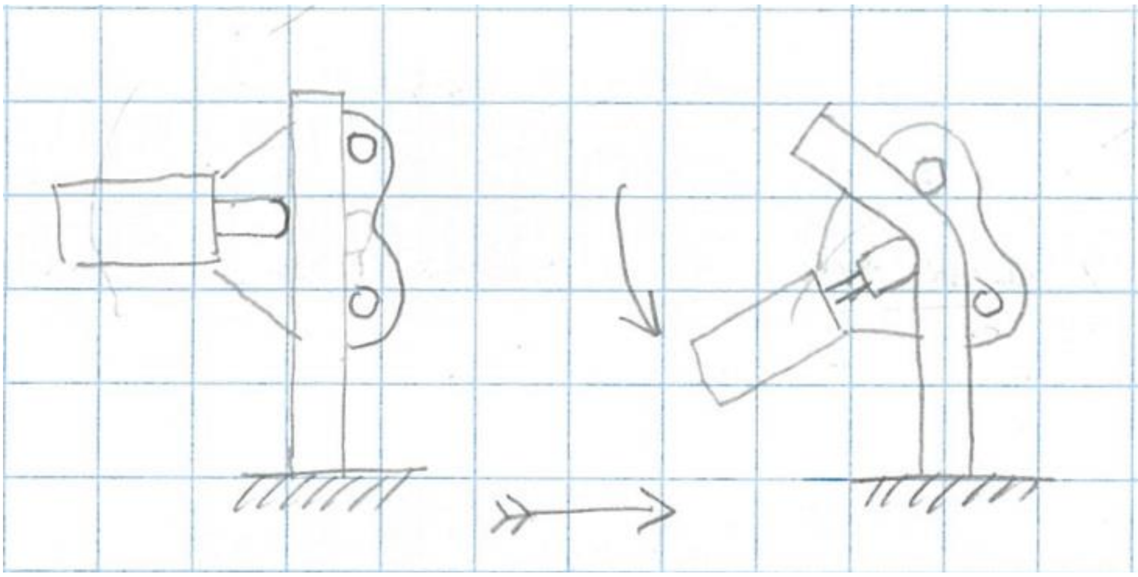

Figure 2.33: Linear rebar bending of partially embedded rebar

2.9 Research Conclusion

Conducting this research has defined what is needed regarding user interaction, what the New Zealand construction standards require, and the possible methods that metals can be shaped and cut. The research conducted in this chapter will be used in the conceptual design generation, concept development, and the first principles analysis.

3 Design Concepts and Evaluation

Utilising the research obtained in *Chapter* 2, this section contains ten possible conceptual designs that rebar can be cut and bent. These ten conceptual designs will then be evaluated against the client specifications, the end user experience (ease of cutting and bending), safety, cost of consumable parts, and the predicted complexity of the internal mechanism. The scores will be between 1 and 5; with 1 being undesirable, and 5 is desirable. The chosen conceptual design will then be further developed in the following chapter. The concepts will be grouped into five categories based on their cutting/shearing and bending combinations.

3.1 Category 1: Rotational Cutting and Linear Bending

3.1.1 Concept 1.1

Concept 1.1 (*Figure 3.1*) employs the linear method of bending. The method of cutting employs the use of a cutting disc, similar to that of a 3-inch hand-held grinder. It was realised that the sparks generated from the grinding disc could pose a fire hazard and that the construction site would have to lodge an application with OSH (Operational Safety and Health) for the power tool to be used. However, spark-less cutting discs are available for purchase from the United States. From the feedback gained from the questionnaires, using a cutting disc on rebar would be slow, but it would provide a finish that is flush with the surface. For this concept, the rebar will have to be secured or held down during cutting.

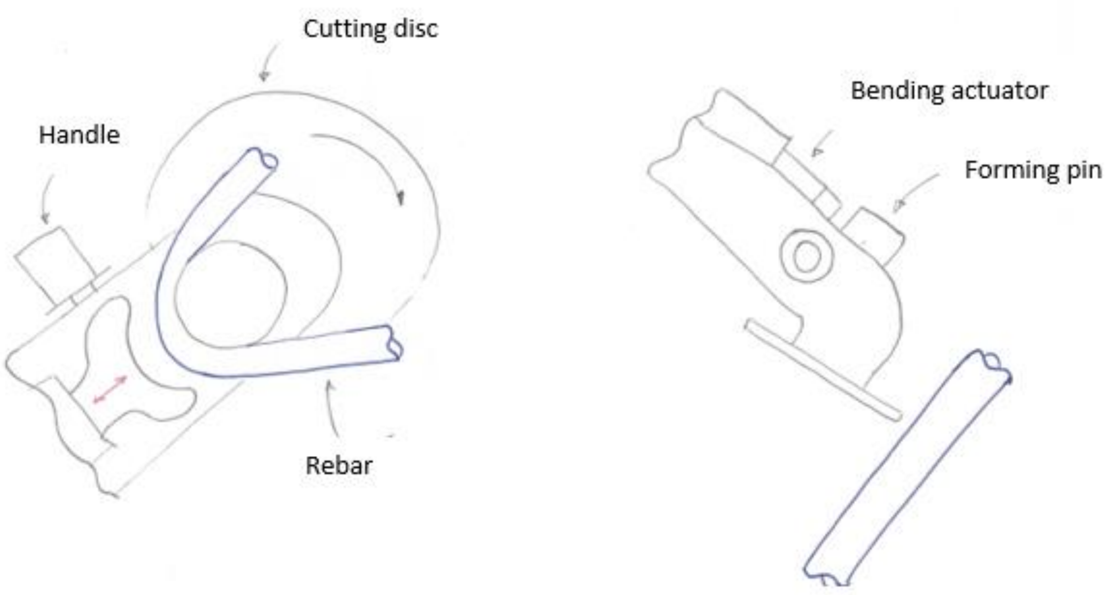

Figure 3.1: Concept 1.1

3.1.2 Concept 1.2

Rebar cutting is achieved by a spark-less cutting disc which gradually moves down at a set speed. Rebar bent by this concept is best suited being operated on the ground. However, it is possible to bend rebar that has been partially embedded in concrete but will be some difficulty in operating the tool, as outlined in *Section 2.8*. Cutting partially embedded rebar would be best suited for this concept; otherwise, the rebar will have to be held with one hand to stop it from moving.

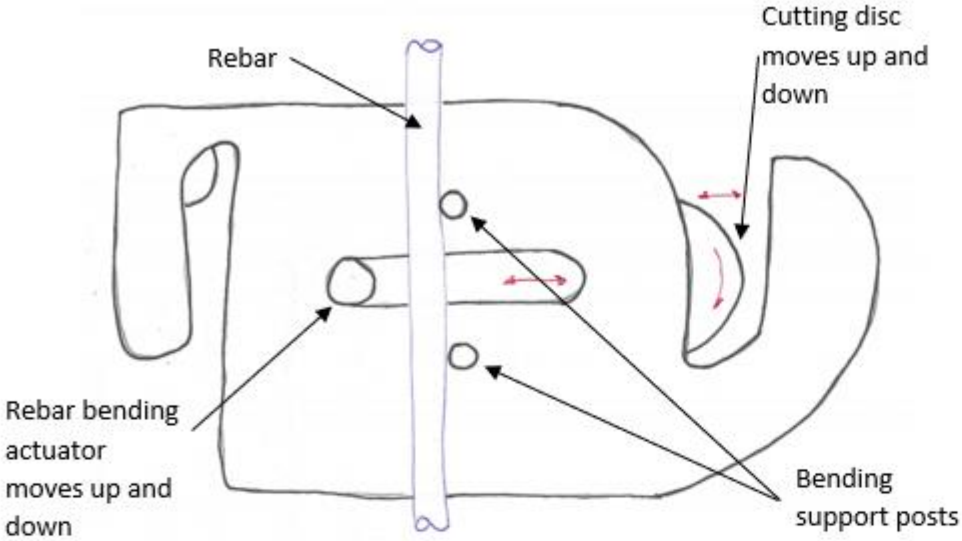

Figure 3.2: Concept 1.2

3.1.3 Evaluation of Category 1

Table 5: Category 1 evaluation table

Concept	Safety	Ease of Cutting	Ease of Bending	Cost of Consumables	Total
1.1	3	2	4	5	12
1.2	4	3	3	5	14

Concept 1.2 was ranked as the better concept from the two in this category. The bending function on both tools are on different planes to the cutting function which mitigates the risk of accidentally cutting rebar or vice versa.

Concept 1.1 provides a handle that allows rebar in different orientations to be bent more comfortably compared to Concept 1.2; therefore, a score of 4 was awarded to Concept 1.1 in terms of ease of bending. Regarding running costs, both concepts use a disposable cutting disc, so an equal score of 5 was awarded. However, cutting both loose and embedded rebar on Concept 1.2 is easier than on Concept 1.1; as Concept 1.2 has a jaw to keep the rebar in place. Due to the protective jaw on Concept 1.2, a higher safety score of 4 was given compared to Concept 1.1. The jaw provides a guard in front of the cutting disc, which mitigates the possible risk of injury to the end user’s hands and other body parts.

3.2 Category 2: Saw Cutting and Rotary Bending

3.2.1 Concept 2.1

Concept 2.1 (*Figure 3.3*) cuts rebar via an oscillating blade. This method of cutting is suitable for cutting through metals, wood, tiles, ceramics, and plastics, and is found on small hand-held power-tools, used for small jobs around the home, so its effectiveness is unproven in an industrial environment. The primary concern of this method is the amount of time it takes to cut through a 20 mm rebar and the vibration of the tool. The vibration of the tool could cause discomfort to the user with prolonged use. Unlike a circular blade or a grinding disc, the oscillating blades do not produce any sparks when cutting metallic materials.

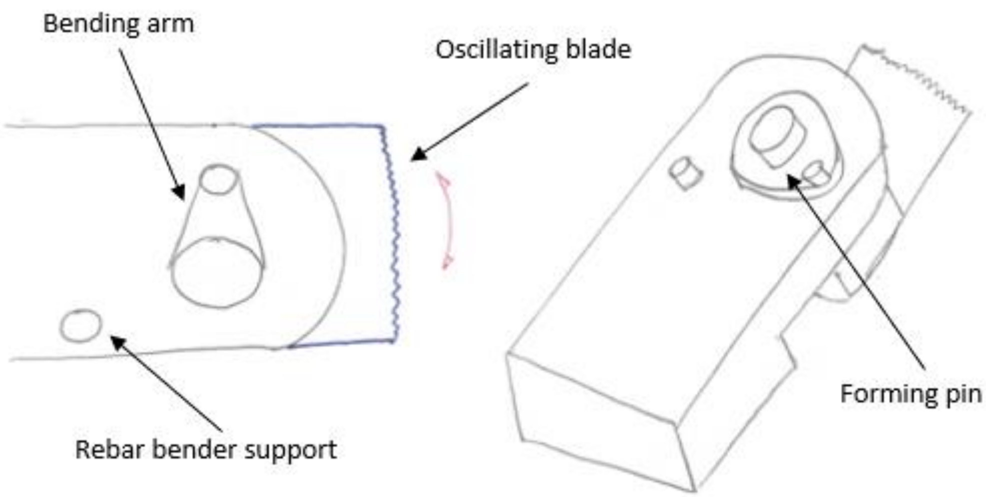

Figure 3.3: Concept 2.1

3.2.2 Concept 2.2

Concept 2.2's method for cutting rebar is similar to the method used on a jig-saw (*Figure 3.4*). This concept is designed so that the rebar is cut on the ground with the user pushing down on the handle. As pressure is exerted on the handle, the oscillating blade moves down and cuts through the rebar. This concept eliminates the user from having to carry the power tool while operating it. However, the drawback is that the rebar can only be cut while it is not set in concrete or in a horizontal position. Bending is performed by standard radial bending and does not require any actuation of the handle to operate the bending function. The bending function is operated by a toggle switch on the side of the tool.

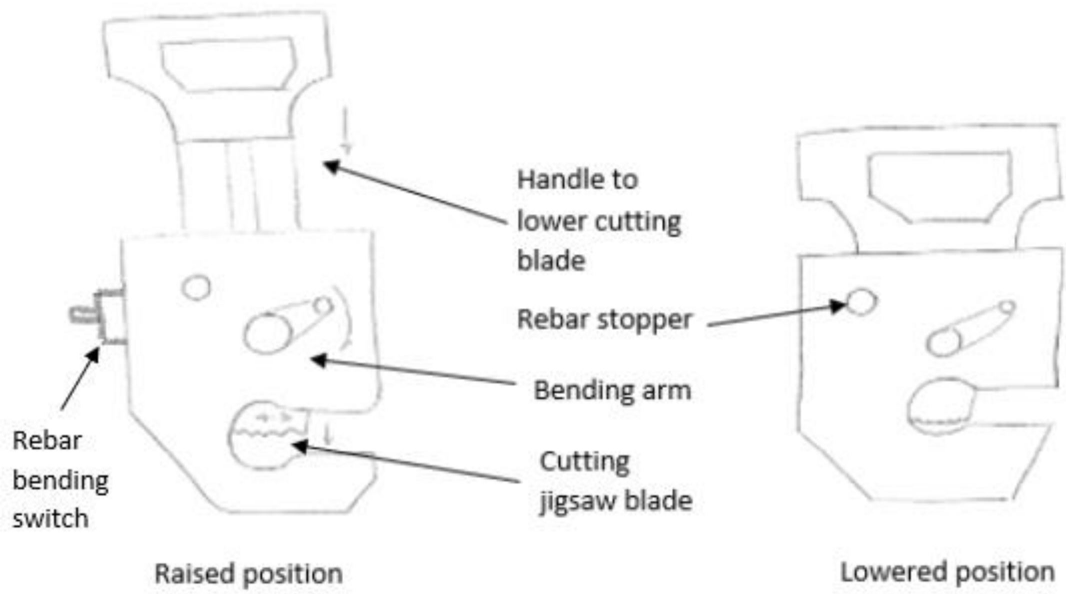

Figure 3.4: Concept 2.2

3.2.4 Evaluation of Category 2

Table 6: Evaluation of category 2

Concept	Safety	Ease of Cutting	Ease of Bending	Cost of Consumables	Total
2.1	5	2	5	2	14
2.2	3	3	5	4	15

Concept 2.2 has been ranked as the better concept from the two concepts in category 2. Concept 2.1 uses a high-speed oscillating blade (faster than that of a jigsaw blade) that could cause discomfort from prolonged use compared to Concept 2.2 due to its vibration a score of 2 was awarded in the ease of cutting category. Concept 2.2 was awarded a score of 3 in the same category, with an oscillating jigsaw blade, as it also poses a vibration problem. However, Concept 2.2 allows the user to cut loose rebar greater accurately; as the blade is pressed down on the rebar it would also hold it in place.

Concept 2.1 is far safer compared to Concept 2.2; this is because the oscillating blade on this tool is designed not to penetrate skin if accidental contact is made, thus receiving a score of 5 regarding safety.

Both conceptual designs share the rotary method of bending, and both are not on the same plane as the cutting function. Therefore, both concepts have an equal score of 5.

However, the most significant factor between the two concepts is the cost of a replacement blade, according to Mitre 10 (2018) the oscillating blade costs in the region of 70 New Zealand Dollars (NZD), compared to the standard jigsaw blade roughly 3 NZD per blade.

3.3 Category 3: Linear Shear and Linear Bending

3.3.1 Concept 3.1

Concept 3.1 (*Figure 3.5*) uses the method of linear bending. Here the bending pin can be altered for different minimum bend diameters. The shearing mechanism is linked to the bending mechanism for simplicity, and weight saving measures; however, this would mean that the shearing blades would operate whenever the user is bending rebar.

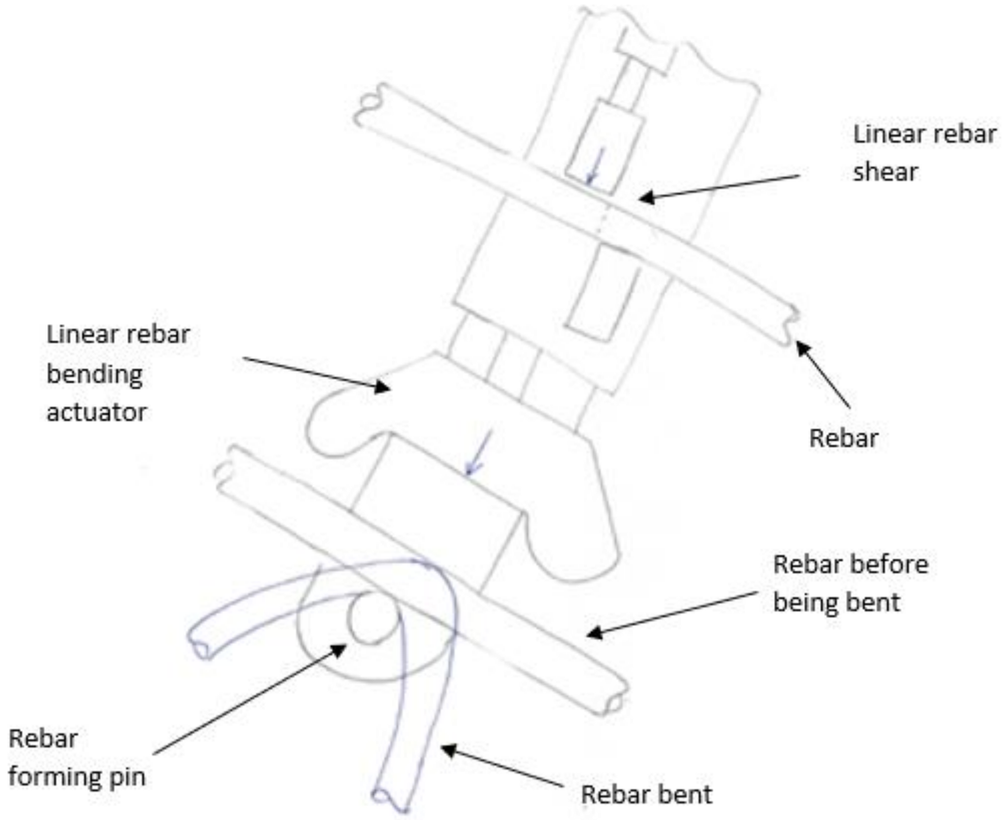

Figure 3.5: Concept 3.1

This linear method of bending could pose a problem; if the bar is set in concrete and bent in situ, it would mean that the power tool would bend with the bar (*Figure 3.5*). This method of bending would make the tool more inconvenient and tiresome to handle, especially if a significant number of rebars is to be bent.

3.3.2 Concept 3.2

This concept explores the possibility of combining the linear method of bending with rebar shearing. For shearing to be achieved by the bending ram and the forming pin would need to be exchanged with a shearing blade. However, the limitations of linear bending have already been highlighted in *Section 2.5.1*.

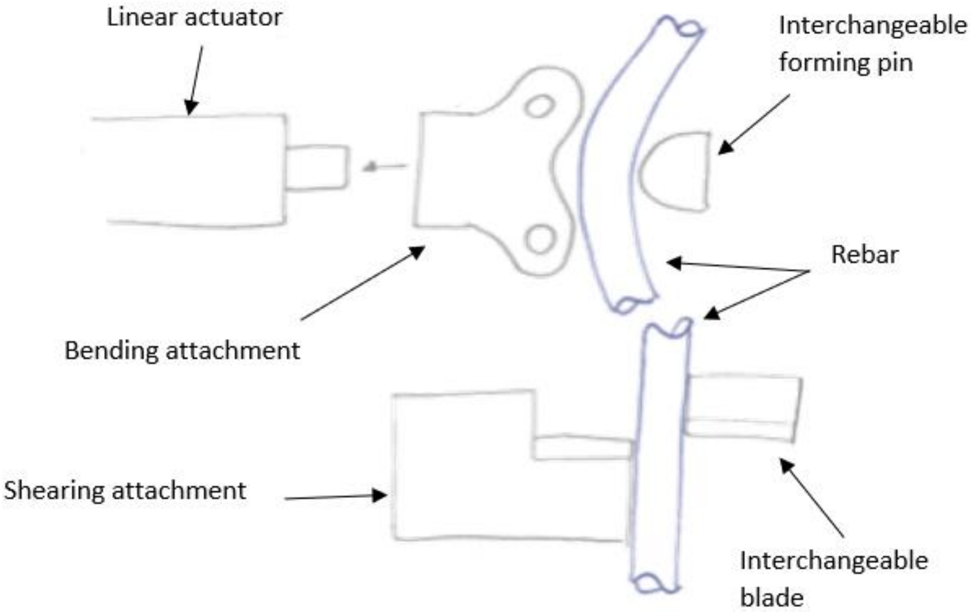

Figure 3.6: Concept 3.2

3.3.4 Evaluation of Category 3

Table 7: Evaluation of category 3

Concept	Safety	Ease of Cutting	Ease of Bending	Cost of Consumables	Total
3.1	3	3	3	5	14
3.2	4	2	2	5	13

Concept 3.1 has the highest rank score of the two concepts in category 3. Regarding the scores for ease of cutting and bending, concept 3.1 scored higher (a score of 3 was awarded in both categories) due to their lack of loose attachments compared to Concept 3.2; allowing the user to switch between bending and shearing with the least disruption.

Concept 3.2 was given a score of 4 in terms of safety; the high score is due to the concept's ability to remove the blade attachment when the tool is not in use. Concepts 3.1 was awarded a score of 3 due to the blades being constantly exposed. Both concepts scored the same in terms of cost as they all have the same shearing blades.

3.4 Category 4: Rotational Shearing and Rotary Bending

3.4.1 Concept 4.1

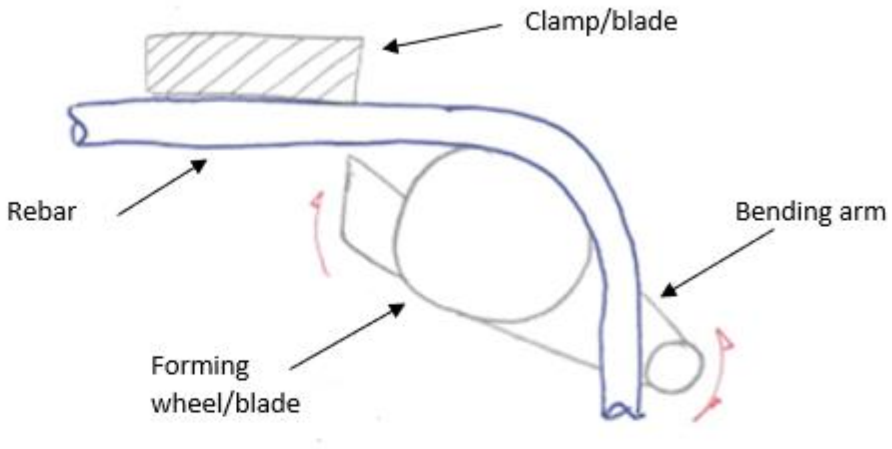

Figure 3.7: Concept 4.1

Concept 4.1, (*Figure 3.7*), eliminates the need to remove or exchange parts in-order for shearing to be performed. The forming wheel and the bending arm will have the ability to move independently of each other. The forming wheel has an attached blade which rotates to shear the rebar. The clamps holding the rebar in place for bending will also act as shearing blades. When the user wishes to shear the rebar, the forming wheel will rotate in a clockwise direction and shear the rebar.

3.4.2 Concept 4.2

Concept 4.2 uses the same radial method of bending as the previous concept. In this concept, however, the bending arm that also acts as a shearing blade. The rebar is placed in the slot (*Figure 3.8*), and the arm rotates around and forces the rebar up against the end of the slot. For different rebar diameters, the forming wheel will have to be removed and changed with the minimum bending diameter that corresponds with the rebar diameter.

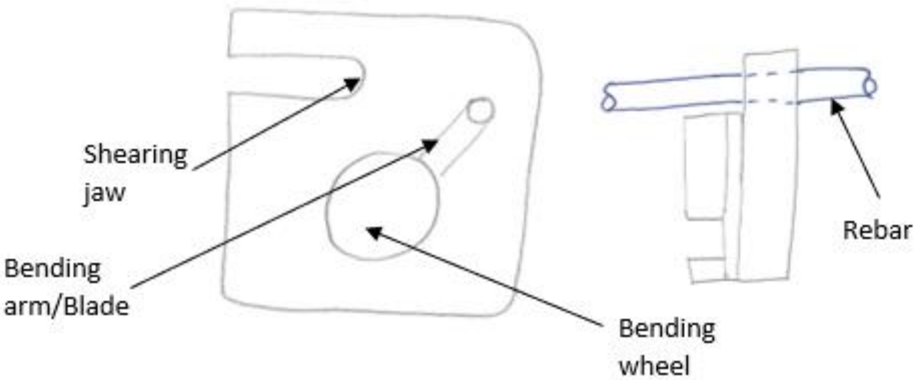

Figure 3.8: Concept 4.2

3.4.5 Evaluation of Category 4

Table 8: Evaluation of category 4

Concept	Safety	Ease of shearing	Ease of Bending	Cost of Consumables	Total
4.1	3	2	3	2	10
4.2	3	5	5	2	13

From the two concepts in category 4, Concept 4.3 is the highest ranked concept. Concept 4.3 separates the shearing and bending functions, mitigating the risk of an accidental bend or shear of the rebar, or vice versa. Therefore, it scores higher than Concept 4.2 regarding ease of shearing and bending; where both shearing, and bending is done in the same plane. The shearing function of Concept 4.2 is only awarded a score of 2; as feeding the rebar into the tool would be cumbersome.

Concept 4.2 also presents a complex mechanism, as the forming wheel (also acting as the blade) shares the same shaft as the bending arm. The mechanism would be complicated as both these components move independently of each other. Both concepts were scored low (a score of 2 each) in terms of cost due to the need of custom-made blades.

Regarding the safety of the two concepts, both have scored the same as the bending and shearing functions of both these concepts are exposed providing an equal amount of risk for injury to the end user.

3.5 Category 5: Rotational Shearing and Rotary Bending

3.5.1 Concept 5.1

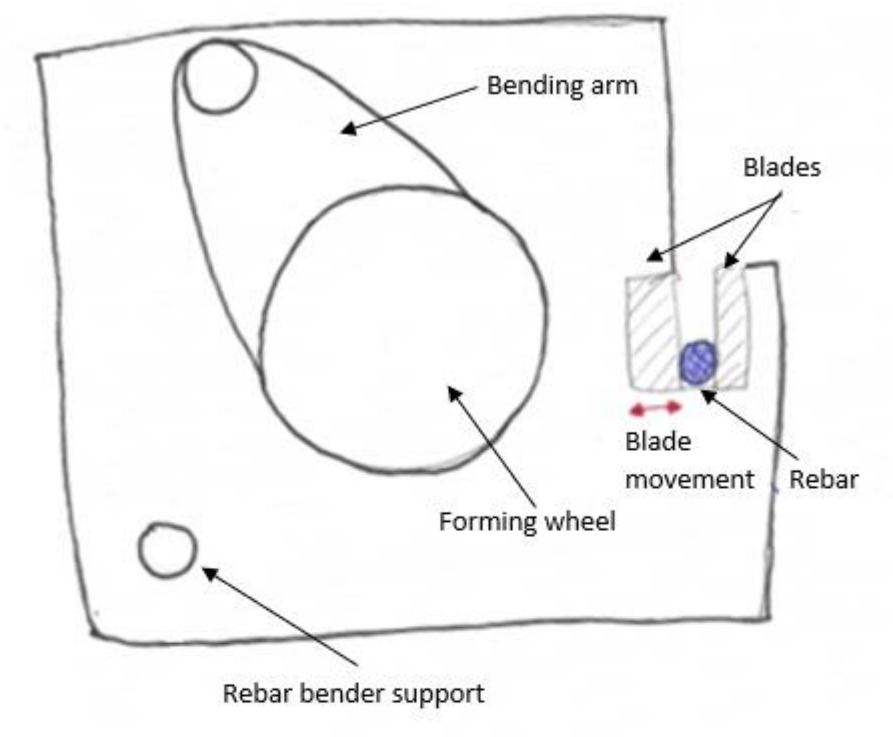

Figure 3.9: Concept 5.1

Concept 5.1 (*Figure 3.9*), does not combine the shearing and bending functions, this allows that rebar to be bent and sheared in a different plane. This layout reduces the risk of the user accidentally shearing the rebar when it needs to be bent and vice versa. However, the downfall of the concept is that it may require two separate mechanisms for bending and shearing, although such mechanisms would be simple.

3.5.2 Concept 5.2

The rebar is placed between the two bending pins and is guided by the two support pins that are fixed to the body. The two bending pins are fixed on a turntable, as the turntable turns the rebar is bent. For the minimum bend diameter to be met, the bending pin that forms the diameter on the rebar can be changed when required. Shearing is performed by one of the bending pins that doubles as a cutter. The rebar is placed in the jaw of the bending pin, and when the jaw moves down into the turntable, the rebar is cut. However, this method will create two shearing planes on the rebar, meaning that an off-cut will become lodged in the jaw of the cutter. This could pose as a potential problem as the off-cut could jam the cutter.

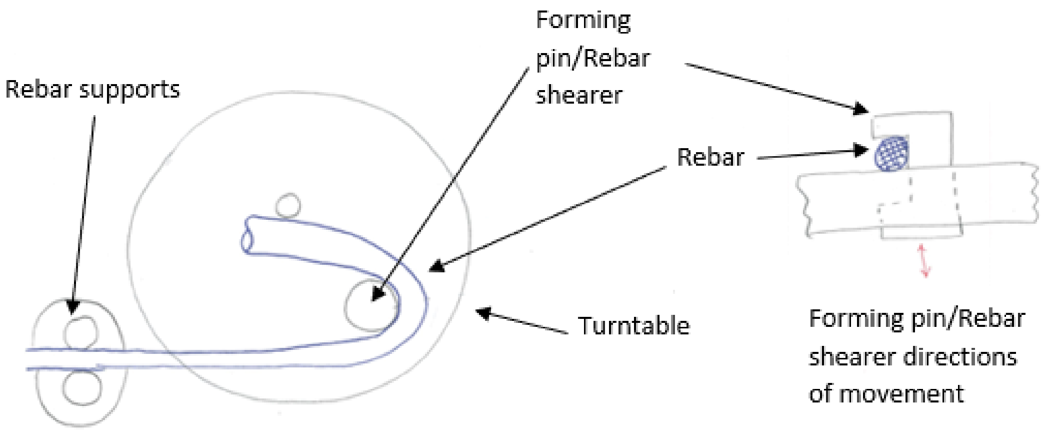

Figure 3.10: Concept 5.2

3.5.3 Category 5 Evaluation

Table 9 Evaluation of category 5

Concept	Safety	Ease of cutting	Ease of bending	Cost of consumables	Total
5.1	3	4	4	4	15
5.2	2	3	3	2	10

Concept 5.1 has achieved the highest score in category 5. From the user's perspective it is the easiest to use, and it has the least risk of accidently bending or shearing the rebar as these functions are in different planes. Therefore, a score of 4 was awarded for ease of bending and cutting. Regarding the safety of Concept 5.1, it was awarded a score of 3 as the cutting jaw is constantly exposed which increases the risk of injury. As for running costs of Concept 5.1, it was awarded a score of 4 as it uses shearing blades which are cheaper than other blades such as jigsaw blades, circular saw blades, etc.

Concept 5.2 combines the shearing and bending functions in the same single plane, which creates the risk of accidentally shearing the rebar when it needs to be bent (or vice versa). However, this configuration would allow rebar to cut and bent without re-orientating the rebar. Due to the risk of accidental bending or shearing, Concept 5.2 is awarded a score of 3 for ease of cutting and bending. In regard to safety, Concept 5.3 was awarded a score of 2, this is because the rebar is pulled into the tool during the bending process, which could cause injury to the user if their hands are in contact with the rebar. It would also mean that the tool will move during bending if the rebar was attached to a structure. Concept 5.2 also scored a 2 regarding cost of consumables, as custom blades would have to be manufactured.

3.6 Concept Evaluation

Each of the five concepts from the previous five categories will be evaluated based on the predicted complexity of the internal mechanism, and client specifications; specifically, regarding bending and cutting. The specifications are that the tool must be able to bend 20 mm rebar 180° in 15 seconds and cut rebar in 10 seconds. The concepts that can meet the client's specifications will receive a score of 5, if the concept is unable to, it will receive a score of 1. The predicted complexity of the mechanism is ranked between 1 to 5; 1 being complex, and 5 being simple.

It is expected that concepts that cut rebar using a cutting disc or sawing motion will require more than 10 seconds to cut compared to shearing. Bending will be judged on whether the concept is able to bend all rebar sizes 180° without prior adjustment to the tool. Linear rebar benders may not be able to achieve this, as the bend angle range would depend on the diameter of rebar, the travel of bending actuator and the width of the post on either side of the actuator. Therefore, not all rebar sizes would be able to be bent 180° with a linear bender.

Table 10: Concept evaluation table client specifications

Concept	**Bending rebar 180°**	**Cutting 20 mm rebar in 10 seconds**	**Complexity**	**Total**
1.2	1	1	2	4
2.2	5	1	2	8
3.1	1	5	5	11
4.2	5	5	3	13
5.1	5	5	5	15

Concept 5.1 meets the client's specifications and may provide the least complicated internal mechanism to drive the shearing and bending functions; therefore, it was given a score of 5 regarding complexity. Concept 3.1 is one of the simpler designs, using both a linear bend and a shear; both functions could be driven from the one actuator, but unfortunately it does not meet the client specifications of the bending rebar 180°.

The concepts that have a cutting disc (Concepts 1.2 and 2.2) will require a high-speed motor for the discs to cut through rebar. The disc also needs to be lowered and raised during cutting. As it is most favourable to have one electric motor, a mechanism will need to be designed to accommodate the movement of the blades and still maintain contact with the motor; therefore, both concepts scored a 2 regarding complexity. Both of these concepts only scored 1 in terms of cutting rebar in 10 seconds, as it is believed that a battery-powered tool will require more than 10 seconds to cut through the entire cross-section of a 20 mm rebar.

Concept 4.2 would most likely require a two-speed gearbox for bending to be performed safely and within the provided power output of the battery-operated motor (it is reasonable to assume that bending 20 mm rebar will require a significant amount of torque). Therefore, it was awarded a score of 3, as a two-speed gearbox would be complicated to design. It also means that there is a risk that the user will forget to switch to the appropriate speeds for either shearing or bending, which could damage the tool.

3.7 Conceptual Design Conclusion

From the ten conceptual designs evaluated in *Table 10*, Concept 5.1 is chosen. In this concept, the rebar is bent and sheared in two different locations on the tool mitigating the risk of accidentally bending when shearing is required (or vice versa). Having the bending and shearing functions separated would allow the bending and shearing functions to operate at their respective speeds without the need of two gearboxes or a two-speed gearbox. These speeds are necessary so that the power remains low enough for the tool to be battery-operated, as it is reasonable to assume that a large shear force and torque will be required to shear and bend 20 mm rebar.

This concept also uses the radial bending method which allows the user to estimate the bend angle of the rebar efficiently. Having a shearing blade, it will cost less to replace compared to grinding or circular saw blades options presents. With these characteristics, it was deemed to be the most suitable concept for further development.

4 Concept Development

From the previous chapter, Concept 5.1 was chosen for further development. This rebar bender and cutter will most certainly be over the mass of 1.4 kg (the ideal mass for single hand operation), and it may be difficult to handle due to the mass distribution of the tool. Therefore, the ergonomics of the bender and cutter must be considered and incorporated into the final design. However, this concept development is not limited to the ergonomics of the tool, but also the embodiment of the shearing, bending, the internal mechanism, and the method in which the mechanism will be driven will also be defined in this chapter.

4.1 Ergonomics

With the high loads that will be applied to this tool, it is foreseeable that the tool will require a significant amount of material and therefore would have a high mass. The weight of the rebar bender and cutter will require the tool to be operated on the ground, and the rebar will need to be brought to the tool to be trimmed or bent. As for moving the tool around the construction site, it will require the person to lift the tool from below the waist if the tool weighs around 25 kg (*Figure 4.1*); if the tool mass exceeds the 25 kg limit, it will require a two-person lift.

Figure 4.1: Lifting and lowering weights (Warren, 2016)

Two handles are located on each side of the tool (*Figure 4.2*). The diameter of the handles on the tool will need to be between 30-50 mm and a handle length “not less than 100 mm” (Hand Tool Ergonomics, 2018) is needed to provide adequate room for the hand. The material of the handle will need to be made of silicon to give the user a comfortable grip on the tool.

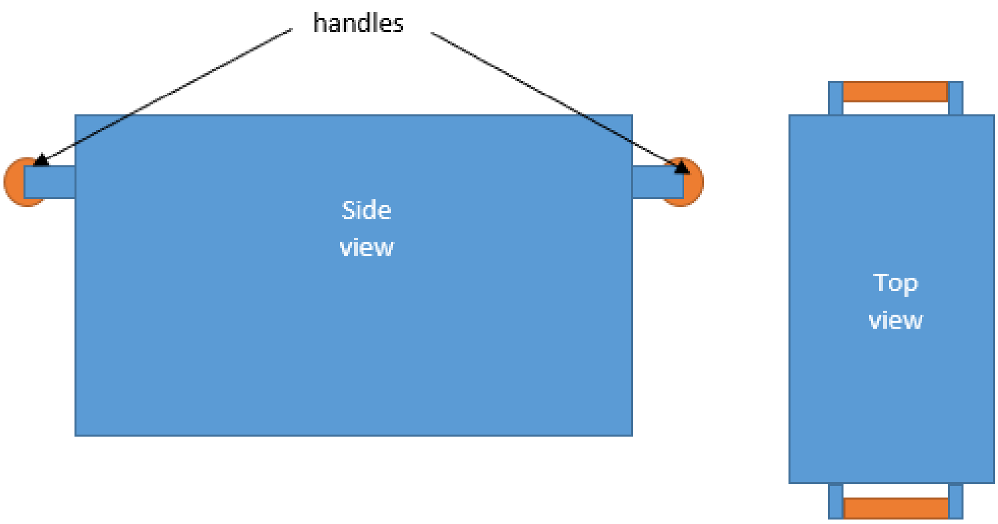

Figure 4.2: Schematic showing handles located on either side

The placement of the handles (*Figure 4.2*) will allow the bulk of the tool to be close to the person's body, which will allow the user to carry the tool with relative ease compared to having the handles mounted on the other two sides of the tool. The handles in this orientation will also allow the tool to be carried by two people without being too close to one another.

4.2 Hydraulics versus Mechanical

Before designing the internal mechanism and the layout of the rebar cutter and bender, a choice had to be made between using a mechanical or a hydraulic transmission. The advantages and disadvantages of each system were considered.

Hydraulic transmissions allow greater freedom in terms of functional design, as it does not require a mechanical pathway, unlike a gear-train where the mechanism dictates the location of the tool's functions. The system also has a higher efficiency compared to a geared transmission; however, this is only true if the geared transmission is complex and contains a large number of gears. The hydraulic transmission provides step-less speed control which would be useful when trying to bend accurately.

However, hydraulics does come with its limitations the first being the cost. A hydraulic power pack (electric motor, pump, control valves, and tank) would cost at least $1500 (Hyspecs, personal communication, January 3, 2018). A hydraulic power tool would require maintenance over time, but unlike a geared system, it requires some training. For instance, if the hydraulic oil requires changing, the system would need to be bled to remove air. According to Casey (2017), the main drawback with hydraulics is that the surrounding temperature and the temperature generated by the tool affects the performance. As the temperature rises, the viscosity of the oil will decrease, leading to a reduction in pressure. As the tool is most likely to cut several hundred pieces of rebar per day (depending on the size of the building), it will generate a lot of heat, meaning it would need a cool-down period. Waiting for the tool to cool down would mean that the efficiency of the site would decrease which, in turn, increases the running costs for the company.

The second option is a mechanical gearbox. Unlike a hydraulic system, the temperature does not affect its performance. Its efficiency, however, is dictated by the complexity of the mechanism. A mechanical system would suit applications where a constant speed is required. The maintenance of a gearbox is much simpler compared to a hydraulic transmission as it would only require greasing of moving parts. This maintenance could be performed anywhere unlike hydraulics, where it would require a controlled environment free of dust, dirt, and other contaminants. The only major drawback of using a gearbox would be its mass, depending on the size of the components, and number of parts.

Comparing the hydraulic transmission to a mechanical transmission, the gearbox would be the better choice as it is more reliable, easy to maintain, and able to work continuously regardless of the temperature. As for the tool's mass, the mechanical system may be similar to that of a hydraulic transmission. While speaking to one of the technicians at Hyspecs, a power pack would weigh roughly 10 kg, and an actuator would weigh between 10 – 14 kg (Hyspecs, personal communication, 3 January 2018). This estimate does not include the tool's housing or other components, but as the tool is dealing with an extremely high amount of force, it can be assumed that the components will be relatively heavy.

4.3 Bending Function

The tool will have one gear train, where a shearing mechanism will be driven off the bending transmission, which means that the two functions would operate simultaneously.

The internal mechanism determines both the bending arm and cutting jaw locations. As partially embedded rebar would most likely not be bent, and that most rebar is first cut to size then placed in position means that bending and cutting rebar would be performed on the ground.

As rebar is being bent on the ground, the location of the arm is not as critical; however, the rotary direction of the arm is essential. In order to avoid injury and inconvenience to the end user, the arm will rotate away from the user, thus bending the rebar away from the user's body. In order to switch between different minimum bending diameters, a screw will need to be removed which will allow the user to change forming wheels. Each forming wheel has two diameters (*Figure 4.3*). The wheel will need to be flipped over to bend the rebar. Having two diameters per forming wheel minimises the number forming wheels that need to be carried or purchased.

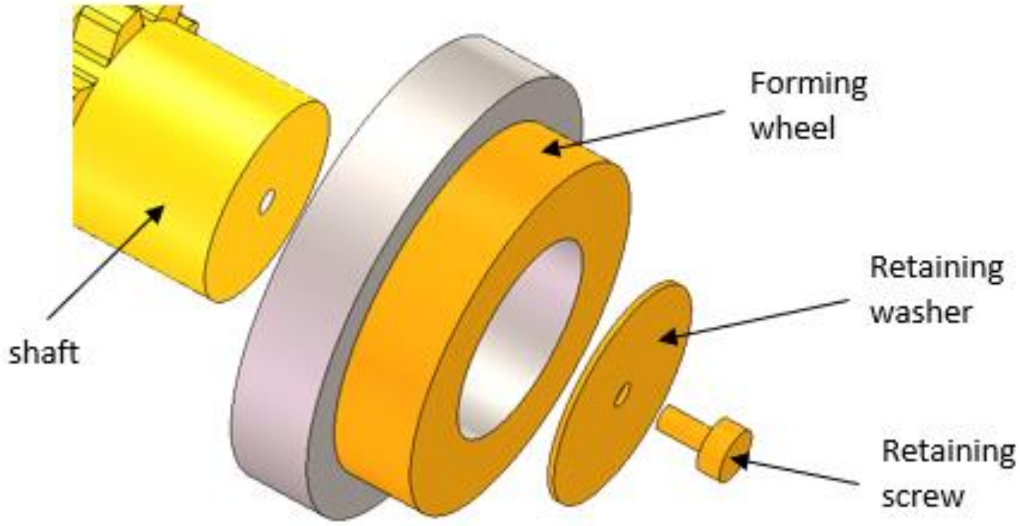

Figure 4.3: The forming wheel will be secured with the use of a thumb screw and washer

4.4 Shearing Mechanism

Several different ideas for driving the cutter were generated. The first idea (*Figure 4.4*) was to use a cam (driven by the same shaft that drives the bending arm) to shear the rebar. It was thought that the mechanical advantage of that the cam might be enough so that a secondary gearbox would not be required, but the frictional forces due to the rubbing between the cam blade and the rebar proved to be too high. Due to the high frictional force and the resulting additional torque required, this idea was also dismissed.

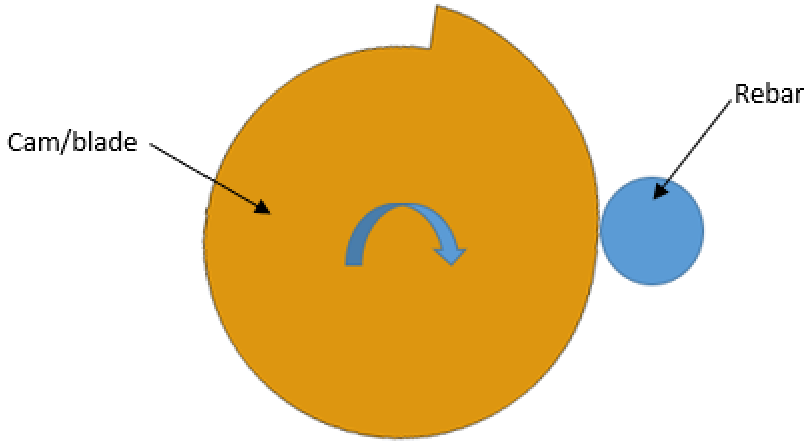

Figure 4.4: Cam used as shearing blade, the blue circle represents the rebar

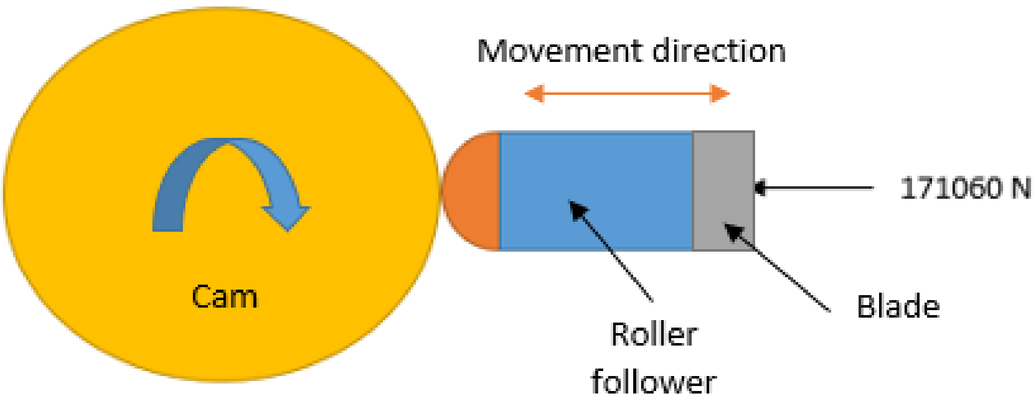

Figure 4.5: Cam and follower system for shearing rebar

The second idea was to use a cam and roller follower system (*Figure 4.5*); the cam would be driven off the same shaft that drives the bending arm, and the roller follower would be used to shear the rebar. However, it was found that the contact stress between the roller and the cam was much too high. The third idea was to use a crank and slider system, but this also proved to be impractical as the torque requirement was too high. The fourth and final idea was to combine the cam and follower idea with a linkage system of the crank and slider mechanism (*Figure 4.6*); this would reduce the amount of force acting on the cam, it would allow the rebar to be sheared without the need of a second gearbox, and it would maintain a relatively low torque requirement from the gearbox.

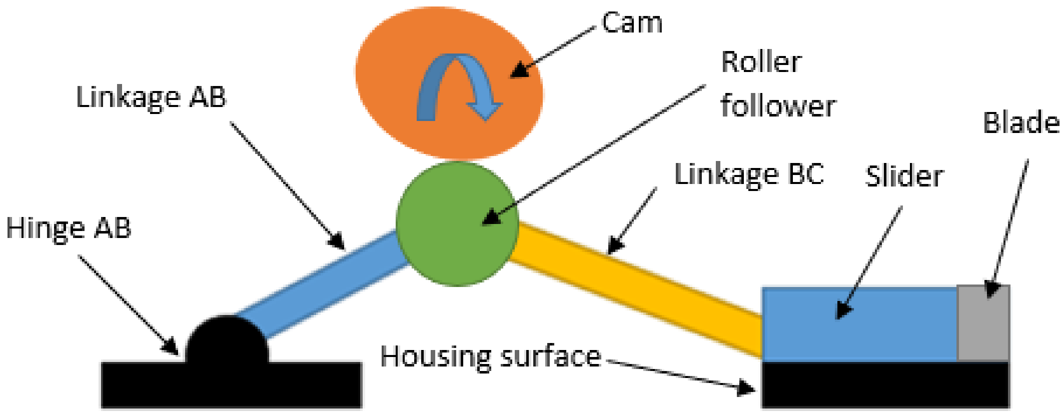

Figure 4.6: Combination of linkage system with cam and follower system

The final layout and shape of the tool is determined by knowing the locations of the handles, the power source, the motor type and, the mechanism defined for both shearing and bending (*Figure 4.7*). The shape of the housing is based on the geometry of the internal mechanism, user interaction, and the method in which rebar is bent and sheared. A box-shaped housing will also allow the tool to have better stability when rebar is being bent or sheared.

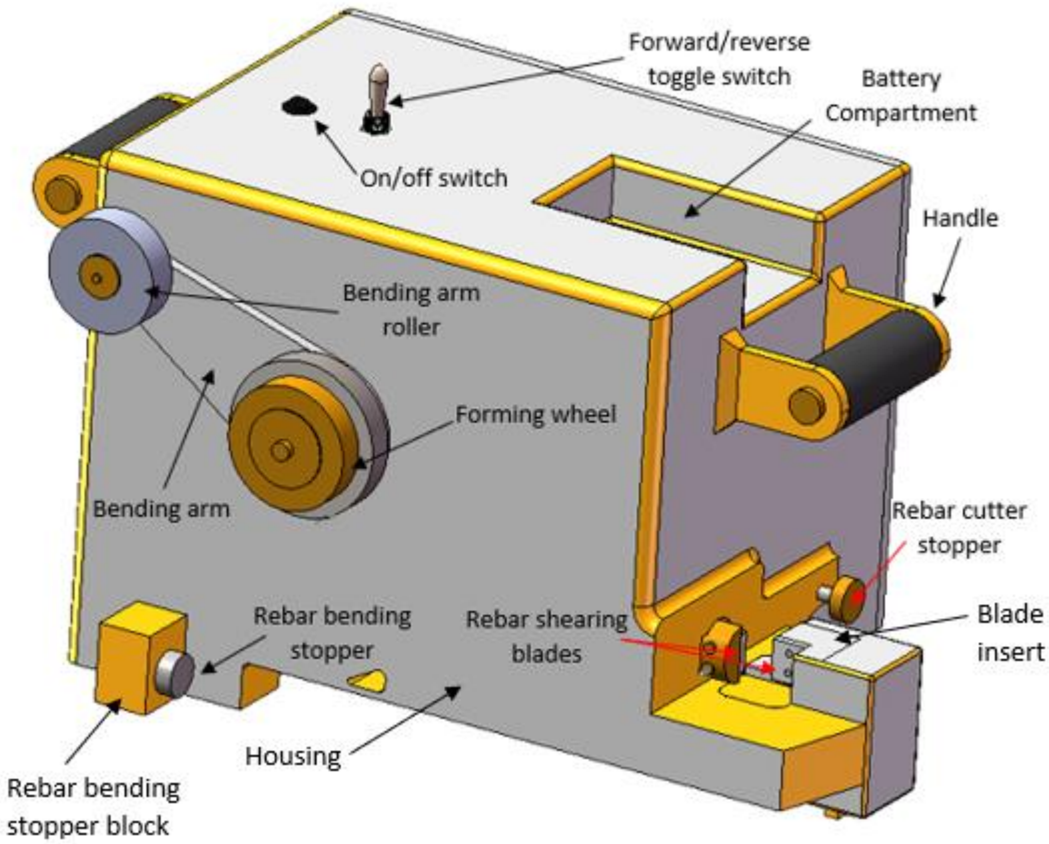

Figure 4.7: Layout of prototype rebar cutter and bender

4.5 Development Conclusion

This development phase has concluded the shearing mechanism will be driven from the same transmission as the bending arm. It was also decided that the tool will utilise a mechanical system as opposed to a hydraulic system due to the operating temperature limitations. With these decisions, the mechanism and the shape of the final design were developed. *Figures 4.8* and *4.9*, show the placement of the rebar during bending and shearing respectively. The shape and ergonomics of the tool will need to be further developed through a collaboration with a product designer in future work. The following chapter will focus on detailing the final design shown in *Figure 4.7*.

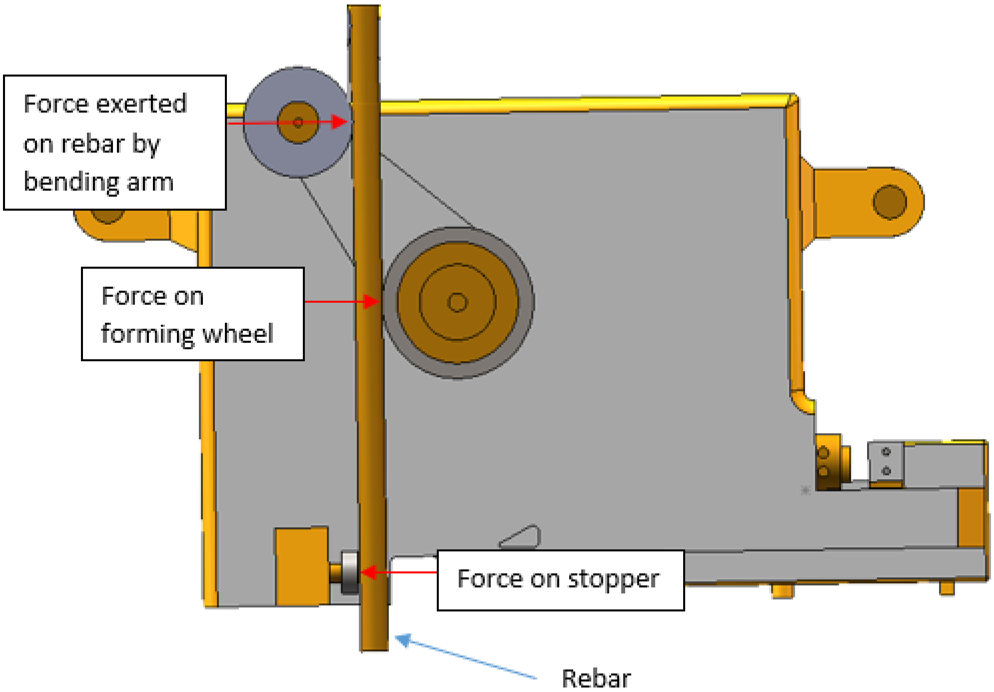

Figure 4.8: Tool bending rebar. Forces exerted on the rebar stopper, forming wheel and bending arm roller

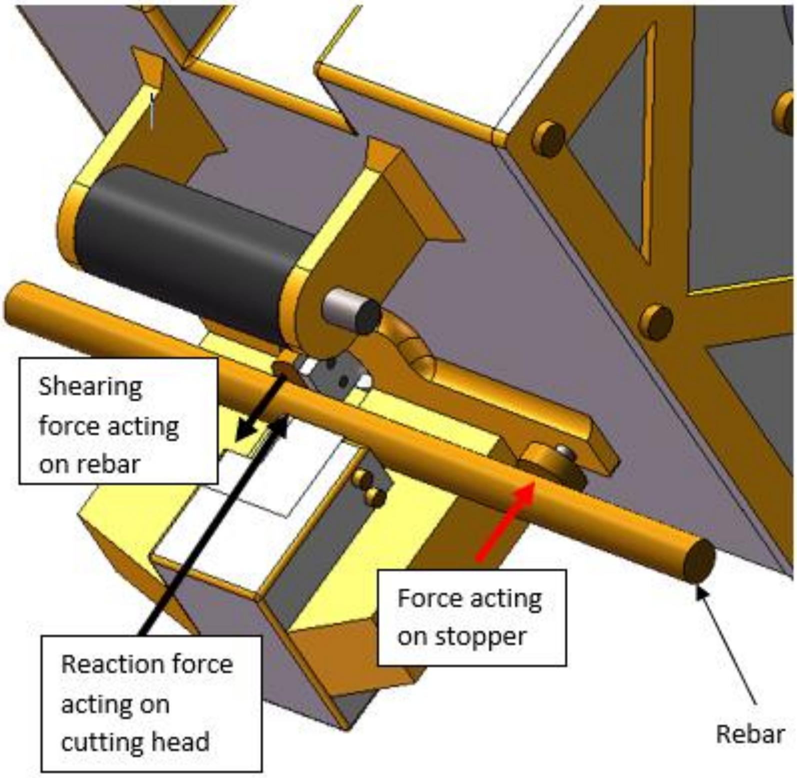

Figure 4.9: Rebar being sheared. Forces are acting on the slider blade, cutting head, and the stopper

5 First Principles Analysis

From *Chapter 4* a final design was developed in which the method of shearing and bending was defined as well as the mechanism that will be driving these functions. The analysis performed in this chapter will involve the simplification of the individual components to their basic shape to determine the average stress or force that it will experience. It will be assumed that forces will be evenly distributed or divided where appropriate. A Solidworks FEA will be used (in the following chapter) to determine the stresses, and the part will be modified accordingly if required. This section will only show the final iteration of the first principle calculations. This chapter will cover materials selection, the calculation of stresses and forces of the shearing mechanism, housing, and other transmission components.

5.1 Materials Selection

5.1.1 Shearing Mechanism and Bending Arm

The slider and linkages will need to be constructed of a material with a high yield stress, as that load would be transmitted throughout the shearing mechanism. Although most of the stress will be exerted on the blade, the slider, linkages, pins and bushings must be able to cope with any high stress resulting from the load. It was decided that D2 steel would be suitable for the slider, and linkages as it has a high yield stress of 1.86 GPa. The pins connecting the linkages will be made of L2 steel, and the bushings that cover the pins will be made of nickel aluminium bronze (C63000), as these materials can cope with high-stress applications.

Bending will most likely result in a much lower load compared to shearing. However, the bending arm would also be subjected to the harsh construction environment. With such a harsh environment this would mean that the material must be corrosion resistant. Stainless steel with its high its corrosion resistance, and along with its high strength capabilities, it would be most suitable; cast ASTM A747 stainless steel will be used to construct the bending arm.

5.1.2 Forming Wheel, Bending Arm Roller, Blade Insert, Cam and Follower

The forming wheel, bending arm roller, blade insert, cam, and follower (*Figures 4.8* and *5.1*) will most likely experience extremely high stresses. The rebar will be pressing against the forming wheel and the bending arm roller, in which only a small contact area will receive the force exerted by the rebar. The cam pressing down on the follower will have a similarly small contact area. The Hertzian stress calculation which was performed in order to determine the stresses these four components will experience, which assisted in selecting a suitable material (see *Sections 5.2.1*, *5.2.2* and *5.4.4*). After calculating the stresses, ASSAB PM30 SuperClean steel was chosen for its high yield stress (3.5 GPa compressive stress). This steel is used in the manufacturing industry for forming operations.

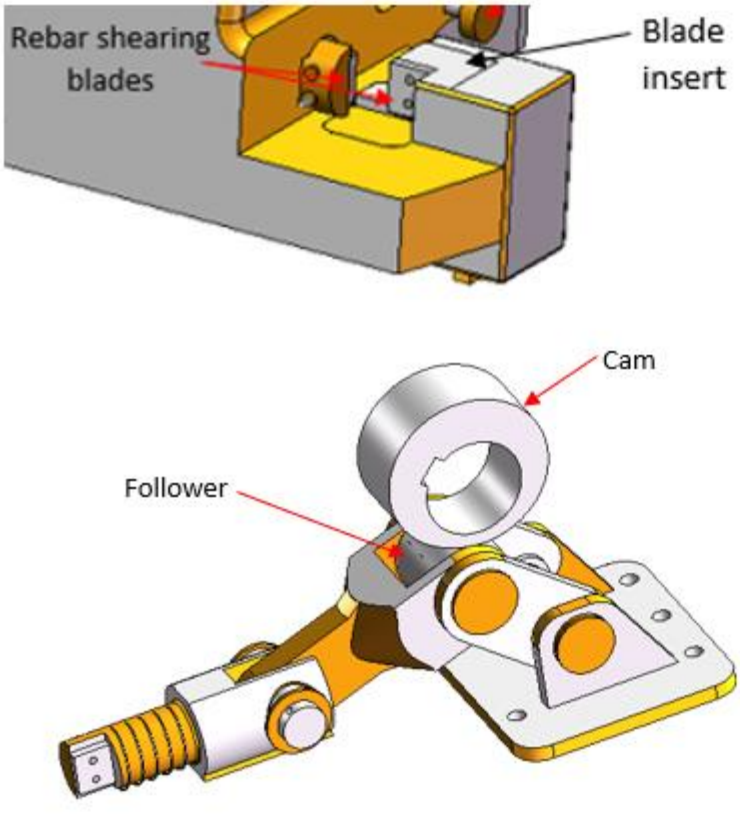

Figure 5.1: Materials selection for cam, follower, and blade insert

5.1.3 1024:1 Gearbox Components

The materials for the cycloidal discs were chosen with the knowledge that there will be contact stress loading from the central disc pins and the pin holes on the cycloidal disc. As the contact stresses will only have a small area of contact between the two parts, it was anticipated that a material with a high yield stress would be required. The steel for the cycloidal discs will be AISI 4142 as it has a higher yield stress when heat-treated compared to AISI 4140. The central disc steel will be AISI 4140 steel (which can also be heat-treated to different grades in order to obtain better mechanical properties), and a high yield stress bushing material will be used for the pins of the central disc (copper beryllium

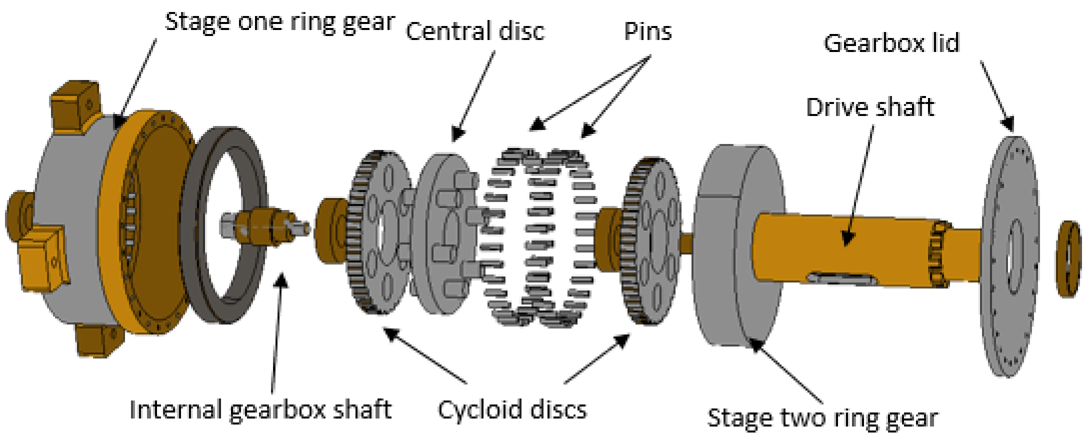

Figure 5.2: Gearbox components

The stage one ring gear, which also acts as the body of the gearbox, will be constructed of aluminium alloy 5056-H18. As most of the other components of the gearbox are made of high strength steel, the body and also the stage one ring gear will be made of this aluminium alloy to save weight.

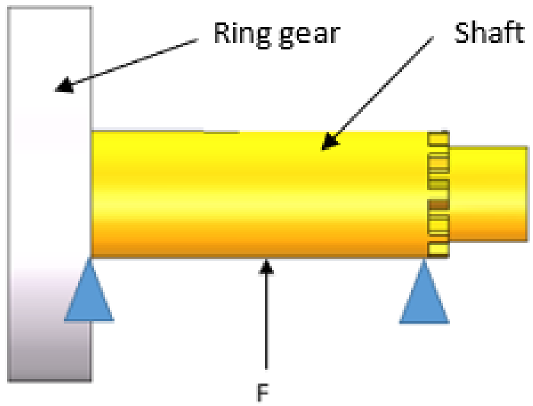

Figure 5.3: Schematic of force acting on second stage ring gear

The second stage ring gear (which is also the output shaft) drives the bending arm and will experience a high force exerted from the shearing mechanism (*Figure 5.3*). With the anticipated torque to bend and cut the rebar, an aluminium output shaft would be large, and a coupling device (connecting the output shaft from the gearbox to the main shaft) that could withstand both the torque from bending and the force from shearing would most likely require a significant amount of space and other components. It would be much simpler to have the second stage ring gear and the main shaft cast or machined as a single part. 6580 alloy steel will be used for this part, as it has a high yield stress, and is used in shaft applications.

The materials to be used for the pins (mounted on the ring gears to act as teeth) will be L2 steel (also known as silver steel). L2 steel was chosen as it has excellent wear resistance and high strength and hardness, which is required of the gear teeth. L2 steel can also be heat-treated to improve its mechanical properties if required.

The material for the internal shaft of the gearbox was more difficult to select, as the shaft is not driving anything (the central disc and two cycloidal discs spin freely). The shaft would only act as a support and to move the cycloidal discs around the ring gear. As the shaft will have high loads and torque applied from the cycloidal discs and motor; it was decided to use 6580 alloy steel (the same material as the second stage ring gear) as it is used in shafts and has a high yield stress (the occurring yield stresses will depend on the diameter).

5.1.4 Housing

The housing (*Figure 4.7*) being the largest of all the components, will require the material to be as light-weight as possible. The housing also experiences a large amount of stress, meaning that the material will also have to have high strength. Using the CES program and the material indices for a flat plate, a graph relating yield stress and density was drawn (*Figure 5.4*). From *Figure 5.4* it can be seen that magnesium alloys have similar yield stress to aluminium alloys but with inherently lower density. Knowing that the case will be subjected to the loads from shearing and bending 20 mm thick rebar, EA65RS-T4 magnesium alloy was selected as it has the highest yield stress that could be sourced. Magnesium alloys can be cast using sand casting, which means that the housing will be more rigid compared to a housing made up of multiple components. The magnesium alloy will need to undergo galvanic anodising in-order to improve its corrosion resistance which is essential as it will be operated in a rather harsh construction site environment, with a high possibility of water exposure from external sources such as rain.

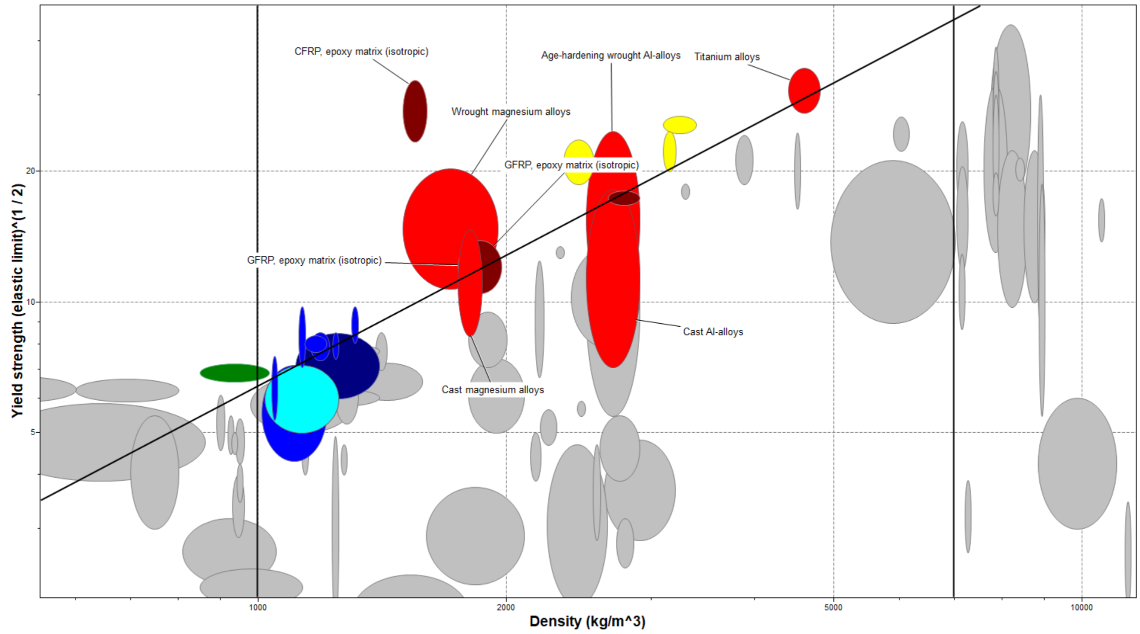

Figure 5.4: CES EDUPACK yield stress versus density materials graph

5.2 Rebar Shear Force

Knowing the cross-sectional area of the circular cross-section and using the ultimate tensile stress from *Figure 2.18*; the maximum shear force is 171.1 kN (*Appendix G15*).

The shear force calculated has been checked against a rebar cutter manufacturer's value of 166.6 kN (Cordless 20 mm Rebar Cutter Machine (Be-RC-20b), 2018). This shear force is for an orthogonal blade (*Figure 5.5*), in other words, a flat blade. The larger shear force of 171.1 kN will be used for the rest of the analysis as it is a more conservative value. Off-the-shelf blades and standard bolts will be used, so no Solidworks or first principles analysis will be performed on these components. Orthogonal blades are most commonly found and will be used on this tool being designed.

Figure 5.5: Rebar blades ("Rebar Blades", 2009)

5.3 Rebar Plastic Bending Moment

To calculate the required bending force to deform rebar permanently, the plastic bending moment, M_P, must first be determined. A formula for calculating the plastic bending moment is derived for a circular cross-section, *Equation 5.3.1* (see *Appendix G16*).

$$M_p = \frac{\sigma_Y \left(3c^4 sin^{-1}\left(\left|\frac{1}{c}\right| y_y\right) - y_y\left(2y_y^2 - 5c^2\right)\sqrt{c^2 - y_y^2}\right)}{6y_y} \tag{5.3.1}$$

Using 30 mm (minimum bend radius plus the maximum distance from the neutral axis to the edge of the 20 mm rebar) as the radius of curvature and the yield stress of the rebar (600 MPa) from *Figure 2.18*. These values can then be substituted into *Equation 5.3.1*, which gives a plastic bending moment of 800 Nm (see *Appendix G16* for calculations).

5.3.1 Contact Stresses of Bending Arm and Forming Wheel

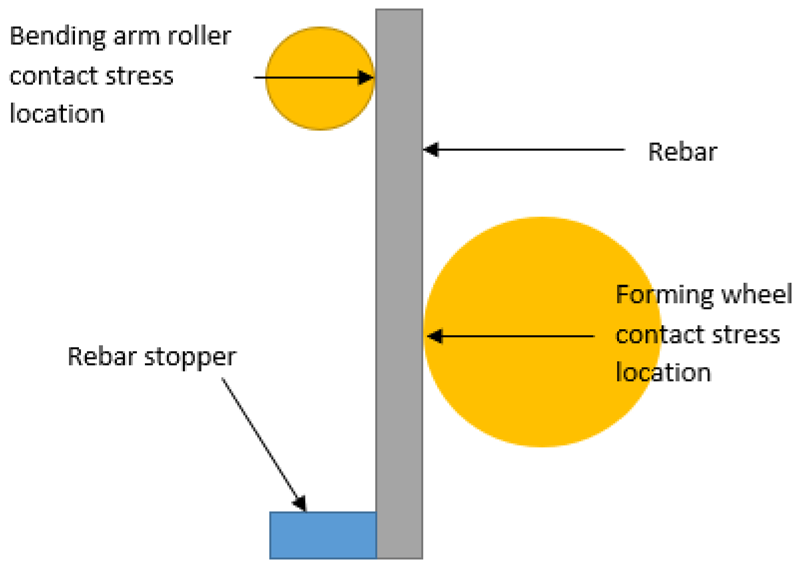

Figure 5.68: Locations of contact stresses between rebar forming wheel and bending arm roller

As the rebar is bent, the forming wheel will have a large force exerted on it (*Section 5.4*). The contact area between the rebar and forming wheel is expected to be small; therefore, the contact stress between the two bodies will be high. The forming wheel and rebar can be assumed to be two perpendicular cylinders (*Figure 5.7*).

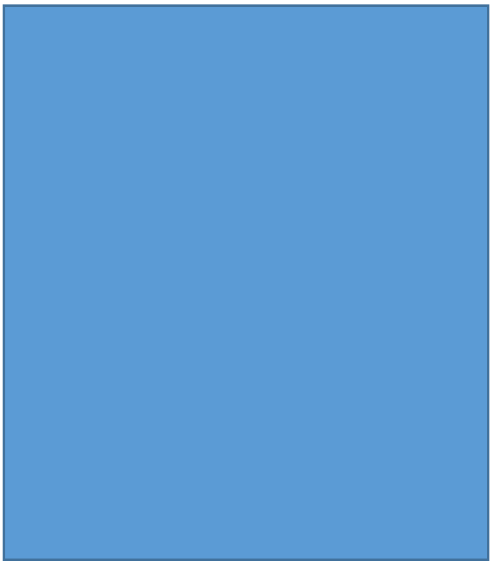

Figure 5.7: Contact stress between two cylinders perpendicular orientation (IHS EDSU, 2000)

The material properties of the rebar and forming wheel are already known. For the forming wheel and roller on the bending arm, ASSAB PM 30 SuperClean steel will be used as these components will experience high stresses. Using the Hertzian Contact stress theory, and the physical and material properties of rebar and the forming wheel; a contact stress of 2.47 GPa is calculated (see *Appendix G3* for calculations).

The contact stress between the rebar and the roller on the bending arm can also be calculated using Hertzian Contact Stress theory. From the material and physical properties of the rebar and bending arm roller, the Hertzian contact stress is calculated to be 2.02 GPa. The contact stress is high, but this is expected as there is a significant amount of force acting on a small contact area between the rebar and the bending arm roller (see *Appendix G4* for calculations).

5.4 Bending Arm Stresses

Knowing that the bending moment to deform the rebar plastically is 800 Nm, and the length between the contact points of the forming wheel and the bending arm roller, the force required to achieve this can be calculated to be 5332.9 N (see *Appendix G14.1*). *Figure 5.7* illustrates how the rebar will be bent. From *Figure 5.9*, a beam diagram can be drawn to show the reaction forces of the forming wheel and the bending arm roller.

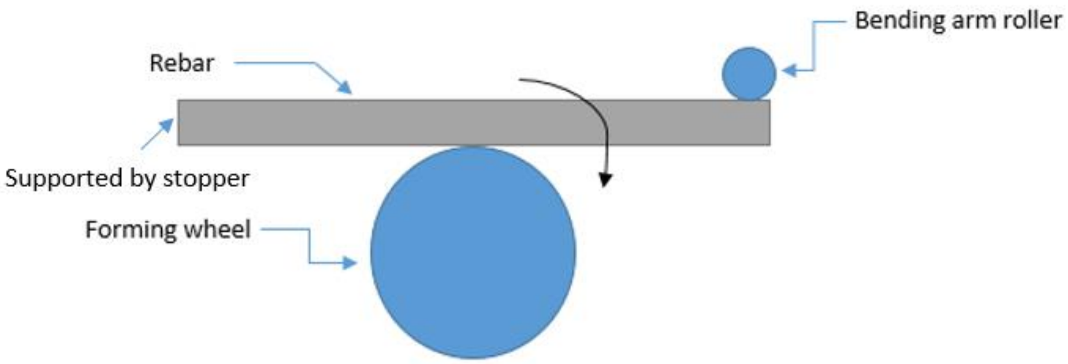

Figure 5.8: Diagram of rebar being bent

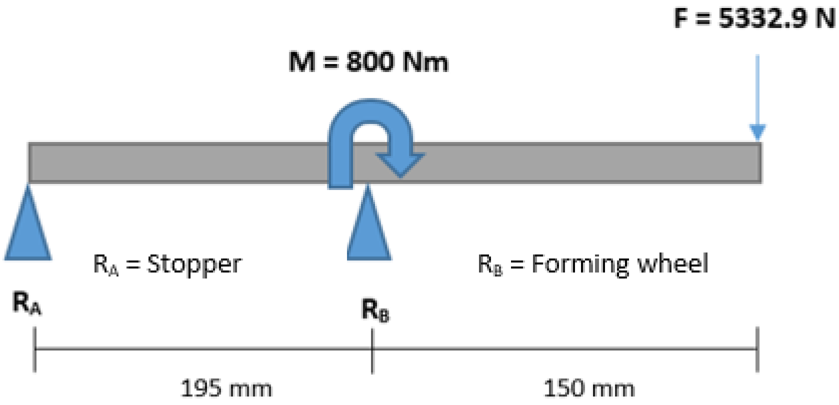

Figure 5.9: Beam diagram depicting loads on the rebar

The force required to bend the rebar is calculated to be 5.3 kN. Knowing the required force to bend the rebar, the reaction forces from the forming wheel (R_B) and the rebar stopper (R_A) are determined to be R_B = 13.5 kN and R_A = -8.2 kN (see *Appendix G14.1*). Knowing the forces acting on the forming wheel, bending arm, and rebar stopper, the stresses can now be calculated for each of these components. In order to calculate the stress experienced by the bending arm, the arm is first simplified to resemble a cantilever beam (*Figure 5.10*) as this will give a more conservative stress value.

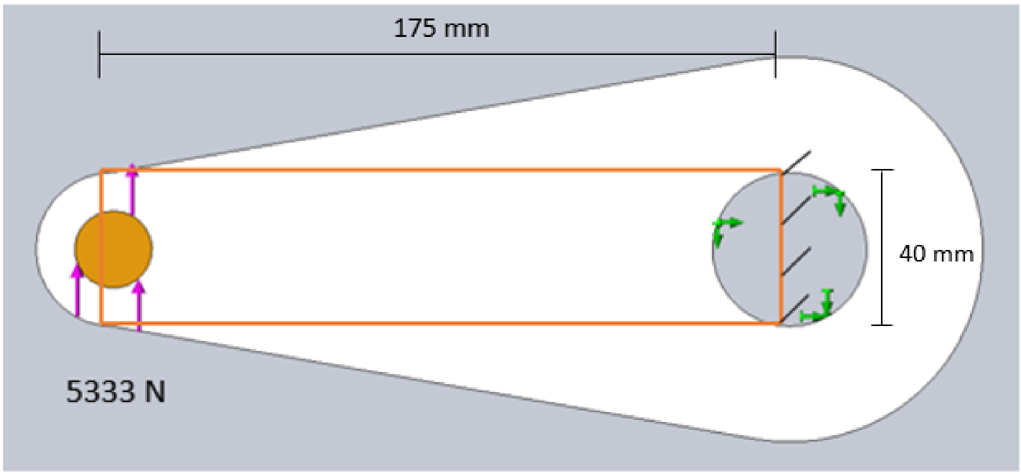

Figure 5.10: Bending arm with simplified cantilever

The bending arm will be constructed of Cast ASTM A747 steel as mentioned previously in *Section 5.1.1*. Knowing the length between the bending arm roller, the centre of the shaft, and the force required to bend the rebar gives a bending stress of 350 MPa. The bending stress is lower than the allowable stress of ASTM A747 (446 MPa).

Due to the force bending the rebar, the bending arm will also most likely experience torsional shear stress (*Figure 5.11*).

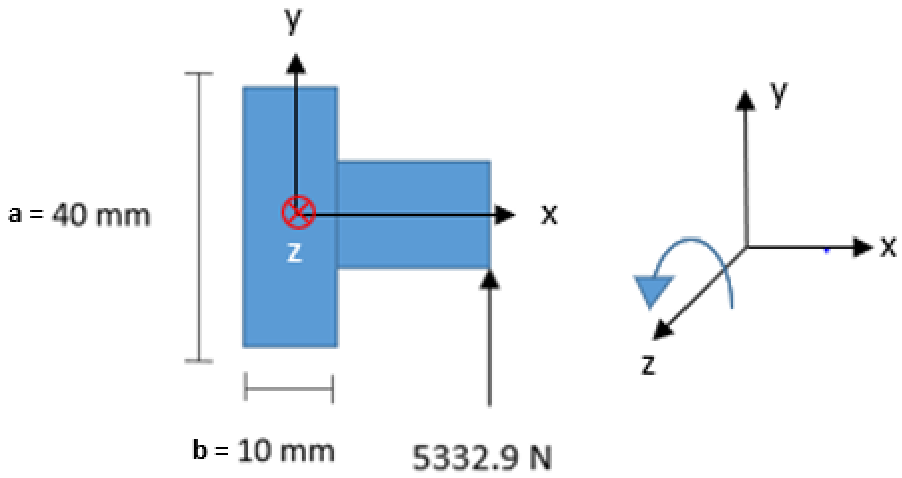

Figure 5.11: Force acting on bending arm roller

Using the dimensions of the cantilever beam and the torque generated by the force on the roller support, the torsional shear stress can be calculated, which yields a shear stress of 119 MPa. Comparing this value to the allowable shear stress of, $\tau_{all} = 223.3\ MPa$, the arm will not shear due to twisting when under load (see *Appendix G14.2* for calculation).

5.5 Powertrain

5.5.1 Drive Shaft and Components Design

The first step in designing the shaft is to determine the length of the shaft. This is achieved by using the dimensions of the case (*Section 5.6.1*), gearbox and motor. It is also important to note that only either bending or shearing of the rebar is ever performed at any given time. The bending moments experienced by the shaft due to shearing and bending the rebar will have to be determined in order to design the shaft. Assuming there is a uniformly-distributed load in the bore of the gearbox lid and the shaft support of the housing, the length of the shaft is taken between half the thickness of gearbox lid and shaft support of the housing. Starting with the forces acting on the shaft created when the tool is shearing (*Figure 5.12*), the reaction forces are F_A = 30.3 kN and F_B = 32.6 kN (see *Appendix G2*).

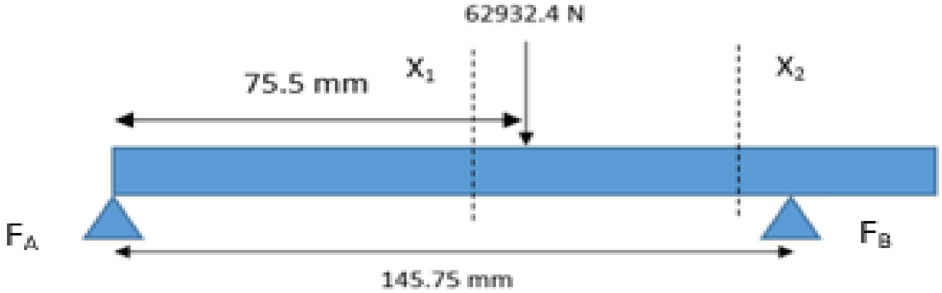

Figure 5.12: Loading of drive shaft when rebar is being sheared

The forces acting on the shaft created when the tool is used for bending is shown in *Figure 5.13*. The calculation of the reaction forces F_A (-4.4 kN), F_B (23.3 kN), bending moment and shearing diagram can be found in *Appendix G2.1*.

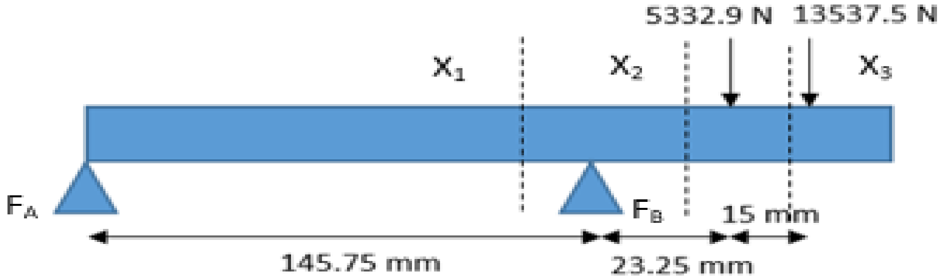

Figure 5.13: Loading of drive shaft when rebar is being bent

In order to design the shaft, the shaft design standard AS1403-1985 will be used (see *Appendix G2.2*). The drive shaft will be constructed of 6580 steel. Having taken into consideration the factor of safety of 1.5, stress concentrations, bending moments, torque, and ultimate tensile stress, the diameter of section AB of the drive shaft is 64 mm (*Figure 5.14*). However, the diameter will need to be increased to 66 mm for the cam to maintain contact with the follower on the shearing mechanism.

Section BC of the shaft (*Figure 5.14*) has two stress raisers, a spline, and a step. For this section of the shaft, the larger bending moment of 649.71 Nm (see *Appendix G2.1*) will be used, which will provide a larger support for the forming wheel. The final diameter of this section of the shaft is 45 mm which will be rounded up to 50 mm.

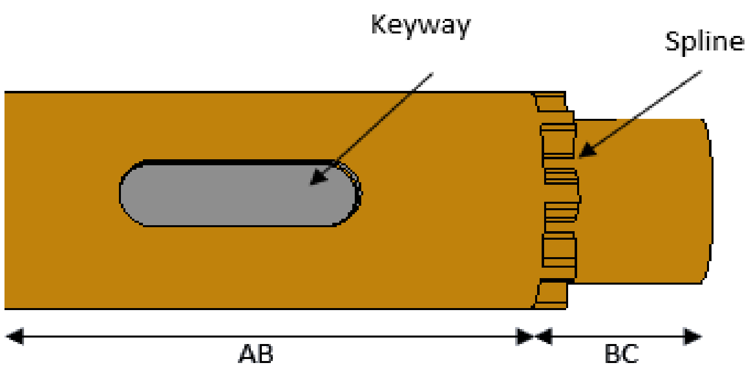

Figure 5.14: Drive shaft that operates both bending and shearing functions of the tool. Also, part of second stage ring gear.

The keyway on section AB of the shaft is the next feature to be designed (see *Appendix G2.3*). From the keyway chart from standard BS4500, a key size can be determined from the diameter of the shaft. The dimensions of the key are used to determine the bearing and shear stresses and select the material for the key. The main body of the key will be the same length as the cam. The ends of the key and the keyway will be rounded as this would make machining easier.

The bearing stress due to the force exerted on the side of the keyway (*Figure 5.16*) is indicated in red in *Figure 5.15*. The depth of the key in the shaft is 7.5 mm, and the length of the cam is 50 mm, which defines the bearing area. The force (8.5 kN) acting on the key and shaft are calculated using the torque of 280.14 Nm and the radius of the shaft.

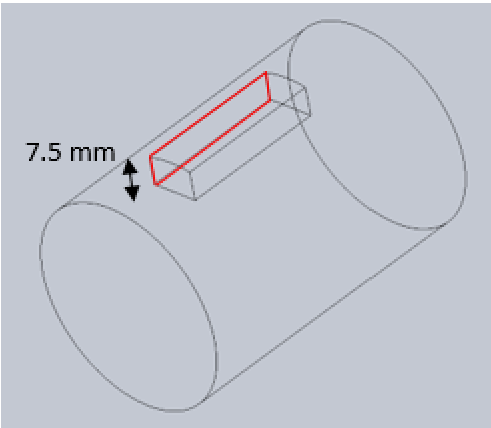

Figure 5.15: Bearing stress exerted on wall of shaft and key

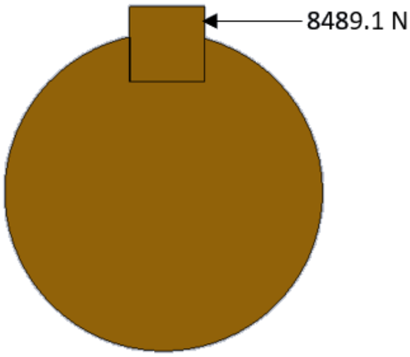

Figure 5.16: Force from shaft torque acting on key

The key will be made of 1018 carbon steel. 1018 steel has a yield stress of 530 MPa; applying the factor of safety (1.5), the allowable stress is 353.3 MPa, and the allowable shear stress is 176.6 MPa. The bearing stress between the key and the shaft is 21.4 MPa (see *Appendix G2.3*) which is lower than the yield stress of 1018 steel used on the key. The shear stress experienced by the key needs to be determined to ensure it falls below the allowable shear stress. The shear area indicated in red is shown in *Figure 5.17*.

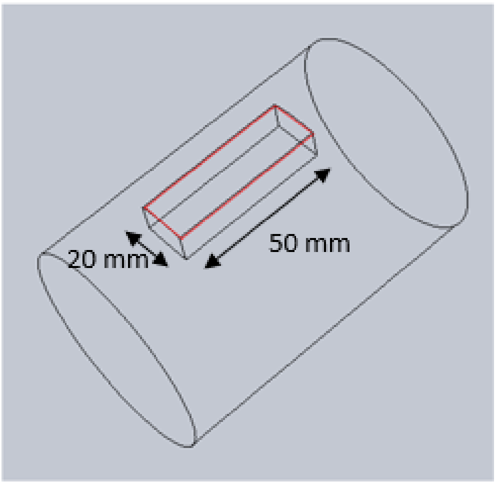

Figure 5.17: Shear plane of the key on the surface of the

The width of the key is 20 mm, and the length is 50 mm. These dimensions provide the shear area (located on the surface of the shaft) in which the shear stress is found to be 8.48 MPa. This shear stress is below the allowable shear stress of 1018 steel (τ_s = 176.6 MPa). The bearing stress between the cam and the key wall also needs to be checked (*Figure 5.18*). The depth of the key in the cam is 4.9 mm, and the length of contact between the key and cam is 50 mm as mentioned previously.

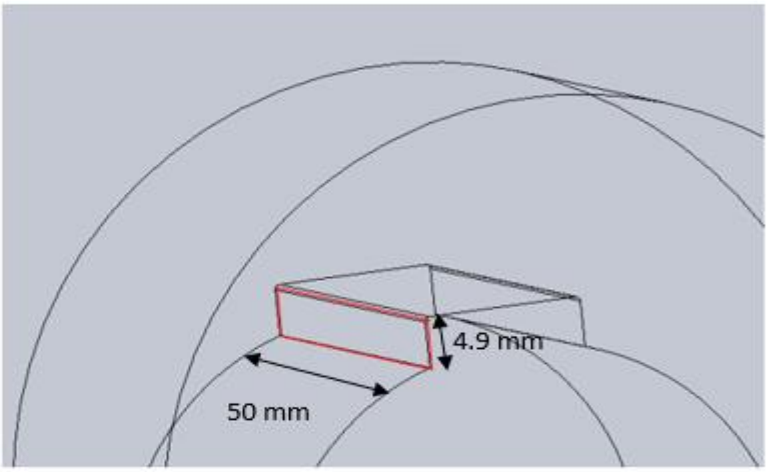

Figure 5.18: Bearing area (indicated by the red box) of cam and key wall

The bearing stress on the cam is 34.6 MPa, meaning that the bearing stress on the cam and key are below the allowable stress of both materials.

The spline that drives the bending arm is the final part of the shaft to be designed (see *Appendix G2.4*). An involute spline centred to the diameter of the shaft (*Figure 5.19*) will be utilised for this shaft. Splines are commonly used in shafts where axial movement is required. However, in this scenario, this is not required; in order to create a tighter fit for the splines of the shaft and bending arm (*Figure 5.19*), the clearance will be removed.

Figure 5.19: Spline centred to diameter (Beardmore, 2013)

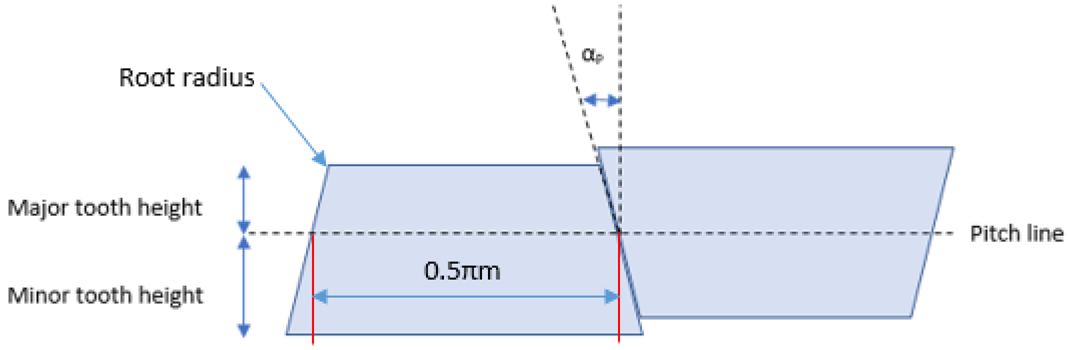

Figure 5.20: Dimensioning system of the spline

The module (7.12) is determined by using a spline with 8 teeth and a pressure angle of 30°. With the module, the root radius, minor, and major tooth height are calculated to be 2 mm, 5.4 mm and 3.6 mm respectively. However, this would give a total tooth height of 9 mm leaving 1 mm protruding over section AB of the shaft. The decision was made to reduce the tooth height to 8 mm to mitigate the risk of stress concentrations occurring. The same dimensions for this spline will be used on the bending arm. In order to calculate the stress experienced by the spline, the spline 'tooth' could be approximated as a cantilever (*Figure 5.21*). The dimensions of the spline teeth are determined in *Appendix G2.4*.

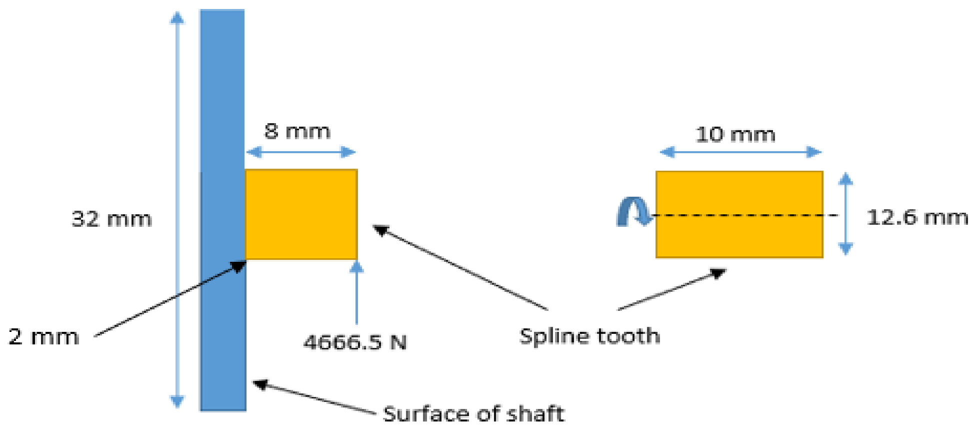

Figure 5.21: Bending stress of the spline tooth

From this cantilever approximation of the spline tooth, the stress that it will experience is 232 MPa, which is below the allowable stress of 6580 steel.

5.5.2 1024:1 Gearbox Components

The cycloidal gearbox designed by Mirko Blagojevic, Nenad Marjanovic, Zorica Djordjevic, and Blaza Stojanovic will be used for this power tool, as it is the most compact two-stage cycloidal gearbox available. Unfortunately, this gearbox is not commercially available; meaning it will need to be designed. It has been calculated previously that the torque required for bending the rebar is 933.3 Nm, and from *Section 5.3*, the torque required for shearing is 280.25 Nm (*Section 5.5.4*). However, the maximum output of the gearbox would be 1536 Nm as the motor torque output is 1.5 Nm; the gearbox will be designed for the maximum torque.

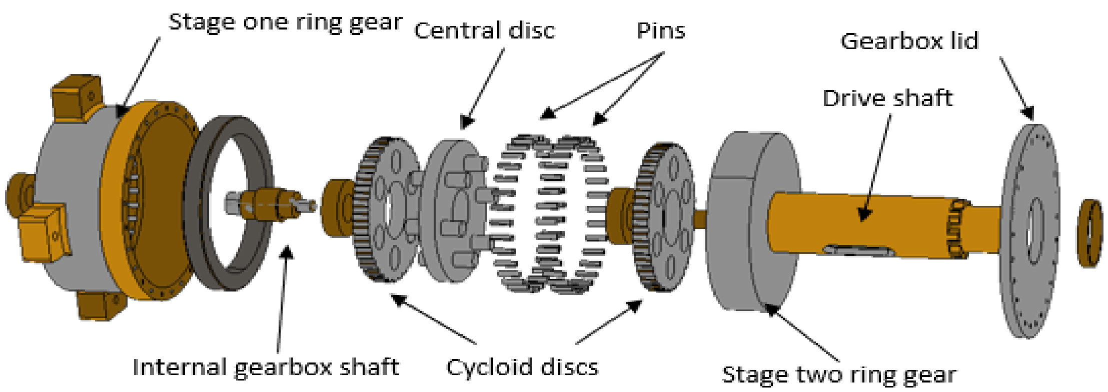

Figure 5.22: Exploded view of gearbox components

5.5.2.1 Stage One and Two Cycloidal Discs

To obtain a gear ratio of 1024:1, each stage of the gearbox will have a reduction ratio of 32:1. Knowing the ratios of each stage and the input torque, the torques of both cycloidal discs will be calculated with the equations supplied by Blagojevic et al. Both cycloidal discs will have equal torques. The cycloidal discs will have a diameter of 164 mm as they will need to accommodate 32 lobes. The added benefit of a large diameter is that it will reduce the amount of force and stress acting on the disc.

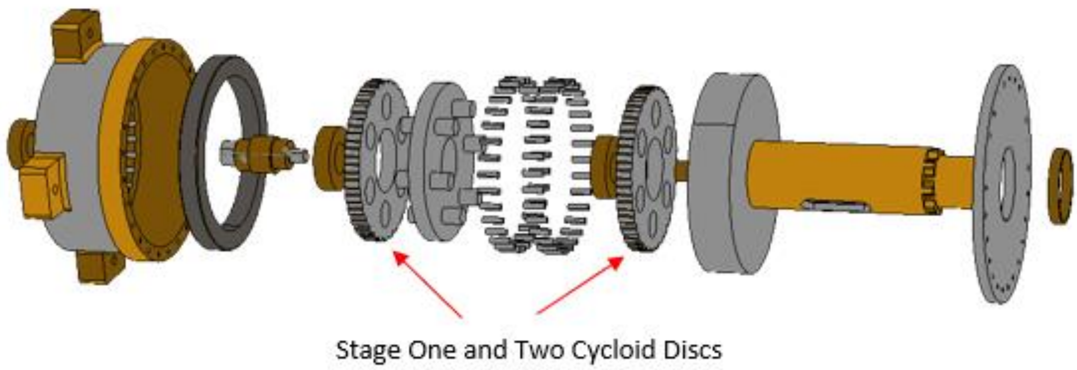

Figure 5.23: Components under consideration

Knowing the torque that each cycloidal disc experiences is 1537.45 Nm (*Appendix G1.6*), the force acting on the teeth on the cycloidal disc can be calculated. It is important to note here that the cycloidal disc engages three pins at any given time (*Figure 5.24*). Assuming the forces are evenly divided, the force per tooth and pin is calculated to be 6.3 kN.

With the forces known, the teeth of the cycloidal disc are approximated as a cantilever to calculate the bending stress of the tooth (*Figure 5.24*). The thickness of the cycloidal disc is 16 mm to increase the contact area to lower the contact stress (the Hertzian Contact Stress between the cycloidal disc and central disc pin bushing is calculated in *Appendix G1.6*).

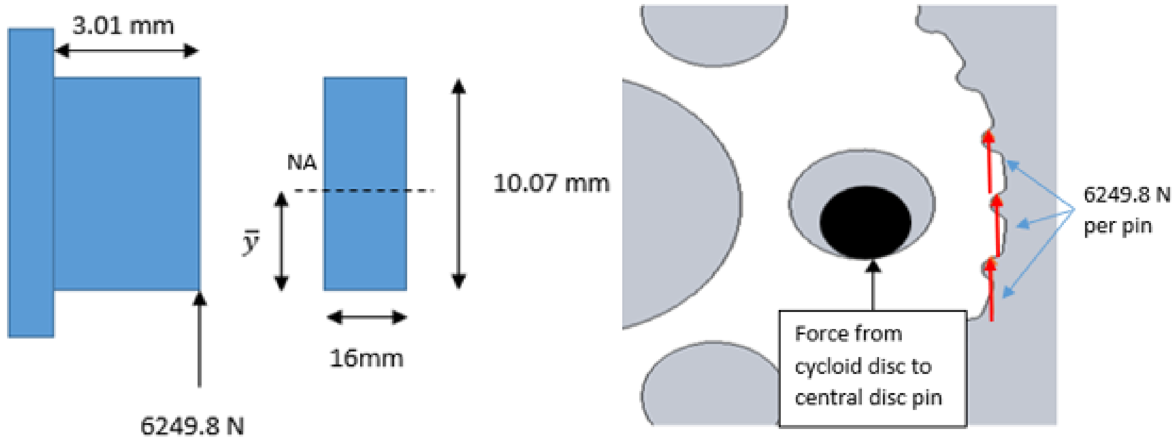

Figure 5.24: (Left) Bending of cycloidal tooth is equivalent to cantilever beam, NA denotes neutral. (Right) Forces acting on the teeth of the cycloidal disc axis.

The bending stress calculation (*Appendix G1.6*) shows that the bending stress (69.5 MPa) is below the allowable stress of 644 MPa of 4142 steel (quenched and tempered). The tooth on the cycloidal disc will also experience shear stress, which is calculated to be 36.5 MPa and which is below the allowable shear stress of 322 MPa.

One final stress that needs to be determined for the cycloidal disc is the contact stress between the pins and central disc (*Figure 5.25*). The cycloidal disc has six holes in which only three are engaged at any one time; it is also assumed that each pin exerts an equally divided force onto the walls of the holes.

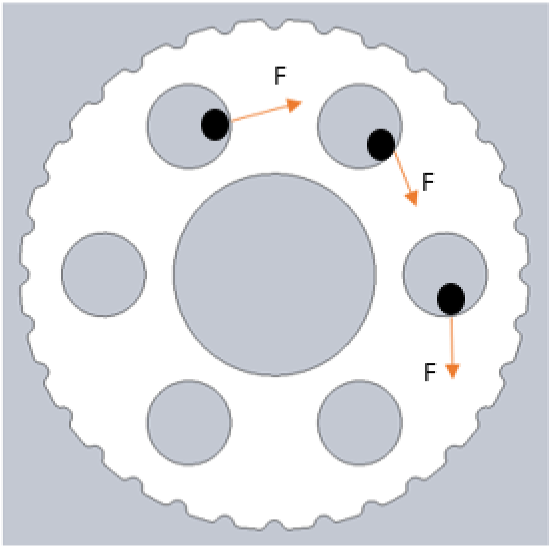

Figure 5.25: Cycloidal disc of stage 1 and 2 showing forces from the pins acting on the holes

Using the Hertzian Contact Stress Theory for a cylinder within a cylinder, the contact stresses between the two parts can be calculated (*Appendix G1.6*). The bushing and cycloidal disc material properties of copper beryllium (*Appendix D7*) and 4142 steel (*Appendix D9*) are used respectively.

Before the contact stress can be calculated, the forces acting between the pin and the hole walls will need to be determined. Knowing the torque of the cycloidal disc, the forces acting at the holes and the pins of the central disc is found to be 9.3 kN. The diameters of the holes and the bushings are 27 mm and 21 mm, respectively. With this information, the calculation yields a contact stress of 588.3 MPa, which is lower than the allowable stress of 4142 steel (644 MPa) and copper beryllium (643.3 MPa).

5.5.2.2 Central Disc

The calculation to determine the central disc pin diameters (see *Appendix G1.7*) was completed using the allowable stress of 4140 steel heat-treated to condition U ($\sigma_{all} = 493.3\ MPa$). The pins will be approximated as cantilevers with a length of 20 mm (*Figure 5.28*). The length of the pins will allow a clearance of 4 mm between the cycloidal disc (16 mm thick) and central disc (*Figure 5.27*) while still engaging with the two cycloidal discs on either side.

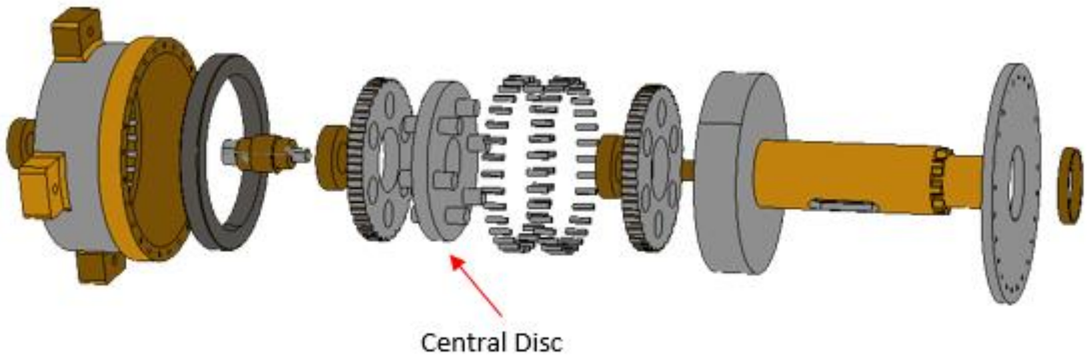

Figure 5.26: Components under consideration

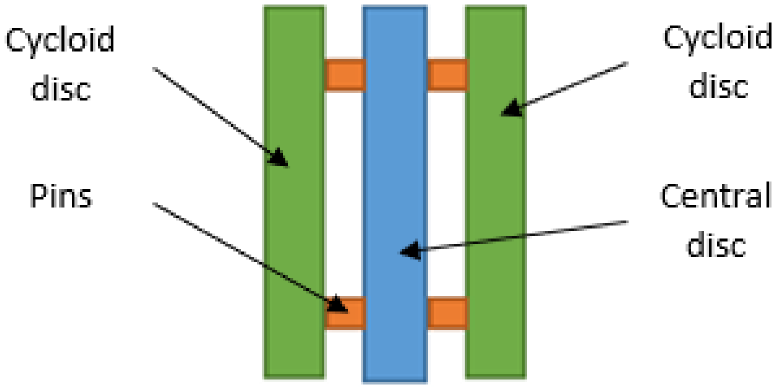

Figure 5.27: Schematic of central disc, pins and cycloidal disc showing 4mm between the discs

The minimum diameter of the pin was calculated to be 16 mm, but it was then increased to 17 mm to fit bushings from the SKF catalogue. Unfortunately, the bushing materials that were offered were of insufficient strength to cope with the contact stresses. As 17 mm is a standard internal diameter, it was then used for the internal diameter of the custom beryllium copper bushing. The thickness of the custom bushing is 2 mm, a similar thickness to the bushings offered in the SKF catalogue.

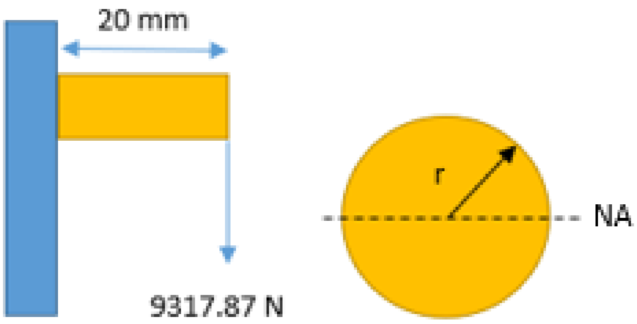

Figure 5.28: Central disc pin approximated as cantilever beam. NA denotes neutral axis

In order to determine the thickness of the central disc, an approximation was made to turn a section into a rectangular wall as indicated in *Figure 5.29*. As the cycloidal discs press down on each side of the central disc pins, a bending moment created by the combined force on the three pins is 27.9 kN. To simplify the analysis of the central disc, the total force will be loaded onto one pin to create the bending moment.

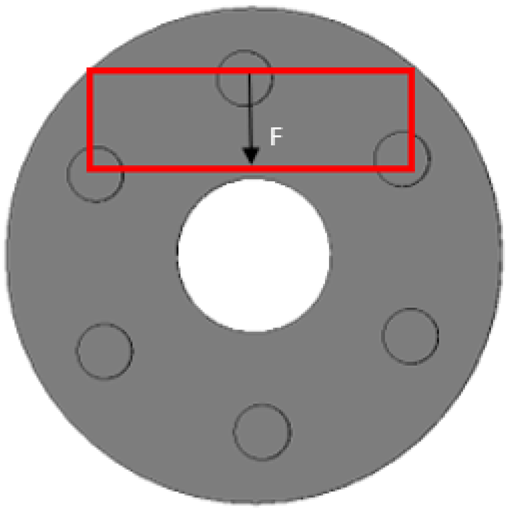

Figure 5.29: Central disc wall (red) approximation

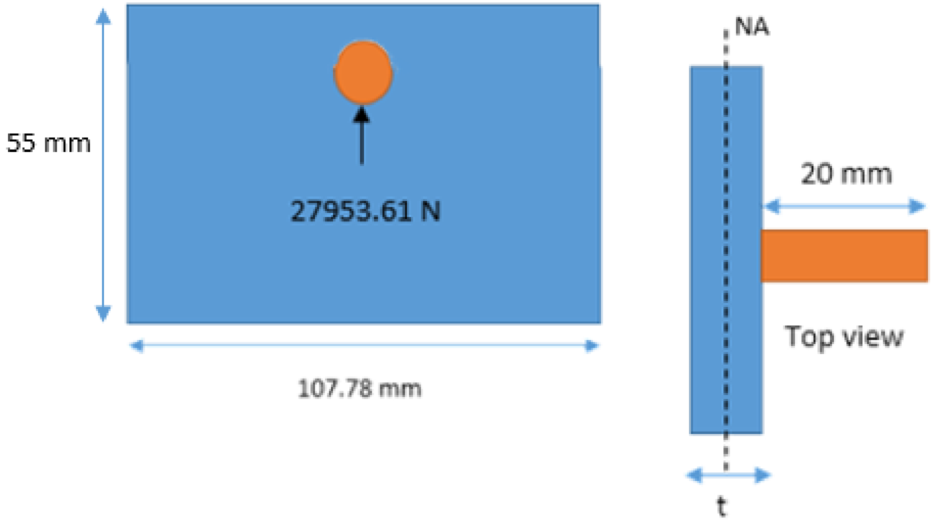

Figure 5.30: Schematic of approximated wall of central disc. NA denotes neutral axis.

From the calculation (see *Appendix G1.7*), the minimum thickness of the central disc is 10 mm. The thickness 't' of the central disc was later increased to 16 mm to fit the selected outer bearing better.

The two cycloidal discs are 180° out of phase (this is done to reduce vibration), meaning only three pins on opposite ends have a force exerted on them. This loading condition could cause some torsional shear stress on the central disc. Using the dimensions in *Figure 5.30*, the torsional shear stress is 68 MPa (see *Appendix G1.7*), which is lower than the allowable shear stress of 4140 steel (246.6 MPa).

5.5.2.3 Internal Gearbox Shaft Design

The internal shaft of the gearbox is different from most shafts as it does not drive any of the components in the gearbox. This is attributed to that fact that none of the components are connected to the shaft via a keyway or other fixtures. It also requires a 3 mm eccentricity to allow the cycloidal discs to move in a cycloidal fashion. As a standard for eccentric shafts could not be found, shaft design standard AS1403-1985 will be used as a guide (see *Appendix G1.2*).

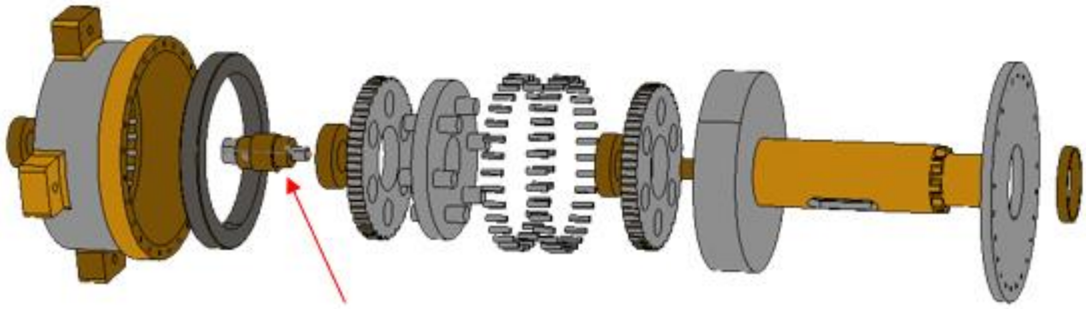

Figure 5.31: Components under consideration

Before the standard could be used, the forces and the bending moments on the shaft need to be calculated. Starting with the forces exerted on the shaft by the cycloidal discs of stage one and two (the torques on both cycloidal discs are equal), the loading conditions can be simplified down to *Figure 5.32*, where F_A represents the force on the shaft, F_B is the reaction force from the central disc pins, and a total force of 18.7 kN act on the cycloidal disc teeth from the ring gear.

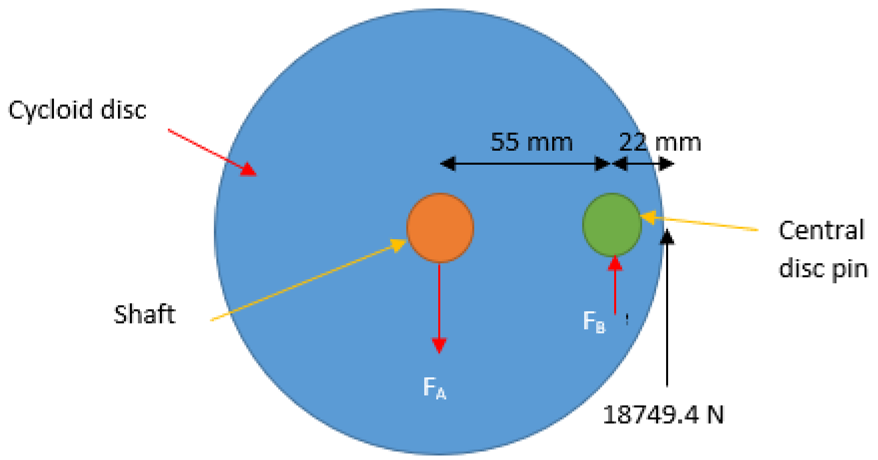

Figure 5.32: Forces from cycloidal disc to shaft

To calculate the forces acting on the shaft in *Figure 5.32*, the situation can be treated as a beam (*Figure 5.33*).

Figure 5.33: Equivalent beam diagram of forces exerted by cycloidal disc

The reaction force F_B, is 27.9 kN and the reaction force F_A, is determined to be 9.2 kN. As both the cycloidal discs have the same torque, the force exerted on the shaft (*Figure 5.34*) from the second cycloidal disc will be the same (*Appendix G1.1*).

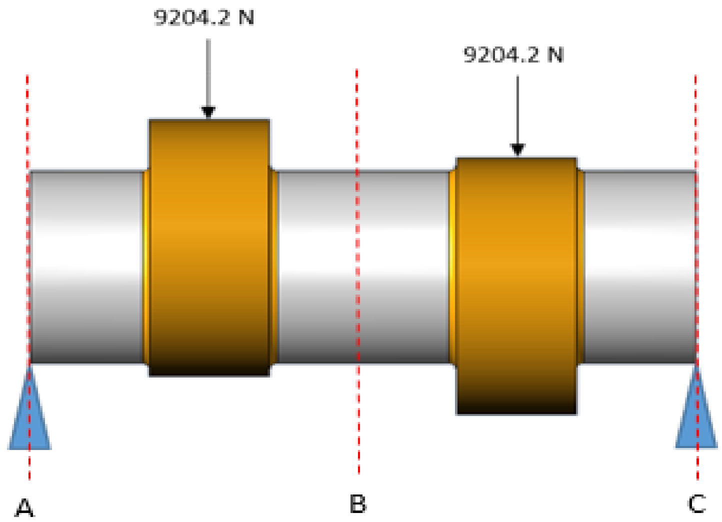

Figure 5.34: Gearbox shaft showing loading condition

Once the initial diameter of the shaft is calculated, a 3 mm eccentricity will be added to offset each section where the cycloidal discs will be located to accommodate the required eccentricity.

The bending moments on the shaft are virtually symmetrical, meaning that the diameter of the shaft will be uniform. It must be noted that one side of the shaft will need to accommodate an internal keyway so that the electric motor can drive the gearbox (*Section 5.5.2.4*).

Determining the final diameter of Section AB of the internal gearbox shaft, the two stress raisers need to be considered. Section AB of the internal shaft has a stepped section (for the eccentric movement of the cycloidal disc) and an interference fit from the bearing (*Figure 5.34*). The shaft diameter of this section is calculated to be 30 mm. The bending moment in section BC of the shaft is identical. Therefore, the diameter of section BC is the same as section AB of the internal shaft (see *Appendix G1.2* for shaft calculation).

5.5.2.4 Internal Keyway Design

The final part of the shaft that needs to be designed is the internal keyway (*Figure 5.35*) that allows the motor to drive the gearbox. The key will be made of 304 stainless steel as it is readily available key steel with a yield stress of 205 MPa and a shear stress of 102.5 MPa. No factor of safety is used as the forces acting on the key would be small. It would also be more beneficial if the key failed as opposed to damaging the motor or the gearbox.

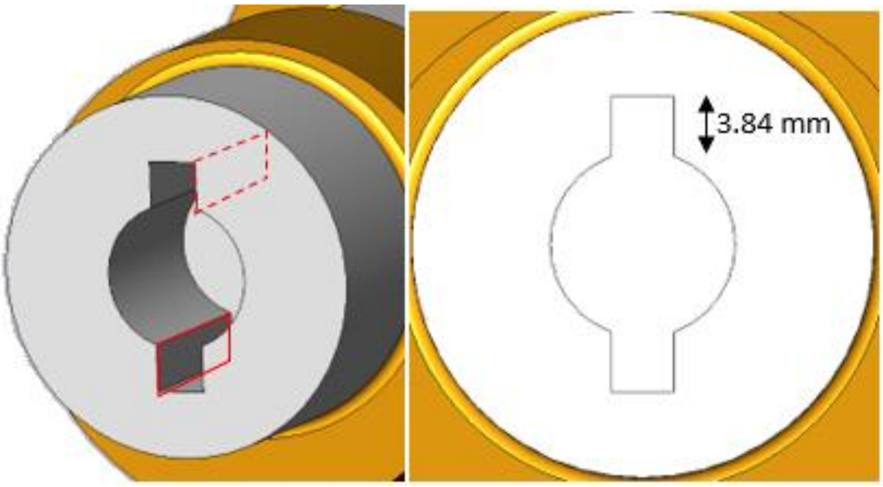

Figure 5.35: Internal keyway to allow motor to drive gearbox. Red box indicates bearing area between key and shaft.

Firstly, the forces acting on the key and the internal wall of the shaft need to be calculated. The force acting on the key is calculated by using the radius of the motor shaft (12 mm) and the maximum torque that the motor can produce (1.5 Nm). Knowing this torque, the total force generated is 250 N. As it is a double-sided key, a double shear scenario is in place, meaning the forces are divided evenly on each end of the key (*Figure 5.36*). As the forces are small, it would be better to assign an arbitrary set of dimensions and calculate the bearing and shear stresses between the key and the shaft.

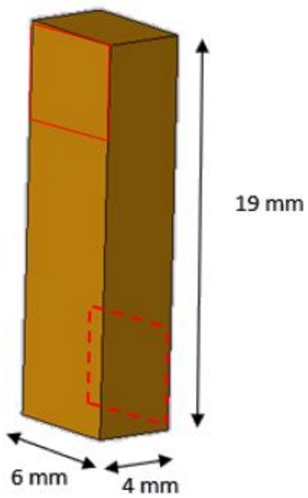

Figure 5.36: Motor keyway dimensions. The red box indicates bearing area between key and shaft

From the calculations, the bearing (5.4 MPa) and shear (5.2 MPa) stresses are below the allowable stresses of the key's material (see *Appendix G1.3* for calculation).

5.5.2.5 Stage One Ring Gear Body and Pins

The first stage ring gear (which also acts as the body of the gearbox) has several different forces acting on it. First, calculating the forces exerted by the central disc onto the body. As the first cycloidal disc exerts a force onto the central disc, the central disc then exerts an equal and opposite force on the second cycloidal disc as shown in *Figure 5.38*, and can be further simplified to a beam diagram in *Figure 5.39*.

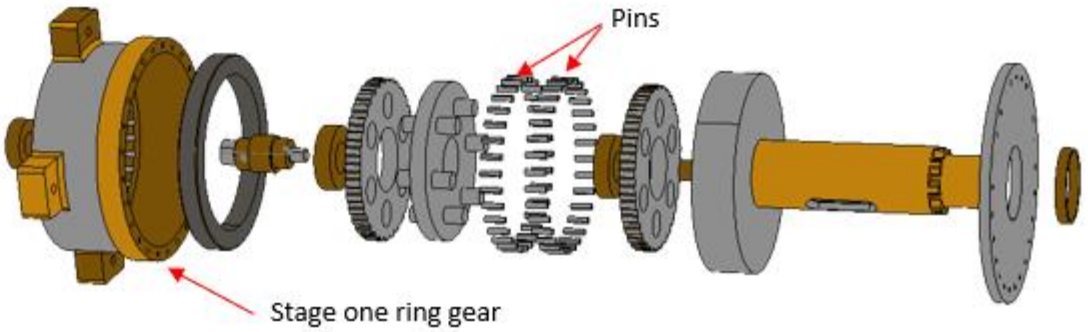

Figure 5.37: Components under consideration

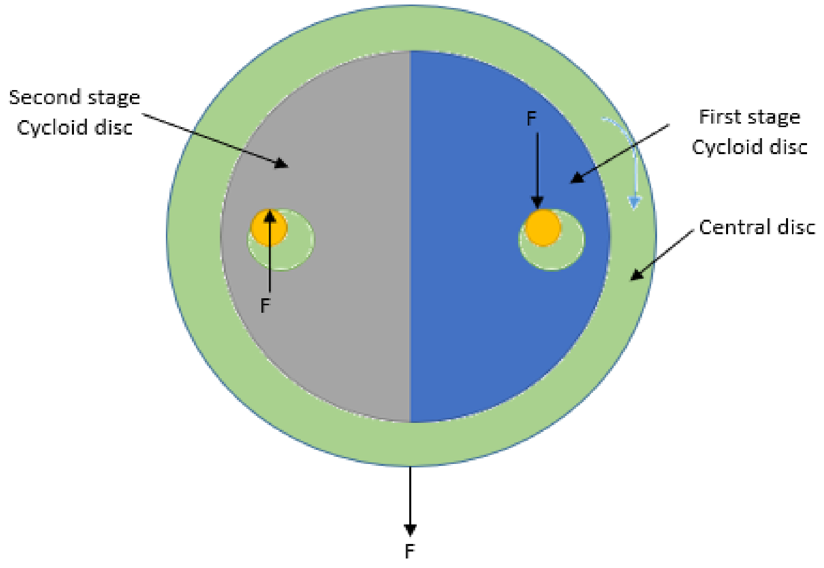

Figure 5.38: Equal and opposite forces exerted on the central disc. First stage cycloidal disc (blue) exerting force onto central disc pin (yellow). Central disc pin exerts force onto second stage cycloidal disc (grey).

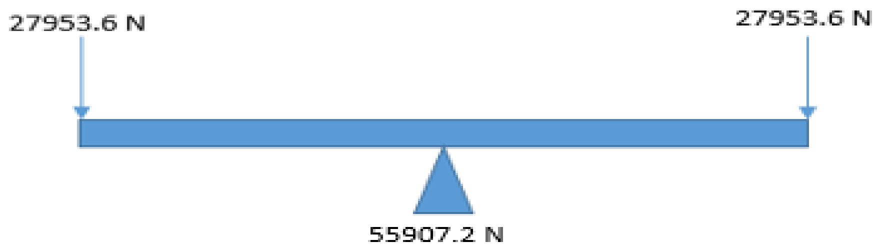

Figure 5.39: Equivalent loading of central disc on beam

The total force of 55.9 kN is exerted onto a bearing that is press-fitted onto the body of the gearbox (*Figure 5.40*).

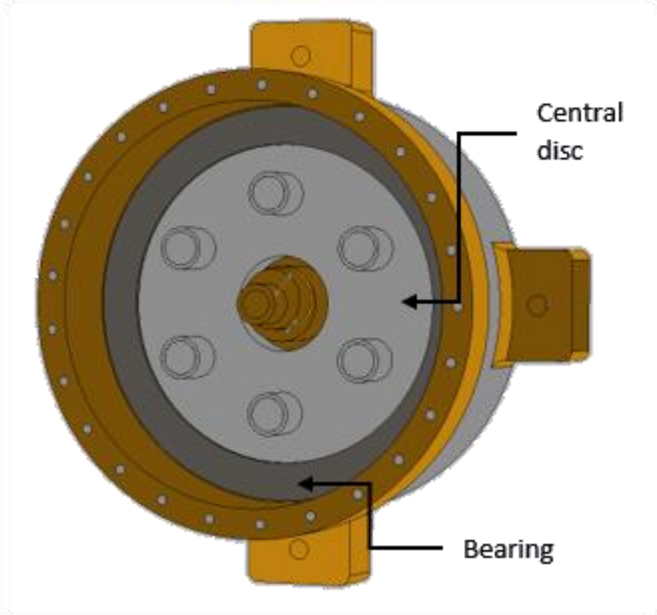

Figure 5.40: Central disc and bearing press fitted into stage one ring gear. Note the central disc is not in contact with the shaft

Using the projected area of the bearing and the force acting on the bearing, the bearing stresses exerted on the body of the gearbox are determined to be 13.9 MPa (*Appendix 1.4.2*), which is below the allowable stress of Al 5058-H18 (271 MPa). The force from the bearing also causes a bending moment on the gearbox body (*Figure 5.41*).

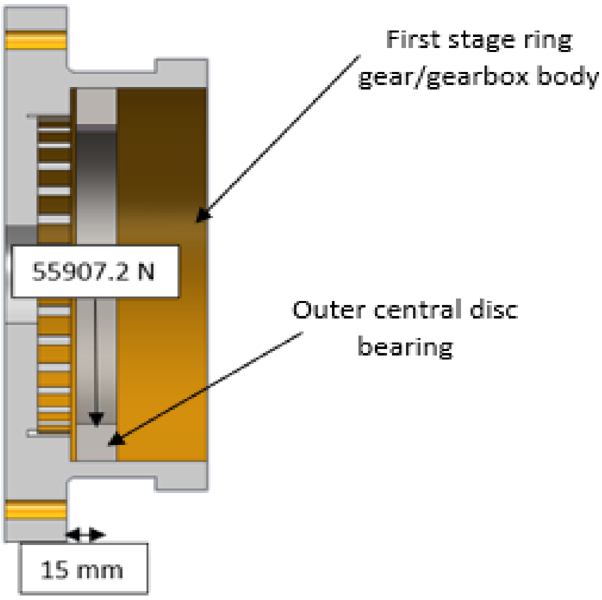

Figure 5.41: Central disc forces acting on bearing causing bending moment on gearbox body

The bending stress caused by the central disc is 3.23 MPa (*Appendix 1.4.1*), which is below the allowable stress of the aluminium alloy (271 MPa).

The next components to be designed are the ring gear pins to be made of L2 steel. Knowing the material properties and that the same forces acting on the cycloidal disc teeth will act on the pins, the dimensions of the pins can be determined.

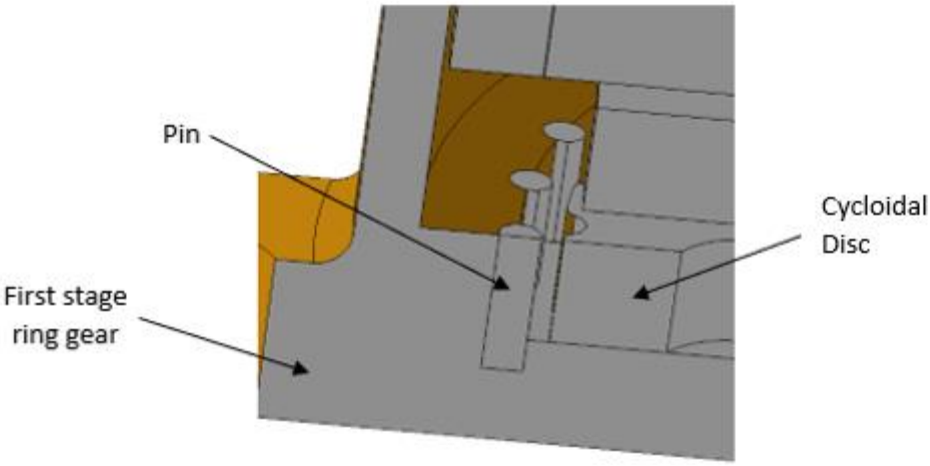

Figure 5.42: Ring gear showing fitted pins

The pins will be interference fitted into the ring gear, and only half the pin will be exposed to the cycloidal disc (*Figure 5.42*). With a pin diameter of 6 mm, the length of the pin can be calculated with respect to the allowable shear stress of L2 steel ($\tau_{all} = 170\ MPa$).

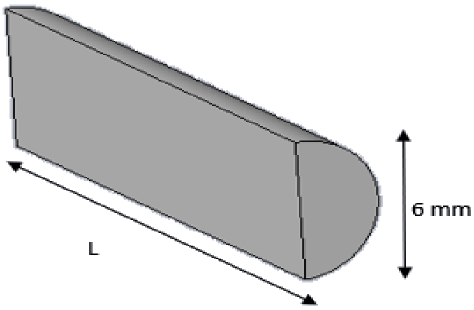

Figure 5.43: Shear area of exposed section of ring gear

From the calculation, the minimum exposed length of the pin is 10 mm (*Appendix G1.4.*3), but the length of the exposed pin is required to be 16 mm to match the thickness of the cycloidal disc. The shear stress in the pin semi-circle cross-section (*Figure 5.43*) also needs to be checked; it is calculated that a shear stress of 589.4 MPa exists. This shear stress is greater than the allowable shear stress, which means L2 steel will need to undergo heat treatment to improve its mechanical properties. According to Pope (1997, p.265), L2 steel can be heat-treated to achieve a yield stress of 1792.6 MPa, which gives an allowable shear stress of 597 MPa and an allowable tensile stress of 1195 MPa. This means that the current dimensions can be maintained. The bearing stress between the pins and ring gear also needs to be checked; Solidworks was utilised to obtain the bearing area. The calculated bearing stress is 50.6 MPa (*Appendix G1.4.3.1*).

To determine the minimum thickness of the ring gear; an approximation was made to turn the ring gear into a flat wall fixed at one end (*Figure 5.44*). The load of three pins is applied on the "tooth" of the ring gear.

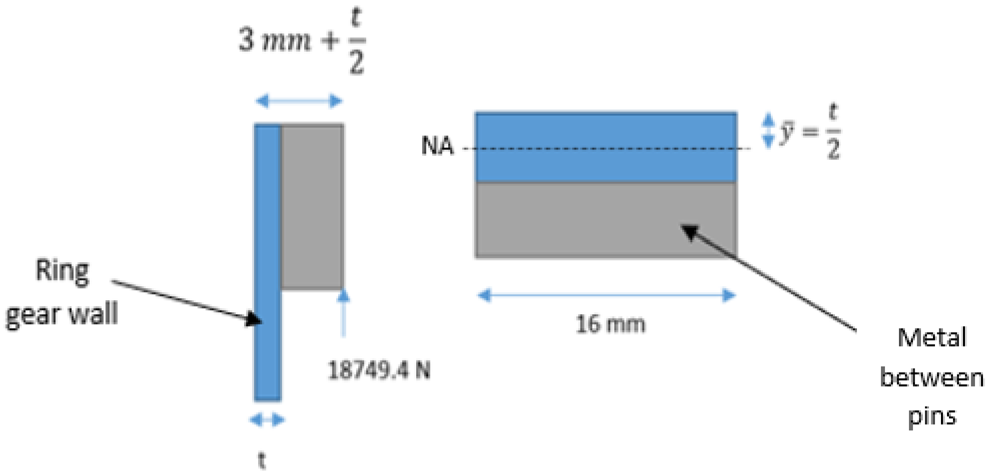

Figure 5.44: First stage ring gear wall loading approximation

Knowing the allowable stress of 5056-H18 aluminium alloy, a calculation is performed, yielding a minimum thickness 't' of 20 mm (*Appendix G1.4.4*).

5.5.2.6 Stage One Ring Gear Bending of Feet and Body

The feet and the bolt diameter to secure the gearbox to the housing of the gearbox are the next items to be designed. Using the upwards force from the shaft during shearing (as it is the highest force that occurs), the force from the first-stage ring gear torque, and the force from the internal gearbox shaft that exerts on the second stage ring gear, will give the loading conditions on the feet and the shear force on the bolts.

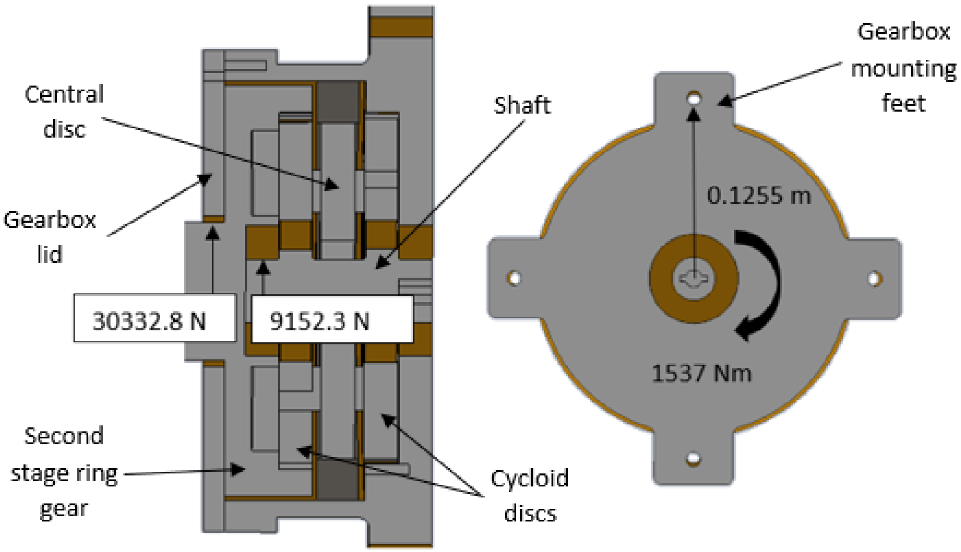

Figure 5.45: Forces and torques on first stage ring gear body

To calculate the bolt diameters used to secure the gearbox to the housing, the net force in the upwards direction is 39.5 kN (*Figure 5.45*), and the force per foot due to torque is 12.9 kN (see *Appendix G1.4.5*). The bolts are made of grade 10.9 steel which has a yield stress of 940 MPa. With an allowable stress of 626.6 MPa and an allowable shear stress of 313.3 MPa, the diameter of the bolts is calculated to be 8.3 mm. However, as 8.3 mm bolts do not exist for this grade of steel, the next largest bolt diameter of 10 mm will be used instead.

The top and bottom feet of the gearbox may also be affected by bending due to the loading from the shaft during shearing (calculation in *Appendix G1.4.6*). The bolt holes in the feet are a source of stress concentration (*Figure 5.46*) and will be taken into account in the analysis.

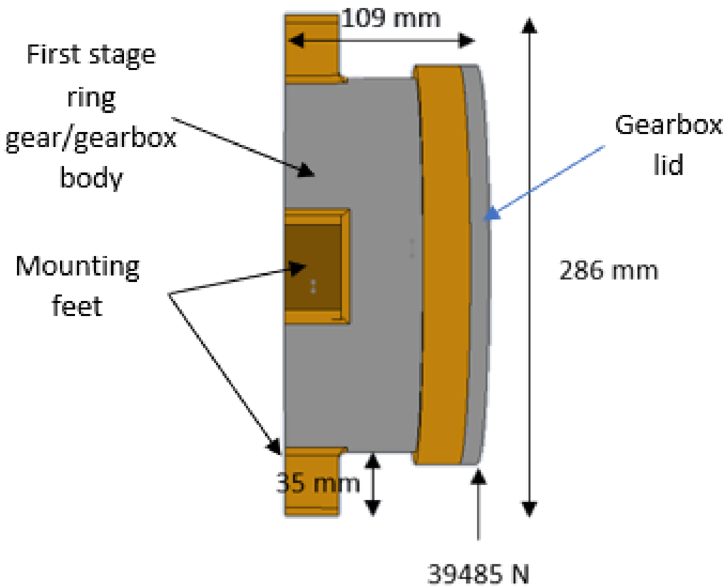

Figure 5.46: Force exerted on the front of gear box could cause the top and bottom feet to bend

The gearbox body is simplified as a T-plate. *Figure 5.47* shows a free body diagram.

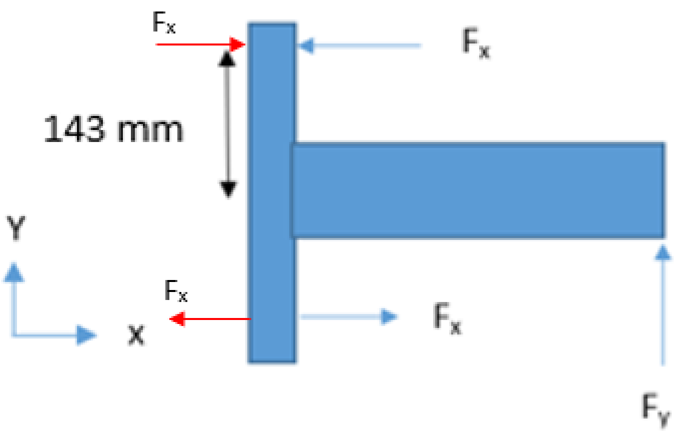

Figure 5.47: Free body diagram of gearbox body. The red arrows indicate reaction forces from the housing

The forces in the x-direction acting on the top and bottom feet need to be determined in order to calculate the bending stress. Knowing that the bending moment caused by the 39.5 kN force is the sum of the two moments created by the two forces acting in the x-direction; the force acting in the x-direction can be calculated. The force has a uniform triangular distribution (*Figure 5.48*). The maximum point force 'F' can be calculated by finding the centre of the triangular force distribution. This force is then used to determine the bending stress of the mounting feet.

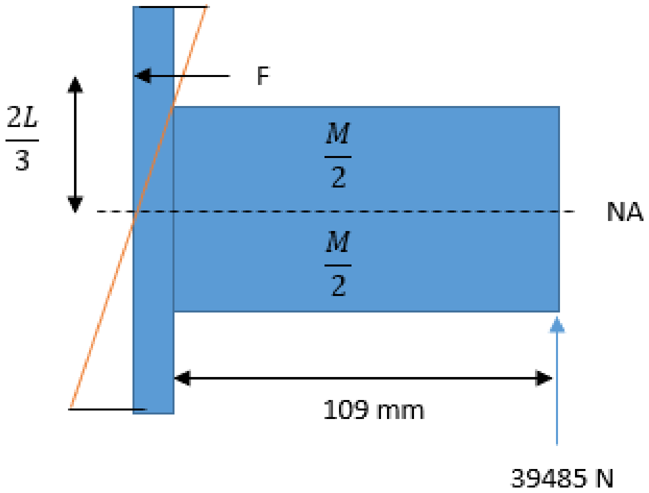

Figure 5.48: Force distribution of the first stage ring gear

Knowing the diameter of the bolt hole, either the width or thickness of the foot can then be arbitrarily assigned until a stress below the allowable stress of the aluminium alloy (271 MPa) is found (*Figure 5.49*). Using D = 10 mm, w = 55 mm, t = 30 mm and the bending moment $M = 22573\ N(0.035\ m) = 790\ Nm$, the bending stress was calculated to be 257.4 MPa which is below the allowable stress (271 MPa) of the aluminium alloy (*Appendix G1.4.6*). The dimensions will be used on all four of the mounting feet on the gearbox.

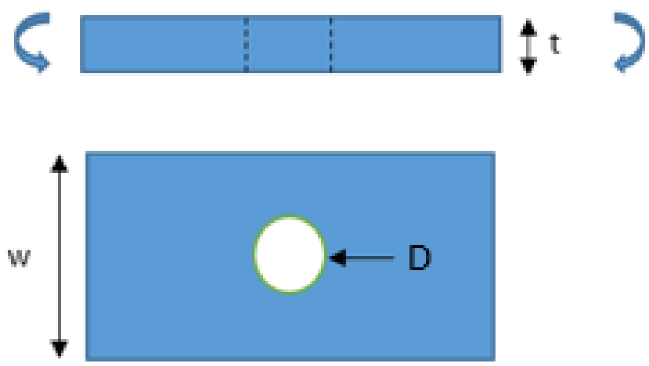

Figure 5.49: Gearbox foot in bending with bolt hole

Bending of the gearbox body will also likely occur from the force exerted by the shaft when rebar is being sheared. Assuming a uniform wall thickness of 8 mm (the thinnest section of the gearbox) and the maximum length of the gearbox (109 mm), the stress caused by bending is 16.4 MPa, which is below the allowable stress of the aluminium alloy (see *Appendix G1.4.7* for calculation).

5.5.2.7 Stage Two Ring Gear

The second stage ring gear will be made of 6580 steel. It should be noted that according to the 6580 steel datasheet (see *Appendix D10*), for a circular section with a diameter between 161 mm and 250 mm, the yield stress of the steel is 700 MPa. The shaft that forms part of the ring gear is discussed in *Section 5.5.1*. The diameters of this shaft are 66 mm and 50 mm.

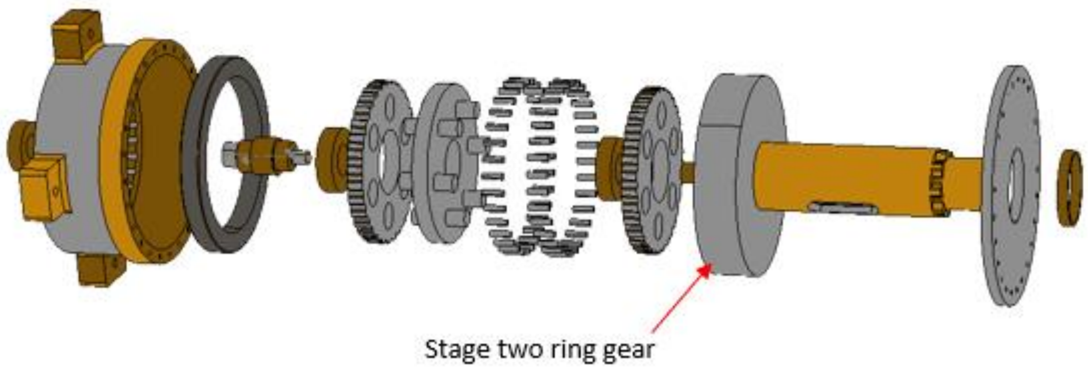

Figure 5.50: Components under consideration

The same approach used to determine the wall of the first stage ring gear will also be used here. The respective section of the ring gear can be approximated as a wall fixed at one end (*Figure 5.44*). Then, the combined force of the three pins (18.7 kN) is applied to the steel between the pins of the ring gear. This steel between the pins acts as a support to each pin; the force will cause a bending moment about the wall. From the calculation, using the allowable stress of 6580 steel (466.6 MPa), the minimum thickness of the stage two ring gear wall is 13 mm (see *Appendix G1.5.1* for calculation).

Next, the bearing holder is to be designed. A bearing will be press-fitted into the second stage ring gear (*Figure 5.51*). The force from the internal gearbox shaft will exert a radial force of 9.25 kN. This will most likely produce a very small bending moment, so it would be more practical to arbitrarily assign a wall thickness and determine whether the bending stresses will exceed the allowable stress of the material.

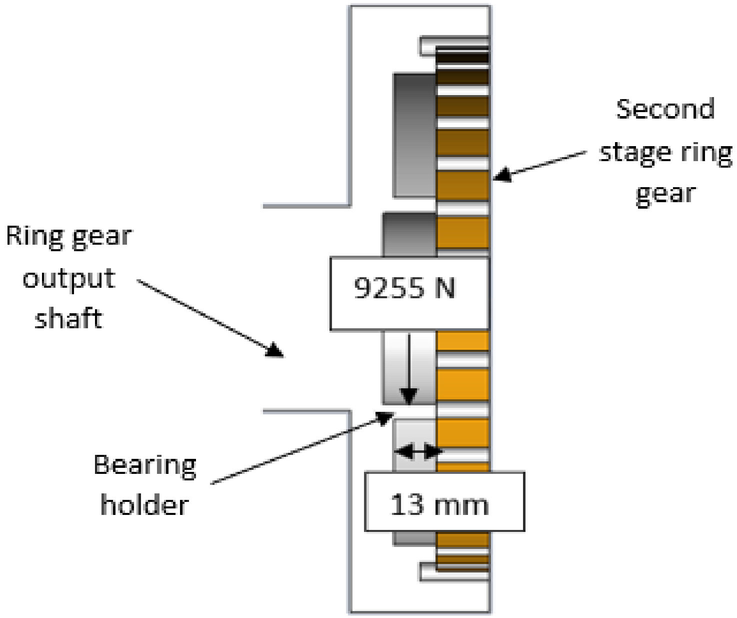

Figure 5.51: Cross-section of second stage ring gear, showing the bearing holder with force indicated

The internal diameter of the bearing holder is 62 mm; however, the outer diameter has been arbitrarily assigned to 72 mm to provide a 5 mm thick holder around the bearing. The maximum bending stress on the bearing housing is 7.3 MPa which is below the allowable stress of 6580 steel (see *Appendix G1.5.2*).

5.5.2.8 Gearbox Lid Design

Next to be calculated is the diameter of the machine screws that secure the lid to the gearbox (see *Appendix G1.5.3*). The net force acting on the lid is 39.8 kN (*Figure 5.45* and 5.53). It is assumed that this force will divide evenly between the screws that secure the lid in place. As space is limited on the front of the first-stage ring gear, it was decided that multiple screws will be used to distribute the force. The screws need to be able to fit within the 14 mm thickness of the first stage ring gear lip.

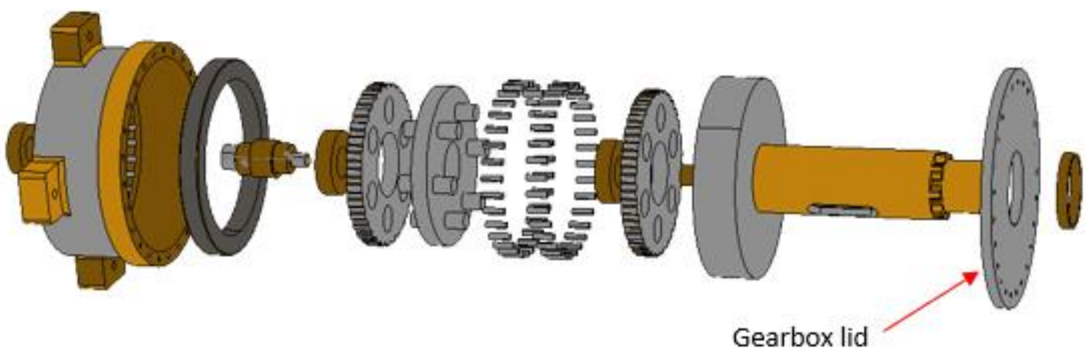

Figure 5.52: Components under consideration

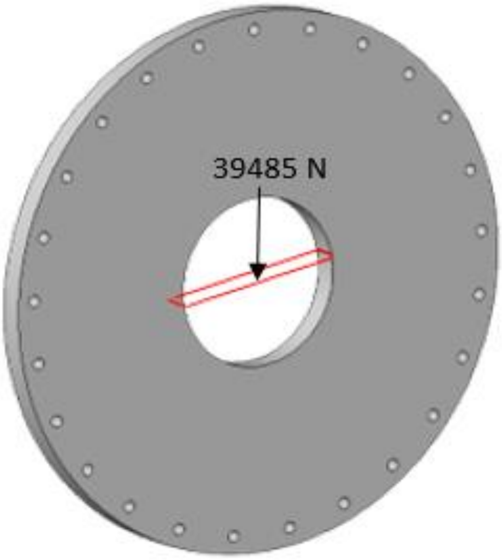

Figure 5.53: Gearbox lid a load of 39485 N acting on half of the bore. The red square indicated projected bearing area.

Class 4.8 machine screws will be used; the steel has an allowable shear stress of 113.3 MPa. Using the allowable shear stress, the screw diameter is calculated to be 5 mm.

The thickness of the lid of the gearbox needs to be determined. Using the net force of 39.5 kN, the outer diameter of the bushing (72 mm), and the allowable stress of the aluminium alloy 5056-H18 (271 MPa), the minimum thickness of the lid becomes 2 mm. However, a thickness of 2 mm is quite small, and a more reasonable thickness of 10 mm is used instead in order for a bushing to be fitted onto the lid.

Due to the slow speed of the drive shaft, a bronze (ASTM B505) bushing will be fitted. The bushing is 3 mm thick, which gives a lid bore diameter of 72 mm. The bearing stress is checked between the bushing and the lid (54.8 MPa), and between the shaft and the bearing (59.8 MPa). Both bearing stresses are below the allowable stress of the aluminium alloy 5056-H18 (271.3 MPa) and ASTM B505 (92 MPa).

5.5.3 Shearing Mechanism Linkage Force and Stress Analysis

The slider requires a displacement of 20 mm in order to shear the smaller rebar sizes. The linkages will have the following starting angles: $\angle BAC = 40°$, $\angle ABC = 119.9°$, and $\angle BCA = 20.14°$ at first contact with the rebar. When the mechanism is fully extended, the angles will be $\angle BAC = 19°$, $\angle ABC = 150.956°$, and $\angle BCA = 10.04°$.

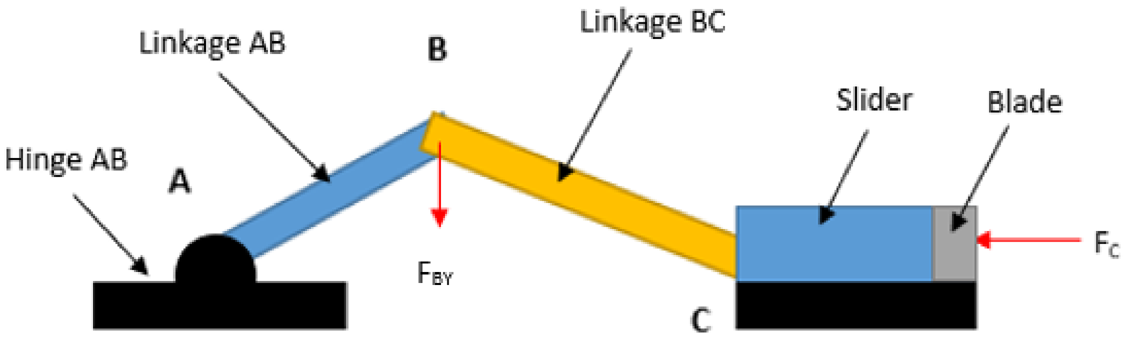

Figure 5.54: Schematic of linkage system to move cutting blade

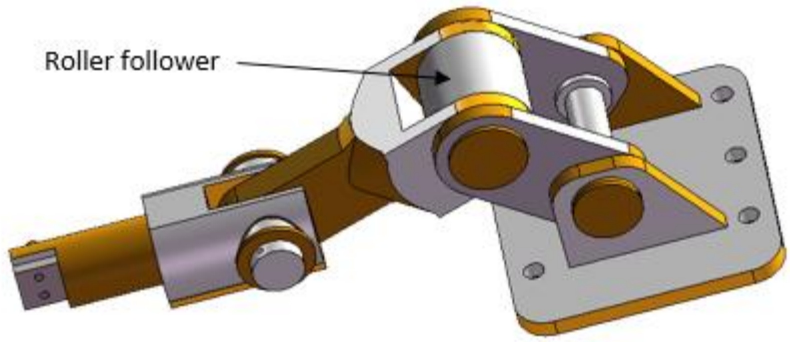

Figure 5.55: Solidworks model of the cutting mechanism

Knowing the force to shear the rebar; trigonometry is used to determine both the forces exerted on each of the linkages and the amount of force required for the cam to push down at point B, F_{BY} (*Figure 5.56*). The most significant force the mechanism will experience will be at the beginning of the shearing phase of the rebar.

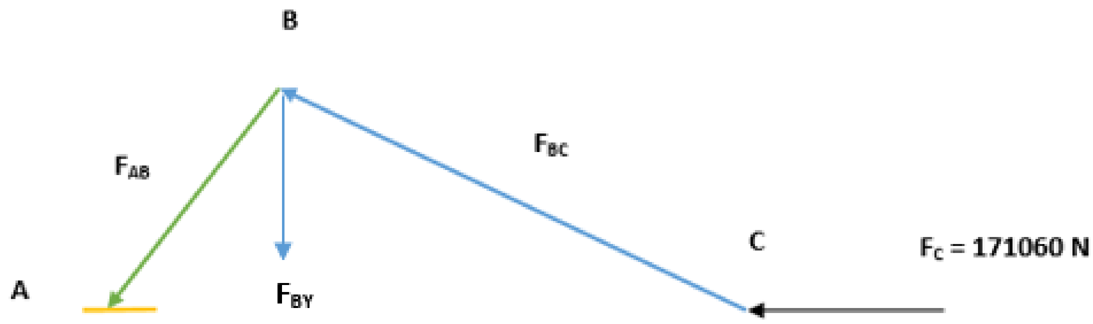

Figure 5.56: Force diagram of linkage system

The forces on each of the linkages are (*Appendix 7.4.1*): F_{AB} = 90.8 kN (linkage AB), F_{BC} = 182.2 kN (linkage BC), and F_{BY} = 62.7 kN (the force required to push the roller follower down). It should be noted that the value of F_{BY} is the starting force required to push the follower down and will decrease as the mechanism reaches top dead centre. These forces will be used to determine the dimensions of the linkages.

5.5.3.1 Slider

The dimensions of the linkage system were assigned arbitrarily but were finalised after several iterations. Calculations were performed for the finalised dimensions to ensure the stresses were below the yield stress of the material.

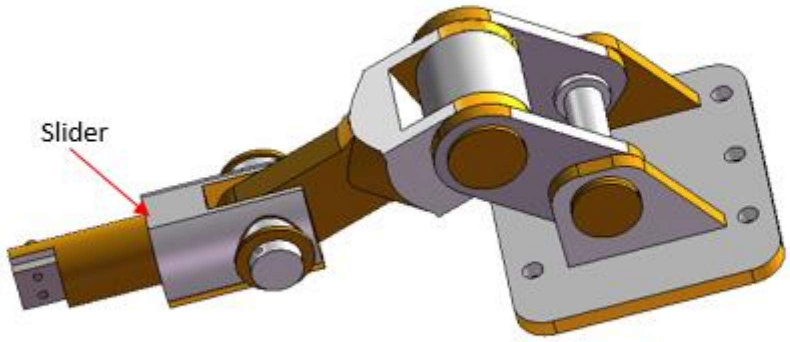

Figure 5.57: Components under consideration

The dimensions of the rebar shearing blade used for this tool will be the same blade used for the Cobalt International RC-22 rebar cutter, as both tools have the same shearing motions.

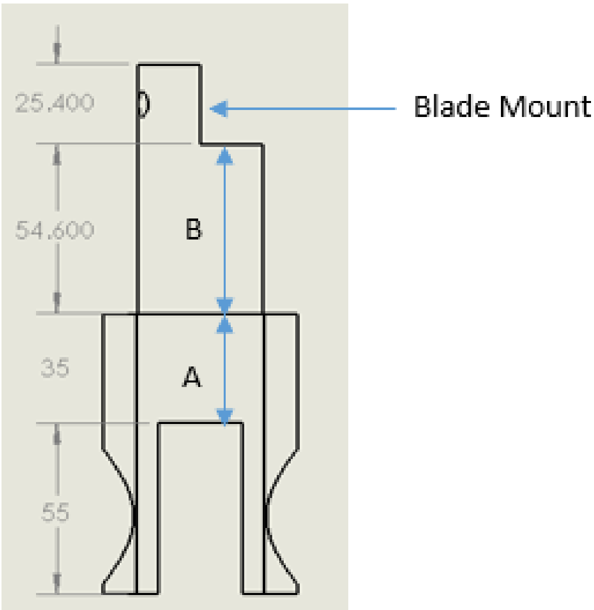

Figure 5.58: Dimensions of the slider

Beginning with the blade mount; the compressive and tensile stress will need to be calculated as the load creates a bending moment of 2538.2 Nm (*Figure 5.59*).

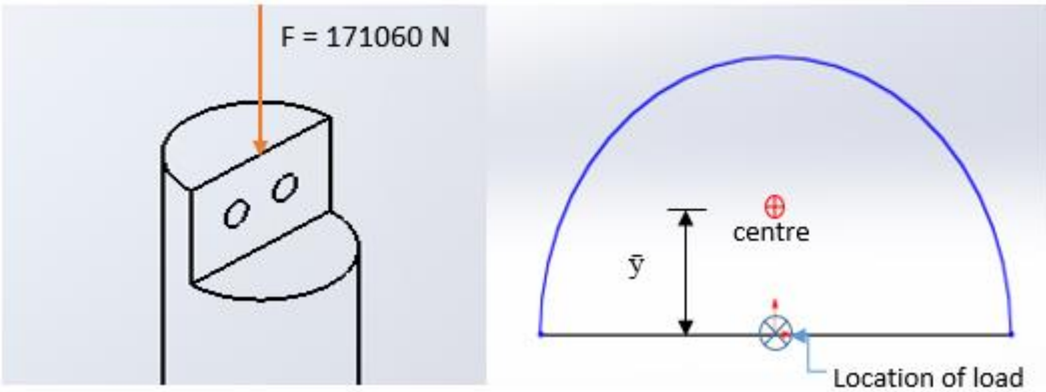

Figure 5.59: Location of load on slider

Both the compressive (-71 MPa) and tensile (615 MPa) stresses are below the allowable stress of the D2 tool steel (1.2 GPa), see *Appendix G7.1.1* for calculations.

Column theory can be used to determine the critical load and stress, also known as the buckling load and stress. The blade mount is the same as a column fixed at one end with a load applied at the top (*Figure 5.60(a)*).

Figure 5.60: Effective lengths of different loading conditions (Beer, Johnston, Jr, DeWolf, & Mazurek, 2006)

The calculations yield a critical compressive stress value of 17.3 GPa, which can be ignored as the blade mount would have buckled before 17 GPa could be reached. From the calculations, the critical force is 21.8 MN which is much higher than the applied force of 171.1 kN, meaning that the blade mount will not buckle (*Appendix G7.1.2*).

The loading in section A of the slider is similar to the loading condition represented in *Figure 5.60(b)*. The calculation yields a critical stress of 406 GPa and a critical force of 12.3 MN, which is much lower than the applied force of 171.1 kN.

Section B has the same loading condition as shown in *Figure 5.60(a).* The critical load and stress are calculated to be 21.8 MN and 17 GPa, respectively. The critical stress of both sections A and B are well above the yield stress of the material and are of no interest as the slider would have buckled before the critical stresses would be reached. The critical loads on the slider are far higher than the applied load of 171.1 kN, meaning that the slider will be able to withstand the applied load.

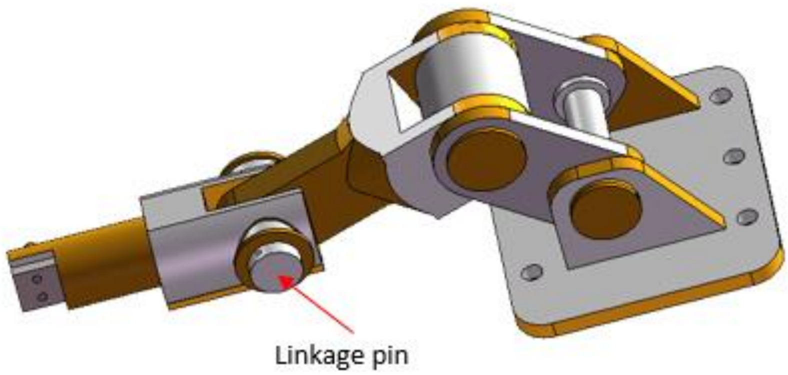

Figure 5.61: Components under consideration

Knowing the forces acting on the components of the shearing mechanism, the dimensions of the bottom half of the slider and the diameter of the pins can be determined. The pin connecting linkage BC with the slider will be made of L2 steel; the pin will most likely fail due to shear. The pin is supported on each side by the slider, meaning that a double shear will occur.

The allowable stress of L2 (non-heat treated) steel is $\sigma_{All} = 340\ MPa$; which also gives an allowable shear stress of $\tau_{All} = 170\ MPa$. Using the allowable shear stress, the minimum diameter of the pin connecting the slider and link BC can be found to be 30 mm. Bushings instead of roller bearings will be used as the speed of the mechanism is slow (maximum velocity of the slider is 0.0015 ms^{-1}). The diameter of the pin holders needs to be large enough to accommodate the pin and bushing, which will be discussed in *Section 5.5.3.2.*

5.5.3.2 Linkage BC

The thickness of link BC was calculated for the linkage acting directly on the 30 mm diameter pin (*Figure 5.63*), as this would give a more conservative thickness. The yield stress of L2 steel (material of pin) will be used since the allowable stress is lower than that of D2 steel. Using the allowable stress of L2 steel as the minimum bearing stress and the diameter of the pin (30 mm), the thickness of linkage BC is determined to be 20 mm (*Appendix G7.1.3* and *G7.2.1*).

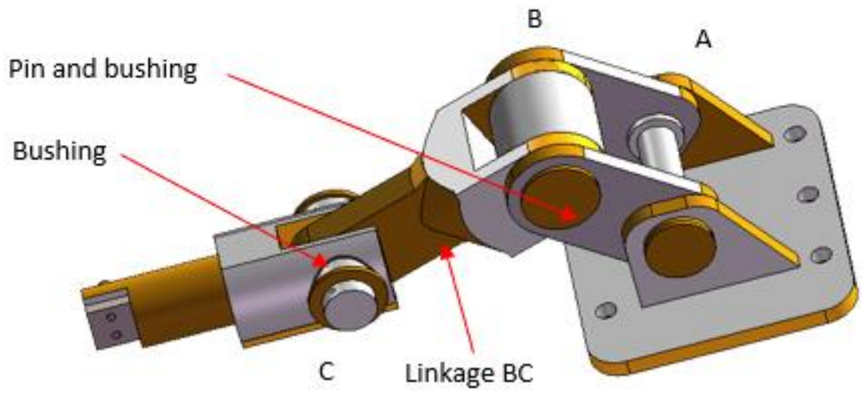

Figure 5.62: Components under consideration

Figure 5.63: Bearing area is approximately the projected area of the pin (Beer, Johnston, Jr, DeWolf, & Mazurek, 2006)

As the bushings (that encase the pins) also experience high bearing loads, it was decided that a bushing wall thickness of 5 mm (giving an outer bushing diameter of 40 mm) would provide a suitable amount of material to wear through before a replacement is required. The outer bushing diameter will be used on the pin supports of the slider and linkage BC. The bearing stress acting on the bushing will be calculated and compared to the allowable stress of nickel aluminium bronze ($506.6\ MPa$). According to the calculation (see *Appendix G7.2.1*), using the highest force exerted by linkage BC (182.2 kN), the bearing stress experienced by the bushing is 227 MPa, which is below the allowable stress.

Column theory can also be applied to the analysis of linkage BC. The linkage is hinged on both ends, similar to *Figure 5.60(b)*. Knowing the maximum force acting on the linkage (182.2 kN) and the equivalent length (0.14 m), these values can be used to determine whether or not buckling of the linkage will occur. For this calculation, the linkage will be simplified to a rectangular block. As the linkage has a rectangular cross-section, the critical load will have to be calculated in x- and y-directions (*Figure 5.64*).

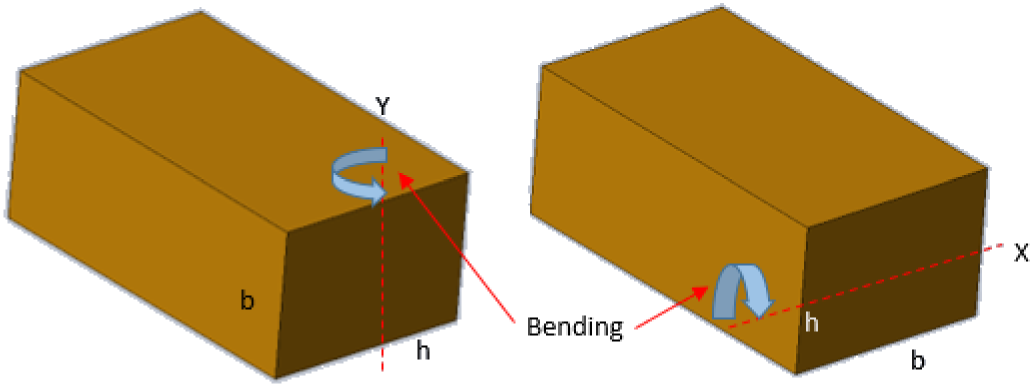

Figure 5.64: Two possible directions of buckling about Y (left) and X (right)

Figure 5.65: Loading on the simplified linkage BC

The critical forces in bending about y- and x-directions are 3.52 MN and 22 MN respectively and are above the applied force (182.2 kN) indicating that this linkage will not buckle (see *Appendix G7.2.2*).

The diameter of the pin located at point B (*Figure 5.62*), which supports both the roller follower and linkage AB, needs to be determined. The maximum force (182.2 kN) that the pin will experience will come from linkage BC. As the force is the same on both ends of the linkage, the pin at point B will have the same diameter as pin C connecting the slider to linkage BC.

Bending will most likely occur on the base due to the force acting on linkage BC's pin supports; therefore, the bending calculation was performed on one side of the base of link BC hinge, as it is symmetrical (*Figure 5.66*).

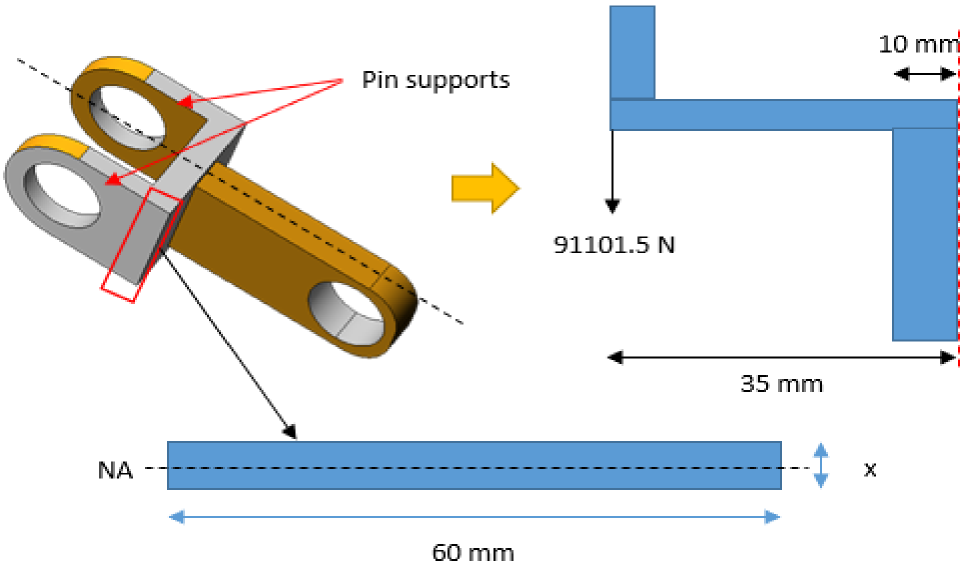

Figure 5.66: Half section of linkage BC. Showing base of linkage BC that will experience bending

Knowing the allowable stress of D2 steel (1.2 GPa), the distance from the bottom edge of the base to the neutral axis, and the bending moment, the minimum thickness of the base 'x' is calculated to be 15 mm (see *Appendix G7.2.3* for calculation).

5.5.3.3 Linkage AB, Pins and Bushing

Moving onto linkage AB, the diameter of the hole where linkage BC and AB meet (indicated by point B in *Figure 5.62*) will have the same diameter as linkage BC (40 mm). The two linkages AB are used on the shearing mechanism (*Figure 5.67*); it is assumed that the forces (*Section 5.5.3*) are evenly divided between the linkages (45.4 kN each). First, the diameter of the pin connecting linkage AB to the hinge is calculated using the allowable shear stress of L2 steel; this gives a pin diameter of 22 mm (see *Appendix G7.3.1* for calculation).

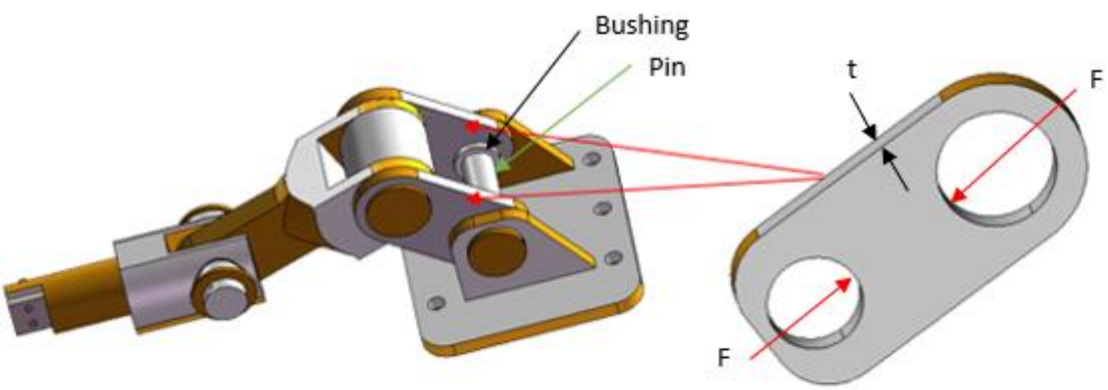

Figure 5.67: Linkage AB with forces, F, and thickness, t, indicated. Bushing (opposite bushing hidden), and pin

The thickness of the plates is determined by the bearing area acting on the pin, with the bearing stress being the allowable stress of L2 steel. The calculation yields a thickness of 10 mm (see *Appendix G7.3.1*).

A bushing with a 5 mm wall thickness encases the pin which creates a total outer diameter of 32 mm. The bearing stress is then calculated again to ensure that it is under the allowable stress (506.6 MPa) of the bearing material. The bearing stress is found to be 206 MPa (see *Appendix G7.3.1*).

Column theory is also applied to linkage AB to determine the maximum force that could be applied to the linkage before it buckles. As linkage AB has a rectangular cross-section, the critical force needs to be calculated about both x- and y-direction (*Figure 5.64*). The loading condition of linkage AB is shown in *Figure 5.60(b). K*nowing the dimensions and the equivalent length (75 mm) of linkage AB, the critical buckling force about the x-axis is determined to be 1.84 MN and 66.3 MN about the y-axis. The critical force of linkage AB is well above 45.4 kN, meaning that the linkage will not buckle (*Appendix G7.3.2*).

5.5.3.4 Hinge AB

The second to last part to analyse of the shearing mechanism is the hinge. The forces acting on linkage AB are divided into their x- and y-components (*Figure 5.69*).

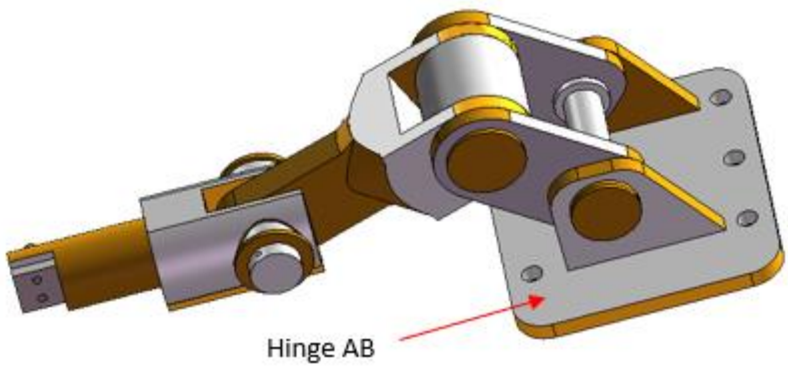

Figure 5.68: Components under consideration

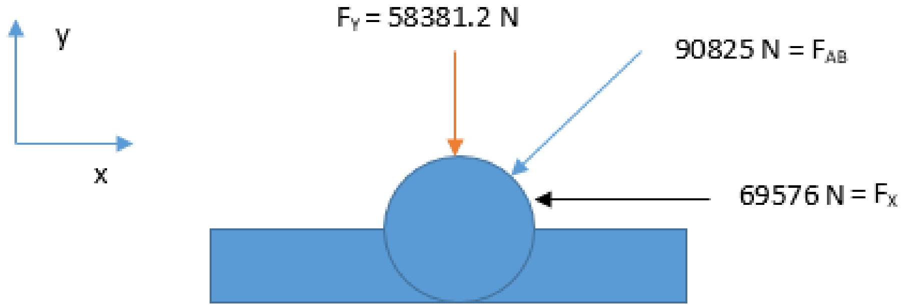

Figure 5.69: x- and y-component forces acting on hinge AB created by linkage AB

It is assumed that the two supports of hinge AB will share the applied force evenly. Each of the supports can be approximated as a cantilever beam for a simplified analysis.

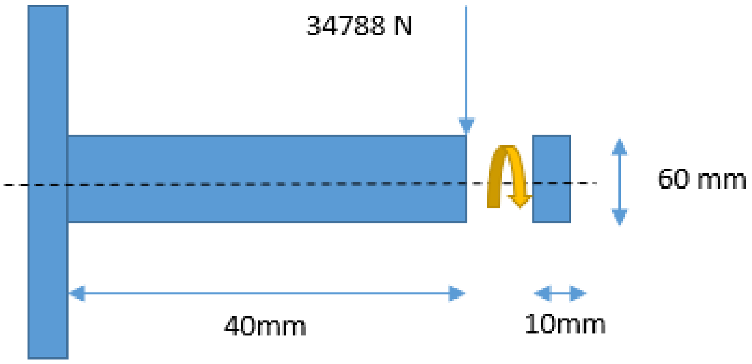

Figure 5.70: Hinge AB simplified to cantilever

Knowing the dimensions of the bushings, pins, and clearances, the dimensions of the supports of hinge AB (*Figure 5.70*) will be used to determine the bending stress of hinge AB. The calculated bending stress (see *Appendix G7.4.2*) is 232 MPa which is below the allowable stress of D2 steel (1.2 GPa).

The next step is to determine the thickness of the base of hinge AB. In order to determine the thickness, it is assumed that only one end of the base is fixed. The width of the base is determined by the thicknesses of the other linkages, and space for the bolts. NA indicates the neutral axis of the plate in *Figure 5.71*.

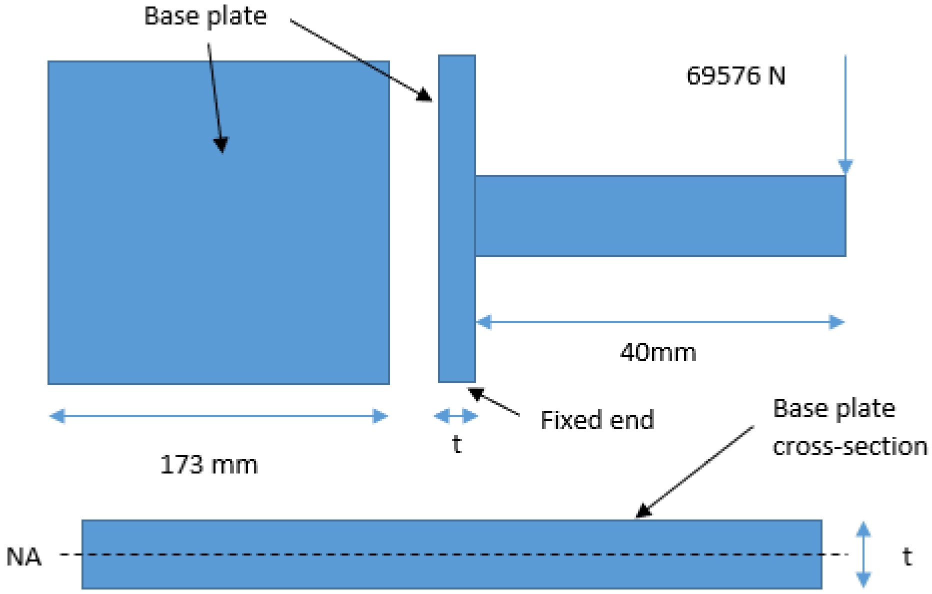

Figure 5.71: Bending of hinge AB base

Knowing the allowable stress of D2 Steel, and the bending moment, the thickness of the base is found to be 10 mm (see *Appendix 7.4.3*).

To calculate the diameters of the bolts that will be used to secure the hinge to the case, an assumption is made that the forces in the x-direction evenly load the bolts (*Appendix G7.4.4*). Each bolt will experience 13915.2 N of force. A grade 8.8 will be used to secure hinge AB to the housing ($\sigma_{all} = 426.6\ MPa, \tau_{all} = 213.3\ MPa$); with the allowable shear stress, the minimum diameter of the bolts is calculated to be 10.5 mm. However, 10.5 mm diameter bolts are not available, so the next largest bolt of diameter 12 mm will be used instead.

5.5.3.5 Return Spring

The final part of this mechanism is the spring that will push the whole shearing mechanism back to ensure constant contact between the cam and the roller follower. To calculate the spring constant required, the mass of the linkages and the slider need to be known. Using Solidworks, the total mass of these components is 5.53 kg. Placing the total mass of the mechanism at point B (*Figure 5.73*), the force required to push the mechanism up against the cam, F_c, is calculated to be 306.8 N (see *Appendix G7.5*).

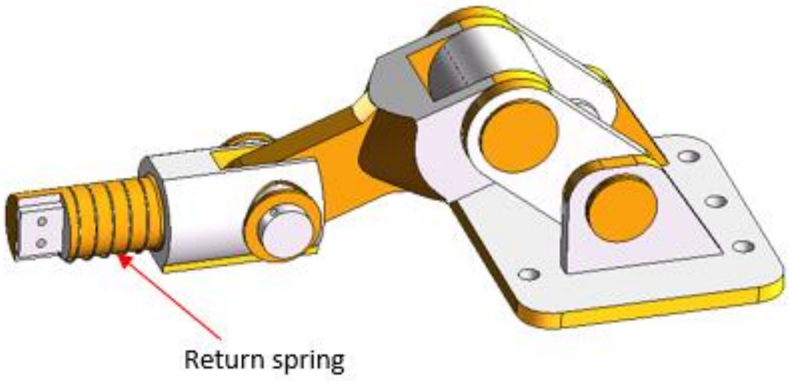

Figure 5.72: Components under consideration

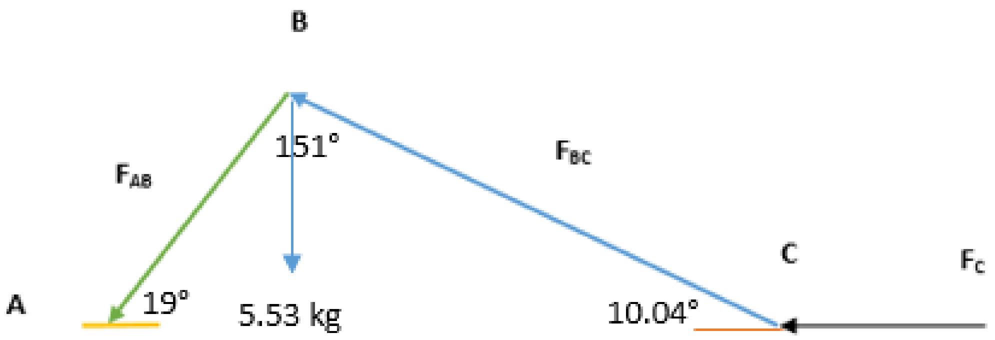

Figure 5.73: Force diagram for required spring constant when mechanism is fully extended.

Knowing the distance between the wall of the housing and the slider when the linkage system is fully retracted, gives a clearance of 50 mm for the spring to be fitted. Knowing the force; an estimated spring constant can be calculated using *Equation 5.5.16*. The slider moves 20 mm from the initial position of the linkage system to the final position as shown in *Figure 5.73*. An estimated spring constant of 15348.8 Nm^{-1} is determined using the aforementioned values (*Appendix G7.5*). This spring constant will change depending on the free length of the spring. From the Spring Store catalogue, a spring with a 13000 Nm^{-1} spring constant and a free length of 63 mm was chosen (PC190-2000-6250-MW-2500-CG-N-IN). A total spring displacement of 33 mm is required for the spring to fit between the wall of the housing and the slider and compress 20 mm. Knowing these values, the amount of force that the spring will be pushing back on the mechanism is 429 N (see *Appendix G7.5*), which is higher than the required 306.8 N. This means that the spring can push the mechanism back and keep the follower in contact with the cam. The extra force from the spring is negligible to the rest of the components. For example, at the starting position of the shearing mechanism, the force from the spring is 169 N. This means that linkage BC will have a compressive force of 182381 N; comparing this to the original force of 182201 N, the difference is negligible.

5.5.4 Cam and Follower

The calculations for designing the cam needs to take into account the cam and follower's eccentricity which affects the speed of the slider and the pressure angle. First, the equations defining the rise and return profile of the cam need to be selected. *Figure 5.76* shows the chosen curves H-5 and H-6 as they are the most suitable for the rise and return motion of the cam. The displacement curves of H-5 and H-6 provide a smooth convex profile. A trial rise angle range (0°-150°) is selected for the equations that are given in *Figure 5.76.* The pressure angle, α_P, can be calculated using the prime radius, R_p (*Figure 5.75*), the governing equations of the H-5 curve and the eccentricity. Only the rise section of the curve (H-5) will be used for the calculations as it is the curve that is under load.

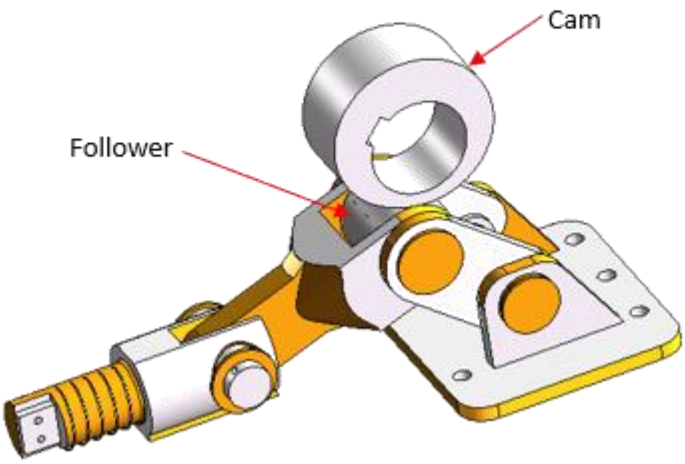

Figure 5.74: Components under consideration

Figure 5.75: Dimensions of cam and follower (Norton, 2002)

The maximum pressure angle will occur at the mid-rise of the cam. The eccentricity, ε, at mid-rise is 8.144 mm due to the lateral movement of the shearing mechanism's roller follower. Using this information, the maximum pressure angle is 4.16° (see *Appendix G7.6* for calculations).

Figure 5.76: Harmonic curves (Kloomok and Muffley, as cited in Mabie and Reinholtz, 1987)

A check needs to be performed to determine if the profile contains any cusps by calculating the radius of curvature, ρ, at the peak of the cam (at 150°) as this is where a cusp is most likely to occur. When $\rho = 0$, a cusp will form, if $\rho > 0$, the cam profile is convex, and when $\rho < 0$, the cam profile is concave.

With the displacement, acceleration and velocity equations for curve H-5, the radius of curvature is calculated to be 13.8 mm. As the radius of curvature is greater than zero, this means that no cusps will form, and the cam is convex, allowing the roller follower to move smoothly with the cam.

5.5.4.1 Contact stress

The contact stresses between the cam and the follower need to be determined to allow the selection of a suitable material. The cam and roller follower can be approximated as two parallel cylinders. The stress experienced by the cam and roller follower is expected to be high. In order to calculate the contact stress (see *Appendix G7.6*), the smallest radius of curvature located at the peak of the cam will be used. Generic steel values of Poisson's ratio, Young's modulus and a length of 50 mm were used to estimate the stress experienced by the cam and follower, and the contact stress was found to be 2.21 GPa. Adding a factor of Safety of 1.5, the yield stress of the material will need to be approximately 3.32 GPa. The only material that could be found with a similar yield stress is ASSAB PM 30 SuperClean steel, with a compressive yield stress of 3.5 GPa. Using the values provided by the datasheet (*see Appendix D2*) the actual contact stress between the cam and follower is 2.36 GPa. The contact stress is slightly above the allowable stress of the PM30 steel (2.33 GPa). However, a small difference between the maximum stress and the allowable stress is of little consequence.

5.5.4.2 Torque and Velocity

The maximum torque occurs when the pressure angle is at its maximum. Knowing the follower's radius, the base circle radius and the maximum pressure angle of the cam (at mid-rise), the force of 46 kN required to push down on the linkage system, the maximum torque required to turn the cam is calculated to be 280.25 Nm.

The maximum rise velocity also occurs when the pressure angle is at its maximum. Using the velocity in the y-direction, V_{BY}, and the velocity diagram (*Figure 5.77*) derived from the shearing mechanism's force diagram (at half rise), the velocity of the slider, V_c, is calculated to be 0.00158 ms^{-1} (see *Appendix G7.6*). The velocity is higher than the minimum speed (0.0012 ms^{-1}) to shear 20 mm rebar within 10 seconds, which also means that the rise angle range of 0-150° is acceptable.

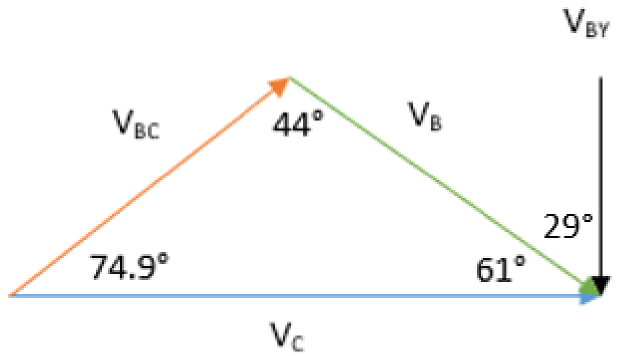

Figure 5.77: Velocity diagram when the cam is at half rise

5.5.5 Power Calculations and Motor Selection

From the shearing force and bending moment values shown in *Sections 5.2* and *5.3*, it is possible to calculate the amount of power required to bend and shear the rebar. Shearing cannot be assumed as the function that requires the most power; there is also the bending function to be considered. Knowing the torque, and the required time (15 seconds) to bend the rebar by 180°, the power can be calculated and compared with the power required to shear.

The force required to bend the rebar is 5.3 kN, and knowing the bending arm length (175 mm), the torque required to bend the rebar can be determined. With the rotational velocity and torque of the bending arm, the minimum required power to bend the rebar is 293.2 W (see *Appendix G9*). The power to shear can be determined in a similar method. Knowing the maximum slider velocity (0.00158 ms^{-1}), and the shear force (171.1 kN), the power required to shear the rebar is calculated to be 270.3 W (see *Appendix G9*).

Comparing the bending and shearing power, it is evident that bending requires more power. Using a factor of safety of 1.5 (to ensure that the motor has sufficient power to overcome any friction losses) a motor with a minimum power output of 439 W is required. From *Table 11*, the only suitable pancake motor (from the Printed Motor Company) is the GPM16LRD 005108 motor. The motor produces enough torque and power to bend and shear the rebar, and it also has a voltage rating low enough to allow a battery to be used as the power source (see *Chapter 7*).

Table 11: Brushed pancake motor specifications ("Brushed Pancake Motors", 2018)

Motor Model	**Rated Terminal Voltage [V]**	**Power [W]**	**Rated Continuous Torque [Nm]**	**Rated Speed [RPM]**
GPN12 005062	37.5	200	0.64	3000
GPM16LR 005016	24.0	221	0.84	3000
GPN16LR 005078	36	324	1.30	3000
GPM16LRD 005108	28	550	1.50	3000

5.5.6 Bearing Selection

Bearings will be required in the gearbox due to high rotational velocities experienced by the shaft and other components. Bearings will be selected from the NSK and SKF catalogues. According to the NSK and SKF catalogues, as there are no axial forces, the equivalent dynamic load is equal to the radial forces applied to the shaft.

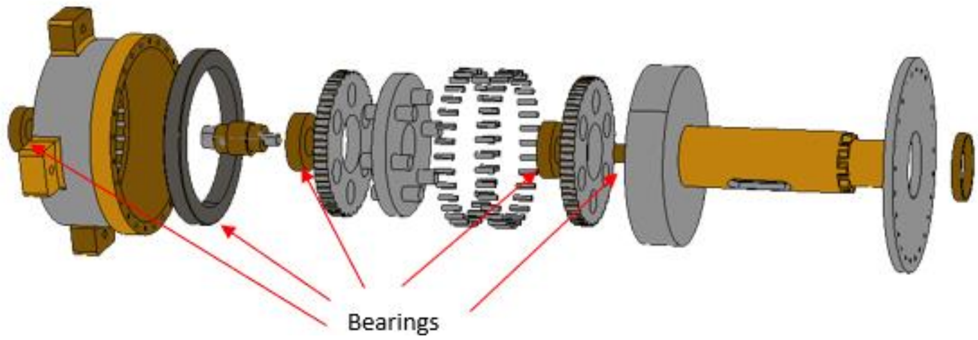

Figure 5.78: Components under consideration

Starting with the cycloidal discs, both discs exert a radial force of 9.2 kN on the shaft (as calculated in *Section 5.5.2.3*). From the NSK catalogue, the bearing 6008 ZZVVDDU with a basic dynamic load of 17.8 kN will be used. At the ends of the shaft, the loading is 9.25 kN and 9.15 kN, where the bearing 6206 ZZDDU with a dynamic load of 20.3 kN will be used.

Next, the outer bearing that fits around the central disc of the gearbox is selected. From the SKF catalogue, bearing 61832 will be used. The bearing has a basic dynamic load of 49.4 kN. The calculated force exerted on the bearing is 55.9 kN. However, it needs to be noted that the forces in the gearbox were calculated using the maximum possible torque output (1534 Nm), whereas the maximum torque that will ever be reached is 933.3 Nm (the torque required for bending rebar). The most likely force that will be exerted on this bearing is 33.9 kN.

5.6 Housing and Components Design

To perform the first principles analysis on the housing, the housing was simplified as a rectangular tube (the Solidworks model will be modelled with structural webbing and the actual shape of the housing). From this tube, a multi-load stress calculation was performed to determine the principal stresses on elements K and H (*Figure 5.80*). These stresses will then be compared to the allowable stress of the housing material (Magnesium alloy EA65RS-T4, σ_{all} = 306.6 MPa). As the housing is not 'fixed' to any solid structure and the calculations demand at least one side of an object to be fixed, a calculation needs to be performed on the sides of the housing where no forces are directly acting. This leaves only the back and top wall (*Figure 5.79*) of the housing where the sides can be fixed.

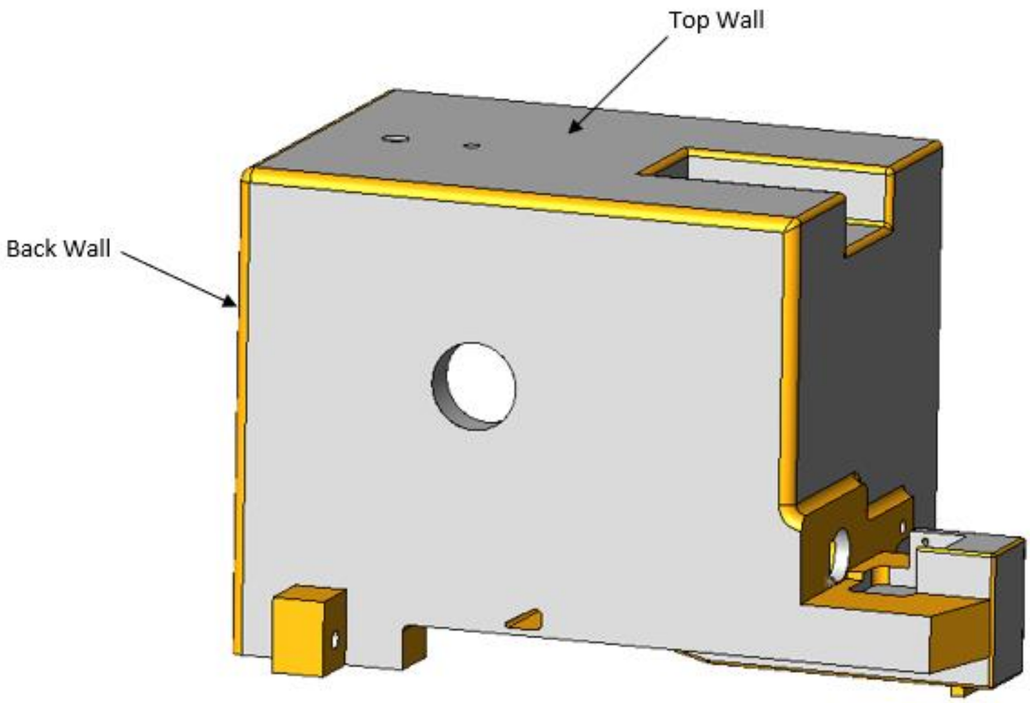

Figure 5.79: Housing constructed of magnesium alloy EA65RS-T4

5.6.1 Housing Back Wall Fixed Analysis

The housing will be analysed with a wall thicknesses of 3.5 mm (a standard plate thickness) to determine the principal stresses. The largest forces will be produced by shearing the rebar and will occur in different parts of the housing. These are the forces due to shearing that will be used for the first-principle analysis. The first calculation will be performed for the housing with the back wall fixed to the yellow wall (*Figure 5.80*).

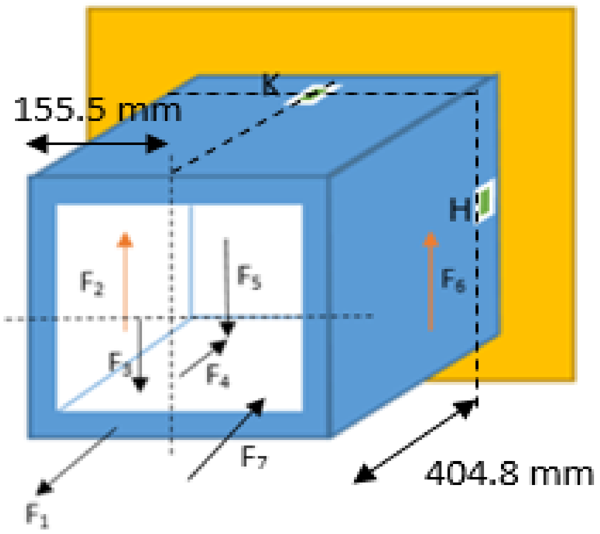

Figure 5.80: Forces acting on rectangular tube approximation of housing. F_1 = 171.1 kN, F_2=32.6 kN, F_3=62.7 kN, F_4=69.6 kN, F_5=58.4 kN, F_6=40.9 kN, F_7 = 4.13 kN

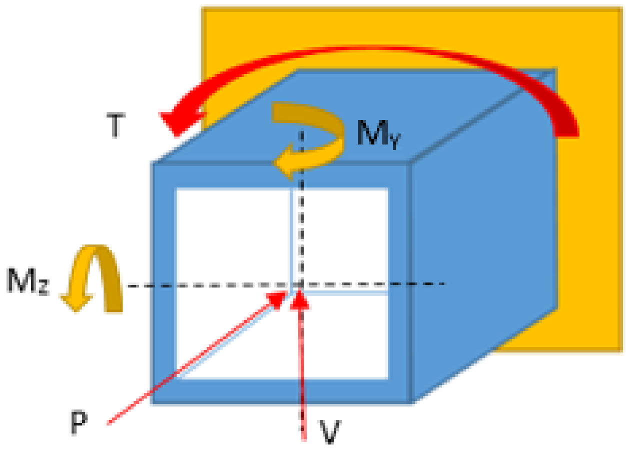

Figure 5.81: Moments and torques caused by forces acting in housing. Where T, P and F are torque horizontal and vertical forces respectively.

Using all the calculated values of shear and normal stresses, the principal stresses for each element can be calculated (*Table 12*).

Table 12: Principal stresses, back wall fixed

	Element K	**Element H**
τ_{max} **[MPa]**	39.44	74.3
σ_{max} **[MPa]**	43.39	54.5
σ_{min} **[MPa]**	-35.49	-94

The maximum shear and bending stresses calculated for elements K and H are below the allowable shear stress and allowable tensile stress of the magnesium alloy, τ_{All} = 153 MPa and σ_{all} = 306.6 MPa respectively. See *Appendix G5* for full calculations.

5.6.2 Housing Top Wall Fixed Analysis

The next orientation of the housing is analysed. For this analysis, the top surface of the housing is fixed (*Figure 5.82*). The same shearing forces are used for this orientation as well.

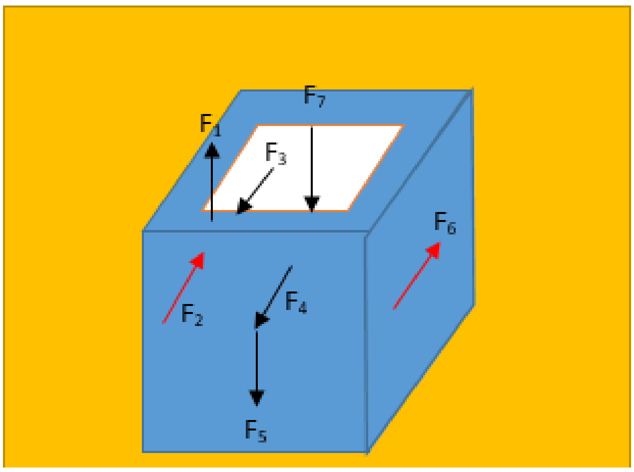

Figure 5.82: Top surface fixed to yellow wall. Forces acting on rectangular tube approximation of housing. F1 = 171.1 kN, F2 = 32.6 kN, F3 = 62.7 kN, F4 = 69.6 kN, F5 = 58.4 kN, F6 = 40.9 kN, F7 = 4.1 kN

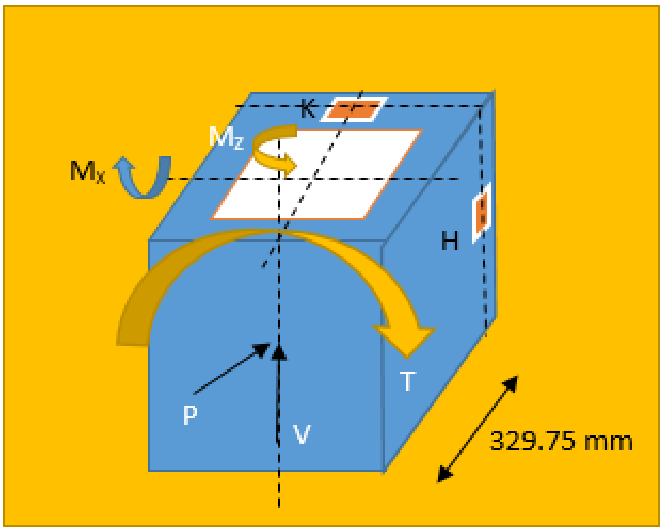

Figure 5.83: Top surface fixed to yellow wall. Moments and torques caused by forces acting in housing. Where T, P and F are torque horizontal and vertical forces respectively.

The same calculation procedure to determine the principal stresses is carried out for the scenario where the top surface of the housing is fixed. The sum of the horizontal forces, P, is calculated to be 13.7 kN, and the sum of all vertical forces is 97.4 kN.

Table 13: Principal stresses with top wall fixed

	Element K	**Element H**
τ_{max} **[MPa]**	81.5	76.2
σ_{max} **[MPa]**	157.6	71.8
σ_{min} **[MPa]**	-5.4	-80.64

According to the maximum normal stress criterion, none of the principal stresses (*Table 13*) exceed the allowable stress of the magnesium alloy, which means that the structure is safe. However, the housing will be modified on the Solidworks simulation package, where structural webbing will be added. For full working see *Appendix G6.*

5.6.3 Cutting Head Design

The next section of the case to be designed is the cutting head (*Figure 5.84*). The cutting head will be cast as part of the housing and provides support for the blade when the rebar is being sheared.

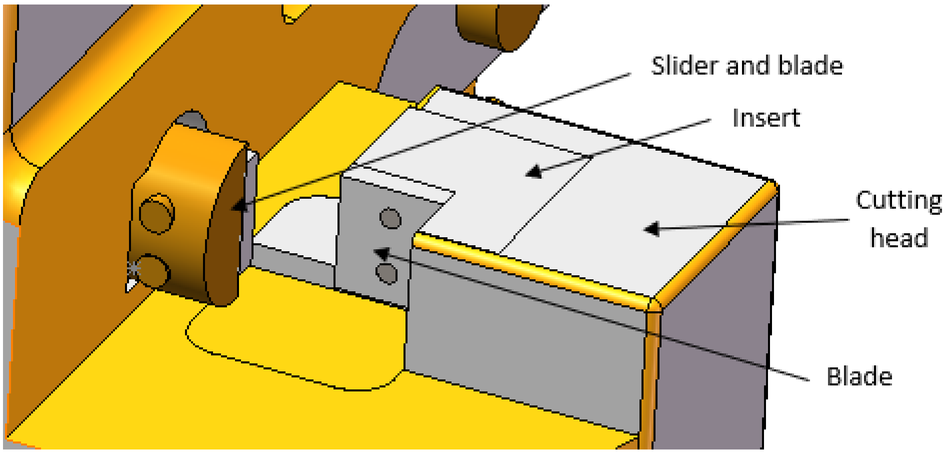

Figure 5.84: Cutting head

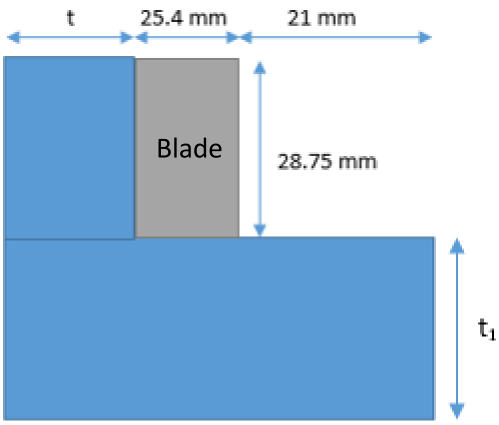

Figure 5.85: Side view of cutting head with dimensions, grey block represents blade

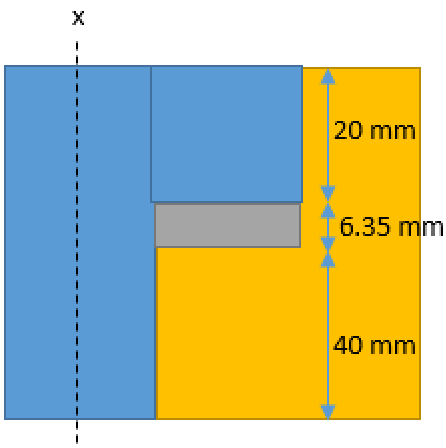

Figure 5.86: Top view of cutting head, showing dimensions and axis of bending

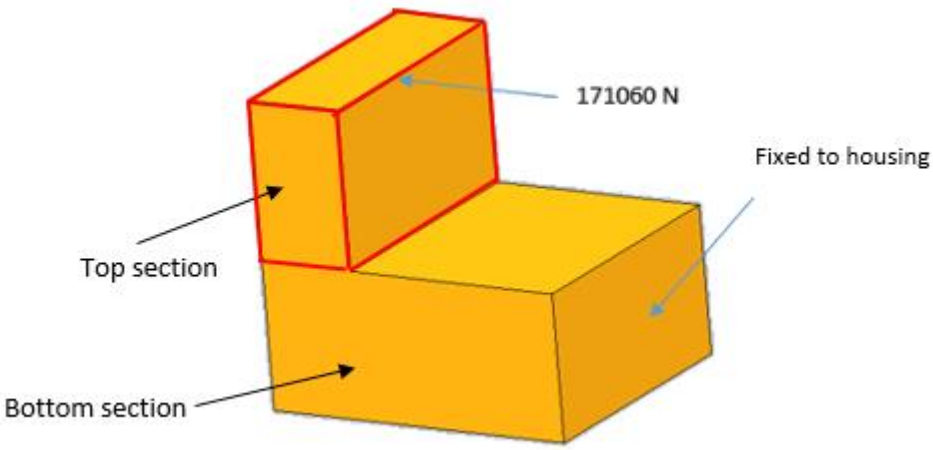

Figure 5.87: Forces acting on the cutting head

The top section (indicated in red in *Figure 5.87*) could be approximated to a cantilever with the bottom portion of the cutting head fixed. A bending moment about the x-axis (*Figure 5.86*) is created by the force required to shear the rebar. Knowing the allowable stress of the magnesium alloy (306 MPa), the thickness can be solved for 't' (see *Appendix G8.1*), which yields a minimum required thickness of 40 mm.

Next, the thickness t_2 (the bottom section of the cutting head) needs to be calculated by the same method. However, the location of the force will create an eccentric loading scenario (*Figure 5.88*).

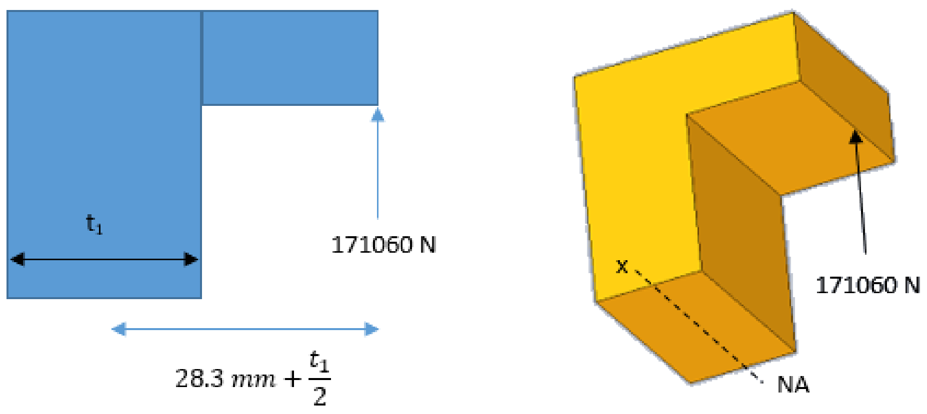

Figure 5.88: Eccentric loading of cutting head

Using the same method of calculation and solving for 't_1', the calculation yields a minimum thickness of 55 mm (see *Appendix G8.2*).

5.6.4 Insert Design

The insert holds the blade in place (*Figure 5.89*) and acts as a barrier between the blade and the cutting head. As shearing requires 171.1 kN of force, it is reasonable to assume that the stresses on this tool would be extremely high, especially for parts of the housing directly supporting the blade. Having the blade directly supported by the cutting head would create an area of high stress. The purpose of this component is to increase the bearing area on the cutting head and to lower the stress. The shape that will be designed here is subject to refinement (as with the parts designed here in the first principles section) using the simulation package in Solidworks. The dimensions of the shearing blade will be used as the starting dimensions for the insert. Assuming the blade is being pushed down onto the insert with the same force required to shear the rebar, the bearing stress between the blade and the insert is calculated to be 938 MPa (*Figure 5.90*). The blade dimensions are shown in *Figures 5.85* and 5.86.

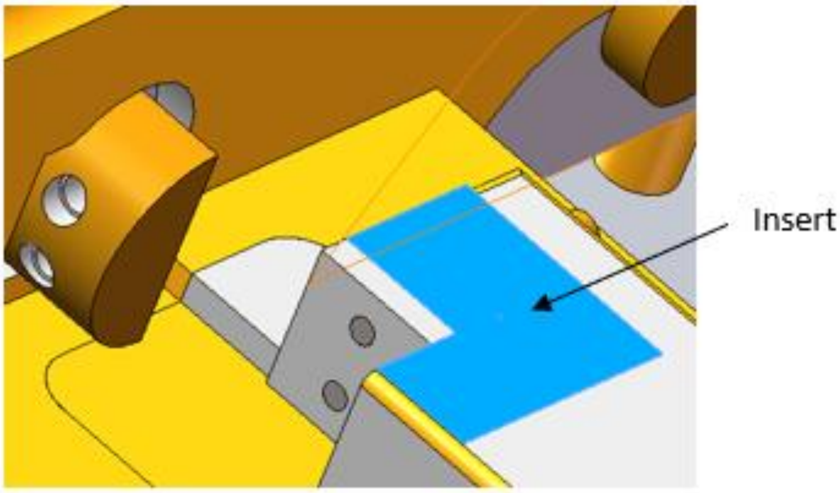

Figure 5.89: The insert with blade (insert is highlighted in blue)

Multiplying this bearing stress by the factor of safety of 1.5 gives the required yield stress of 1.4 GPa. This stress is above the allowable stress of D2 tool steel of 1.2 GPa, but below the allowable stress of ASSAB PM30 SuperClean steel of 2.4 GPa. As mentioned in *Section 5.1.2*, PM30 will be used for the insert.

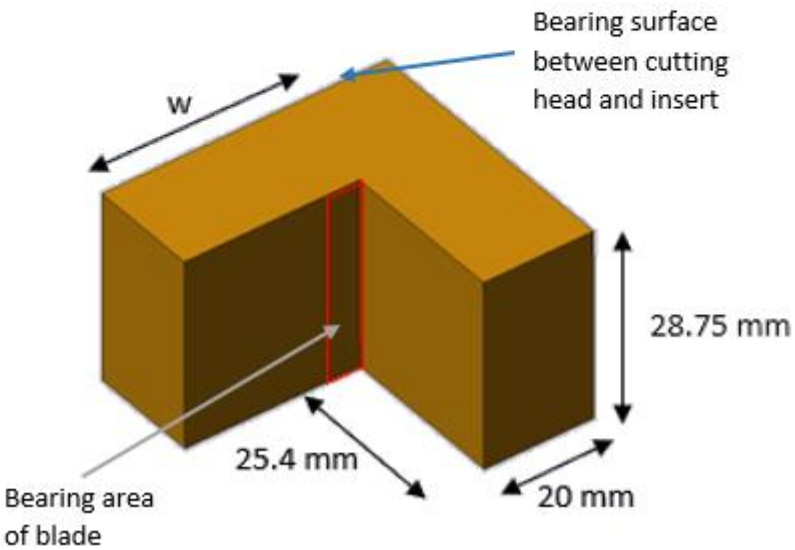

Figure 5.90: Dimensions of insert. The red square indicates bearing area of blade

Using the allowable stress of the housing of 306 MPa, the minimum bearing width between the insert and the cutting head is calculated to be w = 20 mm (*Figure 5.91*). The 20 mm thick wall (perpendicular to 'w') is there to provide an extra bearing surface area, which would make the distribution of stress more even on the cutting head. A Solidworks simulation will have to be performed to determine if this wall thickness is sufficient to distribute the stress, and to modify the insert accordingly if the stresses are above the allowable limit (*Appendix G10* for calculation). It was found that the shape of the insert (*Figure 5.90*) still exerted stress over the allow able stress of the magnesium alloy, Therefore the insert was modified on Solidworks (see *Section 6.4* and *Figure 6.38*).

5.6.5 Rebar Bending Stopper Block, Stopper Screw and Cap Design

The next feature on the housing that experiences a high load is the support block for bending the rebar (*Figure 5.91*). Assuming the rebar makes contact in the middle of the forming wheel, the distance from this point to the housing wall will be 23 mm (*Figure 5.92*). With force being applied away from the surface of the housing, bending of the support block will occur. Knowing the allowable stress of the magnesium alloy, and the force acting on the stopper block, the minimum thickness can be determined.

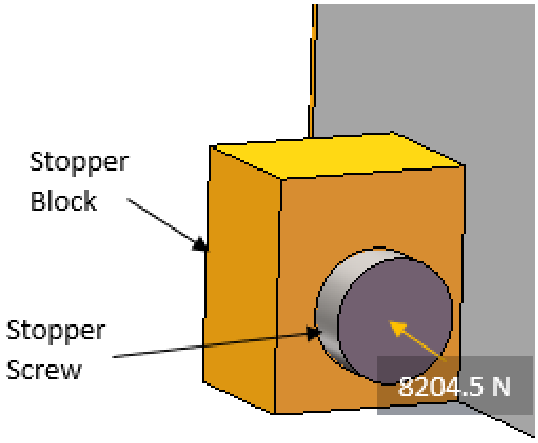

Figure 5.91: Rebar stopper block with stopper screw

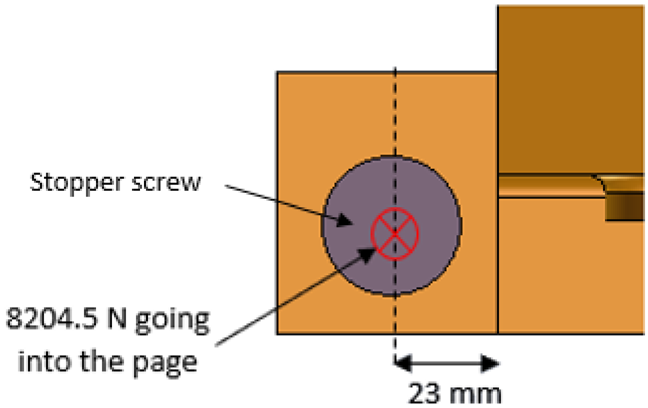

Figure 5.92: Distance from centre of stopper screw to wall of housing

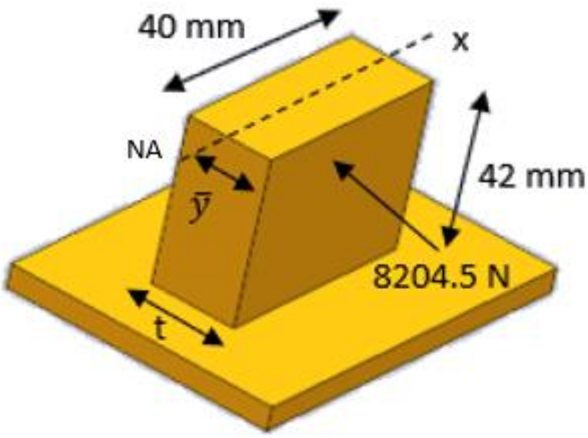

Figure 5.93: Simplified diagram of rebar bending stopper block

There is, however, a possibility that the user may inadvertently place the rebar at the top of the stopper block and not on the stopper screw. To mitigate this risk, the calculation for the block thickness is calculated for the full height of the block (42 mm, *Figure 5.93*). As a result, the minimum thickness of the stopper block is 13 mm (*Appendix G11.1*).

Due to the high forces from the rebar acting on the rebar stopper screw (*Figure 5.94*), the contact stresses between the rebar and the rebar stopper bolt needs to be determined. The loading scenario can be simplified down to a cylinder on a flat plane. The calculation yields a result of 1.22 GPa acting directly on the bolt. As grade 10.9 bolts have a yield stress of 940 MPa, a metal cap with a larger diameter (to reduce the contact stress) will need to be press-fitted over the bolt head to prevent the head from cracking. The cap will be constructed of D2 tool steel, the calculated contact stress between the stopper cap and rebar is 731 MPa (see *Appendix G11.2*) and is below its allowable stress of 1.24 GPa.

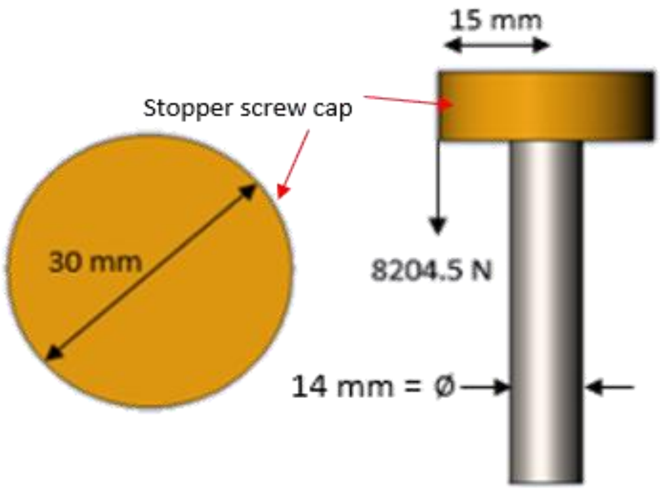

Figure 5.94: Possible loading conditions on bender stopper bolt

There is a high chance that the force applied to the bolt will not be placed in the centre of the bolt. Therefore, bending will most likely occur. Using the bending moment caused by the 8.2 kN force (*Figure 5.94*), the allowable stress of grade 10.9 bolt (σ_{all} = 626.6 MPa), and assuming that the screw is fixed at one end, the minimum diameter of the bolt is calculated to be 14 mm (see *Appendix G11.2*).

5.6.6 Shearing Rebar Stopper Screw and Cap Design

The same calculation to determine the contact stress and diameter of the stopper screw is performed for the rebar shearing stopper screw. First, the force acting on this screw needs to be calculated; this is achieved by treating the rebar as a beam and calculating the reaction forces created by the blade during shearing (*Figure 5.95*).

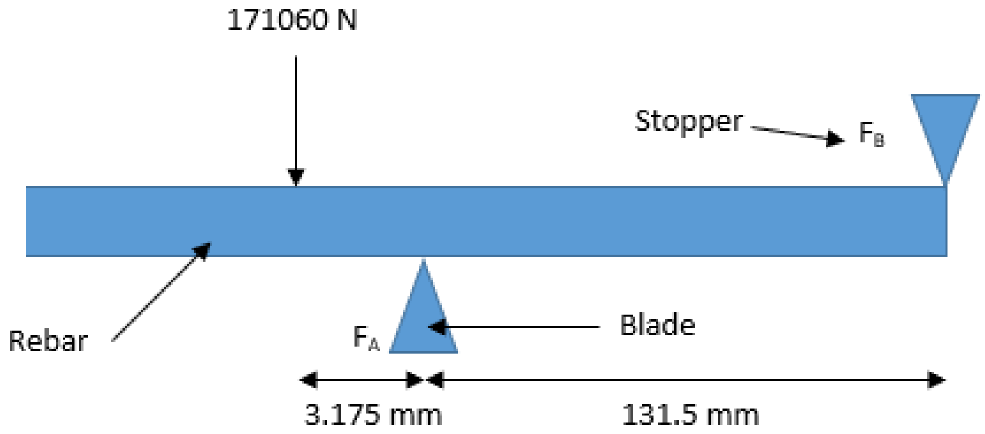

Figure 5.95: Forces created by shearing force. Where F_A is the blade attached to the housing and F_B is the stopper support screw

The reaction forces F_A and F_B are determined to be 166.9 kN and 4.13 kN respectively (see *Appendix G11.3*). With a force of 4.13 kN, and the allowable stress of a grade 10.9 bolt (626.6 MPa); the same calculation procedure is used to calculate the dimensions of this stopper screw. The stopper screw will have a minimum diameter of 10 mm and a bolt-cap (made of D2 steel) diameter of 30 mm. As the cap is the same size as the bending stopper cap and with a lower force acting on it, it can be assumed that the stress will be lower than the allowable stress of D2 steel (see *Appendix 11.3*).

5.6.7 Panel Securing Gearbox and Motor Design

The mounting blocks (*Figure 5.96*) for the gearbox and bolt holes that secure the panel onto the housing is next to be designed (see *Appendix G12* for calculations). The following assumptions are made, the panel is rigid, the mounting blocks are assumed to be uniform rectangular cantilevers, the panel is made of 5056-H18 aluminium alloy, and the forces are distributed evenly. The reason for having the gearbox raised off the surface of the panel is due to the dimensions of the electric motor that is mounted on the exterior of the panel. It should be noted that the panel has already been taken into consideration during the analysis of the housing. The principal stresses of element H show the stresses of the acting on the panel.

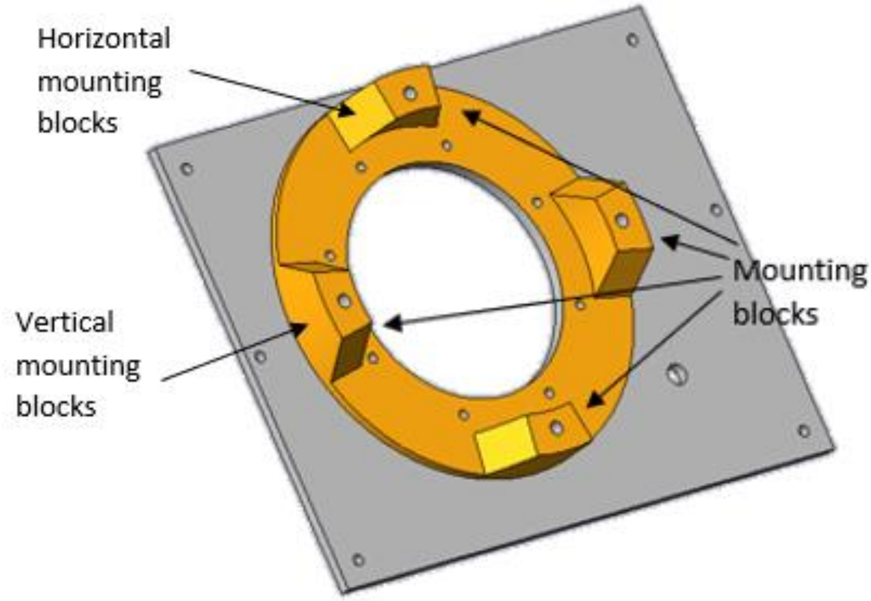

Figure 5.96: Panel securing motor and gearbox

First, the forces acting on the mounting blocks need to be calculated. There are two possible sources of the forces acting on these mounting blocks. The first force comes from the drive shaft when the rebar is being sheared, and the second force comes from the torque of the first stage ring gear of the gearbox. Knowing the upwards net force from the drive shaft (39.5 kN), and the force from torque (12.3 kN), the maximum force acting on a mounting block is 12.9 kN (see *Section 5.5.2.6*) as shown in *Figure 5.97*. The dimensions of the mounting blocks are determined by the dimensions of the motor, and by the dimensions of the finished housing.

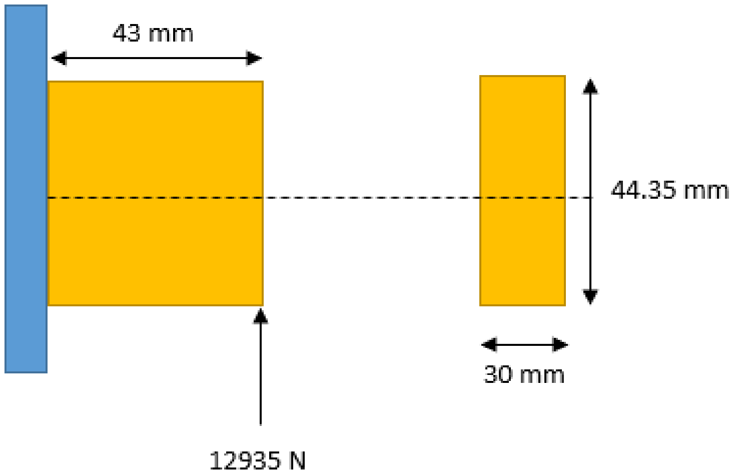

Figure 5.97: Force acting on gearbox vertical mounting block on panel

Knowing the bending moment, and the dimensions of the mounting feet, the bending stress of the vertical mounting blocks is calculated to be 56.7 MPa (*Appendix G12* for calculation).

Bending stress will also occur on the horizontal mounting blocks. However, the force on these mounting blocks will be less, as the force from the torque (3.1 kN per foot) is acting perpendicularly to the force from the main drive shaft (9.87 kN per foot) as shown in *Figure 5.98*. The bending stress of the horizontal mounting blocks caused by the main drive shaft is 64.1 MPa (see *Appendix G12* for calculation).

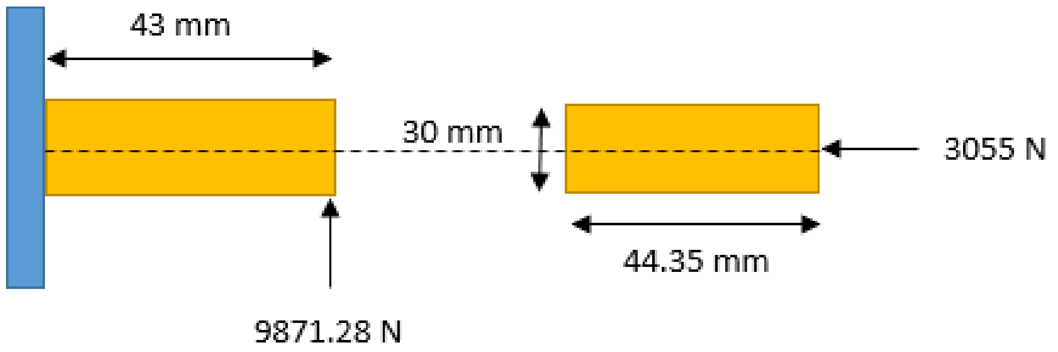

Figure 5.98: Forces acting on gearbox horizontal mounting block on the panel

The stress created by the force 3.1 kN (*Figure 5.97*) does require calculation. The vertical mounting blocks (*Figure 5.97*) are of the same dimensions and have a higher force of 12.9 kN applied in the same direction as the 3.1 kN force shown in *Figure 5.98*.

To secure the panel onto the housing will require six bolts located near the edges of the panel (*Figure 5.99*) with the assumption that the forces are evenly distributed. The maximum force that will be experienced by the bolts will need to be calculated; the bolt closest to the gearbox will most likely experience the greatest amount of force.

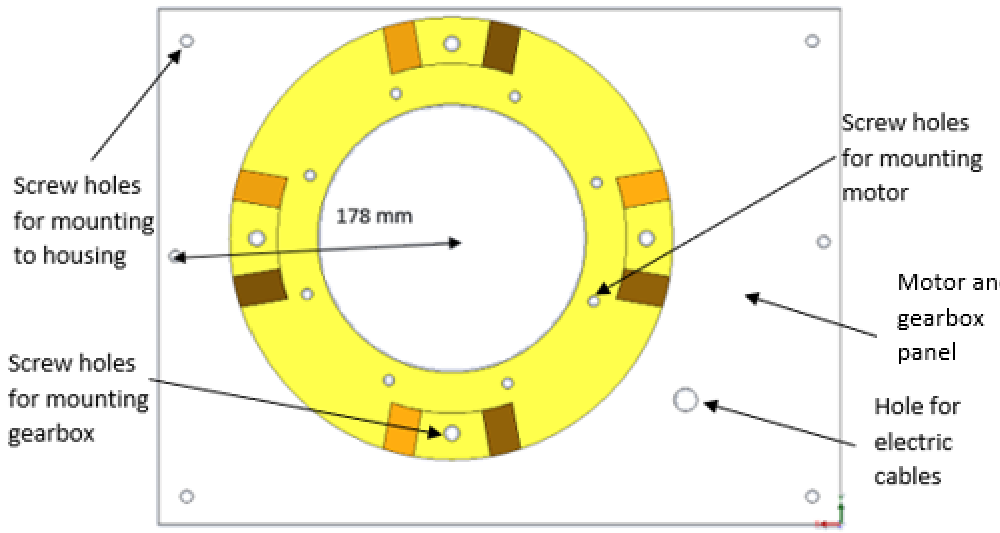

Figure 5.99: Panel showing closest bolt hole to centre of gearbox

Using the highest possible force created by the gearbox torque (8.6 kN) and the force from the drive shaft (39.5 kN), the force acting on each bolt is determined to be 8.1 kN.

With class 8.8 bolts (τ_{all} = 213.35 MPa), the diameter of the six bolts securing the panel the housing can be solved using the allowable shear stress. A minimum bolt diameter of 8 mm is determined. The diameters of the bolts securing the gearbox to the panel were determined in Section 5.5.2.6.

5.6.8 Handle Design

The final parts of the housing are the handles. The handle supports will be cast as part of the housing. From Solidworks, the estimated mass of the tool (including the battery) is 57 kg. From the research gathered in *Section 4.1*, and as the mass of the tool is over the allowable mass for a single person lift, it will require a minimum of at least two handles. These handles will have a silicon rubber exterior with a metal core. The purpose of the metal core is to protect the silicon rubber from wear and tear from the rod running through the handle (*Figure 5.100*). The metal core will be made from stainless steel for its resistance to corrosion.

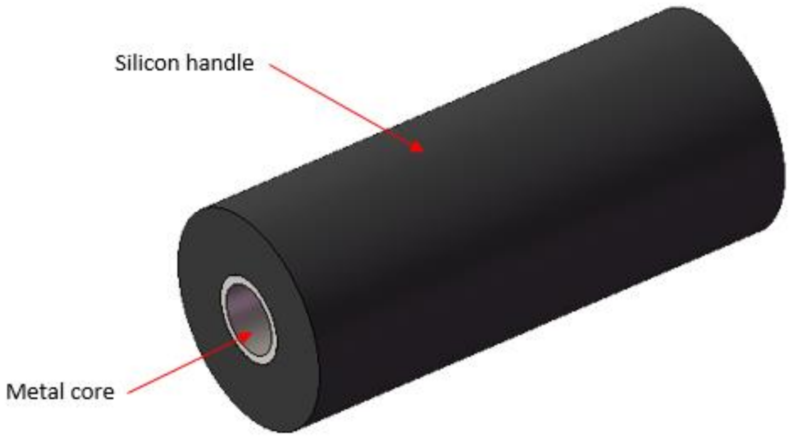

Figure 5.100: Handles of the rebar cutter and bender. Metal core is indicated in grey and silicon indicated in black

The average width of an adult hand is 100 mm as mentioned *Section 4.1*. However, the width of the handle will be 120 mm to give extra room, with a clearance of 40 mm clearance between the rubber handle and the housing for the hand to fit (*Figure 5.102*). Knowing the force due to the mass of the tool, the handle supports and rod (running through the core of the handle) can be designed.

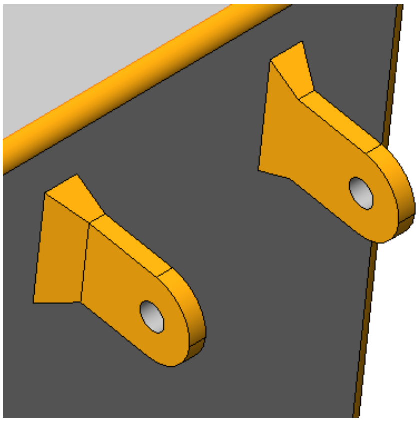

Figure 5.101: Handle supports on housing

Each handle support will be designed with the full weight of the tool acting on it. The worst-case scenario is that the tool is lifted using just one of the handles or by one of its supports, which is a situation that is likely to occur.

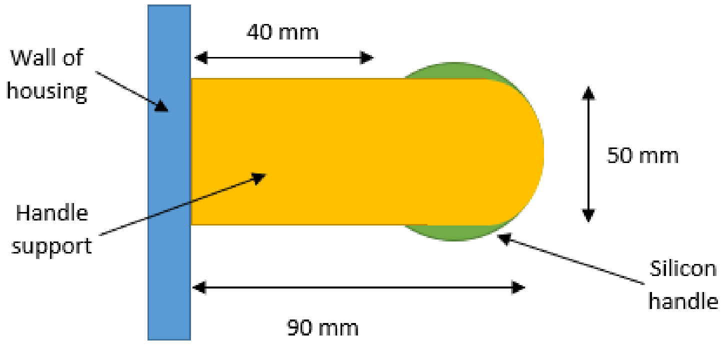

Figure 5.102: Dimensions of the handle support

The handle supports will bend most easily in the configuration shown in *Figure 5.103*. For this orientation to occur, the tool will have to be on its side when the rebar is being bent.

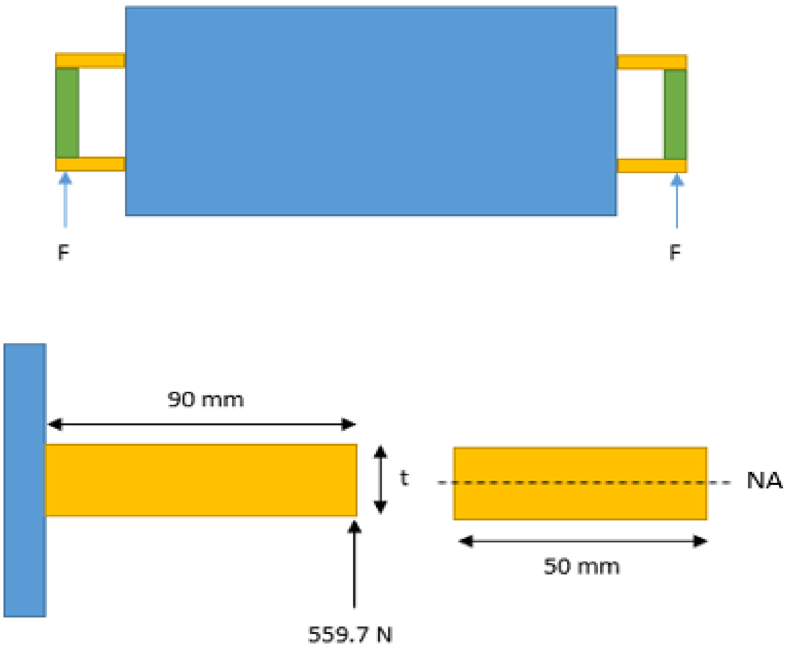

Figure 5.103: Bending of handle support with full weight acting on it when tool is on its side

Knowing the allowable stress of the magnesium alloy and the other dimensions shown in *Figure 5.103*, the thickness ‘t’ of the support, is calculated to be 10 mm (see *Appendix G13.1*).

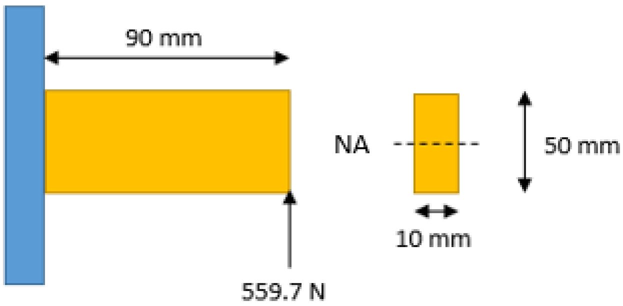

Figure 5.104: Bending of handle support with full weight acting on it when tool is on its side

To check that the bending stresses are below the allowable stress of the handle supports when the tool is carried in the upright position (*Figure 5.104*), the same method of calculation is used (see *Appendix G13.1*) giving a stress of 12 MPa, which is below the allowable stress of magnesium alloy (306 MPa).

The diameter of the rod that will run through the core of the handle needs to be defined. It is assumed that there is a possibility that only one handle will support the entire mass of the tool. As the rod is supported on both sides, a double shear scenario will occur. AISI 1141 medium carbon steel will be used ($\sigma_y = 660$ MPa, $\sigma_{all} = 440$ MPa, and $\tau_{all} = 220$ MPa). Since the forces will be divided equally between the handle supports, the calculation yields a diameter of 1.2 mm (see *Appendix G13.2*). However, it was decided that a bolt of a diameter of 16 mm would be a better option.

5.7 Conclusion of First Principles Analysis

In this chapter, a materials selection for individual components of the tool has been carried out. The materials selection was based on density, strength, and the component's application. Having defined the materials, the forces and torques required to shear and bend 20 mm rebar were calculated based on the 500E rebar material properties in *Section 2.4.3.* The shearing and bending forces were then used to determine the forces acting on shafts, gearbox, shearing mechanism, and the housing. Components with a complex shape, such as the housing, were then simplified to their basic shapes in which the forces were then applied to determine their stresses. In the following chapter, each component will be simulated in Solidworks to obtain a more accurate stress result based on their original shape.

6 Finite Element Analysis

Having calculated the dimensions based on the material properties and forces acting on each component in *Chapter 5* a finite element analysis was performed to determine a more accurate stress experienced by each component. This analysis is required as the first principles analysis calculations were based on the simplified shapes of the individual components. Due to the limitations of Solidworks, some loading conditions were approximated.

6.1 Linkage and Slider Mechanism

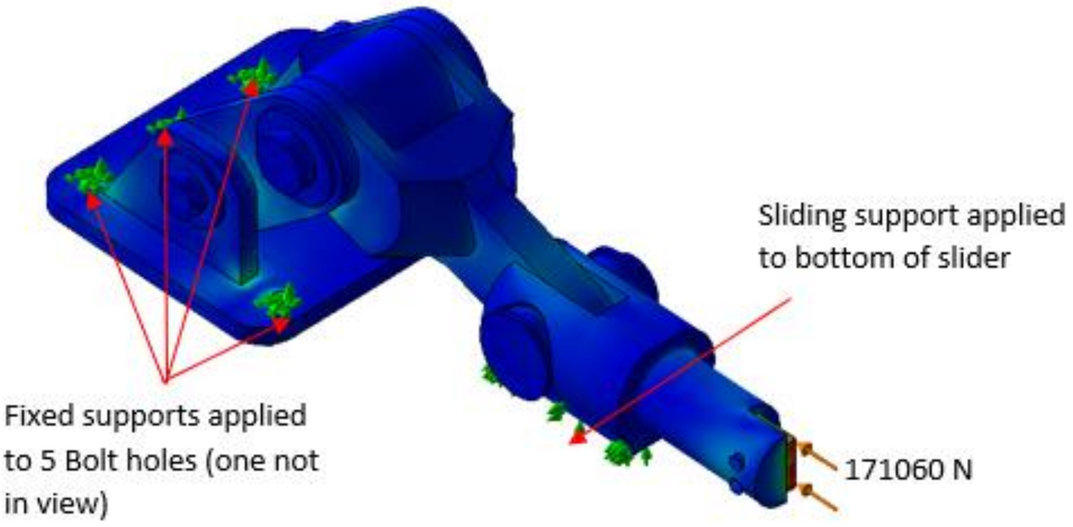

Figure 6.1: Assembled linkage and slider mechanism simulation

The simulation of the linkage and slider mechanism does not include the blade (as this would have been designed to withstand the shear forces). In order to simulate the bearing stress on the bushings and the pins, it was necessary to simulate the whole mechanism (*Figure 6.1*). The hinge plate was fixed at the bolt holes. In addition, the bottom sides of the slider were fixed as a sliding surface (allowing linear movement, but no vertical movement), and the shearing force of 20 mm rebar is then applied to the edge of the blade. From the simulation, all the stresses of the components (bushings and pins) were below the allowable stress of their respective materials. From the simulation, the highest stress the bushings experience is 220 MPa, which is below the allowable stress of nickel aluminium alloy (334 MPa). However, only the top edge of the slider and the corners of hinge AB were slightly above the allowable stress (1.2 GPa) of D2 steel (*Figure 6.2*). As the difference between the simulated stress and the allowable stress were relatively small, no changes to the slider were made.

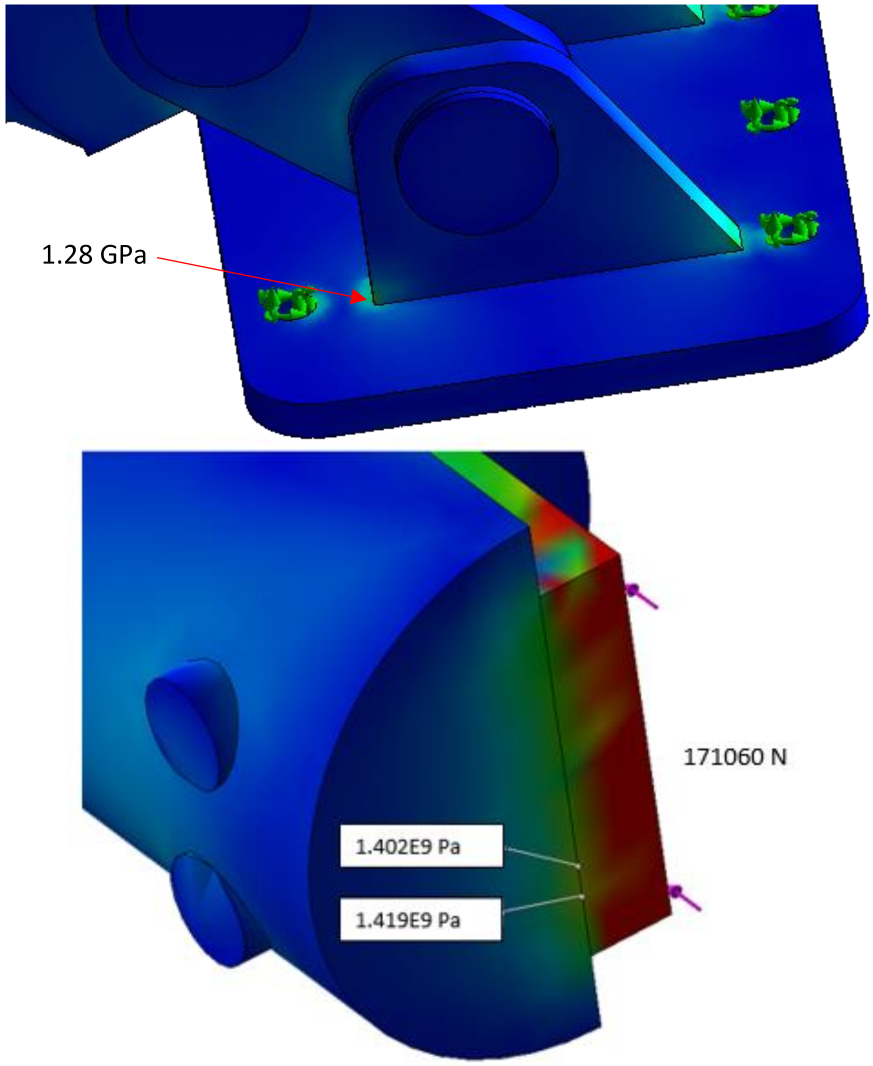

Figure 6.2: (Top) Close up of stress concentration of 1.28 GPa on hinge AB (Bottom) Close up of top of slider showing two nodes indicating a maximum stress of 1.4 and 1.419 GPa

Each linkage was then simulated with the forces calculated in *Section 5.5.3*. Starting with hinge AB (*Figure 6.3*), as the resultant force acting on this hinge is at an angle, the forces are split into two components (F_x = 69.5 kN, and F_y = 58.4 kN). These forces are divided evenly between the two supports with the fixed supports applied to the bolt holes. From the simulation, the highest stresses (860 MPa) occur around the bottom of the bolt holes and the pin supports. This simulation also shows that the highest stress that the bushings experiences is 220 MPa, which is below the allowable stress of nickel aluminium alloy (334 MPa).

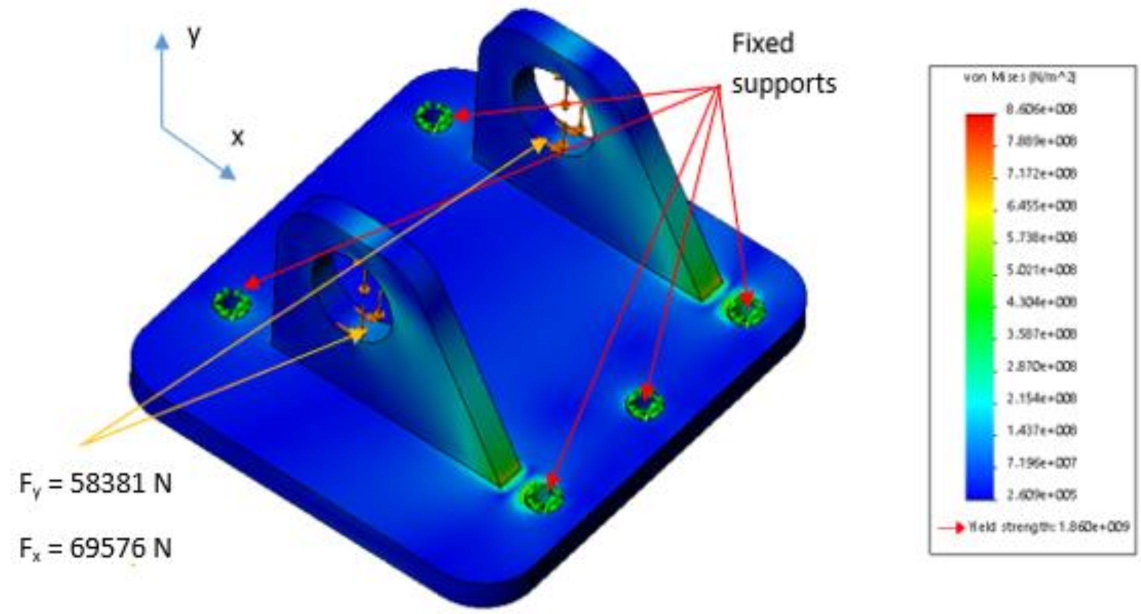

Figure 6.3: Simulation of hinge AB showing maximum stress of 860 MPa

Next, the linkage AB is simulated (*Figure 6.4*). The linkage has a fixed support applied at one end and a force a of 45.4 kN acting at the opposite end (*Figure 6.4*). Note, the forces are divided evenly between the two linkages; therefore, only one simulation was required. From *Figure 6.4*, the highest stress is located at the bottom half of the hole that connects with the AB BC pin (273 MPa). However, the stresses are below the allowable stress of the D2 steel (1.2 GPa).

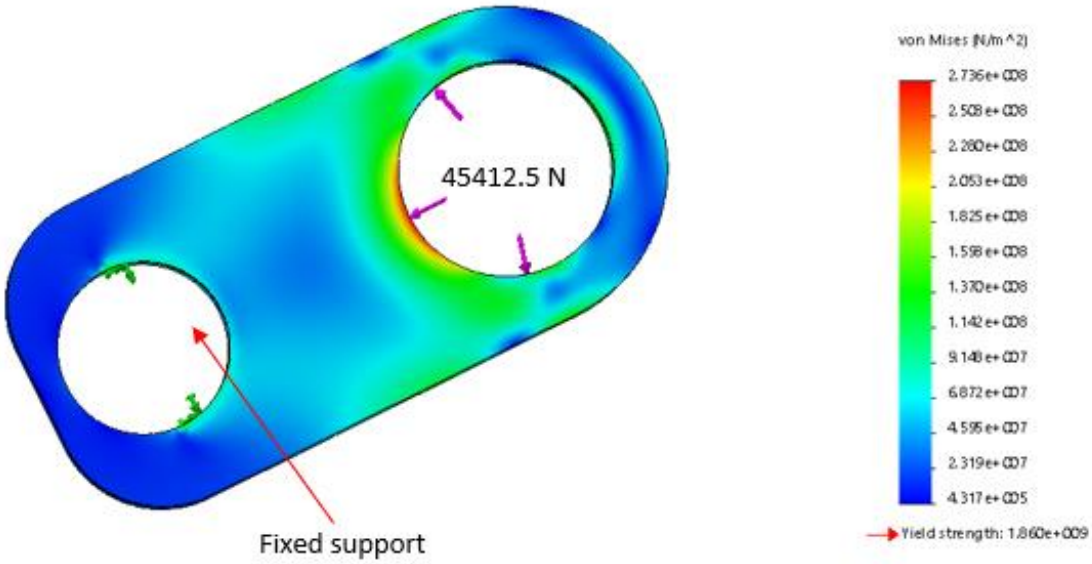

Figure 6.4: Simulation of linkage AB showing maximum stress of 273 MPa

The next simulation is for the linkage BC (*Figure 6.5*). For this simulation, the two pin supports are fixed, and the force of 182.2 kN is applied to the end of the linkage that connects to the slider pin.

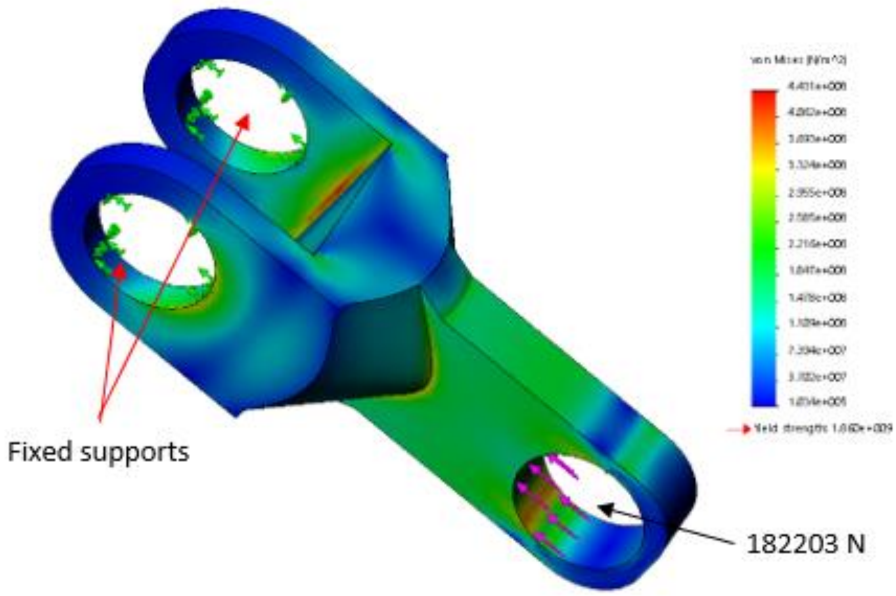

Figure 6.5: Simulation of linkage BC showing maximum stress of 443 MPa

From *Figure 6.5*, the highest stress (443 MPa) occurs around the base of the two supports and the top bearing surface where the force is being applied. There are also some high stresses occurring on the edges of the two supports; however, the stresses are still below the allowable stress of 1.24 GPa.

The simulation is performed by using the force required to shear the rebar (171.1 kN). The force is applied at the location of where the blade will be mounted (*Figure 6.6*). The two pin supports connecting linkage BC are fixed, and the bottom of the slider is chosen to be a sliding surface.

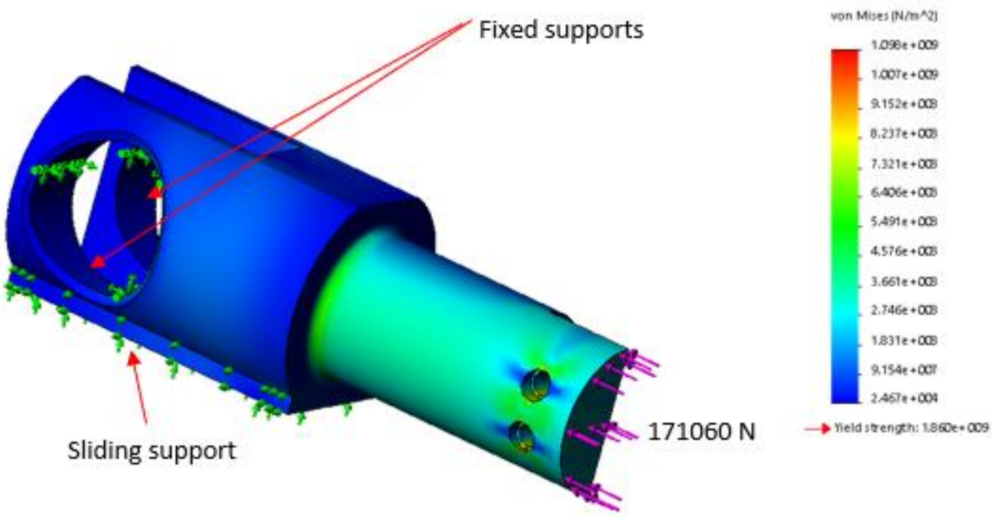

Figure 6.6: Simulation of the slider with 171060 N applied showing maximum stress of 1 GPa

From *Figure 6.6*, the stresses mainly affect the smaller section of the slider. However, the stresses from this section of the slider is roughly 700 MPa. The stress concentrations are located at the edges of the holes that are provided for the screws of the blade, registering values of 1.08 GPa. Although it should be noted that the simulation has no screws in place, this would mean that Solidworks is taking the screw holes as empty space; therefore, the holes will deform which then causes these high stresses.

6.1.1 Column Theory Simulations

To verify the columns theory calculations, further simulations were performed on linkages AB, BC, and the slider. For these simulations, the critical loads calculated in *Section 5.5.3* are used. Beginning with the slider (*Figure 6.7*), a force of 21.8 MN was divided equally and applied to the pin holders, with the top of the slider being fixed. The simulation produced a maximum stress of 315 GPa.

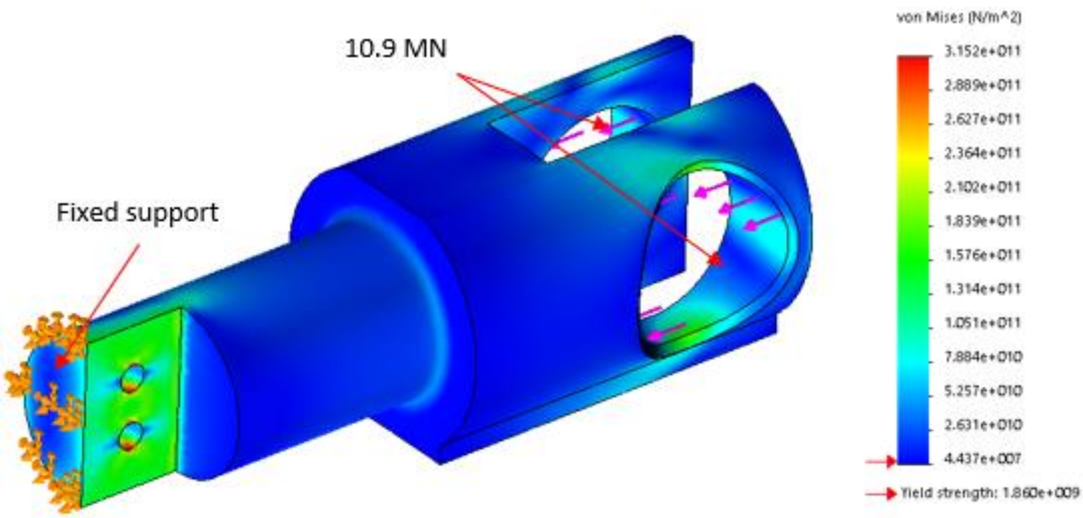

Figure 6.7: Column theory simulation of slider. Maximum stress experienced is 315 GPa

The second simulation is performed on linkage AB (*Figure 6.8*). One end of the linkage is fixed while the other end has the critical force of 66.3 MN applied to it. From *Figure 6.8*, it can be seen that the edges of the pin holes (where the force is applied) produce the highest stresses. The highest stress produced is 399 GPa.

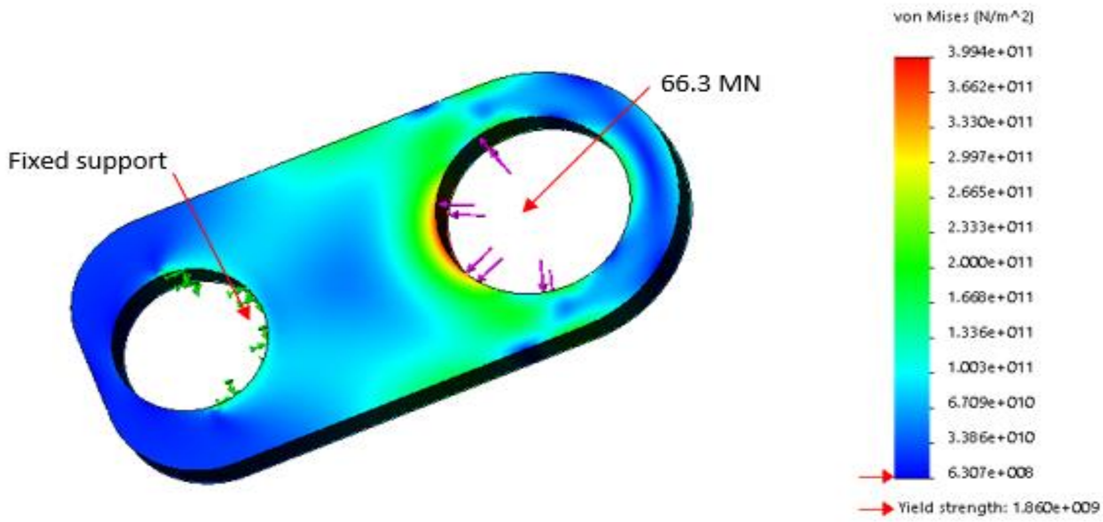

Figure 6.8: Column theory simulation of linkage AB. Maximum stress experienced is 399 GPa

The third simulation is performed on linkage BC (*Figure 6.9*). The two-pronged end of the linkage BC is fixed, and the critical force of 22 MN was applied at the opposite end. The highest stresses occur on the edges of the chamfers and the edges of the holes for the pins. The maximum stress from this simulation produces 47.4 GPa.

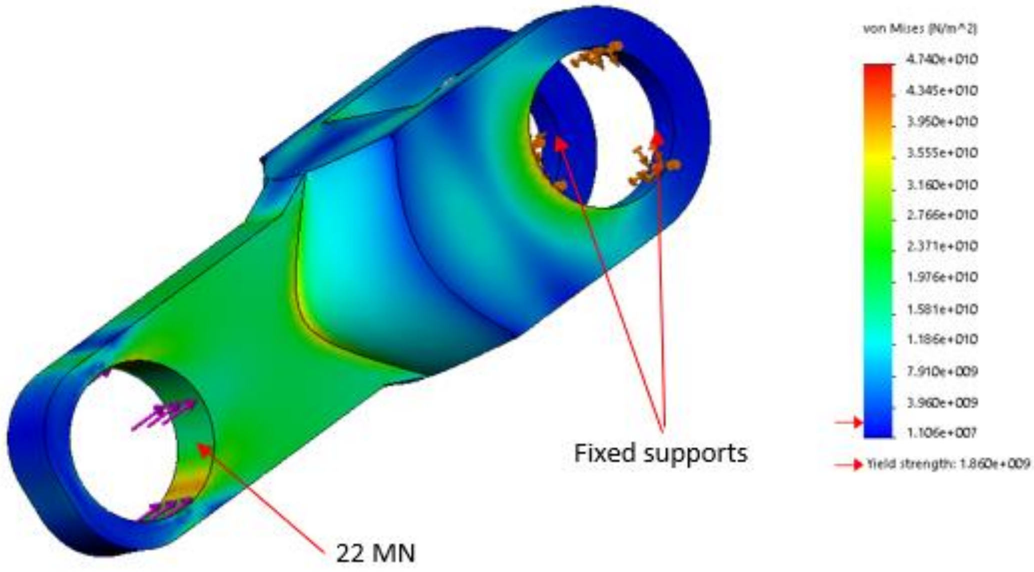

Figure 6.9: Column theory simulation of linkage BC. Maximum stress experienced is 47.4 GPa

6.2 Bending Arm

To simulate the bending arm (*Figure 6.10*), the force required to bend the rebar (5.3 kN) is applied at the roller support. Due to the loading of the arm, it is assumed that only one side of each spline tooth is sharing the load with the shaft.

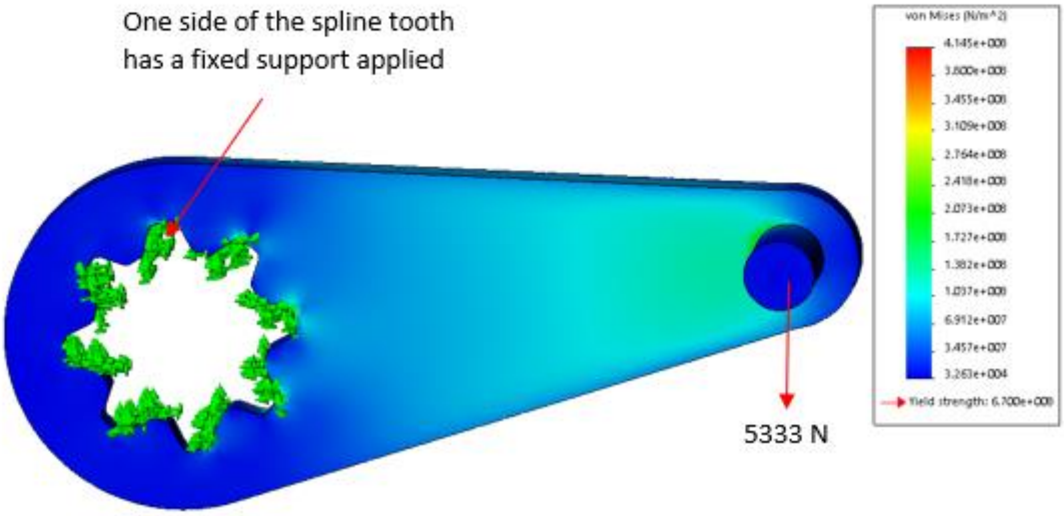

Figure 6.10: Simulation of bending arm. The Stress concentration located on the spline gives a stress of 414 MPa, while the highest stress on the main body of the arm is 238 MPa

The stress indicated in the simulation shows that most of the stress is occurring between the roller support and the spline (238 MPa). However, there are stress concentrations at the spline corners (*Figure 6.11*), but these stresses (414 MPa) are still below the allowable stress of ASTM A747 (446 MPa).

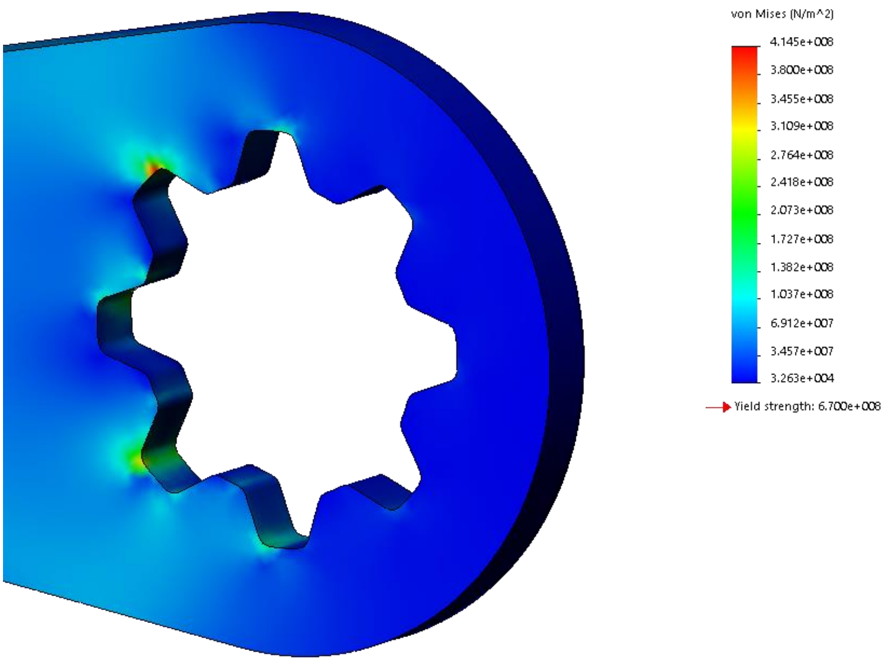

Figure 6.11: Close-up of stress concentration on bending arm showing maximum stress of 414 MPa

Three stress readings were taken away from the stress concentration (*Figure 6.12*) to determine the average stress caused by bending of the spline tooth; the average stress is found to be 239 MPa. The stress values will be compared in *Section 6.5.5.*

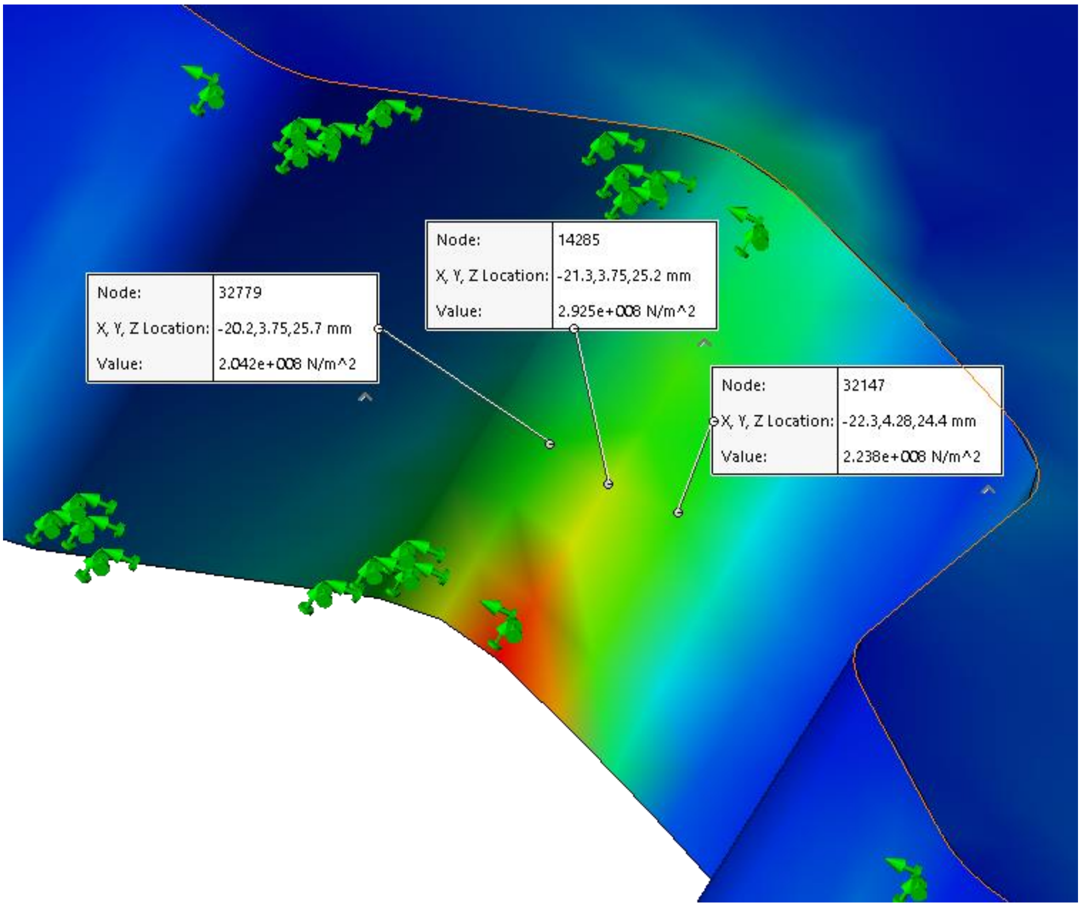

Figure 6.12: Three stress readings taken away from the stress concentration gives an average stress of 239 MPa

6.3 Internal Transmission Components

6.3.1 1024:1 Gearbox Components

Starting with the first stage ring gear (*Figure 6.13* and *6.14*), the forces (see *Section 5.5.2.6*) caused by the torque and by the main drive shaft were applied to the feet of the ring gear. The front section of the structure is fixed, which allows the simulation to show how the rest of the body reacts to these forces. From the simulation, the stresses on the feet (59 MPa) remain well below the allowable stress of aluminium 5056-H18 (271 MPa). The areas of high stress occur at the base of the feet around the fillets; stresses also occur in the interior of the body and on the bearing.

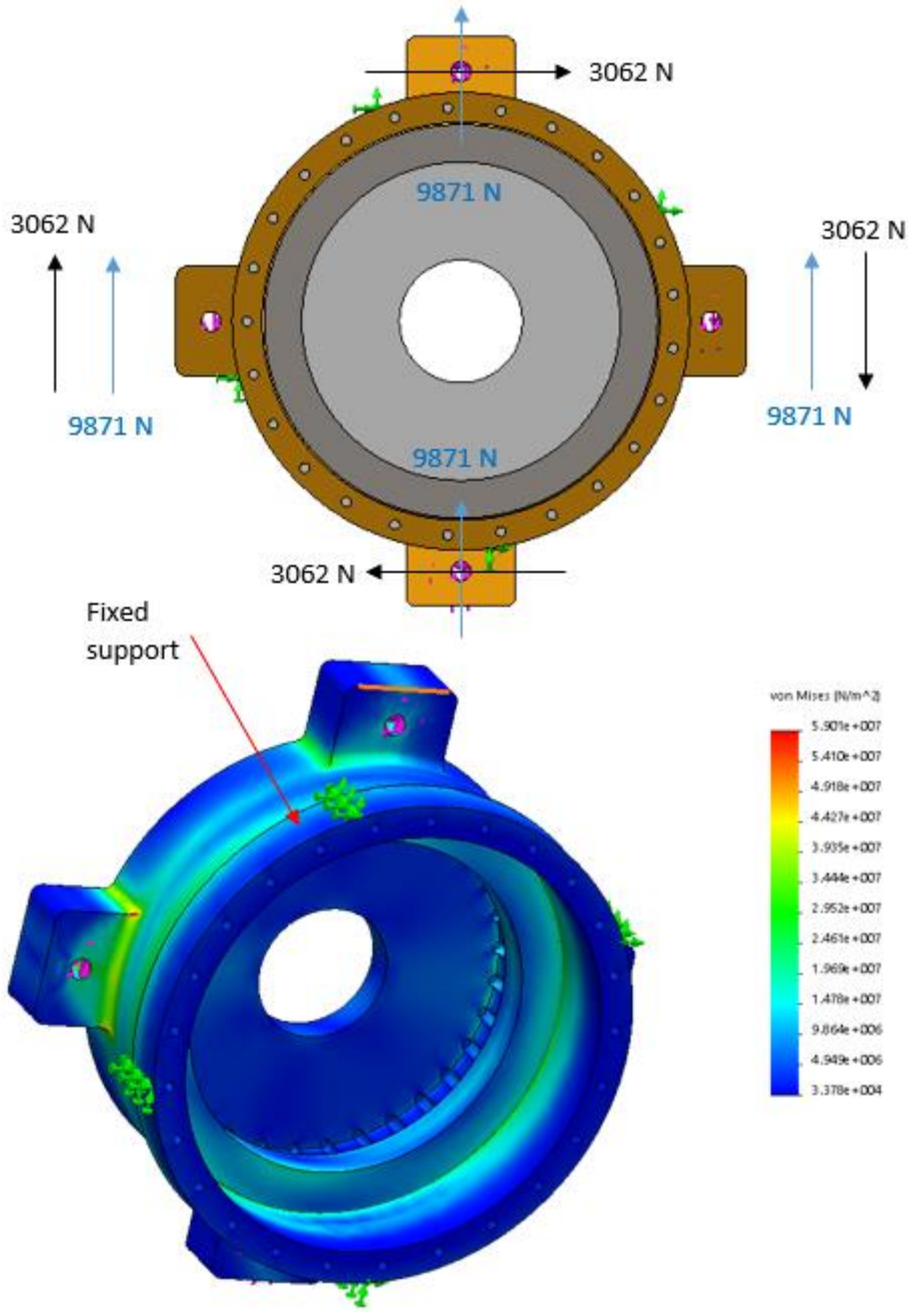

Figure 6.13: (Top) Loading conditions of the mounting feet of first stage ring gear (Bottom) Simulation of first stage ring gear mounting feet showing maximum stress of 59 MPa

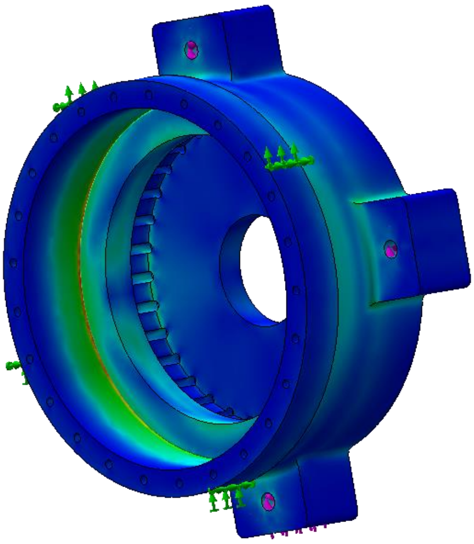

Figure 6.14: Stresses on the interior of the first stage ring gear

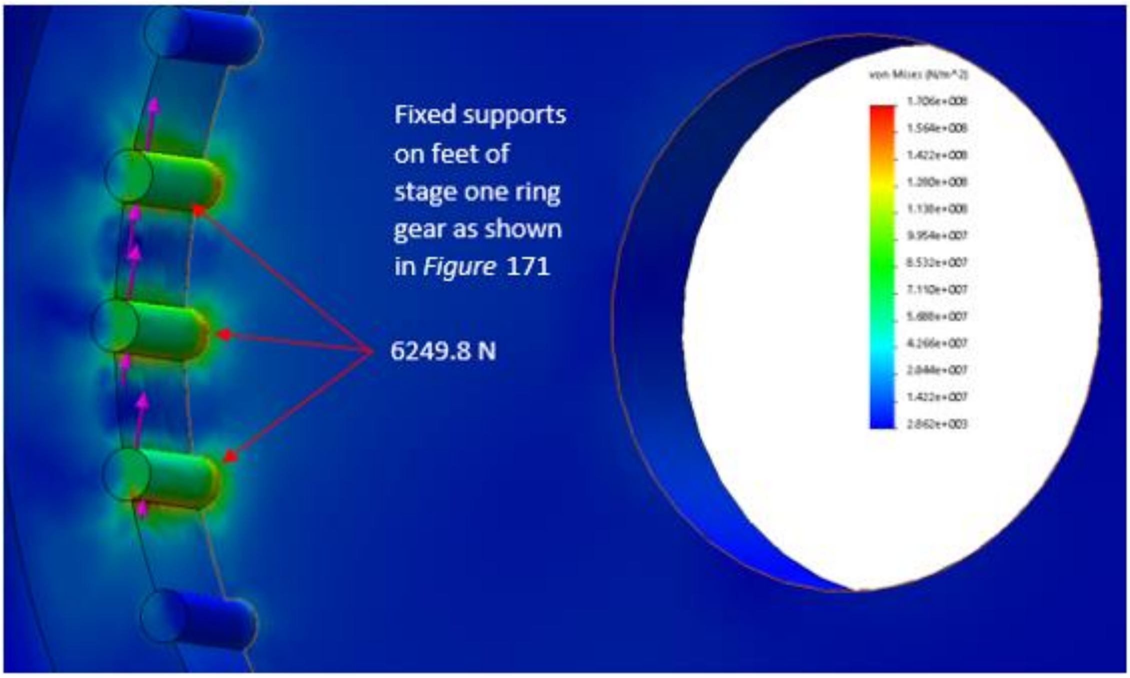

Figure 6.15: Simulation of pins assembled in first stage ring gear showing a maximum stress of 179 MPa

The next part of the first stage ring gear to be simulated are the pins that will act as teeth for the cycloidal disc (*Figure 6.15*). It is again assumed that only three pins are in contact with the cycloidal disc at any given time, and the force is divided evenly between the three pins (6.24 kN per pin). The mounting feet of the first stage ring gear is fixed at the bolt holes to simulate it being attached to the housing. From the simulation (*Figure 6.15*), the highest stresses occur around the edges between the pins and the ring gear. The simulation indicates that there is 180 MPa of stress on both the ring gear and the pins. However, the stress from the simulation is below the allowable stresses of both L2 steel and aluminium 5056 H18 of the pin and the ring gear, respectively.

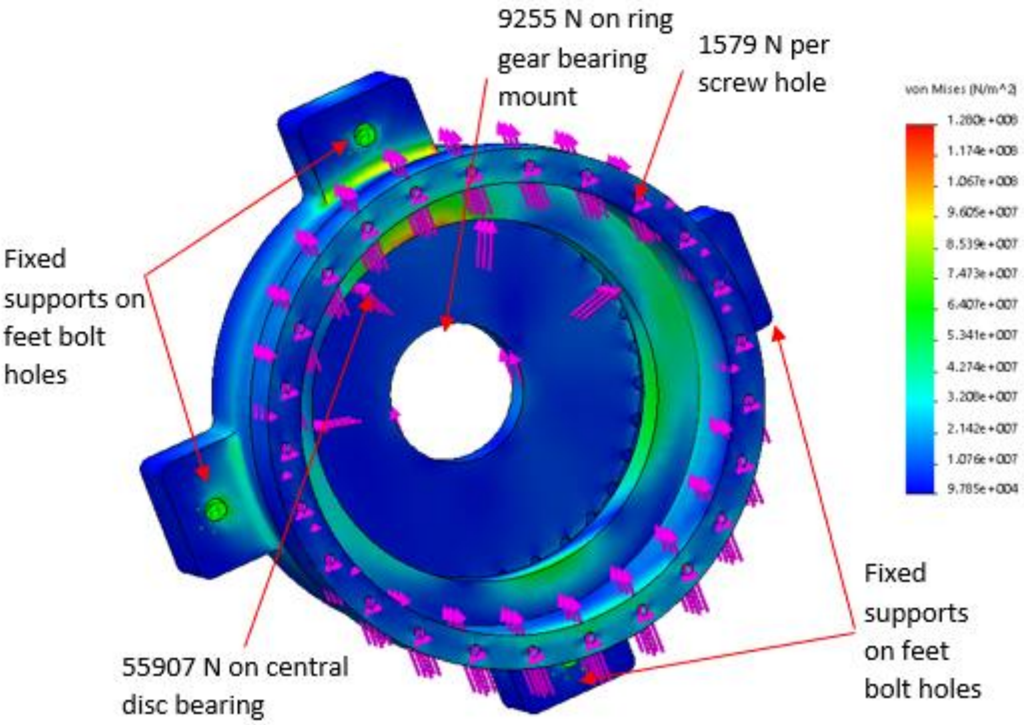

Figure 6.16: Simulation of first stage ring gear with all the forces applied. Maximum stress indicated is 128 MPa

The last simulation for the first stage ring gear (*Figure 6.16*) involves utilising all the possible forces that will be acting on the gearbox when it is in operation. It is assumed that the forces will move around the gearbox as the components within rotate. A simulation is performed for the worst case where all the forces are acting in the same direction. The net force coming from the drive shaft and the internal shaft of the gearbox is divided evenly between the 25 screw holes and is 1.58 kN (per hole). The total force acting on the central disc's outer bearing is 55.9 kN, the forces acting on the three pins of the ring gear are 6.25 kN (per pin). There is also a force exerted by the internal shaft on the rear of the stage one ring gear (9.25 kN). The bolt holes of the mounting feet are fixed to simulate the gearbox being attached to the housing. From the simulation, the areas of high stress occur around the bolt holes and fillets of the mounting feet. The only other stress concentration occurs on the edge of the inner diameter of the bearing for the central disc. None of the stresses computed by Solidworks (128 MPa) is over the allowable stress of the first stage ring gear's material (271 MPa).

The next component of the gearbox to be simulated is the cycloidal disc (*Figure 6.17*). As the dimensions and loading of the two cycloidal discs are identical, only one simulation is required.

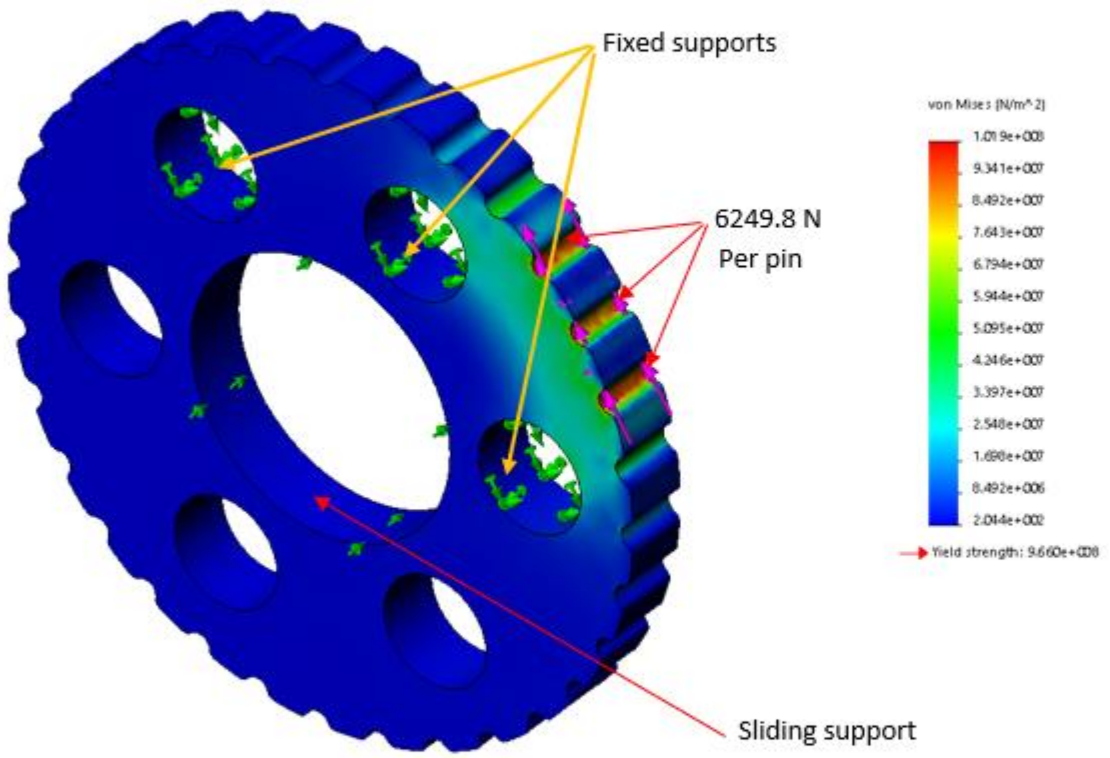

Figure 6.17: Cycloidal disc with 6249.8 N applied to one side of each tooth, simulation showing a maximum stress of 102 MPa

A sliding fixture is applied to the centre of the cycloidal disc, and the three central pin-holes are fixed; this is done to mimic the pins from the central disc pushing against the cycloidal disc. It is assumed that only three teeth of the cycloidal disc are engaged with the ring gear at any given time and that the forces are divided evenly (6.25 kN per tooth). From the simulation (*Figure 6.17*), the highest stress (102 MPa) occurs at the base of the tooth; however, the stresses are below the allowable stress of 640 MPa.

A simulation is needed for the contact stress between the central pin bushing and the cycloidal disc; this was achieved in Solidworks by applying a force onto the previously calculated contact area dimensions between the bushing and the cycloidal disc made of copper beryllium and 4142 steel, respectively (*Figure 6.18*). Having drawn the contact area, a small extrusion of 0.0001 mm was made so that the load (9.32 kN) could be applied onto this area.

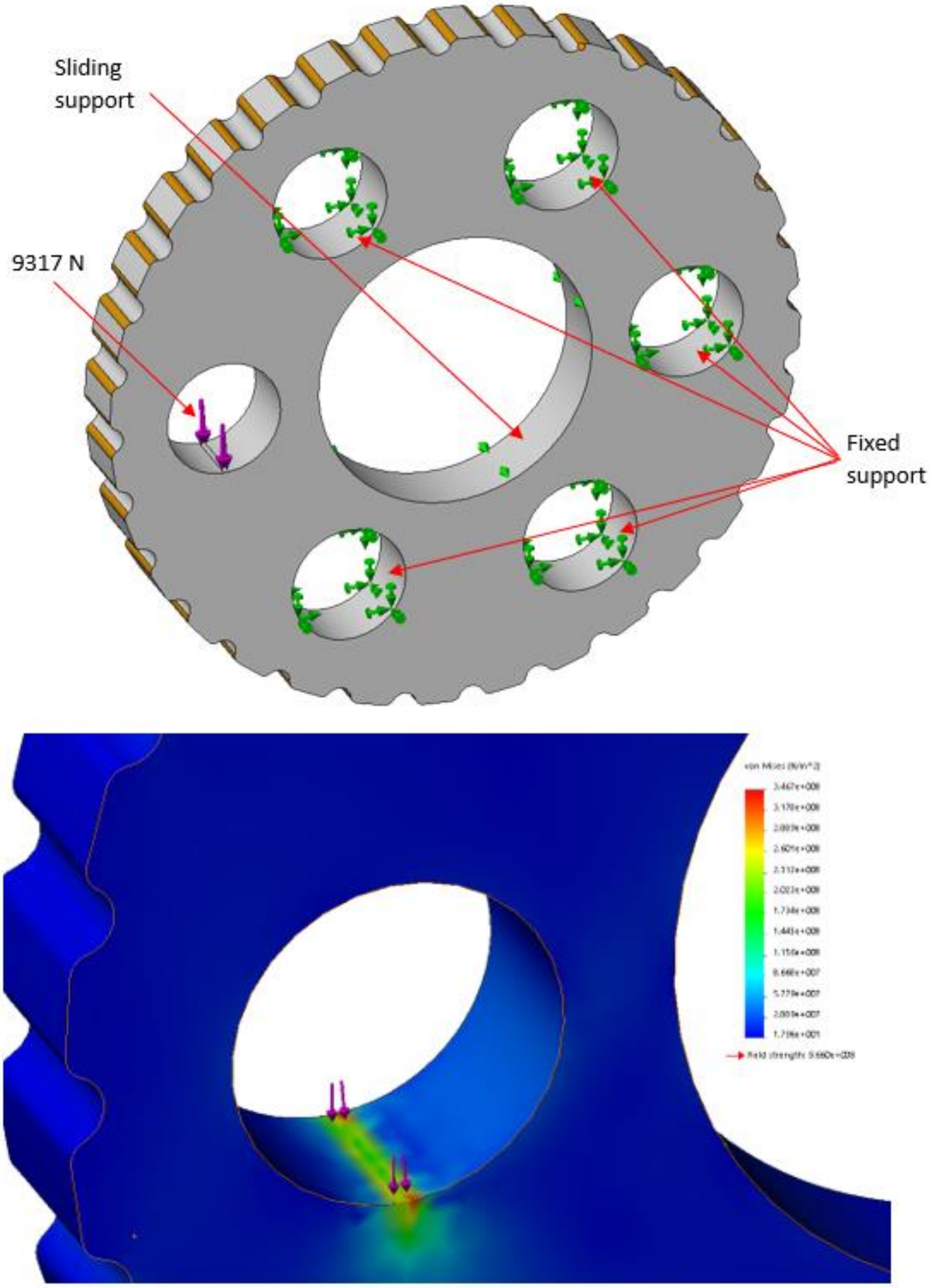

Figure 6.18: (Top) Boundary conditions. (Bottom) Approximation of contact stress between cycloidal disc and central disc bushing, showing maximum stress of 346 MPa

From the simulation, the contact stress between the cycloidal disc and the bushing gives a maximum stress of 346 MPa. The stress produced from this simulation is below the allowable stress of the copper beryllium (643.3 MPa) and the 4142 steel (640 MPa).

The next component simulated is the central disc (*Figure 6.19*). The outer diameter is defined as a sliding support to simulate the outer bearing.

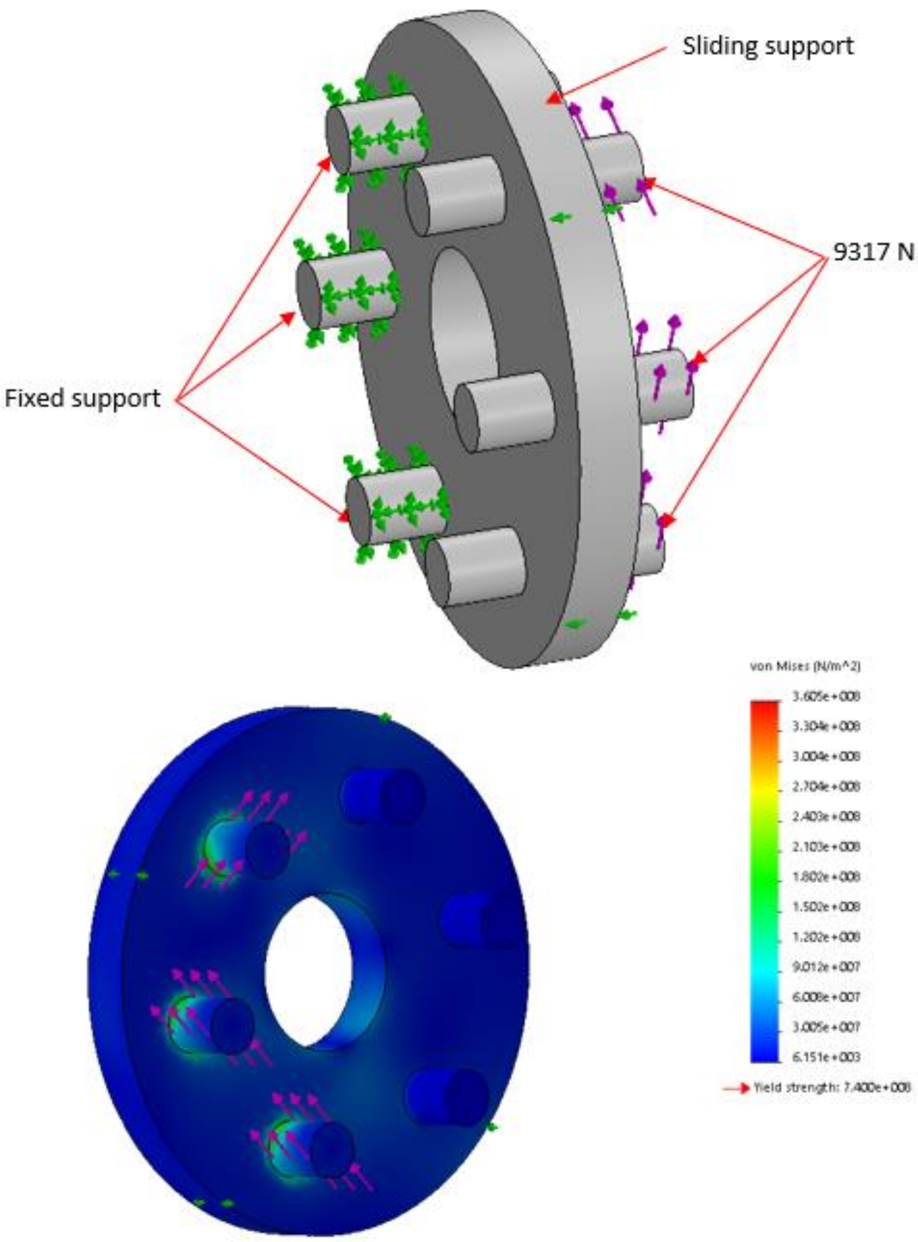

Figure 6.19: (Top) Boundary conditions. (Bottom) Simulation of central disc showing maximum stress of 360 MPa

The three pins on the other side of the central disc are fixed to simulate the load from the cycloidal disc on the opposite side. It is assumed that the forces acting on the three pins from the cycloidal disc are evenly distributed (9.32 kN per pin); however, the force directions could only be approximated as Solidworks has no provisions for controlling the directions of the forces accurately. From the simulation, the highest stress occurs at the base of the pins (360 MPa), but it is below the allowable stress of 4140 steel (493 MPa).

The next component to be simulated is the internal shaft that drives the two cycloidal discs around the ring gear (*Figure 6.20*). In order to simulate this part, both end sections were fixed as sliding supports to act as bearings. A torque of 1.5 Nm was applied as this is the maximum rated torque that the motor can produce. The forces exerted by the cycloidal discs are applied to the two eccentric sections of the shaft and were simulated in both the vertical and horizontal directions (*Figure 6.20* and *6.21*).

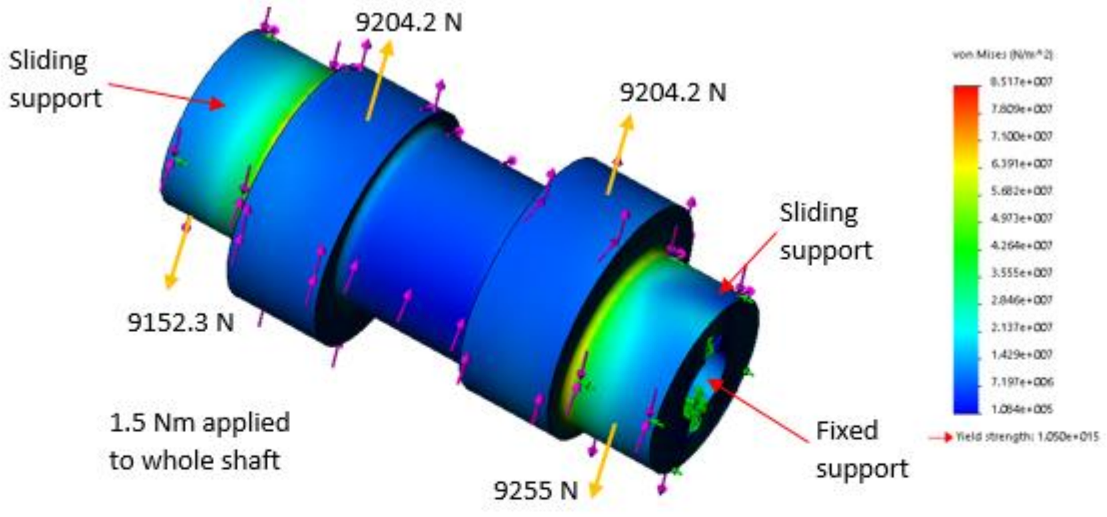

Figure 6.20: Simulation of gearbox shaft with forces from the cycloidal disc applied in the vertical direction

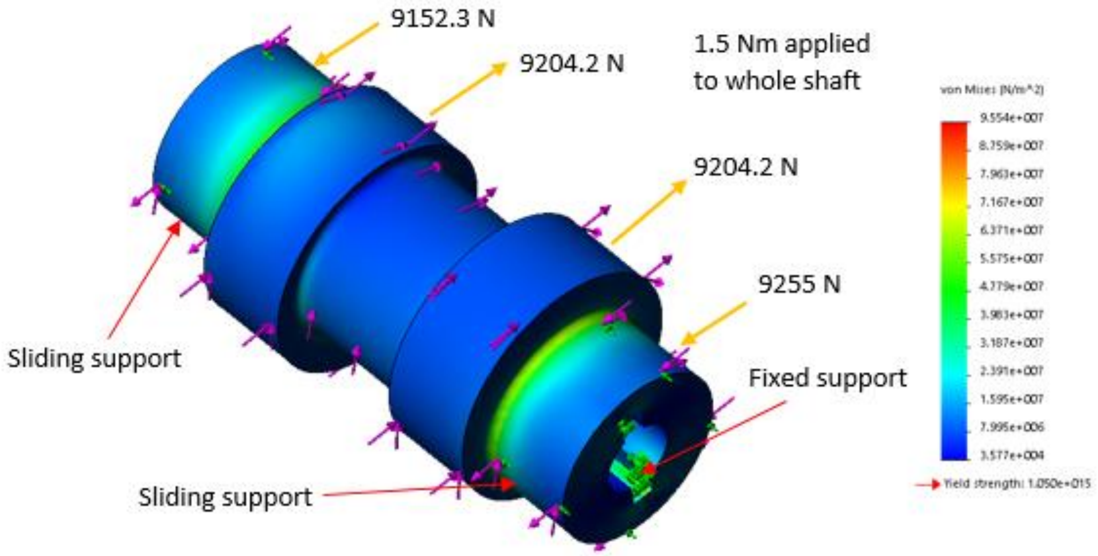

Figure 6.21: Simulation of gearbox shaft with forces from the cycloidal disc applied in the horizontal direction

Both simulations indicate that the stresses are low, with the highest stress occurring when the forces are applied in the horizontal direction (95.5 MPa). The high stresses are mainly occurring at the fillets located near the eccentric sections of the shaft, but are still below the allowable stress of 6580 steel (700 MPa).

The next component to be simulated is the second stage ring gear (*Figure 6.22*). The shaft that also forms part of the second stage ring gear will be discussed in the following section. The simulation conducted here is similar to the simulation performed for the first stage ring gear. The shaft behind the ring gear is fixed, the force from the internal shaft is applied to the bearing holder (9.25 kN), and it is assumed that only three pins engage with the cycloidal disc with the forces distributed evenly (6.25 kN per tooth).

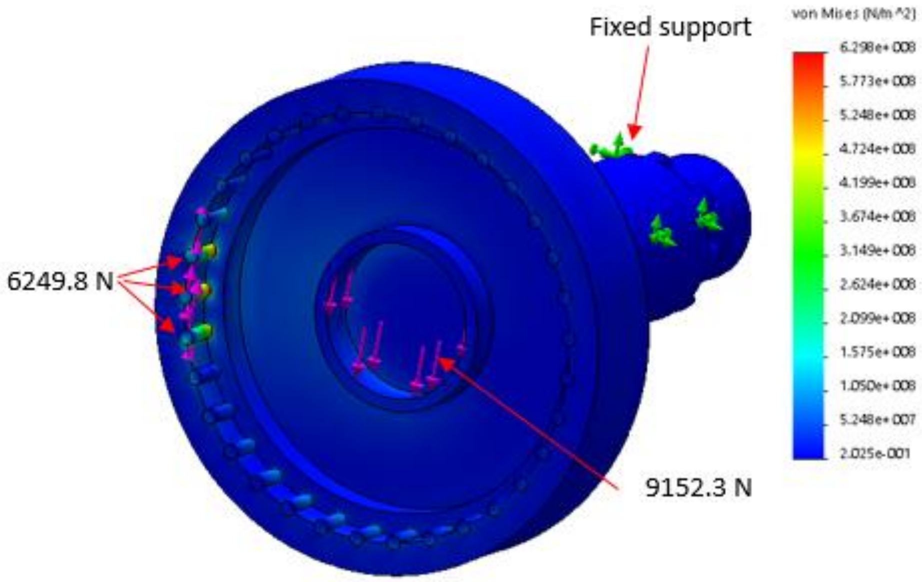

Figure 6.22: Simulation of second stage ring gear with maximum stress of 629 MPa on pins and 468 MPa on the ring gear.

The stress experienced by the second stage ring gear is 468 MPa which is slightly above the allowable stress of 6580 steel. With a factor of safety of 1.5, the allowable stress is 466.6 MPa for diameters over 161 mm. However, since the difference is small, no design changes are necessary. The pins, however, experience a much higher stress (629 MPa), exceeding the allowable stress for L2 steel. This can be remedied by having the L2 steel heat-treated, which changes the yield stress to 1792 MPa (σ_{all} = 1194 MPa).

The final part of the gearbox is the lid of the gearbox (*Figure 6.23*). The screw holes are fixed to simulate the screws holding the lid in place, and a force of 39.5 kN is applied to the bore of the lid to simulate the force from the main drive shaft.

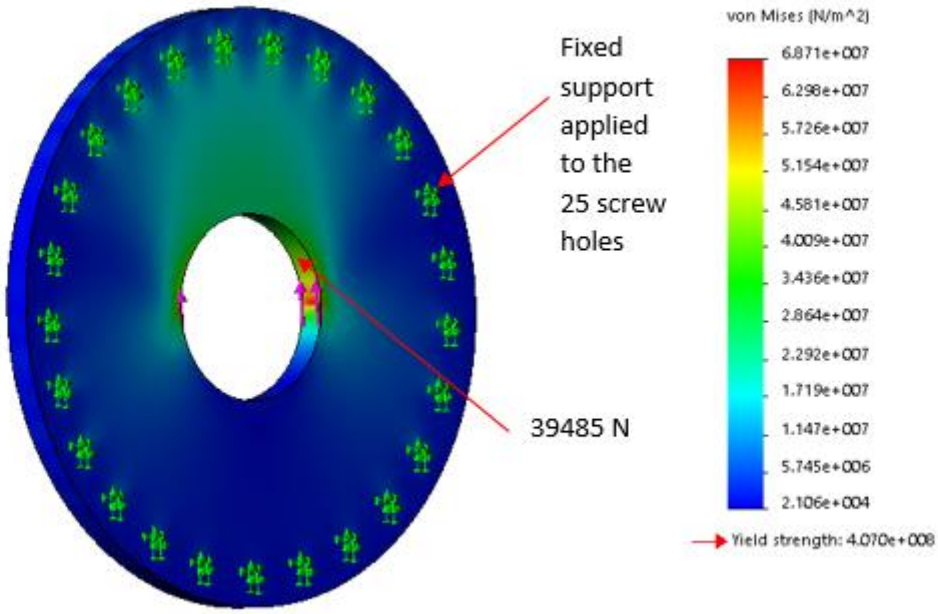

Figure 6.23: Simulation of gearbox lid, showing a maximum stress of 68 MPa

From the simulation, most of the stress can be found at the top half the of the lid. The location of the high stress is on the split line feature (allows the force to be applied to half of the bore). Solidworks assumes this to be an edge rather than a continuous curve. This high stress could potentially be an error. The stress of 68 MPa is experienced by this part and is still well below the allowable stress of aluminium 5056 H18 (271 MPa).

It must be noted that the forces used in both the first principles and the simulations will never be reached. The forces were derived from the maximum possible torque that the motor can produce with a gear ratio of 1024:1. The actual maximum torque reached during operation will be 933.3 Nm as opposed to the assumed 1536 Nm maximum output torque.

6.3.2 Main Drive Shaft, and Keyway

The main drive shaft operates both the shearing and bending functions of the tool. However, only one function is used at any given time. The first simulation on the drive shaft is the bending stress caused by the shearing of rebar (*Figure 6.24*). The shaft is assembled between two fixed plates that represent the wall of the housing and the lid of the gearbox (the housing simulation results will be discussed in *Section 6.4*). Both the key and the cam are assembled onto the shaft so that the force (62.9 kN) can be applied to the correct area.

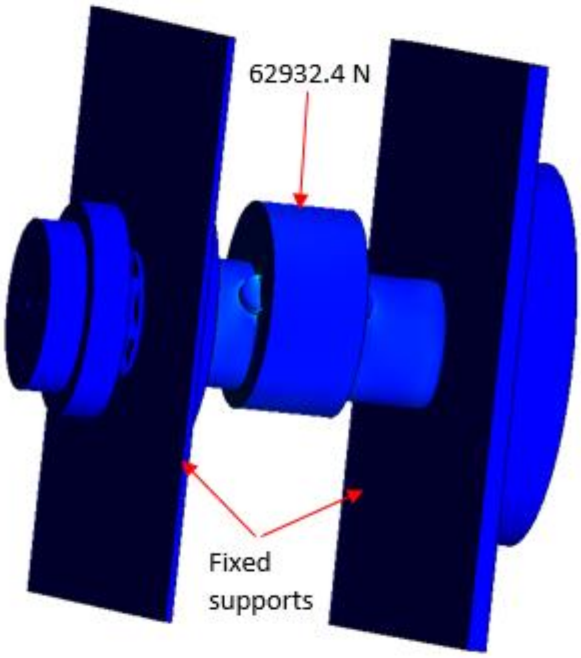

Figure 6.24: Simulation of bending when tool is shearing of main drive shaft.

As expected, the stresses are mainly focused around the edges of the cam and walls. The highest stress that the shaft experiences is 170 MPa, while the cam experiences a stress of 884 MPa, and the key experiences a stress of 536 MPa. The only component in this assembly that exceeds its yield stress is the 1018 steel key (σ_Y = 530 MPa). 1144 carbon steel is selected instead. 1144 steel has a yield stress of 655 MPa which is more than sufficient for the key. The highest stress experienced is at the corners of the cam's keyway; however, the stress (668 MPa) is still below the cam material's allowable stress of 2.4 GPa.

The next simulation on the shaft is the bending stress created by bending the rebar (*Figure 6.25*). The forming wheel is used to allow the force (13.5 kN) to be applied to the correct location of the shaft. The same fixture conditions from the simulation for shaft bending due to the rebar shear is used in this simulation.

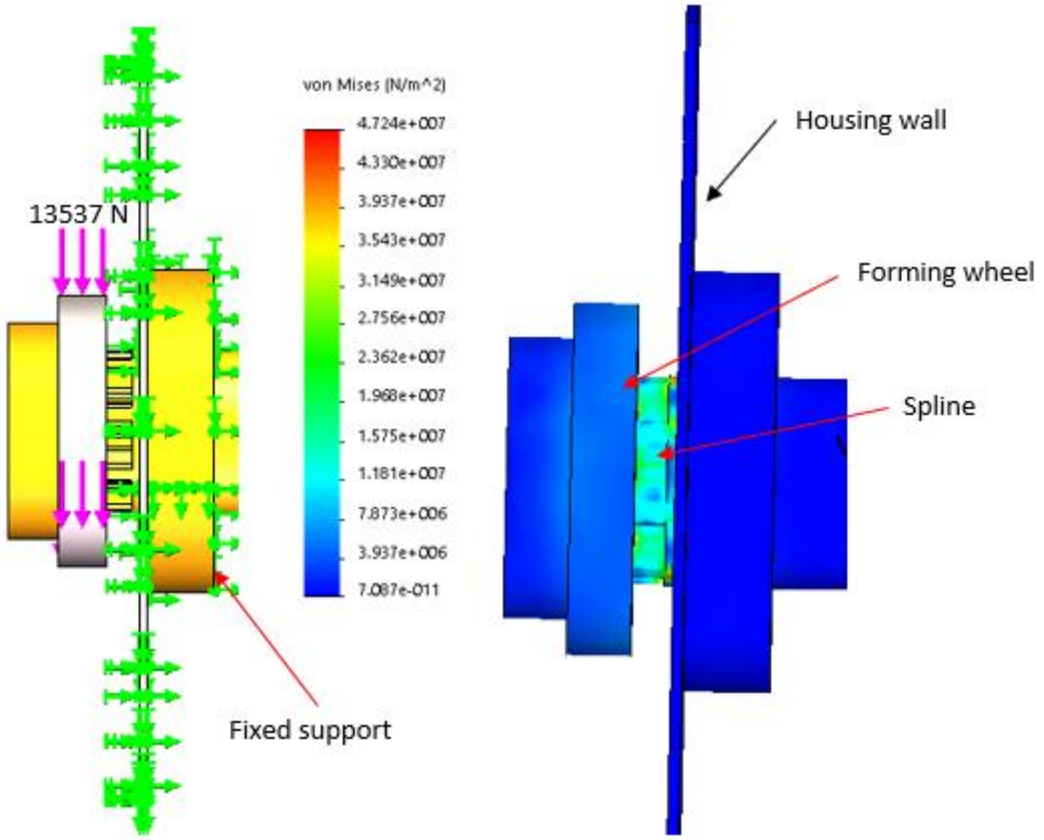

Figure 6.25: (Left) Loading and fixed geometry (Right)Bending simulation of shaft from rebar bending

The simulation shows that the maximum stress experienced by the shaft is 47.2 MPa. From *Figure 6.25*, the stresses are mainly concentrated around the area of the spline.

The next simulation is on the spline itself (*Figure 6.26*). The forces acting on each spline tooth (4.67 kN per spline tooth) were calculated from the maximum operational torque (933.3 Nm) and the radius of the shaft that supports the forming wheel. It is assumed that the forces are distributed evenly between the 8 teeth of the spline. Only one side of the spline experiences this force, this is to simulate the spline driving the bending arm when the rebar is being bent.

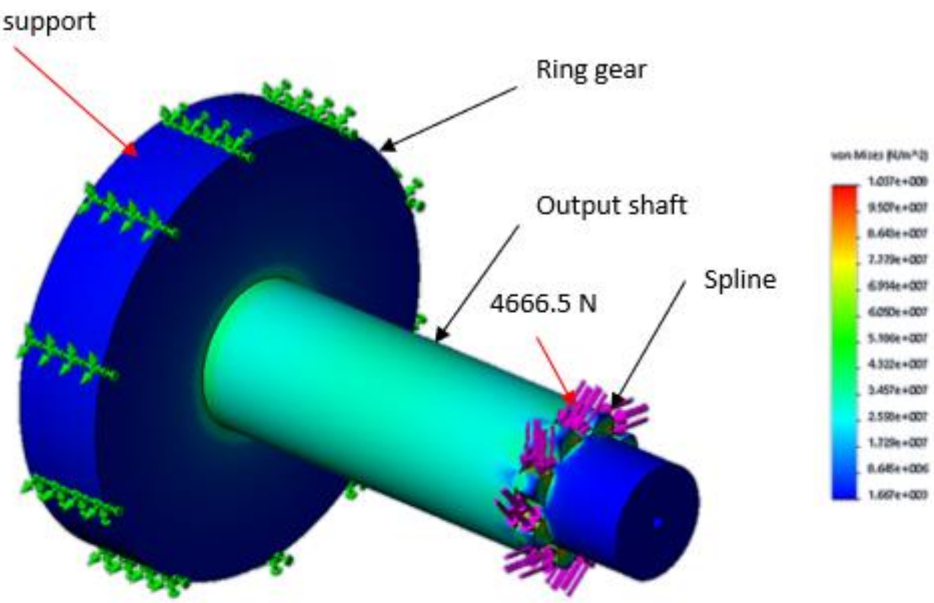

Figure 6.26: Simulation of shaft spline, showing a maximum stress of 103 MPa

From the simulation, it can be seen that the maximum stress that the spline experiences is 103 MPa. The stresses are uniformly distributed across the shaft with the highest stresses occurring at the base and edges of the spline.

The keyway (*Figure 6.27*) is the next feature that needs to be simulated. Using the maximum operation torque (280 Nm, the cam is only used when the rebar is being sheared) and the radius of the shaft (0.033 m), the force acting on the keyway is 8.48 kN.

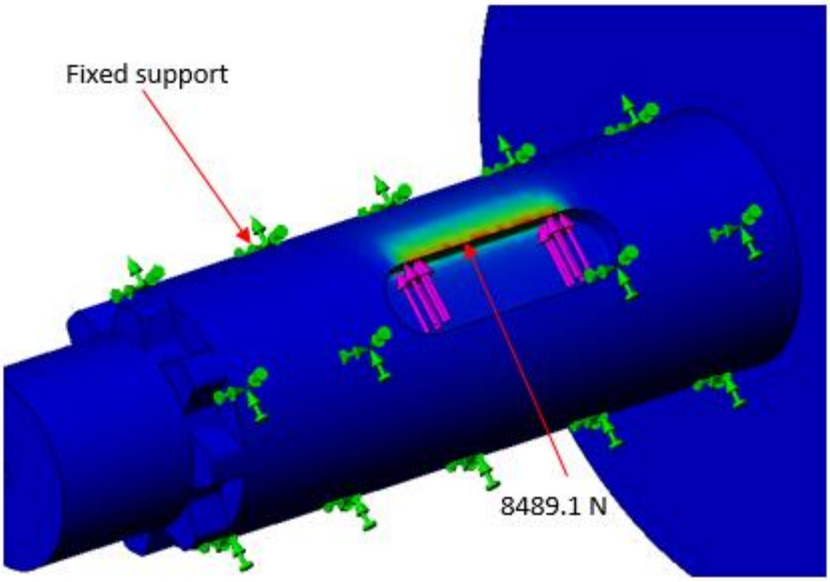

Figure 6.27: Simulation of keyway, maximum stress indicated is 47 MPa

The force is applied to the keyway wall while the shaft is fixed. From the simulation, the highest stresses occur at the top edge of the keyway. However, the stress is below the allowable stress of the shaft.

Finally, the shaft is simulated using the maximum operational torque of 933.3 Nm (*Figure 6.28*). The ring gear section of the shaft will be fixed.

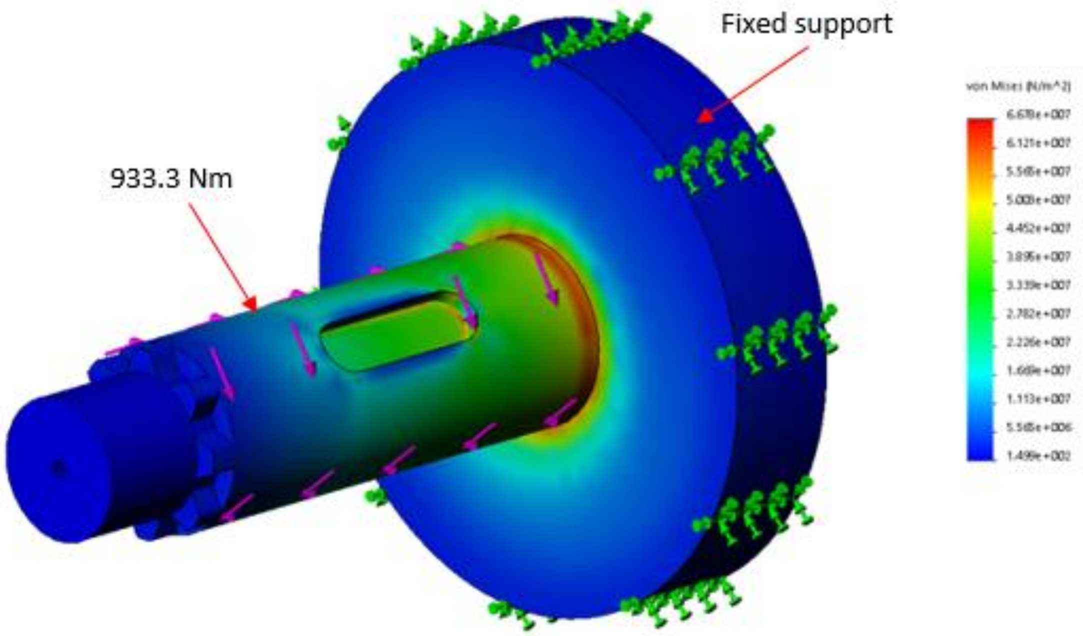

Figure 6.28: Simulation of drive shaft, showing maximum stress of 66.7 MPa

The maximum stress that occurs when the shaft is under the maximum operational torque (933.3 Nm) is 66.7 MPa, with the highest stresses located in the interior of the keyway and at the corner between the shaft and the ring gear. All the stresses from the simulation are below the allowable stress of the 6580 steel (700 MPa).

6.3.3 Contact stresses of Cam, Follower, Forming Wheel, and Bending Arm Roller

To simulate the contact stresses of these components, an approximation had to be made as Solidworks does not have provisions for Hertzian contact stress simulations. The dimensions of the contact area are calculated using the Hertzian stress formulas for the component's respective orientations (see *Section 5.1.2*). These dimensions are then transferred to the component and the forces applied to the calculated areas.

The first simulation is the contact stress between the cam and the follower (*Figure 6.29*). The maximum contact stress occurs at the peak of the cam profile (at 150°). The dimensions calculated in *Section 5.1.2* are used in the simulations. As the two components are parallel to one another, a line contact is formed.

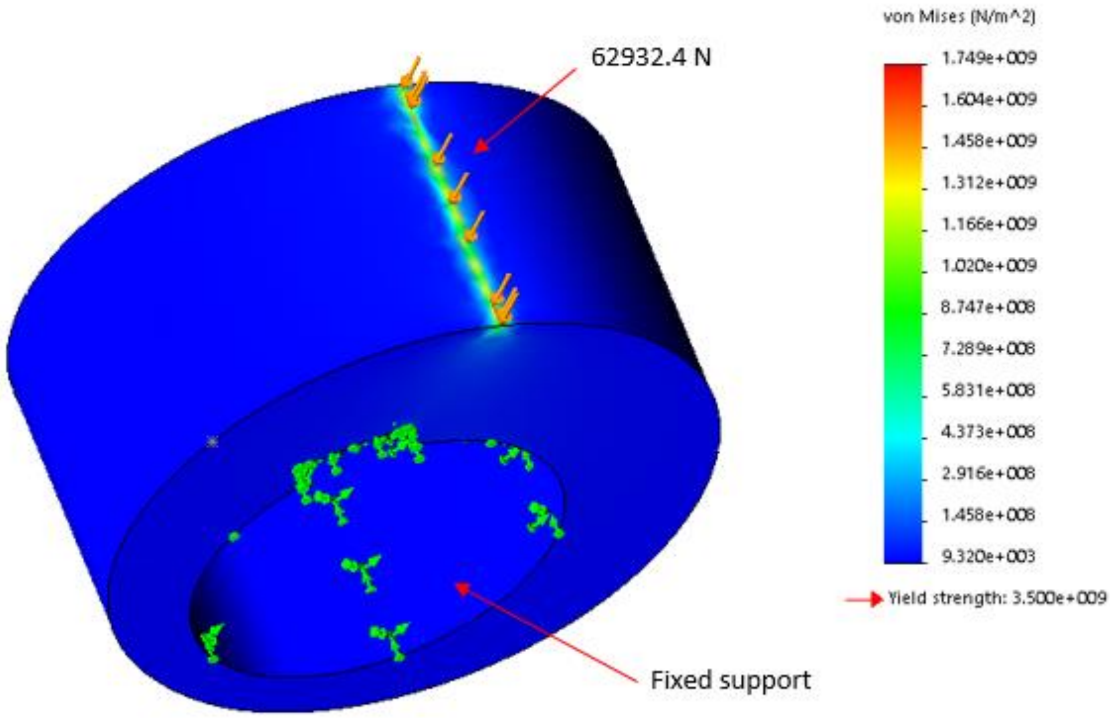

Figure 6.29: Approximated contact stress simulation of cam, showing maximum stress of 1.75 GPa

The cam's bore is fixed along with its keyway to simulate the presence of the shaft of the main drive shaft. A force of 62.9 kN is applied to the contact area. From the simulation, the contact stress is much lower than the allowable stress of 2.3 GPa. The same loading and fixture conditions are used for the follower (*Figure 6.30*).

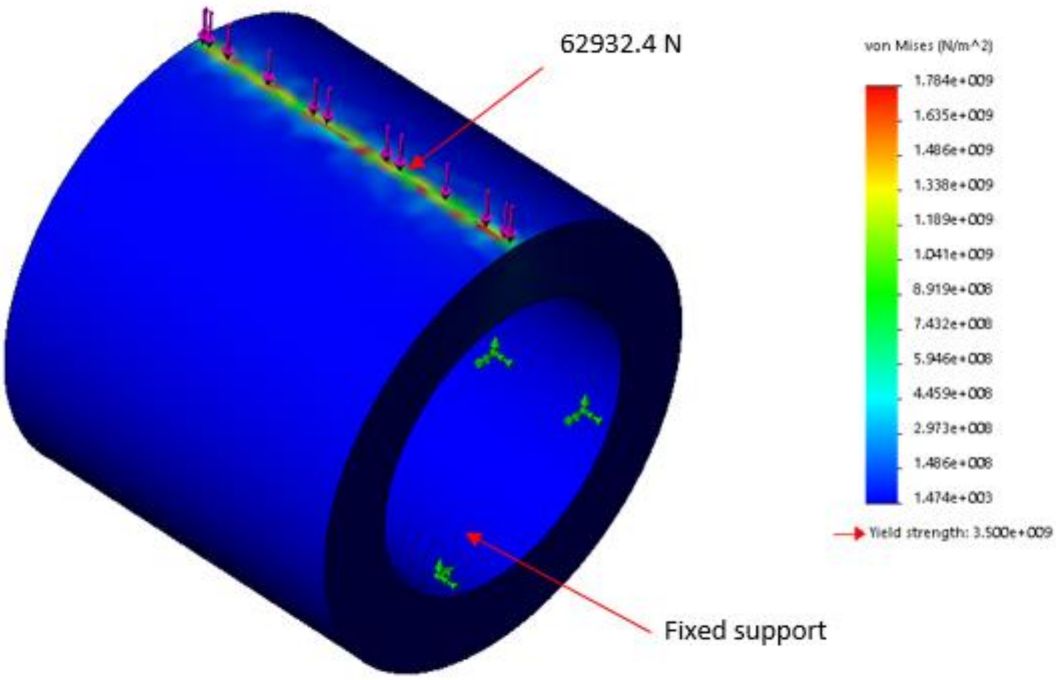

Figure 6.30: Approximated contact stress simulation of follower, showing maximum stress of 1.78 GPa

The same contact dimensions are used, except that the contact area does not run the full width of the follower as the cam is 2 mm shorter. The contact stress is only slightly higher than the cam but remains below the allowable stress (both components are made of the same material).

Next, the forming wheel is simulated (*Figure 6.31*). The contact stress occurs between the rebar and forming wheel which is perpendicular to each other; this gives a contact shape of an ellipse. The same contact area shape occurs between the bending arm roller and the rebar.

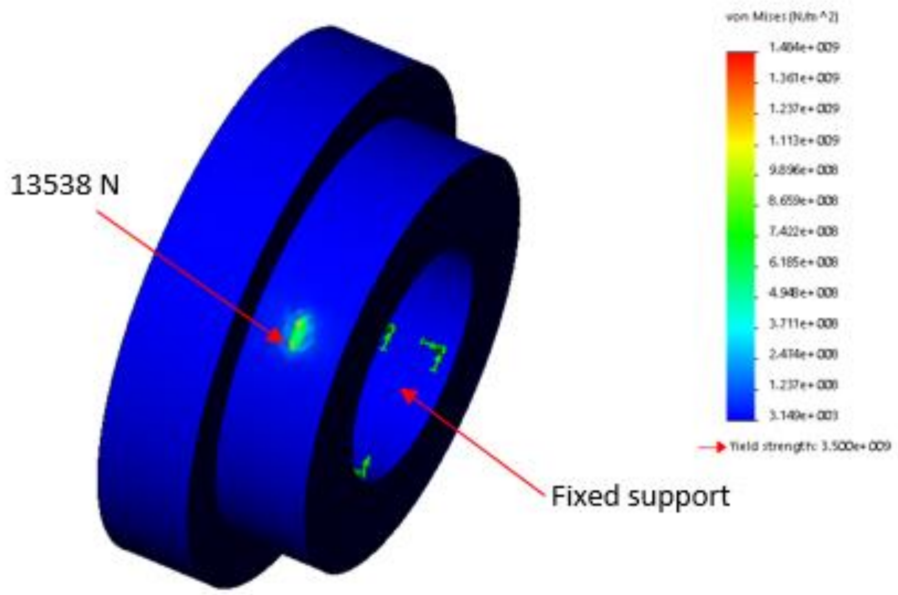

Figure 6.31: Approximated contact stress simulation of forming wheel, showing maximum stress of 1.48 GPa

The contact area for the forming wheel was calculated for the smaller rebar bend diameter (40 mm) as this would give the highest contact stress (*Section 5.1.2*). From the simulation, a force of 13.5 kN was applied to the contact area, and the maximum stress that occurs on the forming wheel is 1.48 GPa, which is below the allowable stress of 2.3 GPa.

The bending arm roller (*Figure 6.32*) has the same simulation settings, except that the force applied to the contact area is 5.33 kN. It should also be noted that as the bending arm roller has a smaller diameter, the contact area is also smaller.

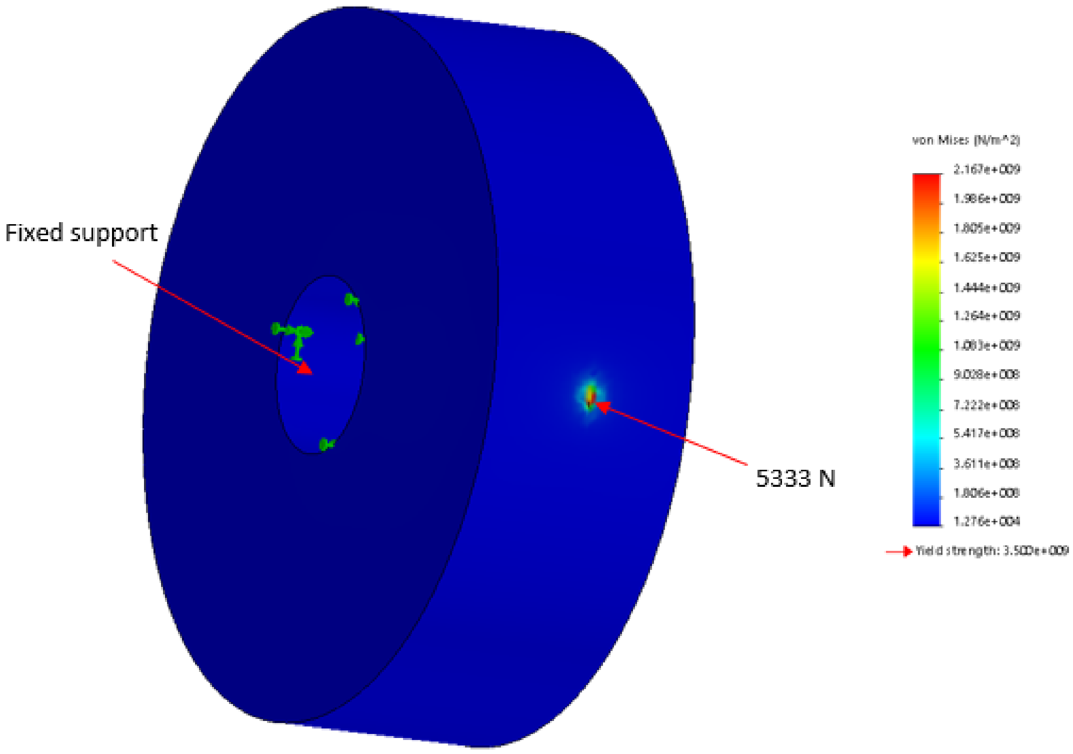

Figure 6.32: Approximated contact stress simulation of bending arm roller, showing maximum stress of 2.16 GPa

From the simulation, the maximum stress that occurs on the bending arm roller is 2.16 GPa. As contact stresses (from the forming wheel and the bending arm roller) are above the ultimate tensile stress of the rebar (700 MPa), the rebar will plastically deform when being bent. However, this deformation is negligible as the contact area is small. The deformation created on the rebar would not affect its mechanical properties.

6.4 Housing

As the housing is not fixed to any wall or solid structure, it was necessary for simulations to be performed for different fixture orientations. The purpose of these simulations is to see how the stresses change depending on the location of the fixture. A fixture will be applied to a wall where forces are not directly acting on it. In this case, the top and rear walls will be used in the simulations; if a fixture is applied to a wall where a force is acting, the force would have a reduced effect on the rest of the housing. The first simulation (*Figure 6.35*) will have the top wall fixed and the forces associated with shearing the rebar applied. Certain components such as the slider, AB hinge, insert, and stopper screws are added in the simulation to apply the forces accurately.

Unlike the first principles calculation, the simulation includes the webbing and other features. The webbing (similar to a truss structure) is the structural support for the housing and allows the forces to be distributed around the housing. With numerous forces acting in multiple directions, it is expected that the stresses on the housing will be high.

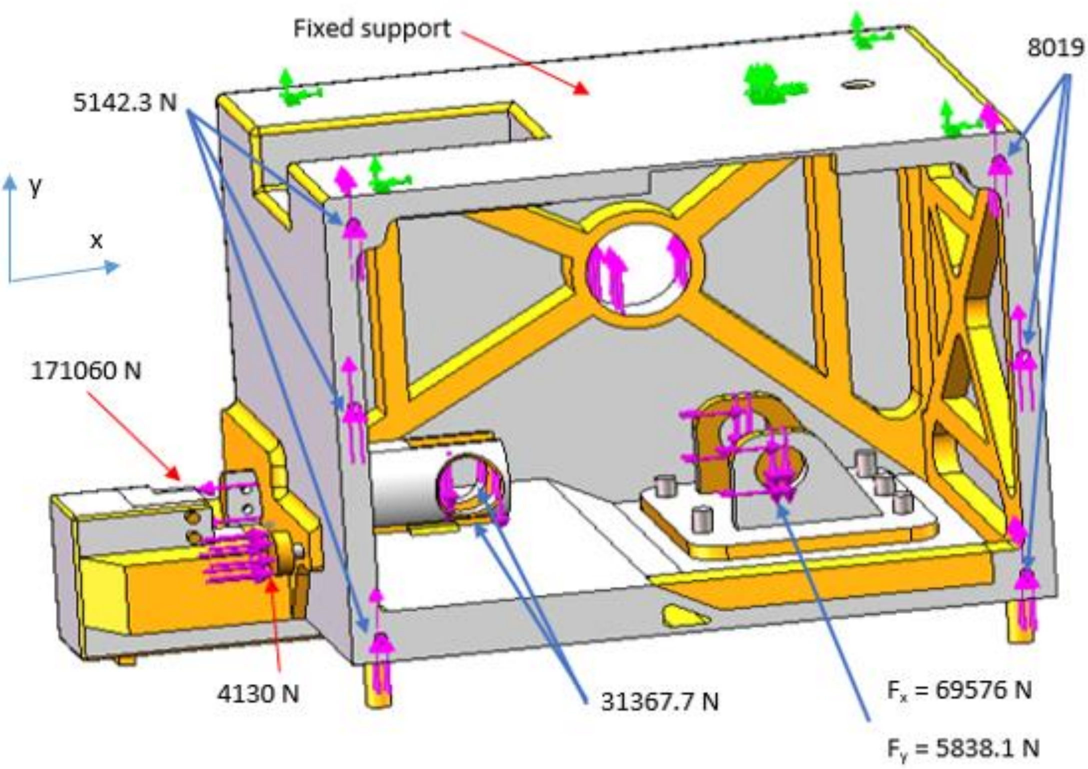

Figure 6.33: Forces acting on housing

A force of 171.1 kN is applied to the insert, 4.13 kN is applied to the shearing rebar stopper, and 31.4 kN is applied to each of the supports of the slider. Hinge AB has two force components that will be divided evenly between the two supports (total force parallel to the housing is 6.95 kN, and the total force perpendicular to the housing is 5.83 kN). A force of 32.6 kN is applied to the shaft bore, and the screw holes that fasten the panel to the housing have 39.5 kN divided equally between the six holes. However, there is also the force created by the torque from the gearbox that also needs to be considered. Using the distance from the centre of the gearbox to the closest screw hole on the panel, the maximum force created by the gearbox torque can be found (see *Section 5.6.7*). However, as the gearbox is exerting a torque, it will mean that one side of the panel will exert an upwards force, while on the opposite side the forces will be acting downwards (*Figure 6.34*).

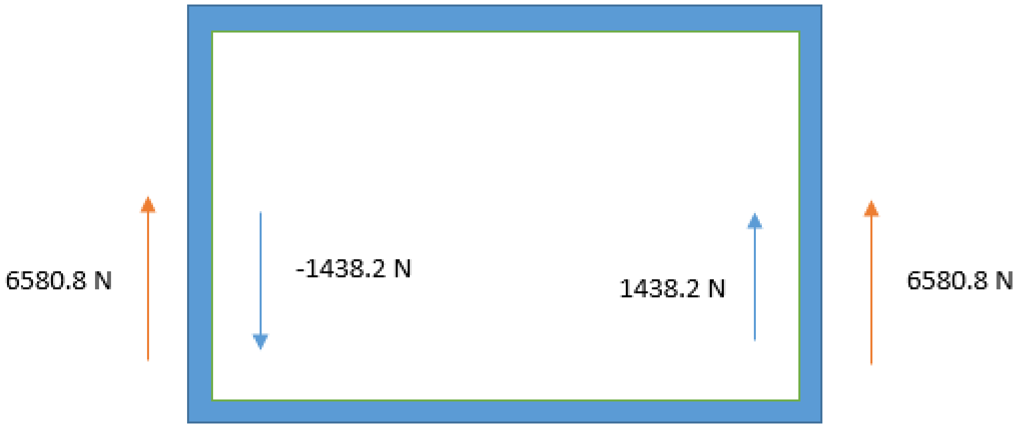

Figure 6.34: 6580.8 N (per screw hole) from the drive shaft is acting on both sides of the housing in the same direction, while the force due to torque, 1438 N (per screw hole), from the gearbox acts in opposite directions

Due to the direction of the forces, a net force of 8.1 kN (per screw hole) will be exerted on the right side while 5.14 kN (per screw hole) will be exerted on the left.

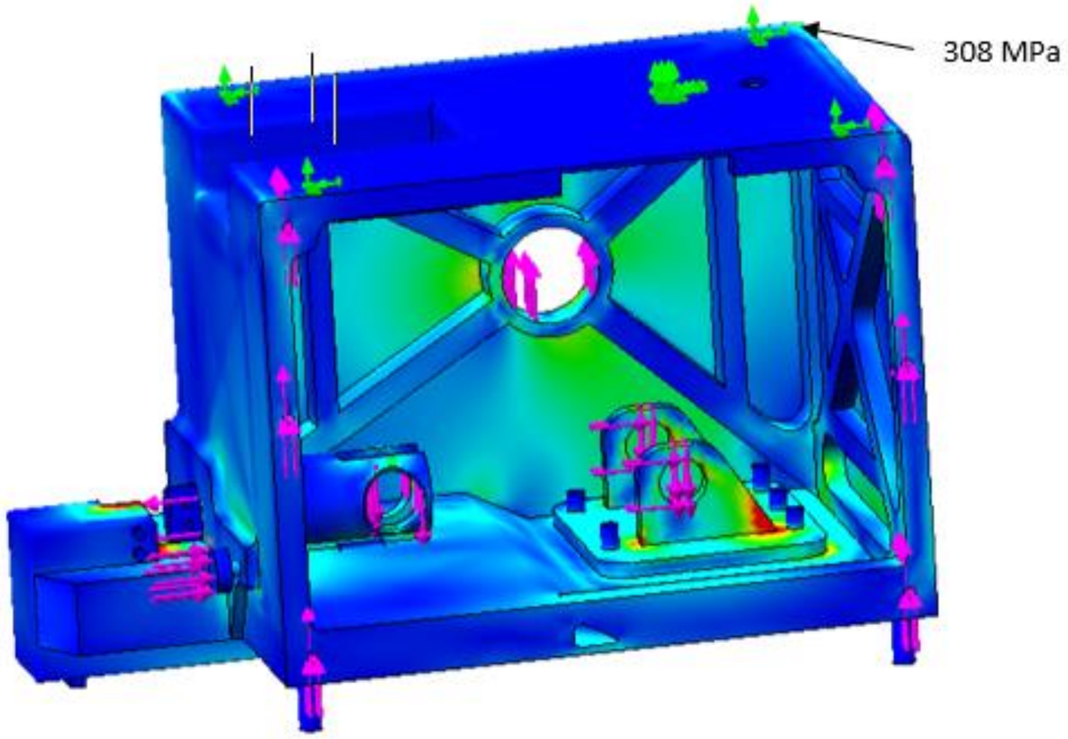

Figure 6.35: Simulation of housing with top wall fixed with forces from shearing rebar applied. Maximum stress experienced by the housing is 308 MPa

From the simulation, the highest stress occurs at one corner of the housing as indicated in *Figure 6.35*. The stress occurring at the corner of the housing is slightly above the allowable stress of the magnesium alloy (306 MPa). As the stress is only slightly over the allowable stress, no action was needed as the difference is negligible as there is a factor of safety of 1.5.

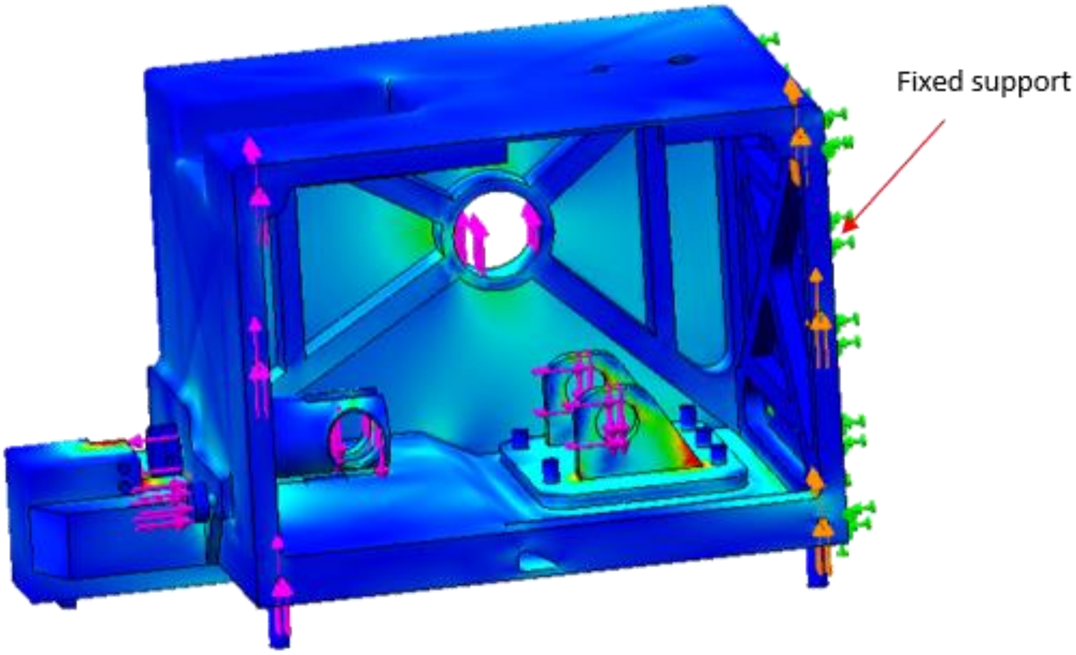

Figure 6.36: Simulation of housing with panel fixed, simulation indicates maximum stress of 289 MPa

The second fixture orientation (*Figure 6.36*) with the same forces, gives a much lower maximum stress of 289 MPa. However, this stress is acting on the cutting head near the insert instead of the back corner.

As part of the same housing simulation, the insert is tested for its maximum stress (*Figure 6.37*). It is expected to be high as the shear force is directly loaded onto it from the blade.

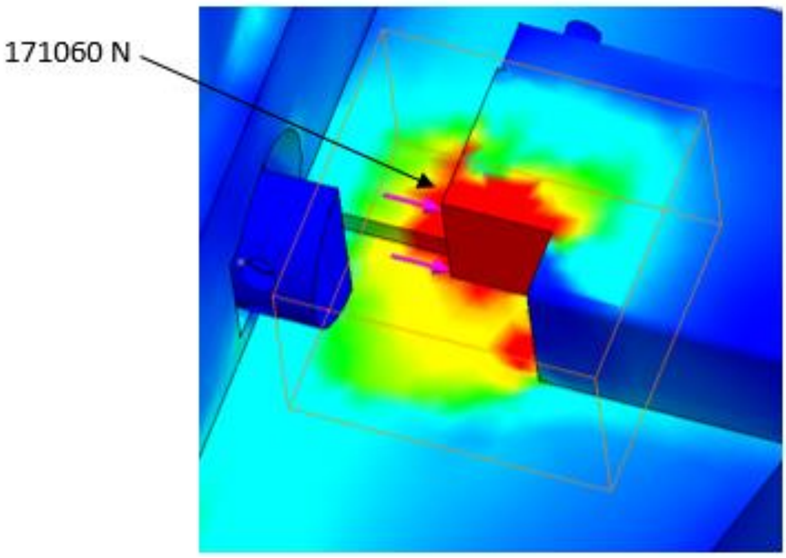

Figure 6.37: Simulation of insert. Shearing force (171.1 kN) exerted onto blade

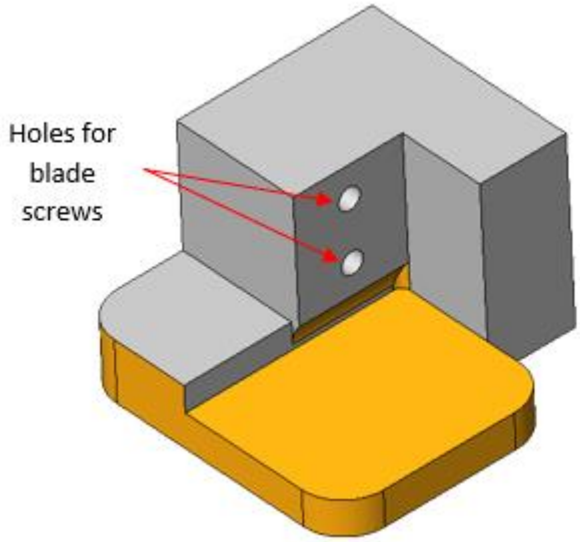

Figure 6.38: Modified insert. Acts as a barrier between the stresses from the blade and the housing

The simulation indicates that the maximum stress experienced by the insert is 2.24 GPa which is just under the allowable stress of 2.3 GPa (ASSAB PM30 SuperClean steel). The basic shape of the insert (designed in *Section 5*.6.4) had to be modified in Solidworks as it was found that the force acting on the insert caused high stresses to occur elsewhere on the cutting head (at the interface between the housing and the insert). This means that the insert's dimensions had to be increased to reduce these stresses at the interface between the insert and the cutting head.

The following simulations are performed to determine the stresses on the housing caused by bending the rebar. Different fixture locations are used for the bending simulations as certain components used for shearing the rebar are no longer exerting forces, which allows panels with no direct forces acting on them to be fixed.

The third simulation has the bottom of the housing fixed (*Figure 6.39*). A force of 8.2 kN is applied to the rebar bending stopper, and a force of 23.3 kN is applied horizontally on the shaft support. The reaction force from the drive shaft (4.41 kN) is assumed to be divided evenly on the six screw holes, and the force created by the maximum possible torque (1536 Nm) of the gearbox is also assumed to be distributed evenly between the screw holes of the housing (1.44 kN per screw hole, calculated for the previous simulation).

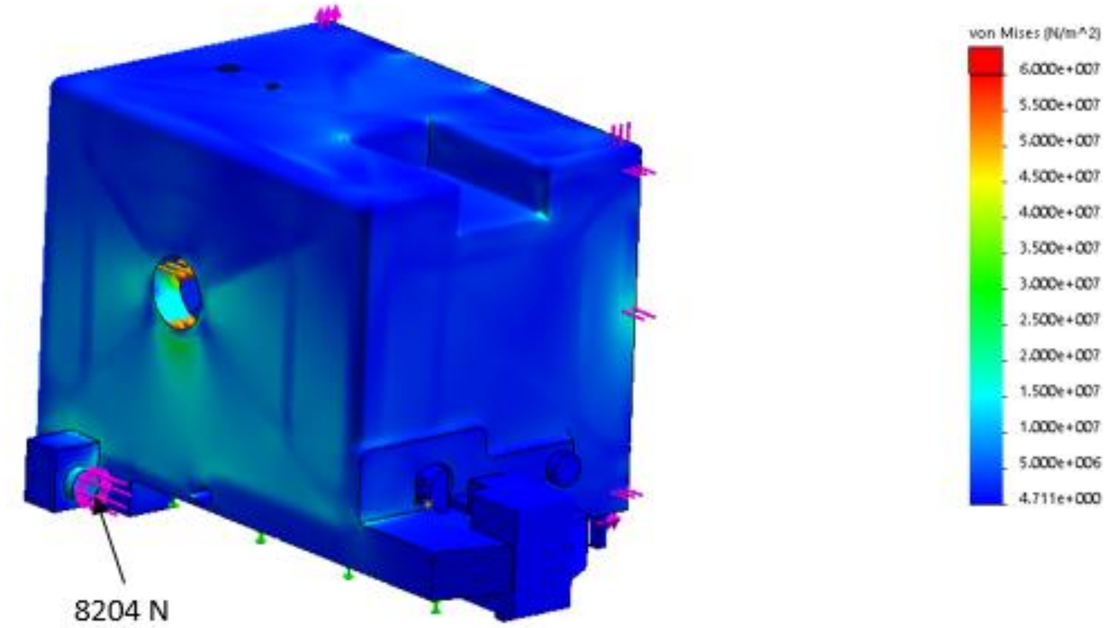

Figure 6.39: Simulation of housing for rebar bending with bottom panel fixed. Maximum stress housing experiences is 51 MPa

From the simulation, the highest stresses are mainly located on the panel that supports the drive shaft and on the corners of the housing where the panel is attached to (*Figure 6.40*). However, the maximum stress (51 MPa) at the corners are below the allowable stress of the magnesium alloy (306 MPa).

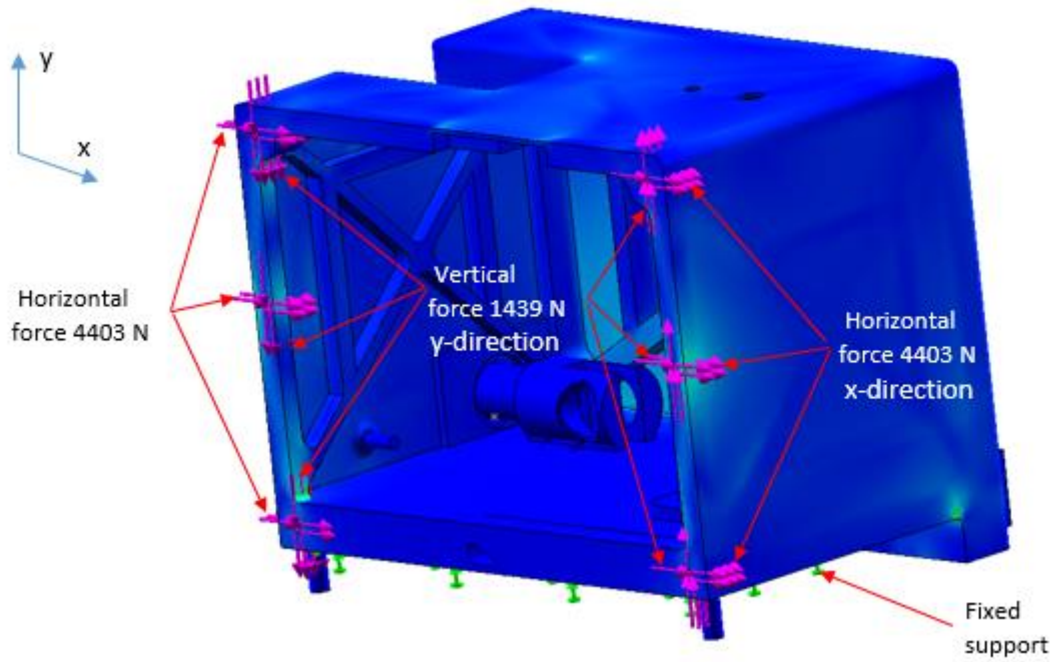

Figure 6.40: High stresses located on the corners of the housing from the same simulation

The next simulation of the housing uses the same forces applied to the same locations. However, this time the fixture is applied to the back wall of the housing (*Figure 6.41*). With this fixture orientation, the stresses are mainly occurring on the corners and the top wall of the housing. The maximum stress that the housing experiences is only 80 MPa, which is well below the allowable stress.

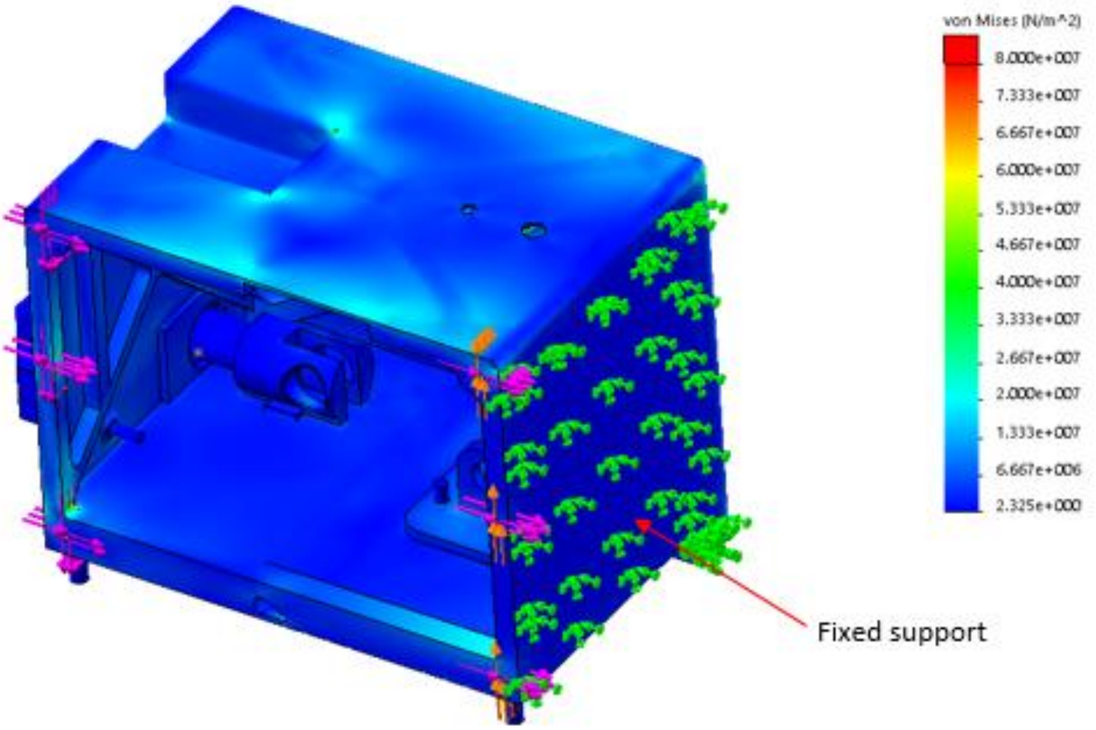

Figure 6.41: Simulation of rebar bending on housing with fixture applied to back wall. Maximum stress experienced by housing is 80 MPa

The next simulation has the top panel fixed with the same loading conditions (*Figure 6.42*). The stresses created by the forces mainly affect the side wall that supports the shaft. However, the maximum stress experienced by the housing is only 50 MPa.

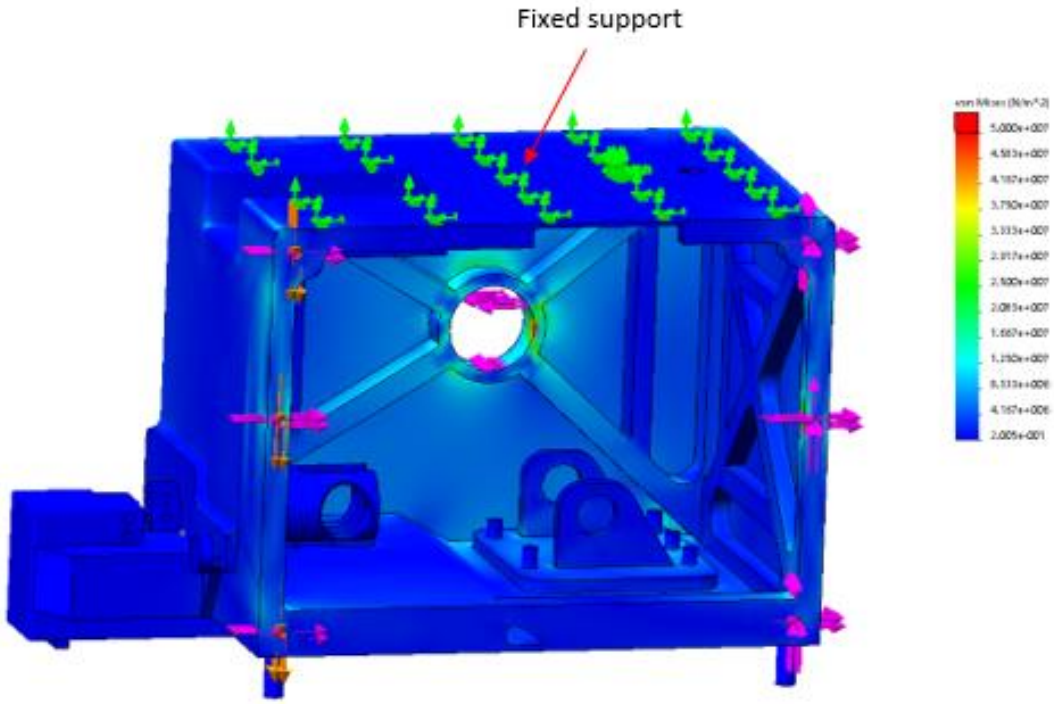

Figure 6.42: Simulation of rebar bending on housing with fixture applied to top wall. Maximum stress experienced by housing is 50 MPa

6.5 Comparison of Finite Element Analysis and First Principles Results

From the simulations in the previous sections, most of the stresses experienced by the individual components are either well below or at the allowable stresses of their respective materials. However, there were a few components where the allowable stress was exceeded, but only by a small margin. As the stress was only slightly over the allowable stress, the difference is negligible. It is expected that the simulation results will differ from the first principles results, as the first principle analysis was based on simplified versions of the components. The purpose of simplifying the components was to make the calculations easier to conduct by hand. A comparison between the FEA and first principle results will be made with the major components of the tool.

6.5.1 Gearbox

Most of the values from the FEA analysis are close to the first principles analysis (*Table 14*). However, there are few components with larger differences, which is due to using approximate shapes in the first principles. The largest difference between the FEA and first principles result comes from the bending of the stage one ring gear. The highest stresses occur around the bottom of the mounting feet. However, the FEA analysis yields an average stress of 20 MPa, which is similar to the first principles result, validating the calculation.

Table 14: Gearbox FEA and first principles comparison

	First Principles Analysis [MPa]	**FEA (highest stress) [MPa]**
Ring gear stage one force on metal between teeth (*Figure 6.15*)	271	179
Ring gear stage two force on metal between teeth (*Figure 6.22*)	466	468
Ring gear stage one bending (*Figure 6.16*)	16	128
Cycloidal disc teeth (*Figure 6.17*)	70	101
Central disc pins (*Figure 6.19*)	493	360
Lid (*Figure 6.23*)	54	68

6.5.2 Shearing Mechanism Linkages

Comparing the first principles result of Linkage AB to the FEA result (*Table 15*), a large difference can be noticed. The high stresses are occurring at the edges of the pin holes; these stress concentrations were not taken into account for the first principles analysis. When the average stress of the component is measured, a stress of 89 GPa is produced, which is close to the first principles result.

The high stresses are mainly occurring on the pin holes and on the corners of linkage BC (*Figure 6.9*). However, when the average stress of the component is measured, an average stress of 10 GPa is found. This is lower than the first principles result, which is expected as the first principles analysis did not take into account the chamfers that were used in the FEA model.

The column theory calculation of the slider was divided into three sections (*Figure 5.58*). In order to compare with the FEA result, the critical stress of the smallest section of the slider (the blade mount section) will be used. The calculated critical stress of the blade mount section is 17.3 GPa; when compared to the FEA result of 315 GPa there is a significant difference. However, the average stress is 29 GPa which is similar to the critical stress calculated in the first principles.

The stress experienced by Hinge AB is close to the FEA result. The difference in stress is due to the FEA model having chamfers added to it (*Figure 6.3*) which reduce any stress concentrations.

Table 15: Shearing mechanism linkages FEA and first principles comparison

	First Principles Analysis	**FEA (highest stress)**
Linkage AB (*Figure 6.8*)	105 GPa	399 GPa
Linkage BC (*Figure 6.9*)	20 GPa	47 GPa
Slider (*Figure 6.7*)	17.3 GPa	315 GPa
Hinge AB (*Figure 6.3*)	1.2 GPa	860 MPa

6.5.3 Housing

To calculate the stress on the walls of the housing, the housing was approximated as a hollow rectangular tube. The calculation does not take into account stress concentrations. The large difference between the first principles and the FEA results (*Table 16*) is due to the stress concentrations on the corners of the housing. However, the average stress of the housing walls from the FEA analysis is 62 MPa (top wall fixed, *Figure 6.35*), and 53 MPa (back wall fixed, *Figure 6.36*) which is much closer to the first principles results.

Table 16: Housing FEA and first principles comparison

	First Principles Analysis [MPa]	**FEA (highest stress) [MPa]**
Back wall fixed (*Figure 6.36*)	55	289
Top wall fixed (*Figure 6.35*)	71	308

6.5.4 Drive Shaft

The keyway bearing stress from the first principles calculation is much smaller than the stress obtained through FEA. It must be noted that the 47 MPa stress occurs along the edge of the keyway (*Figure 6.26*). When an average stress reading is taken from the bearing area of the keyway, a stress of 20.5 MPa is produced.

From the *Table 17,* the first principles stress calculated for the spline is much higher than the FEA result (*Figure 6.27*). This is because the spline tooth in the FEA simulation model is not treated as a cantilever, while the first principles calculation assumes the tooth to be a cantilever.

Table 17: Drive shaft FEA and first principles comparison

	First Principles Analysis [MPa]	**FEA (highest stress) [MPa]**
Keyway (*Figure 6.26*)	21.4	47
Spline (*Figure 6.27*)	232	103

6.5.5 Bending Arm

Table 18 shows that there are differences between the bending stress calculated by the methods of first principles and the FEA results. The higher bending stress calculated using first principles analysis, assumed that the bending arm had a rectangular cross-section; this meant that extra material was removed on either side bending arm (*Figure 5.10*). The first principles calculation gives a much smaller stress value when compared to the FEA result. The 414 MPa stress is due to the stress concentration as shown in *Figure 6.11*. However, the stress reading away from the stress concentration yields a result of 239 MPa (*Figure 6.10*).

Table 18: Bending arm FEA and first principles comparison

	First Principles Analysis [MPa]	**FEA (highest stress) [MPa]**
Bending stress (*Figure 6.10*)	350	238
Spline (*Figure 6.12*)	232	414

6.5.6 Contact Stresses

As Solidworks was not able to simulate the contact stresses of two independent bodies pressing into one another, an approximation was made. In order to obtain the contact stresses, the calculated force acting on that part is applied to a small extruded cut on the surface of the part. This extruded cut area uses the contact area dimensions calculated from first principles. From *Table 19*, the first principles Hertzian contact stress are much higher than the FEA results, as “Hertzian stresses calculated can be overly conservative” (LeCain, 2011).

Table 19: Contact stress FEA and first principles comparison

	First Principles Analysis [GPa]	**Finite Element Analysis (highest stress) [GPa]**
Forming wheel (*Figure 6.31)*	2.47	1.48
Bending arm roller (*Figure 6.32*)	2.02	2.16
Cam (*Figure 6.29*)	2.36	1.74
Cycloidal disc (*Figure 6.18*)	0.588	0.346

6.5.7 Potential Causes in Variation of FEA and First Principles Analysis

From the stress comparisons between the FEA and first principles analysis, these is a noticeable variance in the results. The simulation discretises the component into multiple elements in which it calculates the stress-strain of each element, the stress-strain of each element will then affect the stress-stress of all adjacent elements. The first principles analysis however, assumes the whole component as a single element, therefore only calculating an average stress. The highest stress from the simulation are stress concentrations detected by the Solidworks simulation package. The stress concentrations most likely occur due to the boundary conditions that have been applied in the simulations. For example, in the Solidworks simulation of the housing, the loading conditions are more accurately portrayed with one side of the housing receiving higher forces (*Figure 6.33*). As the forces are not distributed evenly, certain locations of the component will develop much higher stresses. In contrast, for the first principles analysis of the housing, it is assumed that the forces are evenly distributed over the approximated hollow square tubing. As previously mentioned, the first principle analysis only models the components in its simplified form, which will also contribute to the variance between the FEA and first principles results. In conclusion, with the uneven force distributions and major differences in geometry, the results of the FEA simulations will be different when compared to the simplified calculations of the first principle analysis.

7 Circuitry

A battery that supplies 36 V (DeWalt DCB360) will be used to power the tool; however, the motor only requires 28 V. A voltage divider is required to lower the voltage being applied to the motor. To calculate the resistance required, *Equation 7.1* is used. A 100 kΩ resistor is chosen for one of the resistors, which allows the second resistor to be calculated.

$$V_{out} = \frac{V_{in} R_{e2}}{R_{e1} + R_{e2}} \tag{7.1}$$

$$28\ V = \frac{(36\ V) R_{e2}}{100\ k\Omega + R_{e2}}, \therefore R_{e2} = 350\ k\Omega$$

Knowing both the resistor values the circuit diagram can be drawn (*Figure 7.1*).

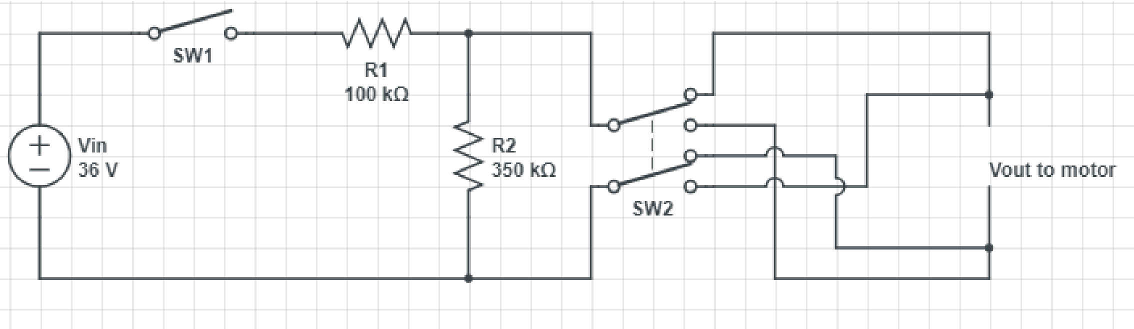

Figure 7.1: Circuit diagram of tool

The circuit has two switches, one for switching (SW1) the tool on and off, while the other one is used as a reverse switch (SW2). SW2 is a double pole toggle switch which means that the tool is only activated if SW2 is held down.

7.1 Battery Attachment

The tool will be powered by a battery as specified by the client. The battery that will be used on this tool and that is widely available in New Zealand will be manufactured by DeWalt. However, this means that the battery mount will have to be taken off an existing power tool and attached to the casing. As the battery mount is of complex design with very small tolerances, copying the battery mount would be too time-consuming. Space for attaching the battery mount will be provided; however, it will have to be detailed in future work.

8 Conclusion and Future Work

Ten conceptual designs were generated based on the research of bending standards, end user feedback, and currently available off-the-shelf rebar cutters and benders. These ten conceptual designs were then evaluated against the needs of the client and the needs of the end user until one concept was selected for further development.

Having developed the concept further, a first principles analysis was conducted along with a FEA analysis. It was found that the average stress of the FEA and first principles analysis were similar but were obviously not the same. There were some large differences between the first principles and FEA stresses, this is due to the stress concentrations on the components created by the uneven force distribution in the simulations. The differences between the geometry used in the first principle and FEA analysis also contributed to the variances in stress.

The prototype rebar cutter and bender that has been designed is by no means the final product (*Figure 8.1*) that will be sold to the public. Future work of this power tool will require further optimisation to reduce its mass (in its present state it would require the minimum of a two-person lift), a more in-depth analysis of the case and the gearbox (both in first principles and ANSYS). These simulations and optimisations should be completed before a prototype is built. Collaboration with a product designer to improve the tool's ergonomics is also required. From the simulations, it is apparent that a topology optimisation could be performed to reduce the mass of the components. A further study should also be conducted to determine if a hydraulic system would be more feasible than the mechanical system designed here. The rebar cutter and bender that has been designed allows rebar to be sheared and bent within 10 seconds with the use of a readily available battery pack. The rebar cutter and bender is portable, but will require a two person lift as prescribed by OSH guidelines.

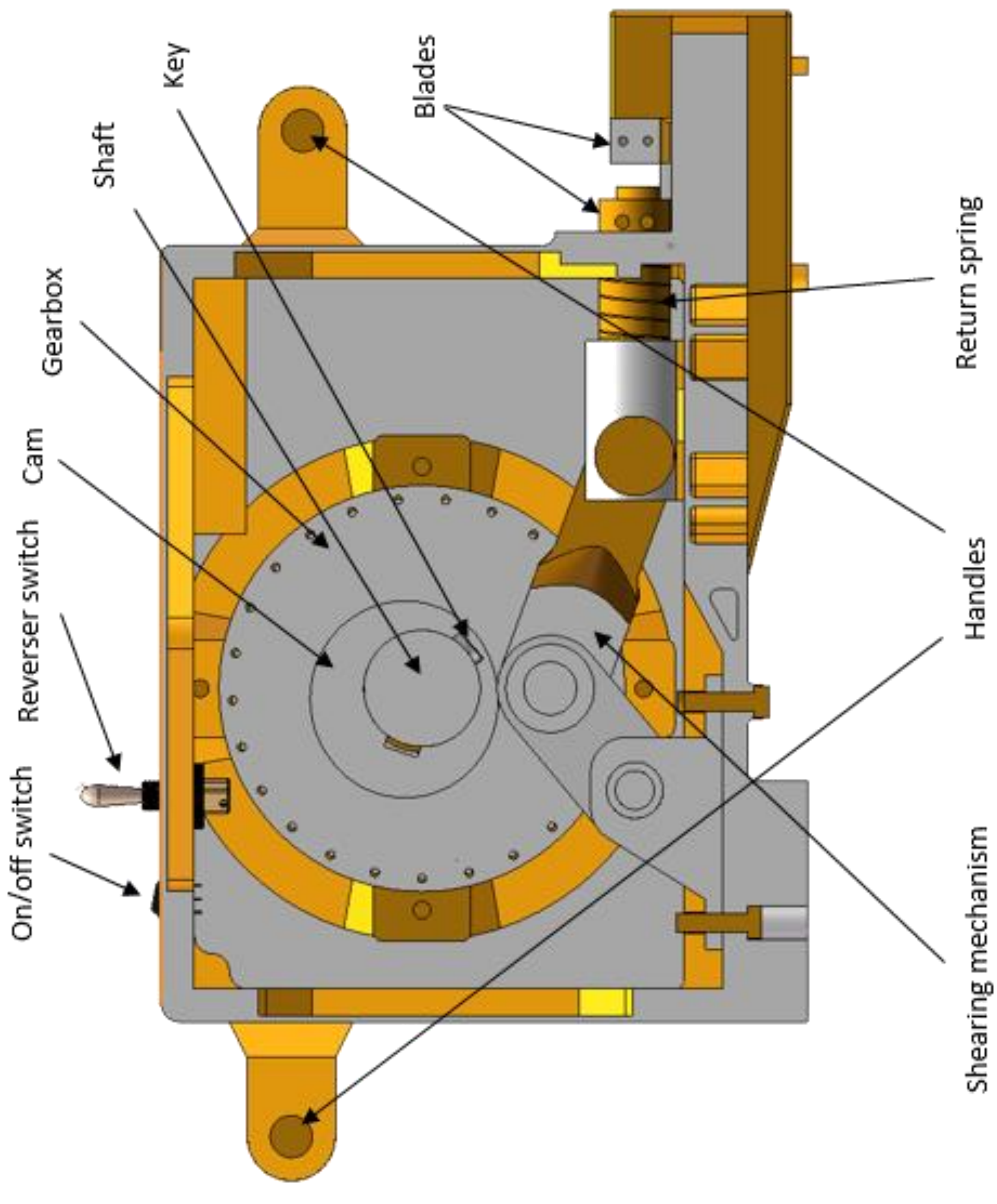

Figure 8.1: Cross-section of rebar cutter and bender

References

Albina. (2018). *Synchronized Incremental Cold Bending*. Retrieved from https://www.albinaco.com/blog/category/steel-bending-methods/synchronized-incremental-cold-bending

Beardmore, R. (2013). *ISO Involute Spline*. Retrieved from http://www.roymech.co.uk/Useful_Tables/Keyways/Splines_Inv.html

Beer, F. P., Johnston, Jr, E. R., DeWolf, J. T., & Mazurek, D. F. (2006). *Mechanics of Materials* (5^{th} ed.). New York, NY 10020: McGraw Hill.

Betons. (2017). *Plain rebar and deformed rebars*. Retrieved from https://www.reinforcing-bar.com/

Biezen, M. (2016). Mechanical Engineering: Internal Forces on Beams (5 of 27) Bending Moments Explained [Video file]. Retrieved from https://www.youtube.com/watch?v=2juoQva4FPY&feature=youtu.be&t=3m1s

Blagojevic, M., Marjanovic, N., Djordjevic, Z., Stojanovic, B., & Disic, A. (2011). A New Design of a Two-Stage Cycloidal Speed Reducer. *Journal of Mechanical Design, 133(8), 1-7.* Retrieved from https://www.researchgate.net/publication/235992854_A_New_Design_of_a_Two-Stage_Cycloidal_Speed_Reducer

Bosch. (n.d.). *14 In. 3/32 In. 1 In. Arbor Type 1A (ISO 41) 36 Grit Metal Stud/Stainless Cutting Bonded Abrasive Wheel.* Retrieved from https://www.boschtools.com/ca/en/boschtools-ocs/cutting-wheels-for-cutoff-machines-type-1a-cwcs1m14sc-27880-p/

British Standards. (n.d.). *BS4500 Keyway Chart.* London, United Kingdom

"*Brushed Pancake Motors"*. (2018). Retrieved from http://www.printedmotorworks.com/brushed-pancake-motors/

Casey, B. (2017). Solving Hydraulic System Overheating Problems. Retrieved from http://www.machinerylubrication.com/Read/680/hydraulic-overheating

Cordless 20mm Rebar Cutter Machine (Be-RC-20b). (2017). Retrieved from ode119.en.made-in-china.com/product/GvYxJSVCgNkn/China-cordless-20mm-Rebar-cutter-Machine-Be-RC-20b-.html

Darali Drives. (n.d.). *Cycloidal Advantage*. New Jersey, America. Retrieved from http://www.darali.com/catalog/page6.pdf

Explosive Forming & Hydro Forming Services Provided at Pacaero. (2018). Retrieved from http://pacaero.com/products/explosive-bonded-metals/explosive-metal-forming-hydro-forming/

Gonzalez, C. (2015). *What's the Difference Between Pneumatic, Hydraulic and Electrical Actuators?* Retrieved from https://www.machinedesign.com/linear-motion/what-s-difference-between-pneumatic-hydraulic-and-electrical-actuators

Gorla, C., Davoli, P., Rosa, F., Longoni, C., Chiozzi, F., & Samarani, A. (2008). Theoretical and Experimental Analysis of a Cycloidal Speed Reducer. *Journal of Mechanical Design 130(11)*, 112604-1 – 112604-8. Retrieved from http://mechanicaldesign.asmedigitalcollection.asme.org/article.aspx?articleid=1449921

Hand tool Ergonomics – Tool design. (2018). Retrieved from https://www.ccohs.ca/oshanswers/ergonomics/handtools/tooldesign.html

HBB-19180DF cordless rebar benders from Stainelec Hydraulic Equipment. (2011). Retrieved from http://www.ferret.com.au/c/stainelec-hydraulic-equipment/hbb-19180df-cordless-rebar-benders-from-stainelec-hydraulic-equipment-n1828346

Hitachi VB16Y 8.0-Amp Portable Variable-Speed Rebar Cutter / Bender. (2018). Retrieved from https://www.amazon.com/Hitachi-VB16Y-Portable-Variable-Cutter/dp/B000066OC3

Hitachi VB16Y 8 Amp Rebar Bender and Cutter. (2018). Retrieved from http://www.cpohitachitools.com/hitachi-vb16y-8-amp-rebar-bender-and-cutter/hitnvb16y,default,pd.html

Hydraulic Actuators: Cylinders. (2005). Retrieved from https://www.slideshare.net/jineshrachana/hydraulics-3634875

Hydroforming of tubes, extrusions, and sheet. (2018). Retrieved from http://www.thefabricator.com/article/hydroforming/hydroforming-of-tubes-extrusions-and-sheet

IHS EDSU. (2000). *Contact Phenomena 1: Stresses, Deflections and Contact Dimensions for Normally-Loaded Unlubricated Elastic Components*. Retrieved from https://www.esdu.com/cgi bin/ps.pl?sess=unlicensed_1180721081637qnr&t=doc&p=esdu_78035d

LeCain, N. (2011). Tutorial of Hertzian Contact Stress Analysis. Retrieved from https://wp.optics.arizona.edu/optomech/wp-content/uploads/sites/53/2016/10/Tutorial_LeCainNicholas.pdf

Mabie, H. H., & Reinholtz, C. F. (1987). *Mechanisms and Dynamics of Machinery* (4th ed.). Virginia: John Wiley & Sons

Makita Power Tools - XCS01Z. (2018). Retrieved from https://www.makitatools.com/products/details/XCS01Z

Mitre 10. (2018). Jigsaw Blade [Brochure]. Retrieved from https://www.mitre10.co.nz/shop/search?q=Jigsaw-Blade%3Arelevance&page=0

Mitre 10. (2018). Multi-Tool Blades [Brochure]. Retrieved from https://www.mitre10.co.nz/shop/search?q=Multi-Tool-Blades%3Arelevance

Molloy, D. (2010, June). Reinforcing Steel. *Build*, 118, 20-22. Retrieved from https://www.buildmagazine.org.nz/assets/PDF/Build118-20-Reinforcing-Steel.pdf

Nanovate High Load Bushings and Bearing Material. (n.d.). Retrieved from http://www.integran.com/products/high-load-bushings

Norton, R. L. (2002). *Cam Design and Manufacturing Handbook* (2nd ed.). Retrieved from https://www.globalspec.com/reference/54773/203279/chapter-7-cam-size-determination

Opinions on Cycloid gear. (2011). Retrieved from http://www.writeopinions.com/cycloid-gear

Integrated Publishing Construction. (n.d.). *Placing and Tying Reinforcing Steel*. Retrieved from http://www.tpub.com/steelworker2/78.htm

Pope, J. E. (1997). *Rules of Thumb for Mechanical Engineers.* Houston, Texas: Gulf Publishing Company.

Preferred Fits and Tolerances Charts (ISO and ANSI Metric Standards). (2018). Retrieved from https://www.amesweb.info/FitTolerance/PreferredTolerances.aspx

Rebar and Mesh Conversion Supplies (Pty) Ltd. (n.d.). Retrieved from http://www.rmcspl.co.za/RMCSPL%20DBC-16H.php

Rebar Blades. (2009). Retrieved from http://www.rebarblades.com/blades/mustang.html

Recycling | New Zealand Steel. (2018). Retrieved from http://www.nzsteel.co.nz/sustainability/recycling/

Rohloff. (n.d.). *Planetary Gear System*. Retrieved from https://www.rohloff.de/en/experience/technology-in-detail/planetary-gear-system/

RMCS. (n.d.). *Rebar Bender DBD-16L*. Retrieved from http://www.rmcspl.co.za/Rebar%20Bender%20DBD-16L.php

Roofing Tools. (2011). *Malco Sheet Metal Saw Blade*. Retrieved from https://www.roofing-tools.com/sheet-metal-saw-blade-c2x11631096

SEISMIC® Pacific Steel. (2018). Retrieved from http://www.pacificsteel.co.nz/products/reinforcing-bar-and-coil/seismic-300e/

Sheet Metal Cutting (Shearing). (2009). Retrieved, from http://www.custompartnet.com/wu/sheet-metal-shearing

Shell rolling procedure. (2013). Retrieved from https://www.slideshare.net/patil_13pramod290/shell-rolling-procedure

Stainelec EDILGRAPPA REBAR BENDERS. (2014). Retrieved from http://www.stainelec.com.au/edilgrappa-rebar-benders.php

Stainlec Hydraulic Equipment. (2014). Retrieved from http://www.stainelec.com.au/images/ogurarebarbender.jpg?357Standards Australia. (1985). Design of Rotation Steel Shafts (AS1404-1985).

The American University in Cairo. (2003). *Cam Design* [Power point]. Egypt. Retrieved from https://www.slideshare.net/rajat_jubilee/chapter-8-29473471

WARDJet. (n.d.). Waterjet University - Pumps. Retrieved from https://wardjet.com/waterjet/university/pumps

Worm Gearbox. (2014). Retrieved from https://wiki.pierobotics.org/wiki/Worm_Gearbox#/media/File:Gearbox_Rev_I_case_removed.png

Warren, G. (2016). Moving and handling: reducing risk through assessment. *Nursing Standard,* 30(40), 49-57. Retrieved from https://journals.rcni.com/doi/pdf/10.7748/ns.30.40.49.s45

Appendix A: Motor Specifications

Printed Motor Works GPM16LRD 005108 (Brushed Pancake Motors, 2018)

Motor Constants	Symbol	Unit	Value
Voltage	Ke	V/krpm	6.5
Torque	Kt	Nm/Amp	0.062
Damping	Kd	Nm/1000rpm	0.14
Friction	Tf	Nm	0.06
Terminal Resistance	Rm	Ohm	0.6

Motor Ratings	Unit	Value
Voltage	V	28
Current	A	26.5
Torque	Nm	1.5
Speed	RPM	3000
Power	W	550

Appendix B: Motor Technical Drawings

GPM16LRD 005108 (Brushed Pancake Motors, 2018)

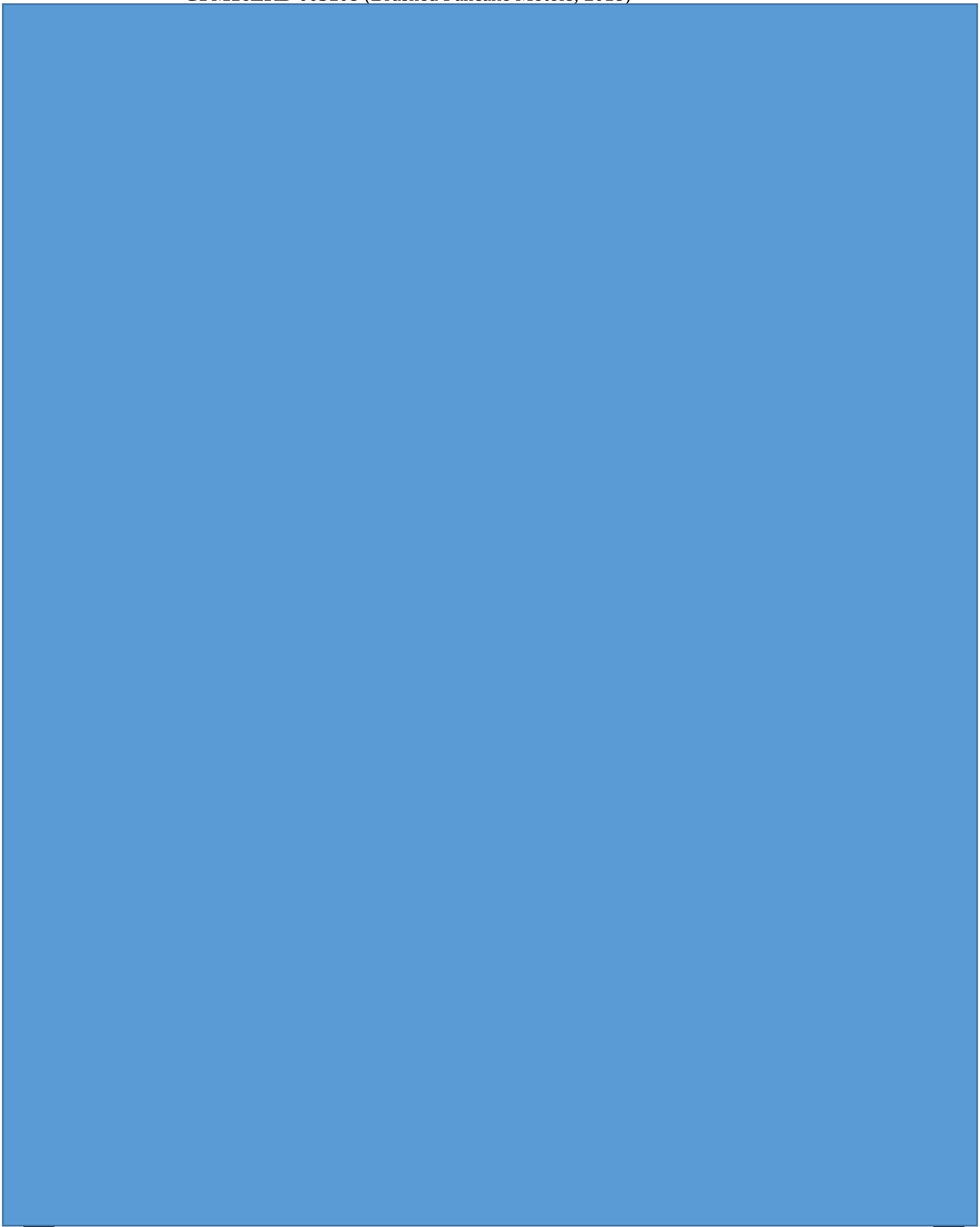

Appendix C: Technical Drawings

C1 Tool Assembly Drawings

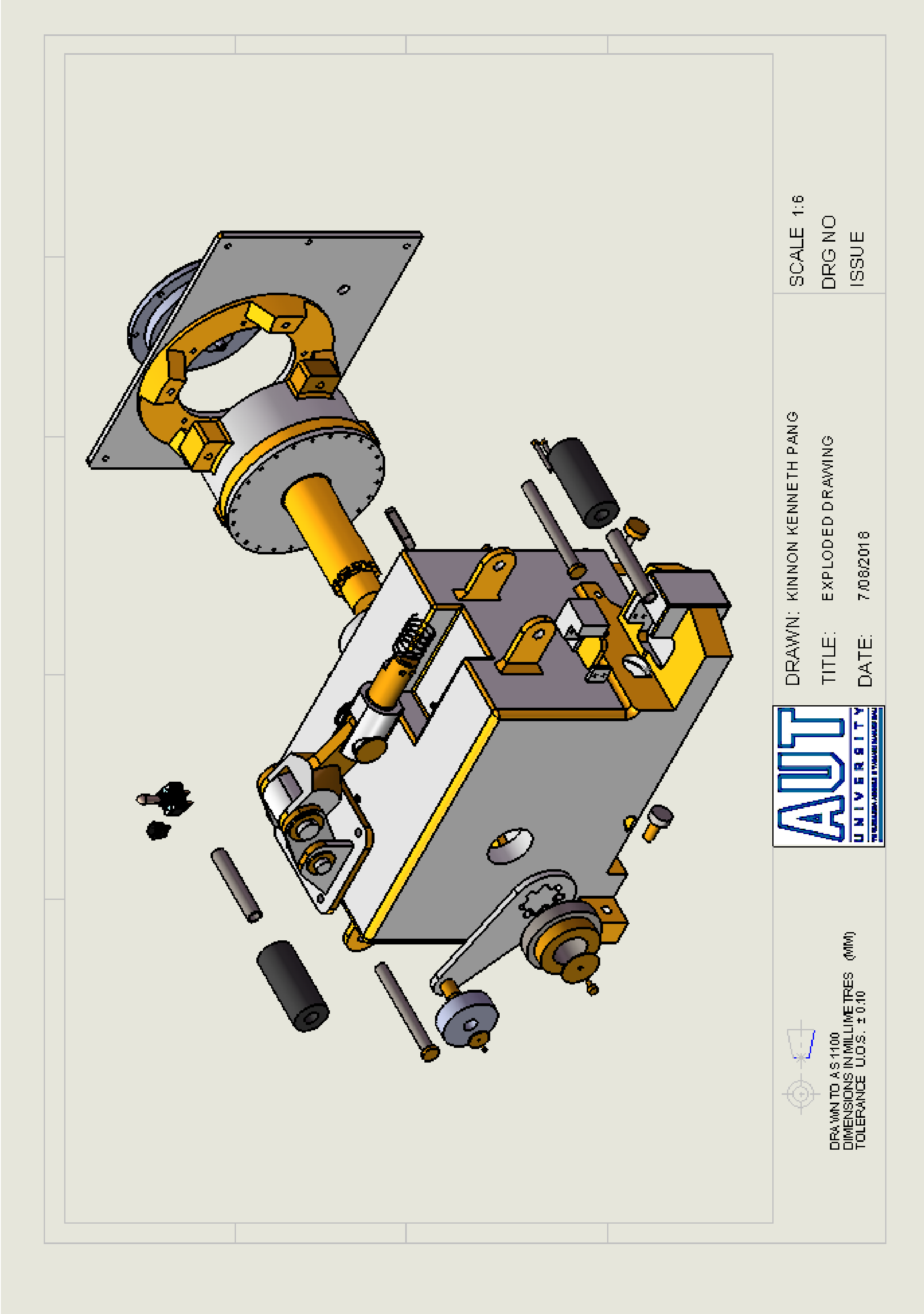

C1.1 Bill of Materials

BOM Table

ITEM NO.	PART NUMBER	DESCRIPTION	QTY.
1	Housing	EA65RS-T4 magnesium alloy	1
2	Shear mechanism		1
3	Insert	ASSAB PM30 SuperClean steel	1
4	Handle bolt	16 mmx2 mmx140 mm Zinc grade 10.9 hex and matching nut	2
5	Handle core	Stainless 304	2
6	Handles	Silicon	2
7	Rebar stopper screw cutting	10 mmx1.5 mmx 50 mm grade 10.9 hex	1
8	Rebar stopper screw bend	14 mmx2 mmx50 mm grade 10.9 hex	1
9	Blade	RC-22 Blade	1
10	Blade screw	M5 screw (information could not be obtained from supplier)	2
11	Back panel	EA65RS-T4 magnesium alloy	1
12	Gearbox		1

BOM Table

ITEM NO.	PART NUMBER	DESCRIPTION	QTY.
13	Cam H5 H6	ASSAB PM30 SuperClean steel	1
14	Cam and shaft key	1018 steel	1
15	Pancake motor		1
16	Motor key	stainless 304	1
17	Forming wheel	ASSAB PM30 SuperClean steel	1
18	Bending arm roller	ASSAB PM30 SuperClean steel	1
19	Retaining thumb screw for forming wheel	M6 x13 mm	1
20	Retaining washer	Zinc plated	1
21	Bending arm	ASTM A747	1
22	Retaining roller screw		1
23	On/off switch		1
24	Reverser switch switch	Double pole toggle swtich	1
25	Retaining washer roller arm	Zinc plated	1

BOM Table

ITEM NO.	PART NUMBER	DESCRIPTION	QTY.
26	m8x125mmx16mm	Grade 8.8	6
27	12mm x 1.75mm x 40mm	Grade 8.8 bolt and matching nut	5
28	10mm x 1.5mm x 90mm	Grade 10.9 bolt and matching nut	4
29	7mm x 1mm x 30mm	Supplied with motor	8
30	Return spring	PC1902-2000-6250-MW-2500-CG-N-IN	1
31	M5x0.8mmx12mm	Class 4.8 philips pan head	25

DRAWN TO AS 1100
DIMENSIONS IN MILLIMETRES (MM)
TOLERANCE U.O.S. ± 0.10

AUT UNIVERSITY

DRAWN: KINNON KENNETH PANG
TITLE: BILL OF MATERIALS
DATE: 07/08/2018

SCALE
DRG NO
ISSUE

C1.2 Motor and Gearbox Panel Assembly

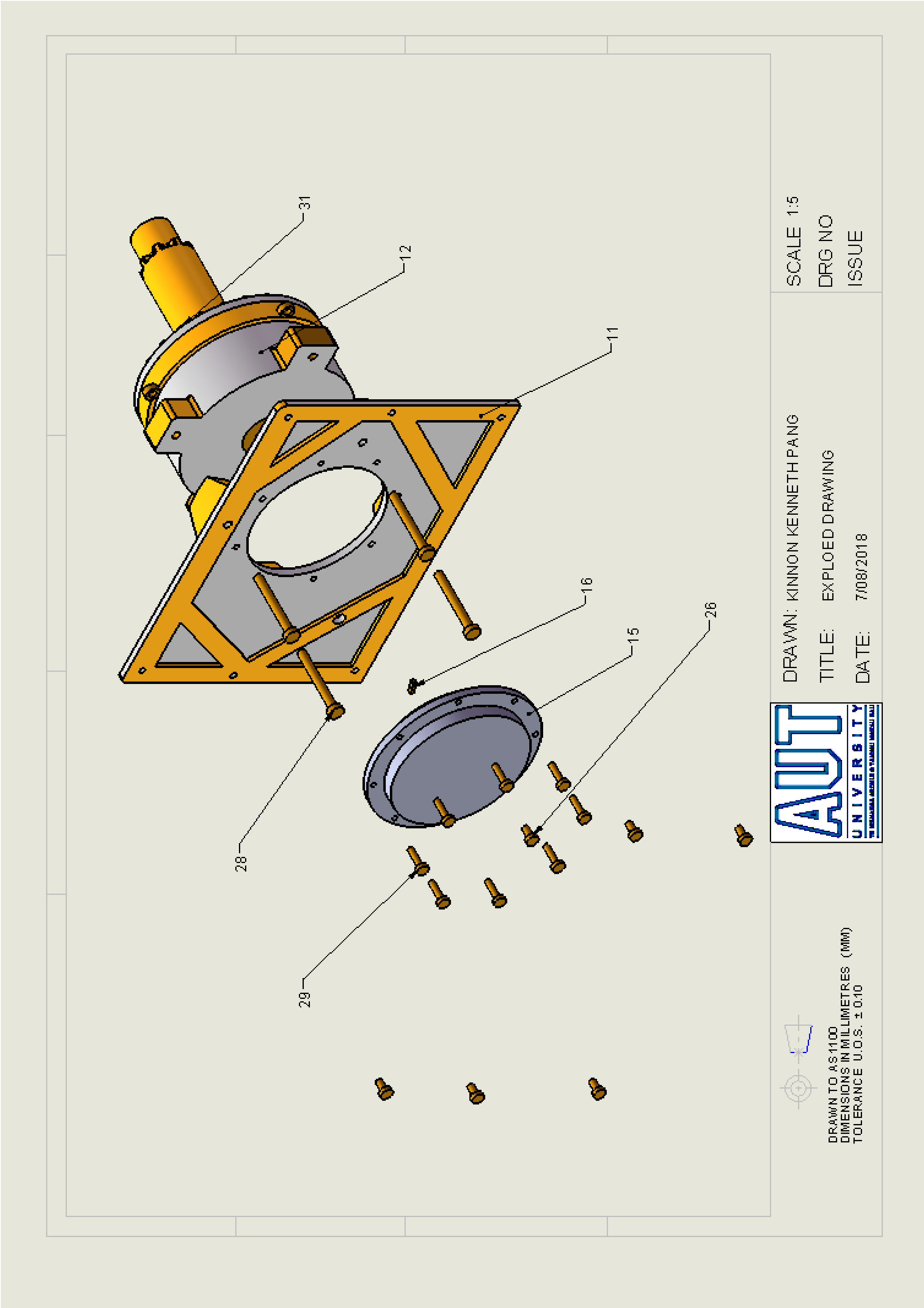

C1.3 Bending Components Assembly

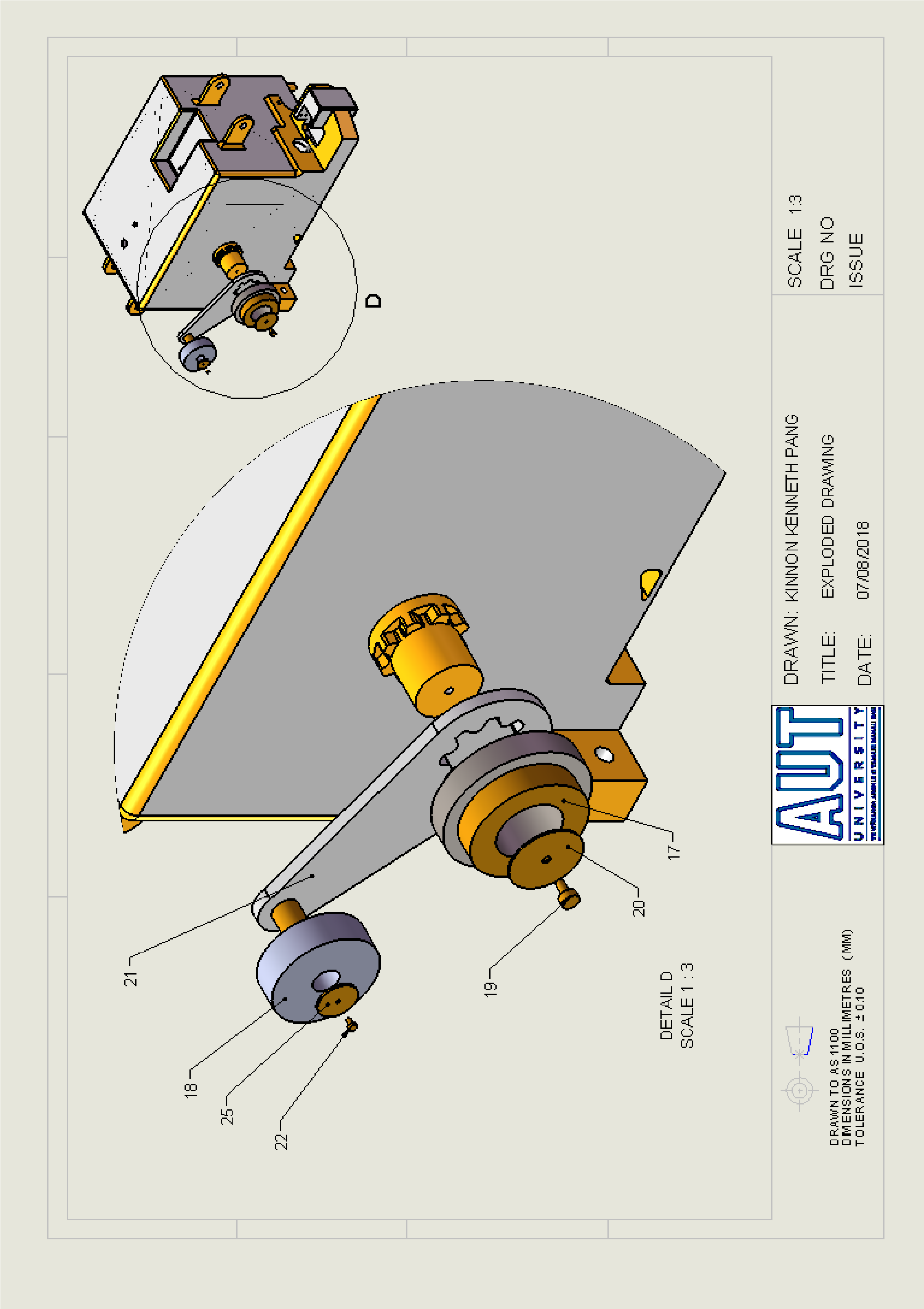

C1.4 Handle Assembly

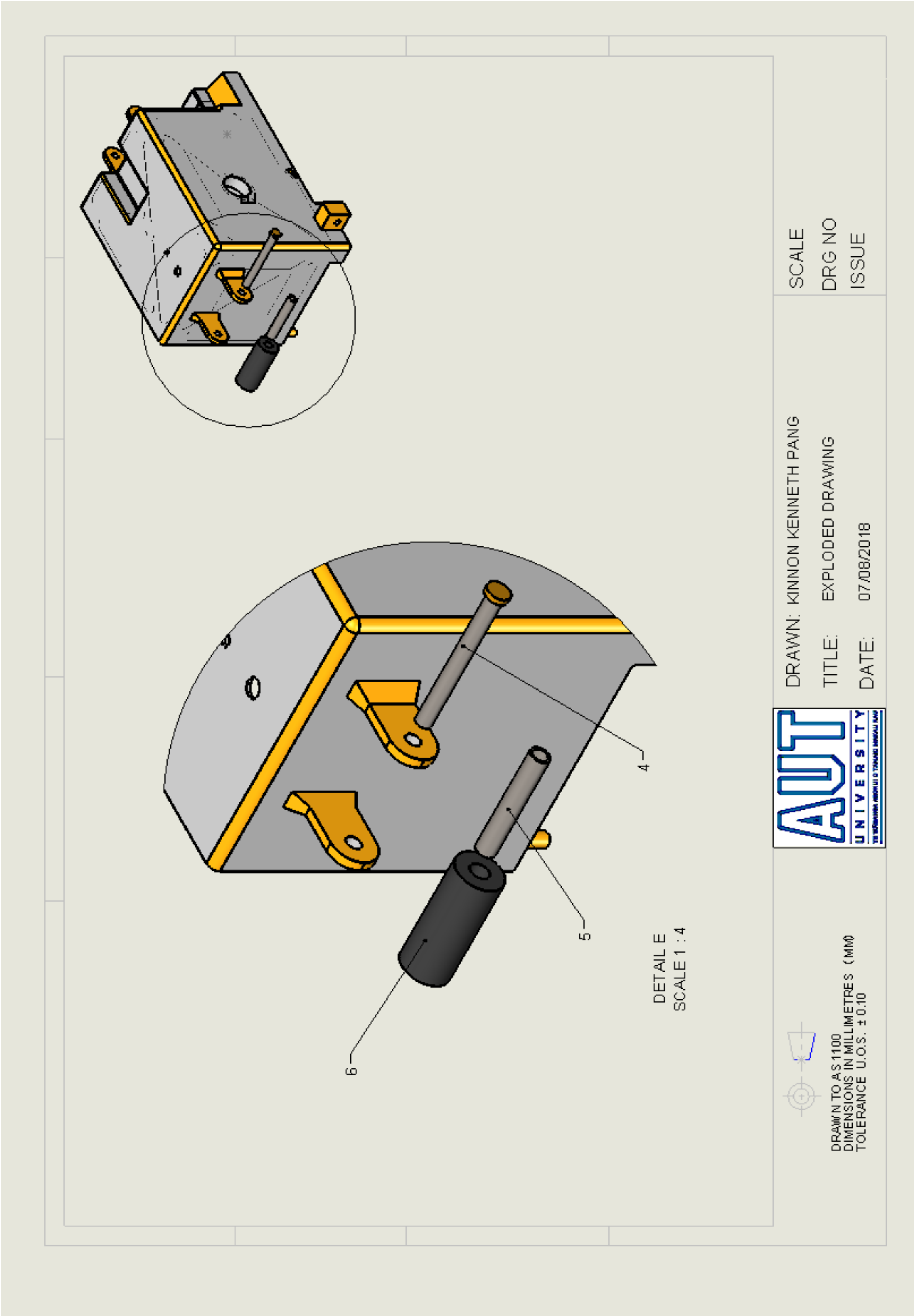

C1.5 Cutting Head Assembly

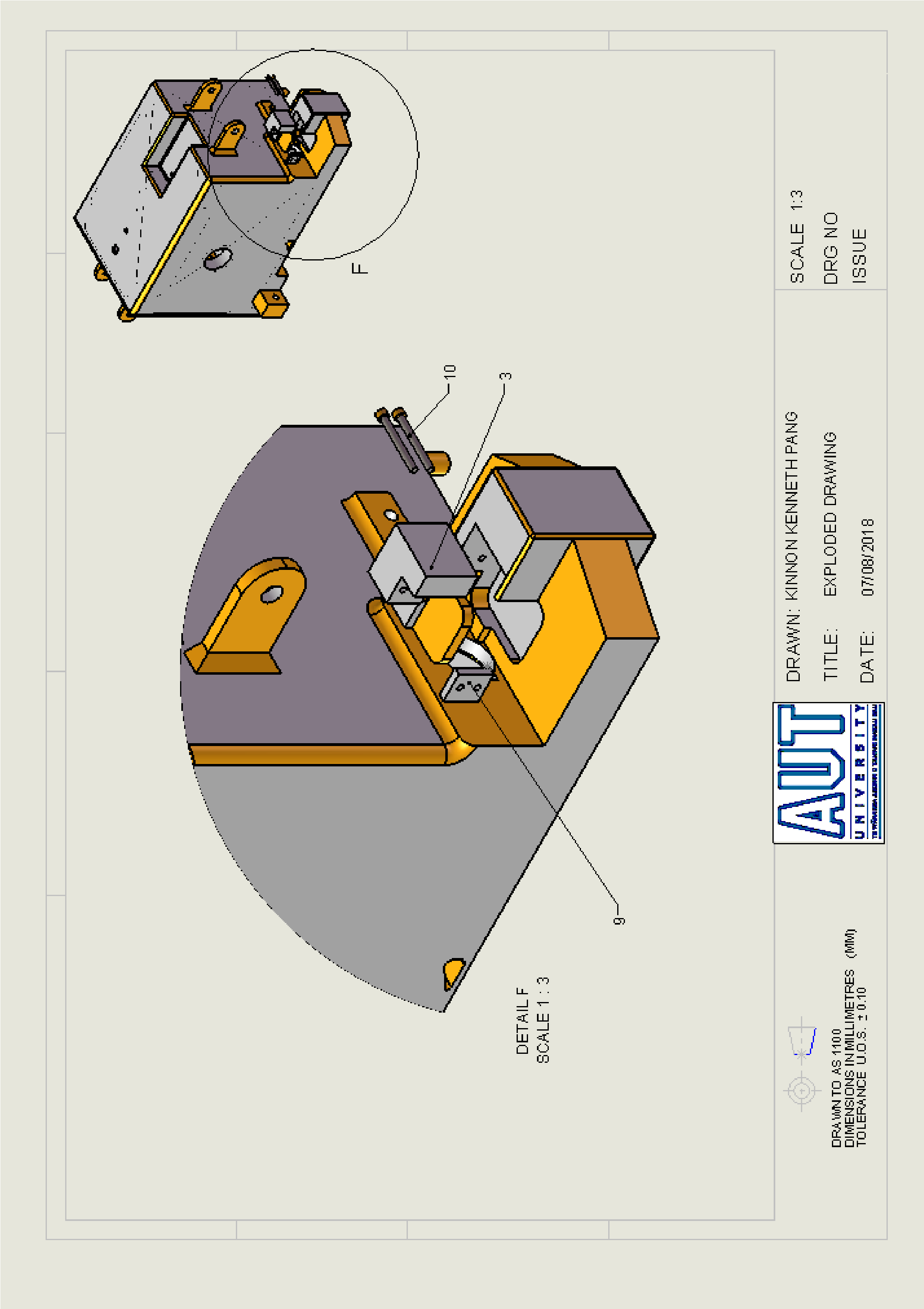

C1.6 Cam Assembly

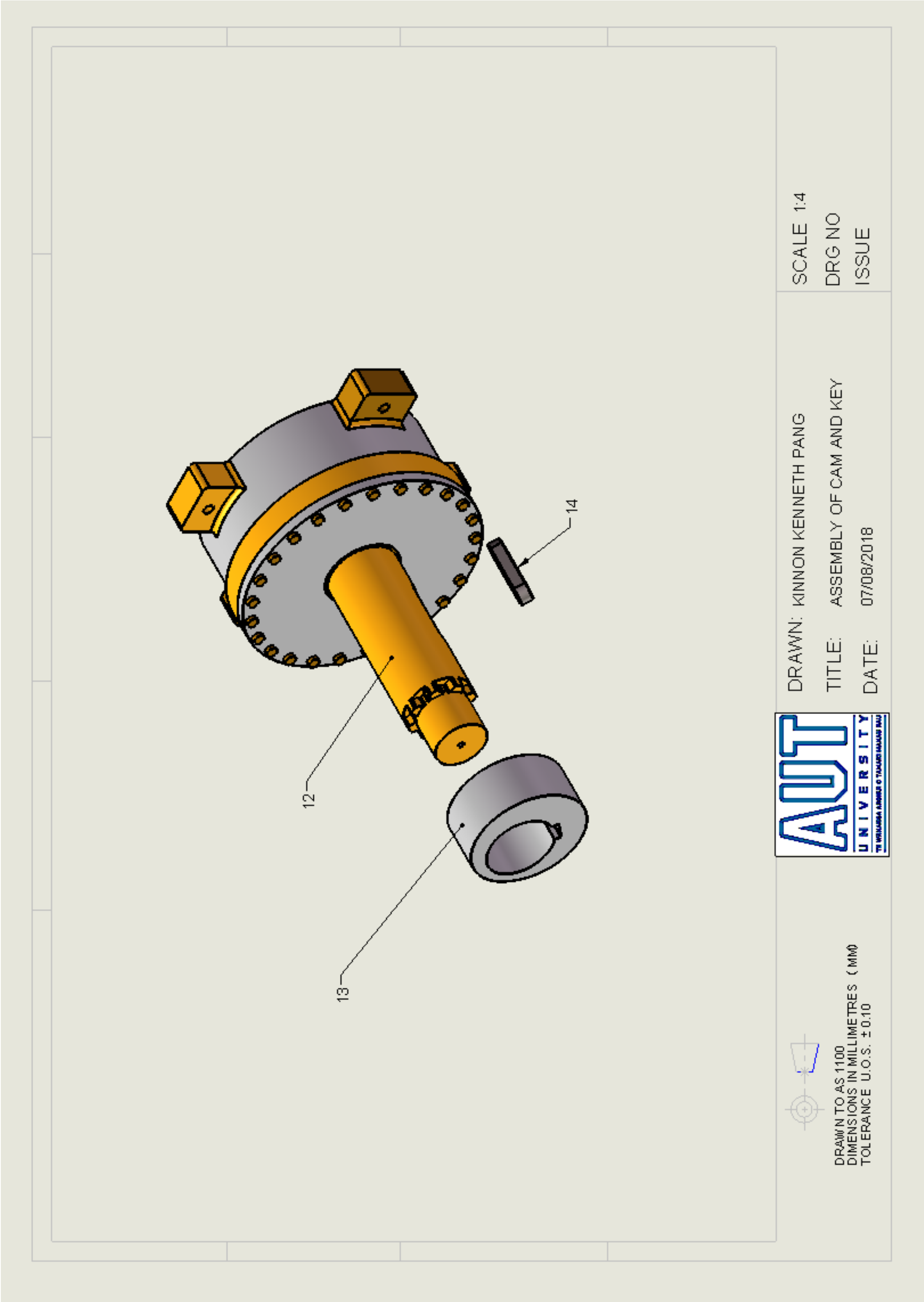

C1.7 Shear Mechanism and Housing Assembly

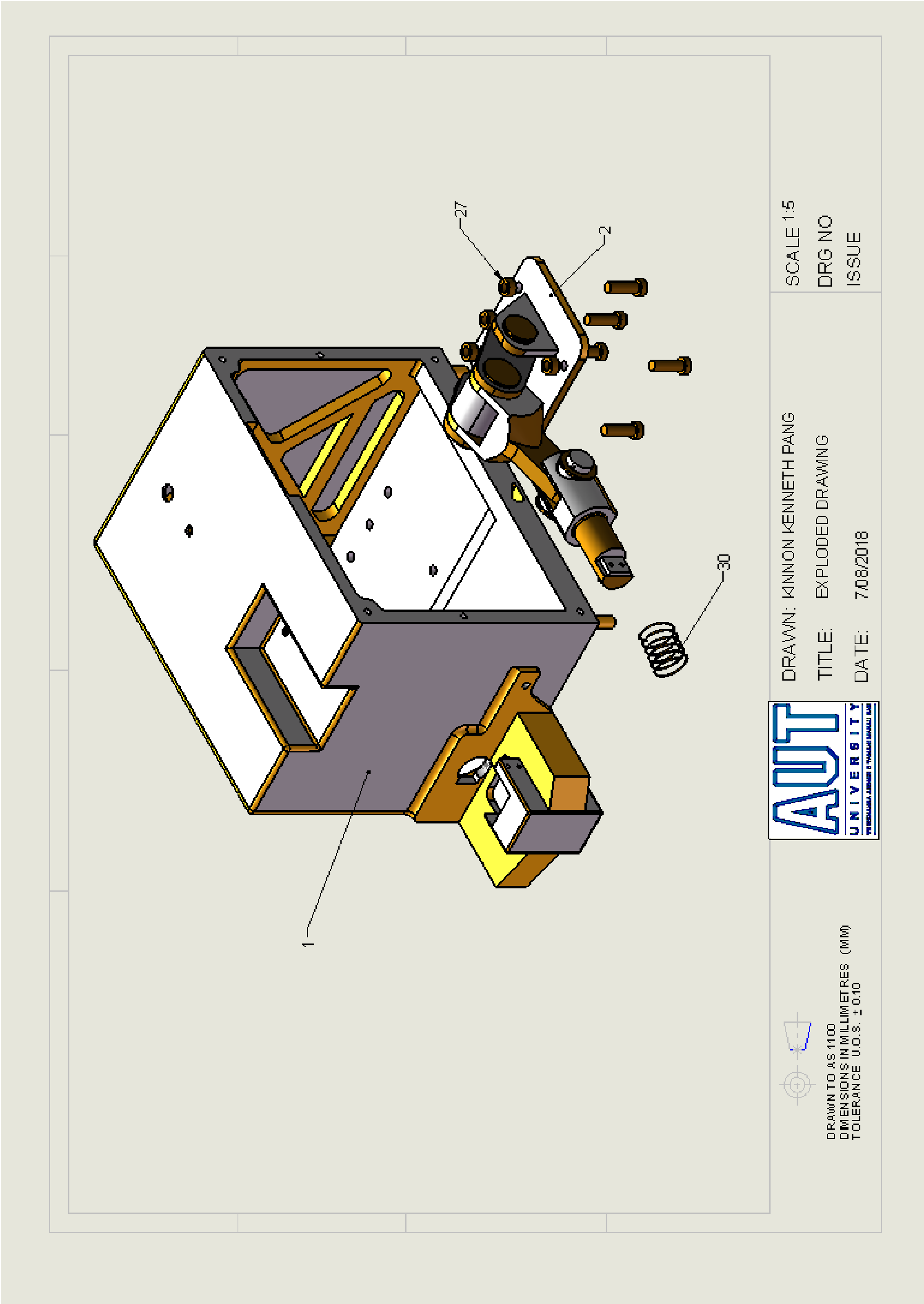

C2: Gearbox

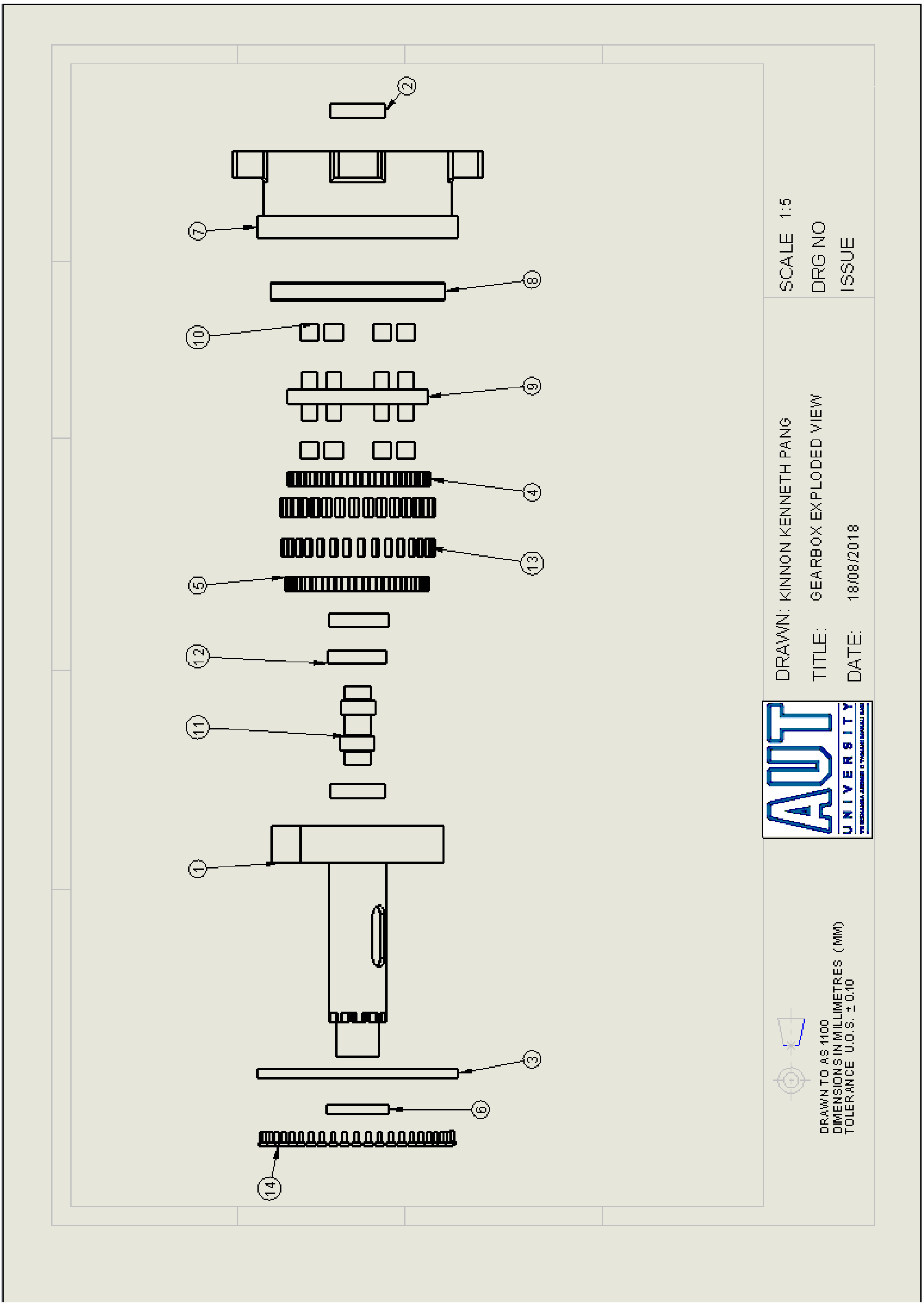

SCALE 1:5
DRG NO
ISSUE
DRAWN: KINNON KENNETH PANG
TITLE: GEARBOX EXPLODED VIEW
DATE: 18/08/2018
AUT UNIVERSITY
DRAWN TO AS 1100
DIMENSIONS IN MILLIMETRES (MM)
TOLERANCE U.O.S. ± 0.10

C2.1 Bill of Materials

ITEM NO.	PART NUMBER	DESCRIPTION	QTY.
1	ring gear stage two	6580 STEEL	1
2	6206zzvvddu bearing		2
3	gearbox lid	5056-H18 Al ALLOY	1
4	cycloid disc s1	4142 STEEL	1
5	cycloid disc s2	4142 STEEL	1
6	bushing for lid	BRONZE ASTM B505 C93200	1
7	ring gear stage one v2 use this	5056-H18 Al ALLOY	1
8	61832 bearing		1
9	central disc v2 use this	4140 STEEL CONDITION U	1
10	central disc pin bushing	COPPER BERYLLIM C17200-TH04	12
11	gearbox shaft	6580 STEEL	1
12	6008zzvvddu		2
13	ring gear pins	L2 STEEL	66
14	lid screws m5 x 0.8 mm x 12 mm	CLASS 4.8	25

DRAWN TO AS 1100
DIMENSIONS IN MILLIMETRES (MM)
TOLERANCE U.O.S. ± 0.10

DRAWN: KINNON KENNETH PANG
TITLE: BILL OF MATERIALS
DATE: 18/08/2018

SCALE
DRG NO
ISSUE

C2.2 Gearbox Assembly Drawing

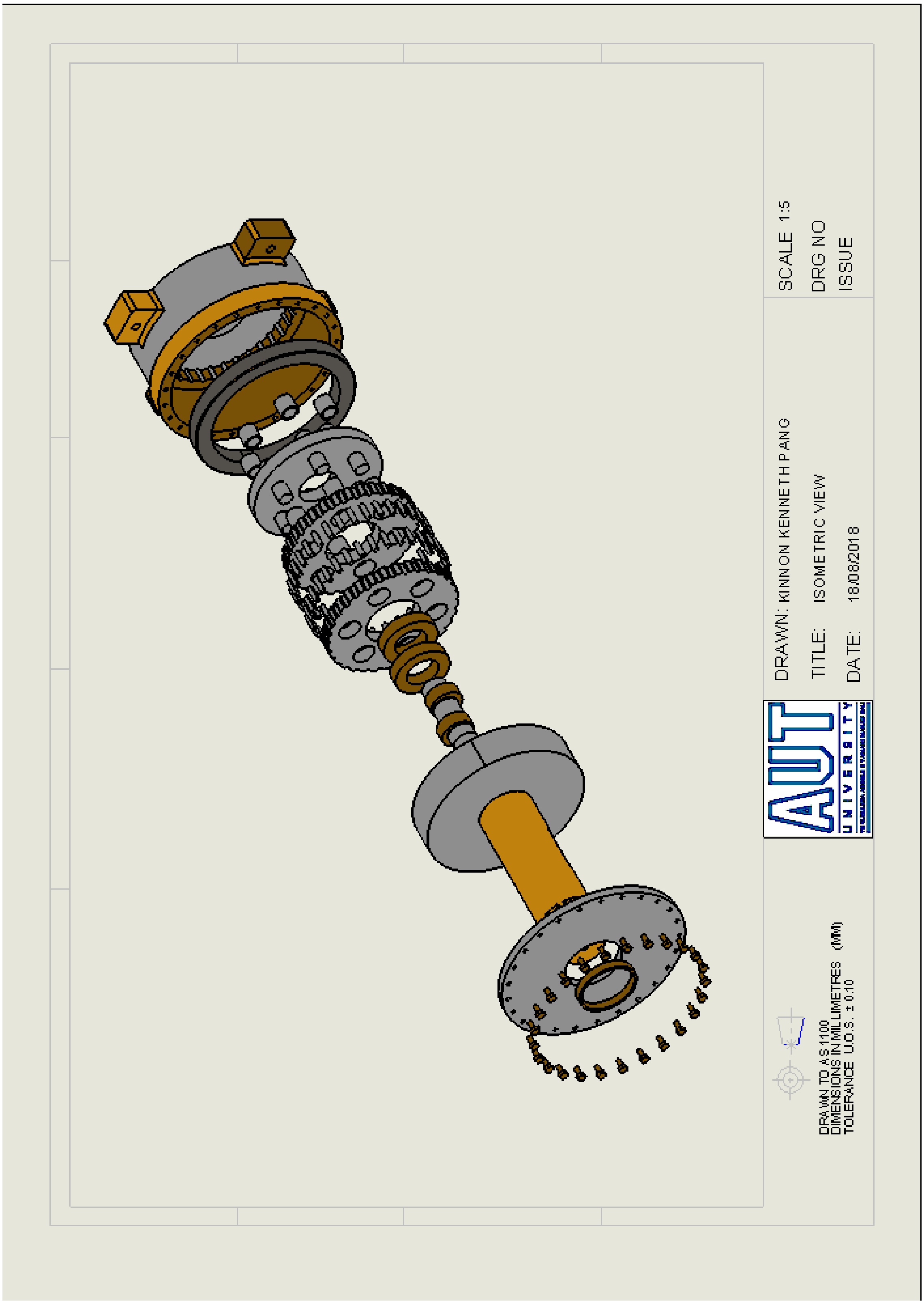

C2.3 Gearbox Lid Bushing

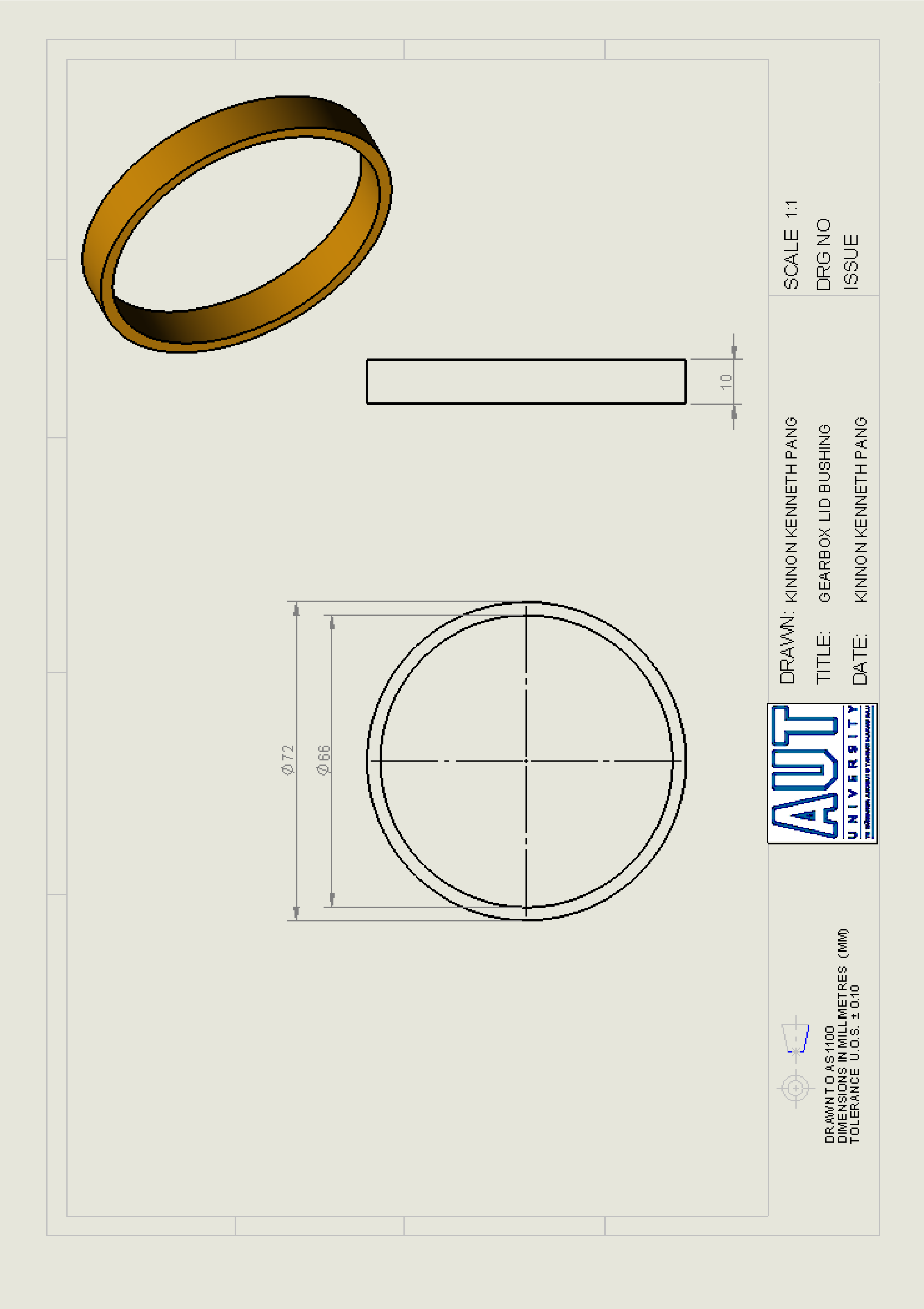

C2.4 Drive Shaft Key

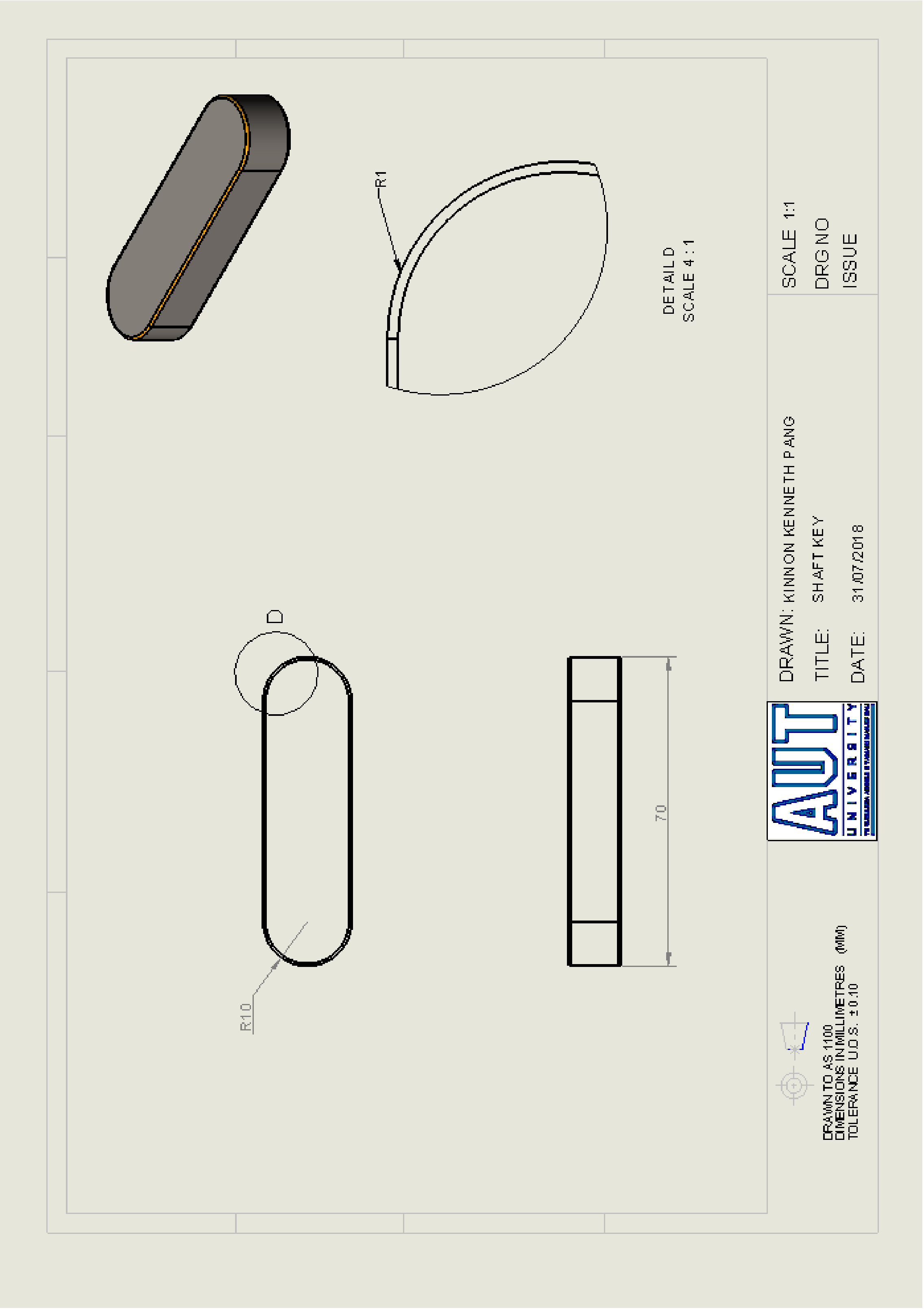

C2.5 Central Disc Pin Bushing

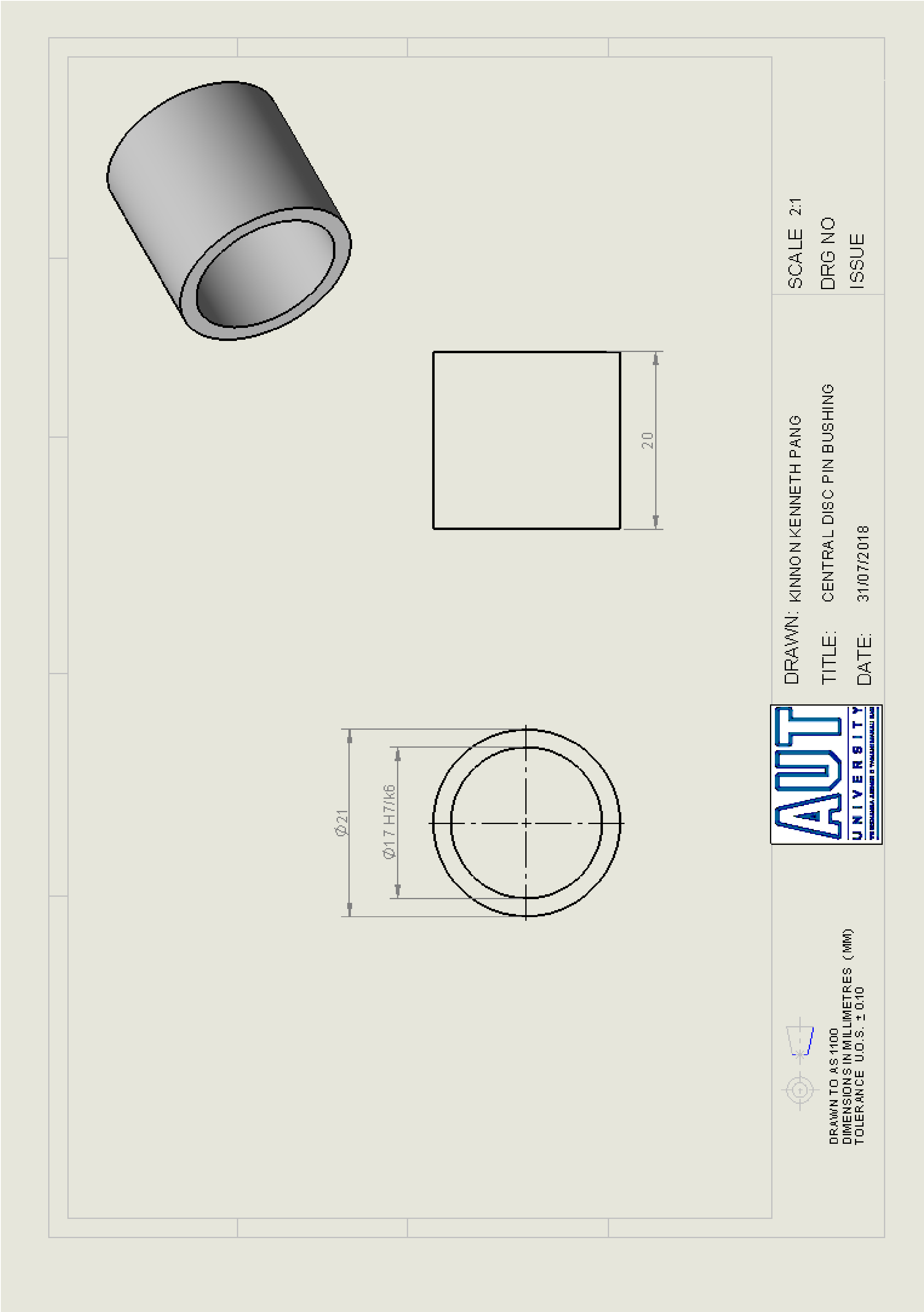

C2.6 Central Disc

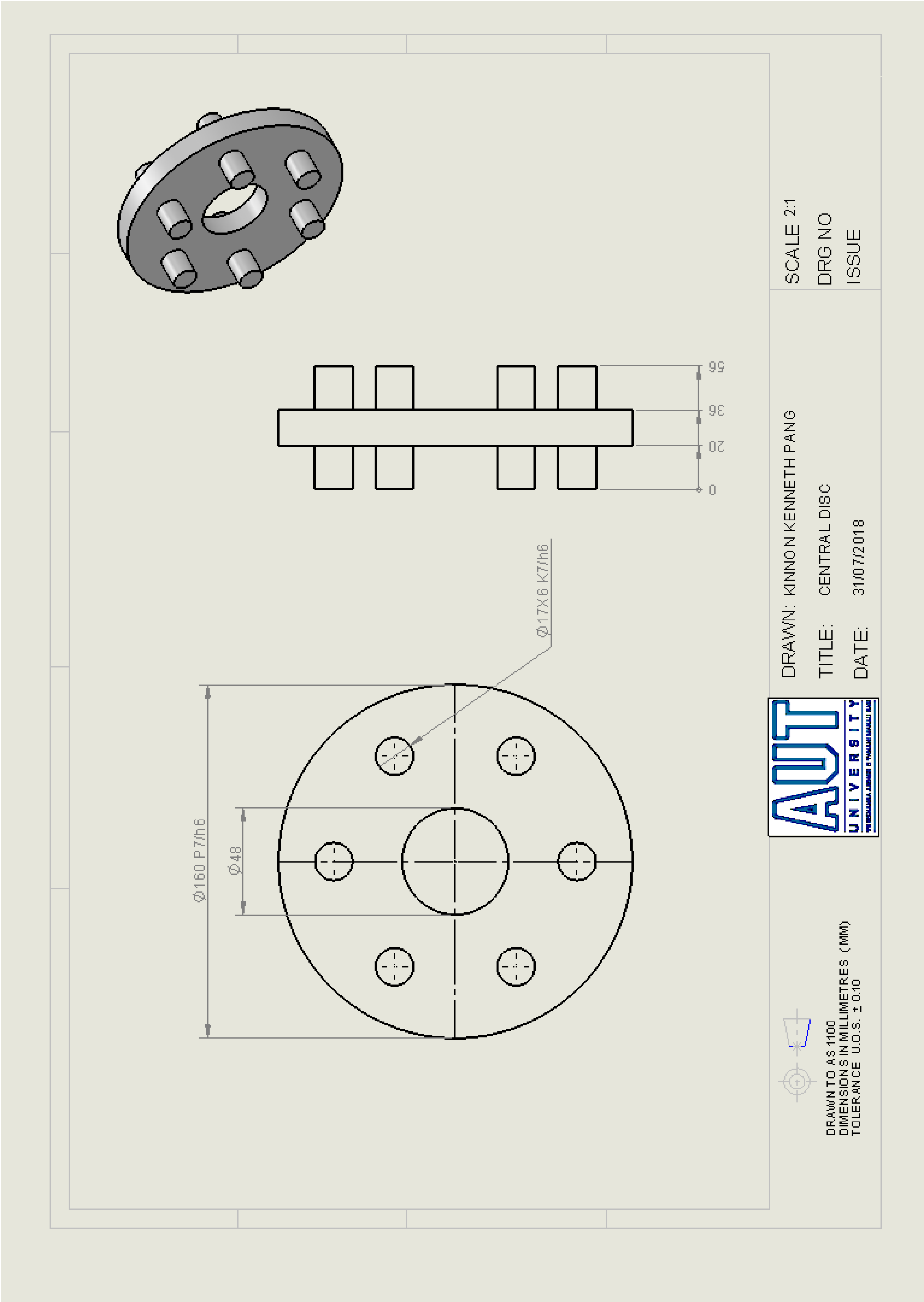

C2.7 Stage 1 and 2 Cycloidal Disc

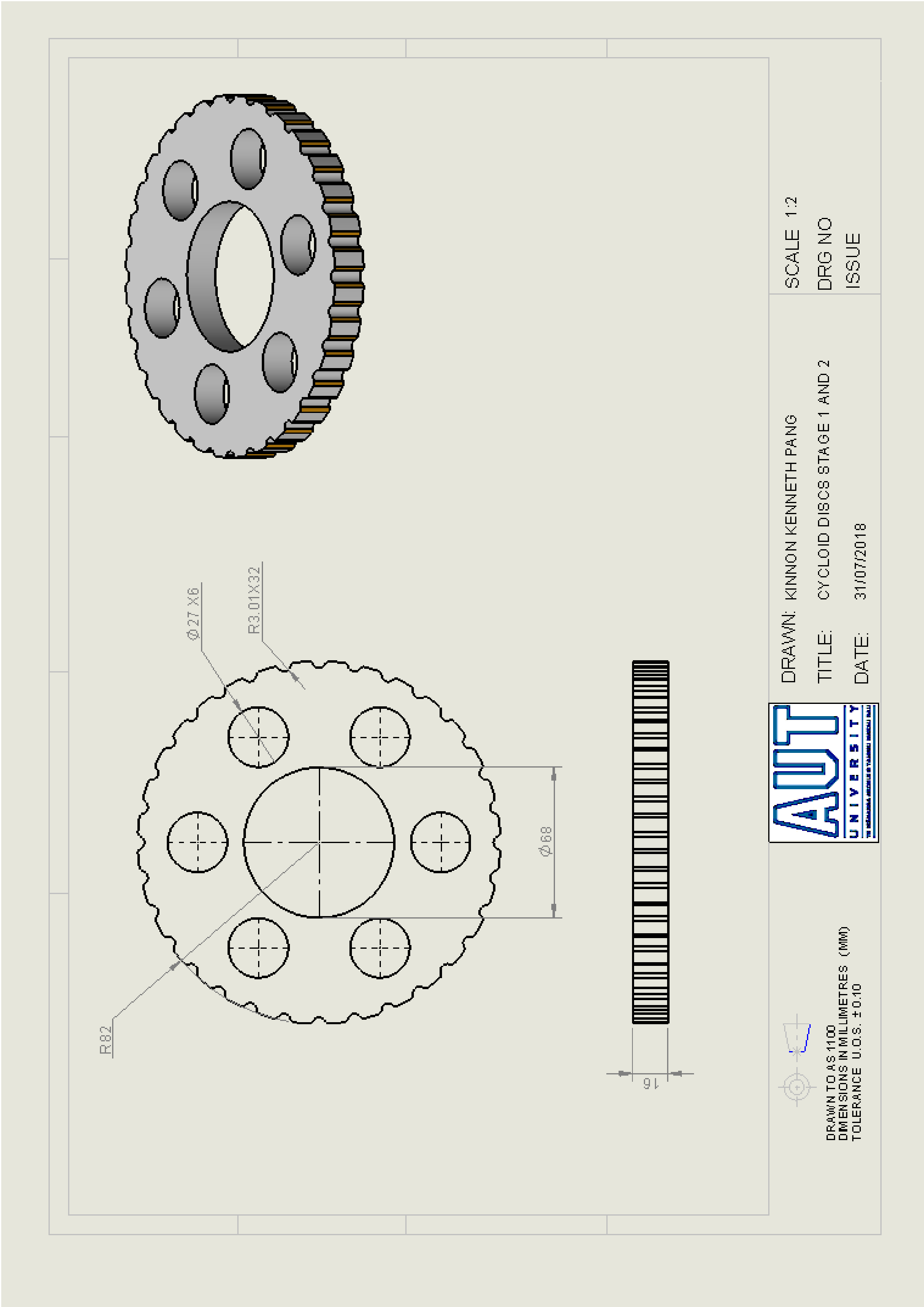

C2.8 Gearbox Lid

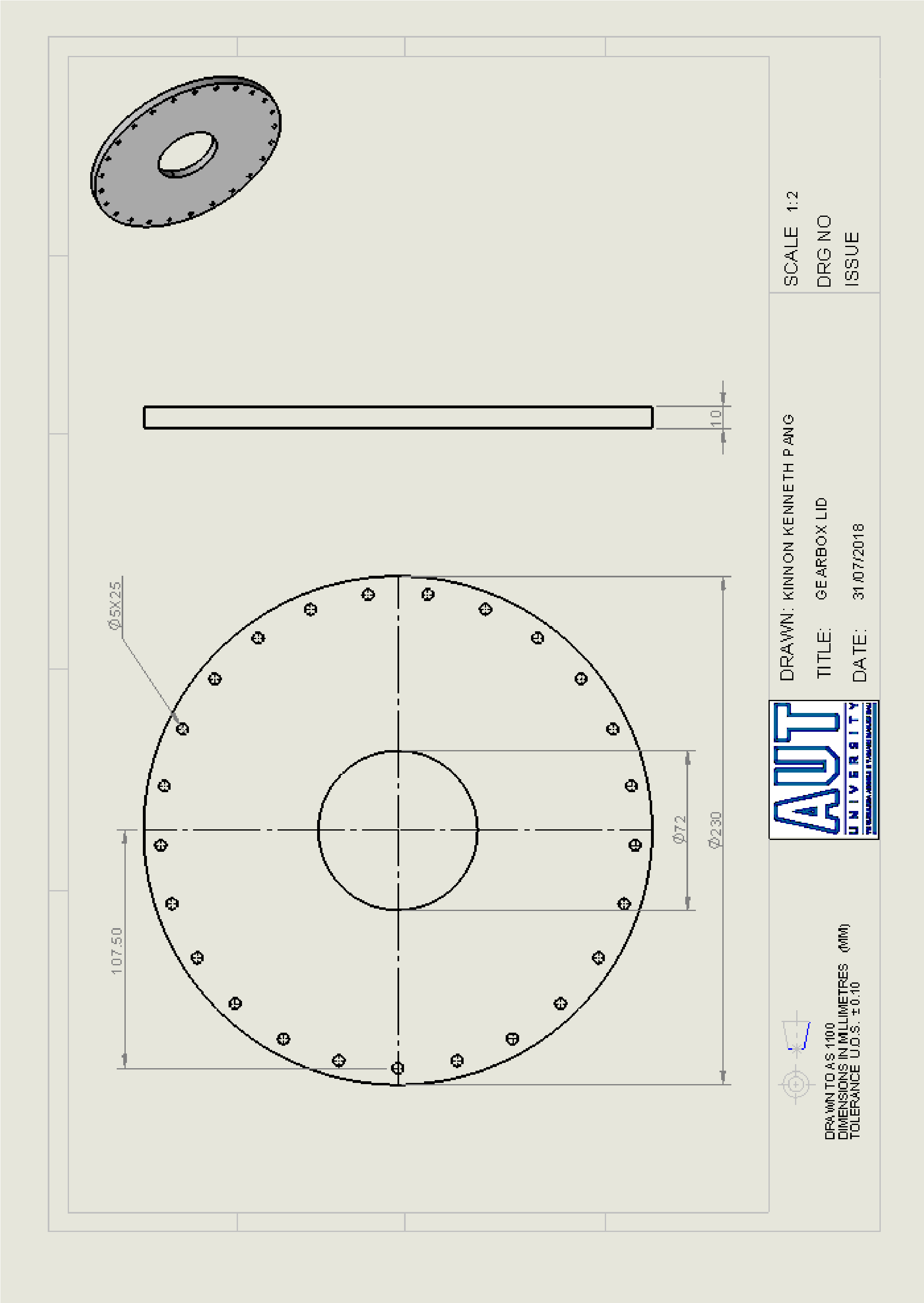

C2.9 Motor Key (Internal for Keyway)

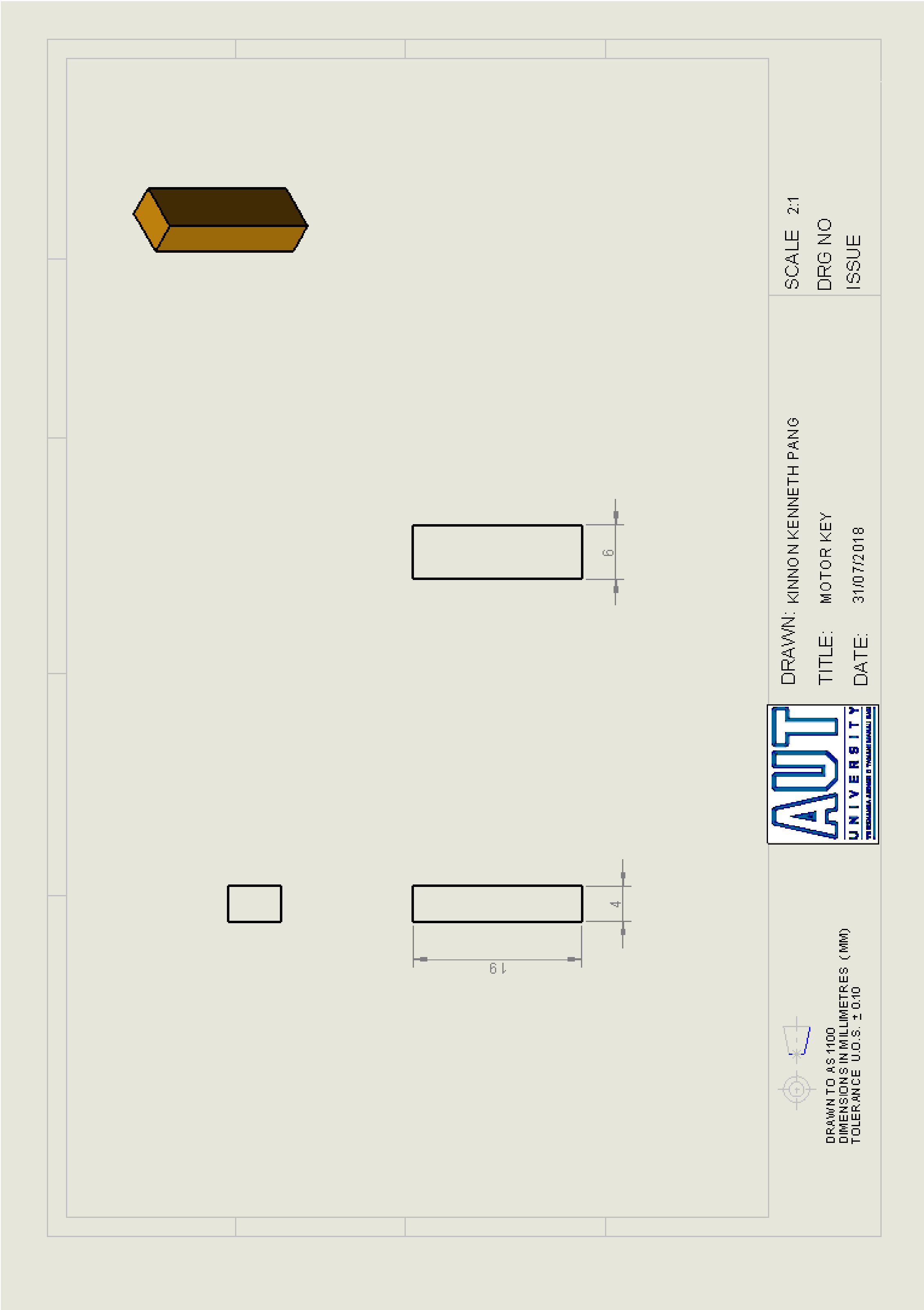

C2.10 Internal Gearbox Shaft

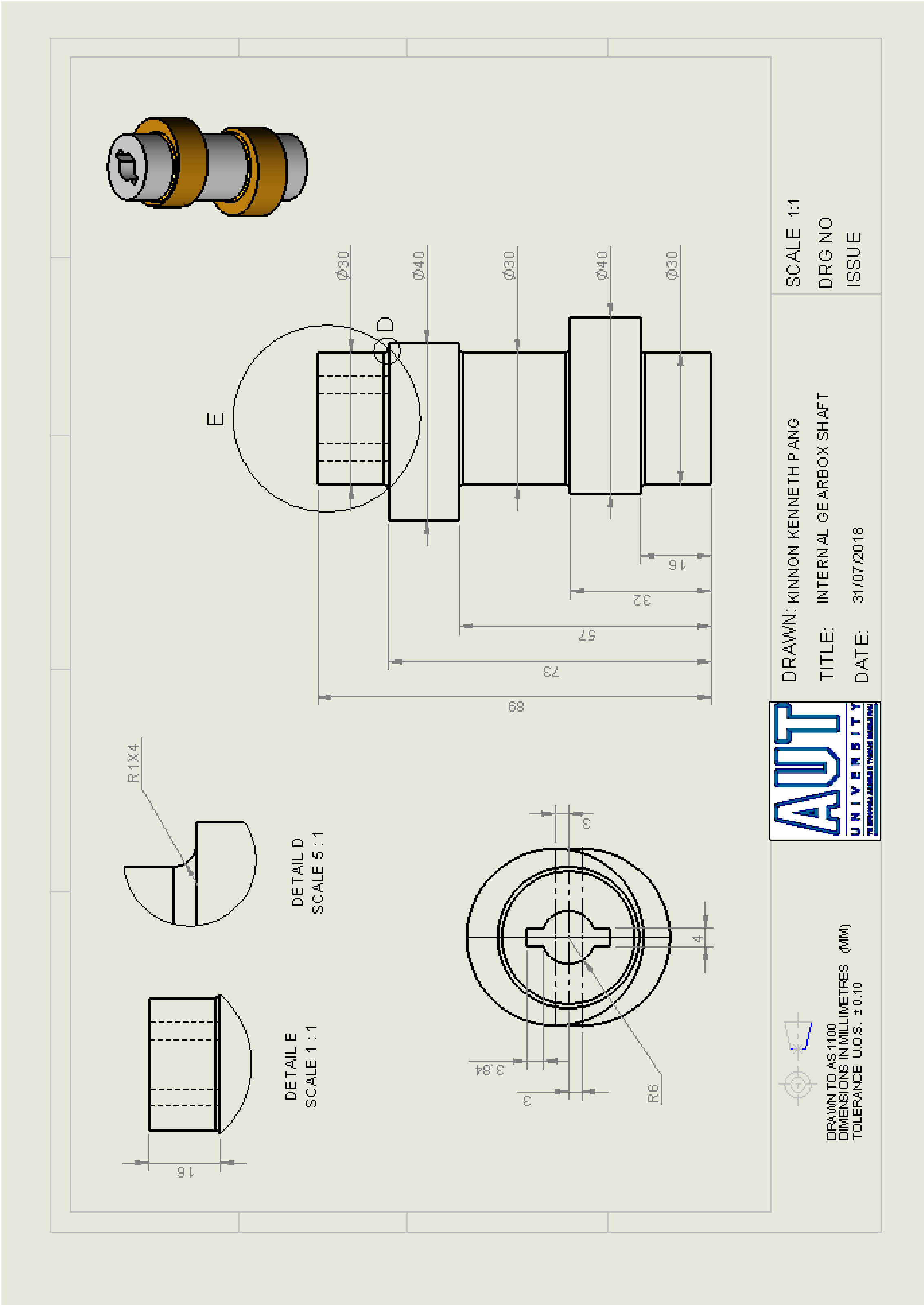

C2.11 Stage 1 and 2 Ring Gear Pins

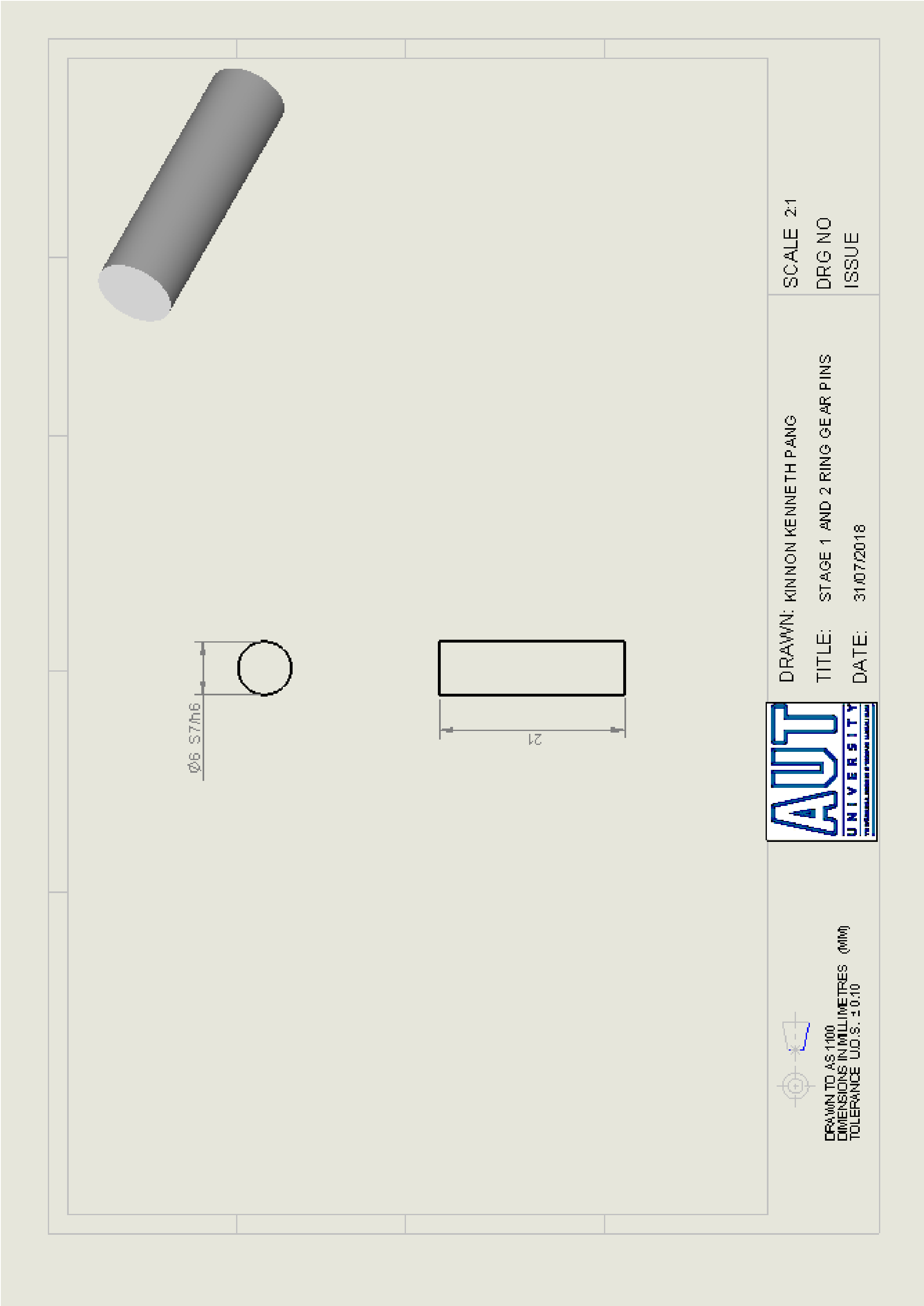

C2.12 Stage 1 Ring Gear

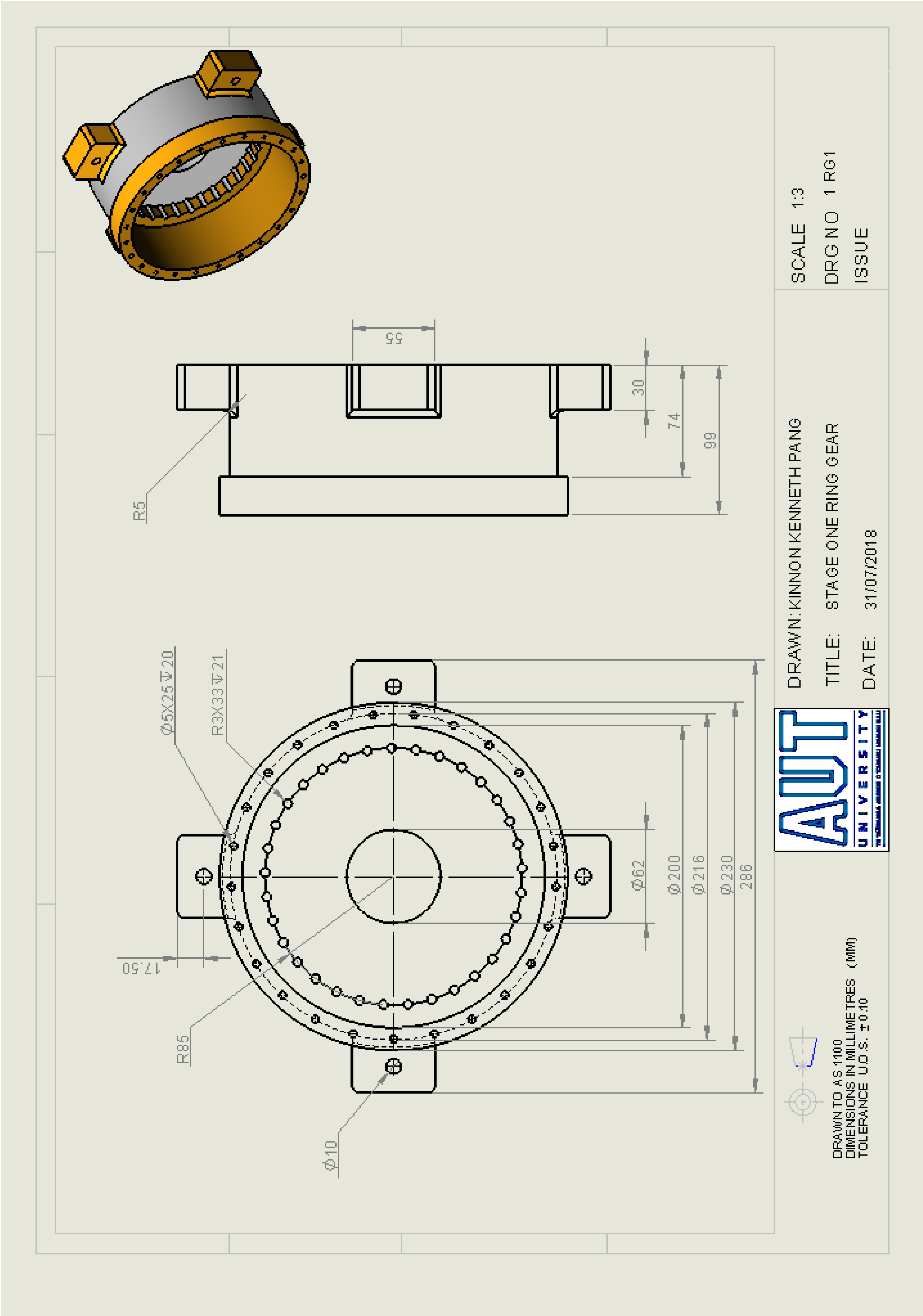

C2.13 Stage 2 Ring Gear

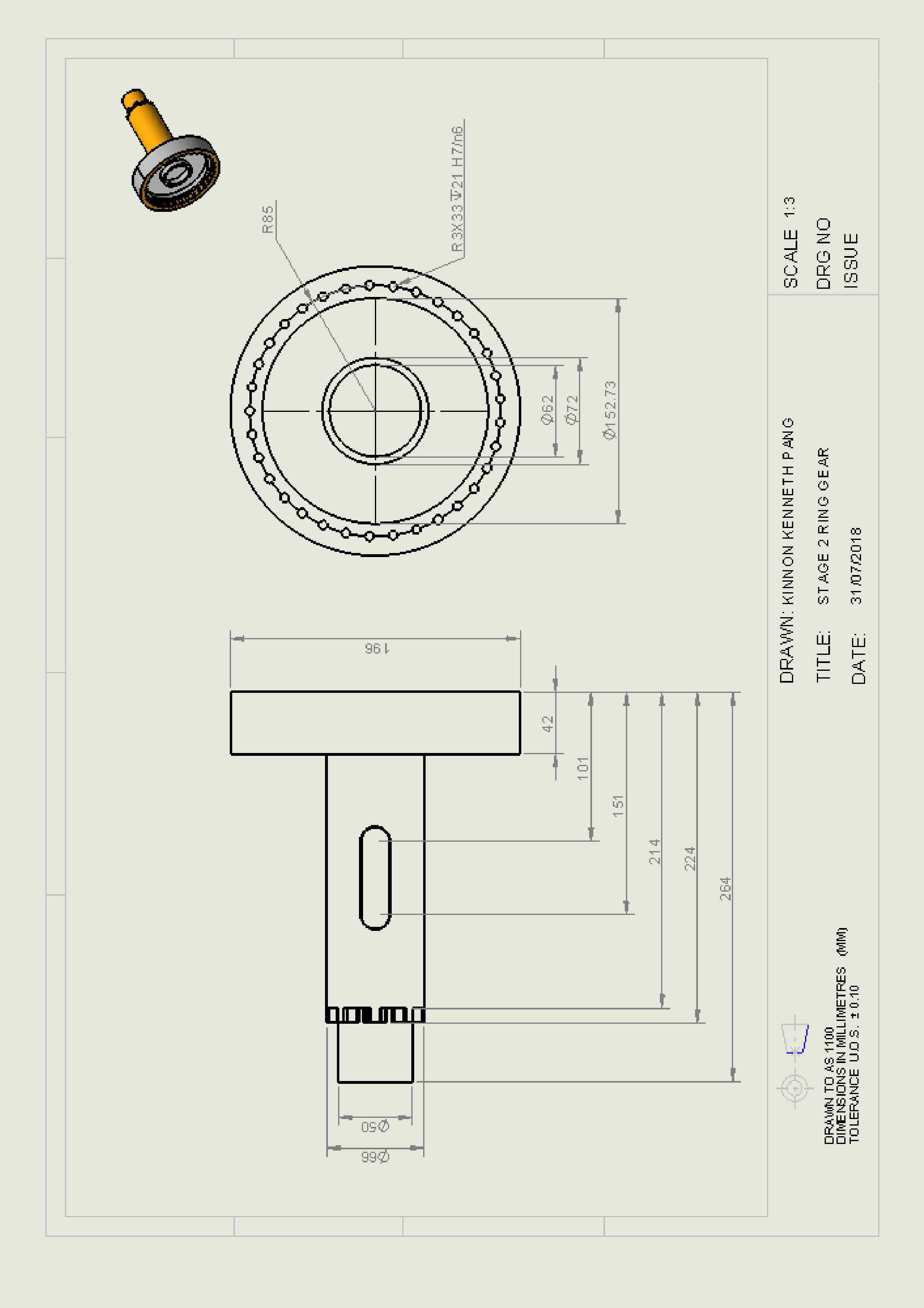

C2.14 Drive Shaft Spline

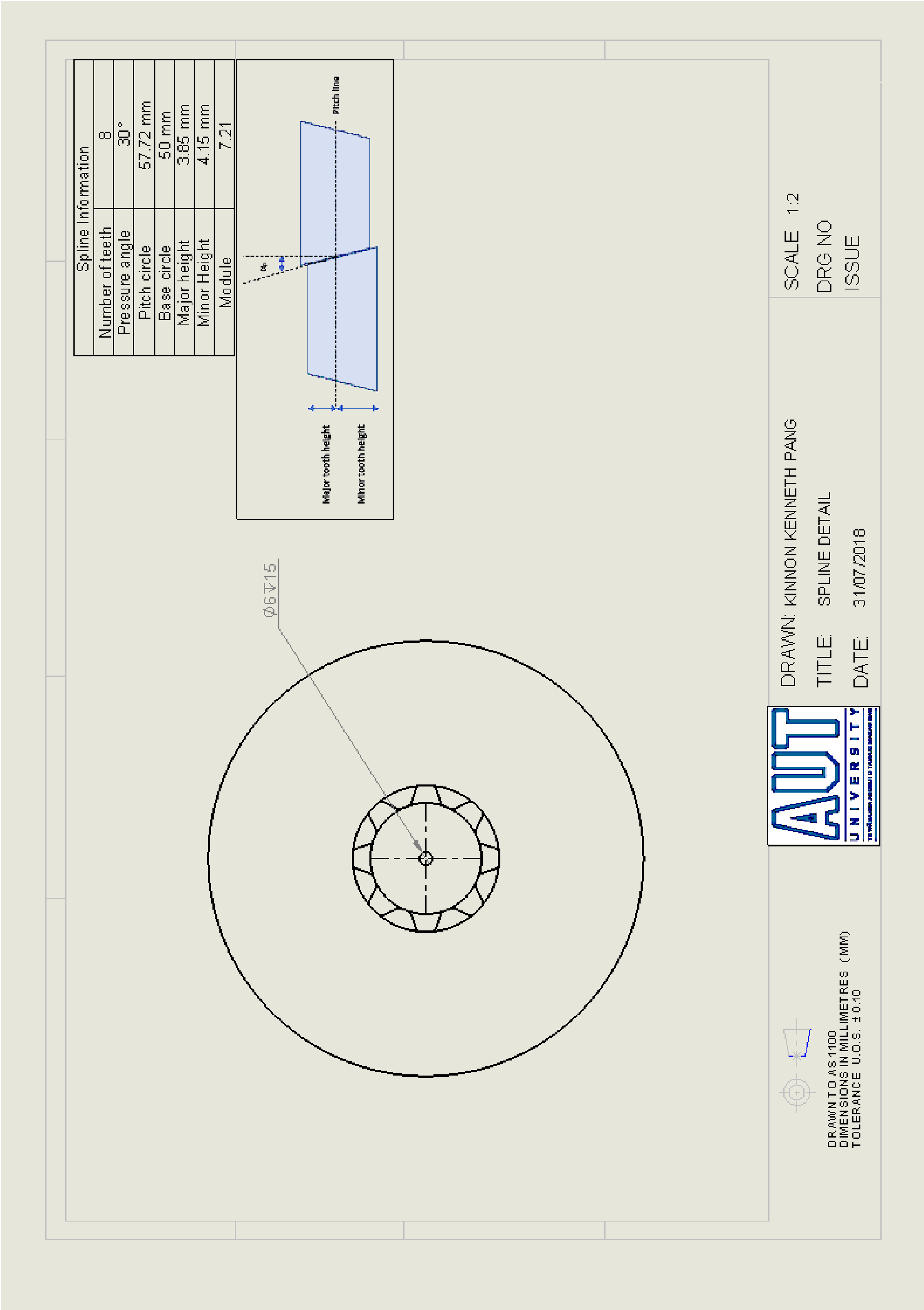

C2.15 Drive Shaft Keyway

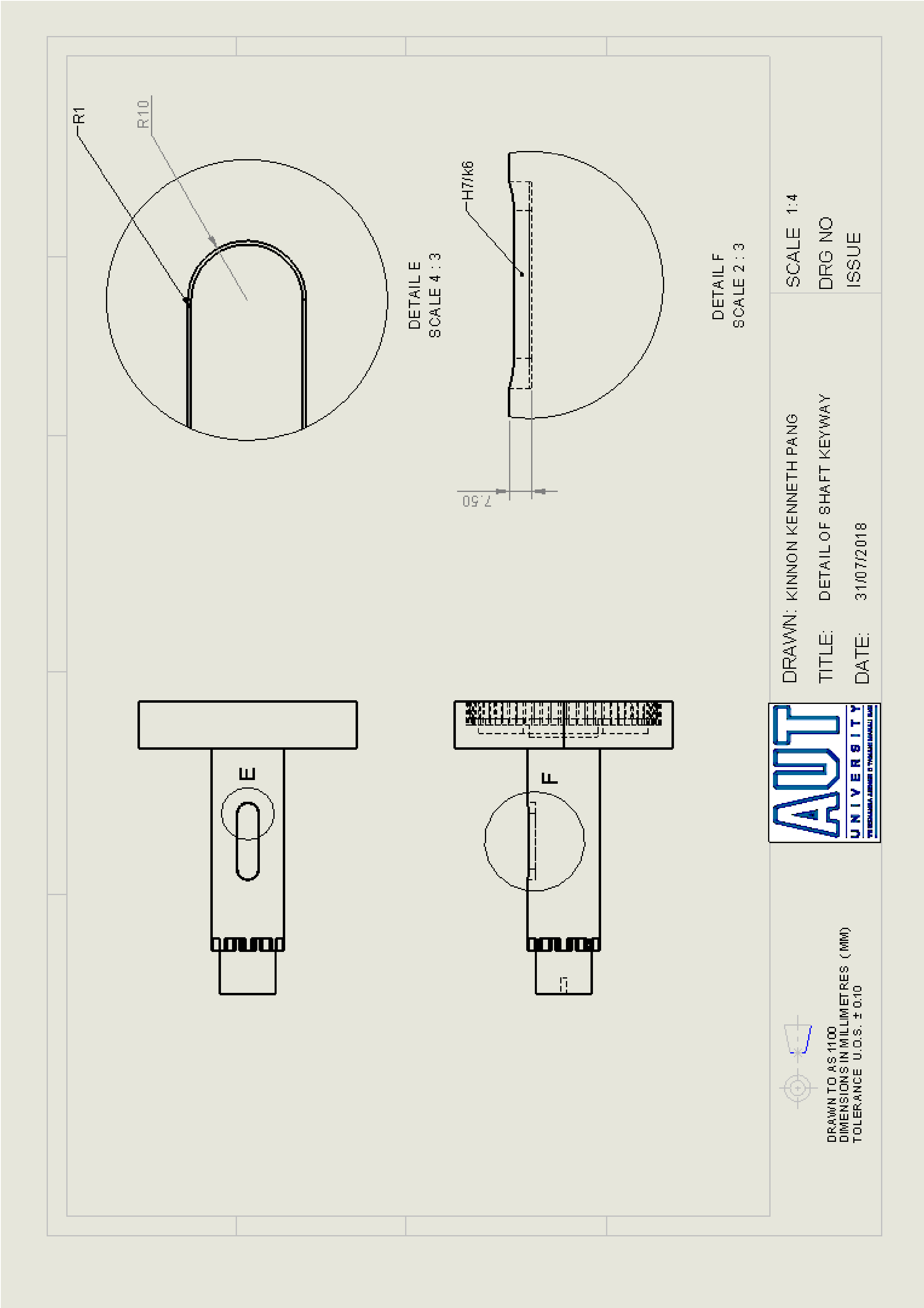

C2.16 Stage 2 Ring Gear Cross-section

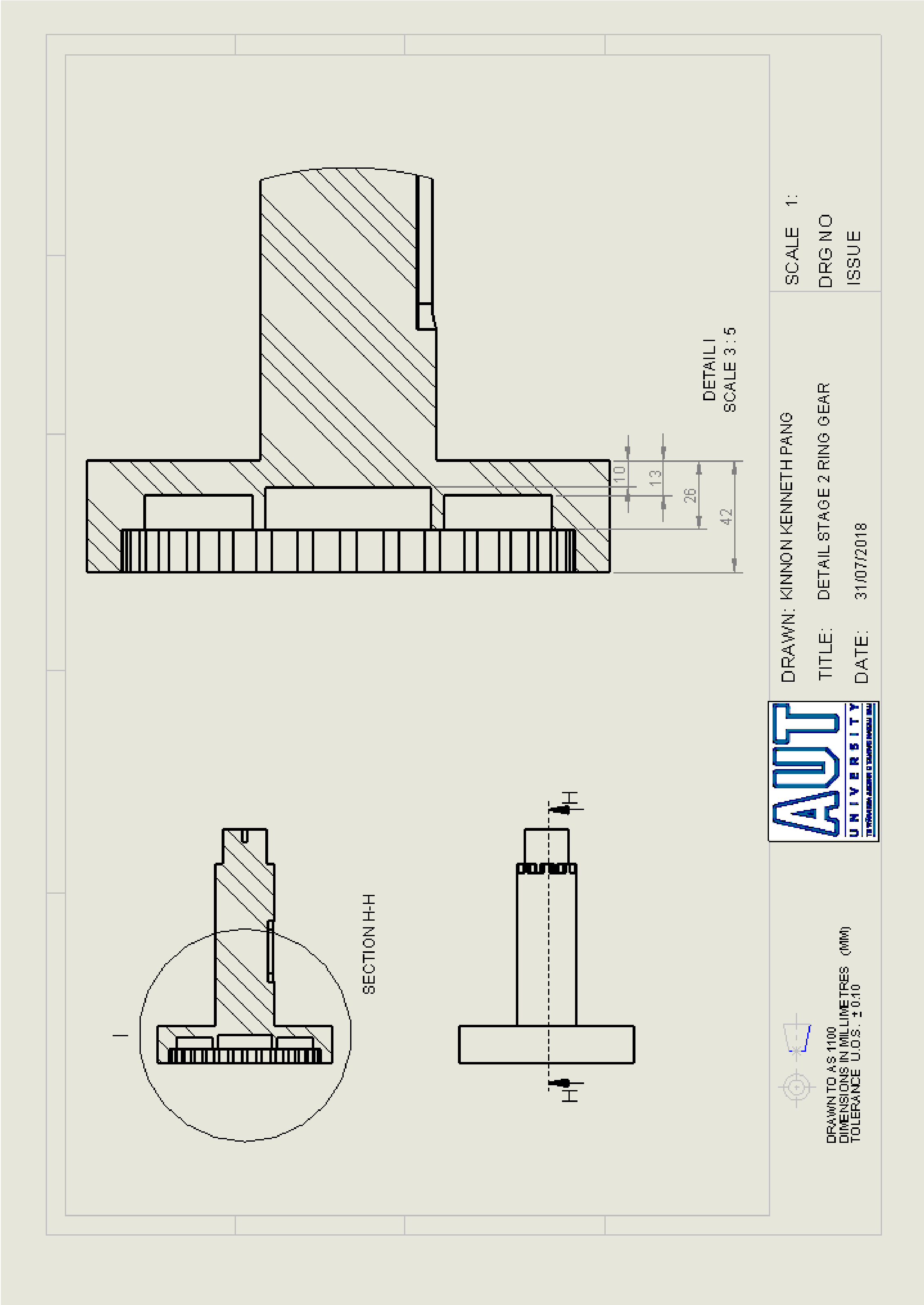

C3 Shearing Mechanism

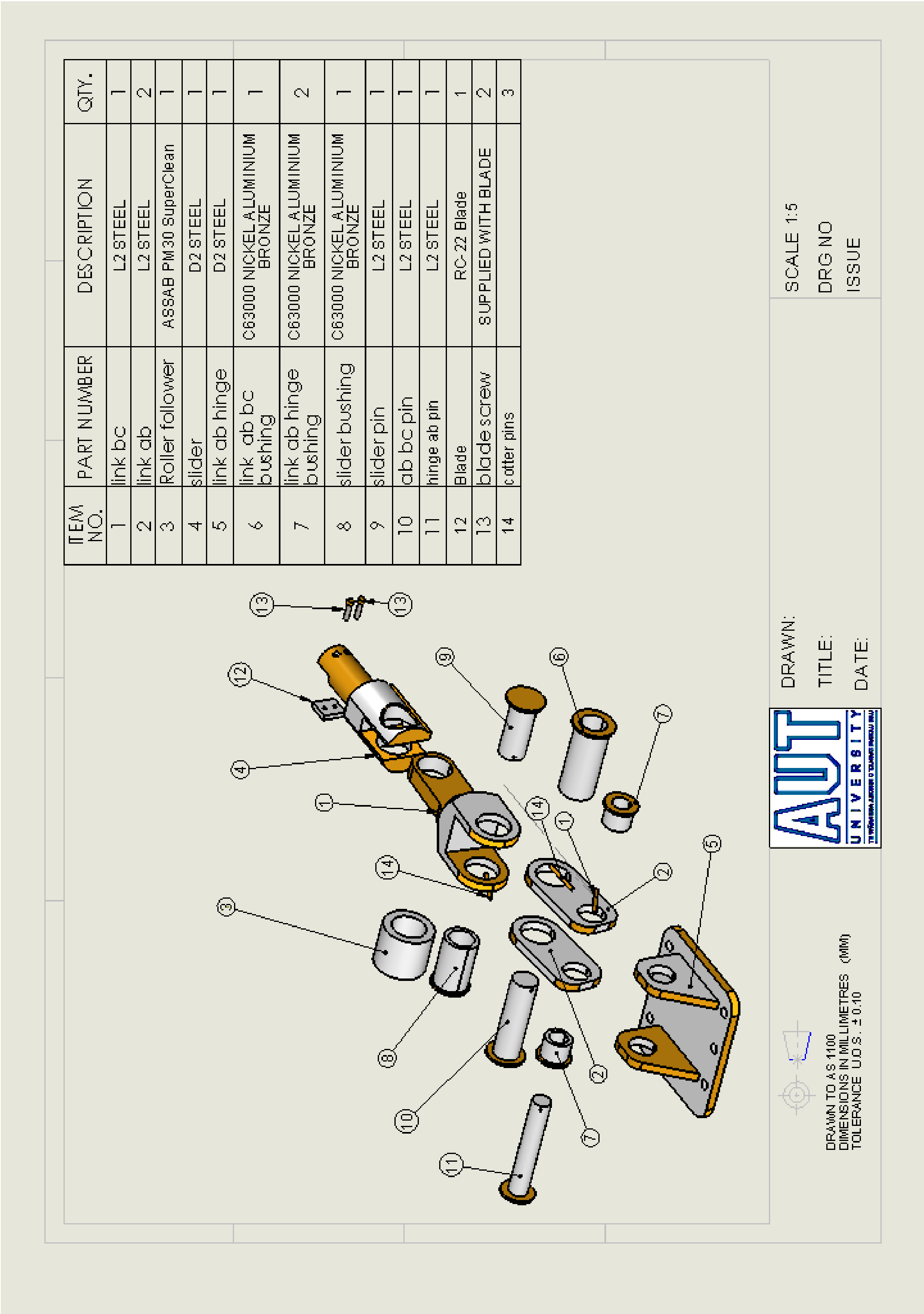

ITEM NO.	PART NUMBER	DESCRIPTION	QTY.
1	link bc	L2 STEEL	1
2	link ab	L2 STEEL	2
3	Roller follower	ASSAB PM30 SuperClean	1
4	slider	D2 STEEL	1
5	link ab hinge	D2 STEEL	1
6	link ab bc bushing	C63000 NICKEL ALUMINIUM BRONZE	1
7	link ab hinge bushing	C63000 NICKEL ALUMINIUM BRONZE	2
8	slider bushing	C63000 NICKEL ALUMINIUM BRONZE	1
9	slider pin	L2 STEEL	1
10	ab bc pin	L2 STEEL	1
11	hinge ab pin	L2 STEEL	1
12	Blade	RC-22 Blade	1
13	blade screw	SUPPLIED WITH BLADE	2
14	cotter pins		3

C3.1 Linkage and Roller Follower Pin

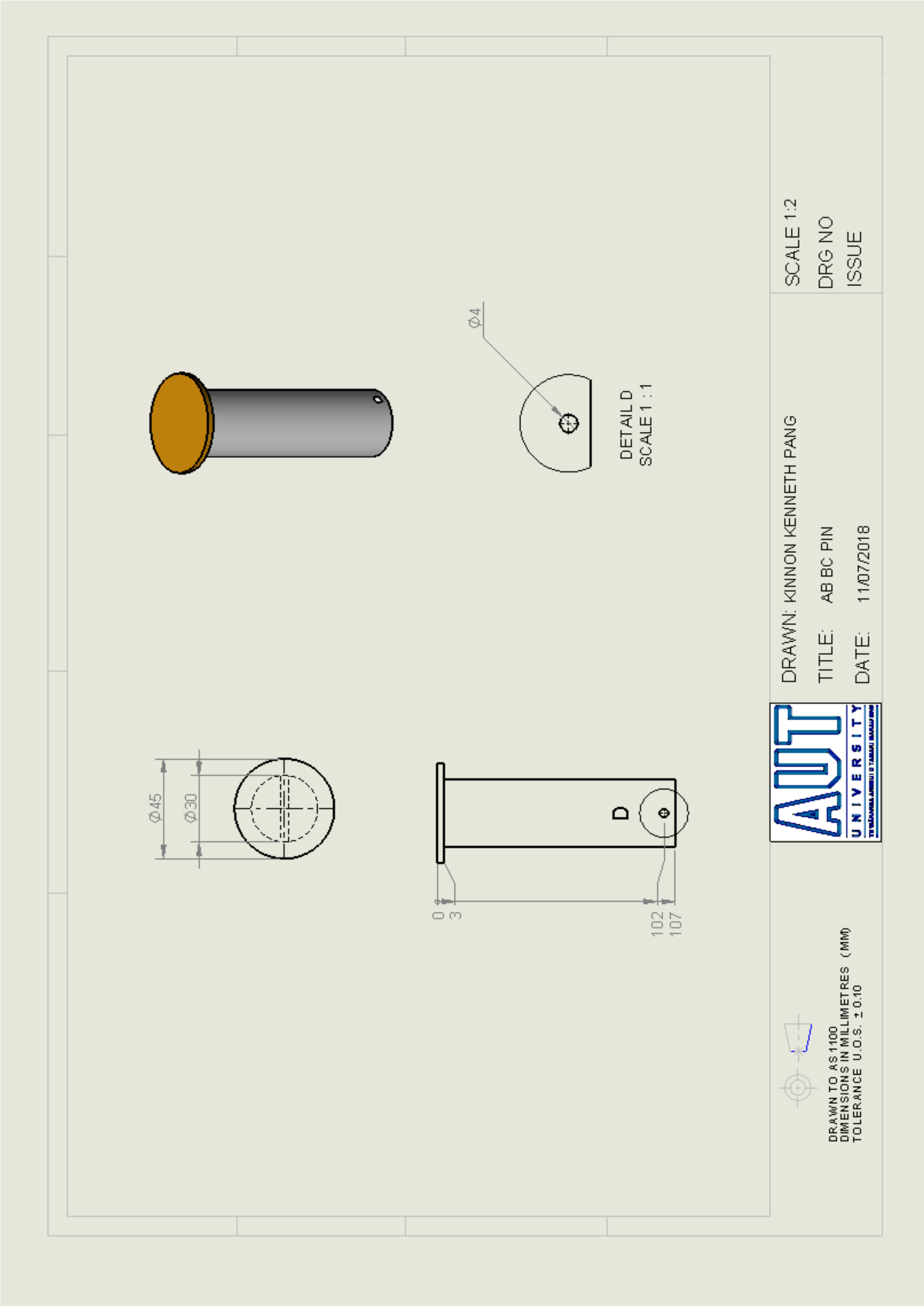

C3.2 Hinge AB Pin

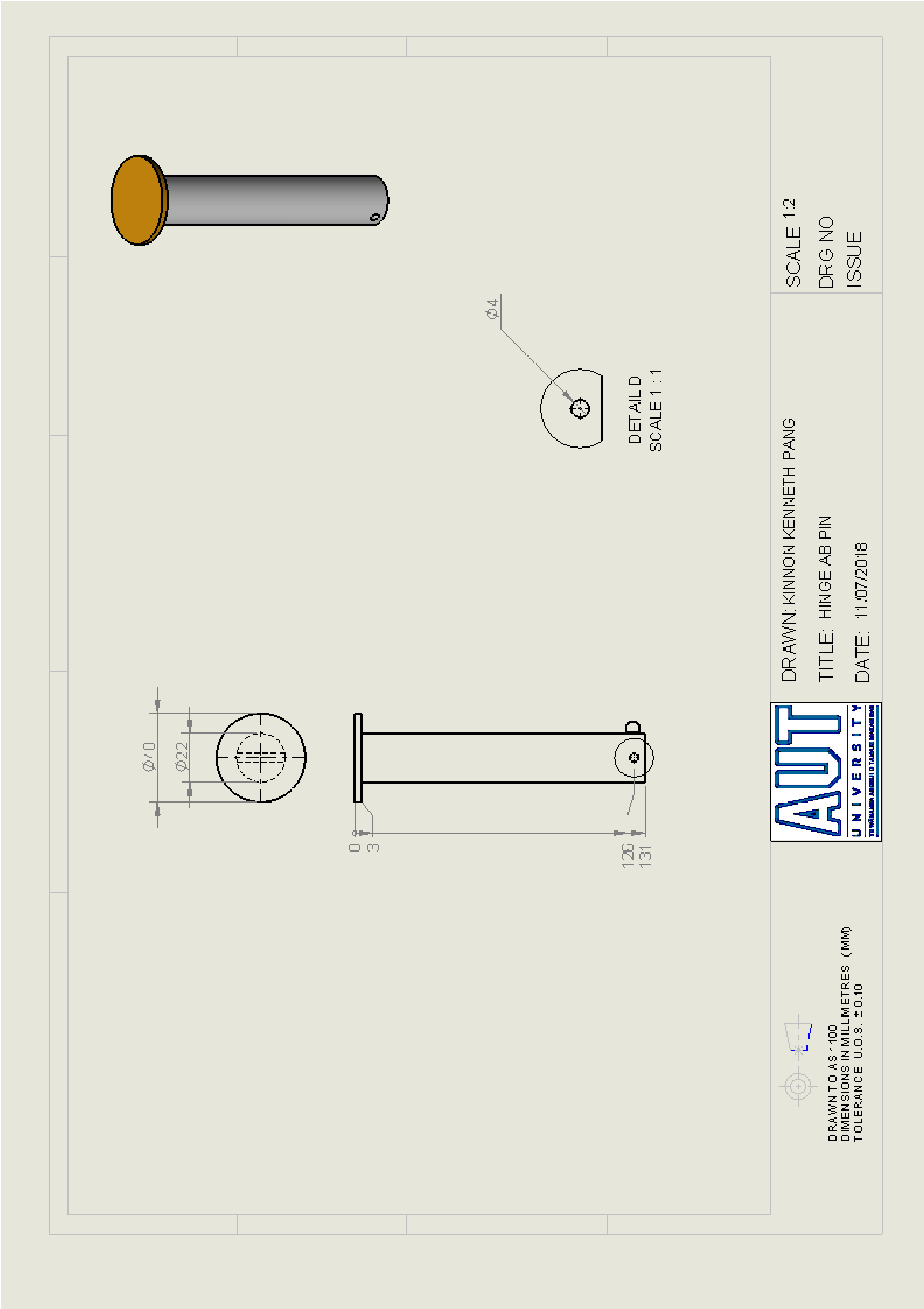

C3.3 Linkage and Roller Follower Bushing

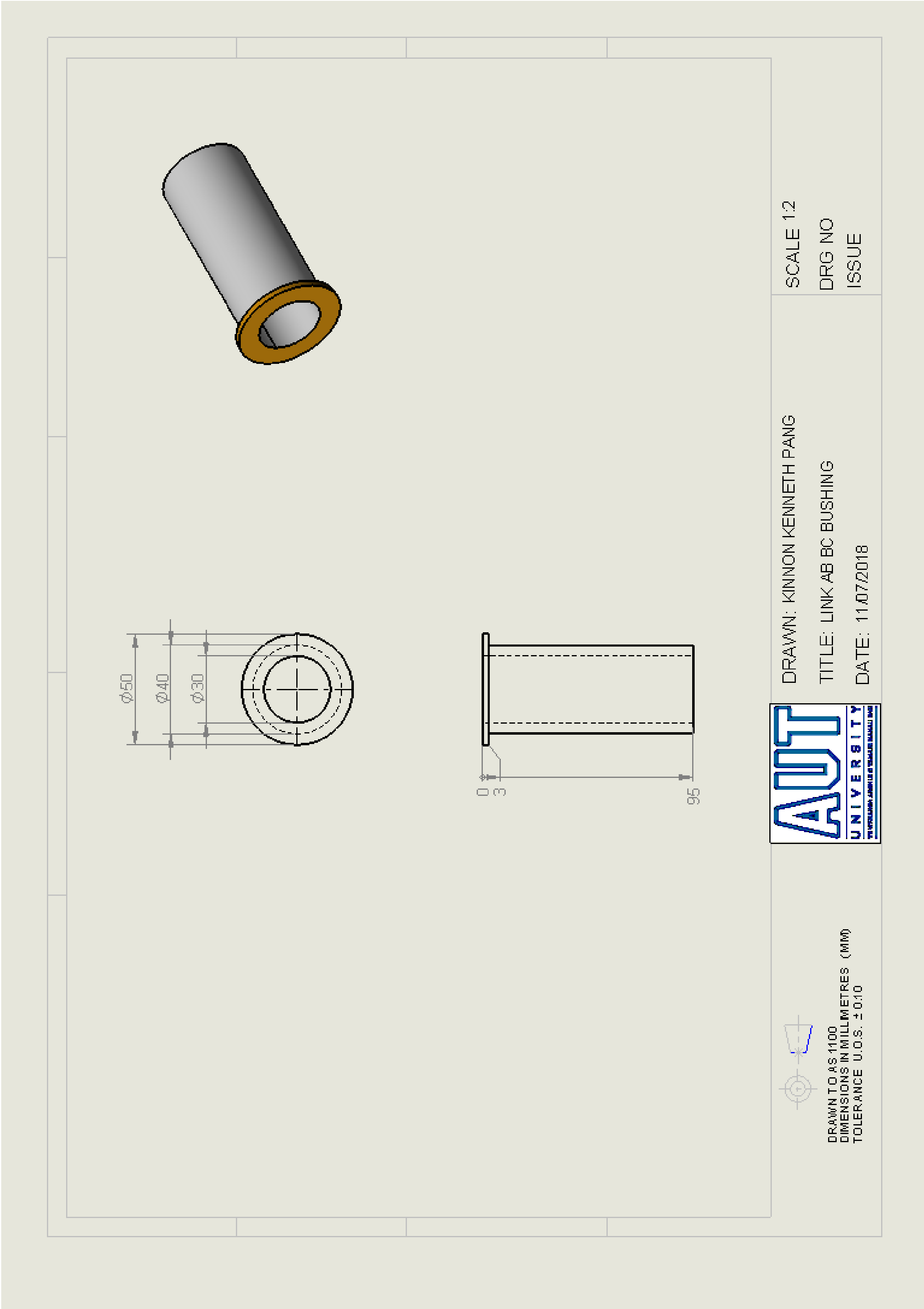

C3.4 Hinge AB Bushing

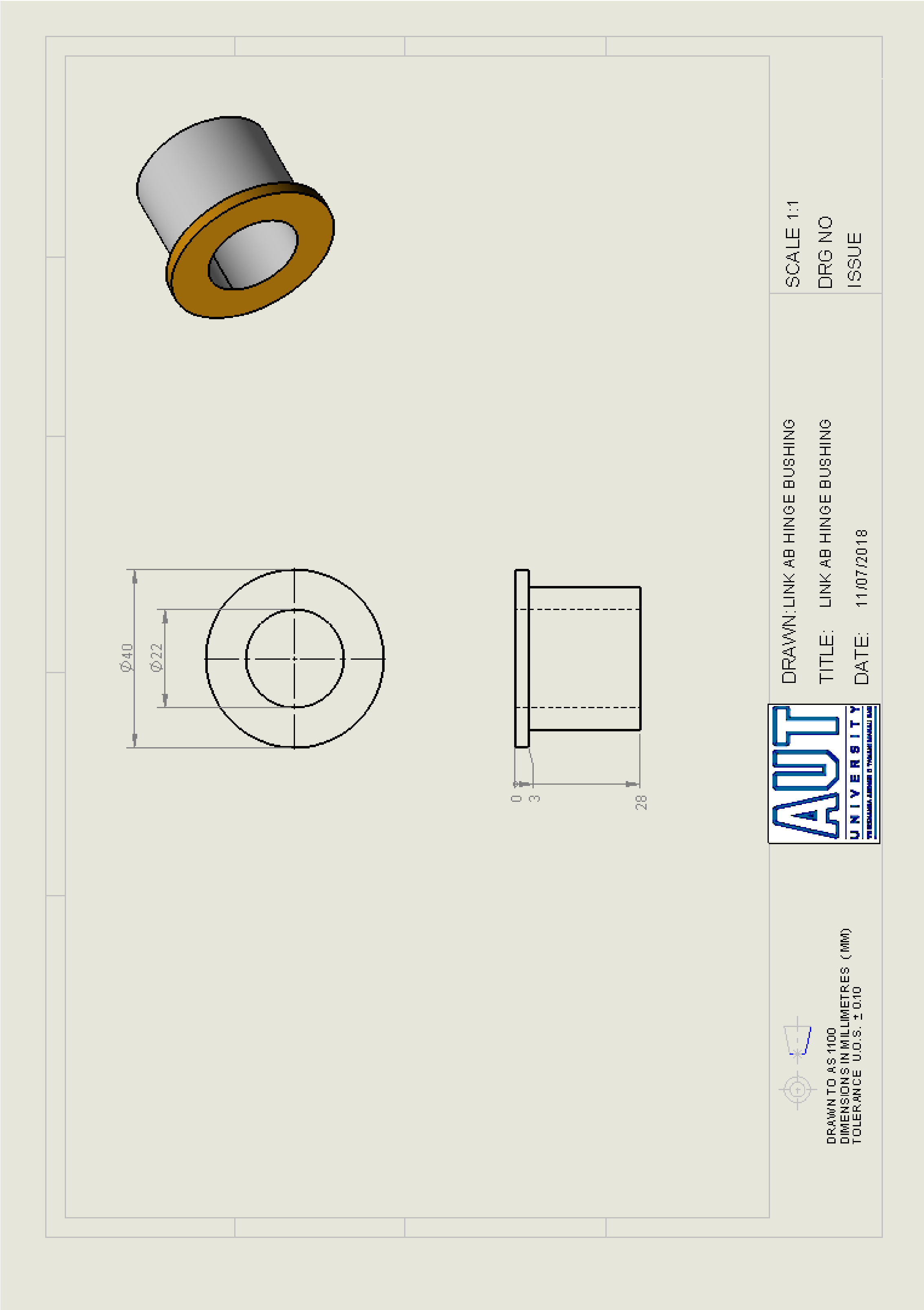

C3.5 Hinge AB

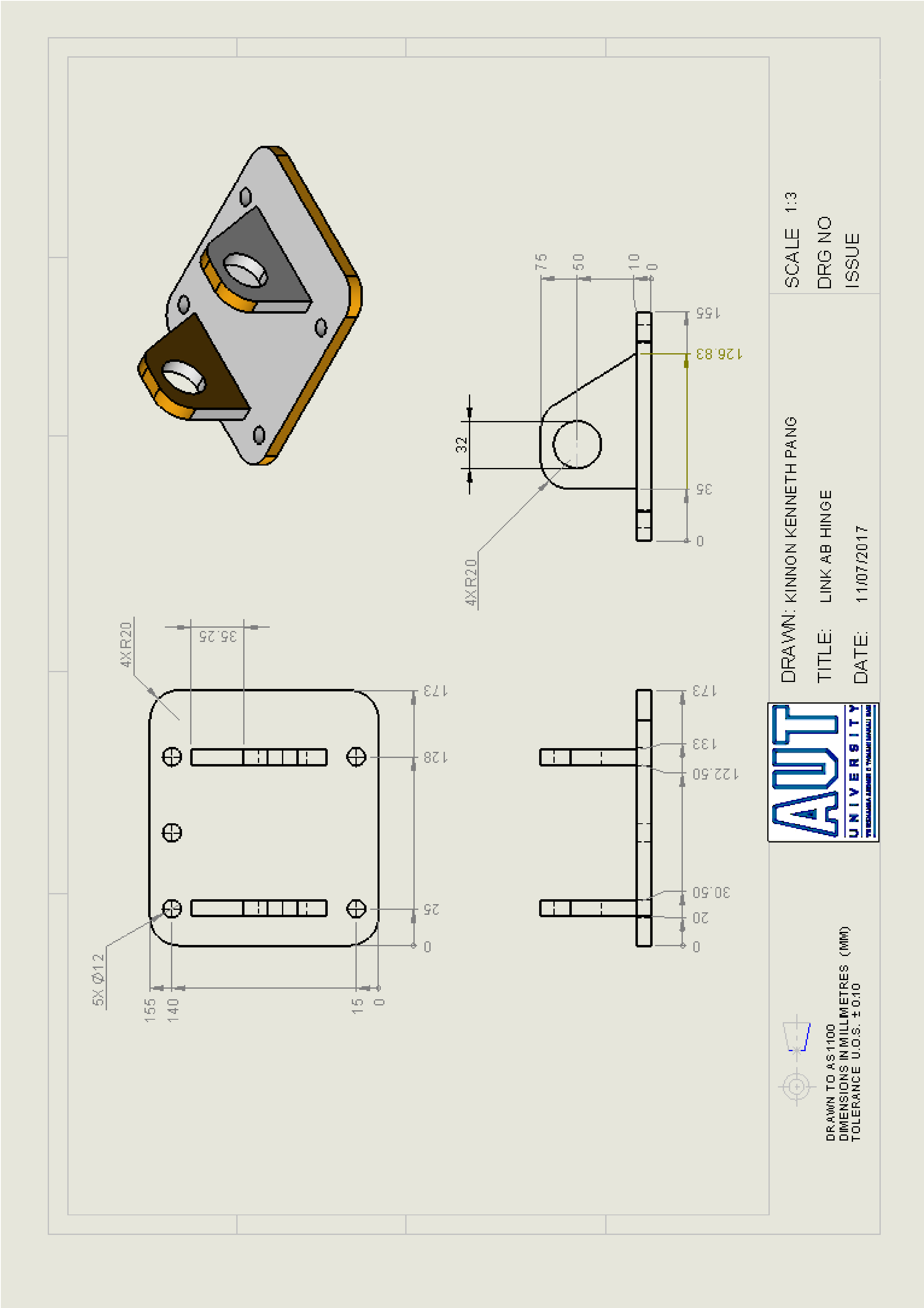

SCALE 1:3
DRG NO
ISSUE
DRAWN: KINNON KENNETH PANG
TITLE: LINK AB HINGE
DATE: 11/07/2017
DRAWN TO AS1100
DIMENSIONS IN MILLIMETRES (MM)
TOLERANCE U.O.S. ±0.10

C3.6 Linkage AB

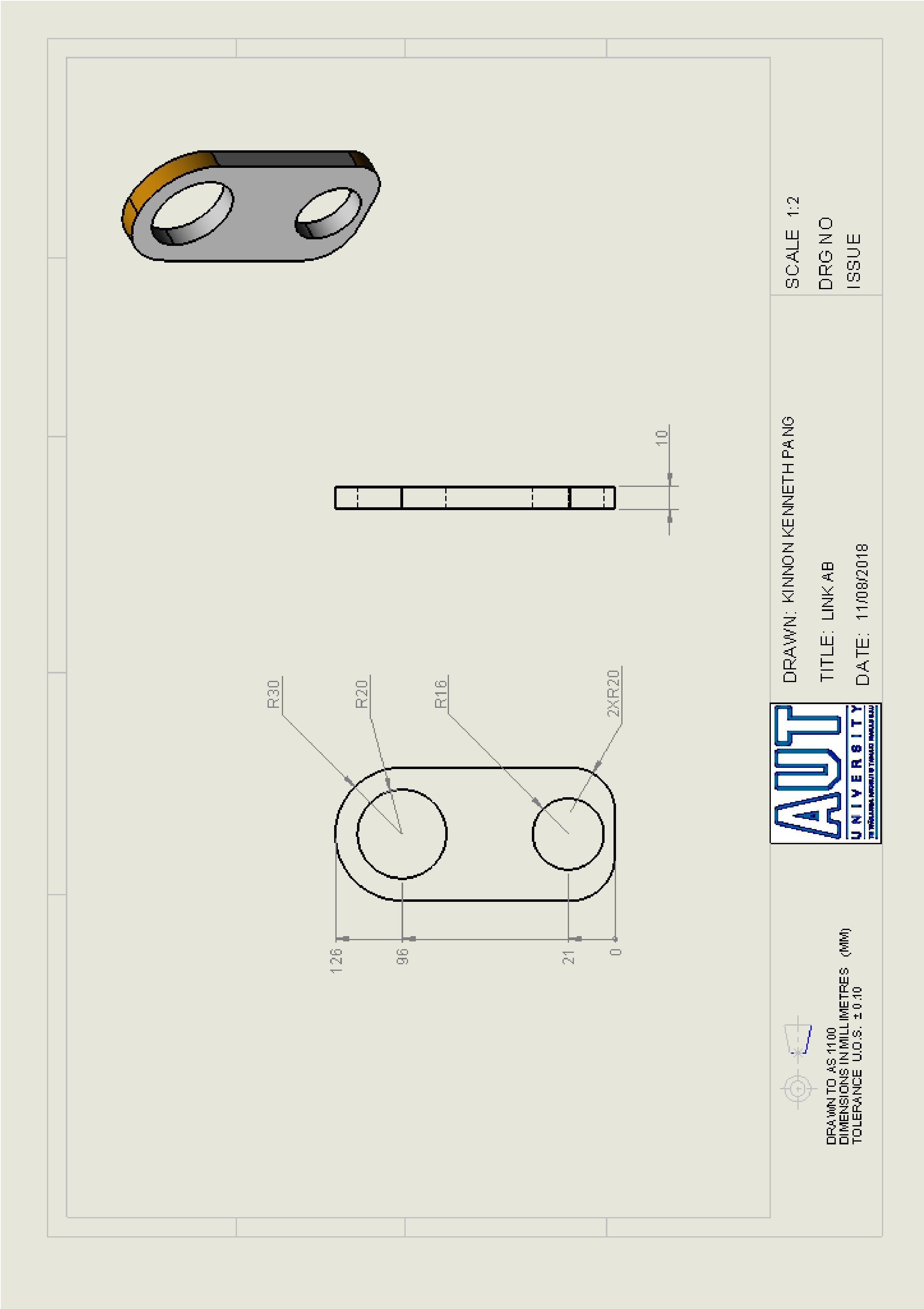

C3.7 Linkage BC

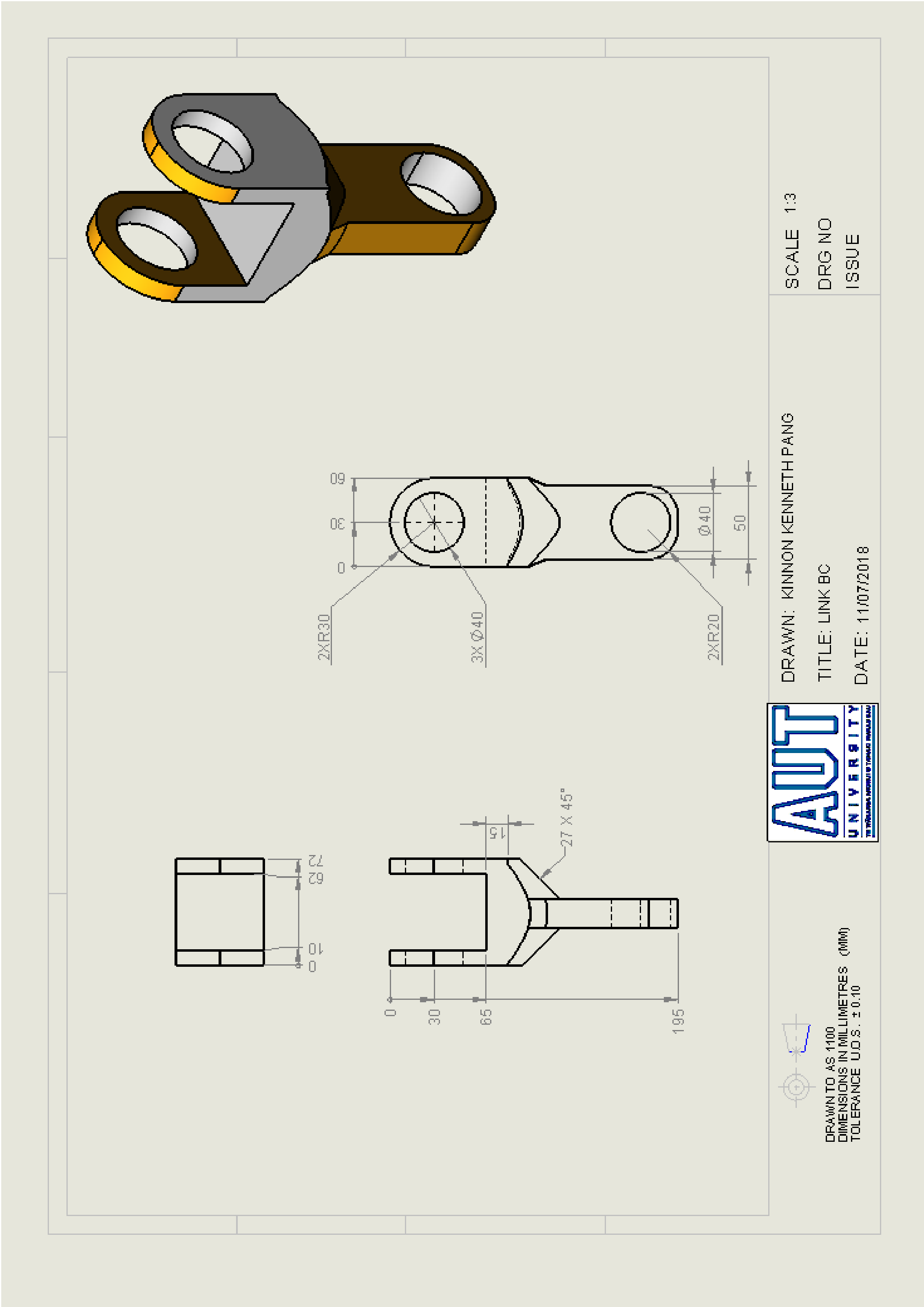

C3.8 Roller Follower

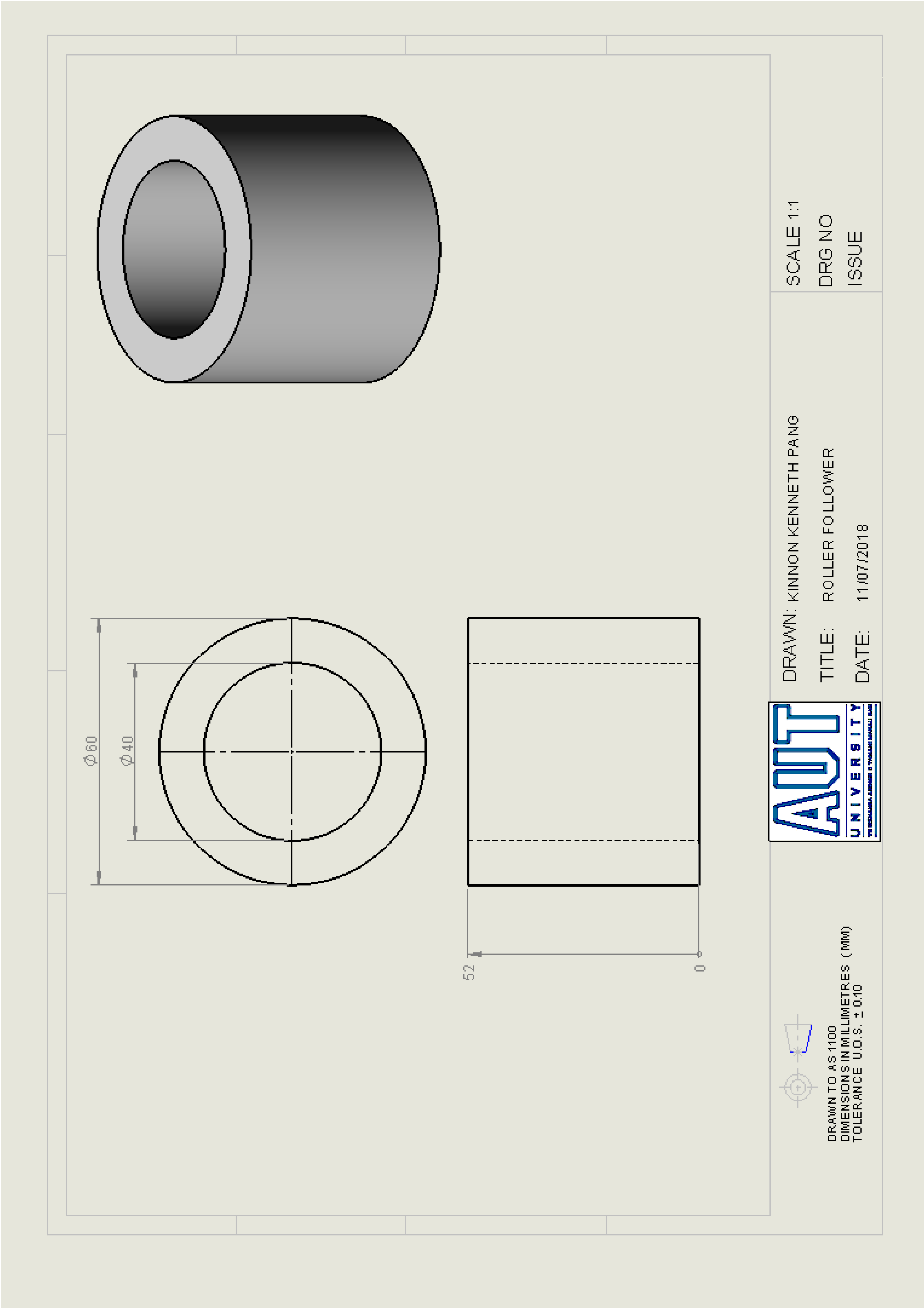

C3.9 Slider Bushing

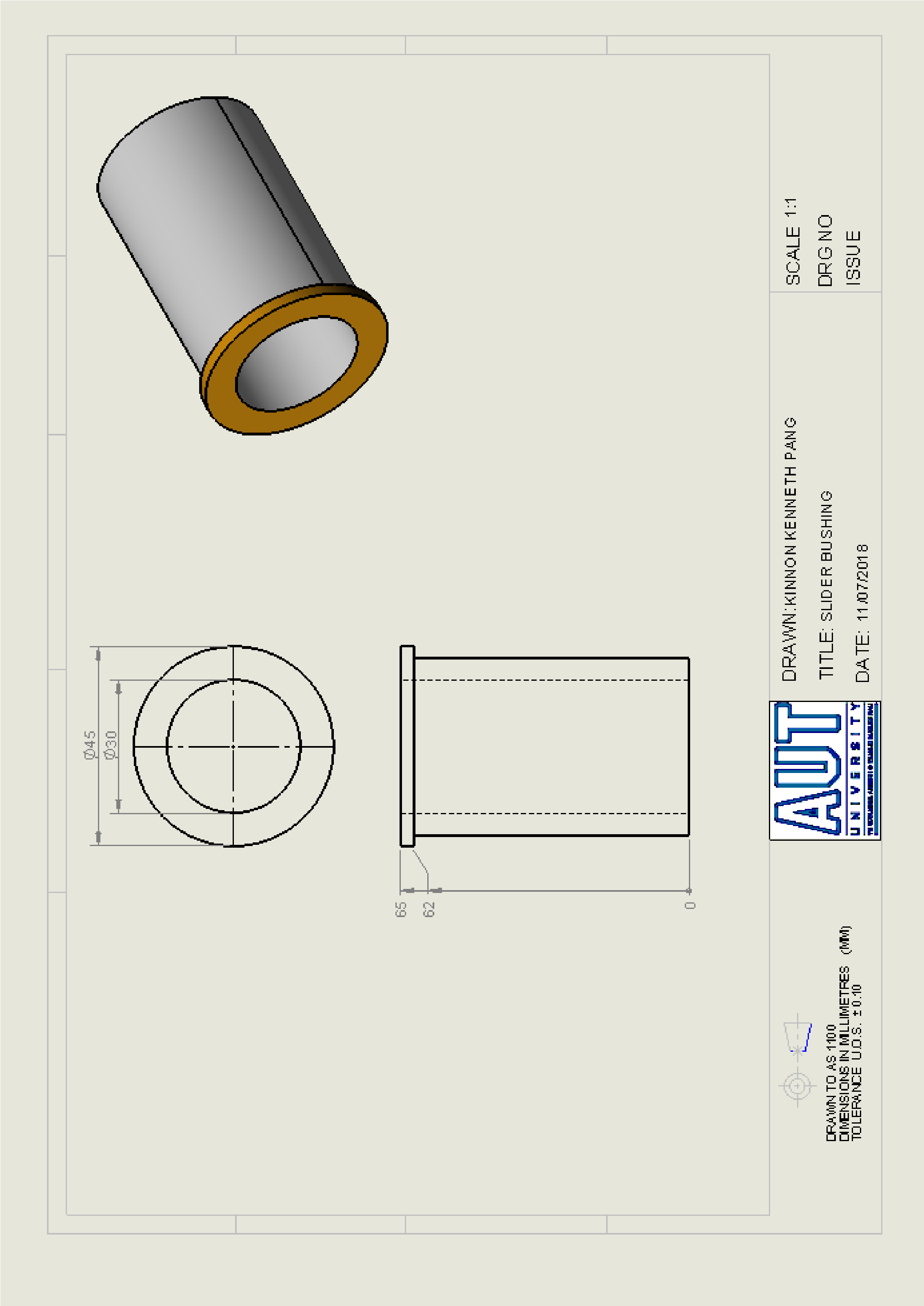

C3.10 Slider Pin

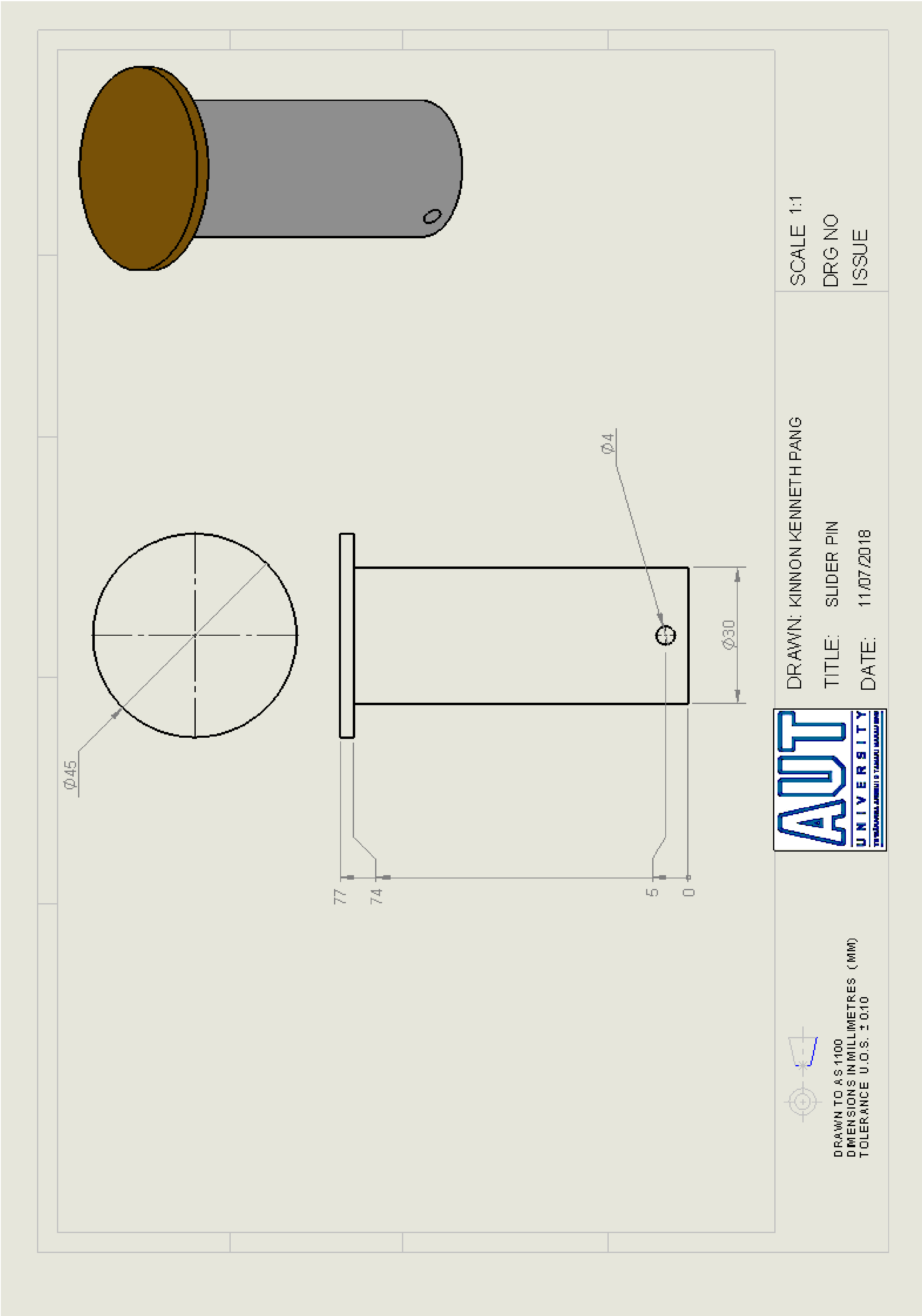

C3.11 Slider

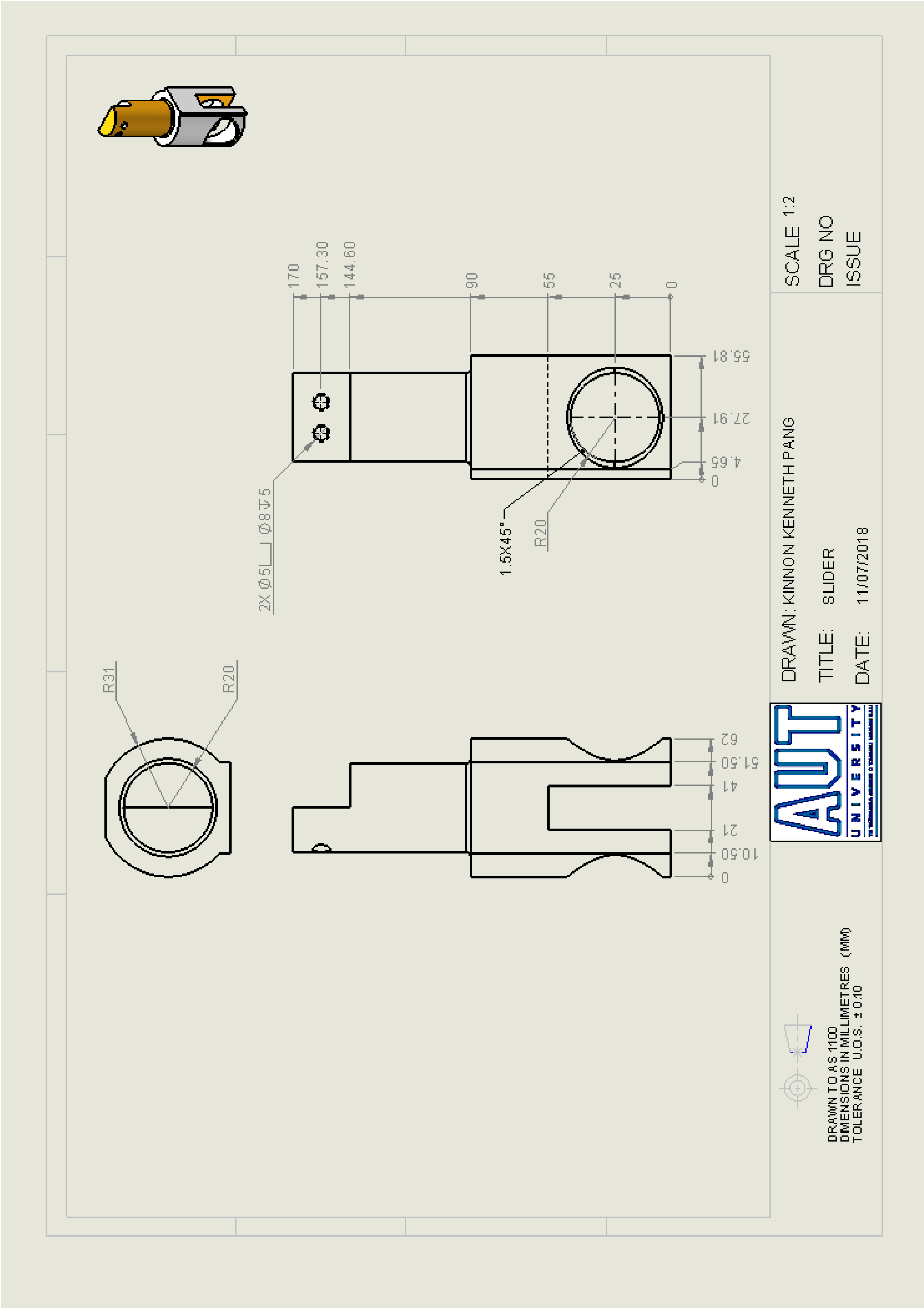
R31
R20
2X Ø5 ⌴ Ø8 ↧5
170
157.30
144.60
90
55
25
0
55.81
27.91
4.65
0
1.5X45°
R20
62
51.50
41
21
10.50
0
SCALE 1:2
DRG NO
ISSUE
DRAWN: KINNON KENNETH PANG
TITLE: SLIDER
DATE: 11/07/2018
DRAWN TO AS 1100
DIMENSIONS IN MILLIMETRES (MM)
TOLERANCE U.O.S. ±0.10

C4 Housing and Housing Components

C4.1 Gearbox and Motor Panel

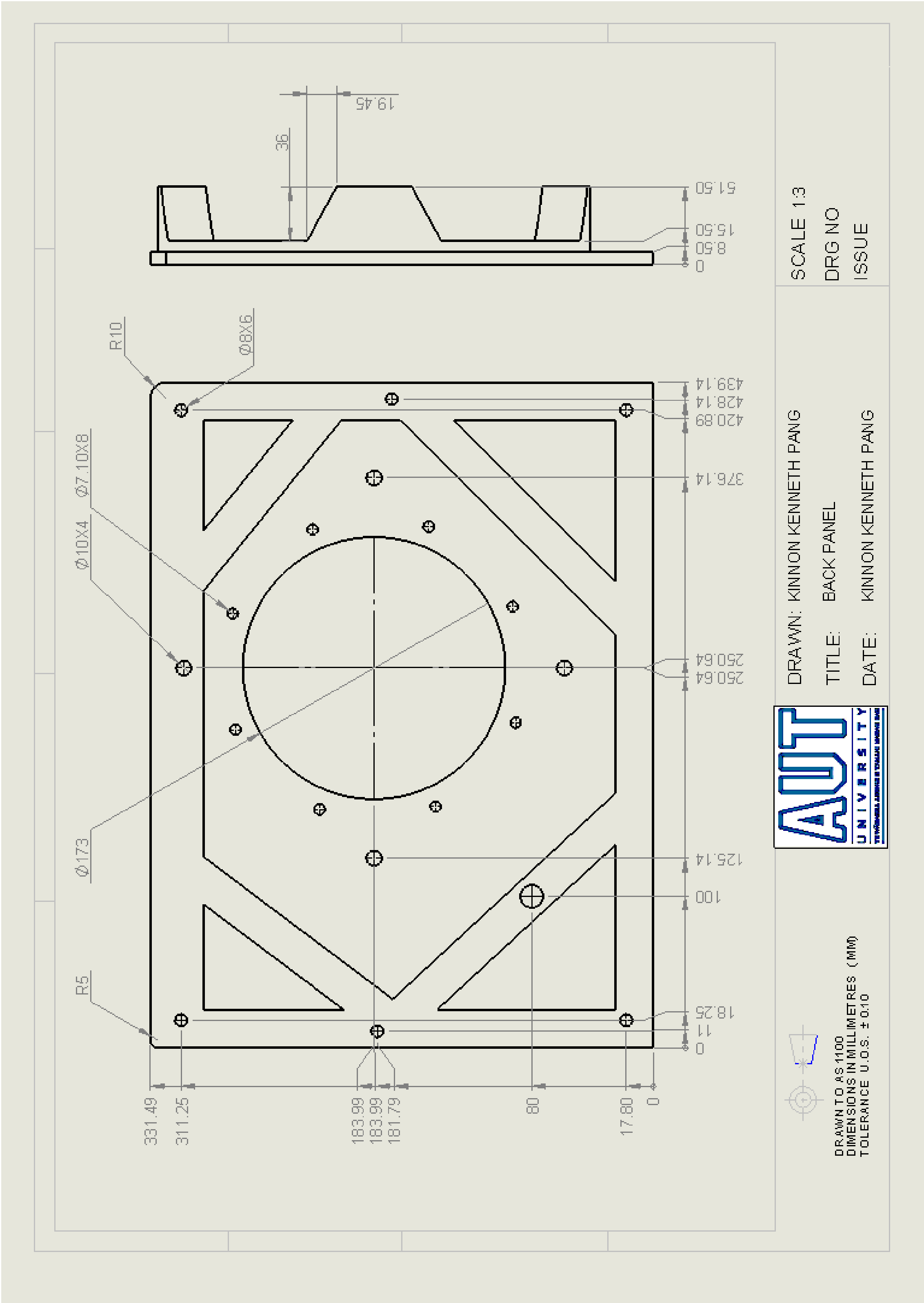

C4.1.1 Gearbox Motor Panel Interior Detail

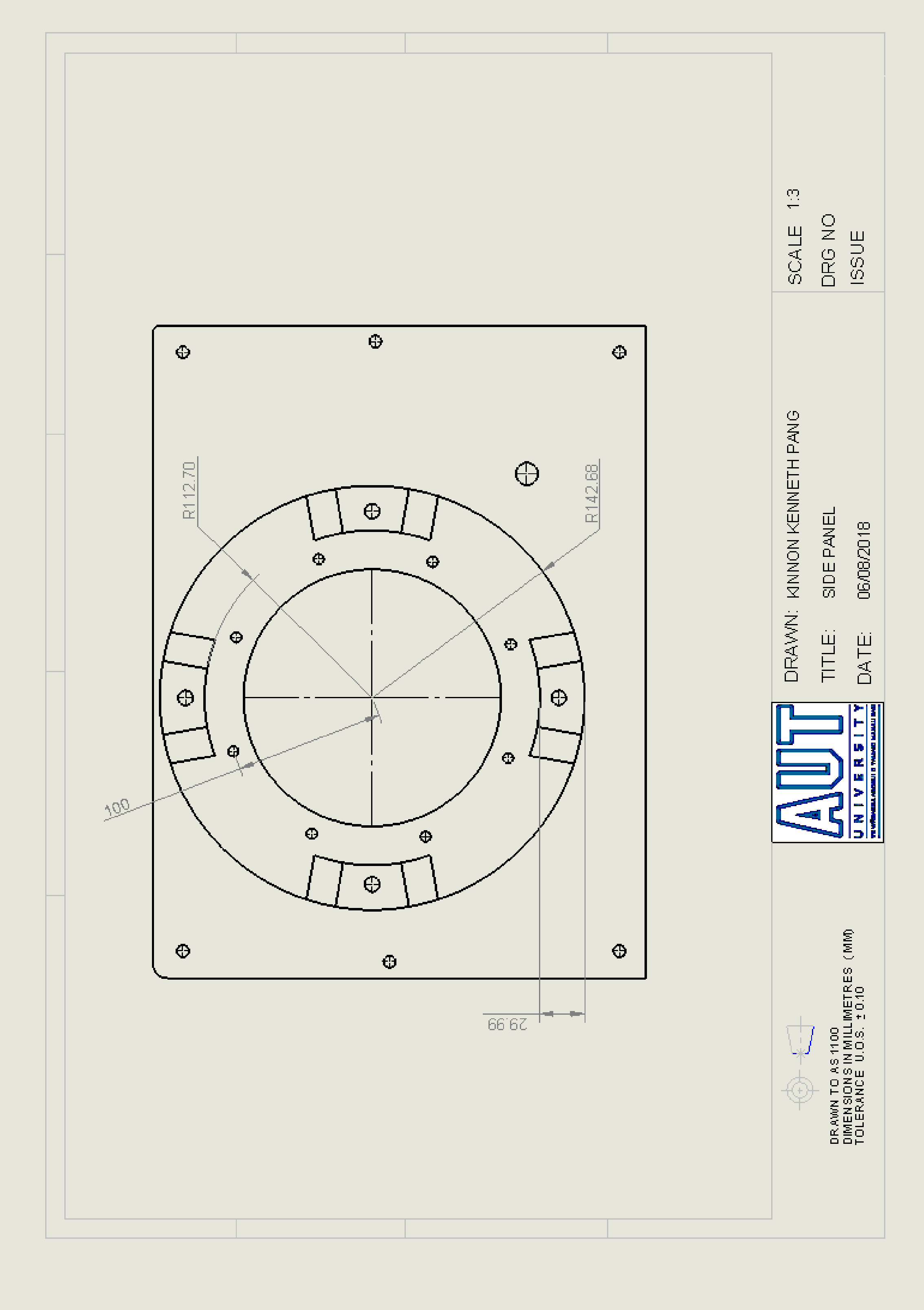

C4.1.2 Gearbox Motor Panel Exterior Detail

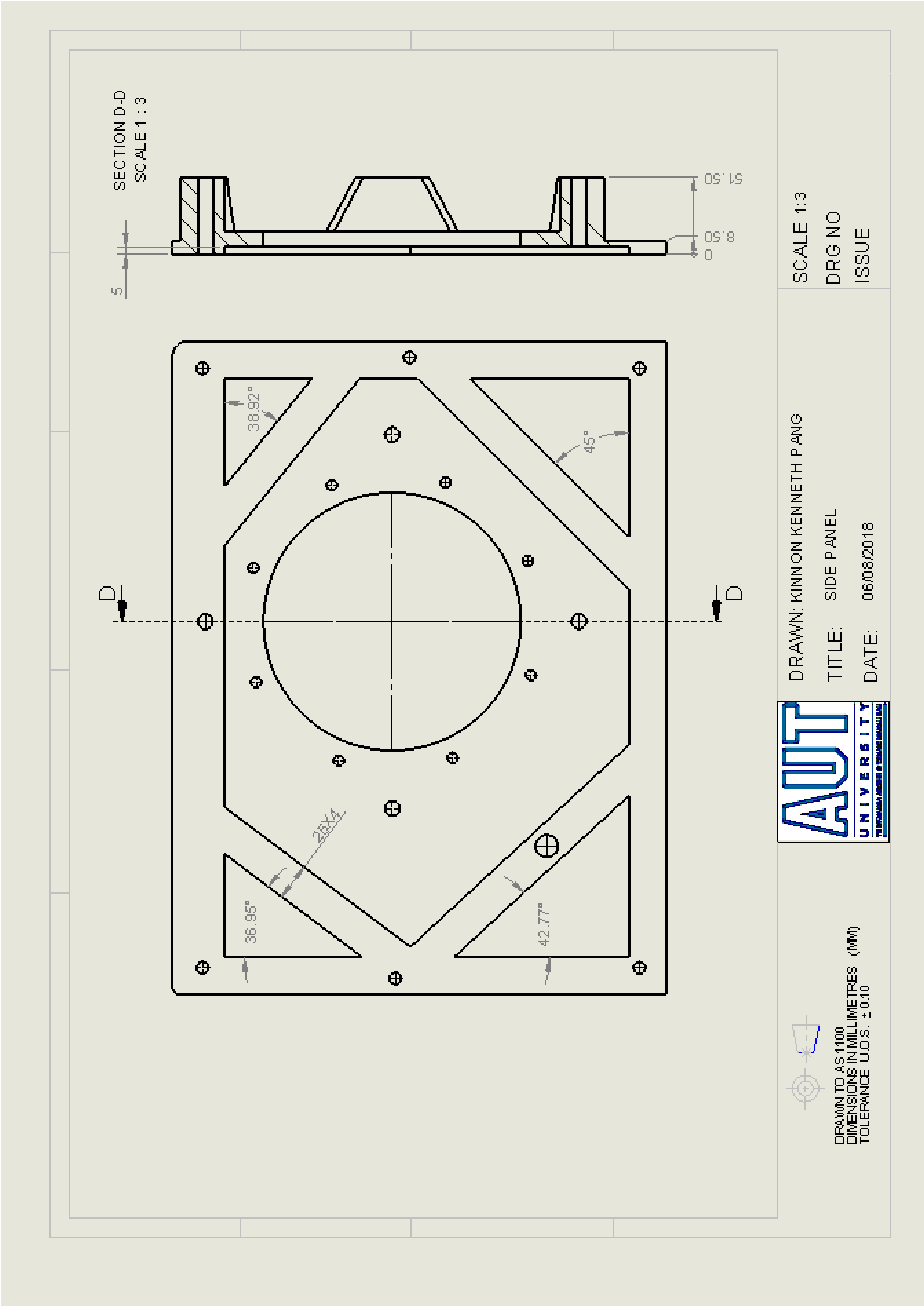

C4.4 Insert

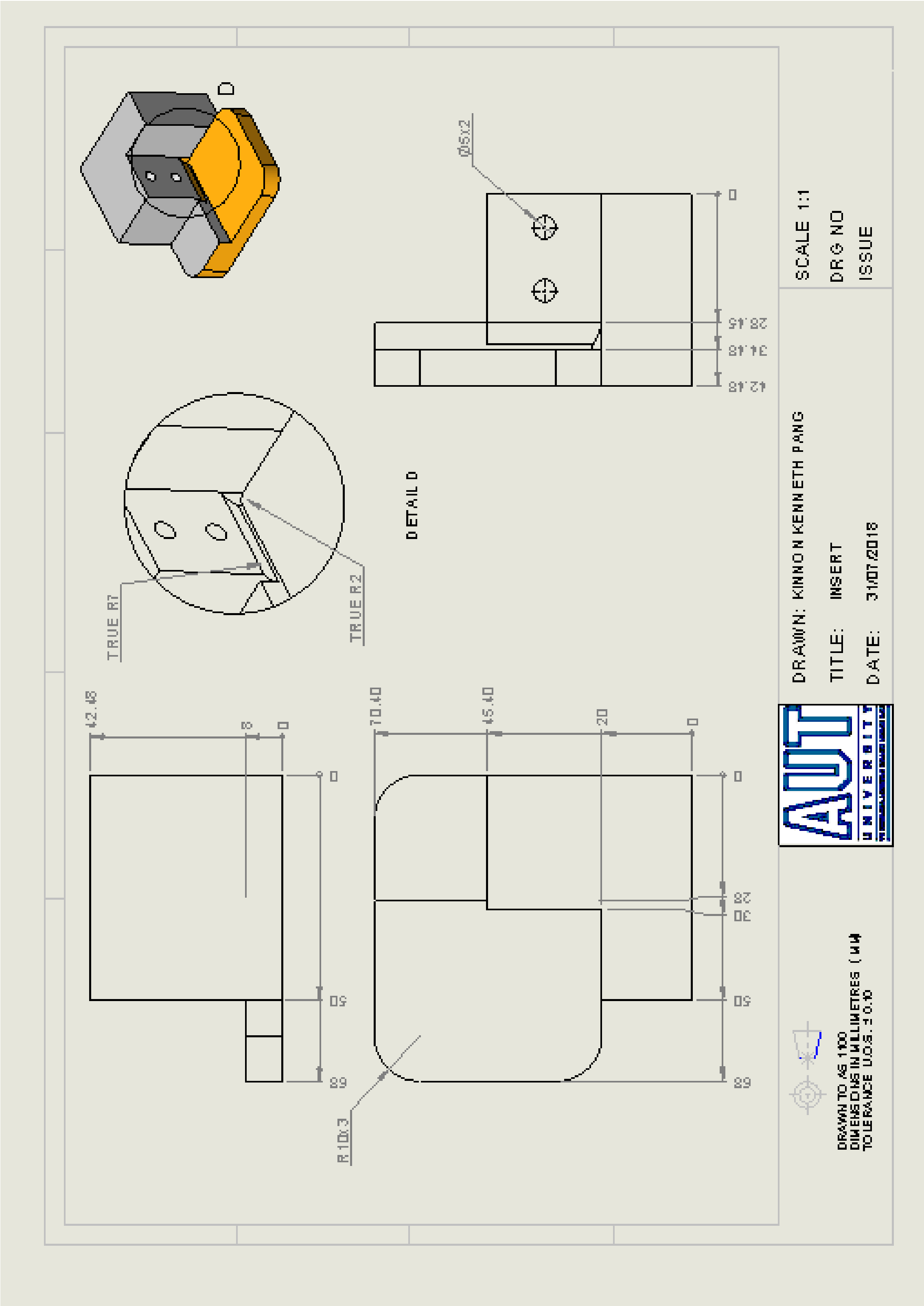
DRAWN: KINNON KENNETH PANG
TITLE: INSERT
DATE: 31/07/2018
SCALE 1:1
DRG NO
ISSUE
DETAIL D
TRUE R1
TRUE R2
R10x3
Ø5x2
D

C4.3 Bending and Shearing Bolt and Cap Assembly

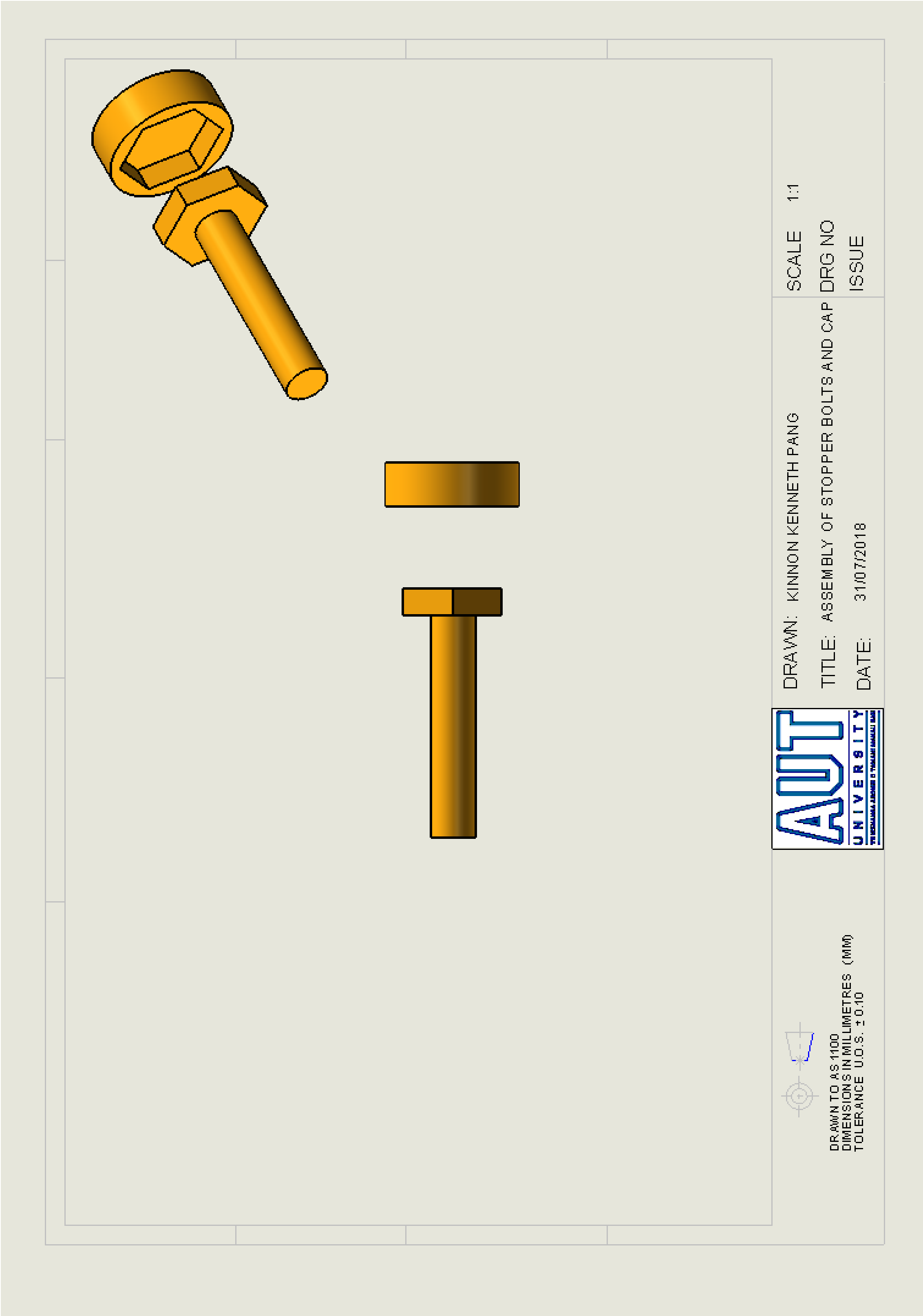

C4.4 Bending Bolt Cap

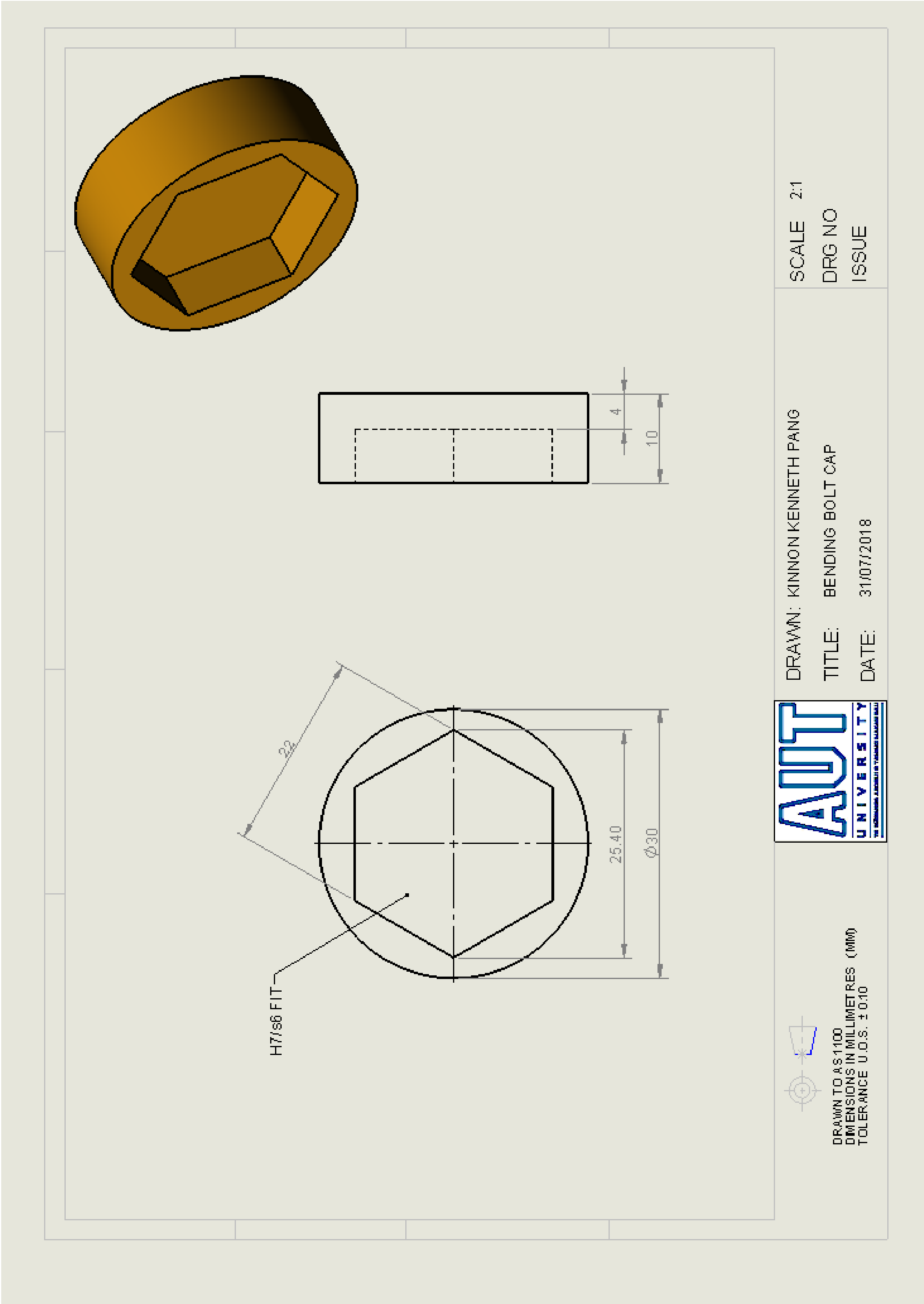

C4.5 Shearing Bolt Cap

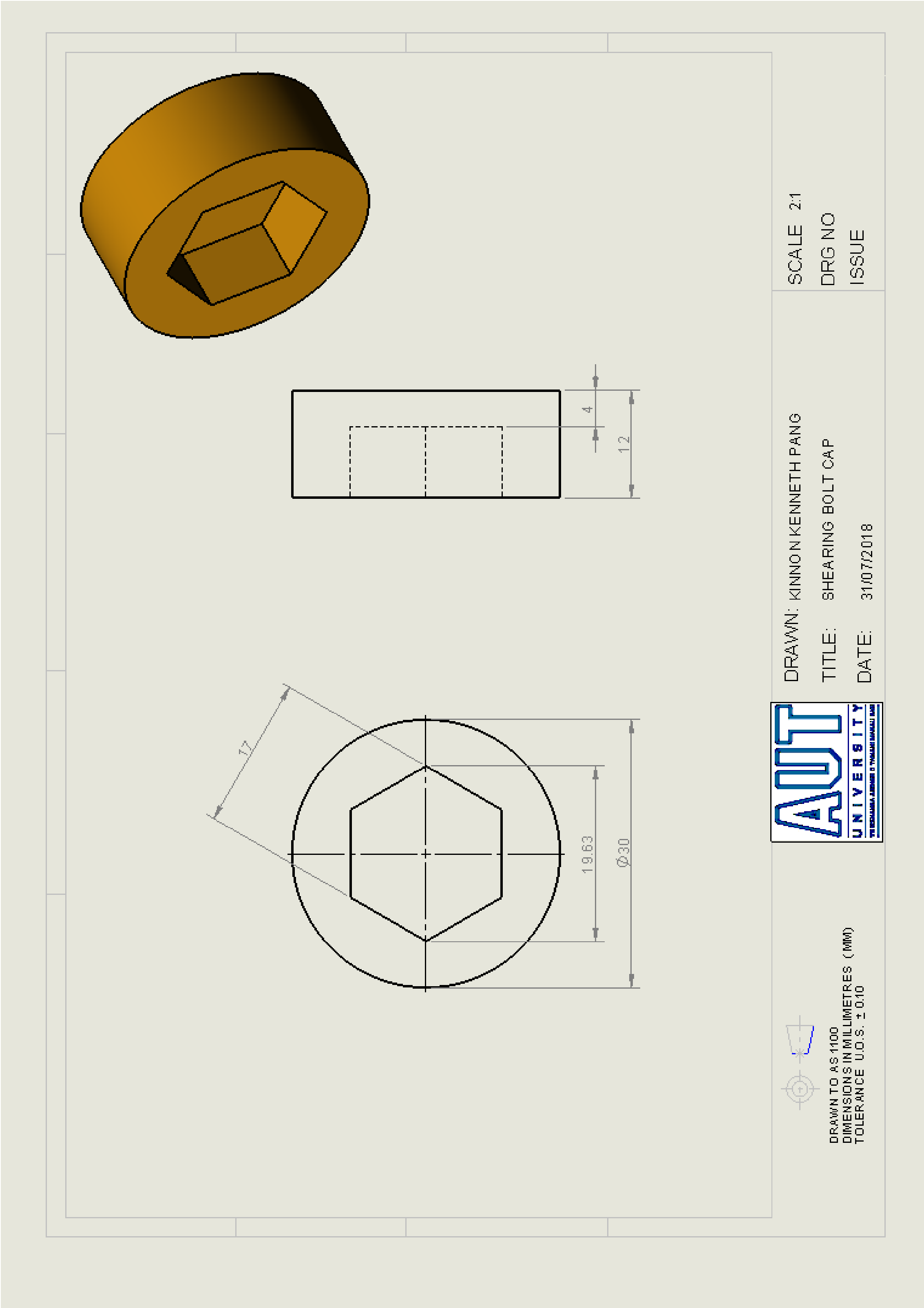

C4.6 Handle Core

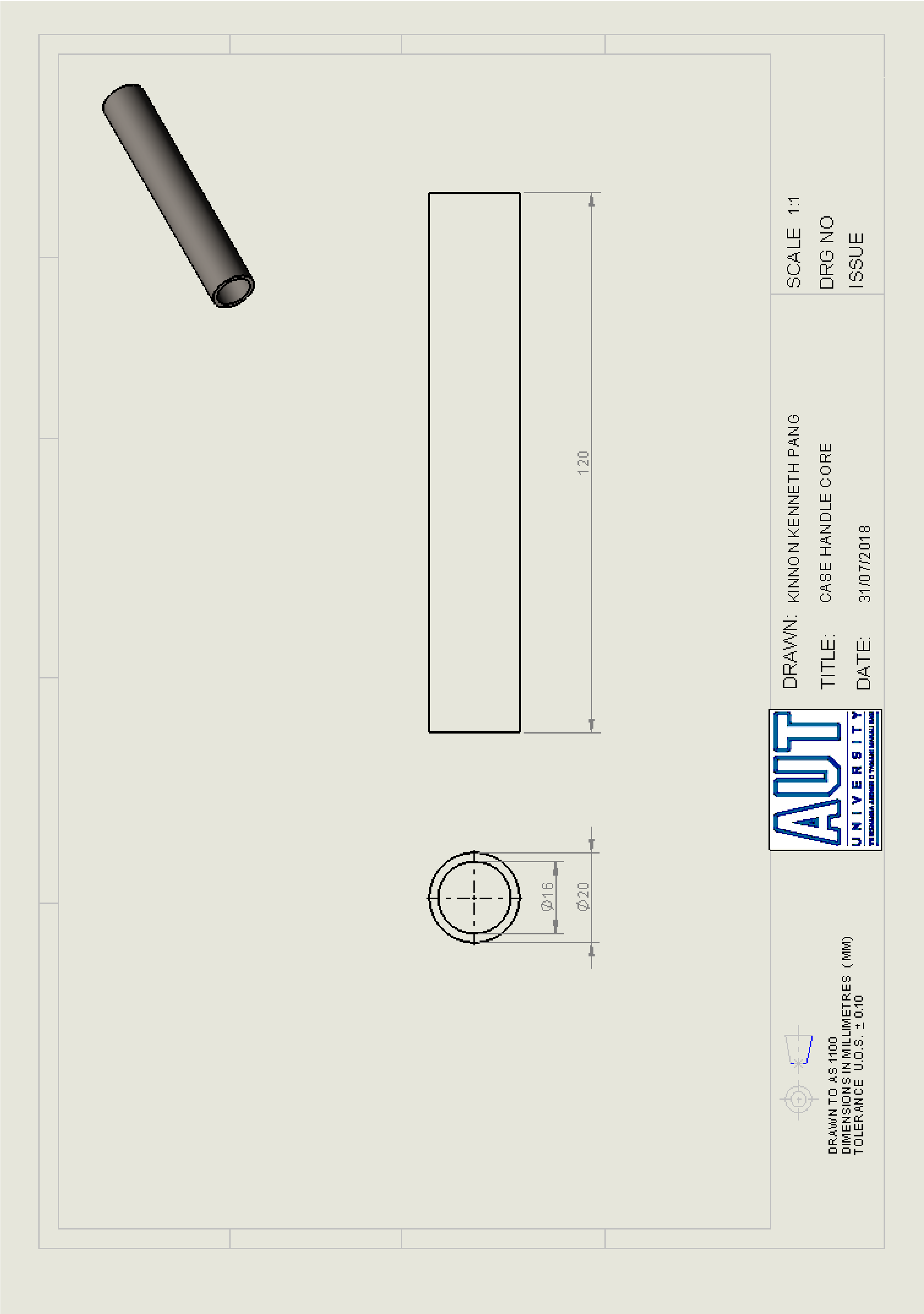

C4.7 Handle

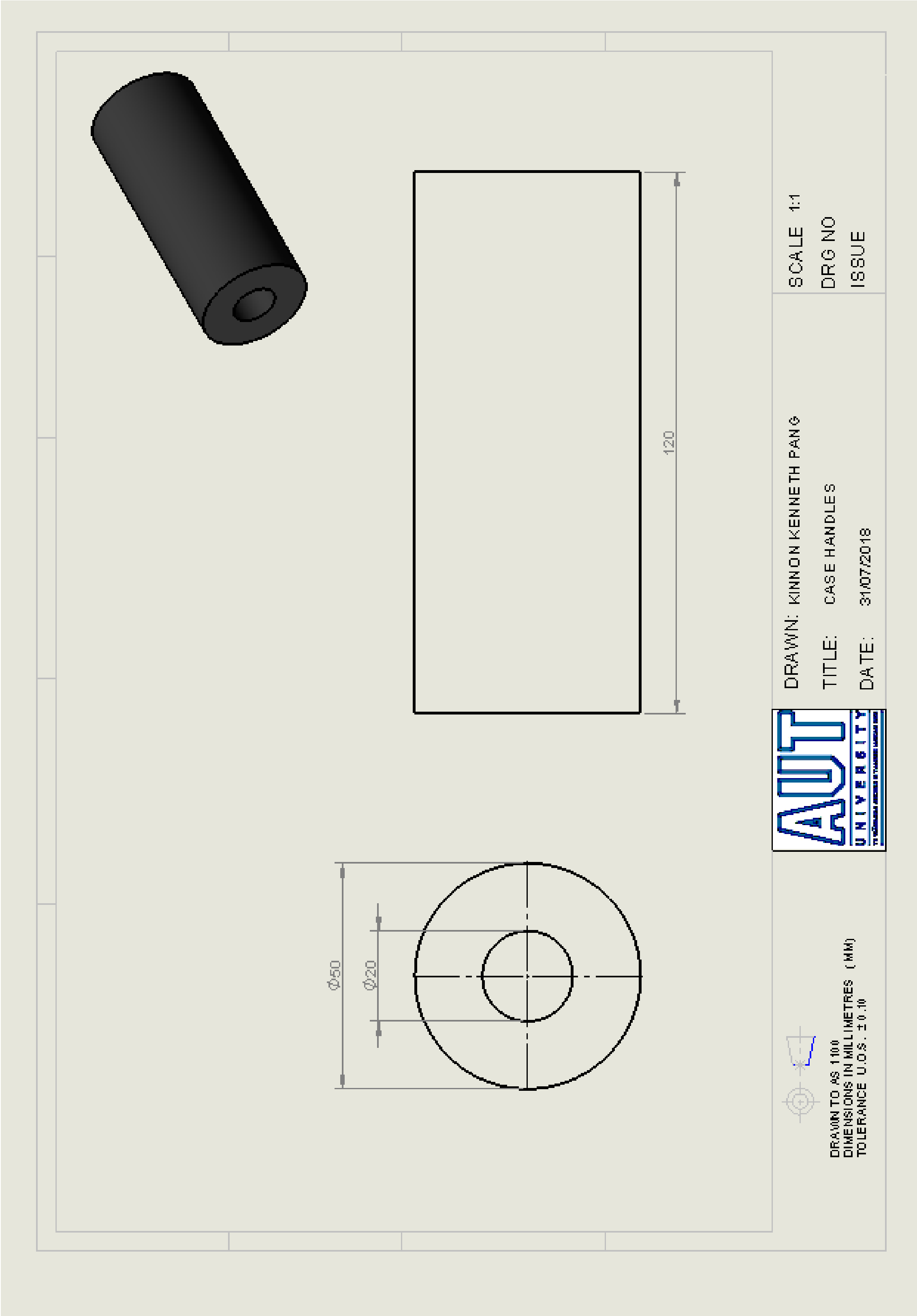
120
Ø50
Ø20
SCALE 1:1
DRG NO
ISSUE
DRAWN: KINNON KENNETH PANG
TITLE: CASE HANDLES
DATE: 31/07/2018
AUT
UNIVERSITY
DRAWN TO AS 1100
DIMENSIONS IN MILLIMETRES (MM)
TOLERANCE U.O.S. ±0.10

4.8 Housing Drawings

4.8.1 Housing Top Exterior

NOTE: Handles supports were removed from the following drawings to allow for better view of housing details.

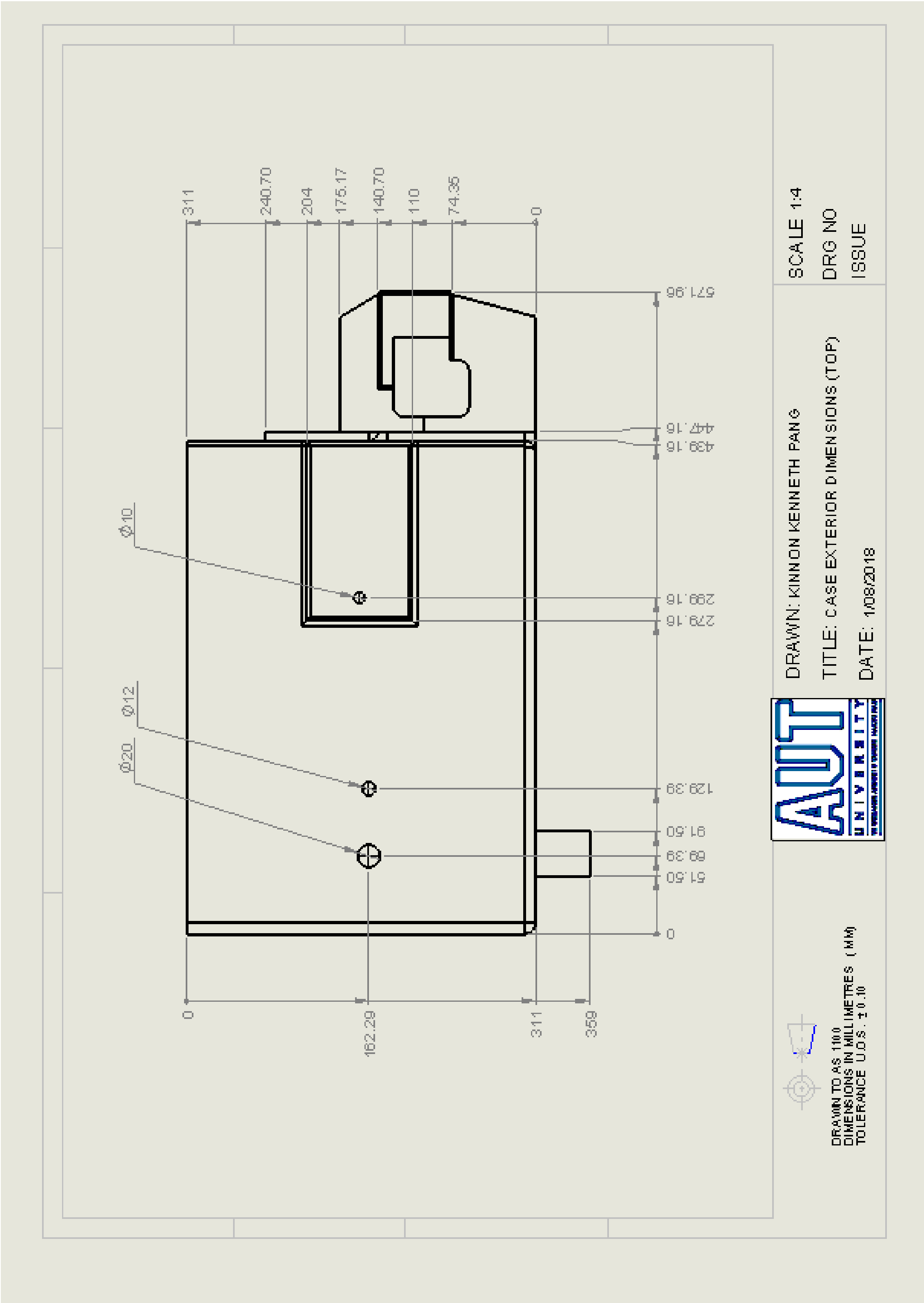

C4.8.2 Cutting Head Detail

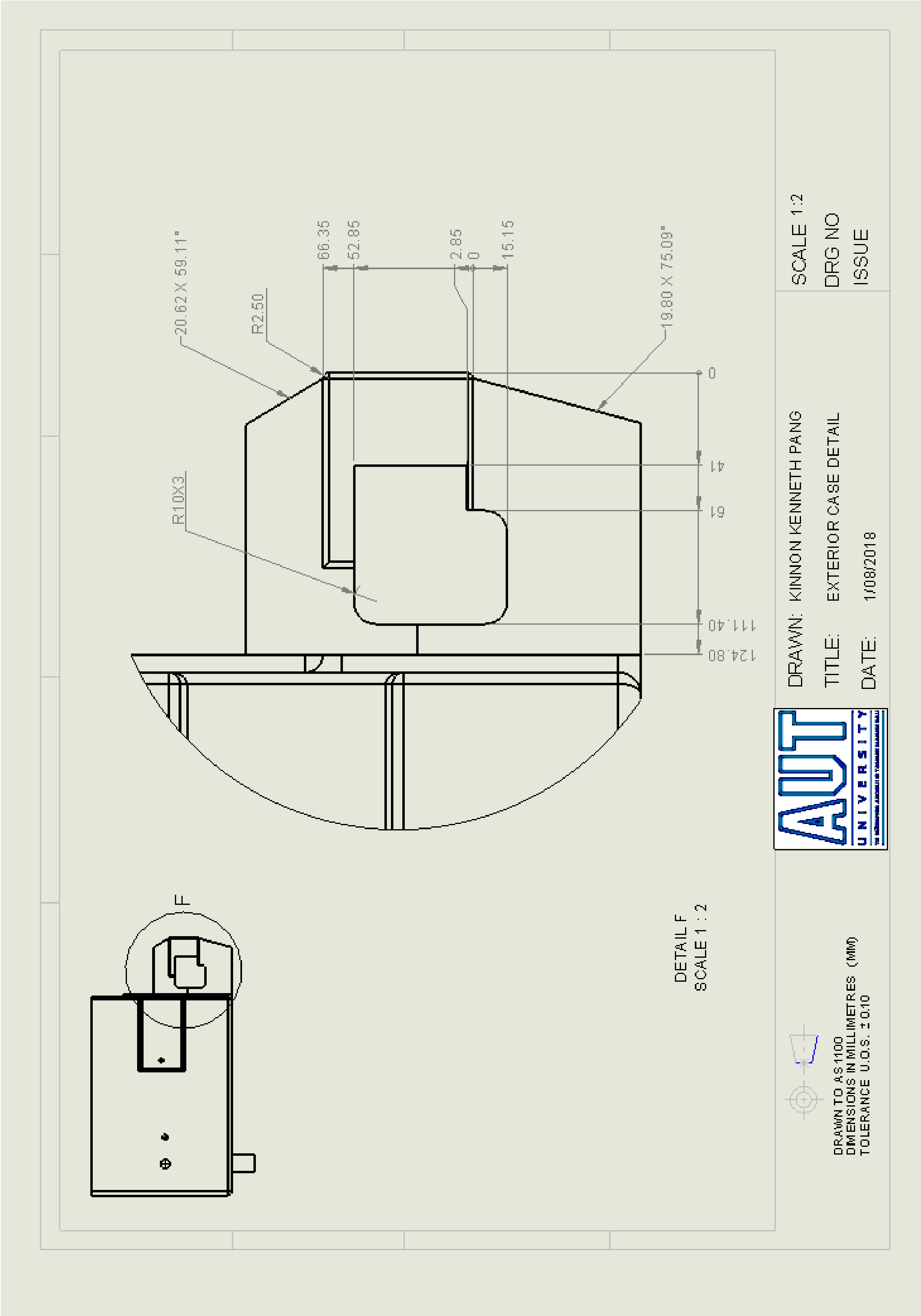

C4.8.3 Housing Front Exterior

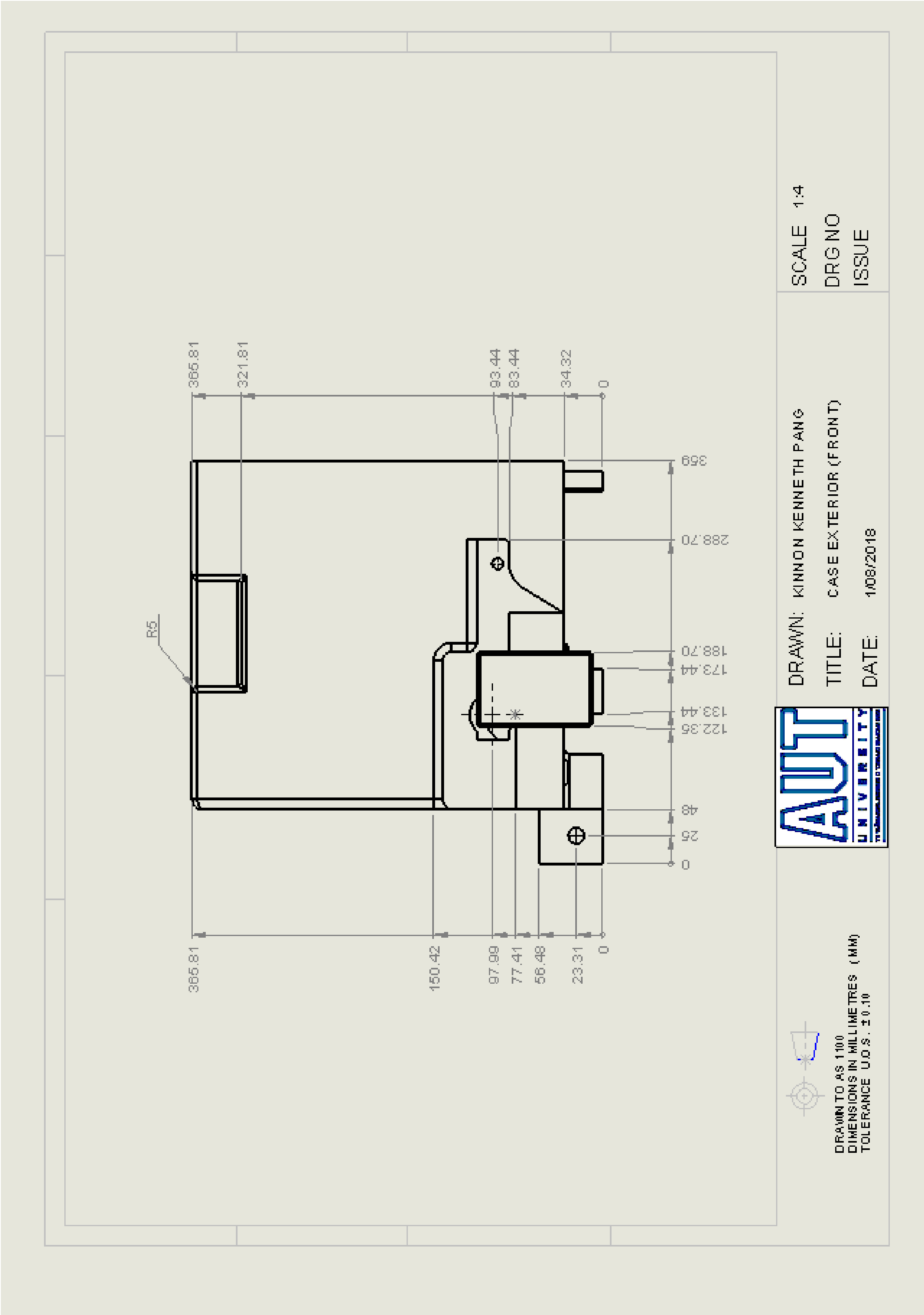

C4.8.3.1 Further Front Exterior Detail

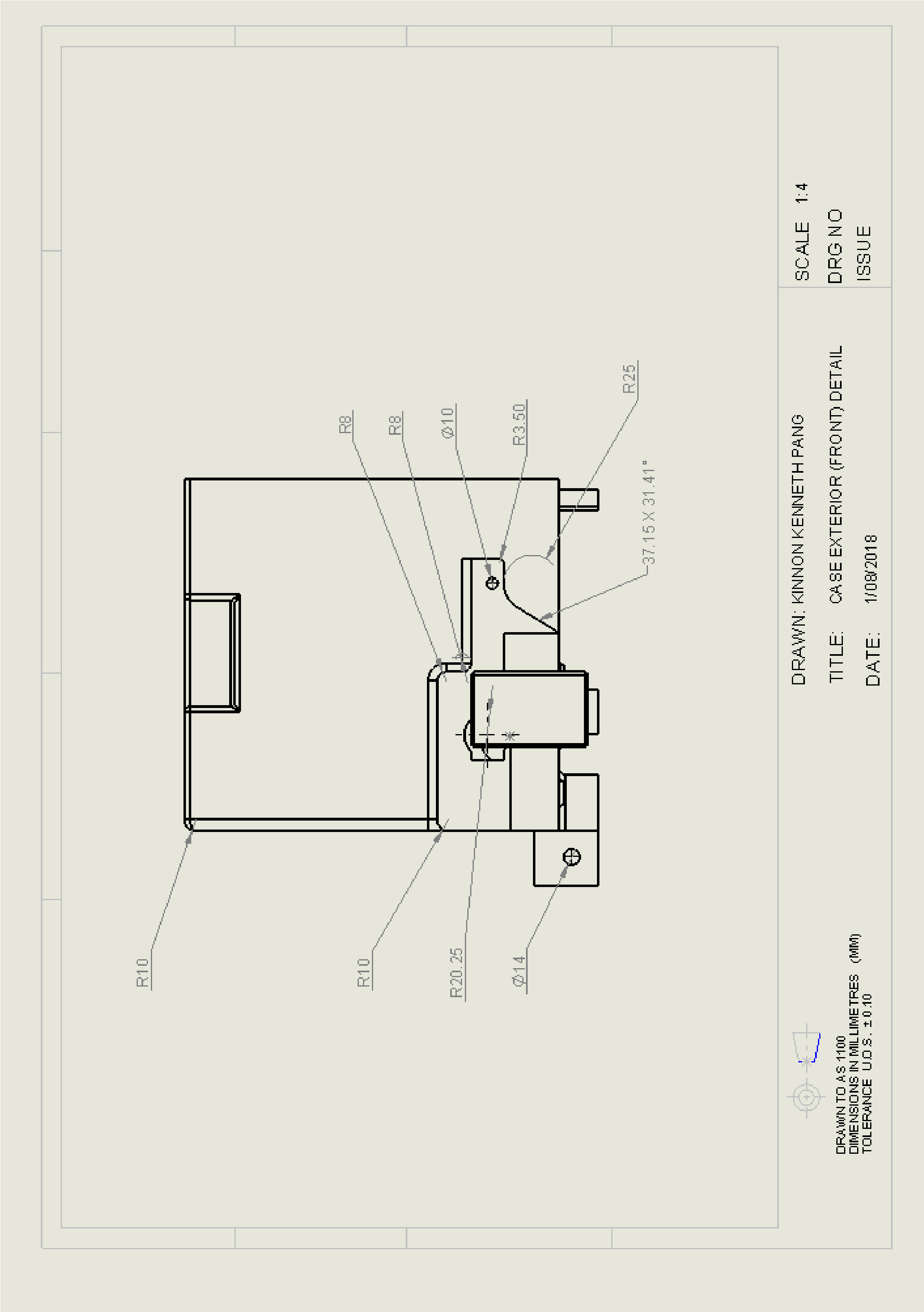

C4.8.4 Housing Bottom Exterior

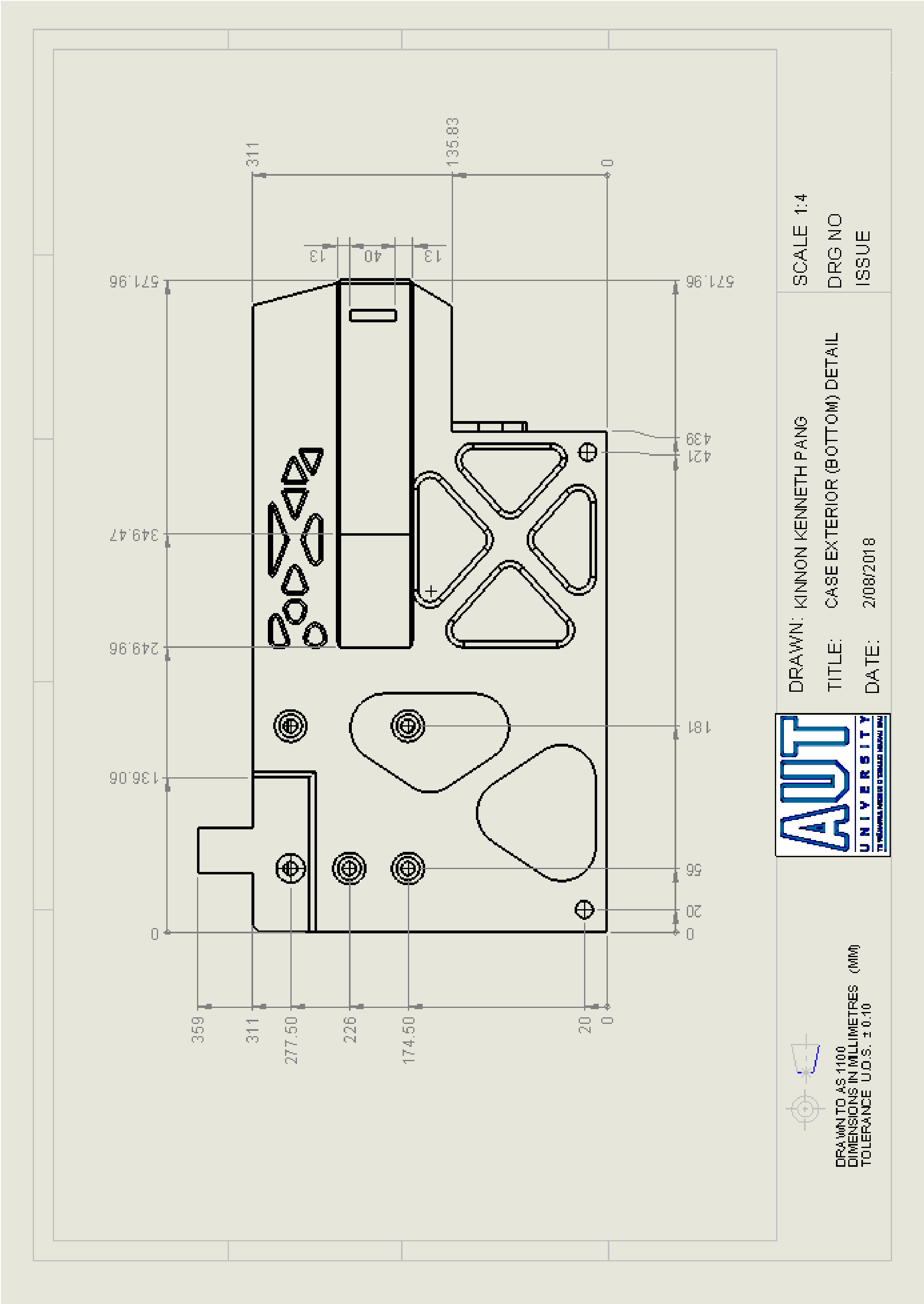

C4.8.4.1 Housing Bottom Exterior (A)

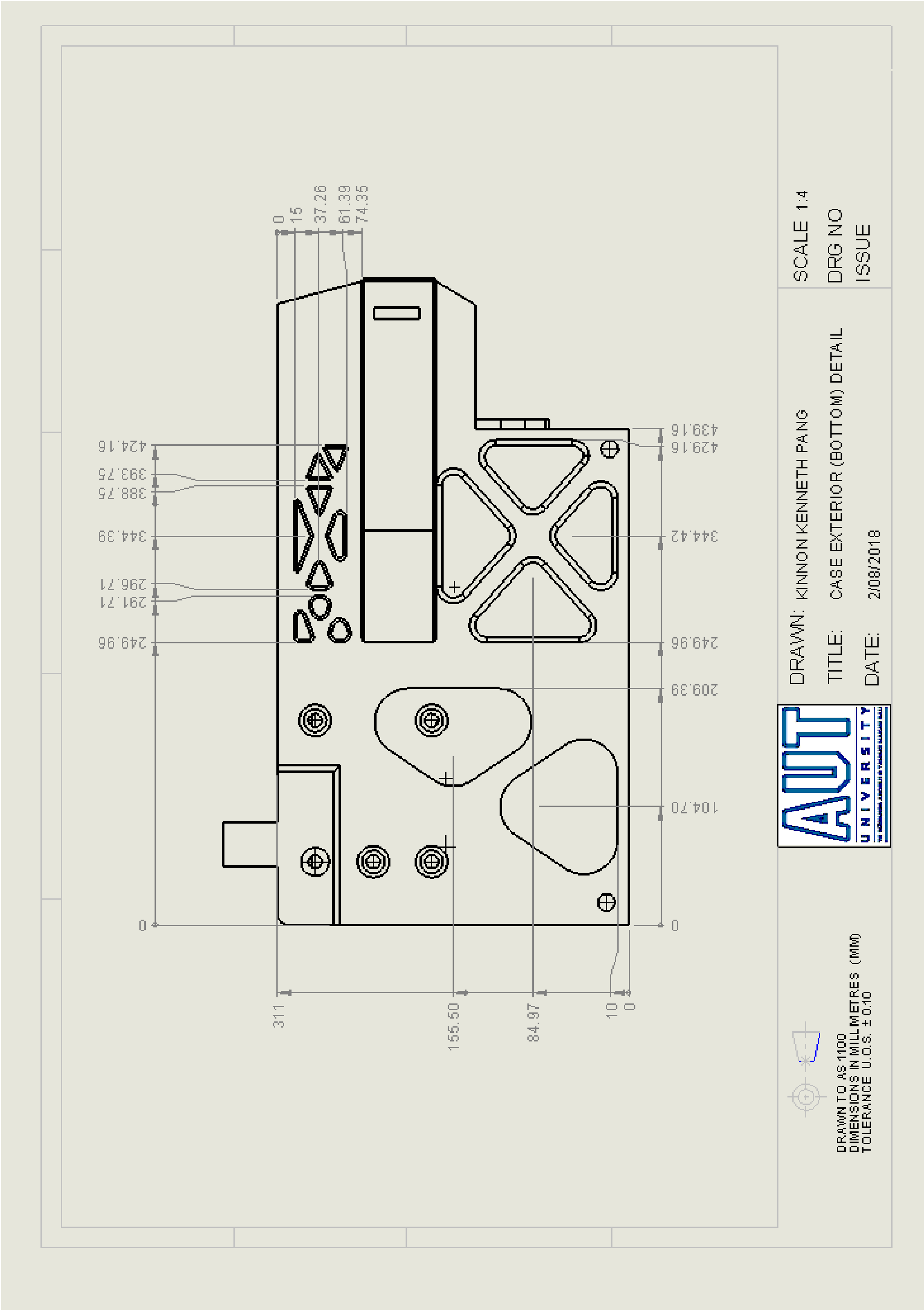

C4.8.4.2 Housing Bottom Exterior (B)

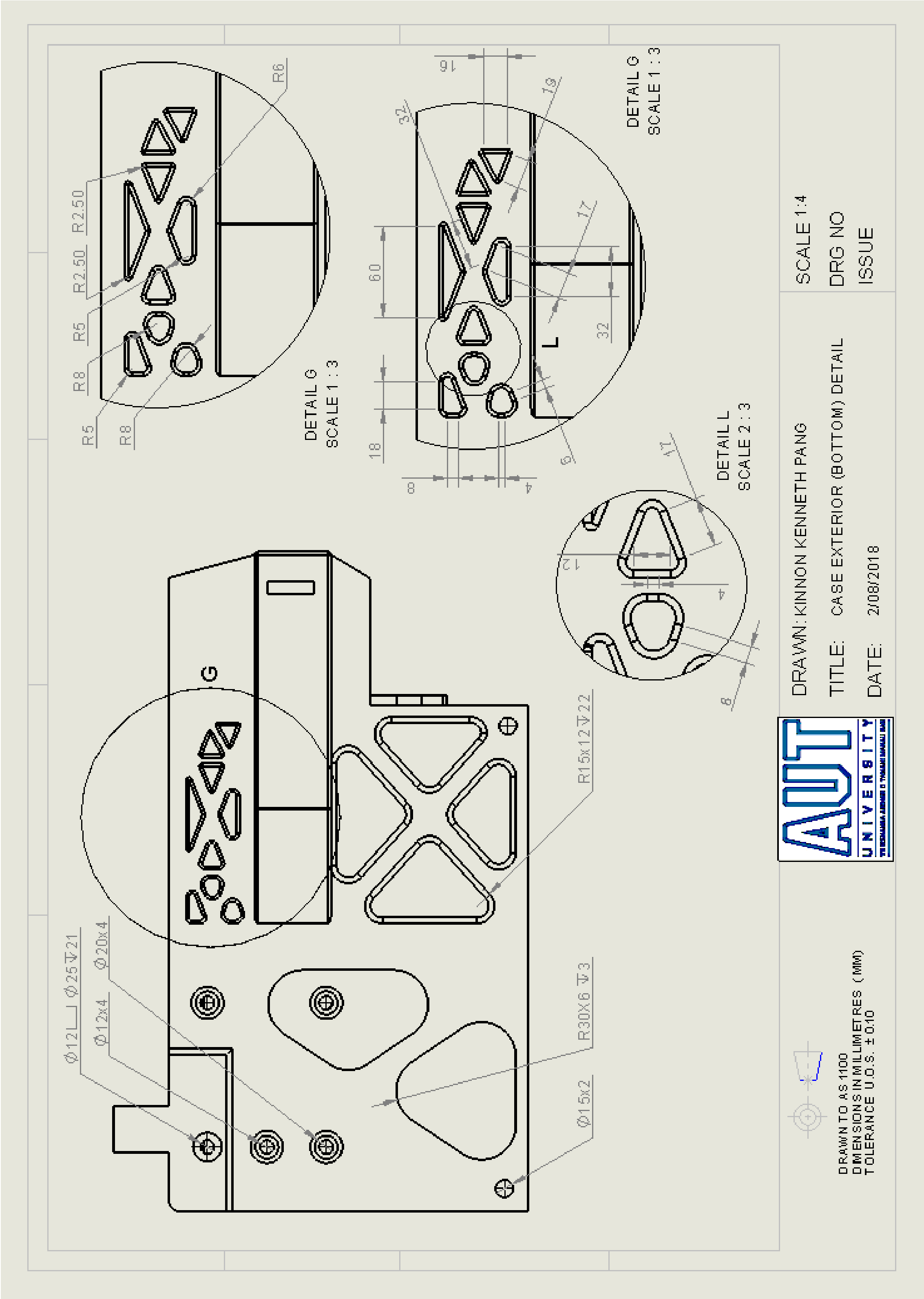

C4.8.4.3 Housing Bottom Exterior (C)

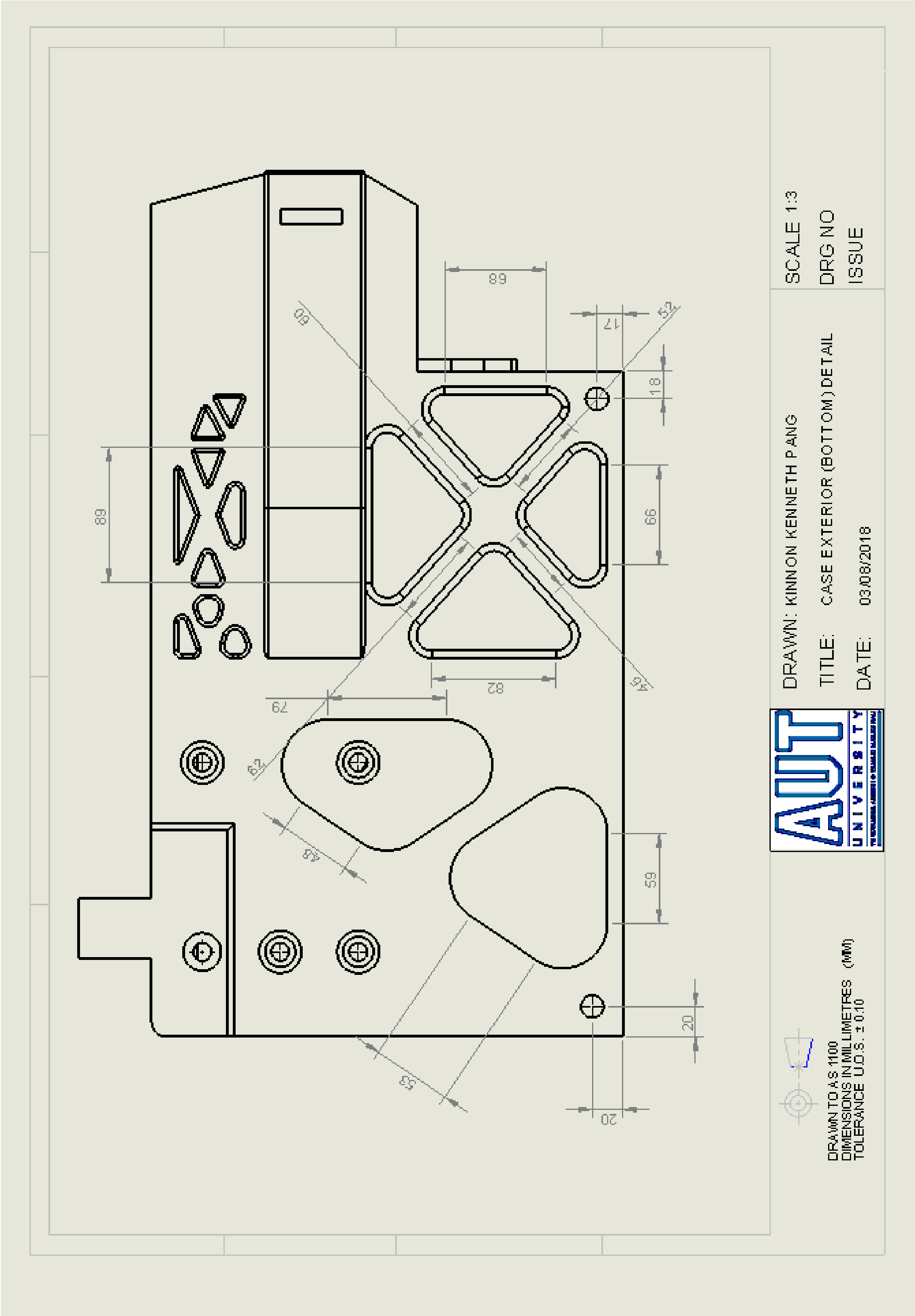

C4.8.5 Housing Exterior Side A

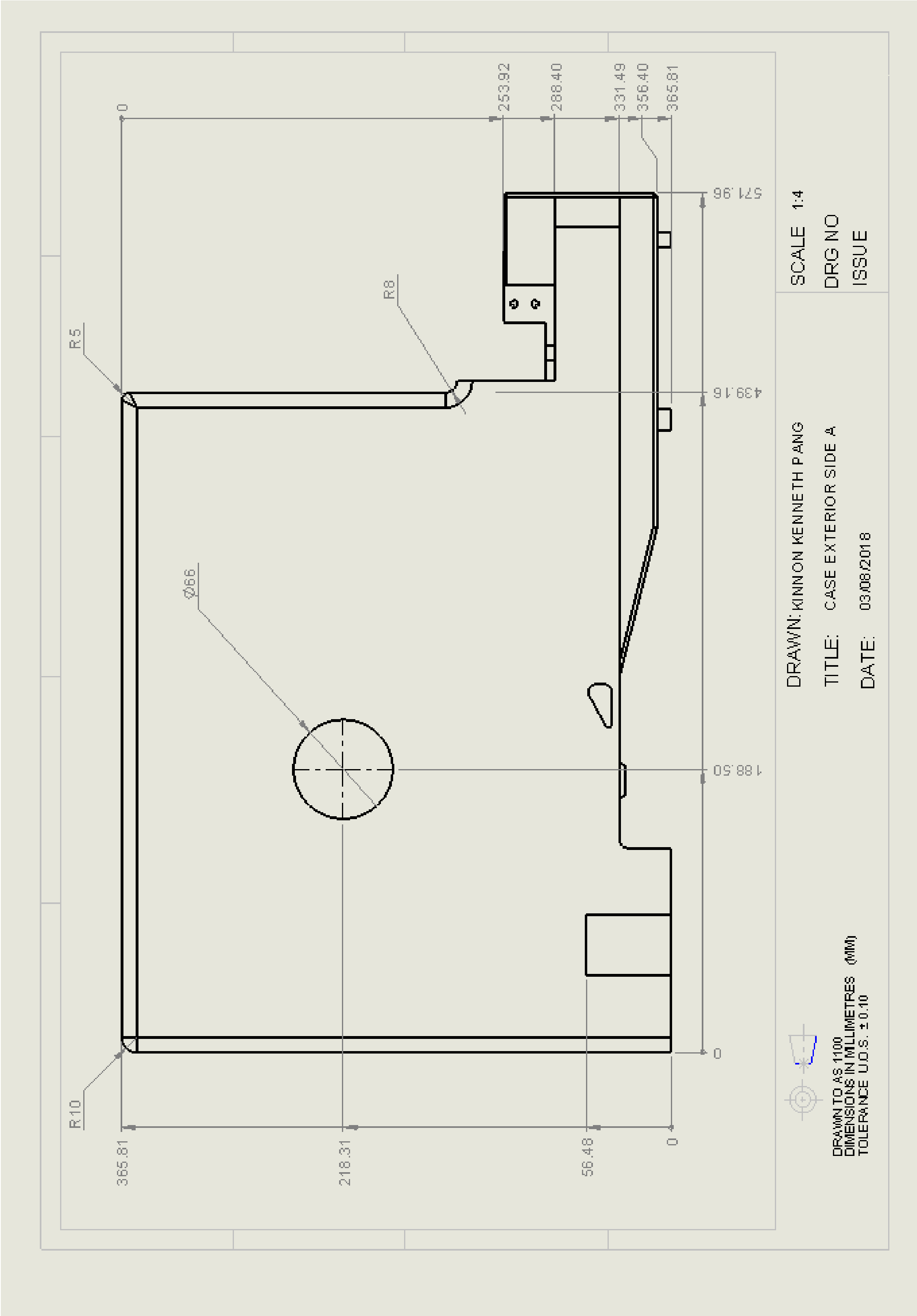

C4.8.5.1 Exterior Side A Cutting Head Detail

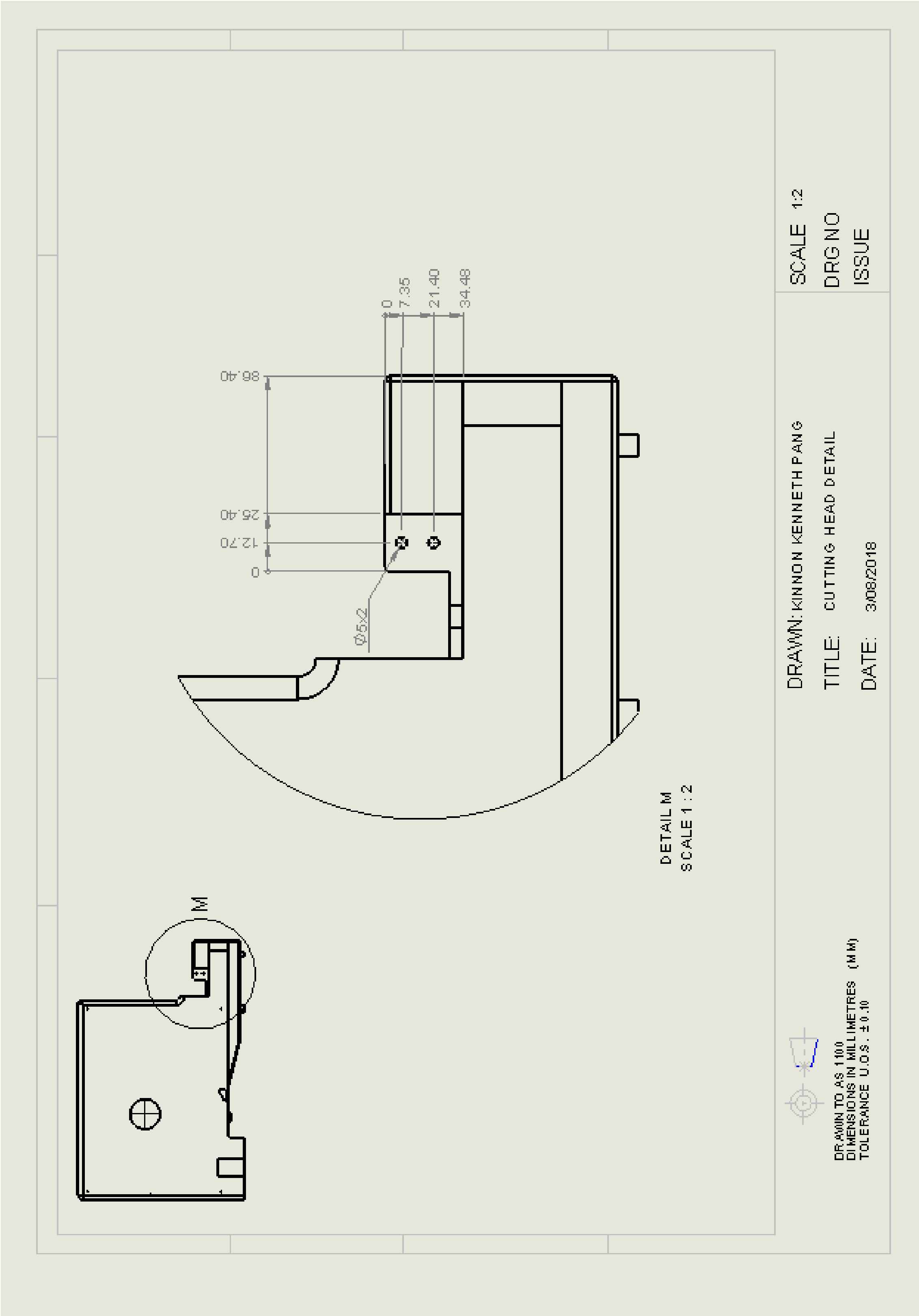

C4.8.6 Housing Exterior Rear

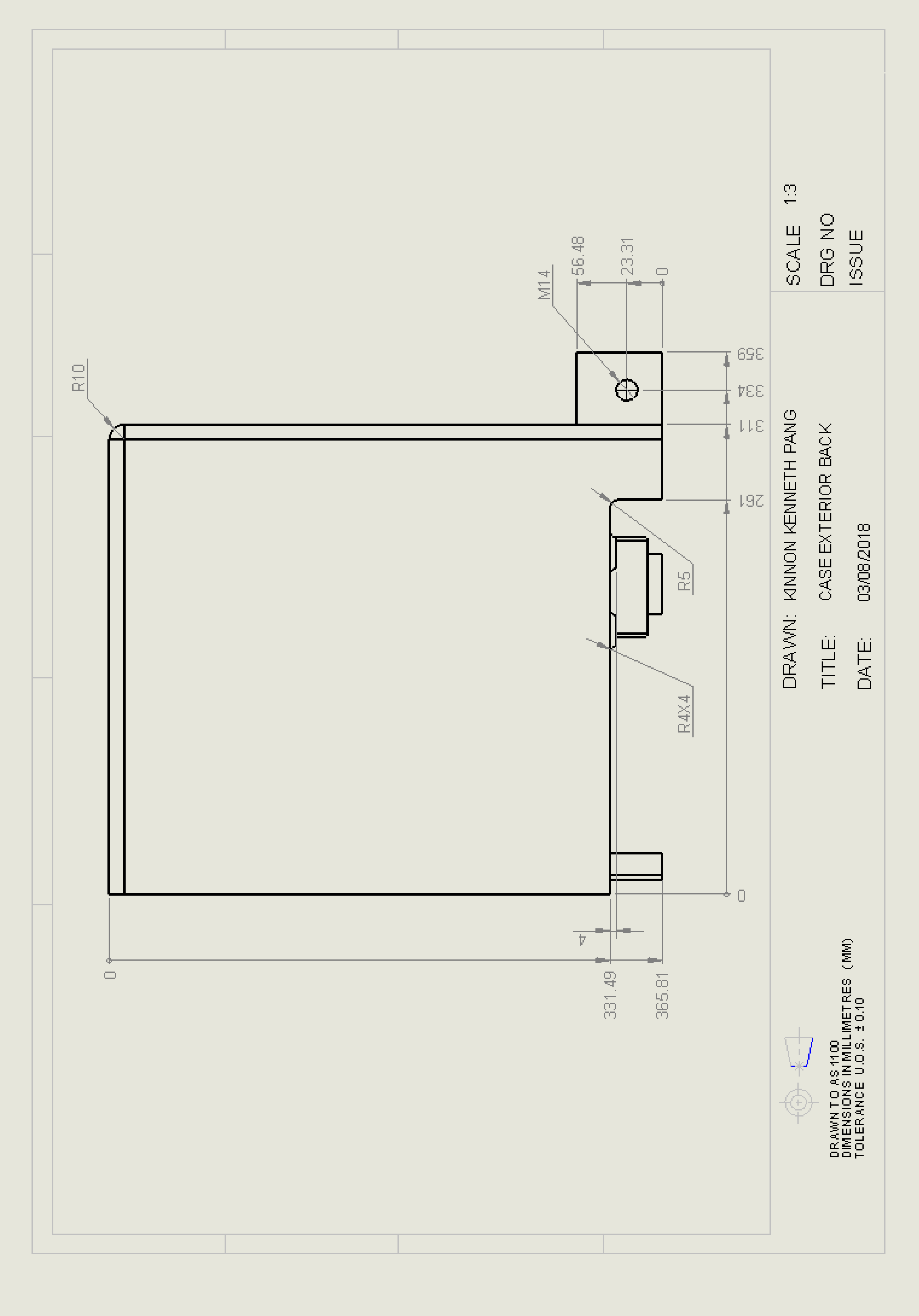

C4.8.8 Housing Exterior Side B

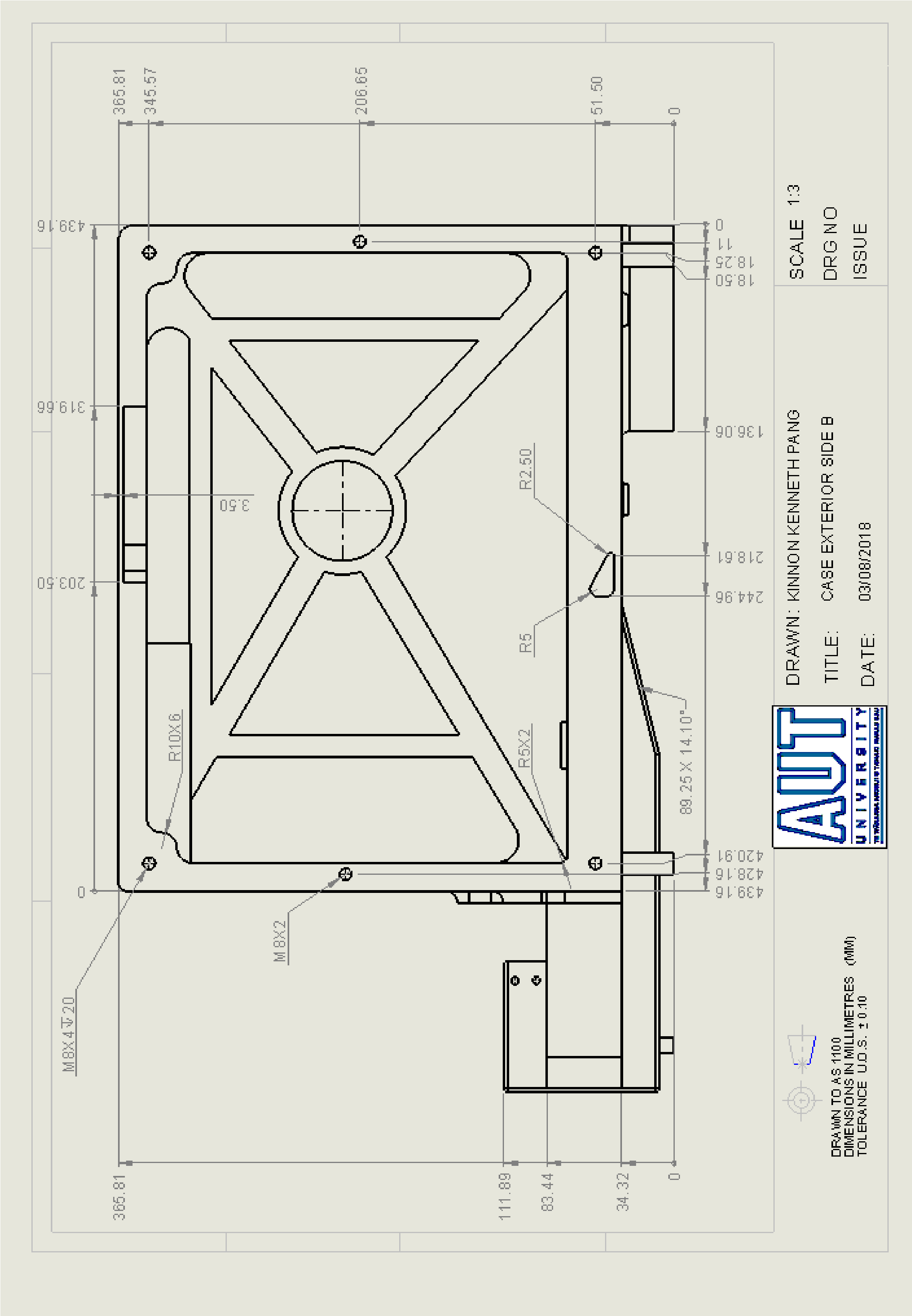

C4.8.9 Interior Looking in From Side B

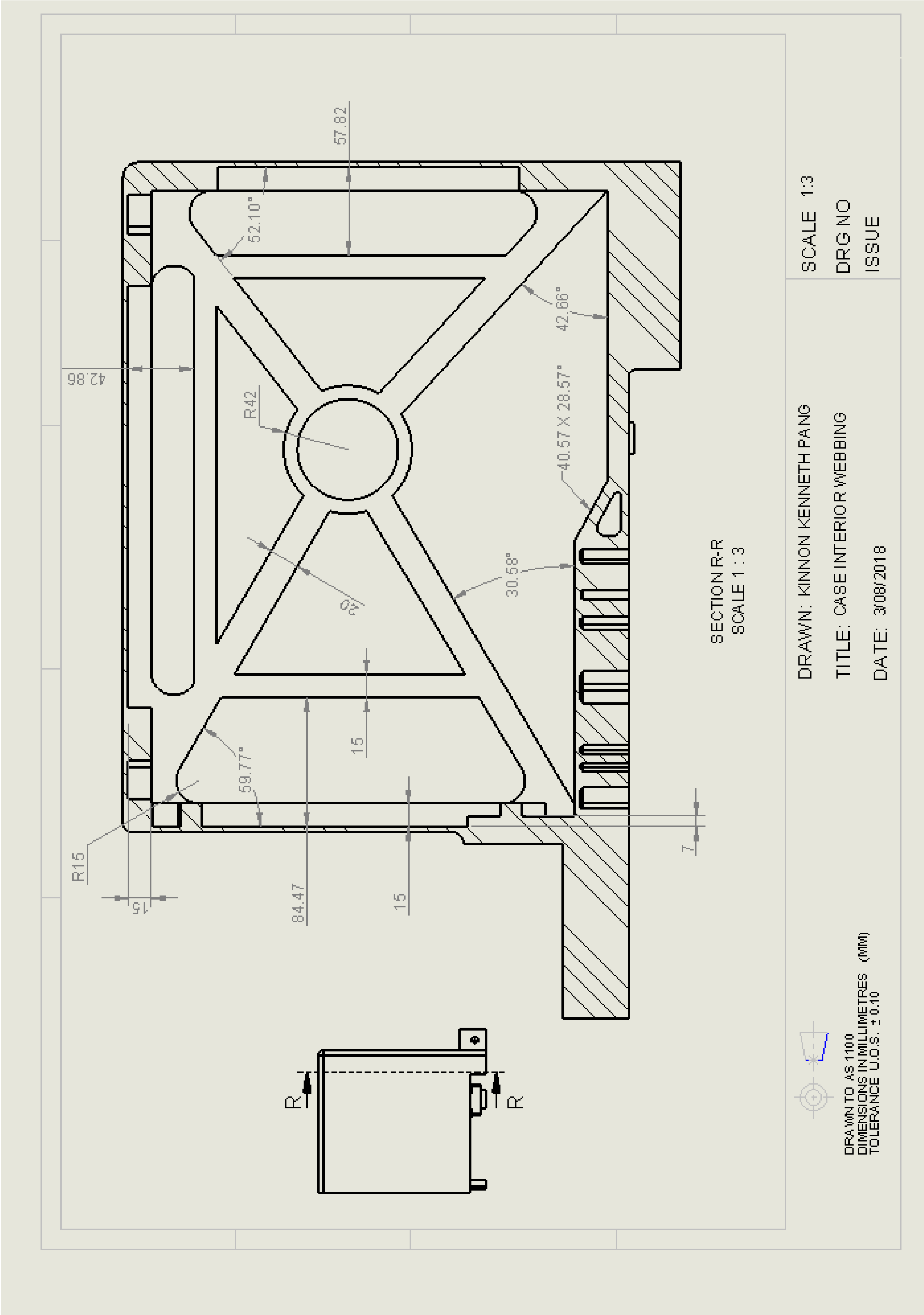

C4.8.10 Housing Interior Top

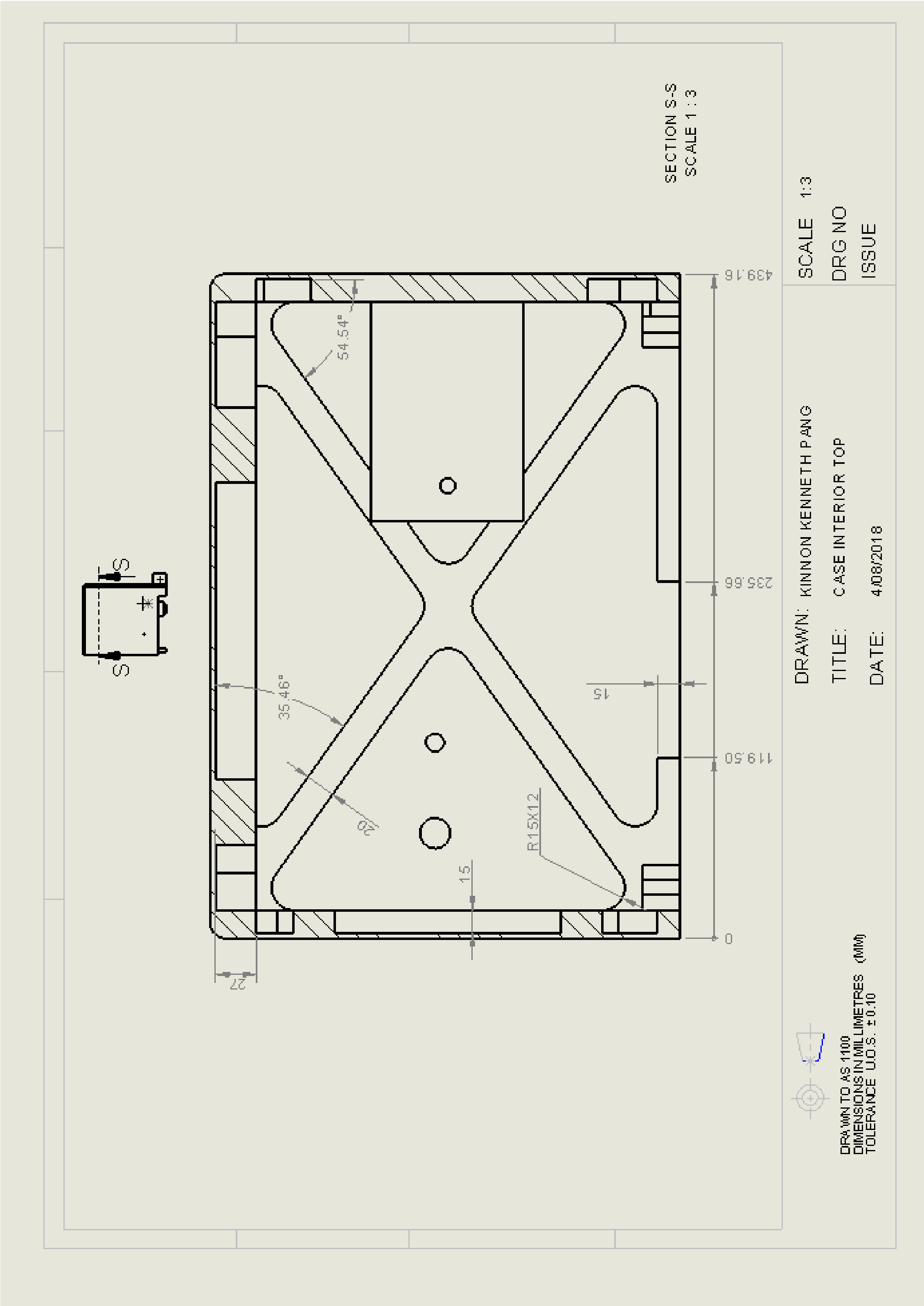

C4.8.11 Housing Interior Front

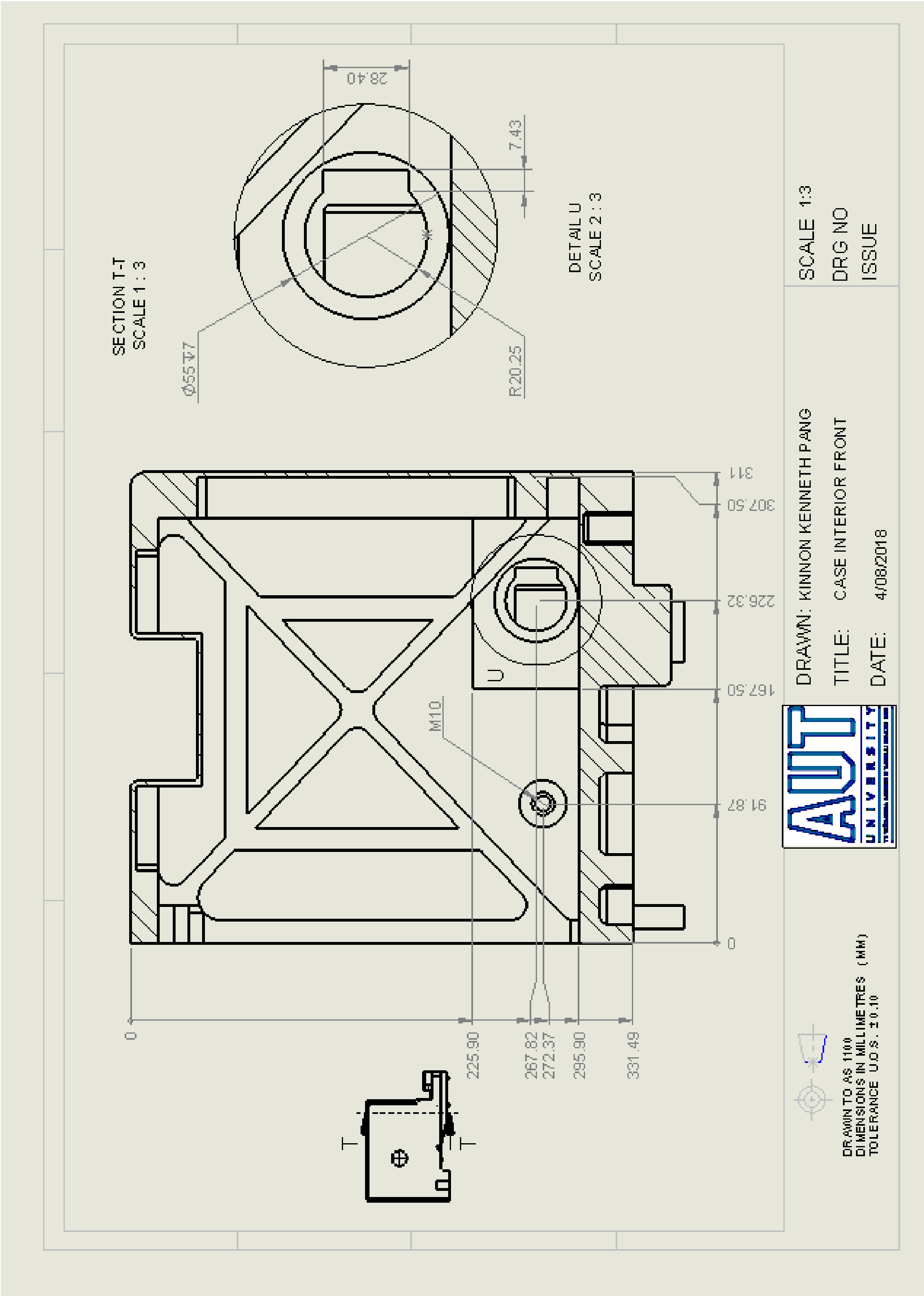

C4.8.12 Housing Interior Rear

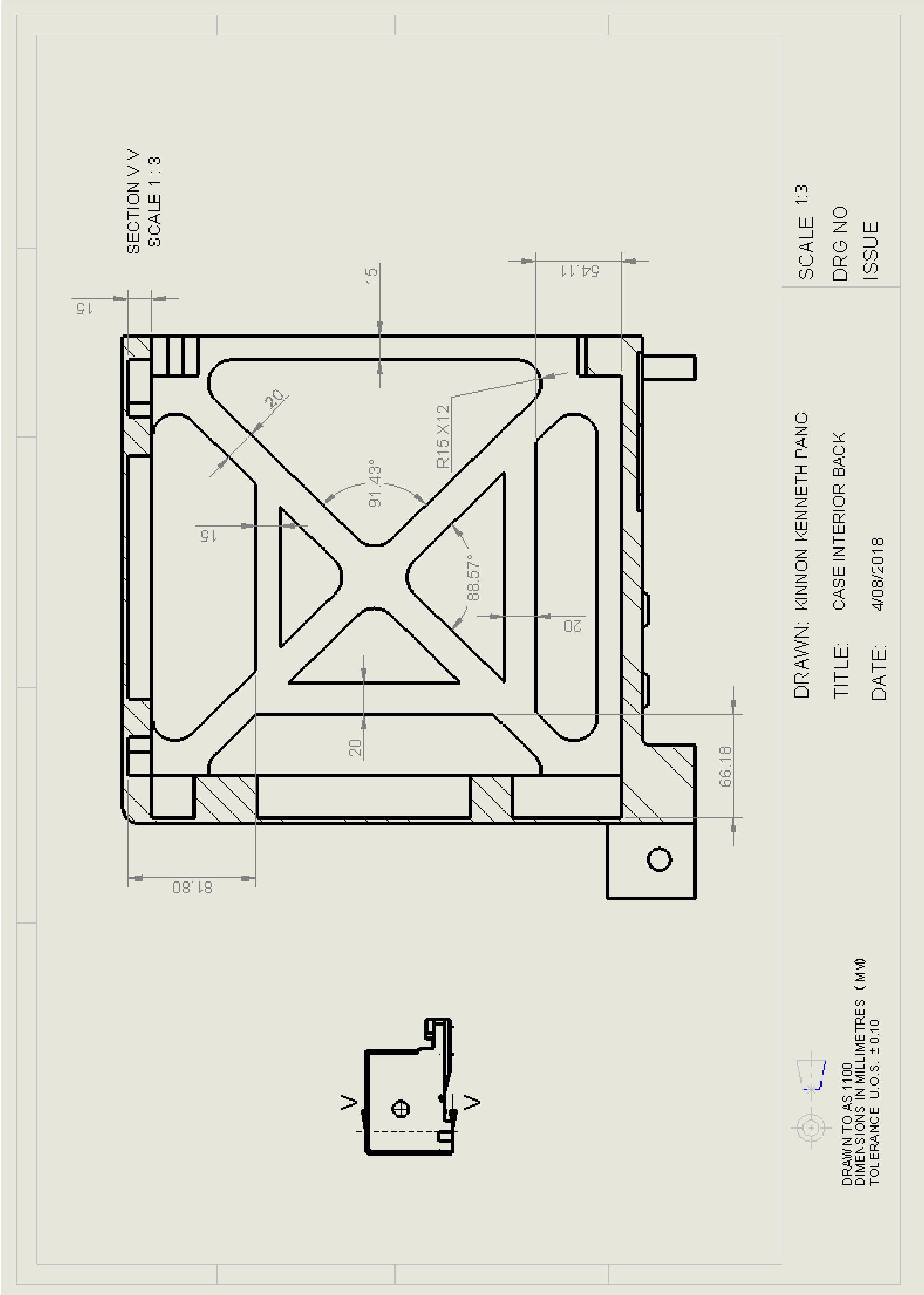

C4.8.13 Slider Guide

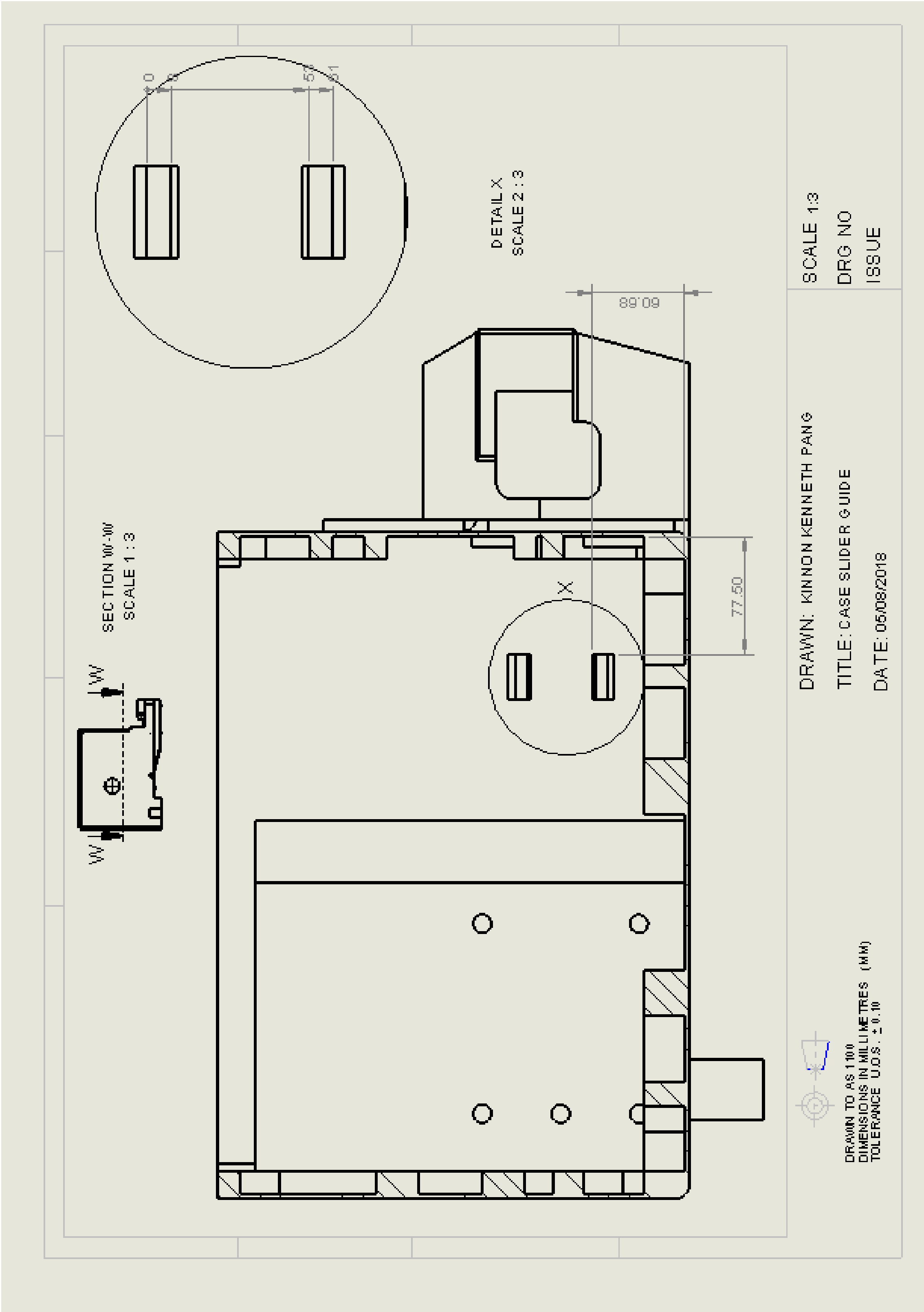

C4.8.13.1 Slider Guide Detail

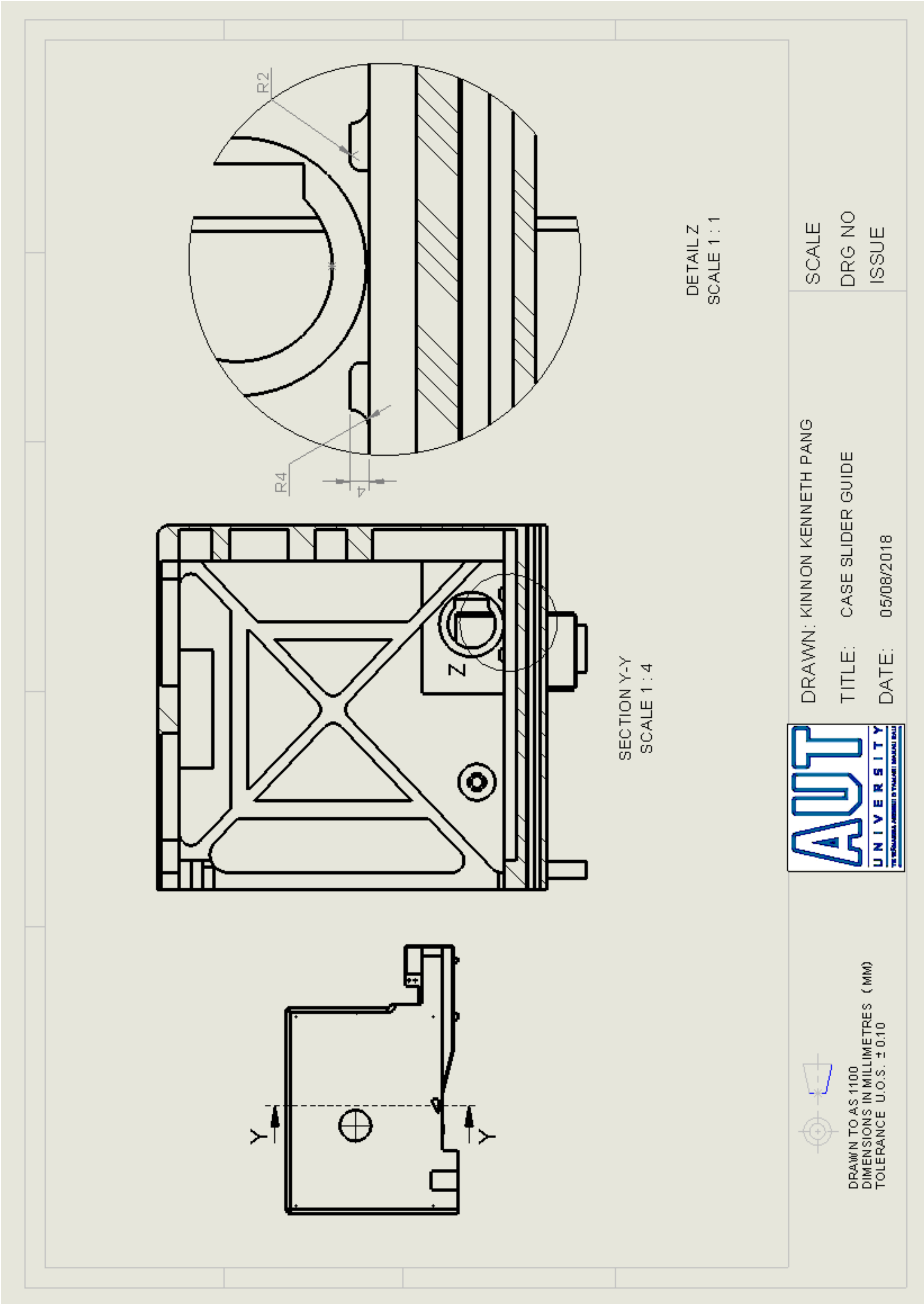

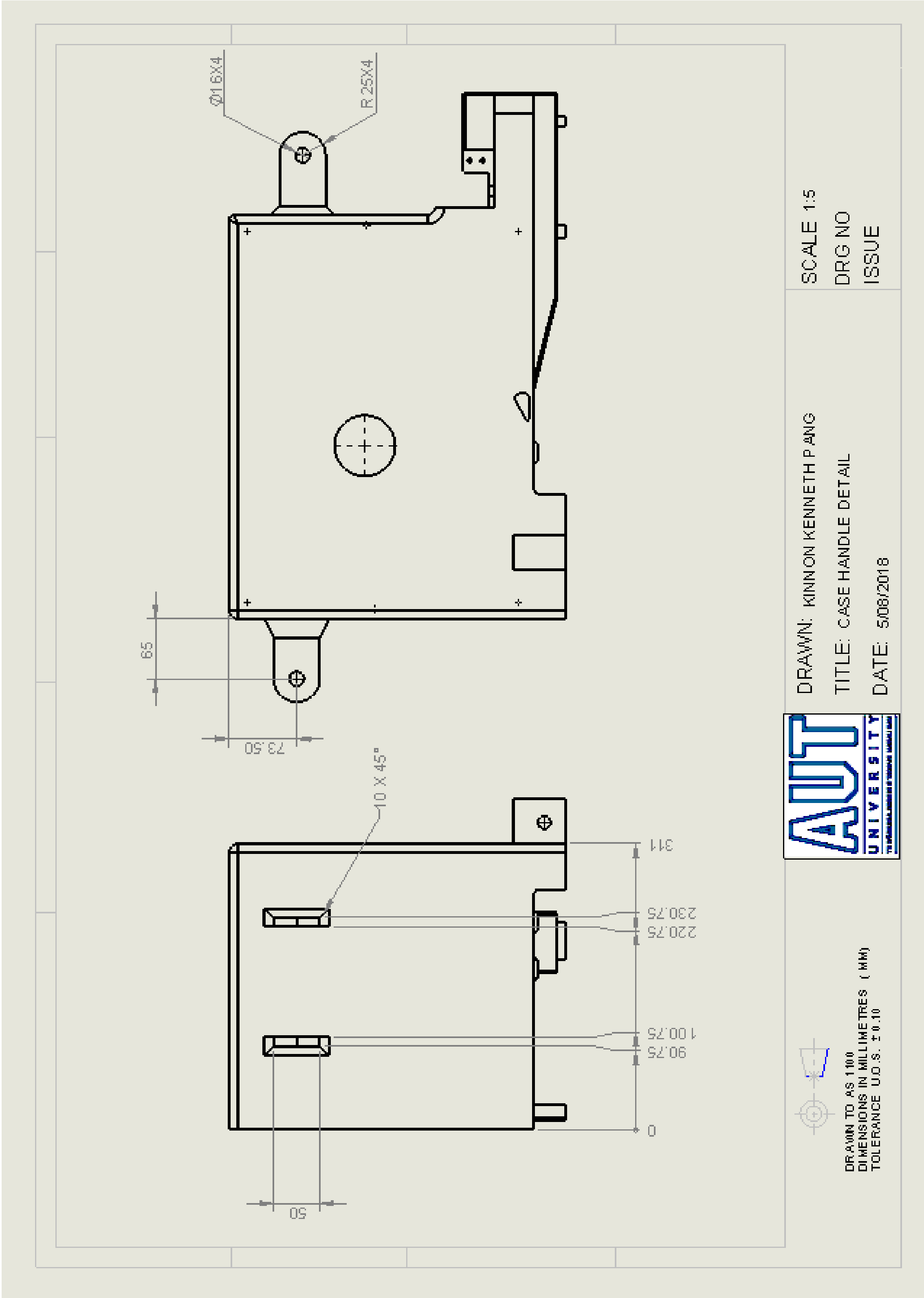
SCALE 1:5
DRG NO
ISSUE
DRAWN: KINNON KENNETH P ANG
TITLE: CASE HANDLE DETAIL
DATE: 5/08/2018
DRAWN TO AS 1100
DIMENSIONS IN MILLIMETRES (MM)
TOLERANCE U.O.S. ±0.10

C5 Bending Components

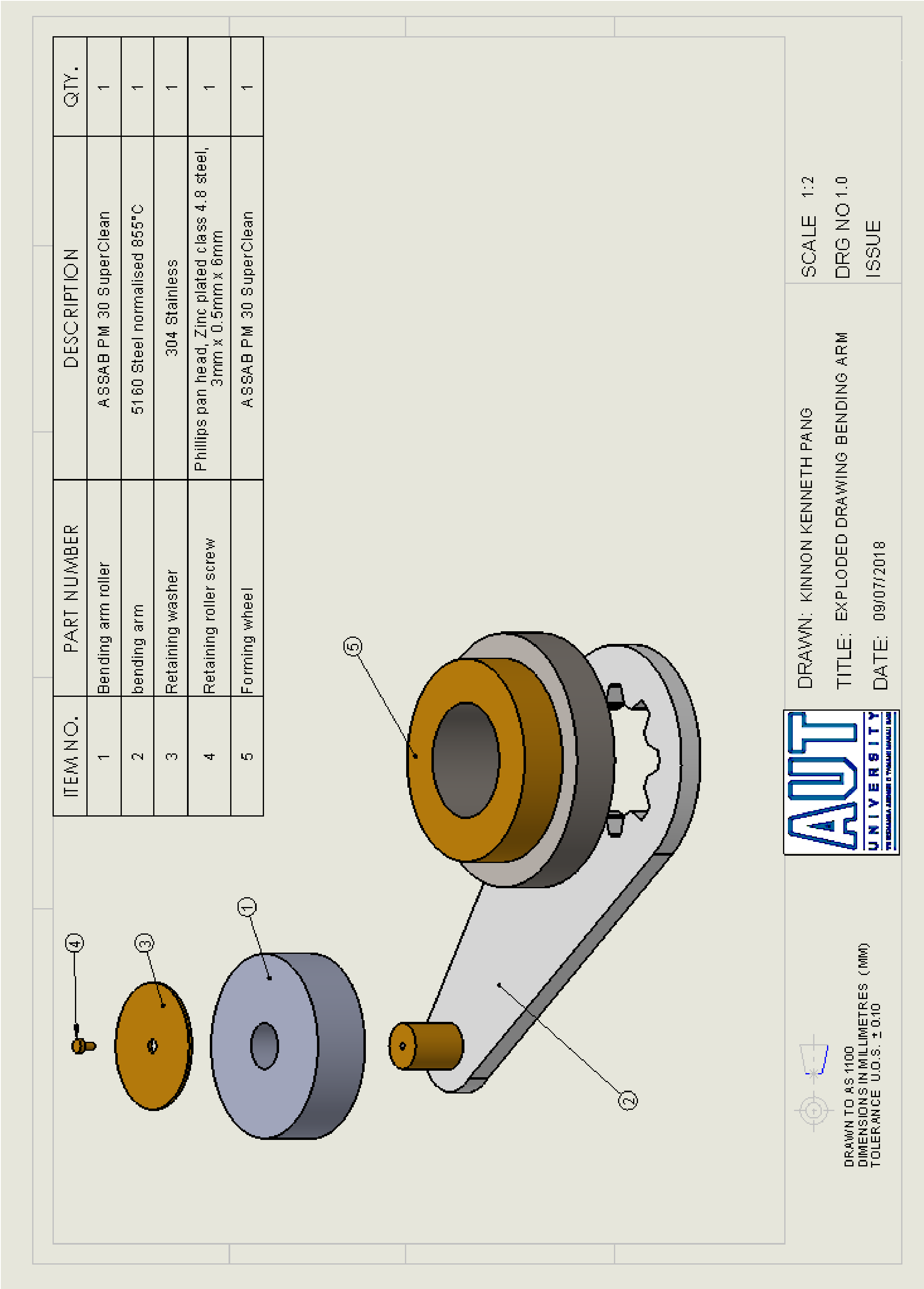

C5.1 Bending Arm Roller

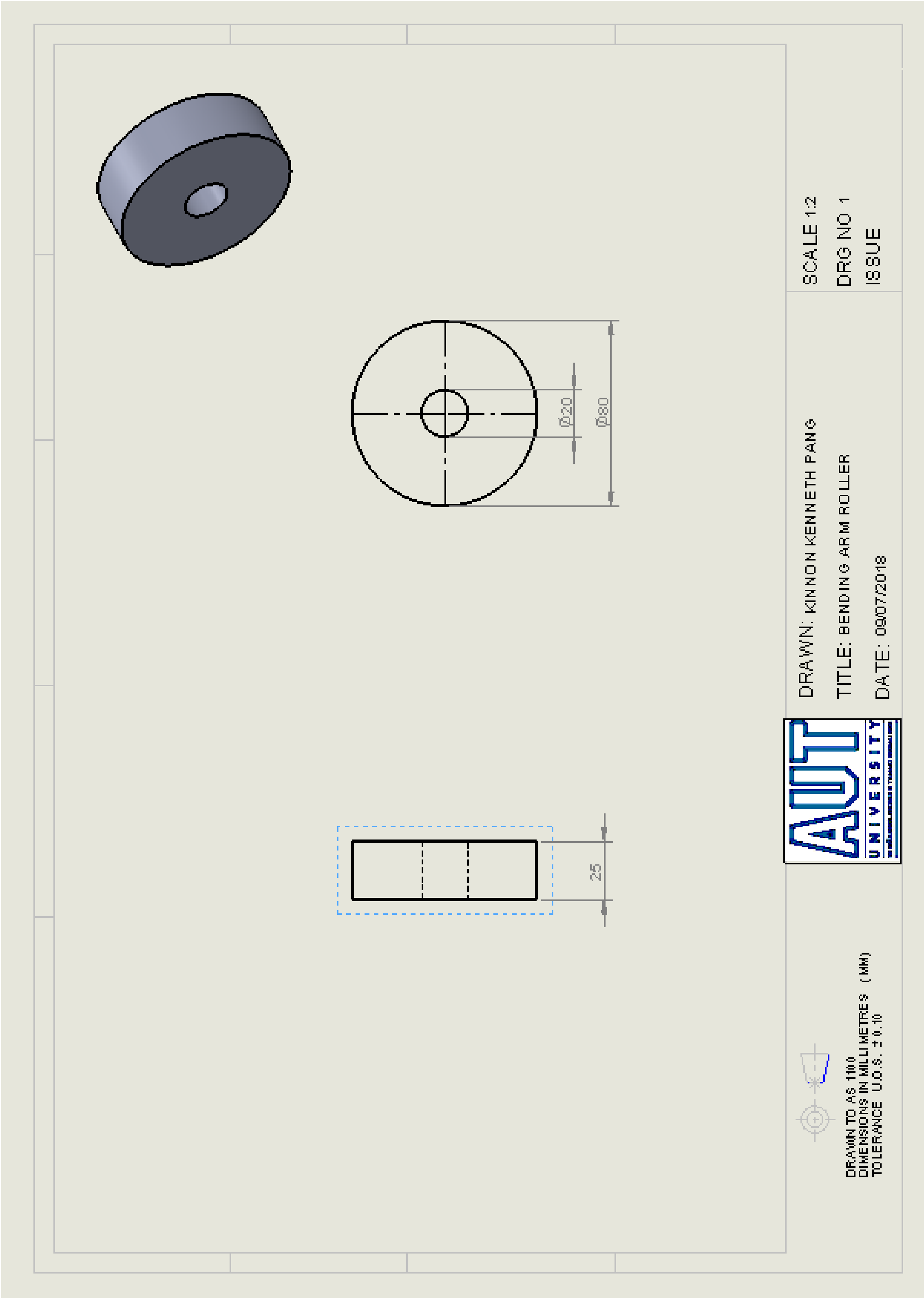

C5.2 Bending Arm

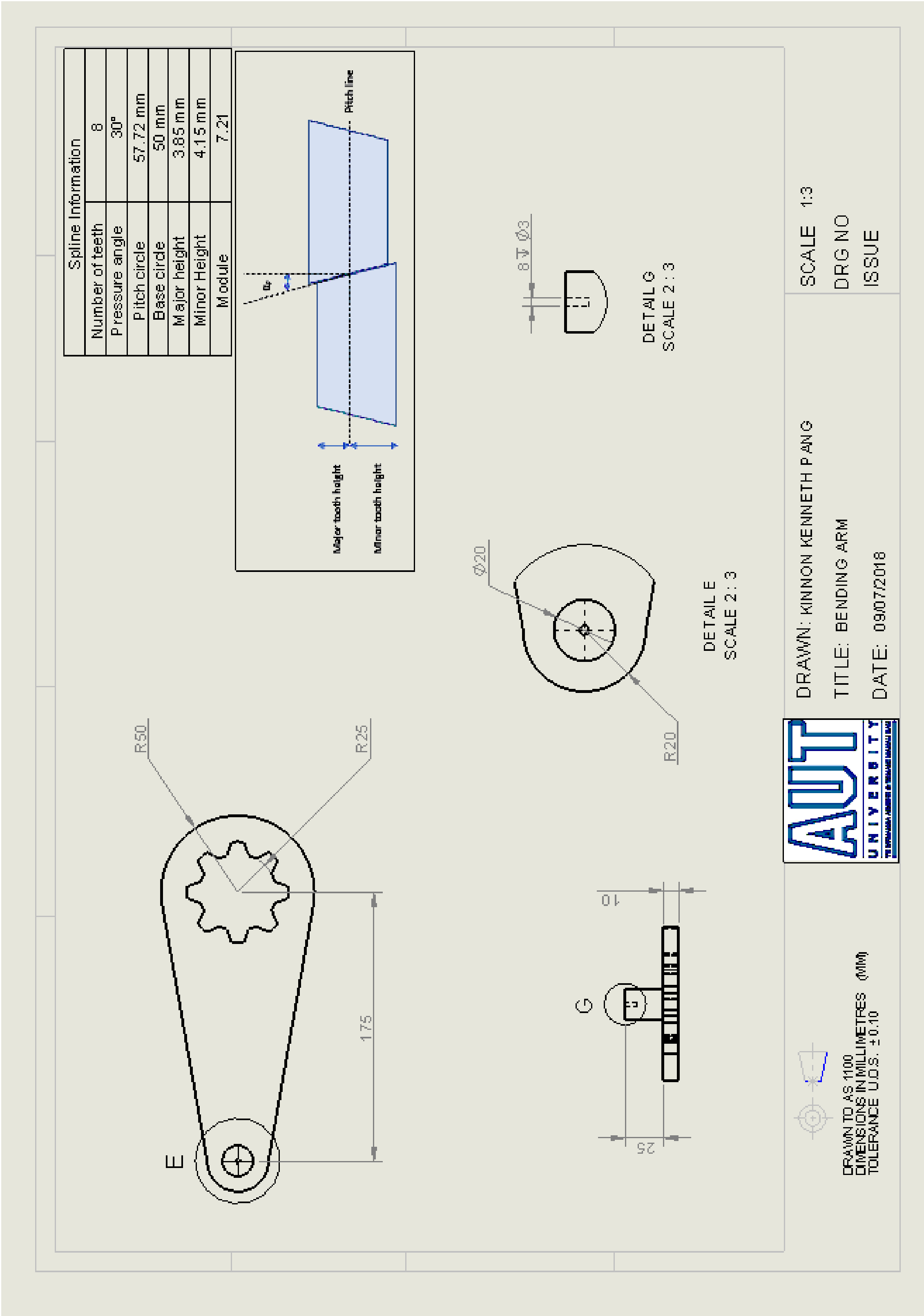

C5.3 Forming Wheel

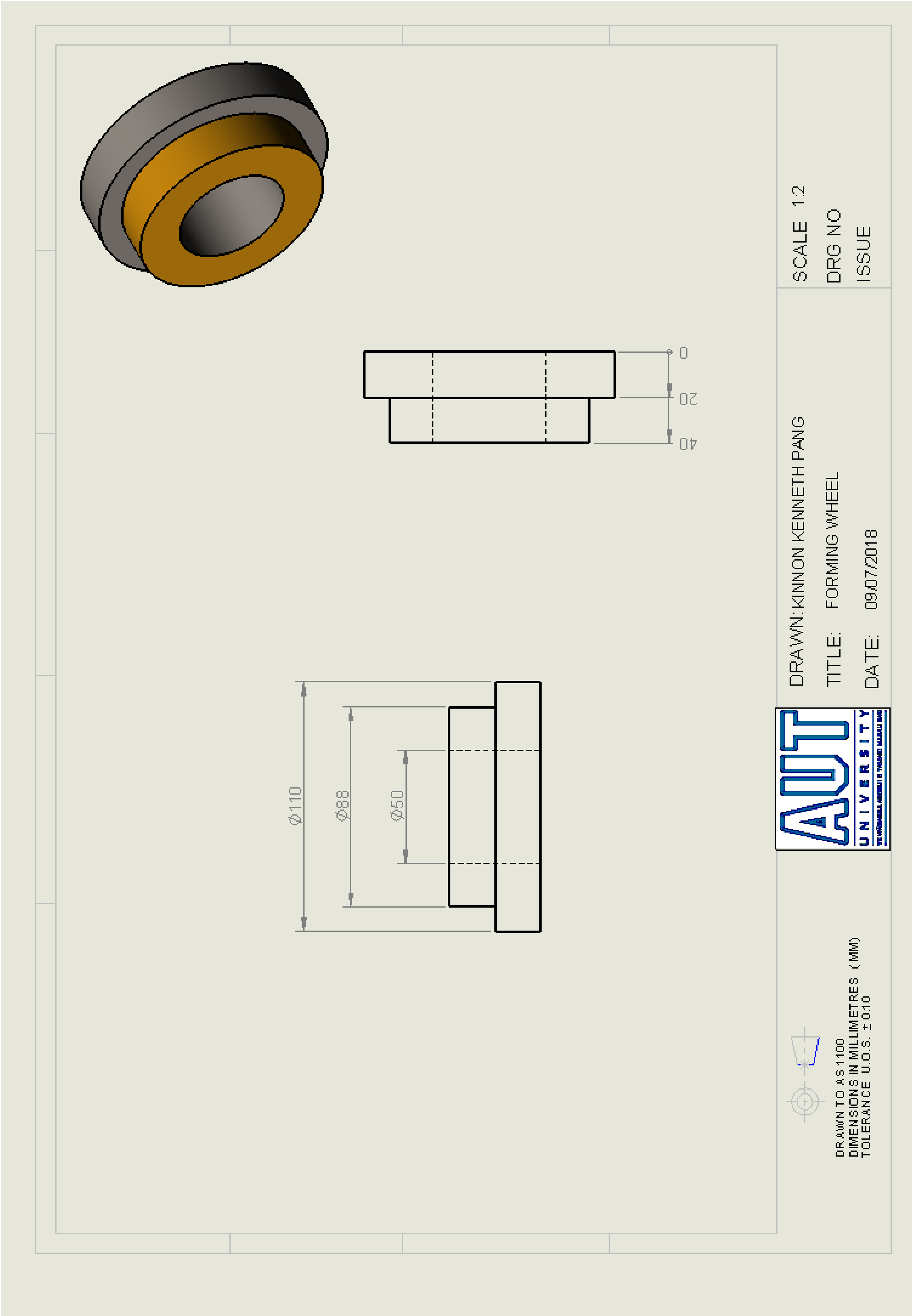

C5.3.1 Forming Wheel Retaining Washer

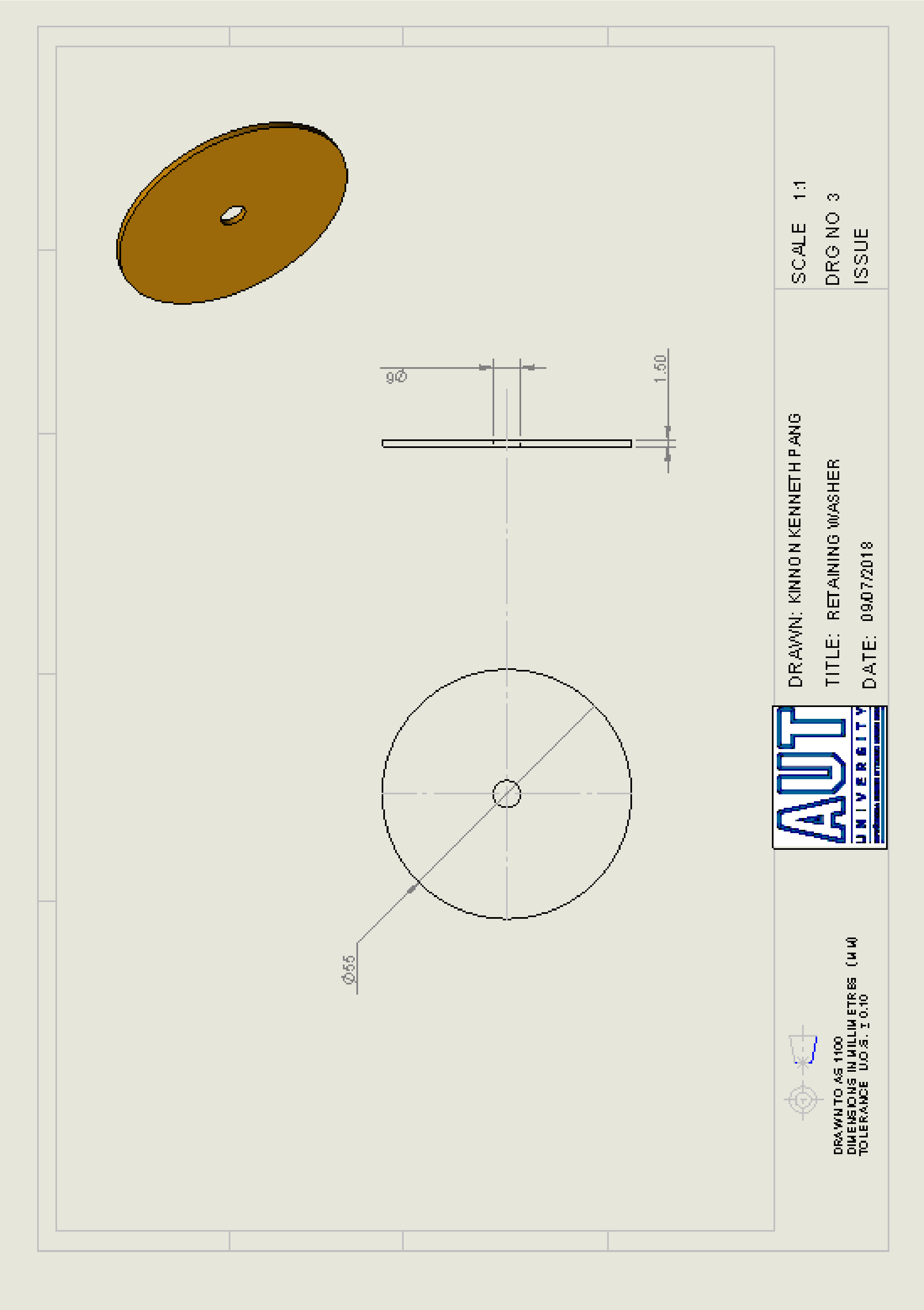

Appendix D: Material Data Sheets

D1 ASSAB PM30 SuperClean

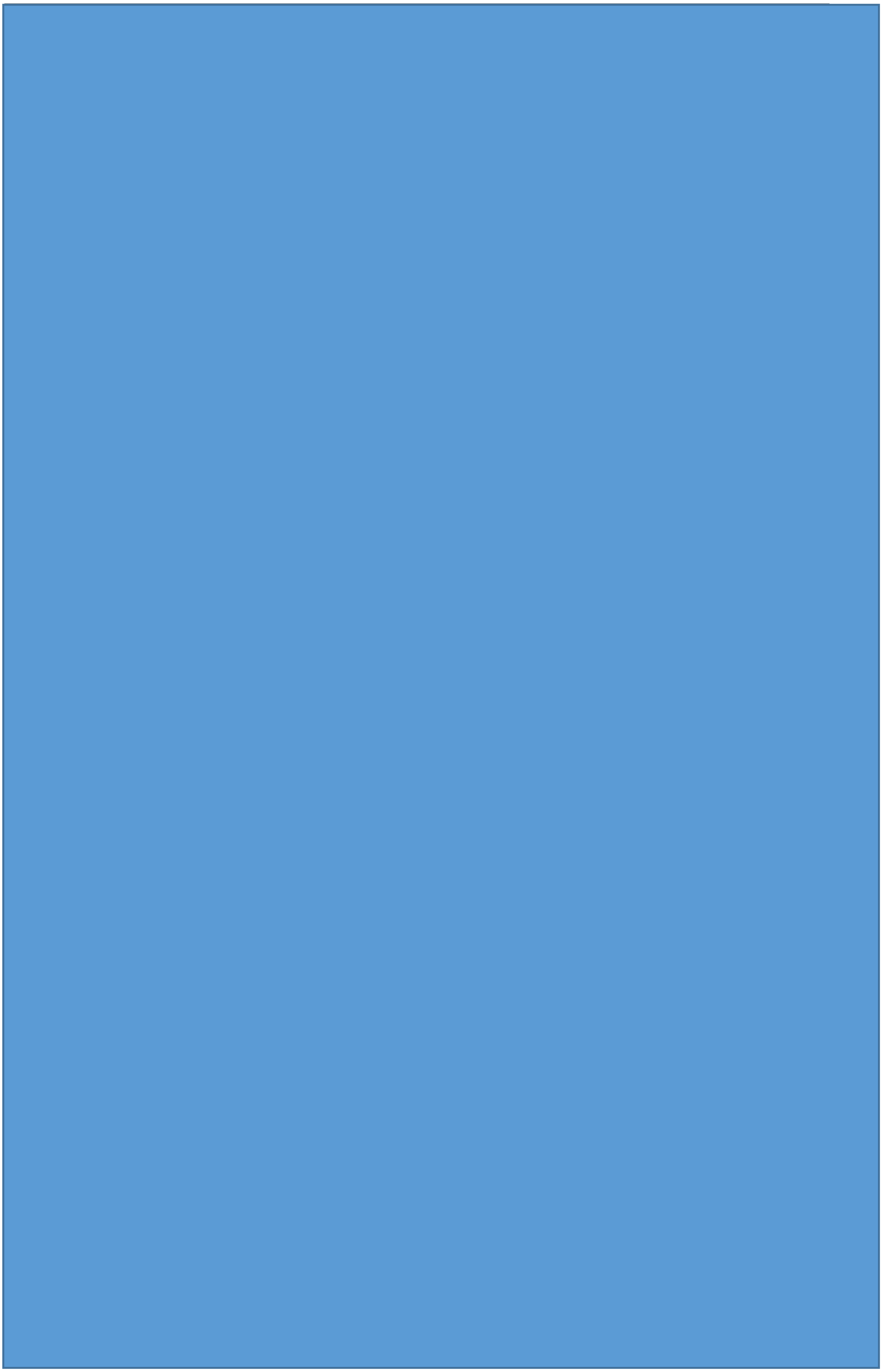

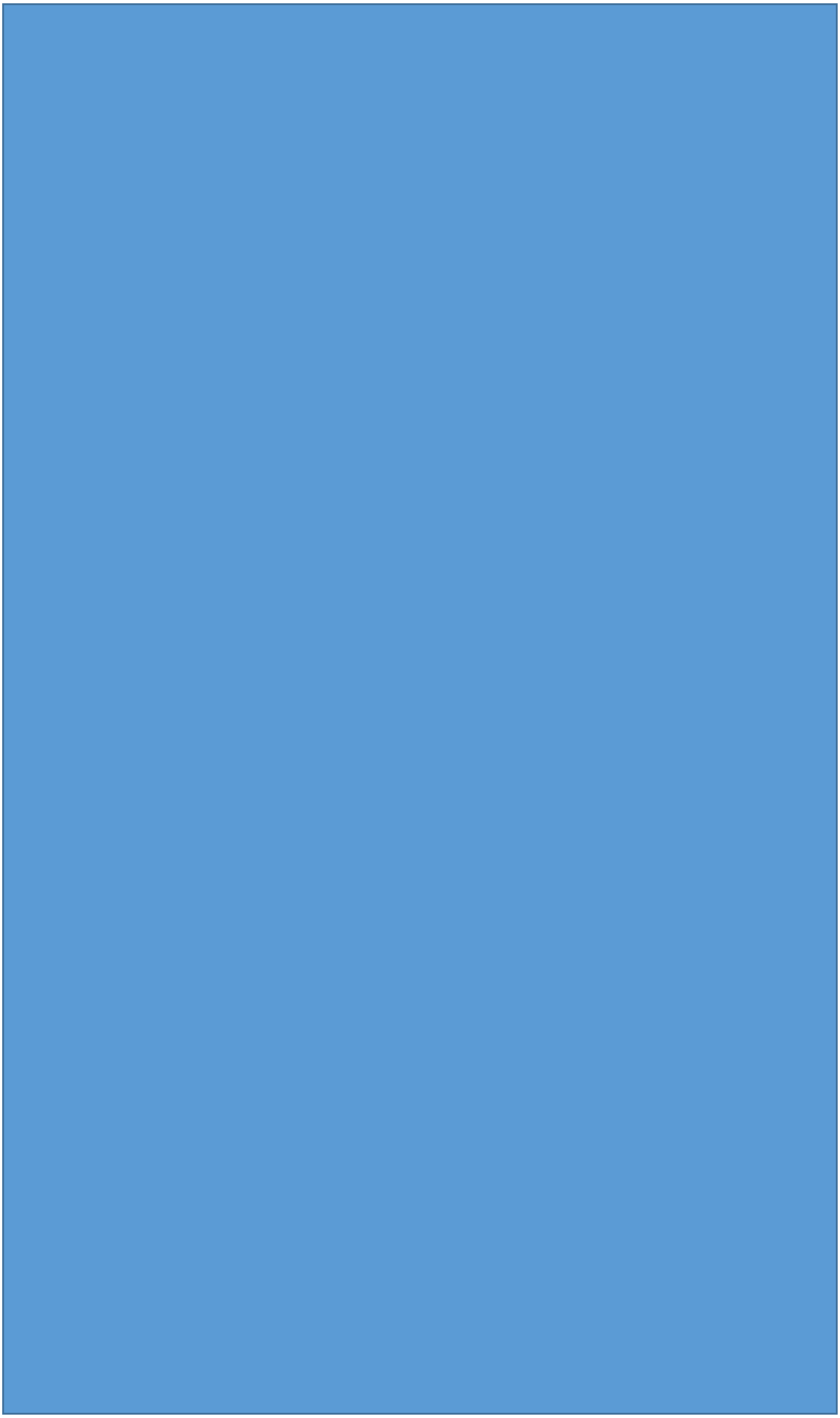

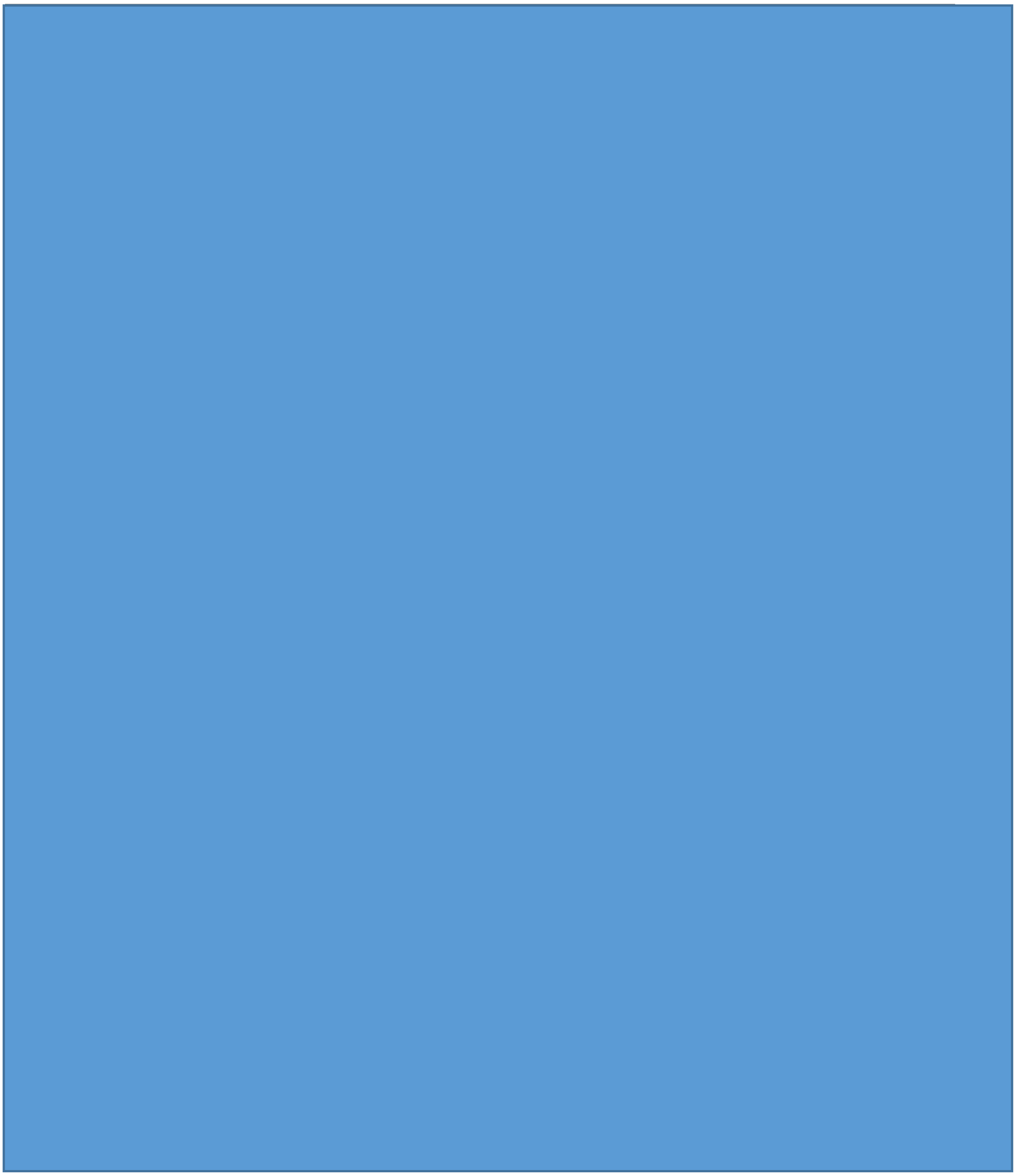

Retrieved from: http://www.assab-japan.com/media/ASSAB_PM_30_SuperClean_Brochure_English.pdf

D2 ASTM B505-C93200

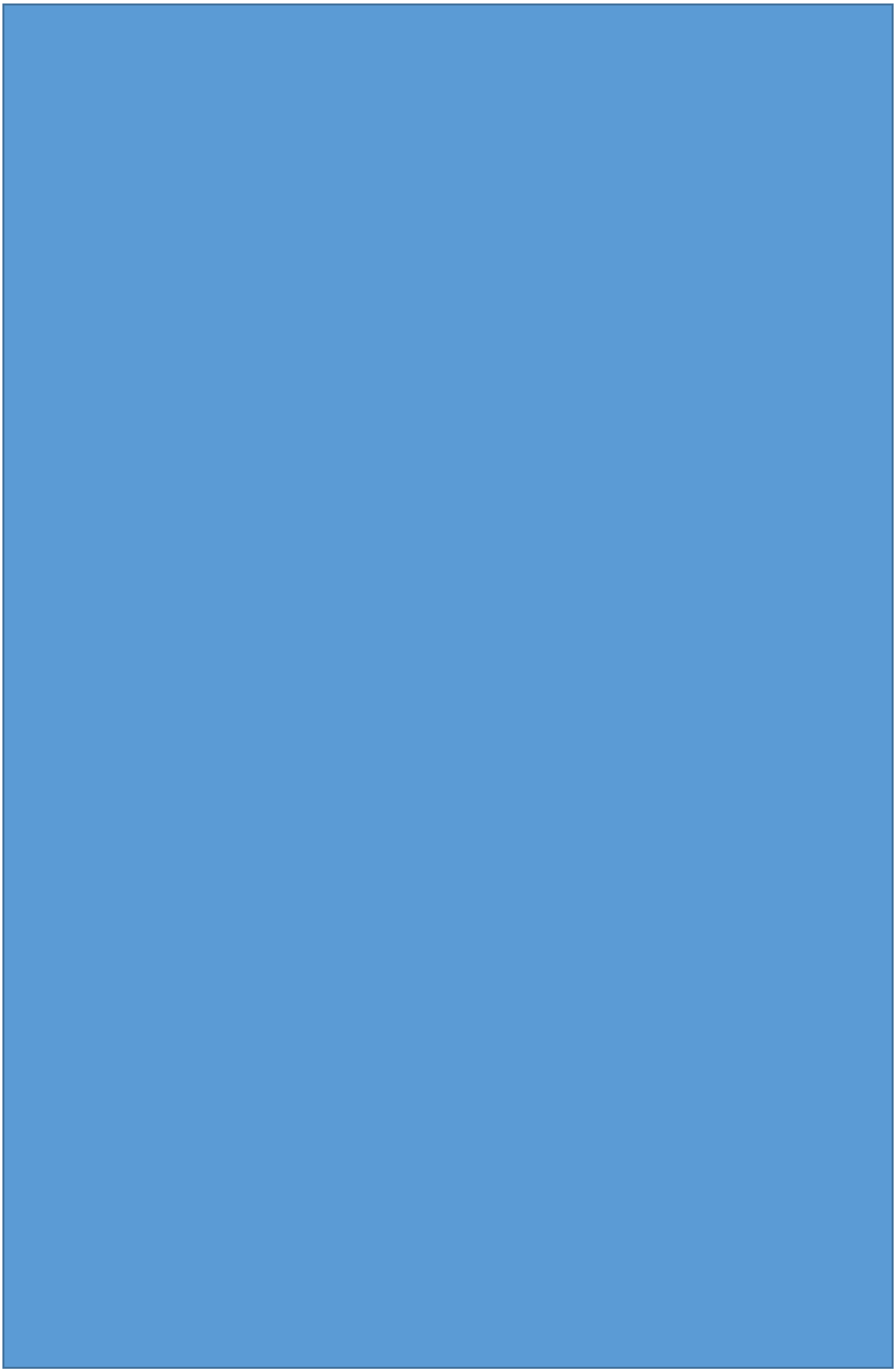

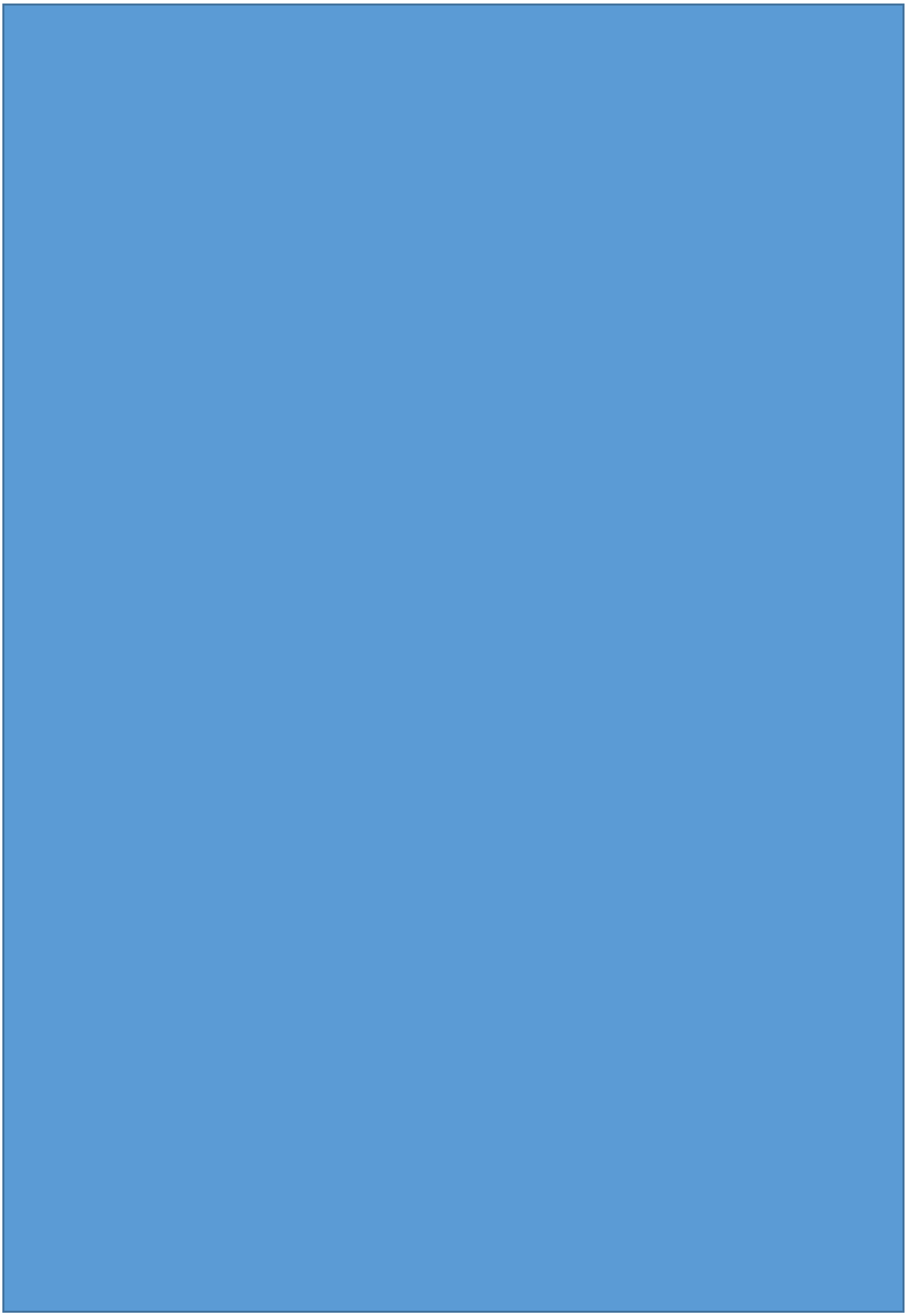

Retrieved from: www.concast.com/c93200.php

<u>D3 ASTM A747</u>

Retrieved from:
http://www.matweb.com/search/datasheettext.aspx?matguid=b402bdddf43c4923961fb01c960501c8

D4 Magnesium EA65RS-T4

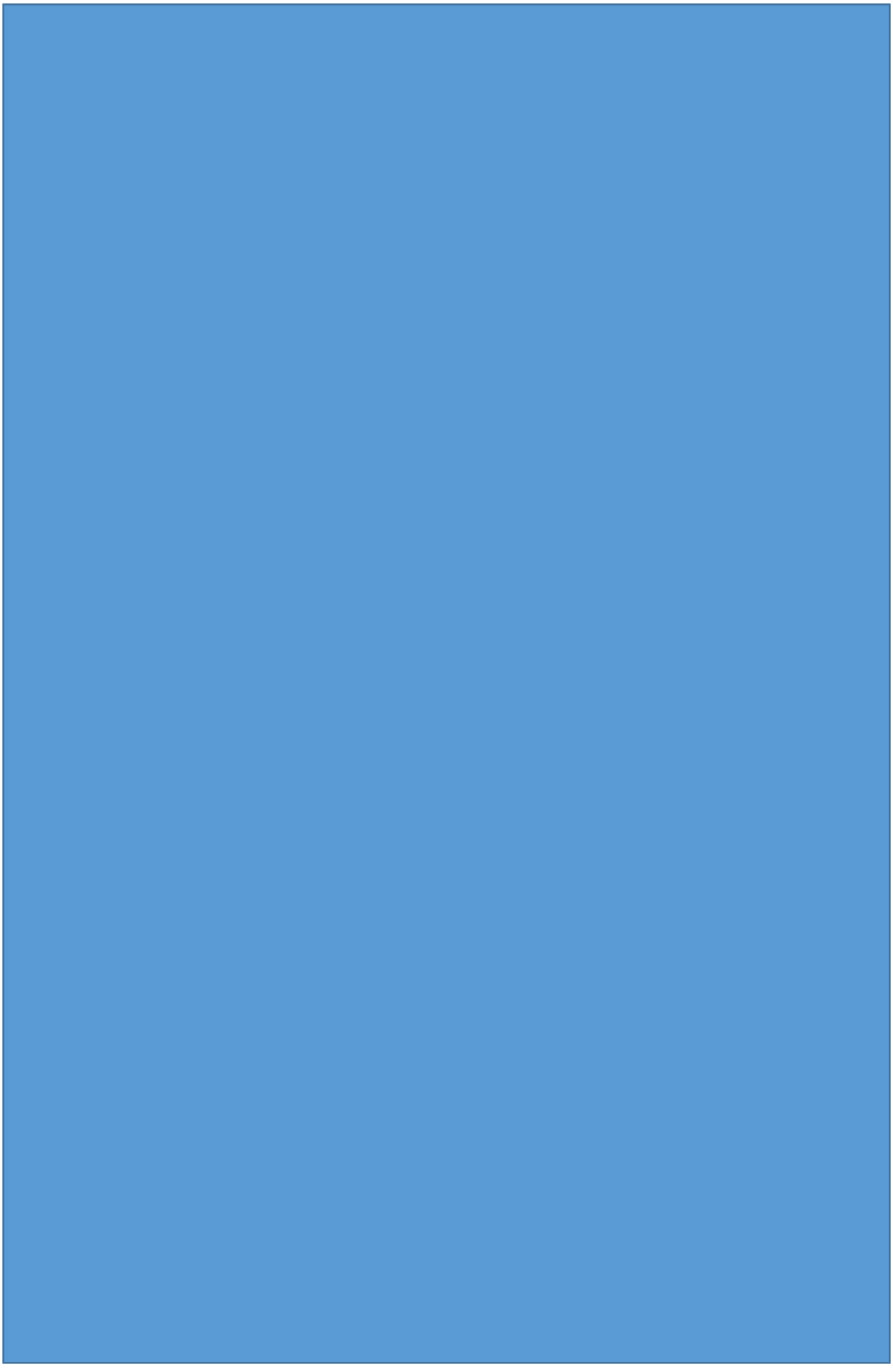

Retrieved from: https://www.azom.com/article.aspx?ArticleID=8683

D5 D2 Steel

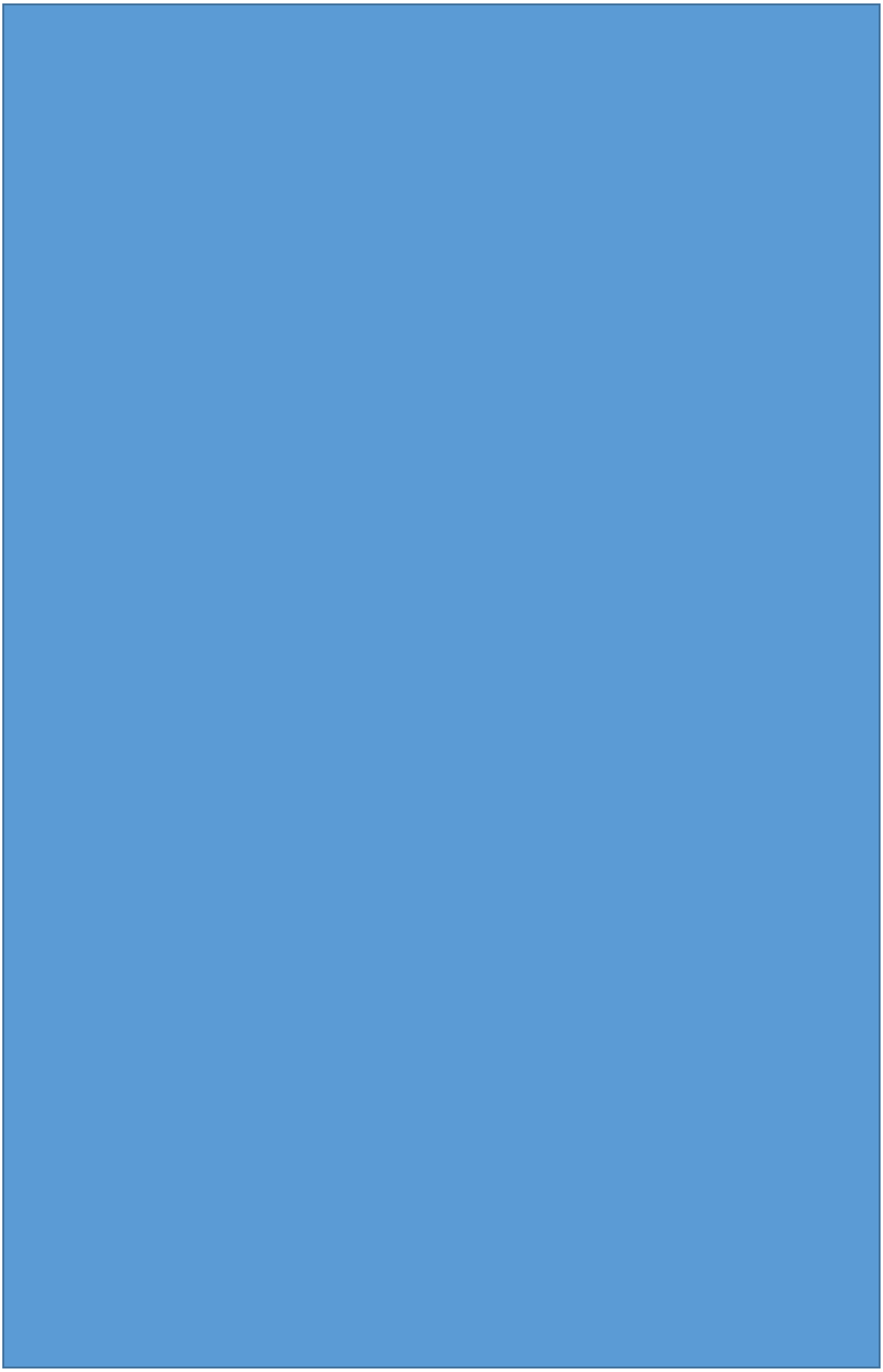

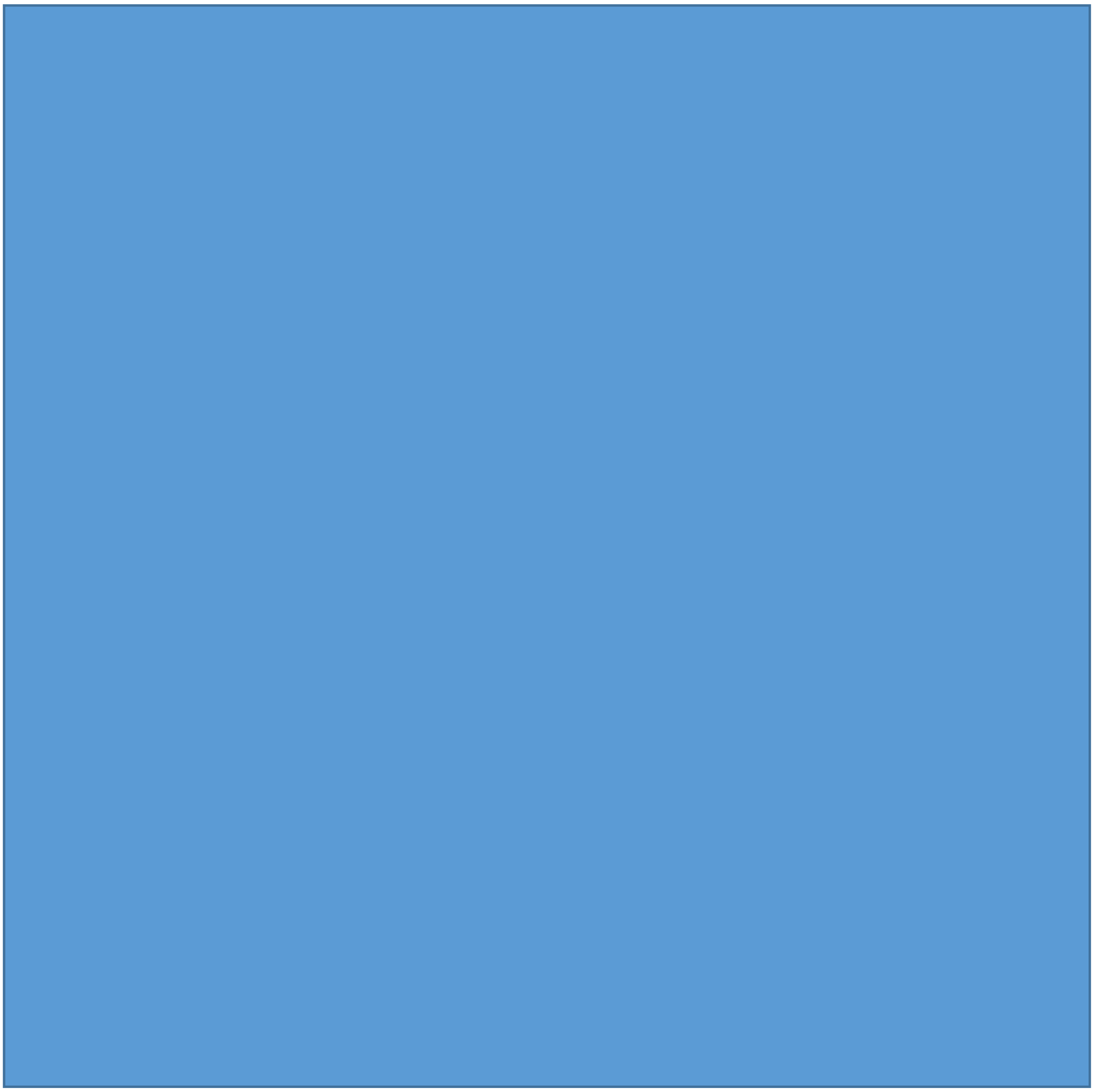

Data from CES EDUPAK

D6 C63000 Nickle Aluminium Bronze

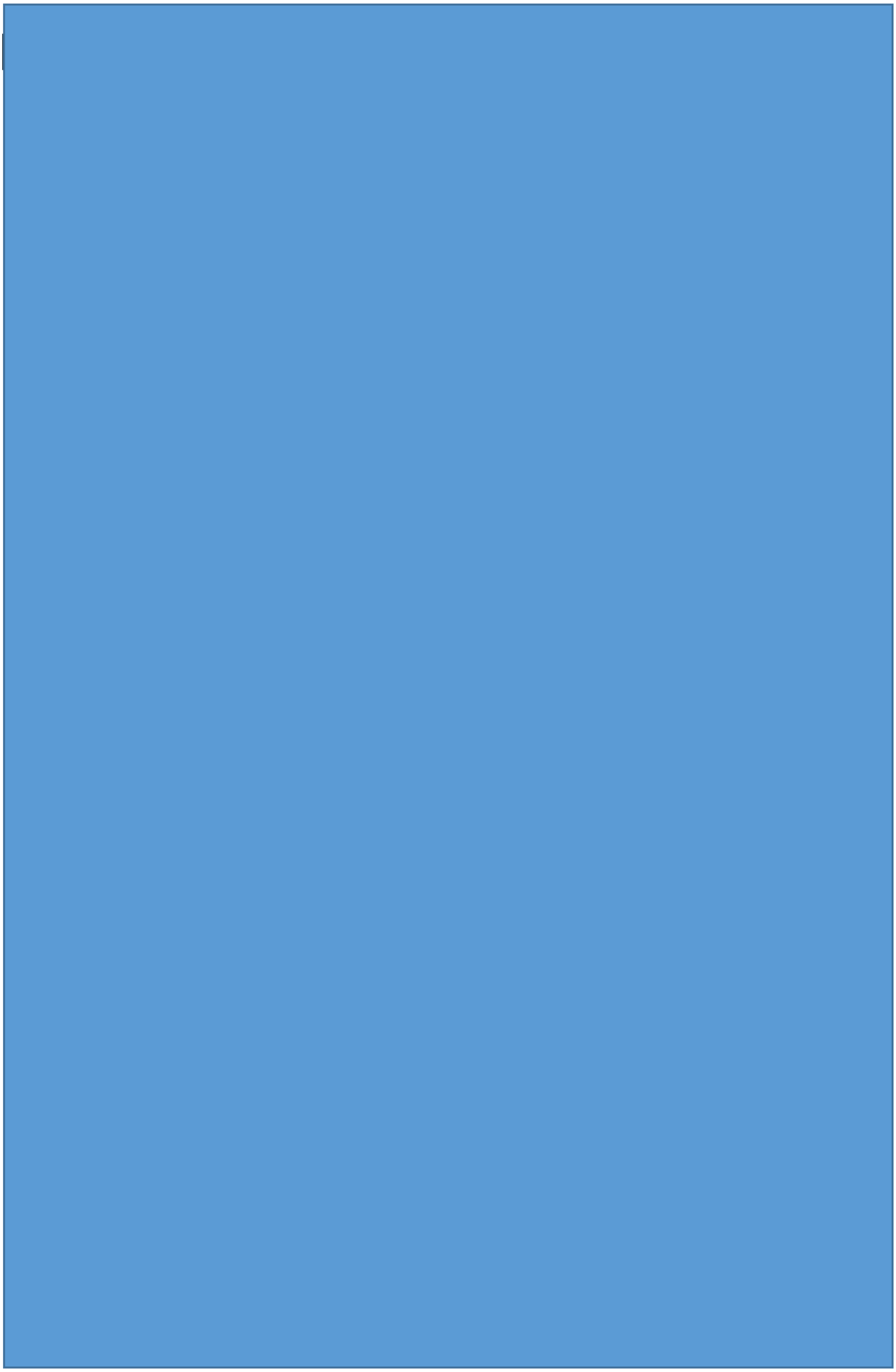

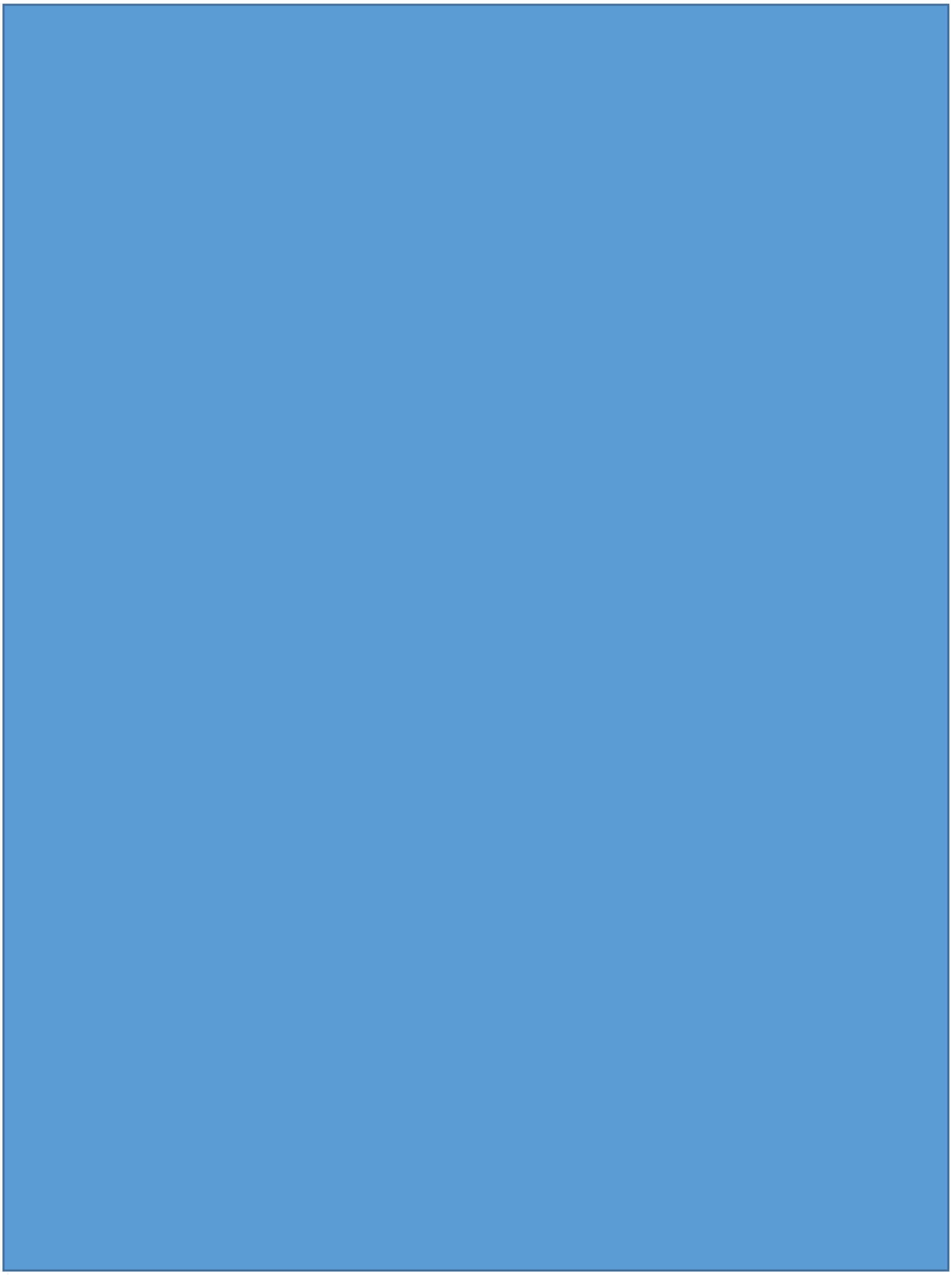

Retrieved from: http://www.spectrummachine.com/c63000-material-data-sheet

D7 Beryllium Copper C17200

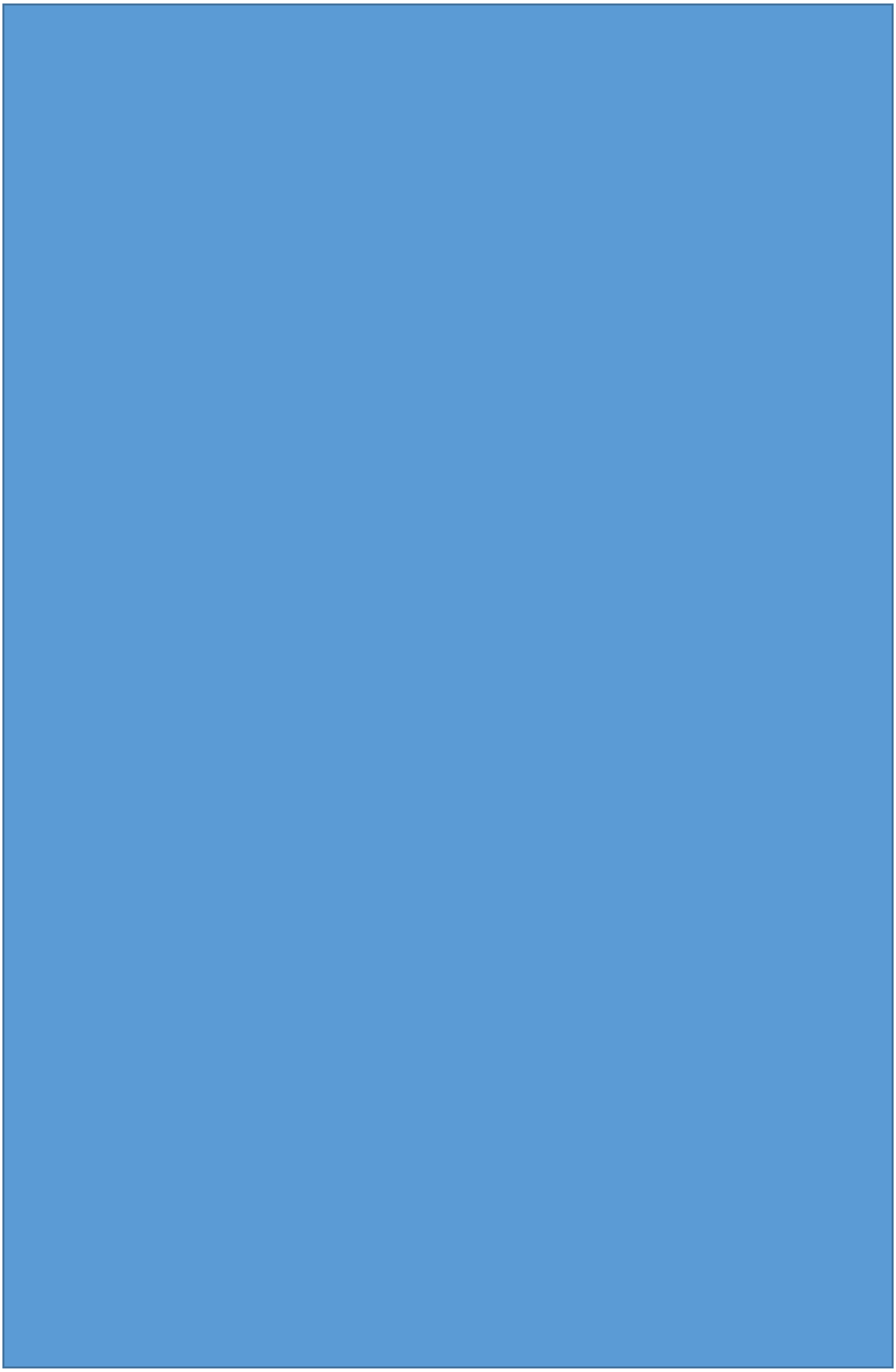

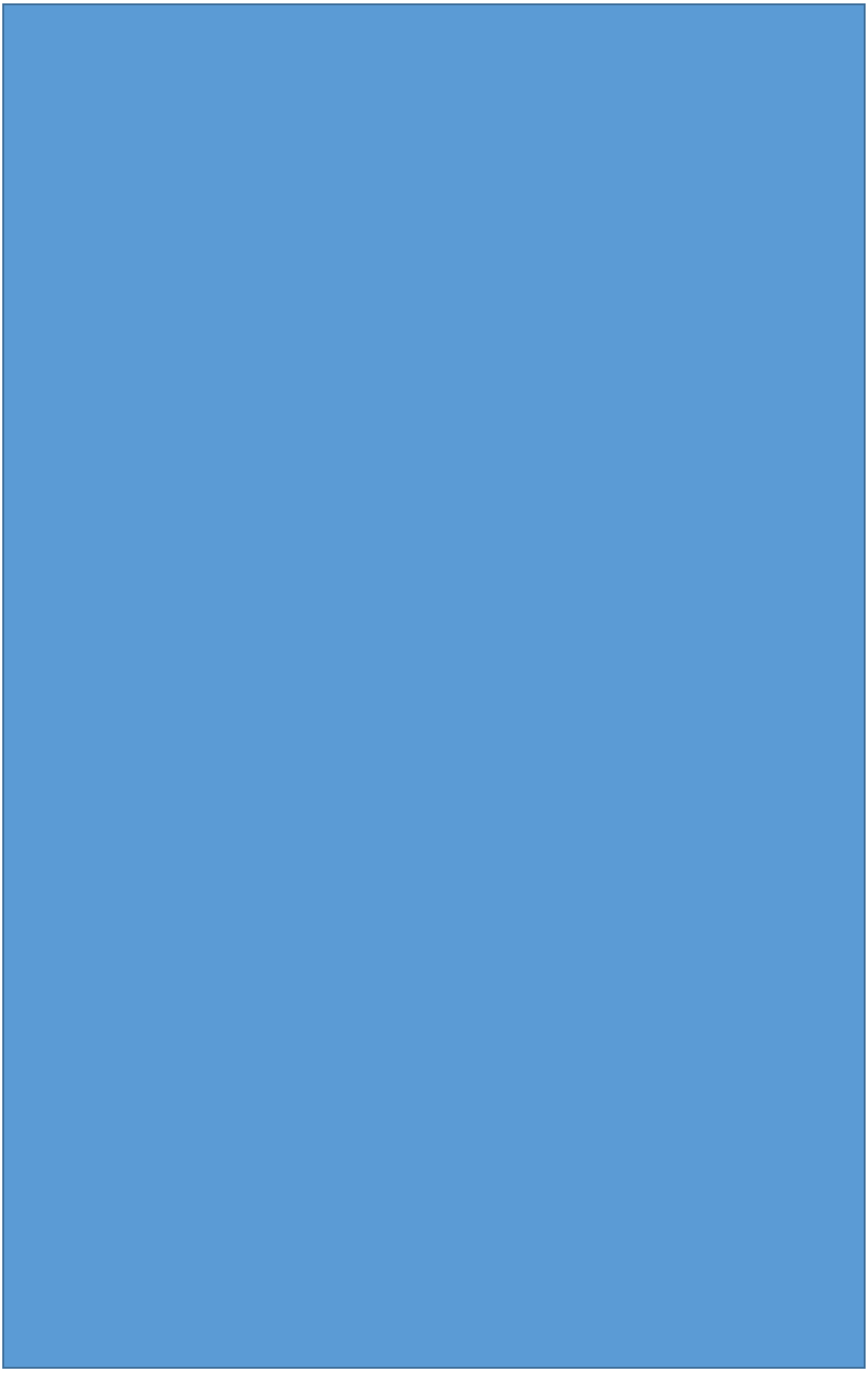

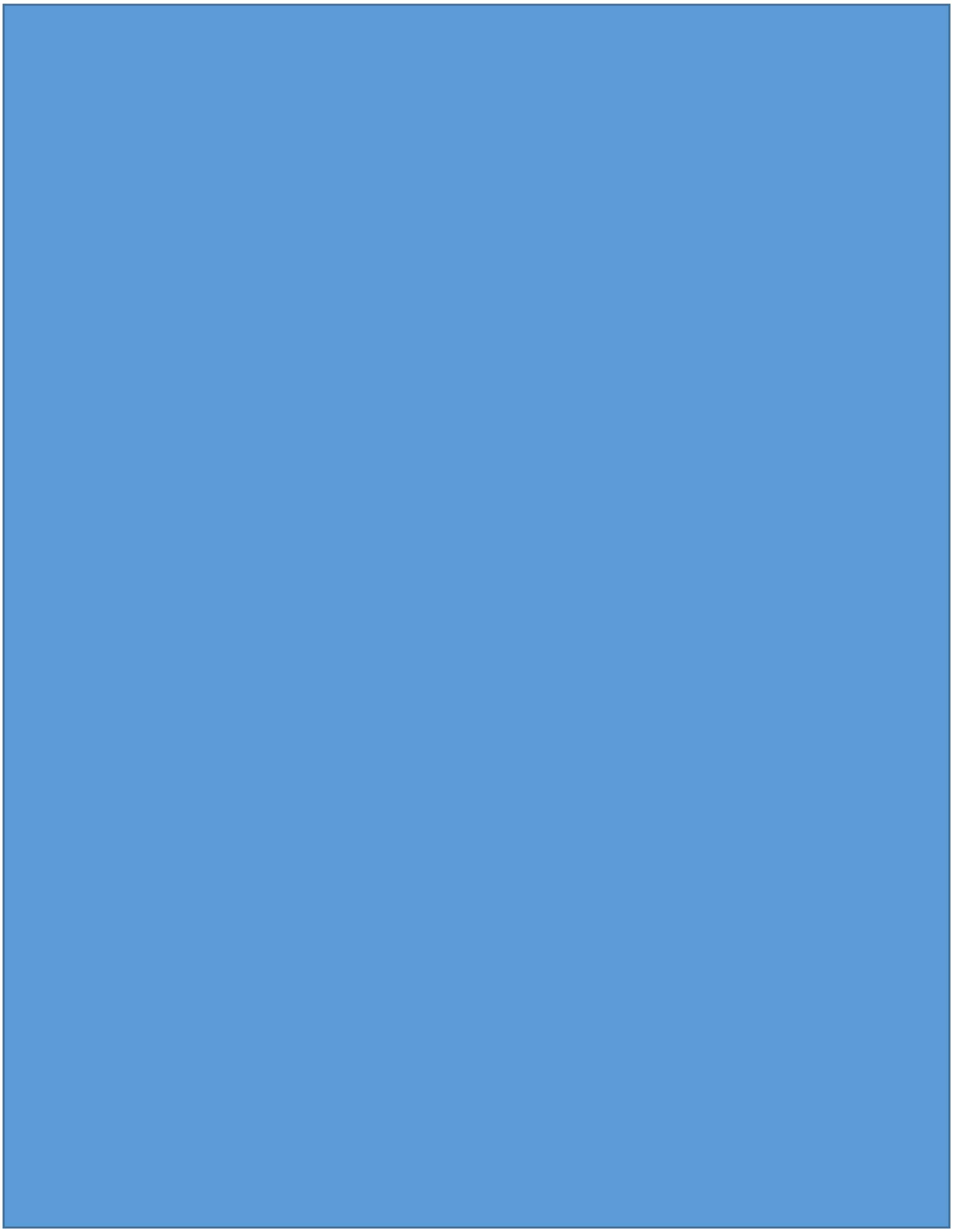

Retrieved from: https://www.azom.com/article.aspx?ArticleID=6326

D8 4140 Steel

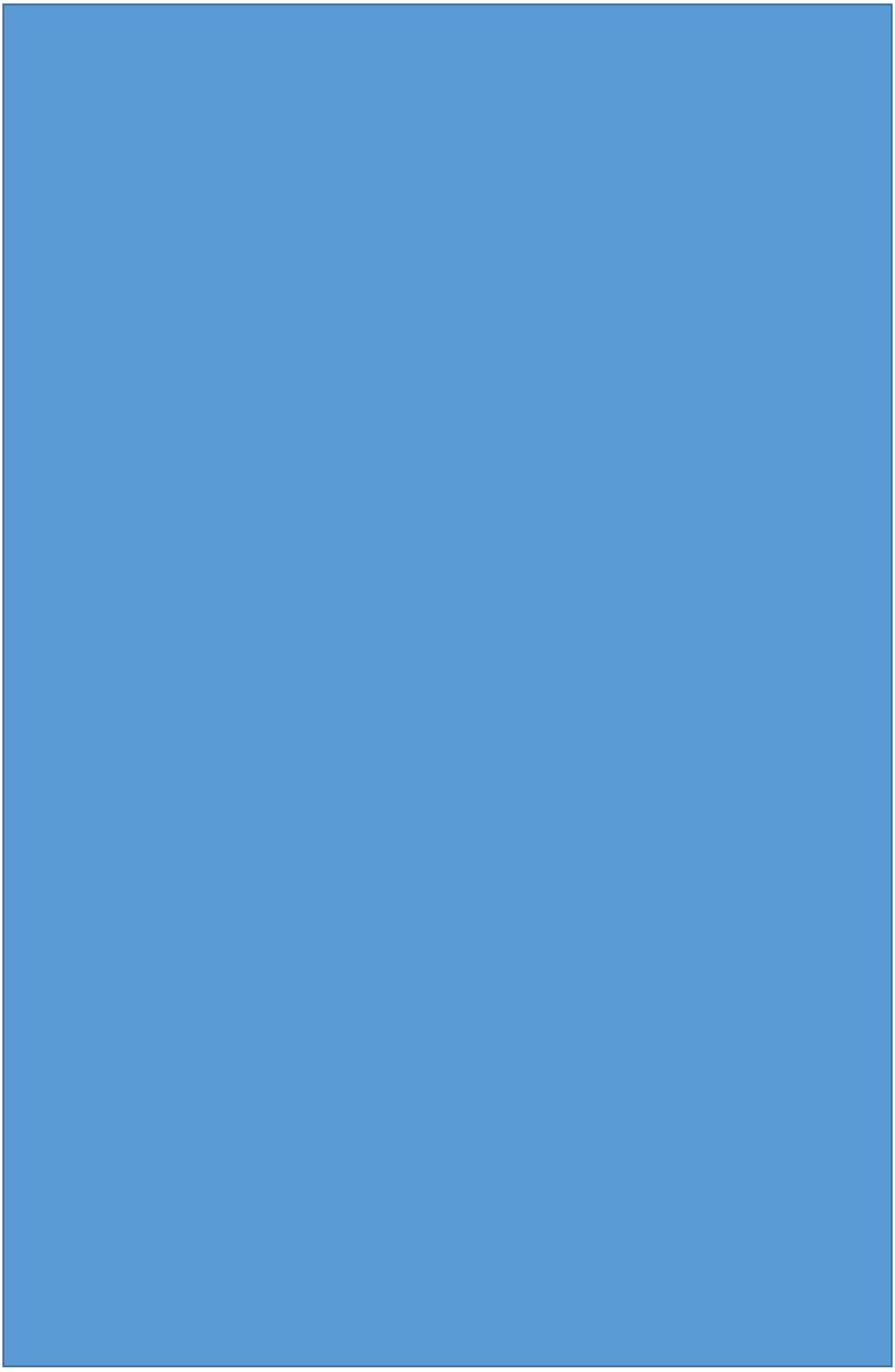

Retrieved from: http://www.atlassteels.com.au/documents/Atlas4140.pdf

D9 4142 Steel

Retrieved from:

http://www.matweb.com/search/datasheet.aspx?matguid=1b012a1ae1d64e409c445a814bfcf9d5

D10 6580 Steel

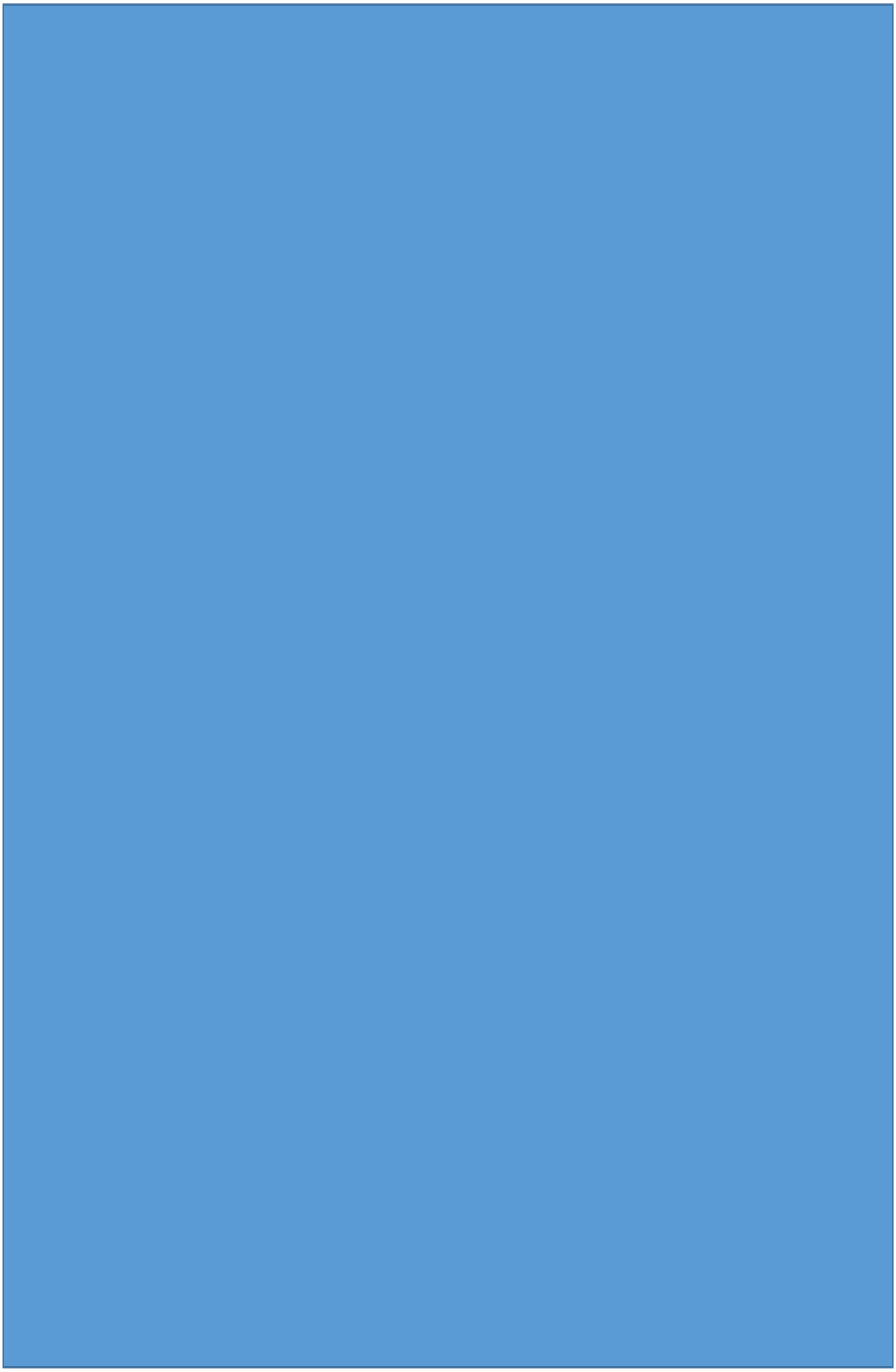

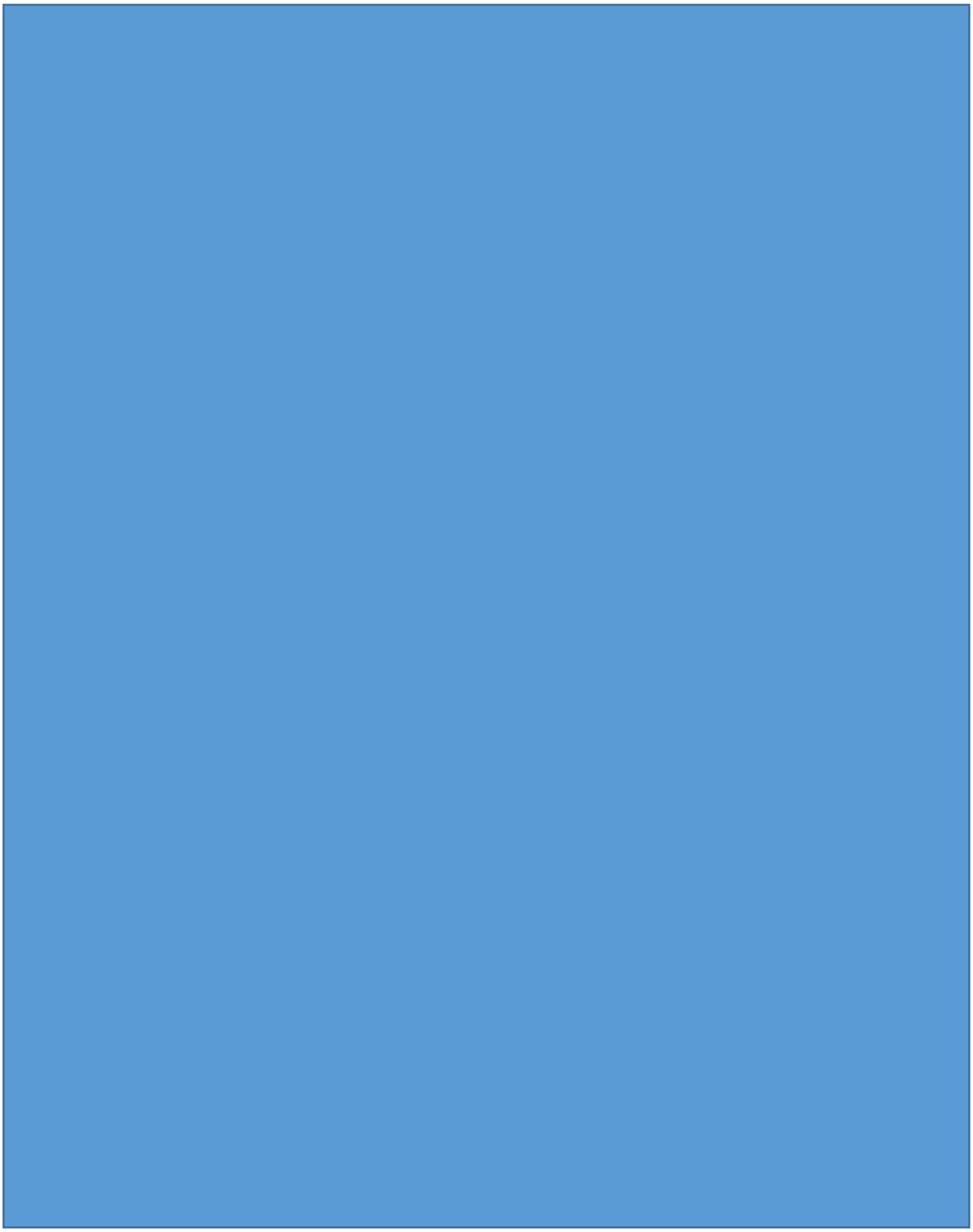

Retrieved from: https://steelselector.sij.si/steels/VCNMO200.html

D11 L2 Steel

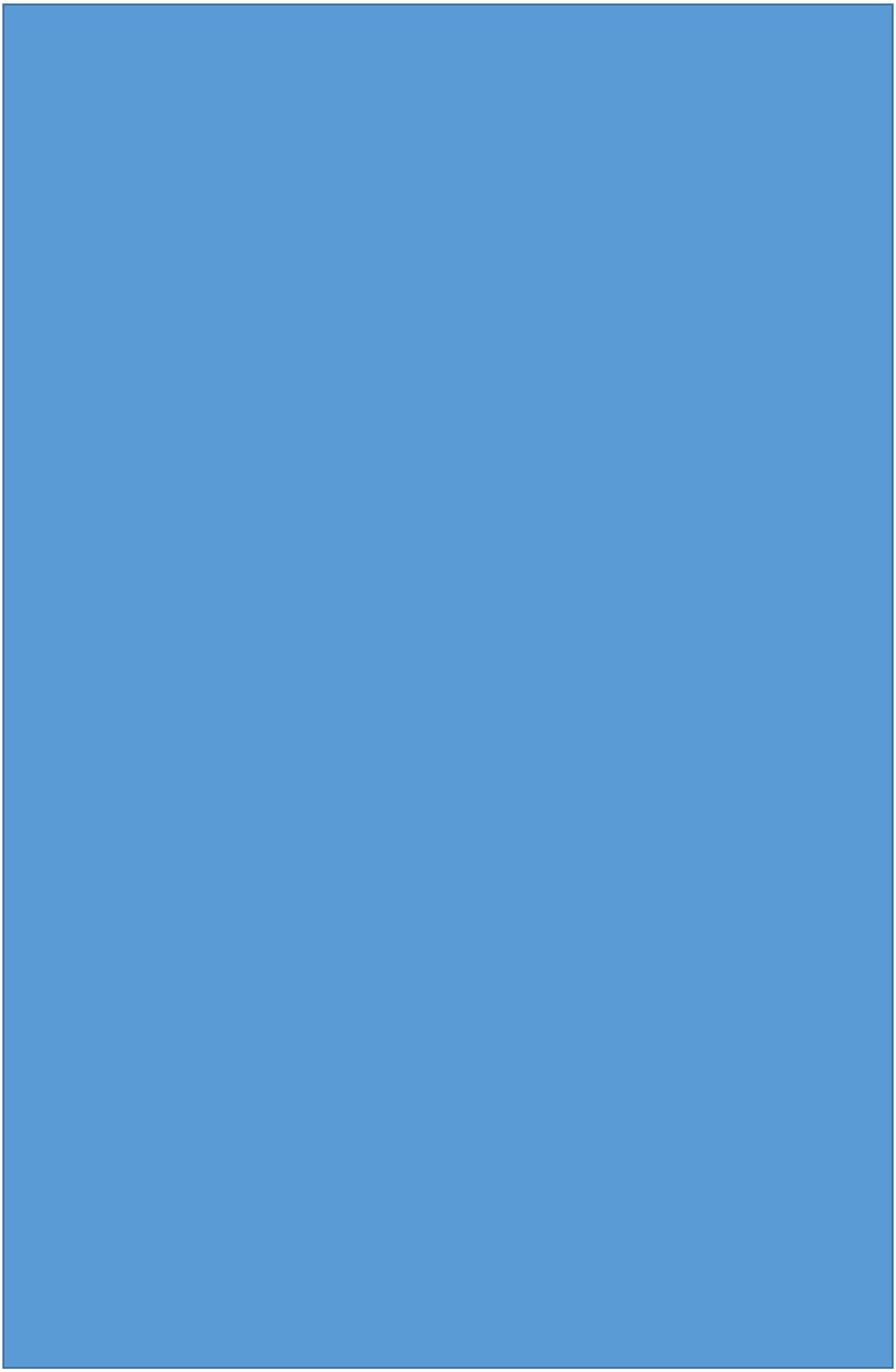

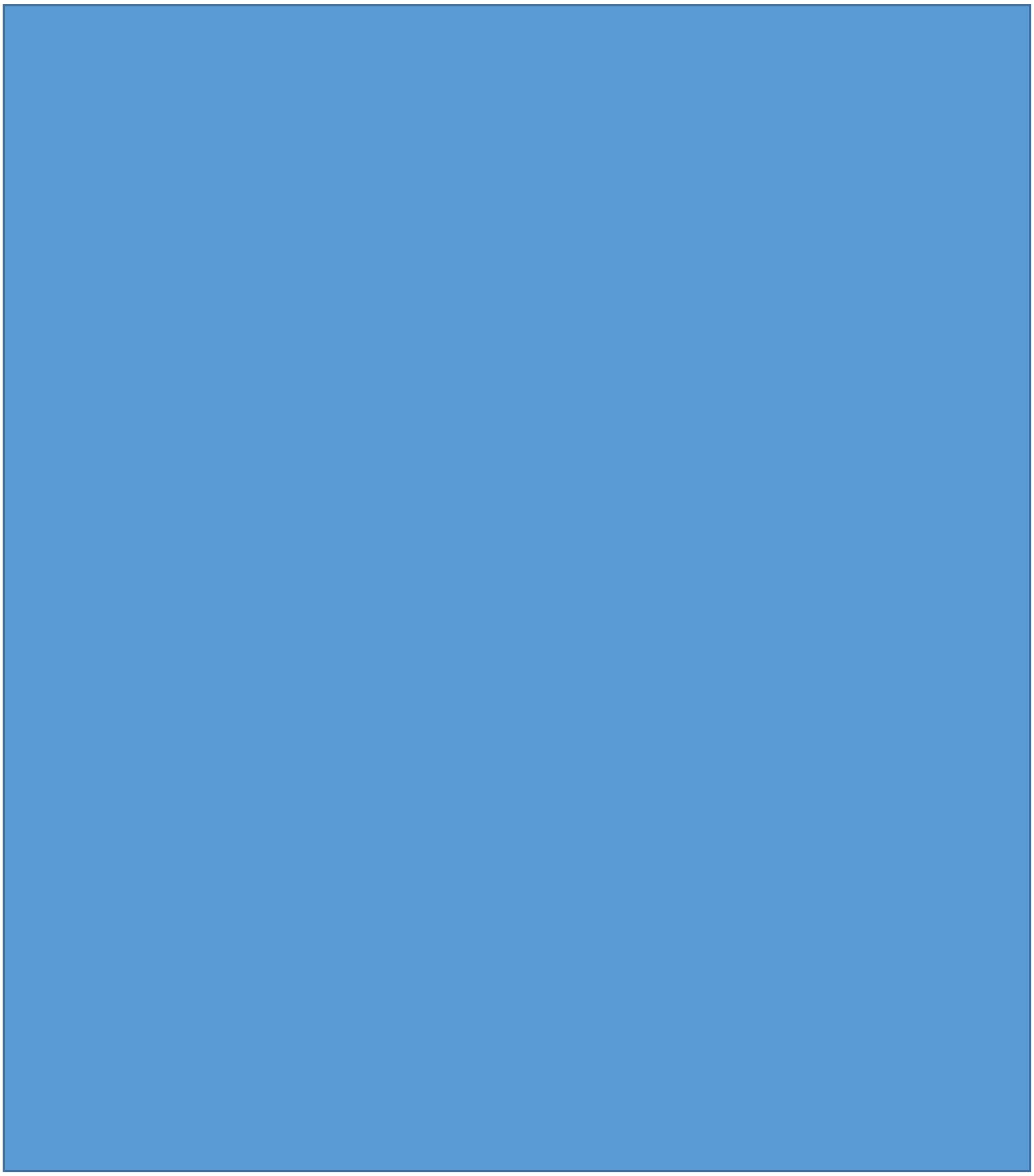

Retrieved from: https://www.azom.com/article.aspx?ArticleID=6241

D12 Aluminium 5056-H18

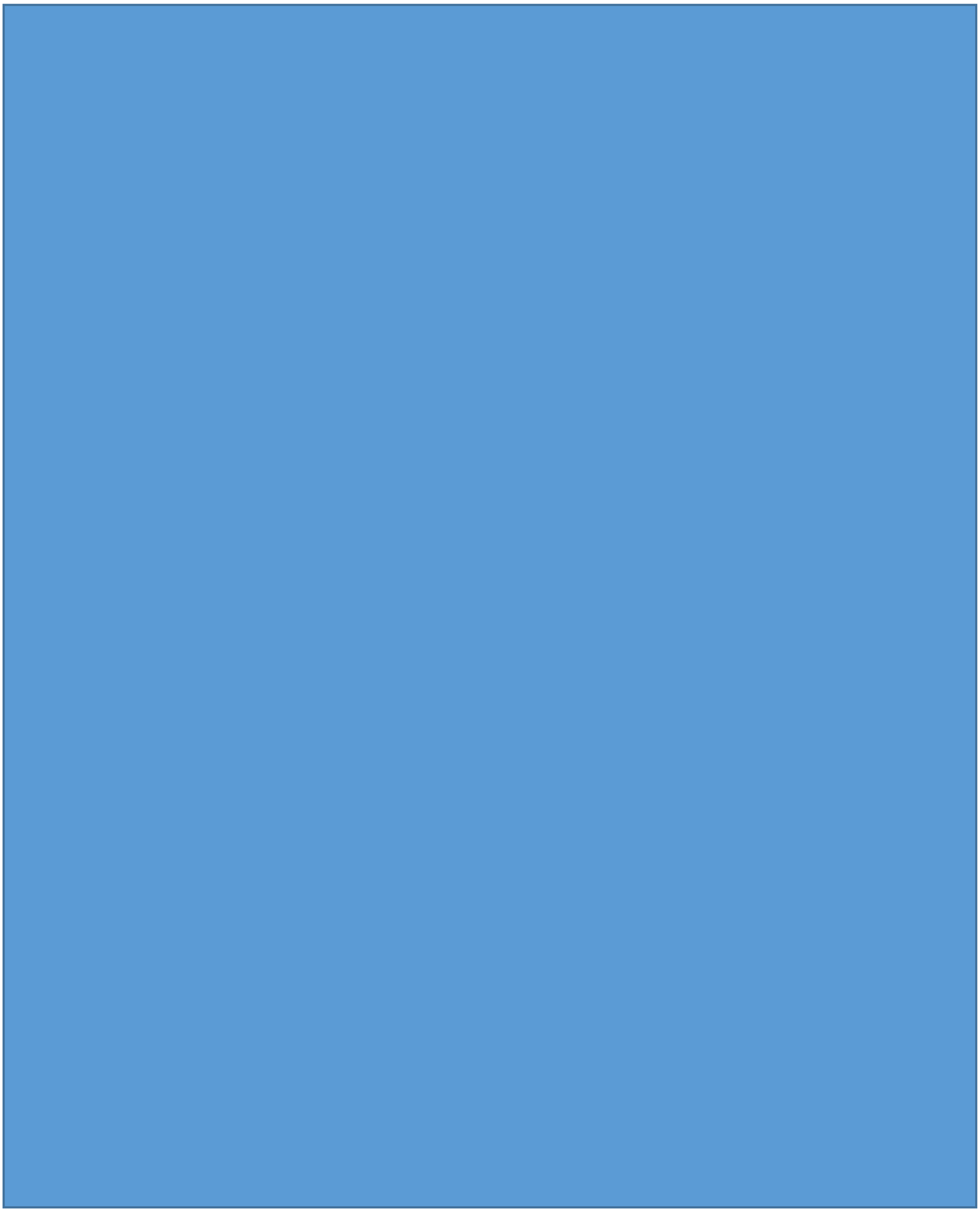

Retrieved from:

http://www.matweb.com/search/datasheet.aspx?matguid=4643f621e29c4dd08ddb763bdf526fc9

Appendix E: Questionnaire and Information Sheet

AUT

Questionnaire

By completing the questionnaire, you give consent for the information entered to be used by AUT university staff and researchers. Please write/type in your answers in the blue boxes. This questionnaire is purely voluntary there is no obligation for you to take part in this research. Once completed please fold and place the questionnaire in the box provided.

What equipment are you currently using to bend and cut rebar?

Are there any special/new features that you'd like to see on new hand-held rebar cutters/benders?

What are some of the things you find annoying or difficult when you're cutting/bending rebar?

Roughly how many rebars do you normally cut/bend per day?

Approved by the Auckland University of Technology Ethics Committee on 7th August 2017, AUTEC Reference number 17/259

When cutting/bending rebar, is the tool placed on the ground, held with two hands, etc.?

Is the rebar bent/cut when it is already set in the concrete?

During your working day, how are you interacting with the rebar cutter/bender? E.g. carrying it upstairs, using lifts, carrying it around the worksite, etc.

What the most common bend angles that you use?

If there was a cordless combination rebar cutter and bender, would you be interested in using such a device?

TE WĀNANGA ARONUI O TĀMAKI MAKAU RAU

Participant Information Sheet

Date Information Sheet Produced:

19/07/2017

Project Title

Design of Portable Rebar Cutter and Bender.

Invitation

Hello, my name is Kinnon Pang, and I am a researcher at AUT University. The purpose of this project is to design a new innovative portable rebar cutter and bender for use on construction sites. The questionnaire is to help me understand what is required, and what will make performing this work easier. The goal is design a device that will increase safety, usability and efficiency on the worksite. This questionnaire is voluntary, there is no obligation to complete.

If you wish to withdraw from the research, then please do not submit a questionnaire. Being an anonymous survey, the individual participants will not be able to withdraw their submitted questionnaire.

This project is also part of the Master of Engineering program at Auckland University of Technology (AUT), a thesis will be produced after the project; names of the participants or companies will not be published in the thesis or be shared with other companies or institutions of higher learning. This project is being completed in partnership with Bay of Plenty Gear Cutters who will be manufacturing the tool once this Master's project is completed.

What is the purpose of this research?

The purpose of this research is to gain the end user's experience in cutting and bending rebar on a construction site. The data collected from the questionnaire will be used in determining specifications and assist in developing and selecting a final design. This research will be used as part of a master's degree research thesis, which will be submitted at the end of the academic year (June 2018).

How was I identified and why am I being invited to participate in this research?

Construction and reinforcing companies, large and small, across New Zealand have been contacted in regards to participating in this research. If you have received this information sheet it means that your company has met the requirements.

Companies that bend/cut rebar in bulk, do not perform ground up construction, bend/cut rebar with a diameter greater than 20mm, bend/cut rebar by hand, or specialise in interior construction have not been invited. The contact details of each company were obtained through the internet, and the Yellow Pages.

How do I agree to participate in this research?

Completing the paper questionnaire, or the online questionnaire will act as consent being given to participate and for the information entered on the questionnaire to be used by university staff and researchers.

Your participation in this research is voluntary and whether you choose to participate will neither give you an advantage nor disadvantage you. However, you personally will not be able to withdraw from the research once the questionnaire is submitted. If you do not wish to participate, please do not submit a questionnaire.

What will happen in this research?

The information collected in the questionnaire will be used in developing a new power tool. Using the information provided by you, a final design final will be developed that will encompass your views, user experience, and knowledge. As participants in this research, the only role you need to perform is to answer the questionnaire in your own time either at home or at work. Once the questionnaire is completed (if it is a paper questionnaire) it will need to be deposited in the box provided or posted back to the address listed under the Primary Supervisor; the box will be there for one week.

What are the discomforts and risks?

There are no risks, no private information about the participants or company information is required. All your views and opinions will not be shared with anyone outside of the university.

What are the benefits?

This research is performed as part of the Master of Engineering program at Auckland University of Technology (AUT), in partnership with Bay of Plenty Gear Cutters to assist in developing a new power tool.

How will my privacy be protected?

All opinions, thoughts, and ideas expressed in the questionnaire will not be shared with anyone outside of the university (AUT) and Bay of Plenty Gear Cutters. The questionnaires will be held by AUT for 6 years; after which the questionnaires will be destroyed or deleted. Names and other contact details of the individual people filling in the questionnaire will not be recorded; only the name of the company and the phone number will be recorded. The names of the companies will not be published when the summary findings are posted online.

What are the costs of participating in this research?

The whole questionnaire will require 15 – 30 minutes to complete, this questionnaire can be completed in your own time either at home or at work.

What opportunity do I have to consider this invitation?

2 days will be given to consider whether you would like to take part in the questionnaire. If you choose to partake, you will be given one week to (7 days) to return the questionnaire (for both the online and paper questionnaire). The date of when the box will be collected will be written on the front of the box.

Will I receive feedback on the results of this research?

A URL will be sent to your company once the project is completed (June 2018)

What do I do if I have concerns about this research?

Any concerns regarding the nature of this project should be notified in the first instance to the Project Supervisor, *Dr Michael Gschwendtner,* ***email:*** michael.gschwendtner@aut.ac.nz, or to the Primary Researcher, Kinnon Pang, **email:** gyp6338@autuni.ac.nz

Concerns regarding the conduct of the research should be notified to the Executive Secretary of AUTEC, Kate O'Connor, *ethics@aut.ac.nz* , 921 9999 ext 6038.

Whom do I contact for further information about this research?

Please keep this Information Sheet and a copy of the Consent Form for your future reference. You are also able to contact the research team as follows:

Researcher Contact Details:

Name: Kinnon Pang BE

Email: gyp6338@autuni.ac.nz

Project Supervisor Contact Details:

Name: Dr Michael Gschwendtner Dipl.-Ing., Dr.-Ing. (Primary Supervisor)

Email: michael.gschwendtner@aut.ac.nz

Address: Auckland University of Technology

School of Engineering, Computer and Mathematical Sciences
Private Bag 92006
Auckland 1142
Auckland

Name: Dr David White PhD, ME, BE, NZCE, Auto-Eng. (Secondary Supervisor)

Email: david.white@aut.ac.nz

Approved by the Auckland University of Technology Ethics Committee on 7th August 2017, AUTEC Reference number 17/259.

Appendix F: Ethics Approval

AUT

AUTEC Secretariat

Auckland University of Technology
D-88, WU406 Level 4 WU Building City Campus
T: +64 9 921 9999 ext. 8316
E: ethics@aut.ac.nz
www.aut.ac.nz/researchethics

7 August 2017

Michael Gschwendtner
Faculty of Design and Creative Technologies

Dear Michael

Re Ethics Application: **17/259 Design and development of portable independently powered combination reinforced steel cutter and bender**

Thank you for providing evidence as requested, which satisfies the points raised by the Auckland University of Technology Ethics Committee (AUTEC).

Your ethics application has been approved for three years until 7 August 2020.

Standard Conditions of Approval

1. A progress report is due annually on the anniversary of the approval date, using form EA2, which is available online through http://www.aut.ac.nz/researchethics.
2. A final report is due at the expiration of the approval period, or, upon completion of project, using form EA3, which is available online through http://www.aut.ac.nz/researchethics.
3. Any amendments to the project must be approved by AUTEC prior to being implemented. Amendments can be requested using the EA2 form: http://www.aut.ac.nz/researchethics.
4. Any serious or unexpected adverse events must be reported to AUTEC Secretariat as a matter of priority.
5. Any unforeseen events that might affect continued ethical acceptability of the project should also be reported to the AUTEC Secretariat as a matter of priority.

Please quote the application number and title on all future correspondence related to this project.

AUTEC grants ethical approval only. If you require management approval for access for your research from another institution or organisation then you are responsible for obtaining it. You are reminded that it is your responsibility to ensure that the spelling and grammar of documents being provided to participants or external organisations is of a high standard.

For any enquiries, please contact ethics@aut.ac.nz

Yours sincerely,

K O'Connor

Kate O'Connor
Executive Manager
Auckland University of Technology Ethics Committee

Cc: kinnonpang@hotmail.com; david.white@aut.ac.nz

Appendix G: First Principles Calculations

A factor of safety of 1.5 is used to obtain the allowable stresses of the materials used in the calculations.

G1 Gearbox Calculations

G1.1 Bending moment and shear force calculations of internal gearbox shaft

Force exerted onto the shaft by the cycloidal disc can be approximated as a simply supported beam (*Figure G1.1.1*).

Figure G1.1.1: Equivalent beam diagram of forces exerted by cycloidal disc

$$F_B = \frac{1537.35\ Nm}{0.055\ m} = 27953.6\ N, F_A = 9204.2\ N$$

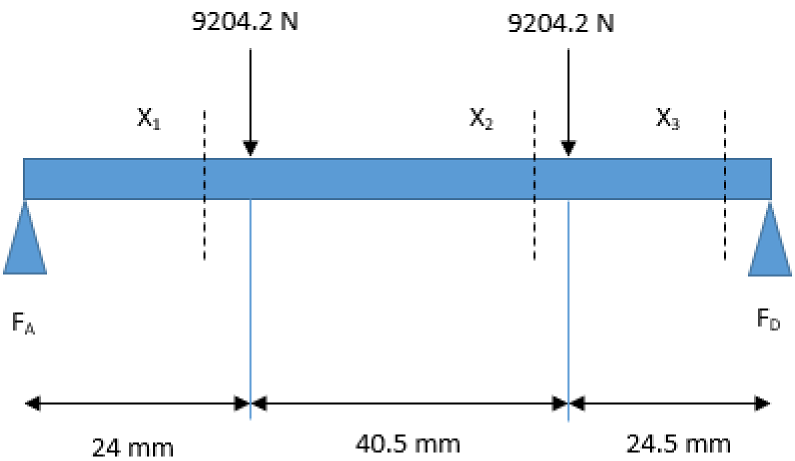

Figure G1.1.2: Equivalent beam loading on gearbox shaft

Sum of forces and moments:

$$\sum +\uparrow F = 0 = F_A + F_D - 9204.2\ N - 9204.2\ N$$

$$\sum + \square M_A = 0 = 9204.2\ N(0.024\ m) + 9204.2\ N(0.0645\ m) - F_D(0.089\ m)$$

$$F_A = 9255.7\ N, F_D = 9152.29\ N$$

Section X1:

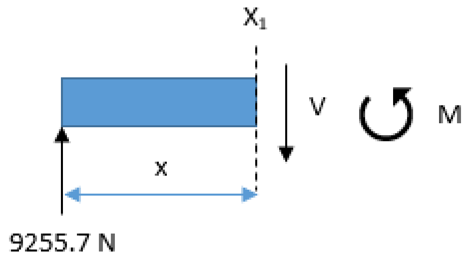

$$\sum +\uparrow F = 0 = 9255.7\,N - V\,, \therefore V = 9255.7\,N$$

$$\sum +\circlearrowleft \mathrm{M}_{X_1} = 0 = (-9255.7\,N)x + M$$

$$@x = 0, M = 0\,Nm$$

$$@x = 0.024\,m, M = 222.137\,Nm$$

Section X2:

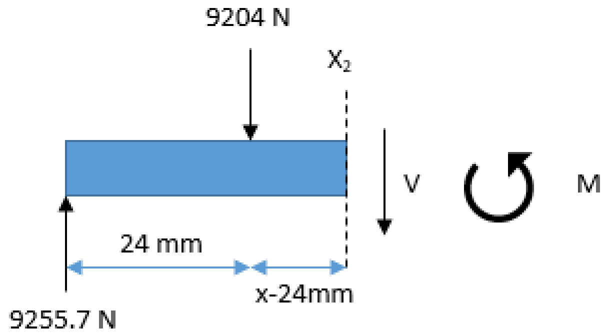

$$\sum +\uparrow F = 0 = 9255.7\,N - 9204\,N - V\,, \therefore V = 51\,N$$

$$\sum +\circlearrowleft \mathrm{M}_{X_2} = 0 = (-9255.7\,N)x + 9204\,N(x - 0.024\,m) + M$$

$$@x = 0.024\,m, M = 222.12\,Nm$$

$$@x = 0.0645\,m, M = 224.186\,Nm$$

Section X3:

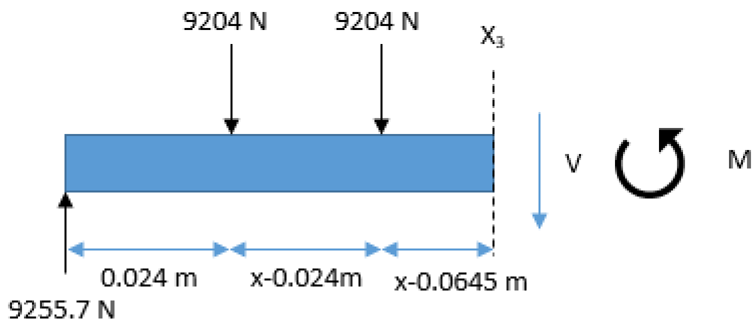

$$\sum +\uparrow F = 0 = 9255.7\ N - 9204\ N - 9204\ N - V\ ,\therefore V = -9153\ N$$

$$\sum +\circlearrowleft \mathrm{M}_{X_3} = 0$$

$$= (-9255.7\ N)x + 9204\ N(x - 0.024\ m) + 9204\ N(x - 0.0645\ m) + M$$

$$@x = 0.0645\ m, M = 224.186\ Nm$$

$$@x = 0.089\ m, M = 0\ Nm$$

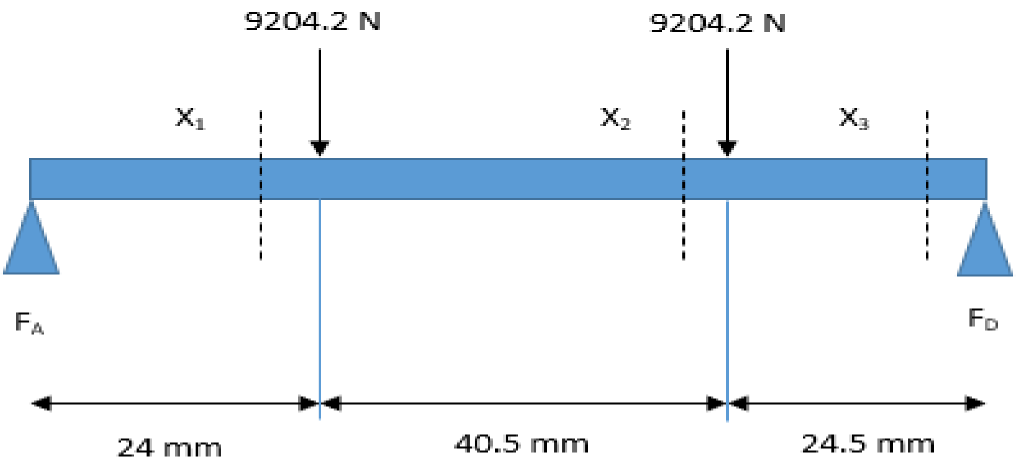

Figure G1.1.3: Equivalent beam loading on gearbox shaft

Using the bending moments and shear forces calculated from each section of the beam, the shear force and bending moment diagrams can be drawn (*Figure G1.1.4*).

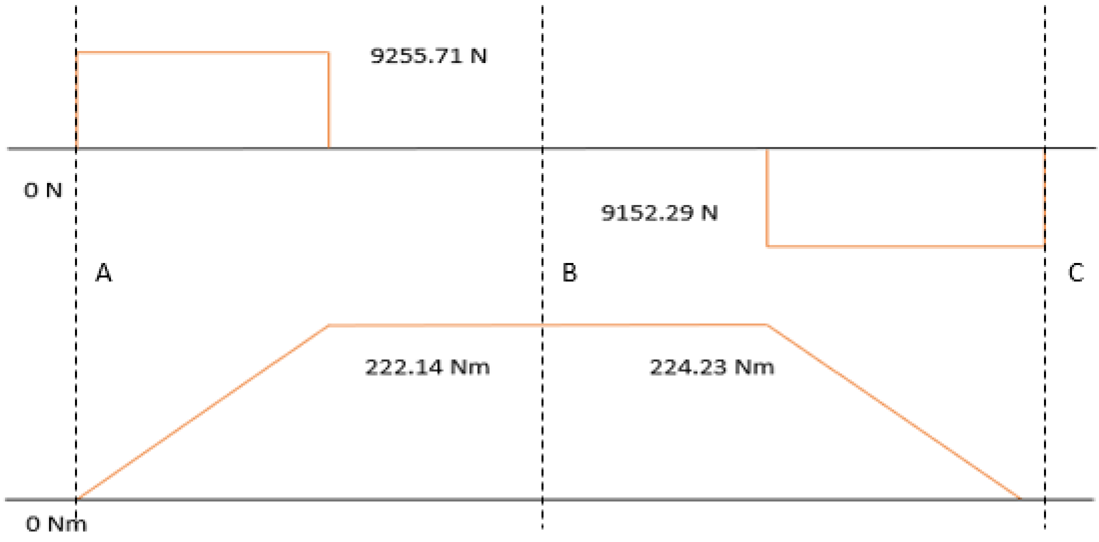

Figure G1.1.4: Shear force (Top) and bending moment diagram (Bottom) of gearbox shaft

G1.2 Internal Gearbox Shaft Design

The first step is to calculate the equivalent torque, T_E, and using *Figure G2.2.1*, the diameter of the shaft can be determined. *Figure G2.2.1* relates the material's ultimate tensile strength (6580 steel σ_{UTS} = 1250 MPa), and equivalent torque to determine the shaft diameter.

$$T_E = 1.15\sqrt{(224.2\ Nm)^2 + 0.75(1.5\ Nm)^2} = 257.8\ Nm$$

As an eccentricity of 3 mm is required, the offset diameters were determined to be 36 mm. However, this diameter was increased to 40 mm to fit the bore of the bearings. 40 mm was then used to calculate the stress concentration factor for a stepped shaft.

Following the procedures in the standard, the first iteration of shaft diameters is listed in *Table G1.2.1*.

Table G1.2.1 First iteration of minimum shaft diameters from A to D

Shaft section	**Diameter [mm]**
AB	30 mm
BC	30 mm

The second and final iteration for the minimum shaft diameters uses the shaft diameters from *Table G1.2.1* as the starting diameter.

<u>Section AB (iteration 2):</u>

Starting diameter: 30 mm

Bending moment at section AB (*Figure G1.1.4*): 224 Nm (rounded up from 222 as such a small difference between the two bending moments are negligible)

Stress raisers: stepped shaft, and bearing interference fit.

From *Figure G2.2.2* the value of K_S for a 30 mm diameter is 1.25. Next, the stress raiser factor for a stepped shaft needs to be determined from *Figure G2.2.5*. The ratio between the previously calculated diameters is used to obtain the correction factor from *Figure G2.2.4*.

$$\frac{D_1}{D} = \frac{40\ mm}{30\ mm} = 1.33$$

The correction factor from *Figure G2.2.4* is 0.055. The Z value to determine the stress raising factor for a stepped shaft from *Figure G2.2.5* needs to be calculated. Where R is the fillet radius of the bearing.

$$Z = \frac{R}{D} + \Delta \tag{G1.2.1}$$

$$Z = \frac{1\ mm}{30\ mm} + 0.055 = 0.088$$

The ultimate tensile stress of 6580 steel (1250 MPa) is greater than the value on the graph, in which case the 1000 MPa will be used as it is the closest value. This gives a stepped shaft stress raising factor of 1.8.

As the shaft has a bearing fitted and being an interference fit, this will also contribute a stress raising factor, and will be determined by *Figure G1.2.1*.

Figure G1.2.1: Stress raising factor for components fitted without key or spline (Standards Australia, 1985)

H7/S6 interference fit are used for medium drive fit for ordinary steel parts or shrink fits on light sections (*Preferred fits*, 2018). This will be used for all bearings fitted on this shaft. The ultimate tensile stress does not appear on this graph either, so 1000 MPa will be used, which gives a stress raising factor of 2.6.

Knowing all the stress raising factors on the shaft, the overall K factor will need to be calculated using *Equation G1.2.2*.

$$K_{overall} = K_{large} + 0.2K_{small} \tag{G1.2.2}$$

Having determined the largest and smallest stress raisers, the overall stress concentration is found to be:

$$K_{overall} = 2.6 + 0.2(1.8) = 2.98$$

The final diameter can now be calculated using *Equation G1.2.3*, where D is the diameter in mm, F_s is the factor of safety, $F_r = 0.45\sigma_{UTS}$ in MPa, K_s is the shape factor, k is the number of components with linear motion, P_q is the maximum axial tensile force in N, T_q is the torque experience by the shaft in Nm, and M_q is the bending moment being experienced by the section under consideration. According to Standards Australia (1985), *Equation G1.2.3* is used for shafts which experience the same torque in both forwards and reverse with over 600 mechanism starts and over 900 revolutions per year.

$$D^3 = \frac{10^4 F_s}{F_r}\sqrt{(K_s K_{overall}(M_q + \frac{P_q D}{8000}))^2 + \frac{3}{16}((1 + K_s K_{overall})T_q)^2} \tag{G1.2.3}$$

$$D^3 = \frac{10^4(1.5)}{0.45(1250\ MPa)}\sqrt{\left(1.25(2.98)(224\ Nm)\right)^2 + \frac{3}{16}\left(\left(1 + 1.05(2.96)\right)1.5\ Nm\right)^2}$$

$$D = 30\ mm$$

<u>Section BC:</u>

Trial diameter from first iteration = 30 mm

Stress raisers: Interference bearing fit, and stepped shaft.

Bending moment at section BC (*Figure G1.1.4*) = 224 Nm

To determine the stress raising factors in section BC (*Table G1.2.2*), the same figures are used from section A. *Equation G1.2.3* is also used to determine the diameter of this section.

Table G1.2.2 Stress raising factors for section BC

Stress raiser	Symbol	Value
Shape factor	K_s	1.25
Stepped shaft factor	K_{step}	1.8
Interference fit factor	K_{fit}	2.6
Overall stress factor	$K_{overall}$	2.96

$$D^3 = \frac{10^4(1.5)}{0.45(1250\ MPa)}\sqrt{(1.25)(2.96)(222\ Nm)^2 + \frac{3}{16}\left(\left(1 + 1.25(2.96)\right)T_q\right)^2},$$

$$\therefore D = 27.9\ mm = 30\ mm$$

As expected from the bending moment diagram (*Figure G1.1.4*) the shaft is uniform. Having determined the shape of the uniform shaft, an eccentricity of 3 mm was added. This was achieved by adding two circular offsets (*Figure 5.34*). The stress concentration factor was already added in the uniform shaft calculations.

G1.3 Internal Key Design

Force exerted onto key is calculated using the electric motor's maximum torque (1.5 Nm) and the radius of the motor's shaft (6 mm):

$$F = \frac{T}{r} = \frac{1.5\ Nm}{0.006\ m} = 250\ N$$

$$Force\ at\ one\ end\ of\ key = 102.5\ N$$

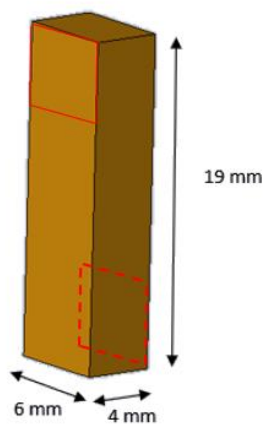

Figure G1.3.1: Motor keyway dimensions. Red box indicates bearing area between key and shaft

Bearing stress: bearing area is 3.84 mm high, and 6 mm in length

$$\sigma_b = \frac{125\ N}{0.006\ m(0.00384\ m)} = 5.4\ MPa$$

Shear stress:

$$\tau_s = \frac{125\ N}{(0.006\ m)0.004\ m} = 5.2\ MPa$$

G1.4 Stage One Ring Gear Body and Pins

G1.4.1 Bearing stress between outer ring gear of central disc on stage one ring gear body:

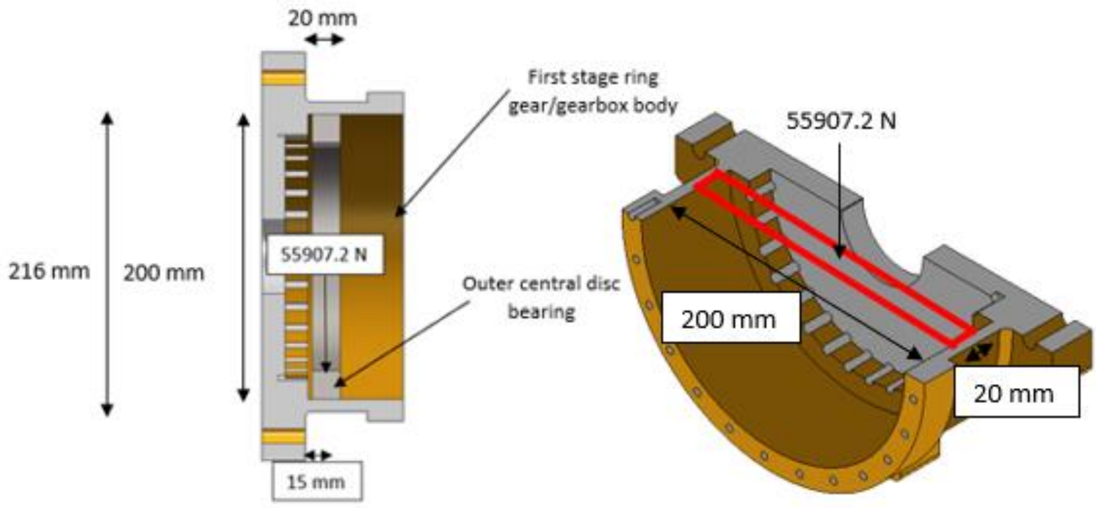

Figure G1.4.1.1: Central disc forces acting on bearing causing bending moment on gearbox body

Bearing stress is calculated using the force exerted by the central disc and the projected bearing area (*Figure G1.4.1.1*).

$$\sigma_B = \frac{F}{A}$$

$$\sigma_B = \frac{55907.2\ N}{0.2\ m(0.02\ m)} = 13.9\ MPa < 271\ MPa$$

G1.4.2 Bending stress of stage one ring gear:

The internal and outer diameter of the gearbox is 200 mm and 216 mm respectively. Knowing the location of the force and the magnitude, the bending moment can be calculated and therefore, the stress due to bending (*Figure G1.4.1.1*).

$$I = \frac{1}{4}\pi(r_o - r_i)^4 = \frac{1}{4}\pi(0.108\ m - 0.1\ m)^4 = 0.000028\ m^4$$

$$\sigma = \frac{M\bar{y}}{I}$$

$$\sigma = \frac{55907.2\ N(0.015\ m)(0.108\ m)}{0.000028\ m^4} = 3.23\ MPa$$

G1.4.3 Shear stress of ring gear pin:

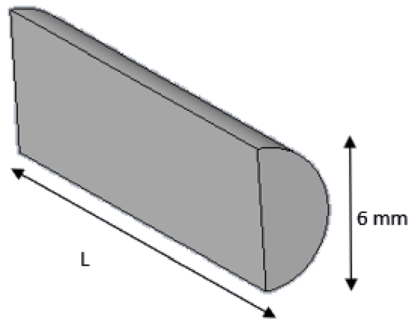

Figure G1.4.3.1: Shear area of exposed section of ring gear pin

The exposed length of the ring gear pin is calculated using the allowable shear stress and the force acting on the pin:

$$170\ MPa = \frac{6249.8\ N}{(0.006\ m)L}, \therefore L = 0.01\ m$$

Shear stress of the smallest shear area (the semi-circular area located at the bottom of the pin) is calculated using the known applied force (6249.8 N) and the radius of the pin (3 mm):

$$\tau = \frac{8F}{3\pi r^2}$$

$$\tau = \frac{8(6249.8\ N)}{3\pi(0.003\ m)^2} = 589.4\ MPa > \tau_{all} = 170\ MPa$$

G1.4.3.1 Pin bearing stress of stage one ring gear:

The bearing stress is calculated using the force applied to the pin and the bearing area (indicated in red in *Figure G1.4.3.2*) on the ring gear (determined by the Solidworks model).

$$\sigma_B = \frac{F}{A}$$

$$\sigma_B = \frac{6249.8\ N}{0.000123\ m^2} = 50.6\ MPa < 271\ MPa$$

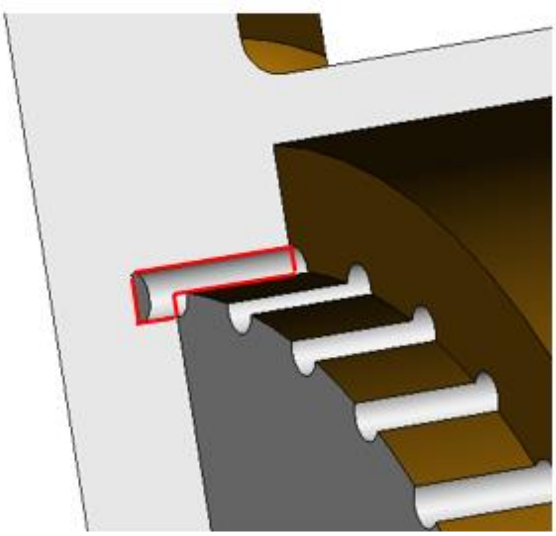

Figure G1.4.3.2: Bearing area on first stage ring gear. The bearing area is also identical to the second stage ring gear

G1.4.4 Wall thickness of stage one ring gear

In order to determine the minimum thickness of the ring-gear, an approximation is made to turn the ring gear into a flat wall fixed at one end (*Figure G1.4.4.1*). The load of three pins is applied on the "tooth" of the ring-gear, as this would be the maximum force that would be applied to the ring gear.

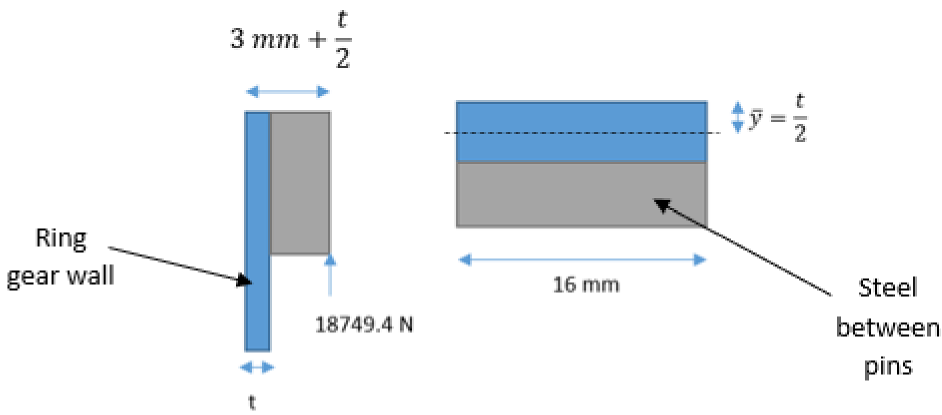

Figure G1.4.4.1: First stage ring gear wall loading approximation

Knowing the applied force on the ring gear (18749.4 N) and the allowable stress of the 5056-H18 aluminium alloy (271 MPa), the thickness, t, can be solved.

$$\sigma = \frac{M\bar{y}}{I}$$

$$271\ MPa = \frac{18749.4\ N\left(0.003\ m + \frac{t}{2}\right)\left(\frac{t}{2}\right)}{\frac{1}{12}(0.016\ m)t^3}, \therefore t = 17.4\ mm \approx 20\ mm$$

G1.4.5 Stage one ring gear feet and body calculations

Bolt diameter that secures the gearbox to the housing is determined by using the maximum force exerted on one bolt and the allowable shear stress of grade 10.9 bolt steel.

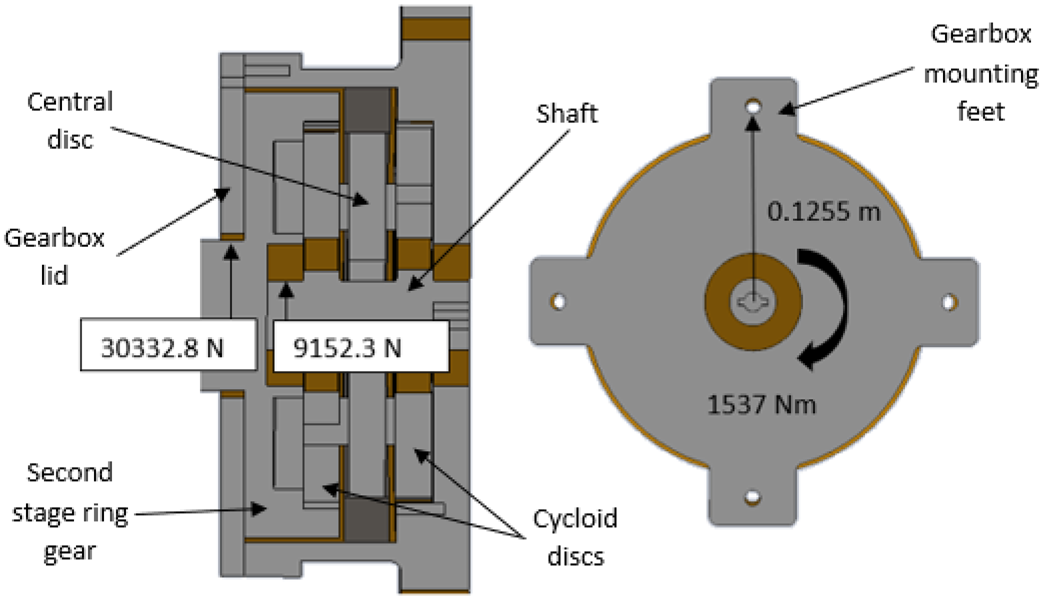

Figure G1.4.5.1: Forces and torques on first stage ring gear body

The net force in the upwards direction (*Figure G1.4.5.1*):

$$F = 30332.8\ N + 9152.3\ N = 3948.1\ N$$

Force due to torque:

$$F = \frac{1537\ Nm}{0.1255\ m} = 12255\ N$$

Maximum force per foot:

$$F_{per\ foot} = \frac{3948.1\ N}{4} + \frac{12255\ N}{4} = 12935\ N$$

Knowing the allowable shear stress of grade 10.9 bolt is 313.3 MPa, and the force acting on each foot, the radius ‘r’ can be solved using *Equation G15.1.1*.

$$313.3\ MPa = \frac{4}{3}\frac{12935\ N}{\pi r^2}, \therefore r = 0.00418\ m, \emptyset = 8.3\ mm$$

This gives a minimum bolt diameter of 8.3 mm; however, 8.3 mm bolts are not available this means the next largest size bolt diameter of 10 mm is selected.

G1.4.6 Bending of stage one ring gear feet

The stage one ring gear has a 39485 N net force acting on its outer edge (*Figure G1.4.6.1*), which will cause bending stresses to occur on the top and bottom feet.

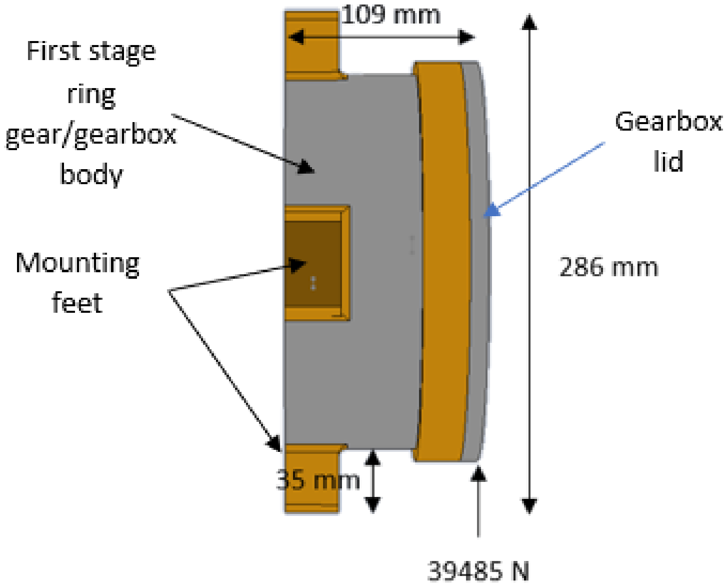

Figure G1.4.6.1: Force exerted on the front of gear box could cause the top and bottom feet to bend

First the bending moment acting on the gearbox body is calculated.

$$M = 39485\ N(0.109\ m) = 4303.87\ Nm$$

The gearbox body is simplified as a T-section, assuming the section where F_y is applied is rigid, the force F_x can be determined. *Figure G1.4.6.2* shows a free body diagram.

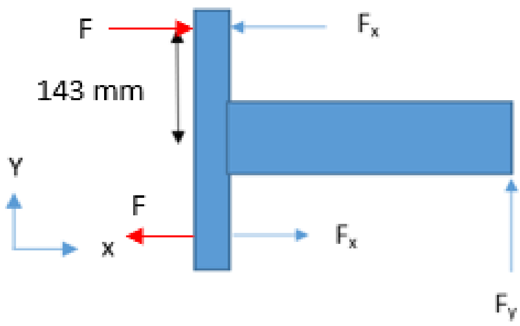

Figure G1.4.6.2: Free body diagram of gearbox body

The bending moment above and below the neutral axis is half the total bending moment caused by force F_y (*Figure G1.4.6.3*). According to Biezen (2016), the uniform triangular distribution (*Figure G1.4.6.3*) is caused by the internal tension and compressive forces. The force and the stress linearly increase as it moves away from the neutral axis.

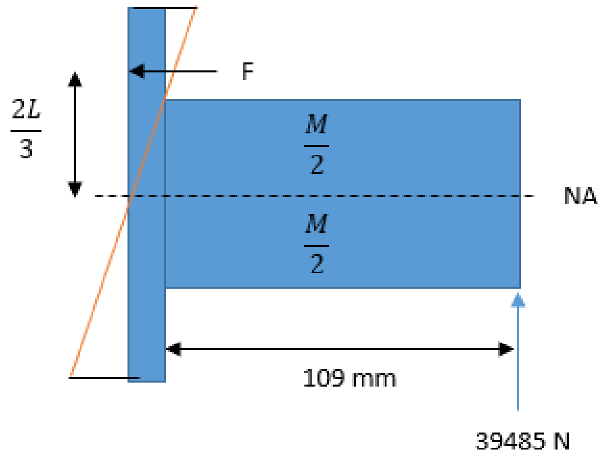

Figure G1.4.6.3: Force distribution of the first stage ring gear

Calculating F_x:

$$\frac{2L}{3} = \frac{2(0.143\ m)}{3} = 0.0953\ m$$

$$F = \frac{4303.88\ Nm}{2(0.0953\ m)} = 22573\ N$$

Knowing the value of F_x, *Equation G1.4.6.1* is used to determine the stress concentration and *Equation G1.4.6.4* to determine the maximum stress taking into consideration of the stress raising factor, K. Where t is thickness, D is the diameter of the hole, and w is the width (*Figure G1.4.6.4*).

$$K = \left(1.79 + \frac{0.25}{0.39+\frac{D}{t}} + \frac{0.81}{1+\left(\frac{D}{t}\right)^2} - \frac{0.26}{1+\left(\frac{D}{t}\right)^3}\right)\left(1 - 1.04\left(\frac{D}{w}\right) + 1.22\left(\frac{D}{w}\right)^2\right) \quad \text{(G1.4.6.1)}$$

$$\sigma = \frac{6M}{(w-D)t^2} \quad \text{(G1.4.6.2)}$$

$$\sigma_{max} = K\sigma \quad \text{(G1.4.6.3)}$$

Using D = 10 mm, w = 55 mm, t = 30 mm and a bending moment $M = 22573\ N(0.035\ m) = 790\ Nm$, the maximum stress can be found (257.4 MPa).

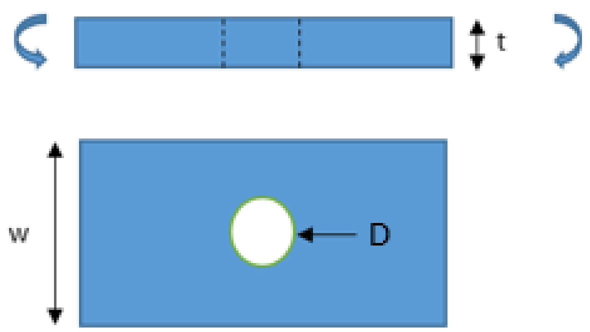

Figure G1.4.6.4: Gearbox foot in bending with bolt hole

G1.4.7 Bending stress of stage one ring gear body

Assuming that the feet are fixed, bending stresses could occur on the stage one ring gear body from the 39485 N force. Using the largest bending moment experienced by the ring gear, the bending stress can be found (*Figure G1.4.6.1*).

$$\sigma = \frac{M\bar{y}}{I}$$

$$\sigma = \frac{39485\,N(0.109\,m)(0.108\,m)}{\frac{1}{4}\pi((0.108\,m)^4 - (0.1\,m)^4)} = 16.4\,MPa < 271\,MPa$$

G1.5 Stage two ring gear

G1.5.1 Wall thickness of stage two ring gear

Approximating the stage two ring gear as a flat wall with one end fixed, the thickness can be calculated. A force of 18749.4 N applied (*Figure G1.5.1.1*) on the metal between the pins.

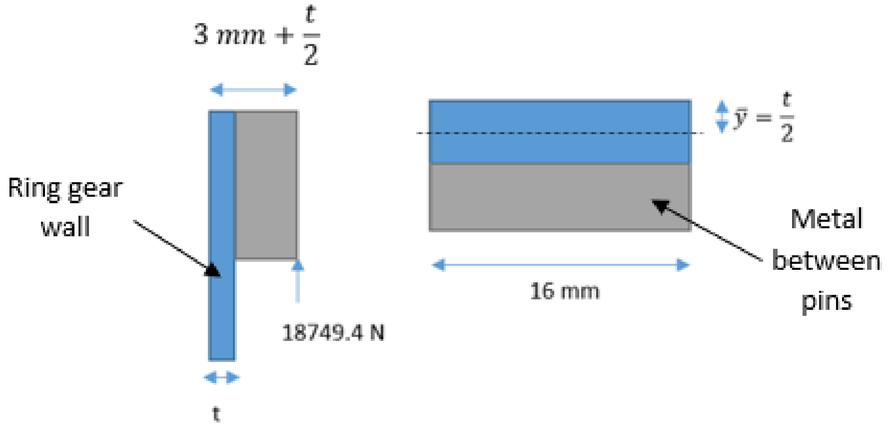

Figure G1.5.1.1: Wall approximation of second stage ring gear

The allowable stress of the steel for the second stage ring gear is 466.6 MPa; using this stress, and *Figure G1.5.1.1* will allow the minimum thickness t to be solved.

$$\sigma = \frac{M\bar{y}}{I}$$

$$466.6\,MPa = \frac{18749.4\,N\left(0.003\,m + \frac{t}{2}\right)\left(\frac{t}{2}\right)}{\frac{1}{12}(0.016\,m)t^3}, \therefore t = 12.5\,mm \approx 13\,mm$$

G1.5.2 Bending stress of stage two ring gear bearing housing

Knowing the force acting on the bearing housing (9255 N), the bending stress can be calculated (*Figure 5.51*).

$$\sigma = \frac{M\bar{y}}{I}$$

$$\sigma = \frac{9255\,N(0.013\,m)(0.036\,m)}{\frac{1}{4}\pi((0.036\,m)^4 - (0.031\,m)^4)} = 7.3\,MPa$$

G1.5.3 Gearbox lid

The bolt diameter to secure gearbox lid is calculated using the allowable shear stress of class 4.8 screws (113.3 MPa), and the force acting on each of the 25 screws. Using *Equation G15.1.1* the diameter can be determined.

$$113.3\,MPa = \frac{4}{3}\frac{39845\,N}{25(\pi r^2)}, \therefore r = 0.00243, \emptyset \approx 5\,mm$$

Thickness of the gearbox lid is calculated using the allowable stress of Al 5056 H18 and the force of 39845 N acting on the lid (*Figure 5.53*).

$$271\,MPa = \frac{39845\,N}{(0.072\,m)t}, \therefore t = 0.002\,m$$

The thickness of 2 mm is deemed to be insufficient to accommodate the bushing that will be fitted to the lid. The thickness of the lid is increased to 10 mm, the bearing stress between the bushing and the gearbox lid needs to be checked.

$$\sigma_B = \frac{F}{A} = \frac{39485\,N}{0.01\,m(0.072\,m)} = 54.8\,MPa$$

Bearing stress between bushing and drive shaft:

$$\sigma_B = \frac{F}{A} = \frac{39485\,N}{0.01\,m(0.066\,m)} = 59.8\,MPa$$

G1.6 Cycloidal Discs

The torque formula (*Equation G1.6.1*) is used to calculate the torques of the first and second stage cycloidal discs.

$$T = T_m R_1 \left(\frac{1}{1 + R_1} + R_2\right) \quad \text{(G1.6.1)}$$

(Blagojevic et al. 2011)

Knowing the reduction ratio of first and second stage is 32:1, the torque on each cycloidal disc is:

$$T = 1.5\ Nm(32)\left(\frac{1}{1+32} + 32\right) = 1537.45\ Nm$$

Using the torque calculated above, the force per tooth can then be calculated:

$$F = \frac{T}{d} = \frac{1537.45\ Nm}{0.082\ m} = 18749.4\ N$$

$$Force\ per\ tooth = \frac{18749.4\ N}{3\ teeth} = 6249.82\ N$$

Approximating the cycloidal disc teeth as cantilever beams, the bending stress can be calculated:

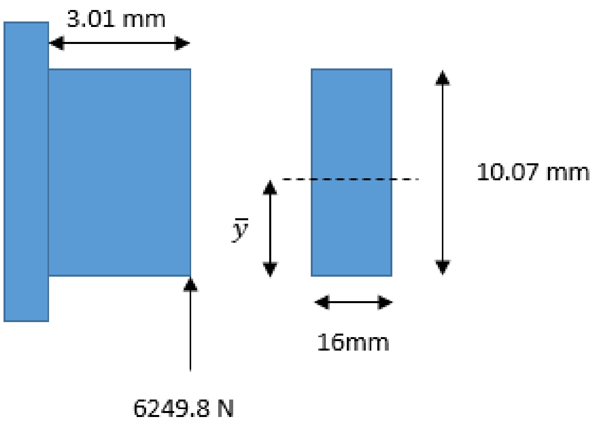

Figure G1.6.1: Bending of cycloidal tooth is equivalent to cantilever beam

$$I = \frac{1}{12}(0.016\ m)(0.01007\ m)^3 = 1.36E - 9\ m^4$$

$$\bar{y} = \frac{0.01007\ m}{2} = 0.005035\ m$$

$$\sigma = \frac{(6249.8\ N)(0.00301\ m)(0.005035\ m)}{1.36E - 9\ m^4} = 69.5\ MPa$$

Contact stress between the central disc pins and holes of cycloidal disc (*Figure 5.25*):

$$F = \frac{1537.45\ Nm}{0.055\ m} = 27953.6\ N$$

$$Force\ per\ center\ disc\ pin = \frac{27953.6\ N}{3\ pins} = 9317.87\ N$$

$$b = \sqrt{\frac{4(9317.87\ n)}{\pi(0.016\ m)} \frac{\frac{1-0.3_1^2}{210\ GPa} + \frac{1-0.3_2^2}{130\ GPa}}{\frac{-1}{0.027\ m} + \frac{1}{0.021\ m}}} = 0.00063\ m$$

$$\sigma = \frac{2(9317.87\ N)}{\pi(0.016\ m)(0.00063\ m)} = 588.3\ MPa$$

G1.7 Central disc

The diameters of the pins of the central disc need to be defined. The central disc pins are approximated as cantilevers (*Figure G1.7.1*).

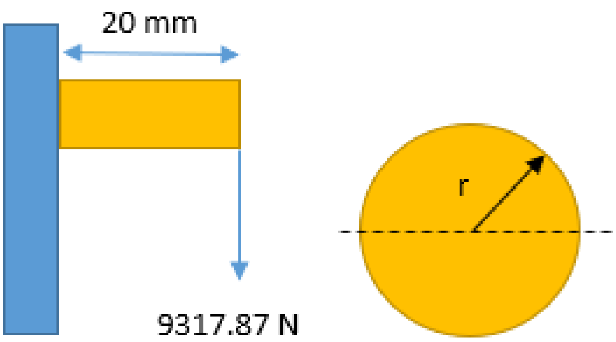

Figure G1.7.1: Central disc pin approximated as cantilever beam

Determining the minimum radius of the central disc pins using the allowable stress (493.3 MPa):

$$\sigma = \frac{M\bar{y}}{I}$$

$$493.3\ MPa = \frac{9317.87\ N(0.02\ m)r}{\frac{1}{4}\pi r^4}, \therefore r = 0.007835\ m, \emptyset = 16\ mm$$

Next, the minimum thickness of the central disc needs to be calculated by using the allowable stress of 4140 steel (493.3 MPa). The central disc is approximated as a rectangular wall (*Figure G1.7.2*). The distance from the bottom edge of the central disc to the neutral axis is:

$$\bar{y} = \frac{t}{2}$$

Where t is the thickness of the central disc (*Figure G1.7.2*). Knowing the allowable stress, bending moment, and the second moment of area of a rectangular cross-section; the thickness of the central disc can be found.

$$\sigma = \frac{M\bar{y}}{I}$$

$$493.3\ MPa = \frac{27953.61\ N\left(0.02\ m + \frac{t}{2}\right)\left(\frac{t}{2}\right)}{\frac{1}{12}(0.10778\ m)t^3}, \therefore t \approx 0.01\ m$$

The minimum thickness of the central disc is 10 mm this is later increased to 16 mm in order to fit the roller bearing.

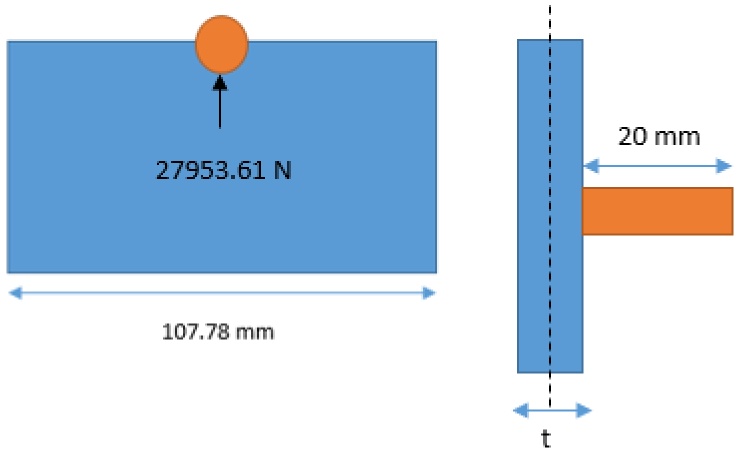

Figure G1.7.2: Schematic of approximated wall of central disc

As the cycloidal discs are 180° out of phase (this is done to reduce vibration), meaning only three pins on opposite ends are loaded. This loading condition could cause some torsional shear stress; the same calculation for the twisting of the bending arm is also done here using the dimensions calculated for the approximated rectangular cross-section (*Figure G1.7.2*). The ratio of length and thickness is calculated to determine c_1 from *Table G14.2.1* as shown below:

$$\frac{a}{b} = \frac{107.78}{16} = 6.735, \therefore c_1 \approx 0.298$$

From the calculation below, the shear stress due to torsion is well below the allowable shear stress of through-hardened 4140 steel.

$$\tau = \frac{27953.61\ N(0.02\ m)}{(0.298)(0.10778\ m)(0.016\ m)^2} = 68\ MPa < \tau_{all} = 246.6\ MPa$$

G2 Bending moment and shear force calculations of main drive shaft (shearing rebar)

Knowing the force exerted on the drive shaft by the roller follower of the shearing mechanism (62932.4 N), the bending moment and shearing diagrams can be drawn.

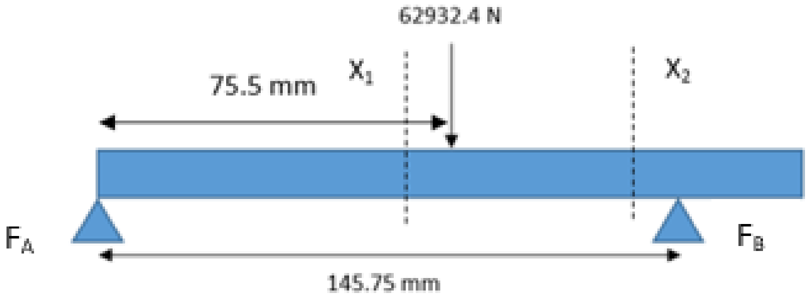

Figure G2.1: Loading of drive shaft when rebar is being sheared

Sum of forces and moments:

$$\sum +\uparrow F = 0 = F_A + F_B - 62932.4\,N$$

$$\sum +\square M_A = 0 = 62932.4\,N(0.075\,m) - F_B(0.14575\,m)$$

$$F_A = 30332.6\,N$$

$$F_B = 32599.6\,N$$

Section X_1:

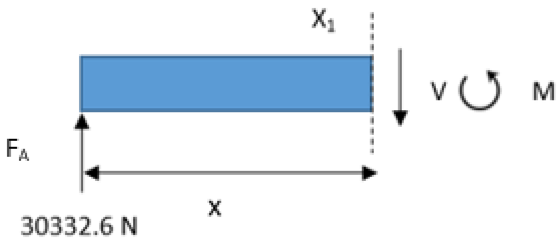

$$\sum +\uparrow F = 0 = 30332.6\,N - V, \therefore V = 30332.6\,N$$

$$\sum +\circlearrowleft \mathrm{M}_{x_1} = 0 = 30332.6\,N(x) + M$$

$$@x = 0, M = 0\,Nm$$

$$@x = 0.075\,m, M = 2290.13\,Nm$$

Section X_2:

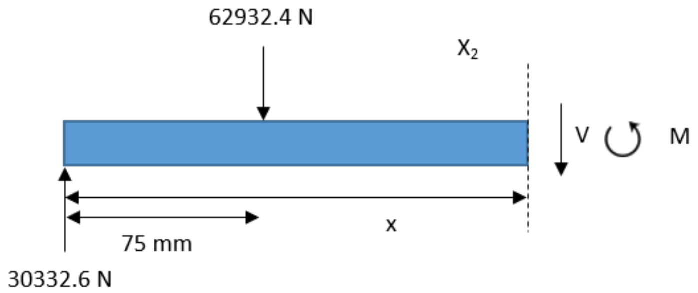

$$\sum +\uparrow F = 0 = 30332.6\,N - 62932.4\,N - V, \therefore V = 32599.6\,N$$

$$\sum + \circlearrowleft \mathrm{M}_{x_2} = 0 = -30332.6\,N(x) + 62932.4(x - 0.075\,m) + M$$

$$@x = 0.075\,m, M = 2290.13\,Nm$$

$$@x = 0.14575\,m, M = 0\,Nm$$

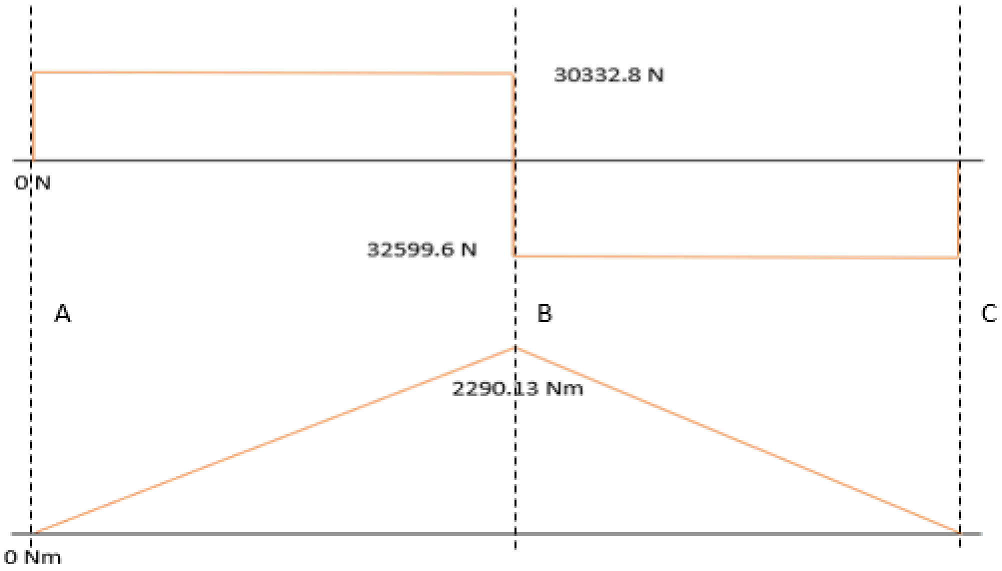

Figure G2.1: Shear force (top) and bending moment (bottom) diagrams of shaft shearing rebar

Using the bending moments and shear forces calculated from each section of the beam, the shear force and bending moment diagrams can be drawn (*Figure G2.1).*

G2.1 Bending moment and shear force calculations of main drive shaft (bending rebar)

The arm exerts a force of 5332.9 N and forming wheel exerts a force of 13537.5 N onto the shaft, when bending rebar. Using these forces, the bending moment and shear force diagrams can be drawn. Firstly, the sum of forces and moments is calculated.

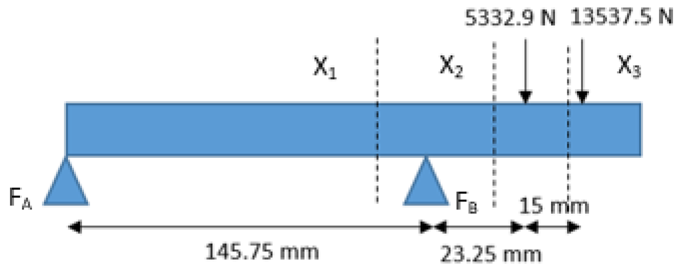

Figure G2.1.1: Loading of drive shaft when rebar is being bent

$$\sum +\uparrow F = 0 = F_A + F_B - 5332.9\,N - 13537.5\,N$$

$$\sum + \circlearrowleft M_A = 0 = -F_B(0.14575\,m) + 5332.9\,N(0.169\,m) + 13537.5\,N(0.184\,m)$$

$$F_A = -4403.4\,N$$

$$F_B = 23273.8\,N$$

Bending moment and shear force for section X_1:

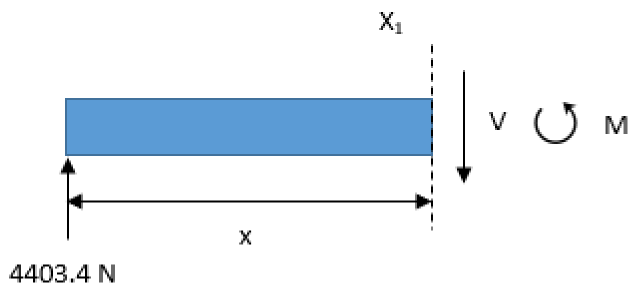

$$\sum +\uparrow F = 0 = -4403.4\,N - V, \therefore V = -4403.4\,N$$

$$\sum + \circlearrowleft \mathrm{M}_{x_1} = 0 = 4403.4\,N(x) + M$$

$$@x = 0, M = 0\,Nm$$

$$@x = 0.14575\,m, M = 641.79\,Nm$$

Bending moment and shear force for section X_2:

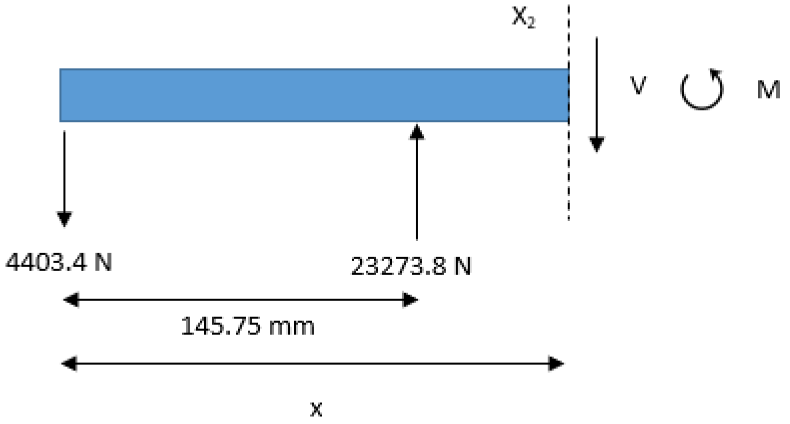

$$\sum +\uparrow F = 0 = -4403.4\ N + 23273.8\ N - V, \therefore V = 18870.4\ N$$

$$\sum +\circlearrowleft \mathrm{M}_{x_2} = 0 = 4403.4\ N(x) - 23273.8\ N(x - 0.145\ m) + M$$

$$@x = 0.145\ m, M = -649.71\ Nm$$

$$@x = 0.169\ m, M = -203\ Nm$$

Bending moment and shear force for section X_3:

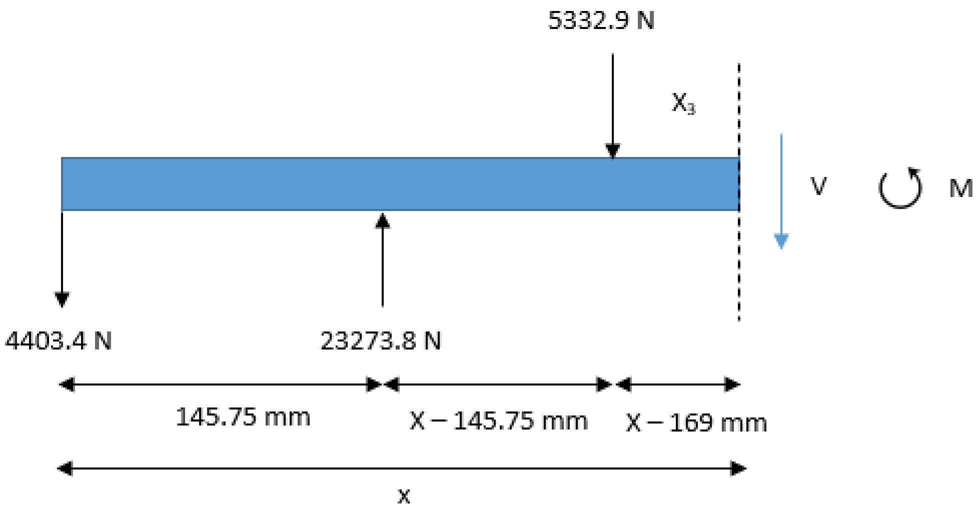

$$\sum +\uparrow F = 0 = -4403.4\ N + 23273.8\ N - 5332.9\ N - V, \therefore V = 18870.4\ N$$

$$\sum +\circlearrowleft \mathrm{M}_{x_3} = 0 = 4403.4\ N(x) - 23273.8\ N(x - 0.145\ m) + 5332.9\ N(x - 0.169) + M$$

$$@x = 0.169\ m, M = -203\ Nm$$

$$@x = 0.184\ m, M = 0\ Nm$$

And section X_3 (Right hand side):

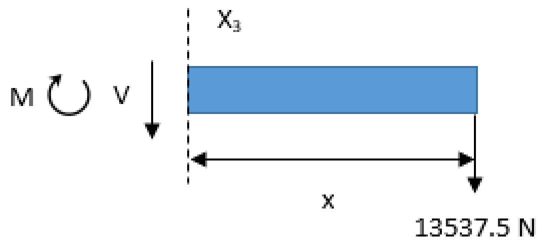

$$\sum +\uparrow F = 0 = -13537.5\ N - V, \therefore V = -13537.5\ N$$

$$\sum + \circlearrowright \mathrm{M}_{x_3} = 0 = 13537.5\ N(x) + M$$

$$@x = 0, M = 0\ Nm$$

$$@x = 0.015\ m, M = -203\ Nm$$

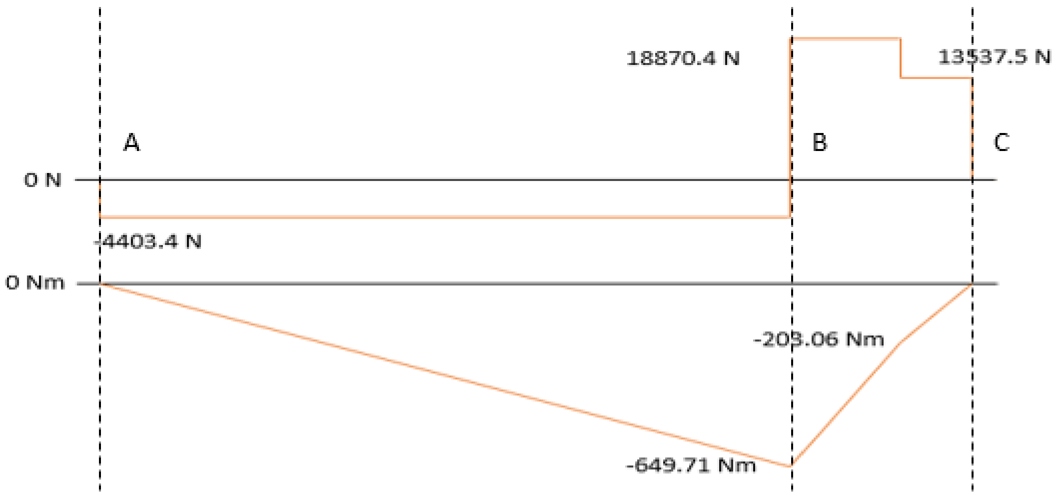

Figure G2.1.2: Shear force (top) and bending moment (bottom) diagrams of shaft bending rebar

Using the bending moments and shear forces calculated from each section of the beam, the shear force and bending moment diagrams can be drawn (*Figure G2.1.2).*

G2.2 Drive Shaft Design

Section AB:

Figure G2.2.1: Trial diameter graph (Standards Australia,

Starting with the section AB (*Figure G2.1*), an equivalent torque (*Equation G2.2.1*) can be calculated using the bending moment and the torque caused by rebar shearing.

$$T_E = 1.15\sqrt{M^2 + 0.75T^2} \quad \text{(G2.2.1)}$$

$$T_E = 1.15\sqrt{(2290.13\ Nm)^2 + 0.75(280.14\ Nm)^2} = 2648.42\ Nm$$

Using *Figure G2.2.1*, the trial diameter is 45 mm. After the first iteration the diameter of the shaft is increased to 62 mm.

Figure G2.2.2: Shape Factor (Standards Australia, 1985)

Using 62 mm diameter, the shape factor can be determined from *Figure G2.2.2,* to be 1.5. The shaft in section AB only has one stress raiser (the keyway). Using *Figure G2.2.3*, the stress concentration factor (using a H7/k6 interference fit and the ultimate tensile stress of the material of 1000 MPa) is 2.3.

Figure G2.2.3: Stress raising factor for keyed components (Standards Australia, 1985)

With these values the final diameter of shaft for section AB can be calculated using *Equation G2.2.2*. According to Standards Australia (1985), *Equation G2.2.2* are for shafts that will experience greater torques in one direction, will have over 600 starts and over 900 revolutions per year.

$$D^3 = \frac{10^4 F_s}{F_R} K_s K \sqrt{\left(M_q\right)^2 + \frac{3}{4}\left(T_q\right)^2} \tag{G2.2.2}$$

$$D^3 = \frac{10^4(1.5)}{0.45(1050\ MPa)}(1.5)(2.3)\sqrt{(2290.13\ Nm)^2 + \frac{3}{4}(280.14\ Nm)^2}$$

$$D = 64\ mm$$

Using the bending moment from section BC (*Figure G2.1.2*), and the torque acting on the drive shaft; the equivalent torque can be calculated. Using both the equivalent torque and ultimate tensile stress of 6580 steel (1050 MPa), a trial diameter of 35 mm is obtained from *Figure G2.2.1*. After the first iteration, the diameter is 44 mm. This diameter will be used in the following second iteration.

$$T_E = 1.15\sqrt{(649.71\ Nm)^2 + 0.75(933.3\ Nm)^2} = 1192.6\ Nm$$

Using *Figure G2.2.2*, the shape factor is determined to be 1.45. The correction and stress factor from the step between section AB and section BC (*Figure 5.14*) is found using *Figures G2.2.4* and *G2.2.5* respectively.

Figure G2.2.4: Correction Factor (Standards Australia, 1985)

$$\frac{D_1}{D} = \frac{66\ mm}{44\ mm} = 1.5$$

From *Figure G2.2.4* the correction factor can be determined to be:

$$\Delta = 0.03$$

The Z value is calculated from *Equation G1.2.1*

Figure G2.2.5: Stepped shaft stress factor (Standards Australia, 1985)

$$Z = \frac{1\,mm}{44\,mm} + 0.03 = 0.0527$$

From *Figure G2.2.5,* the stress raising factor from the shaft step is found to be 1.1. The next stress-raising factor comes from the involute spline used to drive the bending arm. Using the ultimate tensile strength of 6580 steel (1050 MPa), the stress raising factor due to the involute spline can be determined from *Figure G2.2.6.*

Figure G2.2.6: Stress raising factor for splined shaft (Standards Australia, 1985)

From *Figure G2.2.6* the stress raising factor for an involute splined-shaft is 1.7. Knowing the two stress raising factors for this section of the shaft, the overall stress factor is calculated using *Equation G1.2.2.*

$$K_{overall} = 1.7 + 0.2(1.1) = 1.92$$

The final minimum diameter of this section of the shaft is calculated below:

$$D^3 = \frac{10^4(1.5)}{0.45(1050\ MPa)}(1.45)(1.92)\sqrt{(649.71\ Nm)^2 + \frac{3}{4}(933.3\ Nm)^2}$$

The final diameter of the shaft is 45 mm. It will be round up to 50 mm.

G2.3 Keyway Design

The dimensions of the keyway are selected from *Table G2.3.1* using the diameter of the shaft (66 mm).

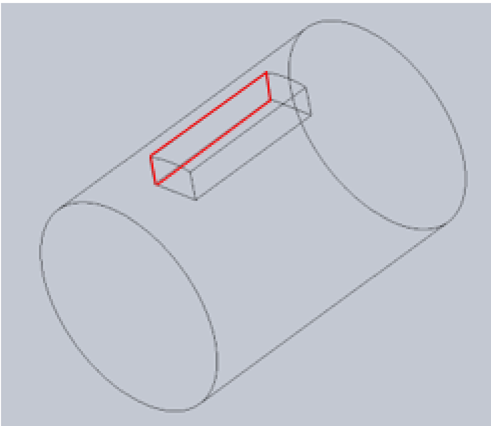

Figure G2.3.1: Bearing stress exerted on wall of shaft and key

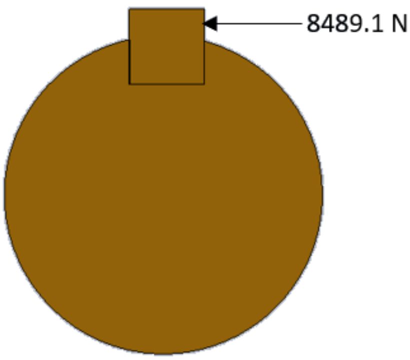

Figure G2.3.2: Force from shaft torque acting on key

The force of 8489.1 N (calculated from the torque acting on the shaft) creates a bearing stress of shaft wall as shown in *Figure G2.3.1.*

$$F = \frac{280.14\ Nm}{0.033\ m} = 8489.1\ N$$

$$\sigma_b = \frac{8489.1\ N}{0.05\ m(0.0075\ m)} = 21.4\ MPa$$

The force also creates a shear plane on the key. The shear area of the key is indicated in *Figure G2.3.4.* Knowing the force and area, the shear stress can be calculated.

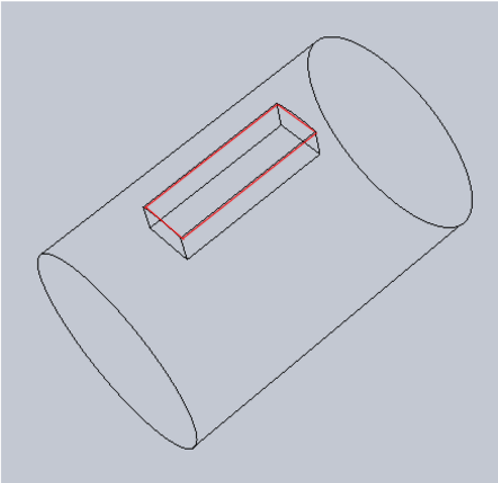

Figure G2.3.4: Shear plane of the key. The red square indicates the shear area on the top surface of the shaft.

$$\tau_s = \frac{8489.1\,N}{0.02\,m(0.05\,m)} = 8.48\,MPa$$

The bearing stress on cam wall is also calculated using the force of 8489.4 N and the bearing area as shown in *Figure G2.3.5*

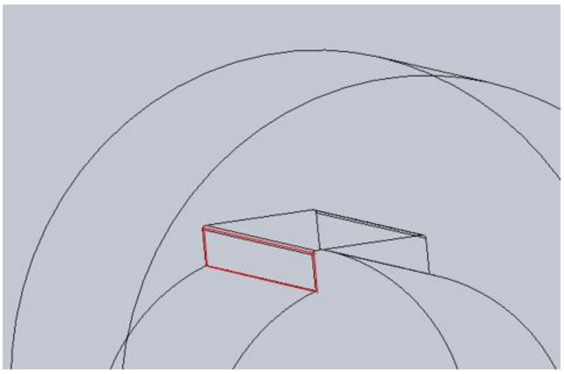

Figure G2.3.5: Bearing area of cam and key wall

$$\sigma_b = \frac{8489.1\,N}{0.05\,m(0.0049\,m)} = 34.6\,MPa$$

Table G2.3.1 BS4500 Keyway Chart (British Standards, n.d.)

G2.4 Spline tooth dimensions

Using the diameter of shaft (50 mm), 8 teeth and the standard pressure angle of 30°, the dimensions of the spline tooth can be calculated from the modulus, m.

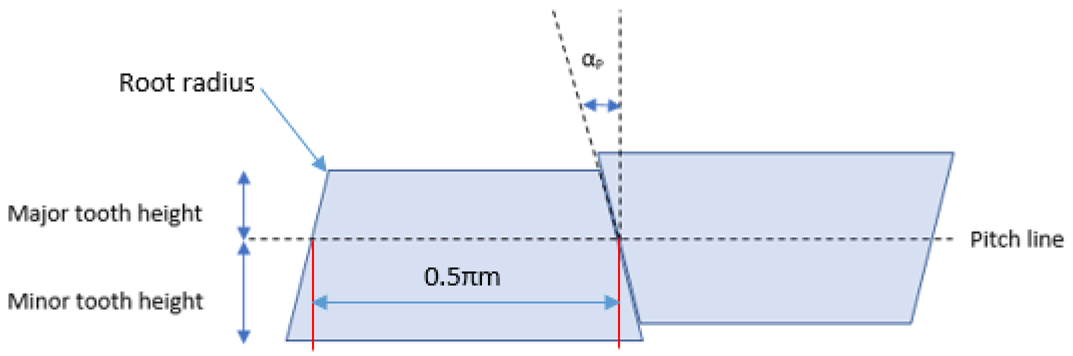

Figure G2.4.1: Dimensioning system of the spline

$$m = \frac{D_{base}}{z \cos \alpha_p} = \frac{50\ mm}{8\cos(30°)} = 7.21$$

$$Minor\ tooth\ height = 0.75m = 0.75(7.21) = 5.4\ mm$$

$$Major\ tooth\ height = 0.5m = 0.5(7.21) = 3.6\ mm$$

$$Root\ radius = 0.2m = 0.2(7.21) = 2\ mm$$

G2.5 Bending stress of spline tooth for shaft and bending arm

Knowing the force (4666.5 N) acting on each of the spline teeth, and the dimensions of the teeth, the bending stress can be calculated. The spline tooth is approximated as a cantilever beam (*Figure G2.5.1*).

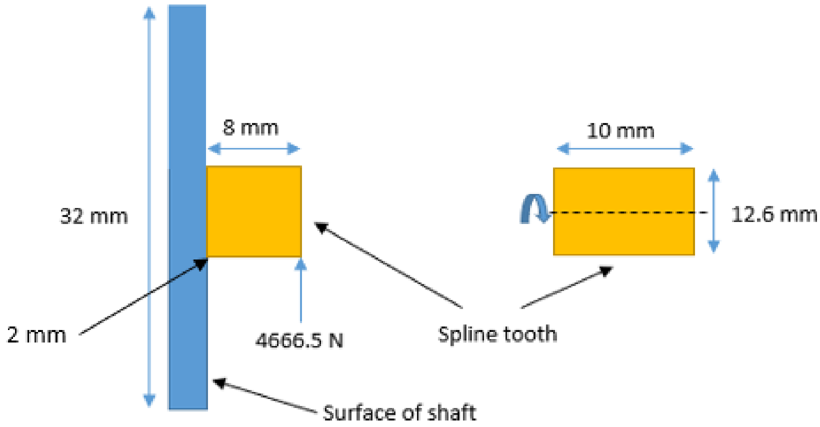

Figure G2.5.1: Bending stress of the spline tooth

$$I = \frac{1}{12}(0.01\ m)(0.01261\ m)^3 = 1.671E - 9\ m^4$$

$$M = 4666.5\ N(0.008\ m) = 37.3\ Nm$$

$$\sigma = \frac{M\bar{y}}{I} = \frac{37.3\ Nm(0.006305\ m)}{1.671E - 9m^4} = 140.7\ MPa$$

Figure G2.5.2: Stress concentration coefficient graph (Beer, Johnston, Jr, DeWolf, & Mazurek, 2006)

To determine the stress concentration factor, the root radius calculated previously will be utilised.

$$\frac{r}{d} = \frac{2\ mm}{12.61\ mm} = 0.15$$

$$\frac{D}{d} = \frac{32.45\ mm}{12.61\ mm} = 2.5$$

$$\therefore K = 1.65$$

Having determined the stress concentration factor, the stress can be determined:

$$\sigma_{max} = 1.65(140.7\ MPa) = 232.7\ MPa$$

The stress is below the allowable stress of both 6580 steel of the shaft and ASTM A747 of the bending arm.

<u>G3 Hertzian Contact stress of forming wheel and rebar</u>

Using the dimensions and material properties of the forming wheel and the rebar, the Hertzian Contact Stress can be calculated. The rebar is assigned as body 1 and the forming wheel assigned as body 2.

Table G3.1: Rebar and forming wheel physical and material properties

	Body 1 (Rebar)	**Body 2 (Forming wheel)**
Poisson's Ratio, υ	0.3	0.3
Material Constant (IHS EDU, n.d., p.32)	$1.4E-12\ \frac{m^2}{N}$	$1.38E-12\ \frac{m^2}{N}$
R_{11}, R_{21}	0.01 m	0.044 m
R_{12}, R_{22}	∞	∞
Youngs Modulus, E (GPa)	200 GPa	240 GPa

$$A_{con} = \frac{1}{4}\left[\frac{1}{R_{11}} + \frac{1}{R_{12}} + \frac{1}{R_{21}} + \frac{1}{R_{22}} - \left[\left(\frac{1}{R_{11}} - \frac{1}{R_{12}}\right)^2 + \left(\frac{1}{R_{21}} - \frac{1}{R_{22}}\right)^2 + 2\left(\frac{1}{R_{11}} - \frac{1}{R_{12}}\right)\left(\frac{1}{R_{21}} - \frac{1}{R_{22}}\right)\cos 2\theta\right]^{\frac{1}{2}}\right] \quad \text{(G3.1)}$$

$$B_{con} = \frac{1}{4}\left[\frac{1}{R_{11}} + \frac{1}{R_{12}} + \frac{1}{R_{21}} + \frac{1}{R_{22}} + \left[\left(\frac{1}{R_{11}} - \frac{1}{R_{12}}\right)^2 + \left(\frac{1}{R_{21}} - \frac{1}{R_{22}}\right)^2 + 2\left(\frac{1}{R_{11}} - \frac{1}{R_{12}}\right)\left(\frac{1}{R_{21}} - \frac{1}{R_{22}}\right)\cos 2\theta\right]^{\frac{1}{2}}\right] \quad \text{(G3.2)}$$

In order to determine the relative principle curvatures (A_{con} and B_{con}) using the radius of the rebar (10 mm) and forming wheel (44 mm) *Equations G3.1* and *G3.2* are used.

$$A_{con} = \frac{1}{4}\left[\frac{1}{0.01\,m} + \frac{1}{0.044\,m} - \left[\left(\frac{1}{0.0.1\,m}\right)^2 + \left(\frac{1}{0.044\,m}\right)^2 + 2\left(\frac{1}{0.01\,m}\right)\left(\frac{1}{0.044\,m}\right)\cos 2(90°)\right]^{\frac{1}{2}}\right]$$

$$= 5.04429\ m^{-1}$$

$$B_{con} = \frac{1}{4}\left[\frac{1}{0.01\,m} + \frac{1}{0.044\,m} + \left[\left(\frac{1}{0.0.1\,m}\right)^2 + \left(\frac{1}{0.044\,m}\right)^2 + 2\left(\frac{1}{0.01\,m}\right)\left(\frac{1}{0.044\,m}\right)\cos 2(90°)\right]^{\frac{1}{2}}\right]$$

$$= 56.3194\ m^{-1}$$

The relative principle curvatures ratio is calculated and then used to determine the coefficients C_a, C_b, and C_f from *Figures G3.1* and *G3.2.*

$$\frac{A_{con}}{B_{con}} = 0.089566$$

Figure G3.1: Contact dimensions for ellipse ratio (IHS EDU, n.d.)

Figure G3.2: Maximum direct surface stress coefficient

Coefficient w (*Equation G3.3*) is calculated in order to determine the dimensions of the ellipse, and the contact stress between the forming wheel and rebar.

$$w = \left(\frac{3F\pi}{4}(k_1 + k_2)(A_{con} + B_{con})\right)^{\frac{1}{3}} \tag{G3.3}$$

$$w = \left(\frac{3(13538\ N)\pi}{4}\left(1.4E - 12\ \frac{m^2}{N} + 1.38E - 12\ \frac{m^2}{N}\right)(5.044 + 56.31)\right)^{\frac{1}{3}}$$

$$= 0.0693$$

$$a_{con} = \frac{C_a w}{A_{con} + B_{con}}\left(\frac{A_{con}}{B_{con}}\right)^{-\frac{1}{3}} \tag{G3.4}$$

$$b_{con} = \frac{C_b w}{A_{con} + B_{con}}\left(\frac{A_{con}}{B_{con}}\right)^{\frac{1}{3}} \tag{G3.5}$$

An elliptical contact area forms when two cylinders are pressed together, the dimensions are determined using *Equation G3.4* and *G3.5*. The contact area dimensions shown in *Figure G3.3.*

$$a_{con} = \frac{1.3(0.0693)}{5.04429 + 56.3194}\left(\frac{5.04429}{56.3194}\right)^{-\frac{1}{3}} = 0.003285\ m$$

$$b_{con} = \frac{1.65(0.0693)}{5.04429 + 56.3194}\left(\frac{5.04429}{56.3194}\right)^{\frac{1}{3}} = 0.000835\ m$$

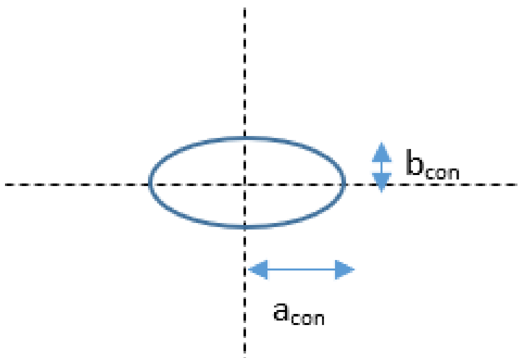

Figure G3.3: Elliptical contact area of two perpendicular cylinders

The contact stress between the forming wheel and the rebar is calculated using *Equation G3.6.*

$$\sigma_{con} = C_f \frac{2w}{\pi^2(k_1 + k_2)} \tag{G3.6}$$

$$= 0.49\frac{2(0.069375)}{\pi^2(1.38E - 12\ \frac{m^2}{N} + 1.4E - 12\ \frac{m^2}{N})} = 2.47\ GPa$$

G4 Hertzian Contact stress of bending arm roller and rebar

The rebar is assigned as body 1, while the bending arm roller is assigned as body 2.

Table G4.1 Bending arm roller physical and material properties (Body 2)

Youngs Modulus, E [GPa]	240 GPa	
Poisson's Ratio, υ	0.3	
Material Constant, k_1	$1.4E-12\ \frac{m^2}{N}$	(IHS EDU, n.d., p.32)
R_{21}	0.04 m	
R_{22}	∞	

Calculating the relative principle curvature (*Equations G3.1* and *G3.2*) using the radiuses of rebar (10 mm) and the bending arm roller (40 mm).

$$A_{con} = \frac{1}{4}\left[\frac{1}{0.01\,m} + \frac{1}{0.04\,m} - \left[\left(\frac{1}{0.0.1\,m}\right)^2 + \left(\frac{1}{0.04\,m}\right)^2 + 2\left(\frac{1}{0.01\,m}\right)\left(\frac{1}{0.04\,m}\right)\cos 2(90°)\right]^{\frac{1}{2}}\right]$$

$$= 5.48059\,m^{-1}$$

$$B_{con} = \frac{1}{4}\left[\frac{1}{0.01\,m} + \frac{1}{0.04\,m} + \left[\left(\frac{1}{0.0.1\,m}\right)^2 + \left(\frac{1}{0.04\,m}\right)^2 + 2\left(\frac{1}{0.01\,m}\right)\left(\frac{1}{0.04\,m}\right)\cos 2(90°)\right]^{\frac{1}{2}}\right]$$

$$= 57.0194\,m^{-1}$$

$$\frac{A_{con}}{B_{con}} = 0.096117$$

$$w = \left(\frac{3(5333\,N)\pi}{4}\left(1.4E-12\,\frac{m^2}{N} + 1.38E-12\,\frac{m^2}{N}\right)(5.48059 + 57.194)\right)^{\frac{1}{3}}$$

$$= 0.035152$$

From *Figure G3.1*, coefficients C_a and C_b can be found:

$$C_a = 1.1$$

$$C_b = 1.13$$

The dimensions of the elliptical contact area are calculated with *Equations G3.4* and *G3.5*:

$$a_{con} = \frac{1.1(0.035152)}{5.48059 + 57.0194}\left(\frac{5.48059}{57.0194}\right)^{-\frac{1}{3}} = 0.00136\ m$$

$$b_{con} = \frac{1.13(0.035152)}{5.48059 + 57.0194}\left(\frac{5.48059}{57.0194}\right)^{\frac{1}{3}} = 0.000291\ m$$

From *Figure G3.3*, coefficient C_f can be found:

$$C_f = 0.79$$

The Hertzian contact stress can be now calculated using *Equation G3.6*:

$$\sigma_{con} = 0.79\frac{2(0.0351516)}{\pi^2(1.38E - 12\ \frac{m^2}{N} + 1.4E - 12\ \frac{m^2}{N})} = 2.02\ GPa$$

G5 Housing calculations (back wall fixed)

A multi-load analysis is used to determine the principle stresses on the housing. The housing is approximated as a square tube (*Figures G5.1* and *G5.2*).

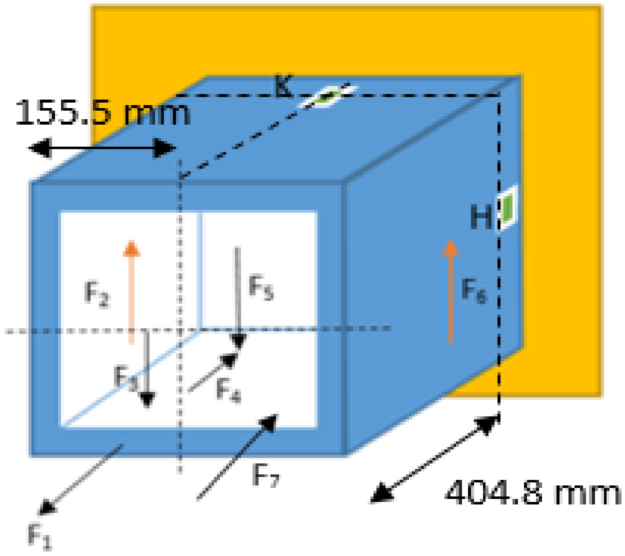

Figure G5.1: Forces acting on rectangular tube approximation of housing. F_1 = 171.1 kN, F_2=32.6 kN, F_3=62.7 kN, F_4=69.6 kN, F_5=58.4 kN, F_6=40.9 kN, F_7 = 4.13 kN

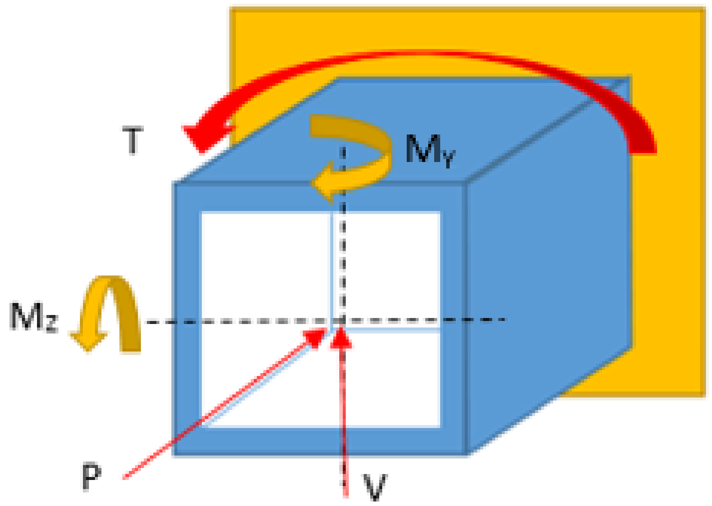

Figure G5.2: Moments and torques caused by forces acting in housing. Where T, P and F are torque horizontal and vertical forces respectively.

Sum of horizontal forces acting on the approximated housing:

$$\sum P = 69576\ N - 171060\ N + 4130.6\ N = -\ 97353\ \text{N}$$

Sum of vertical forces acting on the approximated housing:

$$\sum V = 32599.6\ N + 39485N - 62735.4\ N - 58381.2\ N = -49032\ N$$

The negative values show that the forces are acting in the opposite direction than indicated in *Figure G5.2* and are causing tensile stress. Next, the torsion (about the x axis, coming out of the page) experienced by the housing can be calculated with distances taken from the force to the y-axis.

$$T = 62735.4\ N(0.07232\ m) + 58381.2\ N(0.072\ m) - 32599.6\ N(0.1555\ m) + 80803.6\ N(0.1555\ m) = 16236.2\ Nm$$

The bending moments about the y-axis:

$$M_Y = -171060\ N(0.07232\ m) + 69576\ N(0.072\ m) - 4130.6\ N(0.06213\ m) = -7618.2\ Nm$$

The bending moments about z-axis:

$$M_Z = 62735\ N(0.28617\ m) - 32599.6\ N(0.15418\ m) - 39485\ N(0.15418\ m) + 58381.2\ N(0.09669\ m) + 1534\ Nm = 14017.7\ Nm$$

The second moment of area about y-axis:

$$I_y = \frac{1}{12}(0.3315\ m)(0.311\ m)^3 - \frac{1}{12}(0.3245\ m)(0.304\ m)^3 = 0.000071\ m^4$$

The second moment of area about z-axis:

$$I_z = \frac{1}{12}(0.311\ m)(0.3315\ m)^3 - \frac{1}{12}(0.304\ m)(0.3245\ m)^3 = 0.000078\ m^4$$

To determine the shear stress on the housing due to torsion, *Equation G5.1.1* is used.

$$\tau_s = \frac{T}{2t\mathfrak{A}} \qquad \text{(G5.1.1)}$$

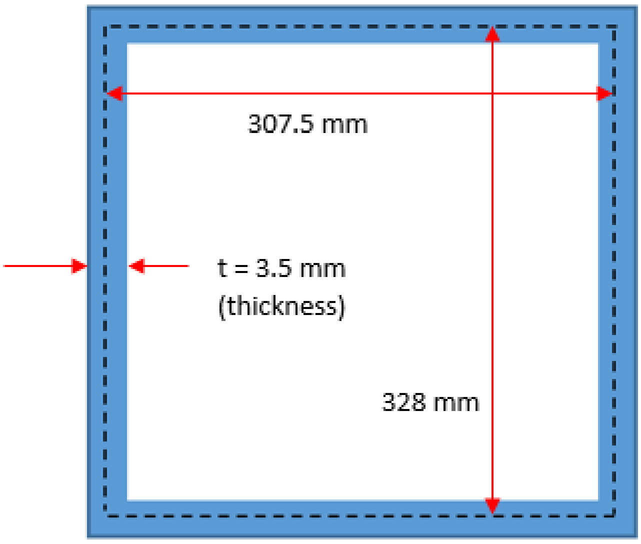

Figure G5.3: Shear area bound by the centre lines of the rectangular cross-section

$$\tau_s = \frac{16236.2\ Nm}{2(0.0035\ m)(0.328\ m)(0.3075\ m)} = 23\ MPa$$

Next, the transverse shear stress for the area shaded in blue (caused by the vertical forces) is calculated using *Equations G5.1.2 and G5.1.3* (*Figure G5.4*).

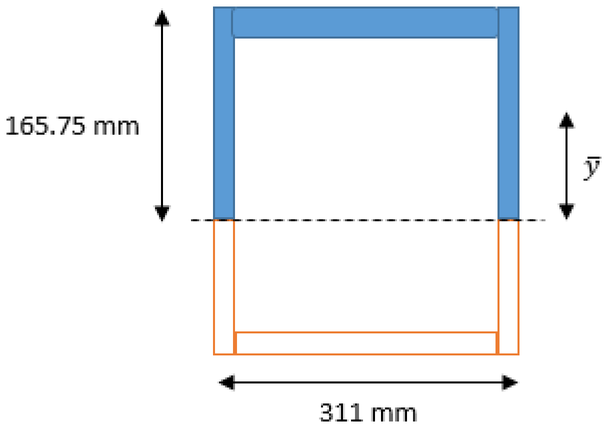

Figure G5.4: Transverse shear of the blue section of the cross-section

$$\tau_s = \frac{VQ}{I_Z t} \tag{G5.1.2}$$

$$Q = \bar{y}A \tag{G5.1.3}$$

$$Q = 0.16575\ m(0.311\ m)(0.082875\ m) - 0.304\ m(0.16225\ m)(0.081125\ m)$$
$$= 0.000271\ m^3$$

$$\tau_s = \frac{49032\ N(0.000271\ m^3)}{0.000078\ m^4(0.0035\ m)} = 48.6\ MPa$$

The normal stresses can now be found for elements K and H using *Equation G5.1.4*. Starting with element K, there are no stresses caused by the moment about y-axis, M_Y, as element K is located on the neutral axis. However, the moment about z-axis, M_Z, does cause a normal stress for element K.

$$\sigma_x = \frac{F}{A} + \frac{M\bar{y}}{I_Z} \tag{G5.1.4}$$

$$\sigma = \frac{-97353}{0.311\ m(0.3315\ m) - 0.3245\ m(0.304\ m)} + \frac{14017.7\ Nm\left(\frac{0.3315\ m}{2}\right)}{0.000078\ m^4}$$
$$= 7.9\ MPa$$

The normal stress for element H can also be calculated using *Equation 5.5.4.*

$$\sigma = \frac{-97353}{0.311\ m(0.3315\ m) - 0.3245\ m(0.304\ m)} + \frac{-7618.2\ Nm\left(\frac{0.311\ m}{2}\right)}{0.000071\ m^4}$$
$$= -39.6\ MPa$$

Using all the calculated values of shear and normal stresses, the principal stresses for each element be calculated. These values can then be represented by the Mohr's Circle (*Figure G5.5*).

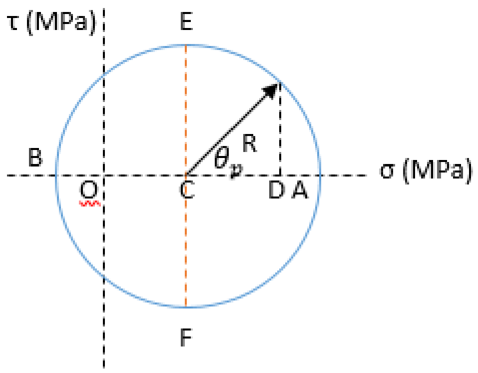

Figure G5.5: Annotated Mohr's Circle

The principal stresses for element K:

$$OC = CD = \frac{1}{2}7.9\ MPa = 3.95\ MPa$$

$$\tau_{max} = R = \sqrt{(3.95\ MPa)^2 + (23\ MPa)^2} = 39.44\ MPa$$

$$\sigma_{max} = OC + R = 3.95\ MPa + 39.44\ MPa = 43.39\ MPa$$

$$\sigma_{min} = OC - R = 3.95\ MPa - 39.44\ MPa = -35.49\ MPa$$

$$\tan 2\theta_p = \frac{23}{3.95}, \therefore \theta_p = 40.1°$$

The principal stresses for element H:

$$OC = CD = -\frac{1}{2}39.6MPa = -19.8\ MPa$$

$$\tau = 48.6\ MPa + 23\ MPa = 71.6\ MPa$$

$$\tau_{max} = R = \sqrt{(-19.8\ MPa)^2 + (71.6\ MPa)^2} = 74.3\ MPa$$

$$\sigma_{max} = OC + R = -19.8\ MPa + 74.3\ MPa = \ 54.5\ MPa$$

$$\sigma_{min} = OC - R = -19.8\ MPa - 74.3\ MPa = -94\ MPa$$

$$\tan 2\theta_p = \frac{71.6}{19.8}, \therefore \theta_p = 37.3°$$

G6 Housing calculations (top wall fixed)

The multi-load analysis is also performed for this orientation where the top wall is fixed (*Figures G6.1* and *G6.2*).

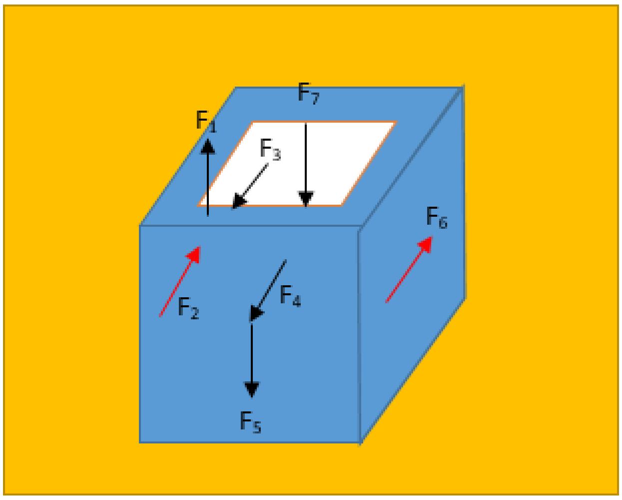

Figure G6.1: Top surface fixed. Forces acting on rectangular tube approximation of housing. F1 = 171.1 kN, F2 = 32.6 kN, F3 = 62.7 kN, F4 = 69.6 kN, F5 = 58.4 kN, F6 = 40.9 kN, F7 = 4.13 kN

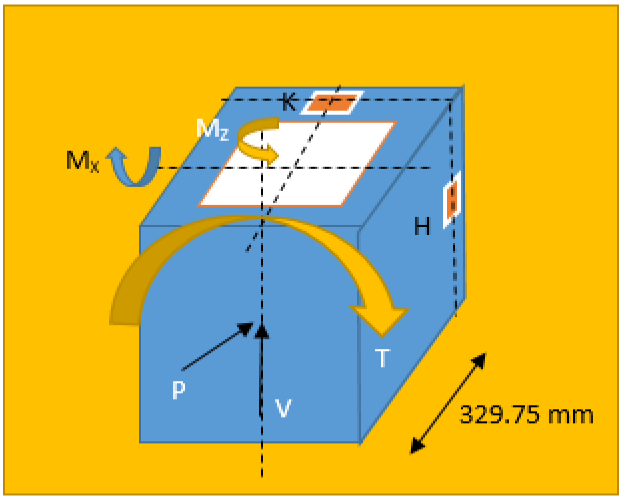

Figure G6.2: Top surface fixed. Moments and torques caused by forces acting in housing. Where T, P and F are torque horizontal and vertical forces respectively.

To calculate the torque, the distances of the forces are taken with reference from the y-axis:

$$T = 4130.6\ N(0.06213\ m) + 171060\ N(0.0598\ m) - 69576\ N(0.072\ m)$$
$$= 5476.55\ Nm$$

The bending moment about the z-axis:

$$M_Z = 39485\ N(0.1555\ m) - 58381.2\ N(0.072\ m) - 32599.6\ N(0.1555\ m) - 62735.4\ N(0.07232\ m) = -7669.7\ Nm$$

The bending moment is acting in the opposite direction indicated in *Figure G6.2*. Next, the bending moment about the x-axis is calculated. Once again, the distance of the forces is taken with reference from the x-axis.

$$\begin{aligned} M_X = {} & -4130.6\ N(0.27063\ m) + 171060\ N(0.26608\ m) - 69576\ N(0.28225\ m) \\ & - 62735.4\ N(0.09998\ m) + 58381.2\ N(0.08857\ m) \\ & + 32599.6\ N(0.03108\ m) + 39485\ N(0.03108\ m) + 1534\ Nm \\ & = 27432.9\ Nm \end{aligned}$$

The second moment of area about the x-axis:

$$I_x = \frac{1}{12}(0.311\ m)(0.3315\ m)^3 - \frac{1}{12}(0.3075\ m)(0.328\ m)^3 = 0.00004\ m^4$$

To calculate the second moment of area about the z-axis, the front face of the rectangular tube is assumed to be rigid and does not deform. This leaves two parallel plates that have a bending moment about the z-axis (*Figure G6.3*). To determine the second moment of area, the parallel axis theorem will be used (*Equation G6.1.1*).

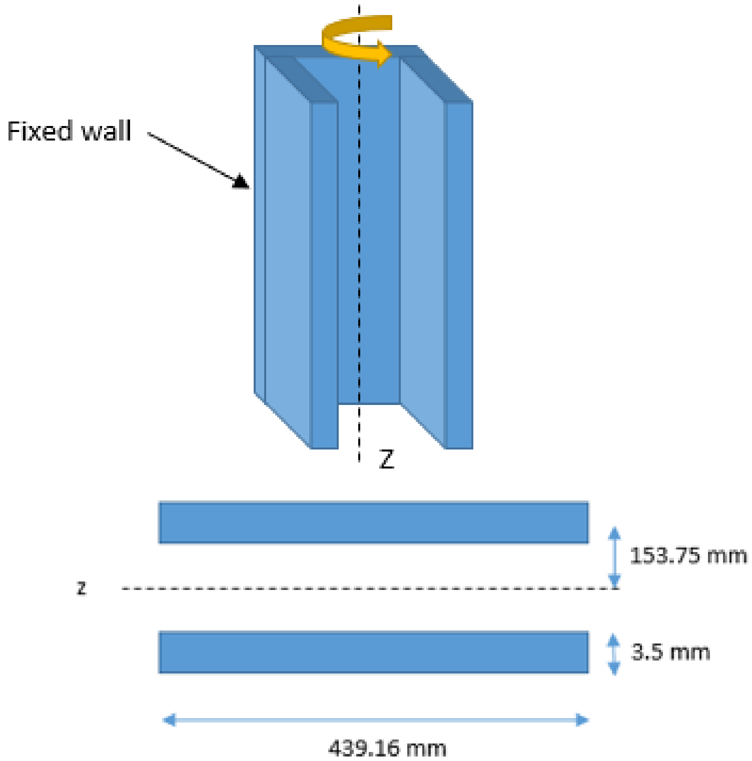

Figure G6.3; Bending of housing about z axis

$$I_{zz} = 2(I_z + Ad^2) \tag{G6.1.1}$$

$$I_{zz} = 2\left(\left(\frac{1}{12}0.43916\ m(0.0035\ m)^3\right) + (0.43916\ m)(0.0035\ m)(0.15375\ m)^2\right)$$

$$= 0.000072\ m^4$$

As there is a torque acting on the housing, this will create torsional shear on the two parallel plates. To determine this shear stress, the polar moment of inertia needs to be calculated (*Equation G6.1.2*).

$$J = I_z + I_x \tag{G6.1.2}$$

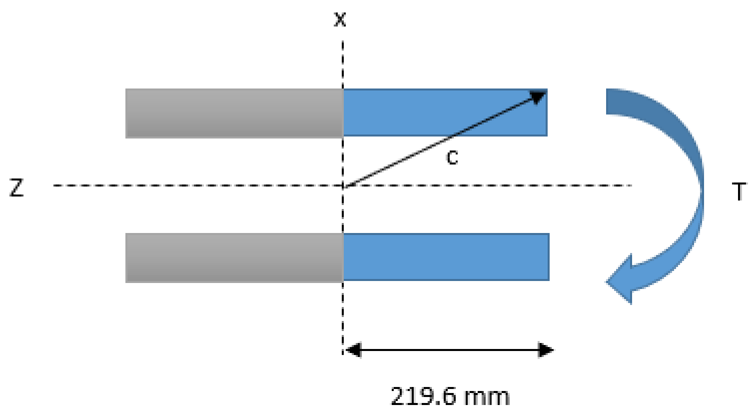

Figure G6.4: Torsional shear of housing

Using *Equation G6.1.2*, the polar moment of inertia about the z- and x-axis needs to be calculated. For the x-axis, only one of the shaded blue sections will be calculated, which will then be multiplied by four times to obtain the total second moment of area. This will give the polar moment of inertia:

$$J = 2\left(\left(\frac{1}{12}0.4316\ m(0.0035\ m)^3 + 0.43916\ m(0.0035\ m)(0.15375\ m)^2\right)\right.$$

$$\left.+\ 2\left(\frac{1}{12}(0.2195\ m)^3(0.0035\ m)\right)\right) = 0.000085\ m^4$$

To calculate the shear stress due to torsion, *Equation G6.1.7* is used. Variable c is the distance from the centre of the housing to a point of interest; in this case the outer most edge of the case as this would give highest shear stress.

$$\tau_s = \frac{Tc}{J} \tag{G6.1.7}$$

$$\tau_s = \frac{5476.5\ Nm(0.4517\ m)}{0.000085\ m^4} = 29.1\ MPa$$

The next shear stress to be calculated is the transverse shear caused by the vertical forces acting in z-direction.

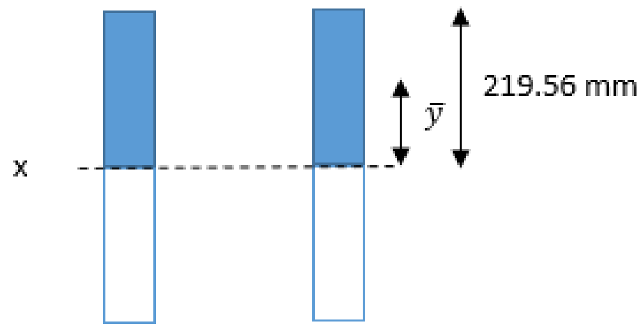

Figure G6.5: Transverse shear of housing

The second moment of area about the x-axis for both sides:

$$I_x = 2\left(\frac{1}{12}0.0035\ m(0.43916\ m)^3\right) = 0.00005\ m^4$$

The second moment of area (*Equation G5.1.3*) of the blue shaded area in *Figure G6.5:*

$$Q = 2\big(0.10979\ m(0.21958\ m)(0.0035\ m)\big) = 0.000169\ m^3$$

Note that the combined thickness of the walls is 7 mm. Using *Equation G6.1.2,* the transverse shear is:

$$\tau_s = \frac{97353.4\ N(0.000169\ m^3)}{0.00005\ m^4(0.007\ m)} = 47\ MPa$$

The normal stresses for the K element can be determined using the bending moment about the x-axis. The bending moment about the z-axis does not cause any stress to element K as it is on the neutral axis (with respect to the bending moment about the z-axis).

$$\sigma = \frac{97353.4\ \mathrm{N}}{2(0.43916\ m)(0.0035\ m)} + \frac{27432.9\ Nm(0.21958)}{0.00005\ m^4} = 152.1\ MPa$$

The normal stresses affecting element H will be calculated using the bending moment about the z-axis, and the corresponding second moment of area about the z-axis (I_{zz}).

$$\sigma = \frac{97353.4\ \mathrm{N}}{2(0.0035\ m)(0.43916\ m)} - \frac{7669.7\ Nm(0.1555\ m)}{0.000072\ m^4} = -8.88\ MPa$$

With the shear and normal stresses known, the principal stresses of each element can be calculated. Starting with element K:

Torsional shear stress: $\tau = 29.1\ MPa$

$$OC = \frac{1}{2}(152.1) = 76.1\ MPa$$

$$R = \sqrt{(76.1\ MPa)^2 + (29.1\ MPa)^2} = 81.5\ MPa$$

$$\sigma_{max} = 76.1\ MPa + 81.5MPa = \ 157.6\ MPa$$

$$\sigma_{min} = 76.1\ MPa - 81.5\ MPa = -5.4\ MPa$$

$$\theta_p = \frac{\tan^{-1}\left(\frac{29.1\ MPa}{76.1\ MPa}\right)}{2} = 10.4°$$

The principal stresses for element H:

Total shear stress:$\tau = 29.1\ MPa + 47\ MPa = 76.1\ MPa$

$$OC = \frac{1}{2}(-8.88\ MPa) = -4.44\ MPa$$

$$R = \sqrt{(-4.44\ MPa)^2 + (76.1\ MPa)^2} = 76.2\ MPa$$

$$\sigma_{max} = -4.44\ MPa + 76.2\ MPa = 71.76\ MPa$$

$$\sigma_{min} = -4.44\ MPa - 76.2\ MPa = -80.64\ MPa$$

$$\theta_p = \frac{\tan^{-1}\left(\frac{76.1\ MPa}{4.44\ MPa}\right)}{2} = 43.3°$$

G7 Shearing mechanism

G7.1 Slider Calculations

G7.1.1 Bending stresses

The bending stresses (due to the location of the force as shown in *Figure G7.1.1.2*) on the blade mount of the slider is determined in order to check it is below the allowable stress of D2 steel.

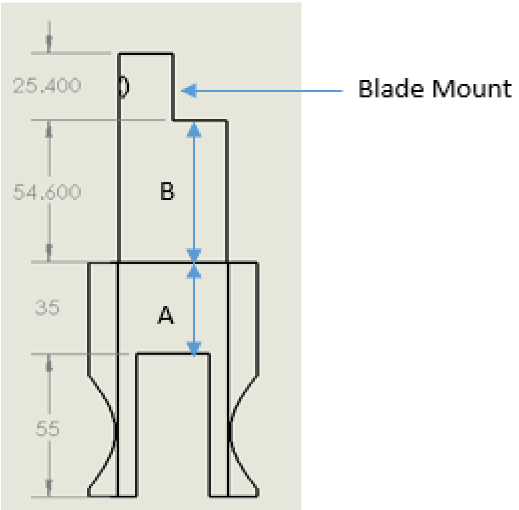

Figure G7.1.1.1; Dimensions of the slider

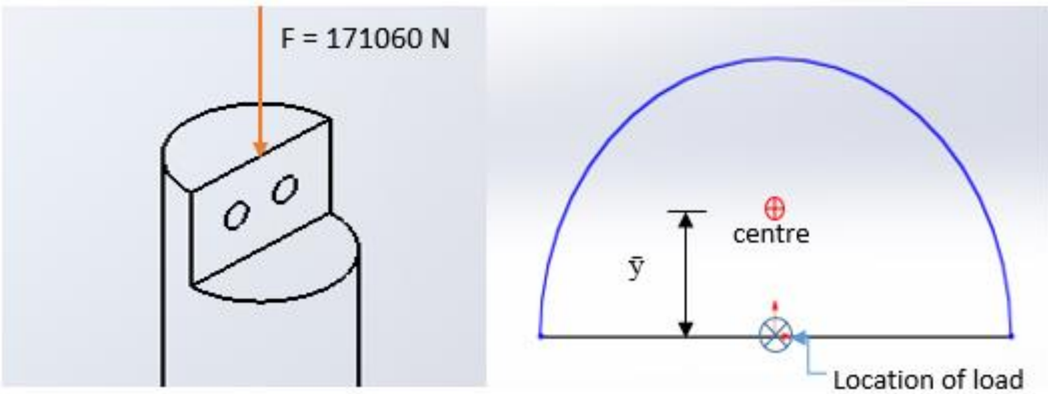

Figure G7.1.1.2: Location of load on slider

The distance from the edge to the neutral axis of the blade mount, (as indicated by ȳ, *Figure G7.1.1.2*) is calculated from the following:

$$\bar{y} = \frac{4r}{3\pi} = \frac{4(0.02\ m)}{3\pi} = 0.008488\ m$$

The bending moment (which accounts for the thickness of the blade of 6.35 mm) and the second moment of area for a semi-circle can then be calculated respectively:

$$M = 171060\ N(0.008488\ m + 0.00635\ m) = 2538.23\ Nm$$

$$I = \frac{1}{8}\pi r^4 = \frac{1}{8}\pi(0.02\ m)^4 = 6.28E-8\ m^4$$

The tensile stress acting on the mount:

$$\sigma = \frac{M\bar{y}}{I} = \frac{2538.23\ Nm(0.008488\ m)}{6.28E - 8m^4} = 342.8\ MPa$$

$$\sigma_{ave} = \frac{F}{A} = \frac{171060\ N}{\pi(0.02\ m)^2} = 272\ MPa$$

$$\sigma_t = \sigma_{ave} + \sigma = 615\ MPa$$

The compressive stress acting on the mount:

$$\sigma_c = \sigma_{ave} - \sigma = -71\ MPa$$

G7.1.2 Column theory

Blade mount section:

The radius of gyration (*Equation G7.1.2.1*) is required to determine the critical stress. Knowing the radius of the blade mount (20 mm) section of the slider, the radius of gyration can be calculated:

$$R = \sqrt{\frac{I}{A}} = \sqrt{\frac{\frac{1}{8}\pi(0.02\ m)^4}{\frac{1}{2}\pi(0.02\ m)^2}} = 0.01\ m \qquad \text{(G7.1.2.1)}$$

Using *Equation G7.1.2.2* and the radius of gyration, the critical stress is determined to be:

$$\sigma_{cr} \frac{\pi^2 E}{\left(\frac{L_e}{R}\right)^2} = \frac{\pi^2(210\ GPa)}{\left(\frac{0.1092\ m}{0.01\ m}\right)^2} = 1.73E10\ Pa \qquad \text{(G7.1.2.2)}$$

The critical load the blade mount can withstand is calculated using *Equation G7.1.2.3*

$$F_{cr} = \frac{\pi^2 EI}{L_e^2} = \frac{\pi^2(210\ GPa)\left(\frac{1}{4}\pi(0.02\ m)^2\right)}{2(0.0546\ m)} = 2.18E7\ N$$

Section A:

The loading in section A is similar to the loading condition represented in *Figure 5.60(b)*, $L_e = L$. First the radius of gyration is calculated (*Equation G7.1.2.1*):

$$R = \sqrt{\frac{\frac{1}{4}\pi(0.031\ m)^4}{\pi(0.031\ m)^2}} = 0.0155\ m$$

Having calculated the radius of gyration, the critical stress can be determined using *Equation G7.1.2.2:*

$$\sigma_{cr} = \frac{\pi^2(210\ GPa)}{\left(\frac{0.035\ m}{0.0155\ m}\right)^2} = 4.06E11\ Pa$$

Finally, the critical load that section A can withstand before buckling occurs is calculated using *Equation G7.1.2.3:*

$$F_{cr} = \frac{\pi^2(210\ GPa)\left(\frac{1}{4}\pi(0.031\ m)^4\right)}{(0.035\ m)^2} = 1.23E7\ N$$

Section B has a similar loading condition as shown in *Figure 5.60(a).* The calculation procedure is the same as the blade mount calculation.

$$R = \sqrt{\frac{\frac{1}{4}\pi(0.02\ m)^4}{\pi(0.02\ m)^2}} = 0.01\ m$$

$$\sigma_{cr} = \frac{\pi^2(210\ GPa)}{\left(\frac{0.0546\ m}{0.01\ m}\right)^2} = 1.7E10\ Pa$$

$$F_{cr} = \frac{\pi^2(210\ GPa)\left(\frac{1}{4}\pi(0.02\ m)^4\right)}{(0.0546\ m)^2} = 2.18E7\ N$$

G7.1.3 Slider pin diameter calculation

Knowing the force of 91101.5 N acting on the pin and the allowable shear stress of L2 steel, slider pin radius, r, can be calculated (*Figure 5.61*). As the pin is supported by the two supports of the slider, a double shear scenario will occur (the force will divide evenly between the two supports).

$$170\ MPa = \frac{4\left(\frac{182203\ N}{2}\right)}{3(\pi r^2)}\ \therefore r = 0.015\ m, \emptyset = 30\ mm$$

G7.2 Linkage BC calculations

G7.2.1 Bearing stress of linkage and bushing

Using the applied force of 182203 N on the pin, and the allowable stress of L2 tool steel the thickness, t, of linkage BC can be solved (*Figure G7.2.3.1*).

$$340\ MPa = \frac{182203\ N}{t(0.03\ m)} = 0.0178\ m \approx 0.02\ m$$

Having found the thickness of linkage BC (20 mm) and the force (182203 N), the bearing stress on bushing can be determined. A bushing with outer diameter of 40 mm encases the slider pin of diameter 30 mm (*Appendix G7.1.3*), knowing the thickness of the linkage and the force, the bearing stress between the bushing and the linkage can be calculated.

$$\sigma_b = \frac{182203\ N}{0.02\ m(0.04\ m)} = 227\ MPa$$

G7.2.2 Column theory

Knowing the dimensions of the linkage, and the material properties of D2 steel, the buckling stress and critical load can be calculated. As the linkage has a rectangular cross-section, this would mean that buckling could either occur about the y- or x-axis.

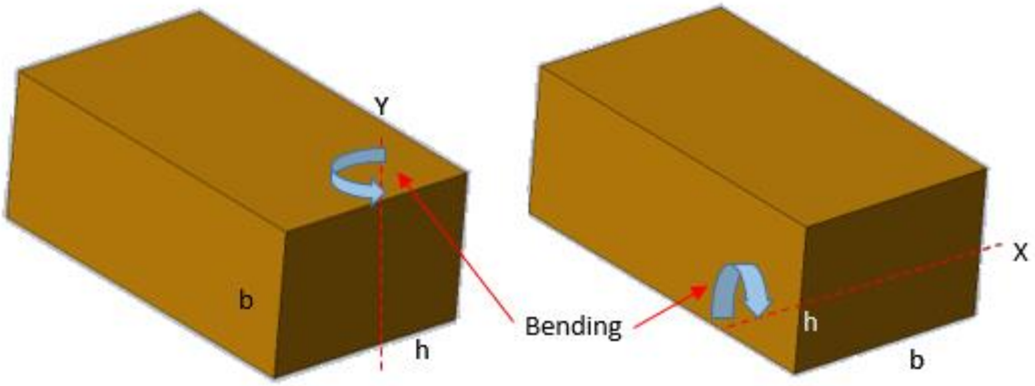

Figure G7.2.2.1; Two possible directions of buckling about Y and X

Buckling about y-axis:

$$I_y = \frac{1}{12}bh^3 = \frac{1}{12}0.05\ m(0.02\ m)^3 = 3.33E-8\ m^4$$

$$F_{cr} = \frac{\pi^2(210\ GPa)3.33E-8\ m^4}{(0.14\ m)^2} = 3.52E6\ N$$

$$\sigma_{cr} = \frac{\pi^2(210\ GPa)}{\left(\frac{0.14\ m}{0.0138\ m}\right)^2} = 2E10\ Pa$$

Buckling about x-axis:

$$I_x = \frac{1}{12}bh^3 = \frac{1}{12}0.02[m](0.05\ m)^3 = 2.08E-7\ m^4$$

$$F_{cr} = \frac{\pi^2(210\ GPa)2.08E-7\ m^4}{(0.14m)^2} = 2.20E7\ N$$

$$\sigma_{cr} = \frac{\pi^2(210\ GPa)}{\left(\frac{0.14\ m}{0.005774\ m}\right)^2} = 3.5E9\ Pa$$

G7.2.3 Linkage BC base bending stress

A force of 91101.5 N creates a bending moment on the base of linkage BC. Knowing the shape of the base and the material properties, the thickness of the base can be determined (*Figure G7.2.4.1*).

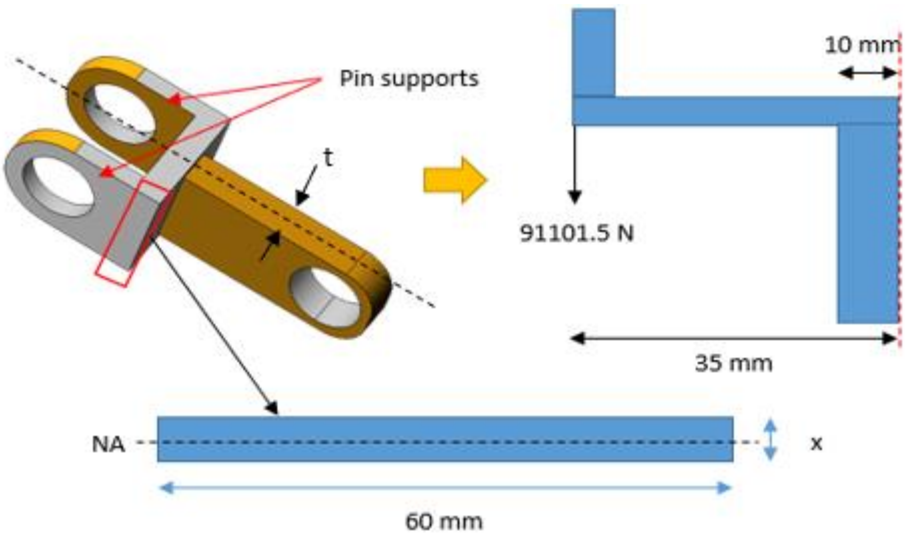

Figure G7.2.3.1: Half side section of linkage BC base

$$M = 91101.5\ N(0.025\ m) = 2277.54\ Nm$$

$$I = \frac{1}{12}bh^3 = \frac{1}{12}(0.06\ m)x^3$$

$$\sigma = \frac{M\bar{y}}{I}$$

$$1.2\ GPa = \frac{2277.54\ Nm\left(\frac{x}{2}\right)}{\frac{1}{12}(0.06\ m)x^3}, \qquad \therefore x \approx 15\ mm$$

G7.3 Linkage AB

G7.3.1 Linkage AB thickness, pin and bushing

Using the allowable shear stress of L2 steel (340 MPa), and the force (45412.5 N) the thickness, t, of linkage AB can be solved (*Figure G7.3.2.1*).

$$340\ MPa = \frac{45412.5\ N}{(0.022\ m)t}, \therefore t = 0.01\ m$$

Using the allowable shearing stress of L2 steel (170 MPa) and the force (45412.5 N) the diameter of the pin can be calculated.

$$170\ MPa = \frac{3}{4}\frac{45412.5\ N}{\pi r^2}, \therefore r = 0.011\ m, \emptyset = 22\ mm$$

The bearing stress on the bushing (which encases the pin giving a total outer diameter of 32 mm) is calculated using the force (45412.5 N), and the projected area.

$$\sigma_B = \frac{F}{A} = \frac{45412.5\ N}{0.01\ m(0.032\ m)} = 206\ MPa$$

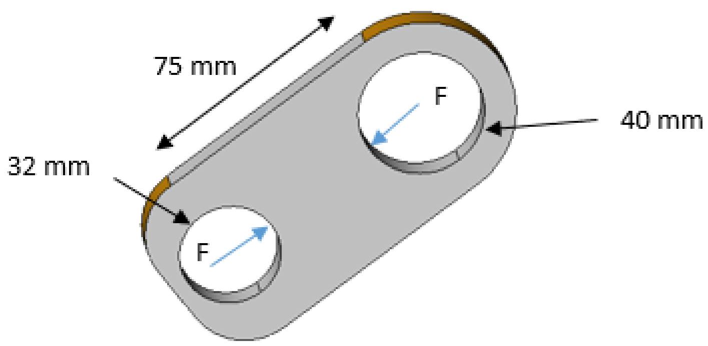

Figure G7.3.2.1: Linkage AB showing dimensions and forces

G7.3.2 Column theory

Knowing the dimensions of linkage AB and the material properties of D2 steel, the critical buckling force and stress can be calculated in x- and y-axis. Starting with the x-axis:

$$I_x = \frac{1}{12}bh^3 = \frac{1}{12}0.06\ m(0.01\ m)^3 = 5E - 9\ m^4$$

$$F_{cr} = \frac{\pi^2(210E9\ Pa)(5E - 9m^4)}{(0.075\ m)^2} = 1.84E6\ N$$

$$\sigma_{cr} = \frac{\pi^2(210\ GPa)}{\left(\frac{0.075\ m}{0.00288\ m}\right)^2} = 3.07E9\ Pa$$

The critical buckling force and stress about the y-axis:

$$I_y = \frac{1}{12} bh^3 = \frac{1}{12} 0.01\ m(0.06\ m)^3 = 1.8E - 7\ m^4$$

$$F_{cr} = \frac{\pi^2 (210E9\ Pa)(1.8E - 7m^4)}{(0.075\ m)^2} = 6.63E7\ N$$

$$\sigma_{cr} = \frac{\pi^2 (210\ GPa)}{\left(\frac{0.075\ m}{0.0173\ m}\right)^2} = 1.05E11\ Pa$$

G7.4 Hinge AB

G7.4.1 Forces on linkages

To determine the forces acting on each linkage, a force diagram is drawn (*Figure G7.4.1.1*).

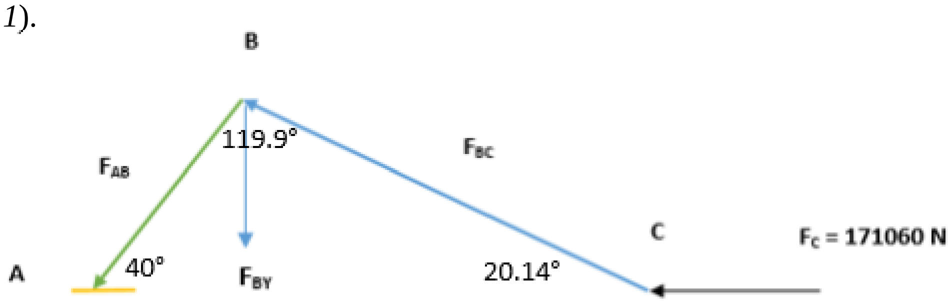

Figure G7.4.1.1: Force diagram of shear mechanism

To determine the force on link BC, the following trigonometric expression is used:

$$F_{BC} = \frac{F_C}{\cos \angle \mathrm{BCA}} = \frac{171060\ N}{\cos(20.14°)}$$

To determine the vertical force at point B, F_{BY}, the following expression is used:

$$F_{BY} = F_C \tan \angle \mathrm{BCA} = 171060\ N \tan(20.14°) = 62734.5\ N$$

To determine the force on link AB, the following expression is used:

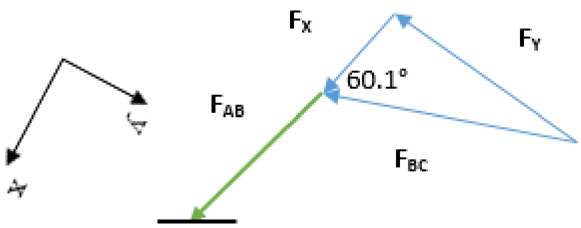

Figure 7.4.1.2: Force acting on linkage AB

$$F_{AB} = F_X = F_{BC} \cos 60.1° = 182201\ N \cos(60.1°) = 90825\ N$$

The force of 45412.5 N is divided evenly between the two linkage ABs.

G7.4.2 Hinge AB supports

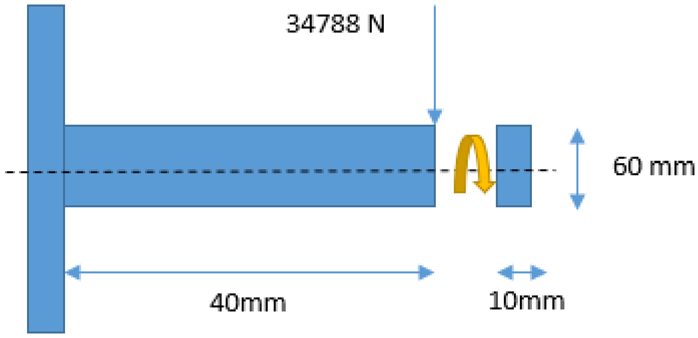

Figure G7.4.1.1: Hinge AB simplified to cantilever

Knowing the horizontal component of the force (34788 N) and the dimensions of the hinge, the bending stress can be calculated.

$$I = \frac{1}{12}(0.01\ m)(0.06\ m)^3 = 1.8E - 7\ m^4$$

$$\sigma = \frac{M\bar{y}}{I} = \frac{1391.52\ Nm(0.03\ m)}{1.8E - 7\ m^4} = 2.32E8\ Pa$$

G7.4.3 Hinge AB base plate

Knowing the allowable stress of D2 steel and the forces acting on the hinge, the base thickness can be determined.

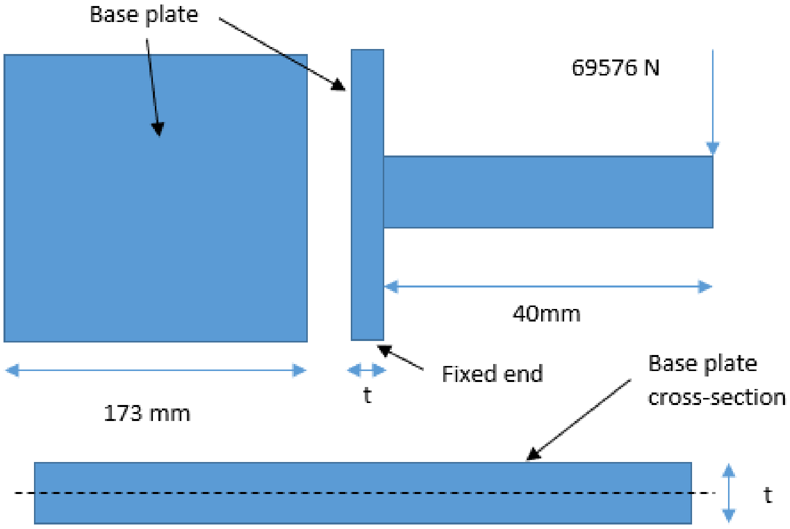

Figure G7.4.2.1: Bending of hinge AB base

Using the dimensions of the base plate of the hinge and the material properties of D2 steel, the thickness, t, of the base plate can be solved for.

$$\bar{y} = \frac{t}{2}$$

$$I = \frac{1}{12}(0.173\ m)t^3$$

$$\sigma = \frac{M\bar{y}}{I}$$

$$1.2\ GPa = \frac{69576\ N(0.04\ m + t)\left(\frac{t}{2}\right)}{\frac{1}{12}(0.173\ m)t^3}, \therefore t = 10mm$$

<u>G7.4.4 Hinge AB bolts</u>

Using the horizontal force component that each bolt will experience (13915.2 N), and the allowable shear stress of the grade 8.8 bolts, the minimum radius, r, can be solved using *Equation G15.1.5*.

$$213.3\ MPa = \frac{4}{3}\frac{13915.2\ N}{\pi r^2}, \therefore r = 5.25mm, \emptyset = 10.5\ mm$$

<u>G7.5 Return Spring</u>

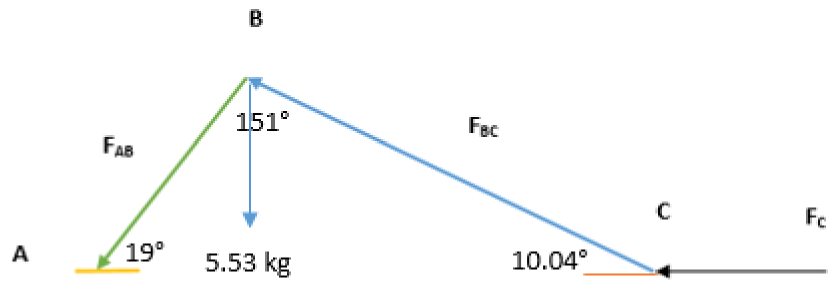

Figure G7.5.1: Force diagram for required spring constant when mechanism is fully extended.

Knowing the total mass of the shearing mechanism, and the force diagram (*Figure G7.5.1*), the estimated spring constant can be calculated.

$$F_c = \frac{54.32\ N}{\tan(10.04°)} = 306.8\ N$$

$$F = -k\Delta x \tag{G7.5.1}$$

$$306.8\ N = -k(0.02\ m), \therefore k = 15348.8\ \frac{N}{m}$$

Using a spring constant of 1300 Nm^{-1} (from spring catalogue) and the compression length (33 mm). The force pushing the mechanism back can be calculated.

$$F = 13000\frac{N}{m}(0.033\ m) = 429\ N > 306.8\ N$$

G7.6 Cam and follower

Maximum pressure angle of the cam:

Using the eccentricity, and prime radius, the governing equations of the H-5 curve, the maximum pressure angle on the cam can be calculated at half rise.

$$\alpha_P = \tan^{-1}\left(\frac{y'(\theta) - \varepsilon_{cen}}{y(\theta) + \sqrt{R_P^2 - \varepsilon_{cen}^2}}\right) \tag{7.6.1}$$

$$\alpha_P = \tan^{-1} \frac{\left(\frac{\pi(0.0237\,m)}{2(150°)}\sin\frac{75°\pi}{150°}\right) - 0.008144[m]}{\left(\left(\frac{0.0237m}{2}\left(1 - \cos\frac{75°\pi}{150°}\right)\right) + \sqrt{0.072\,m^2 - 0.008144\,m^2}\right)}$$

$$= 0.072736\,rad$$

Radius of curvature:

Utilizing the governing equations of the H-5 curve (*Figure 5.76*), maximum rise height, and the angle where the peak of the cam occurs; the radius of curvature at the peak of the cam can be calculated.

$$\rho = \frac{(y^2(\theta) + (y'(\theta))^2)^{\frac{3}{2}}}{y^2(\theta) + 2(y'(\theta))^2 - y''(\theta)y(\theta)} \tag{7.6.2}$$

$$\rho = \frac{\left(\left(\frac{0.0237[m]}{2}\left(1-\cos\frac{150°\pi}{150°}\right)\right)^2 + \left(\frac{0.0237[m]\pi}{2(150°)}\sin\frac{150°\pi}{150°}\right)^2\right)^{\frac{3}{2}}}{\left(\frac{0.0237[m]}{2}\left(1-\cos\frac{150°\pi}{150°}\right)\right)^2 + 2\left(\frac{0.0237[m]\pi}{2(150°)}\sin\frac{150°\pi}{150°}\right)^2 - \left(\frac{0.0237[m]\pi^2}{2(150°)^2}\cos\frac{150°\pi}{150°}\right)\left(\frac{0.0237[m]}{2}\left(1-\cos\frac{150°\pi}{150°}\right)\right)}$$

$$= 0.0138\,m$$

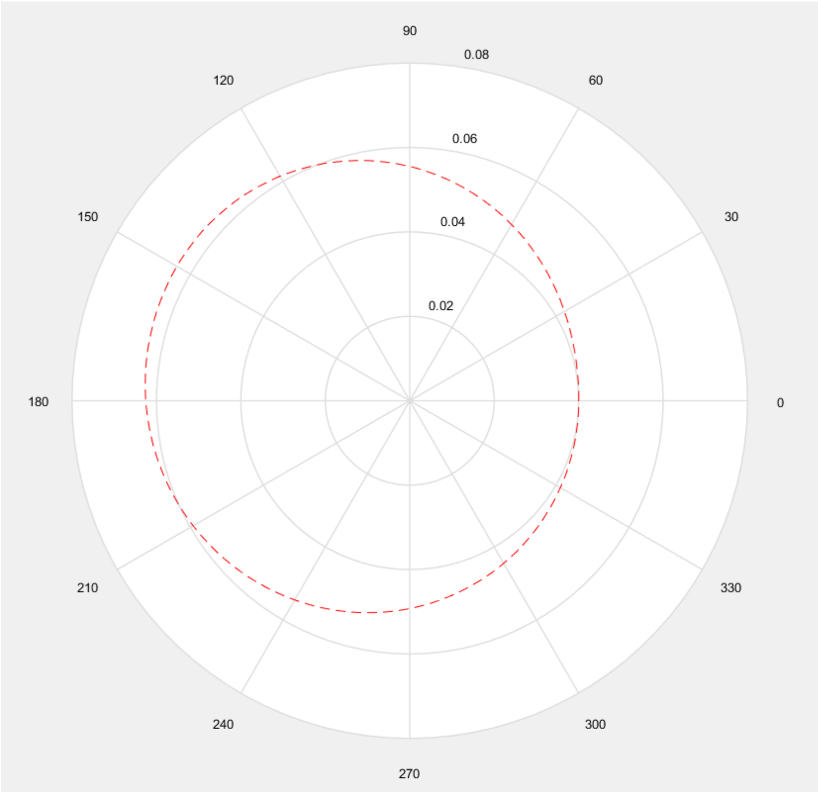

Figure G7.6.1: Cam profile using H-5 and H-6

Hertzian Contact Stress of cam and follower:

Using generic steel material properties an estimate of the half contact width, b, and contact stress, σ_{max}, between the roller follower and can cam can be calculated.

$$b = \sqrt{\frac{2(62932.4\ N)}{\pi(0.05\ m)} \frac{\frac{1-0.3^2}{210\ GPa} + \frac{1-0.3^2}{210\ GPa}}{\frac{1}{0.06\ m} + \frac{1}{2(0.0138\ m)}}} = 0.000362\ m$$

$$\sigma_{max} = \frac{2(62932.4[N])}{\pi(0.000362\ m)(0.05\ m)} = 2.21\ GPa$$

Using the estimated contact stress, a material can be chosen. The re-calculation of the contact stress using ASSB PM30 SuperClean material properties:

$$b = \sqrt{\frac{2(62932.4\ N)}{\pi(0.05\ m)} \frac{\frac{1-0.3^2}{240\ GPa} + \frac{1-0.3^2}{240\ GPa}}{\frac{1}{0.06\ m} + \frac{1}{2(0.0138\ m)}}} = 0.000338\ m$$

$$\sigma_{max} = \frac{2(62932.4[N])}{\pi(0.000362[m])(0.05[m])} = 2.36\ GPa > \sigma_{All} = 2.33\ GPa$$

Torque on drive shaft:

Knowing the force acting on the cam at mid-rise (45992.2 N), the prime radius (r_{12} = 83.8 mm) and the maximum pressure angle (0.072736 rad), the torque acting on the drive shaft can be calculated. Note, r_{12} is the distance between the centres of cam and follower, which also includes the height of rise (*Figure 5.75*).

$$T = F_N r_{12} \sin \alpha_P$$

$$T = 45992.2\,N(0.0838\,m)\sin(0.072736) = 280.25\,Nm$$

Calculating the vertical speed of the follower, and slider:

Knowing the rotational velocity (3 RPM), prim radius, and the maximum pressure angle, the vertical velocity can be calculated.

$$V_{BY} = \omega r_{12} \tan \alpha_P$$

$$V_{BY} = \left(\frac{3\,RPM(2\pi)}{60}\right)(0.042\,m + 0.03\,m + 0.01185\,m)\tan(0.072736)$$
$$= 0.001919\,ms^{-1}$$

Trigonometry is used to calculate the velocity of the slider using *Figure G7.5.2*. V_B and V_C can then be solved:

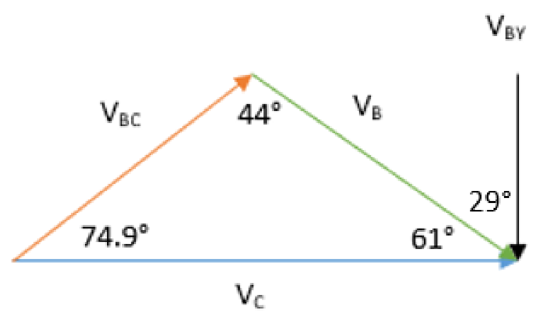

Figure G7.5.2: Velocity diagram when the cam is at half rise

$$V_B = \frac{0.001919\,ms^{-1}}{\cos(0.505971)} = 0.002194\,ms^{-1}$$

Having calculated V_B, the sine rule can be used to determine V_C (velocity of the slider):

$$\frac{V_C}{\sin(0.769254)} = \frac{0.002194\,ms^{-1}}{\sin(1.30751)}, \therefore V_C = 0.00158\,ms^{-1}$$

G8 Cutting Head

G8.1 Bending of top section of cutting head

In order to determine the thickness of the top section of the cutting head (*Figure G8.1.1*), it is assumed that the bottom section of the cutting head is fixed.

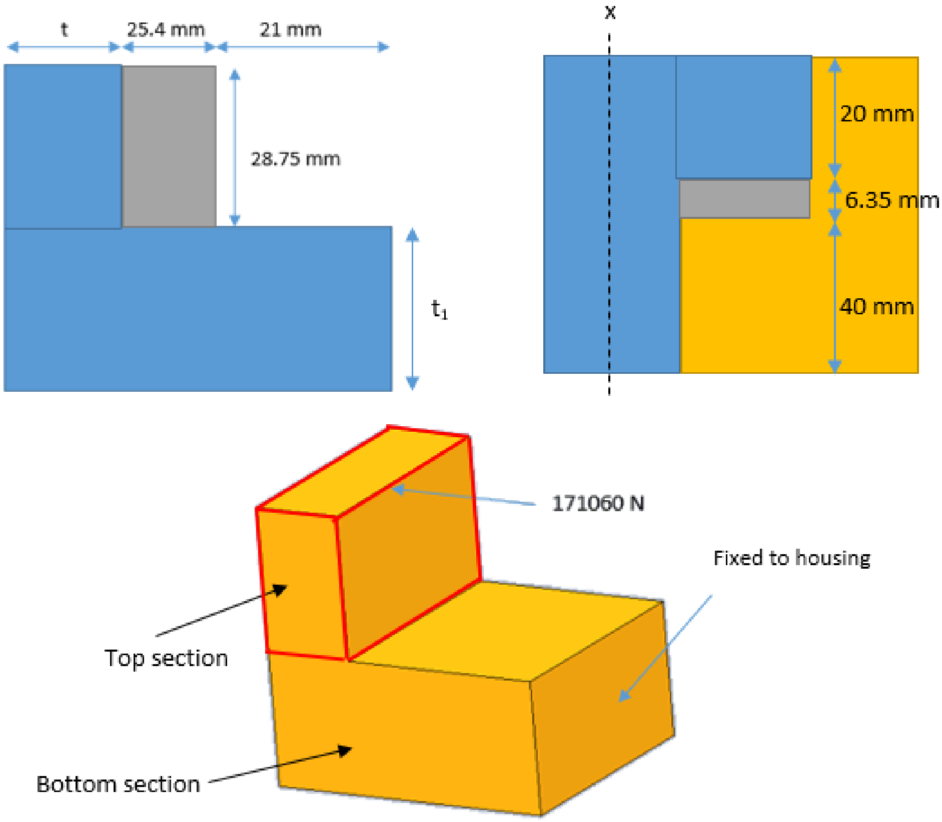

Figure G8.1.1: Bending of top section of cutting head indicated by the red box

Knowing the force (171060 N) acting on the top section of the cutting head, and the allowable stress of the magnesium alloy (306 MPa), the minimum thickness, t_1, can be calculated.

$$M_x = 171060\,N(0.02875\,m) = 4917.98\,Nm$$

$$I_x = \frac{1}{12}bh^3$$

$$\sigma = \frac{M\bar{y}}{I}$$

$$306\,MPa = \frac{4917.98\,Nm\left(\frac{t}{2}\right)}{\frac{1}{12}0.06635\,m\,t^3}, \therefore t = 40\,mm$$

G8.2 Bending of bottom section of cutting head

The thickness, t_1, (the bottom section of the cutting head) needs to be calculated by the same method as in *Section G8.1*. However, the location of the force will create an eccentric loading scenario (*Figure G8.2.1*).

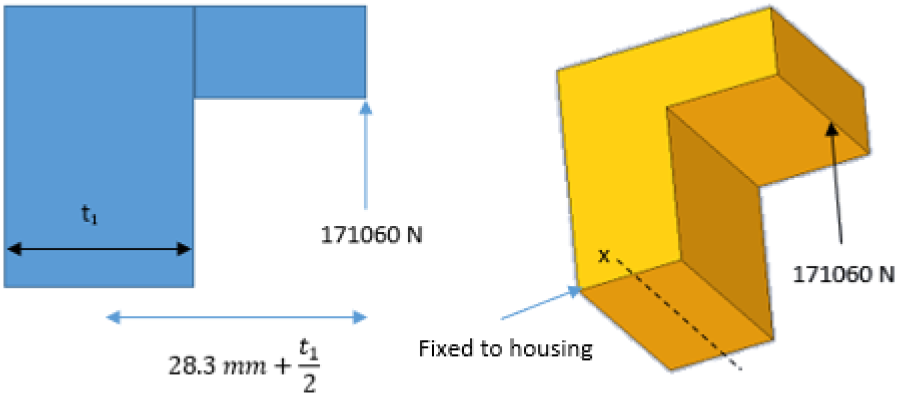

Figure G8.2.1: Eccentric loading of cutting head. Bending of lower section of cutting head

Knowing the force (171060 N) acting on the top section of the cutting head, and the allowable stress of the magnesium alloy (306 MPa), the minimum thickness 't_1' can be calculated.

$$M = 171060\ N\left(0.0283\ m + \frac{t_1}{2}\right)$$

$$I_x = \frac{1}{12}(0.06635\ m)t_1^3$$

$$\sigma = \frac{M\bar{y}}{I}$$

$$306\ MPa = \frac{171060\ N\left(0.0283\ m + \frac{t_1}{2}\right)\left(\frac{t_1}{2}\right)}{\frac{1}{12}(0.06635\ m)t_1^3}, \therefore t_1 \approx 55\ mm$$

G9 Power calculation

Knowing the plastic bending moment of the rebar, the torque can then be calculated and used to determine the power required to bend the rebar.

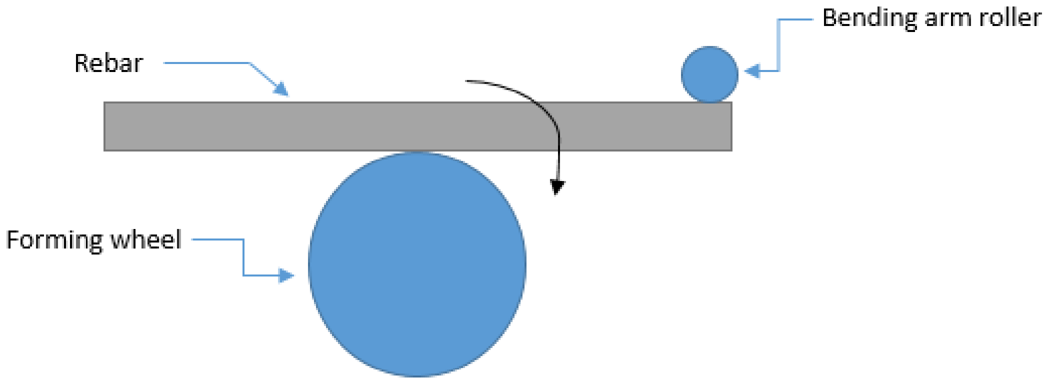

Figure G9.1: Diagram of rebar bending. Arrow indicating direction of bending

$$F = \frac{M_p}{L} = \frac{800\ Nm}{0.15\ m} = 5333.95\ N \tag{G9.1.1}$$

In order to calculate the power required to bend 20 mm rebar, the torque is first calculated using the force required to bend rebar (5333.95 N) and the length of the bending arm (175 mm).

$$T = Fd = 5333.95\ N(0.175\ m) = 933.3\ Nm \tag{G9.1.2}$$

The power for bending can now be determined by using the toque required to bend rebar and the rotational velocity of the arm (3 RPM) the power can be calculated.

$$P_B = T\omega = 933.3\ Nm\left(3\ RPM\left(\frac{2\pi}{60}\right)\right) = 293.2\ W \tag{G9.1.3}$$

The power required for shearing is determined by using the force required to shear rebar (171060 N), and the maximum velocity of the slider, the power required for shearing rebar can be determined.

$$P = F_s V = 171060\ N(0.00158\ ms^{-1}) = 270.3\ W \tag{G9.1.4}$$

G10 Blade Insert

Using the dimensions of the shearing blade, and the force to shear rebar (171060 N); the bearing stress between the blade and the insert can be calculated.

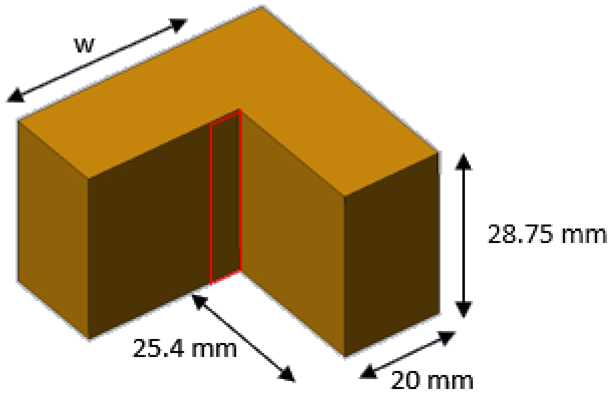

Figure G10.1: The red square indicates bearing area

$$\sigma_B = \frac{171060\ N}{0.00634\ m(0.02875\ m)} = 938\ MPa$$

Using the allow able stress of the magnesium alloy (306 MPa), and the force exerted by shearing rebar (171060 N); the width, w, of the insert can be determined.

$$306\ MPa = \frac{171060\ N}{(0.02875\ m)w}, \therefore w = 20\ mm$$

G11 Rebar stopper block, stopper screw, and stopper cap

G11.1 Rebar stopper block

Assuming the rebar makes contact in the middle of the forming wheel, the distance from this point to the housing wall will be 23 mm. However, the maximum height of 42 mm will be used to give a more conservative thickness.

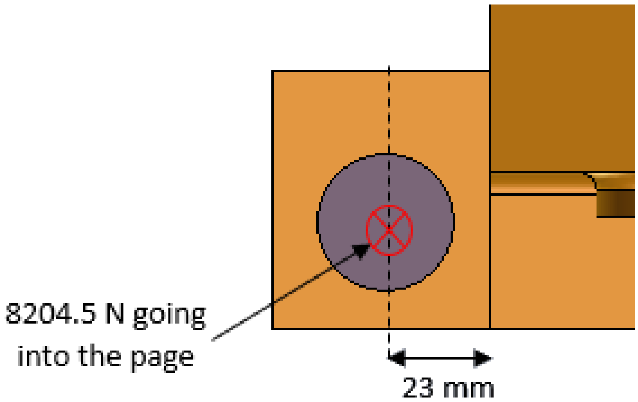

Figure G11.1.1: Distance from centre of stopper screw to wall of housing

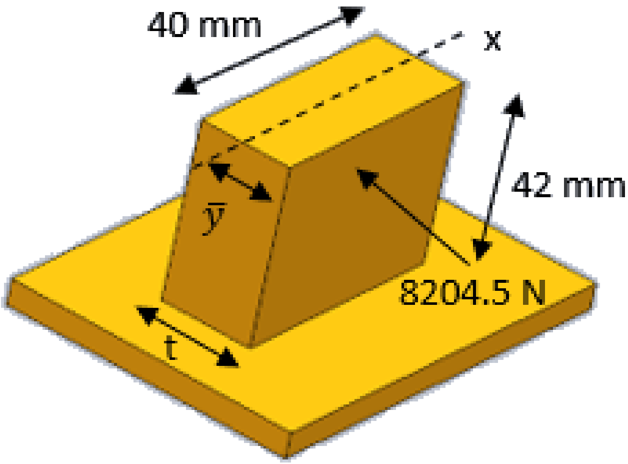

Figure G11.1.2: Simplified diagram of rebar bending stopper block

Knowing the force exerted on the stopper block by the rebar, and the allow able stress of the magnesium alloy, the thickness, t, can be solved.

$$M = 8204.5\ N(0.042\ m)$$

$$I_x = \frac{1}{12}(0.04\ m)t^3$$

$$\sigma = \frac{M\bar{y}}{I}$$

$$306\ MPa = \frac{8204.5\ N(0.042\ m)\left(\frac{t}{2}\right)}{\frac{1}{12}(0.04\ m)t^3}, \therefore t = 13\ mm$$

G11.2 Rebar bending stopper screw

There is a chance that the force applied to the bolt will not be placed in the centre of the bolt. Therefore, bending of the stopper bolt is most likely to occur.

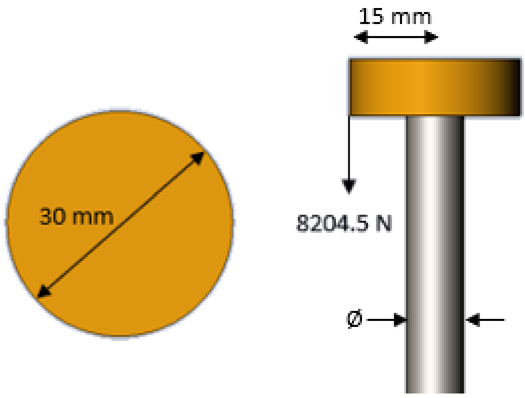

Figure G11.2.1: Possible loading conditions on bender stopper bolt

Using the force acting on the stopper exerted by bending rebar, and the allowable stress of grade 10.9 bolts (626.6 MPa); the radius, r, of the bolt can be solved.

$$\sigma = \frac{M\bar{y}}{I}$$

$$626.6\ MPa = \frac{8204.5\ N(0.015\ m)r}{\frac{1}{4}\pi r^4}, r = 0.0063\ m, \emptyset \approx 14\ mm$$

Contact stress between rebar and bending screw cap

Using the force of 8204.5 N exerted on the stopper by the rebar during bending, and approximating the rebar and the stopper cap to be a cylinder and a plane of length 30 mm. The contact stress between the two bodies can be calculated.

$$b = \sqrt{\frac{4(8204.5\ N)}{\pi(0.03\ m)} \frac{\frac{1-0.3^2}{240\ GPa} + \frac{1-0.3^2}{210\ GPa}}{\frac{1}{0.02\ m} + \frac{1}{\infty}}} = 0.000238\ m$$

$$\sigma = \frac{2(8204.5\ N)}{\pi(0.03\ m)(0.000174\ m)} = 731\ MPa$$

G11.3 Shearing rebar stopper screw and cap

The reaction forces (acting on the stopper, F_B, and the blade, F_A) created by shearing rebar can be calculated using the sum of forces and bending moment equations.

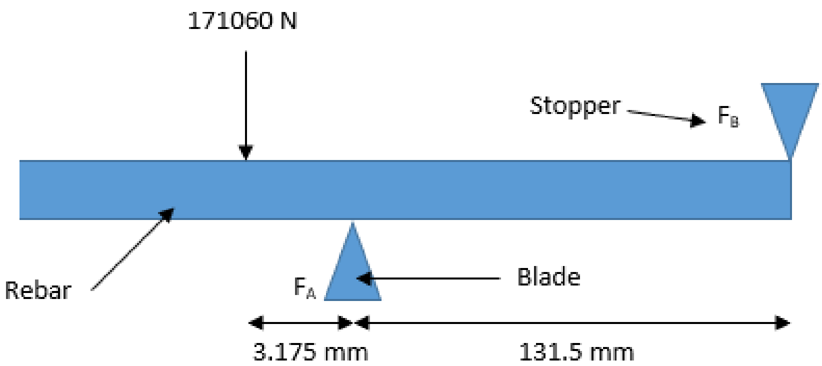

Figure G11.3.1: Forces created by shearing force. Where F_A is the blade attached to the housing and F_B is the stopper support screw

$$\sum +\uparrow F = 0 = F_A - F_B - 171060\ N$$

$$\sum + \square M_A = 0 = -171060\ N(0.003175\ m) - F_B(0.1315\ m)$$

$$F_A = 166930\ N$$

$$F_B = 4130.6\ N$$

Calculating diameter of shearing stopper screw

Knowing the allowable stress of a grade 10.9 (626.6 MPa) and the force exerted on the stopper, the radius of the bolt can be calculated (*Figure 5.94*).

$$\sigma = \frac{M\bar{y}}{I}$$

$$626.6\ MPa = \frac{4130.6\ N(0.015\ m)r}{\frac{1}{4}\pi r^4}, r = 0.005\ m, \emptyset \approx 10\ mm$$

Contact stress between shearing stopper cap and rebar is calculated using force acting on the stopper, the material properties of the rebar and the cap fitted to the stopper bolt.

$$b = \sqrt{\frac{4(4130.6\ N)}{\pi(0.03\ m)} \frac{\frac{1-0.3^2}{240\ GPa} + \frac{1-0.3^2}{210\ GPa}}{\frac{1}{0.02\ m} + \frac{1}{\infty}}} = 0.000169\ m$$

$$\sigma = \frac{2(4130.6\ N)}{\pi(0.03\ m)(0.000174\ m)} = 519.3\ MPa$$

G12 Motor and gearbox panel

Bending stress on vertical gearbox mounting blocks created by the net force from the torque of the gearbox and the vertical forces from the drive shaft.

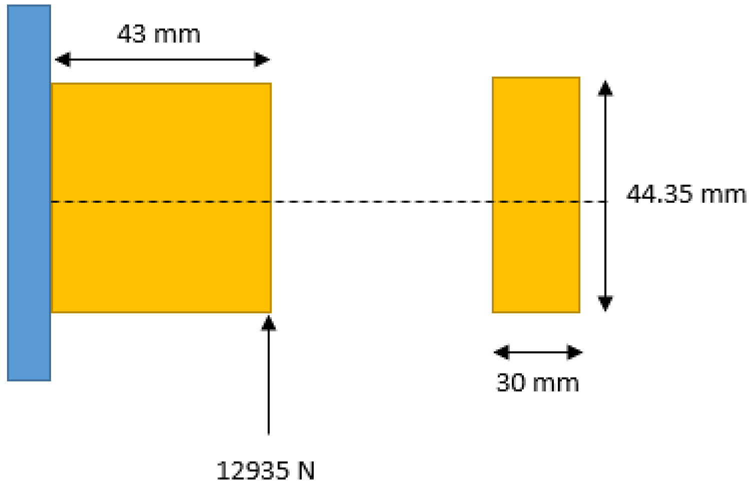

Figure G12.1 Force acting on gearbox vertical mounting block on panel

$$\sigma = \frac{M\bar{y}}{I}$$

$$\sigma = \frac{12935\ N(0.043\ m)(0.02217\ m)}{\frac{1}{12}(0.03\ m)(0.04435\ m)^3 - \frac{1}{4}\pi\left(\frac{0.01\ m}{2}\right)^4} = 56.7\ MPa < 271\ MPa$$

Bending stress on horizontal gearbox mounting blocks:

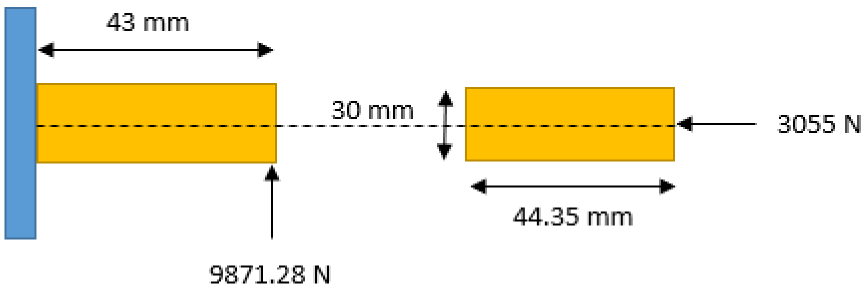

Figure G12.2: Forces acting on gearbox horizontal mounting block on panel

$$\sigma = \frac{M\bar{y}}{I}$$

$$\sigma = \frac{9871.28\ N(0.043\ m)(0.015\ m)}{\frac{1}{12}(0.04435\ m)(0.03\ m)^3 - \frac{1}{4}\pi(0.005\ m)^4} = 64.1\ MPa < 271\ MPa$$

To secure the panel onto the housing will require six bolts located near the edges of the panel (*Figure G12.3*) with the assumption that the forces are evenly distributed.

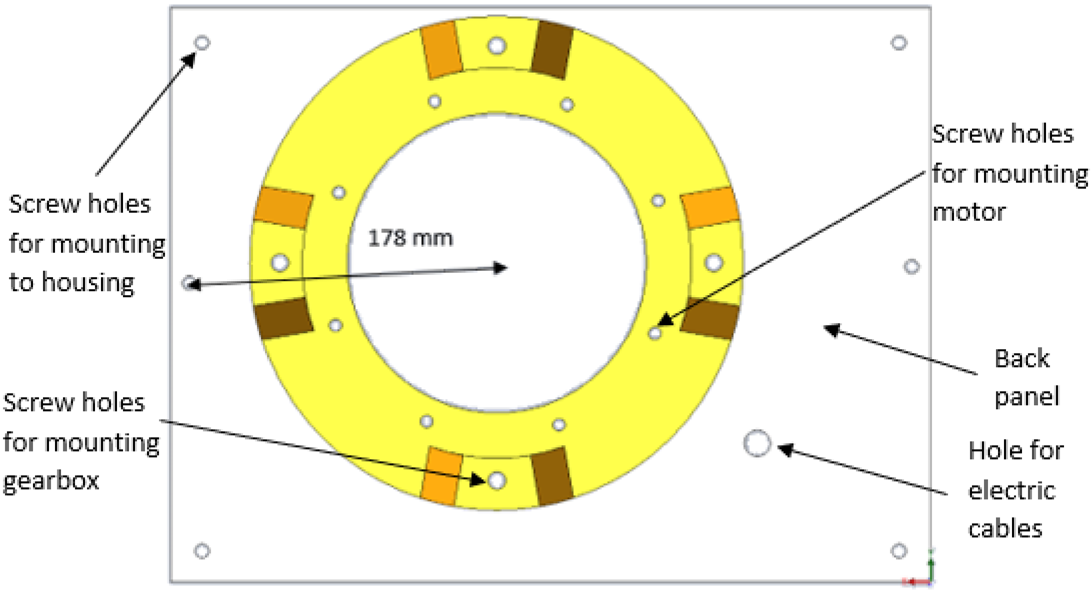

Figure G12.3: Panel showing closest bolt hole to centre of gearbox

Force from first stage ring gear torque:

$$F = \frac{1536\ Nm}{0.178\ m} = 8629.2\ N$$

Force per bolt:

$$F_{bolt} = \frac{39485\ N}{6} + \frac{8629.2\ N}{6} = 8019\ N$$

Using the allowable shearing stress of class 8.8 bolts ($\tau_{all} = 213.35\ MPa$), and the force each bolt will experience (8019 N). *Equation G15.1.5* can be used to determine the diameter of the bolt.

$$213.35\ MPa = \frac{4}{3}\left(\frac{8019\ N}{\pi r^2}\right), \therefore r = 0.004\ m, \emptyset = 8\ mm$$

G13 Handle design

G13.1 Handle support design

Using the total force (due to the total mass of the tool) acting on the handles in the horizontal position, and the allowable stress of the magnesium alloy; the thickness, t, can be determined (*Figure G13.1.2*).

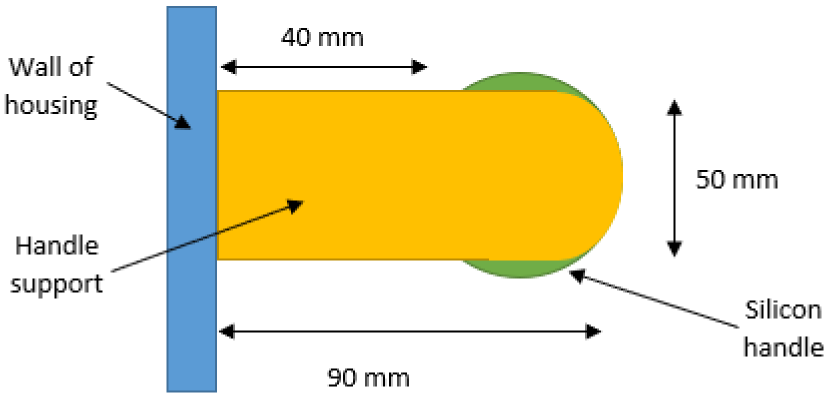

Figure G13.1.1: Dimensions of the handle support

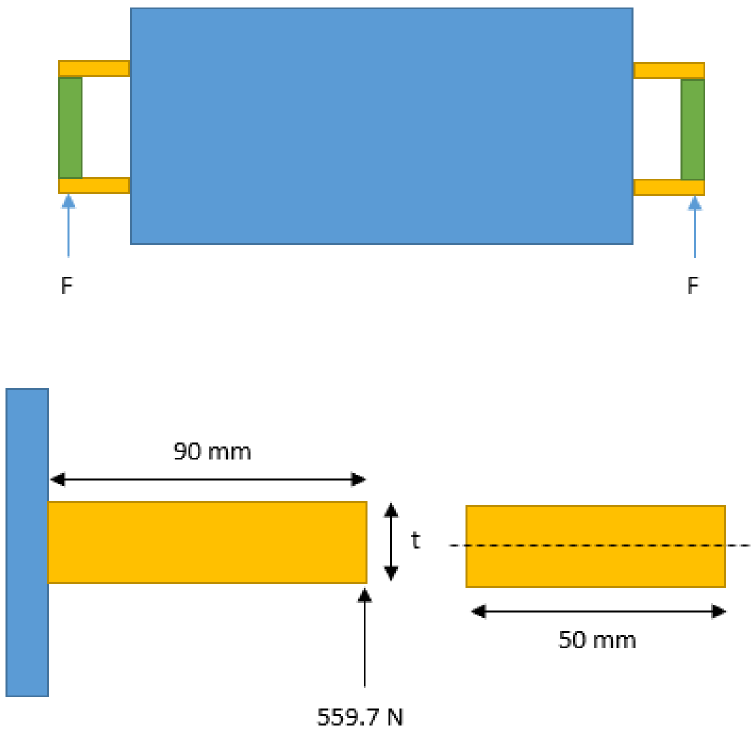

Figure G13.1.2: Bending of handle support with full weight acting on it when tool is on its side

$$\sigma = \frac{M\bar{y}}{I}$$

$$306\text{ MPa} = \frac{559.17\ N(0.09\ m)\left(\frac{t}{2}\right)}{\frac{1}{12}(0.05\ m)t^3}, \therefore t = 0.01\ m$$

Bending stress on handle supports when the tool is upright, using the total force acting on one housing handle, the handle bending stress in the upright position can be checked against the allowable stress of the magnesium alloy.

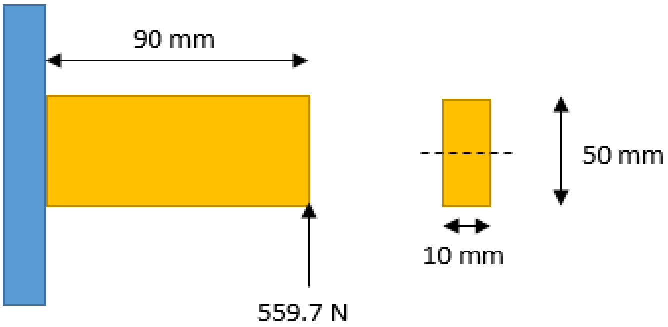

Figure G13.1.3: Bending of handle support with full weight acting on it when tool is on its side

$$\sigma = \frac{M\bar{y}}{I}$$

$$\sigma = \frac{559.7\ N(0.09\ m)(0.025\ m)}{\frac{1}{12}(0.01\ m)(0.05\ m)^3} = 12\ MPa < 306\ MPa$$

<u>G13.2 Diameter of handle bolts</u>

Using the allowable shear stress of AISI 1141 steel, and the total weight of the tool, the minimum diameter of the rod can be determined.

$$220\ MPa = \frac{4}{3}\frac{559.17\ N}{2(\pi r^2)}, \therefore r = 0.000636\ m, \emptyset = 1.2\ mm$$

As a 1.2 mm bolt is difficult to find, a standard 16 mm hex bolt will be used.

G14 Bending arm Calculations

G14.1 Bending stress

Utilizing the plastic bending moment (800 Nm), and the sum of moments and forces; the reaction forces from rebar bender stopper (R_A) and the forming wheel (R_B) can be determined.

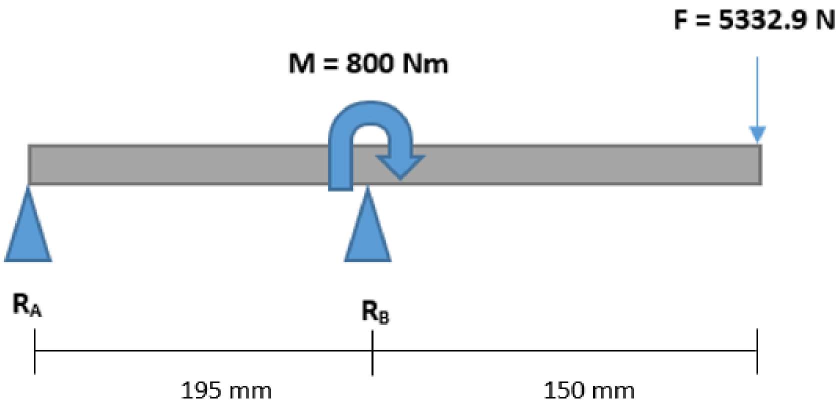

Figure G14.1.1: Beam diagram depicting loads on the rebar

$$F = \frac{M}{L} = \frac{800\ Nm}{0.15\ m} = 5332.9\ N$$

$$\sum F = R_A + R_B - 5332.9\ N = 0$$

$$\sum M_{RA} = -800\ Nm - F_C(0.345\ m) + R_B(0.195\ m) = 0$$

$$R_A = -8205\ N$$

$$R_B = 13538\ N$$

To calculate the bending stress of the bending arm, it was approximated as a cantilever.

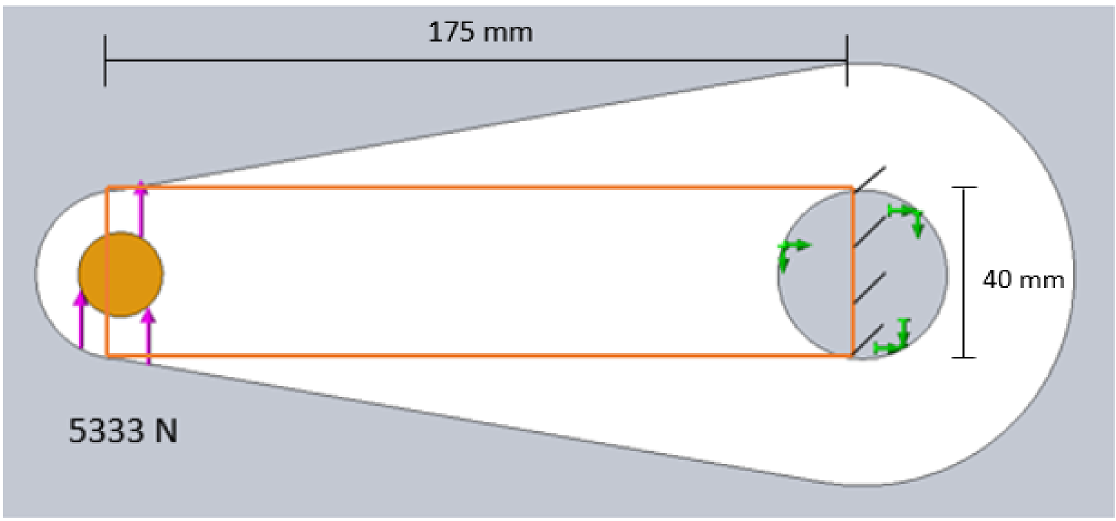

Figure G14.1.2: Bending arm with simplified cantilever

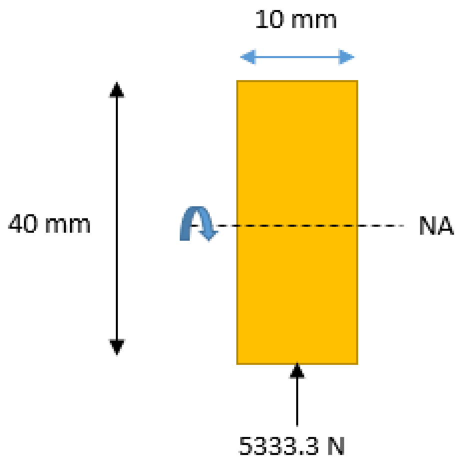

Figure 14.1.3: Cross-section of bending arm cantilever approximation

$$I = \frac{1}{12}bh^3 \tag{G14.1.1}$$

$$I = \frac{1}{12}0.01\,m\,(0.04\,m)^3 = 5.33E - 8\,m^4$$

The stress can then be calculated using the dimensions of the bending arm, force, *Equation G14.1.2*. and *G14.1.1*.

$$\sigma = \frac{My}{I} \tag{G14.1.2}$$

$$\sigma = \frac{5332.9\,N(0.175\,m)0.02\,m}{5.33E - 8\,m^4} = 350\,MPa$$

G14.2 Torsional stress of bending arm

Due to the location of the force acting on the bending arm roller support, torsional stress on the arm is most likely to occur. Therefore, a check must be performed to ensure the torsional shear stress of the arm is below the allowable shear stress of the material.

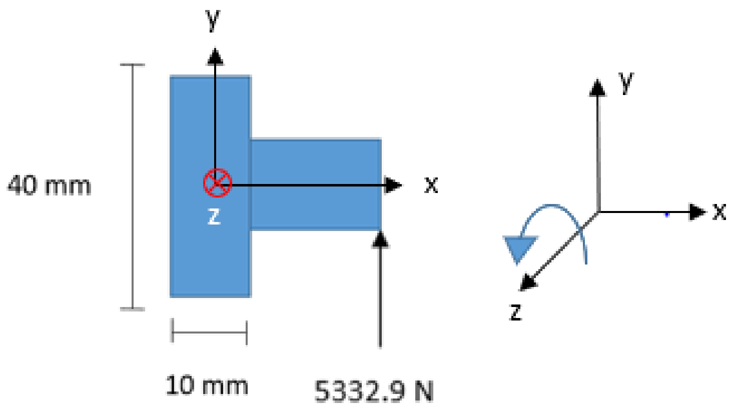

Figure G14.2.1: Force acting on bending arm roller

Where a and b are the long and short lengths of the cross-section respectively. The ratio of a and b are used to select the value of c_1 from *Table G14.2.1*.

$$\tau = \frac{T}{c_1 a b^2} \quad \text{(G14.2.1)}$$

Table G14.2.1 Coefficients for Rectangular Bars in Torsion (Beer, Johnston, Jr, DeWolf, & Mazurek, 2006)

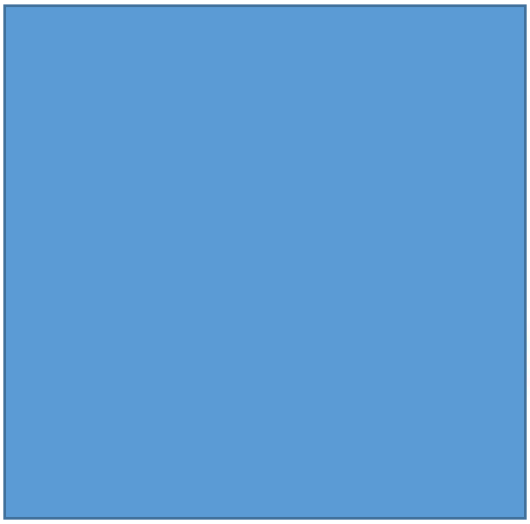

$$\frac{a}{b} = \frac{40}{10} = 4$$

Knowing the magnitude and location of the force, the torsional shear stress can be calculated using *Equation G14.2.1*.

$$\tau = \frac{133.33\ Nm}{0.282(0.04\ m)(0.01\ m)^2} = 119\ MPa$$

G15 Rebar shearing force equation derivation

The average shearing force is determined by deriving a formula, from *Equation G15.1.1*, for a circular cross-section.

$$\tau = \frac{F_s Q}{Iz} \quad \text{(G15.1.1)}$$

The maximum shear stress occurs at the centre of the rebar, which is also the location of the neutral axis, denoted in *Figure G15.1* as N.A. The centroid of the top half of the circle is denoted with the letter C.

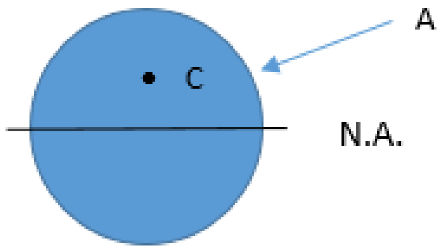

Figure G15.1: Cross-section of rebar

The first moment with respect to the neutral axis of the area A (*Figure G15.1*) is determined using *Equation G15.1.2.*

$$Q = A\bar{y} \quad \text{(G15.1.2)}$$

To determine the distance of centroid 'C' from the neutral axis, *Equation G15.1.3* is used. Note the area, $A = \frac{1}{2}\pi r^2$, is the area of the semi-circular cross-section.

$$\bar{y} = \frac{4r}{3\pi} \quad \text{(G15.1.3)}$$

Substituting *Equation G15.1.3* and the area of the semi-circular cross-section into *Equation G15.12* will give *Equation G15.1.4.*

$$Q = \frac{2r^3}{3} \quad \text{(G15.1.4)}$$

Equation G15.1.4 is then substituted into *Equation G15.1.1*; knowing the formula for the second moment of area (area moment of inertia) of a circular cross-section, and $z = 2r$, the final equation that determines the maximum shear stress in the rebar is derived (*Equation G15.1.5*).

$$\tau_{max} = \frac{4F_s}{3A} \quad \text{(G15.1.5)}$$

G16 Plastic bending moment of rebar

As plastic bending is taking place, Hooke's Laws no longer apply; the only assumptions that can be made are that the material is isotropic, and normal strain, ε_x, varies linearly in the y-direction from the neutral axis. This is described in the following equation and in *Figure G16.1*:

$$\varepsilon_x = -\frac{y}{c}\varepsilon_{max}$$

Where y is some distance from the neutral axis of the cross-section, c is the maximum value of y, and ε_{max} is the maximum strain value.

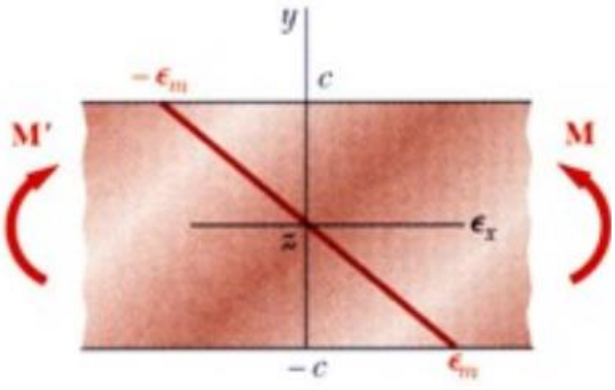

Figure G16.1: Strain distribution (Beer, Johnston, Jr, DeWolf, & Mazurek, 2006)

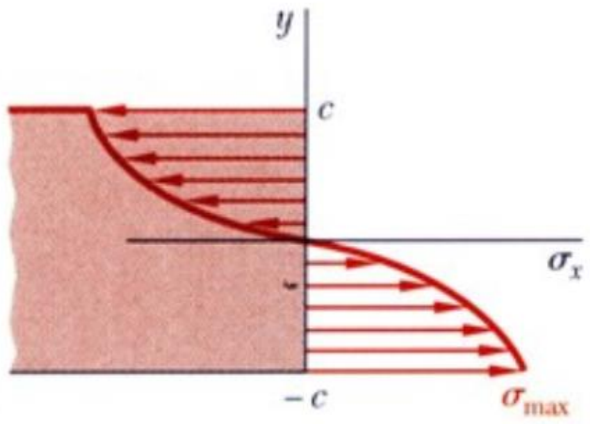

Figure G16.2: Stress distribution (Beer, Johnston, Jr, DeWolf, & Mazurek, 2006)

With bending applied to a bar, a normal stress distribution will appear as shown in *Figure G16.2*. The stress distribution is derived from the normal strain equation mentioned previously, assuming the stress/strain curve is given. To determine the bending moment of the stress distribution, the following general formula is used:

$$M = \int_{-c}^{c} -y\sigma_x dA \qquad \text{(G16.1.1)}$$

Where M is the bending moment, and σ_x is the function of the stress distribution. From *Figure G16.2* one can see that it is an odd function. From this observation the general equation above can be written as the following:

$$M = 2\int_0^c -y\sigma_x dA \tag{G16.1.2}$$

However, as the bar is reaches yield stress, σ_Y, plastic deformation zones form on the top and bottom of the bar, in compression and tension, respectively. This also means that at the core of the bar there is an elastic zone of a certain thickness as shown in *Figure G16.2*.

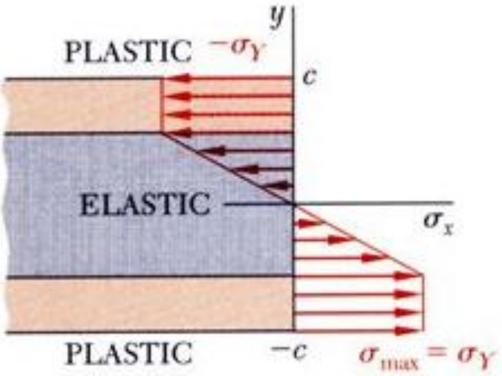

Figure G16.3: Stress distribution of elastoplastic material (Beer, Johnston, Jr, DeWolf, & Mazurek, 2006)

The following equation is then altered accordingly to take the plastic deformation zones into account.

$$M_p = 2\int_0^{y_y} -y\sigma_x dA + 2\int_{y_y}^{c} -y\sigma_Y dA \tag{G16.1.3}$$

Where y_y is the half height of the elastic core. It should also be noted that the strain remains linear even after the bar reaches the yield stress, which allows the following strain relationship to be used in determining y_y.

$$y_y = \epsilon_Y \rho \tag{G16.2.4}$$

Where ε_Y the strain at yield, and ρ is the radius of curvature. The elastic core that exists between the two plastic zones, as shown in *Figure G16.3*, has the following linear stress relationship that changes with the value of y.

$$\sigma_x = -\sigma_Y \frac{y}{y_y} \tag{G16.1.5}$$

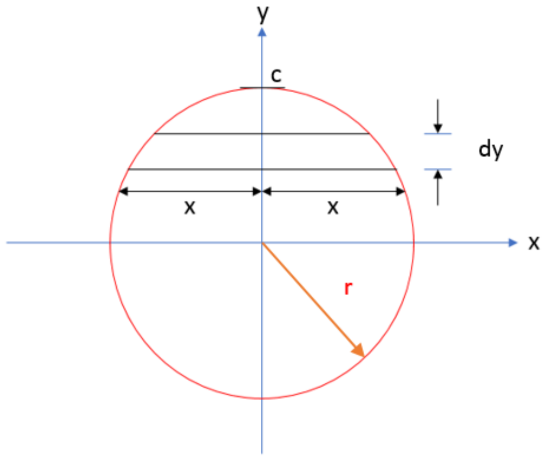

Figure G16.4: Cross-section of rebar

The circular cross-section of the rebar in *Figure G16.4* is given by the equation of a circle, *Equation G16.1.6*.

$$x = \sqrt{r^2 - y^2} \tag{G16.1.6}$$

A rectangular section of the circle is taken with an area determined by dy and $2x$. An equation can then be written in the form of the following:

$$dA = 2xdy \tag{G16.1.7}$$

Substituting *Equation G16.1.6* into *Equation G16.1.7* gives the following:

$$dA = 2\sqrt{r^2 - y^2}dy \tag{G16.1.8}$$

Equations G16.1.8 and G16.*1.5* can then be substituted into *Equation G16.1.3*, integrating the equation gives *Equation G16.1.9*

$$M_p = (-4)\int_0^{y_y} y\left(-\sigma_Y \frac{y}{y_y}\right)\sqrt{r^2 - y^2}\,dy + (-4)\int_{y_y}^{c} y(-\sigma_Y)\sqrt{r^2 - y^2}\,dy$$

And with $c = r$ this yield:

$$M_p = \frac{\sigma_Y\left(3c^4 sin^{-1}\left(\left|\frac{1}{c}\right| y_y\right) - y_y\left(2y_y^2 - 5c^2\right)\sqrt{c^2 - y_y^2}\right)}{6y_y} \tag{G16.1.9}$$